AD NUMBER
AD317764
CLASSIFICATION CHANGES
TO: **UNCLASSIFIED**
FROM: **CONFIDENTIAL**
LIMITATION CHANGES
TO: **Approved for public release; distribution is unlimited.**
FROM: **DTIC Classified Users Only. Controlling DoD Organization: Naval Air Systems Command, Naval Air Weapons Center, Patuxent River NAS, MD.**
AUTHORITY
31 May 1970 DoDD 5200.10 gp-4; ONR, d/n ltr, 26 Oct 1972

AD _____

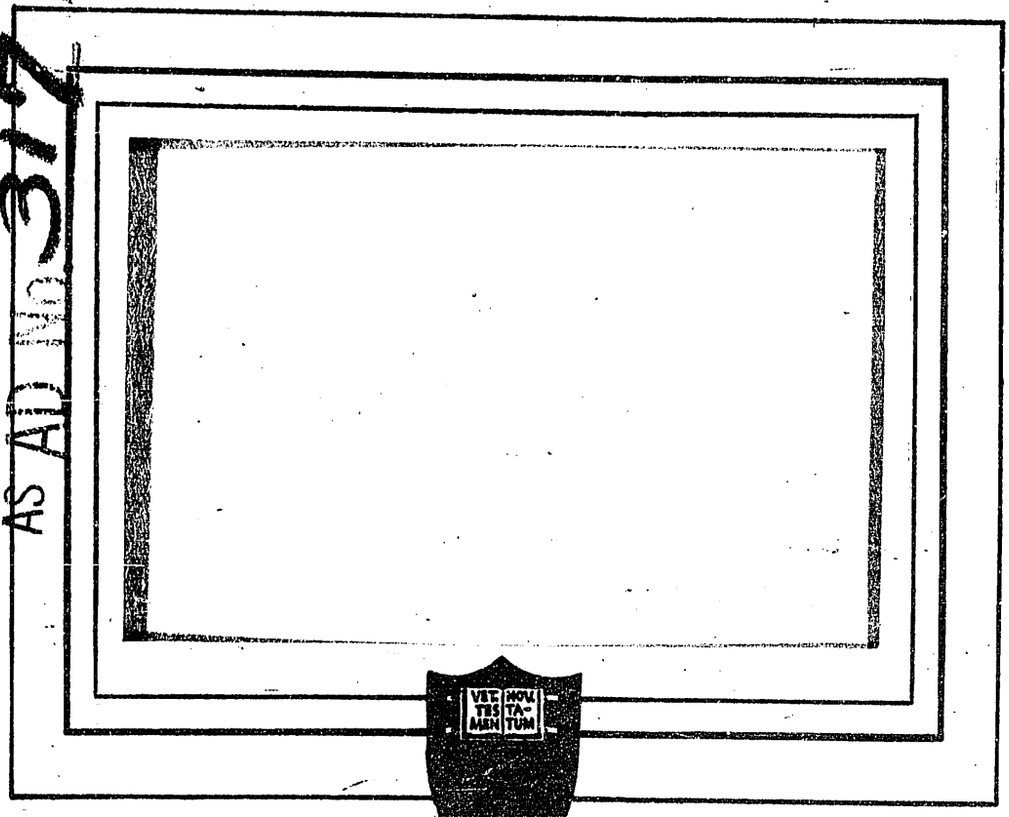

PRINCETON UNIVERSITY

DEPARTMENT OF AERONAUTICAL ENGINEERING

A STUDY OF THE LOW SPEED AERODYNAMIC CHARACTERISTICS OF HIGH-LIFT FLOW CONTROLLED PROFILES AND WINGS

7/16 300

D. J. Dike
H. S. Dunn
D. C. Hazen
R. F. Lehnert

Contract #Noas 55-583-d

Report No. 349 May, 1958

TABLE OF CONTENTS

TABLE OF CONTENTS CON'T.

ACKNOWLEDGEMENTS

The authors wish to extend their gratitude to Mr. M. H. Smith and Mr. M. H. Fisher of the James Forrestal Research Center Library for their many labors in the extensive literature searches necessitated by this project. Recognition is also due Mr. W. R. Willauer, engineer in charge of the smoke tunnel facilities, as well as the members of the technical and analytical staffs of the Subsonic Aerodynamics Laboratory for their great assistance in the experimental phases of this work. In addition, the authors certainly owe their thanks to the many investigators mentioned in the bibliography whose research form the foundation of a good portion of this report.

CONFIDENTIAL

I. SUMMARY

A study ~~has been~~ was made of methods of conducting preliminary estimation of the aerodynamic characteristics of wings and profiles employing various forms of high-lift devices. These high-lift devices include all forms of flow control for which sufficient data are available to form the basis of such semi-empirical methods of estimation. ~~Additionally,~~ those controls for which little data exist are discussed, ~~as fully as possible~~. In all cases an attempt ~~has been~~ was made to study and describe all phenomena basic to the effectiveness of the particular device, and extensive use was made of the smoke tunnel facilities at the Forrestal Research Center ~~has been made for this purpose~~.

~~This report includes~~ are included methods of estimating the ~~two~~ 2-dimensional effectiveness of both leading- and trailing-edge devices applied to arbitrary profiles. These estimations are based on data collected by a large number of investigators, substantiated and extended where necessary by smoke and wind tunnel tests conducted at Forrestal.

An intensive effort was made to develop a technique of predicting the creation and persistance of the leading-edge vortex for the ~~three~~ 3-dimensional case as a function of leading-edge radius, effective Reynolds Number, leading-edge sweep, and aspect ratio. Because of ~~Due to~~ the unavailability of data and the multiplicity of important variables, this approach proved unsuccessful, as did all attempts to rigorously predict the characteristics of wings equipped with high-lift devices, ~~and at the present moment~~ it appears that empirical results based on closely similar configurations form the only adequate means of accurately predicting the low-speed performance capabilities of a given design. This report attempts,

R [C] JM

however, to determine and point out the trends which may give some insight into control design for a given wing as well as indicate areas where further research is apt to be most profitable.

II. INTRODUCTION

High-lift controls such as trailing-edge flaps and, to a lesser extent, slots and slats have been used for a great many years for the purpose of improving the take-off and landing characteristics of aircraft.

As World War II was spreading throughout Europe it became obvious that very short take-off aircraft of the liason and short-haul cargo types could be of considerable tactical use, particularly in operations off unprepared landing strips. This led to the development of aircraft using large, full span slotted flaps, leading-edge slats, and finally, in Germany, to the development of practicable powered controls involving suction and/or blowing. The use of these relatively powerful controls in conjunction with what might be called the low performance type of aircraft has proven quite successful.

It must be remembered, however, that, in applying such controls to a design, the ideal aerodynamic advantage can never be completely achieved. The geometric controls add considerable weight and complexity and thus the speed range (maximum speed minus minimum speed) advantage ideally yielded by such controls is reduced. It has been found to be very disadvantageous to supply energy to the powered form of control through robbing the reciprocating engine. Thus, in aircraft powered with such an engine, it is generally necessary to provide an additional power source. This again can add much weight, especially for the larger aircraft where the blowing or suction must be distributed over a greater span.

Current thinking in the low performance ($<$ 500 knots) field is tending somewhat away from the short take-off and landing (S.T.O.L.) aircraft and toward the vertical take-off and landing (V.T.O.L.). This trend is primarily a result of a re-evaluation of tactical needs, the

V.T.O.L. aircraft being used as an S.T.O.L. when under overloaded conditions. It is probable that the S.T.O.L. aircraft is the more efficient machine if sufficient runway length is available, but this probability has not yet been established as a general truth. It might be pointed out that, although the normal V.T.O.L. operates primarily as a thrusting machine, many of the high-lift devices common to the S.T.O.L. may be incorporated in such a design. For instance, heavy flaps are basic to the performance of the "Vectored slipstream" versions of such aircraft while the ducted fan, the major component for some V.T.O. designs, can be made considerably more efficient through the use of separation controls. Certainly V.T.O.L. and S.T.O.L. aircraft are not mutually incompatible. There is room for much more research in both fields and the problem of flow control must be one of the major phases of such research.

To this point the discussion has been concerned with aircraft in the "low-performance" category, that is, relatively low-speed, non-combat aircraft of the liason or short-haul transport types with basic configurations which, in themselves, are not deleterious to landing or take-off performance. The problem here is thus to make a good low-speed aircraft even better in that respect. At the other end of the scale is the aircraft dedicated to extremely high speeds, quite often with seemingly complete disregard for low-speed performance.

The rapid technological strides made by engine and airframe manufacturers since the original development of the turbojet engine have resulted in aircraft of greater and ever greater high speed capabilities. This trend has been due in large part to the use of thinner and thinner wings, lower aspect ratios, and generally higher wing loadings. It is unfortunate that these

configuration changes, while pushing up maximum speed, have also severely decreased the lifting potential of the airplane and thus radically increased its minimum flying speed. This situation, of course, reflects itself in extremely long take-off and landing runs as well as dangerously high touch-down speeds.

Some current attempts to ease this situation involve the design of larger and larger catapults and arresting gears, the use of drogue-chute landings and, in several cases where the wing section and planform permit, the use of high angle-of-attack take-offs to achieve some lifting thrust. Additionally, much effort is being spent on the development of suitable thrust reversers.

Assuming that wing section and planform are established by high speed considerations, it is widely felt that the most generally applicable solution to the low speed problems connected with high speed aircraft lies in high-lift flow control. Such a control may, in general, be used successfully for both landing and take-off, while the usual power source for such aircraft, the turbojet engine, is, unlike the reciprocating engine, extremely well suited (by virtue of the excess pressure maintained by its compressor) to provide power for a powered form of flow control system. In addition, the high-lift device may be carried as an integral part of the wing and is generally of such a nature as to not aerodynamically damage the aircraft's high speed performance. With the exception of the very special purpose "tail-sitters", it is doubtful that any V.T.O.L. design will rival the more familiar configuration in the very high speed regime for a good many years.

High-lift flow control as applied to the high-speed aircraft certainly maintains some of the problems mentioned previously concerning its use with the "low performance" aircraft. Although the problem of power source is alleviated, the use of powered controls on large aircraft is, because of weight-addition and climb-out considerations, not as yet a completely acceptable solution. As was the case with the low performance aircraft, however, these problems normally simply serve to reduce the net efficiency of the control rather than to make that control actually disadvantageous. Perhaps the one disadvantage to any efficiently designed control is the complexity it adds to the overall design.

Although high-lift flow control may be used to advantage with any aircraft configuration, major interest lies in its use with the very high performance or, on the other hand, the very low performance aircraft. Such controls provide lift increases through effecting changes in profile geometry or through delaying separation by energizing the wing's boundary layer. High-lift controls can be either powered or unpowered and their effects are often described as "boundary layer control (B.L.C.") or "circulation control". Any one control can be designed as a combination of the types above and/or create effects which are neither a pure B.L.C. or circulation. Further, many control systems call for more than one high-lift device.

The effects of such flow controls and flow controls systems are far from being completely understood. Although a large number of different systems have been designed and developed, few inroads have been made toward solidifying knowledge regarding the flow processes involved, the true capabilities of the more basic systems, and the relation of the various

systems to each other as well as to the possible parameters of significance. In the important range near maximum lift very little knowledge can be brought to bear upon the problem of predicting the characteristics of even the uncontrolled two-dimensional profile. The three-dimensional case is still more a question mark, and the addition of controls to this case further complicates the situation.

The field of flow control has been of particular interest to the Subsonic Aerodynamics Group at Princeton University for the past five years. Thus, when approached by the Bureau of Aeronautics and asked to conduct an investigation of the flow mechanisms of high-lift flow controls as applied to wings and profiles, much of the preliminary thinking had already been initiated.

This report represents a summary of the state of aerodynamic knowledge in this important field. The flow mechanisms created by the various control types are discussed. In addition, an attempt has been made to determine and present methods by which the aerodynamic coefficients made possible through use of the various controls can be predicted. The report illustrates that, to a large degree, the effects of all systems are but results of varying mixtures of the same few flow phenomena and hence the different controls can be treated in closely the same manner.

It was impossible with the limited time and budget allotted to this project to launch an extensive experimental study of the subject, since such a program would require years even if the entire facilities of an organization such as a large governmental laboratory were devoted to the problem. In this case, the facilities available were very much less

extensive and so recourse had to be made to limited experimental studies into those regimes that were most lightly covered in the literature. These studies, at the request of the Bureau of Aeronautics, were made to concentrate on the effects of the various leading-edge devices; but it is the intention of this report to deal, insofar as possible, with the effects of all forms of boundary layer and circulation control.

So as to maintain the scope of this report within reasonable limits, no attempt has been made to deal with systems which are primarily low-drag flow controls. Similarly, no attempt has been made herein to study the power requirements or weight addition necessary for operation of the various boundary layer and circulation control systems considered, since, to a very great extent, these will be determined by the specific application considered, certain aircraft configurations being more amenable to some types of systems than others. No evaluation of the relative efficiencies of various systems has been attempted since such a comparison can only intelligently be made within the limitations of a specific design configuration and mission.

The two-dimensional portion of this report is felt to give quite a complete state-of-art aerodynamic summary. As mentioned previously, the concentration here is on leading-edge devices as opposed to the more familiar trailing-edge controls. The important combination of leading-edge and trailing-edge controls has also been considered. Much more correlative difficulty was encountered in the three-dimensional studies and this portion of the report is therefore of a more cursory and qualitative nature than the two-dimensional section.

Considerable elementary and descriptive information has been included in the hope that it will be of assistance in the understanding of the flow mechanisms involved. There are to be found, here and there, some rather speculative statements felt necessary to the proper development of the subject and indicative of little more than the intuitive feelings of the authors. The attempt has been made to state them in such a way that they not be confused with widely documented findings.

A quite complete bibliography covering the field of the aerodynamics of high-lift flow controls may be found at the conclusion of the text. This bibliography has been cross-indexed as to subject and author for the convenience of the reader.

III.

TWO-DIMENSIONAL LIFTING CHARACTERISTICS OF PROFILES

3.1 STALLING CHARACTERISTICS OF BASIC WING SECTIONS

3.1a General Discussion

(The material presented in this entire section draws very heavily on the references given in the Bibliography. Unless a reference is used as a major authority or is directly quoted, it is not specifically mentioned in the text).

In order to gain insight into the complex phenomenon of the three-dimensional stall pattern of a wing, it is valuable to investigate the two-dimensional effects that give rise to these three-dimensional characteristics.

In general, as indicated by inviscid theory, the slope of the lift curve when plotted against the angle of attack is a straight line in the region of low angles of attack, the exact value of the slope varying with the type and condition of the profile under consideration. As the angle of attack is further increased, however, variations from the straight line appear. These may be gradual or sudden depending upon the type of boundary layer separation that occurs, but in every case there are symptoms of the flow mechanism that limits the lift producing capabilities of the profile under consideration. Since these variations are produced by the boundary layer they are functions of all the variables that effect boundary layer growth: Reynolds Number, stream turbulence, surface roughness, distribution of pressure gradient produced by thickness distribution, leading-edge radius, and camber. Thus it is not possible to assign certain types of flow separation to specific airfoils since the character of this separation may totally change with a change of flow conditions.

In order to study the behavior of the boundary layer separation, consider the profile shown in Fig. 1 emersed in a potential flow field at a fairly high angle of attack. The theoretical pressure distribution for this profile is shown in Fig. 2. In the region a to b the flow will normally stay laminar due to the favorable pressure gradient, but after passing the pressure peak at b, instabilities will occur. Depending very much upon the Reynolds Number and the magnitude of the adverse pressure gradient, the boundary layer will follow one of five courses. It may:

(a) remain laminar and attached (generally only if the gradient is small or the distance to flow over the surface is small)

(b) undergo transition from laminar to turbulent flow and remain attached to the profile's upper surface.

(c) undergo transition from laminar to turbulent flow and subsequently separate from the surface.

(d) develop a laminar separation with reattachment of a turbulent flow to the profile's surface at some point downstream.

(e) develop a laminar separation without subsequent reattachment.

The question of whether or not the boundary layer will separate while remaining laminar depends entirely on whether transition to turbulence, which in turn depends on the Reynolds Number, free stream turbulence, surface roughness, etc., will occur before the laminar separation point has been reached. If the boundary layer does become turbulent it is able to withstand a greater adverse gradient than it could in its laminar state and hence separation is delayed. As the flow

proceeds along the upper surface the turbulent boundary layer grows and the boundary layer profile changes, leading to turbulent separation.

These types of boundary layer separation give rise to three general types of stall identified by McCullough and Gault (Ref. 10) as:

1. Trailing-edge stall (preceded by movement of the turbulent separation point forward from the trailing edge with increasing angle of attack)
2. Leading-edge stall (abrupt flow separation near the leading-edge generally without subsequent reattachment)
3. Thin-airfoil stall (preceded by flow separation at the leading-edge with reattachment at a point which moves progressively rearward with increasing angle of attack.

(It should be pointed out that, like McCullough and Gault, throughout this report the stall will be considered as the flow condition which follows the first lift curve peak).

An attempt will be made in the following paragraphs to describe these three types of stall in detail, but it must constantly be born in mind that in general no type can uniquely be assigned to a particular profile since a change in flow conditions (a change in free stream turbulence, free stream velocity, the application of a high lift device, etc.) may easily change the stall characteristics. It can be stated with some conviction that, excepting very thick and very thin profiles that form the limiting cases, both turbulent and laminar boundary layer separation are present at the stall, and stall characteristics depend upon which type becomes dominant. No analytical method for rigorously determining stall type under a given set of circumstances has yet been

satisfactorily developed and the designer must make recourse to experimental data obtained under conditions as closely simulating the design conditions as possible.

3.1b Trailing-Edge Stall

Trailing-edge stall is most commonly associated with relatively thick profiles, i.e., those with thickness ratios ranging upwards from 15%. Since the vast majority of aircraft experience up to the end of World War II had been obtained with aircraft employing such thick wing sections, it is not surprising that this stall phenomenon is better known than the other two types. Fig. 3 presents a series of two-dimensional smoke tunnel photographs of the development of the stall on a NACA 23015 profile which clearly show the basic phenomena involved. It must be pointed out that since these photographs were obtained at a Reynolds Number of only 3.4×10^5 they cannot be expected to agree in detail with wind tunnel data taken at higher speeds. However, it has been found that the smoke tunnel in which these photos were taken (Fig. 15) normally yields, apparently due to a stabilizing influence of tunnel sidewall boundary layer growth, profile stall patterns characteristic of much higher tunnel speeds. Fig. 3 is felt therefore to yield not only a clear demonstration of trailing-edge stall, but also a reasonably good qualitative picture of the higher speed stall characteristics of this particular airfoil.

Fig. 3a shows the profile at zero angle of attack. Although there is no streamline directly on the upper surface of the profile, as can be seen there is one only slightly above, and from it the behavior of the surface flow can be deduced. It can be seen that this streamline remains

laminar to the 42% chord point at which point transition occurs. Due to the turbulent growth, smoke from this streamline attaches to the upper surface at the 74% chord point and becomes a part of the profile boundary layer and wake.

Fig. 3b shows the profile at an angle of attack of 4^{o}. Here it can be seen that the transition point has moved forward to the 31% chord point (it is probable that transition on the profile surface is earlier) and that the turbulent flow attachment point has moved forward to approximately the 57% chord point. It will be noted from the picture that the wake at the trailing edge is becoming very thick and, although it is not clear, it is possible that separation is occurring over about 10% of the trailing edge.

In Fig. 3c the angle of attack has increased to 8^{o} and although the surface flow is not clearly indicated, the growth of the separated region at the trailing edge is evident. Fig. 3d showing the profile at an angle of attack of 12^{o} is possibly more revealing since the upper surface flow is more clearly defined. It can be seen that the transition point of the streamline above the surface has moved to about the 10% chord point and that turbulent attachment occurs very rapidly downstream of this point. The growth of the turbulent boundary layer is clearly indicated up to about the 50% chord point where the smoke has diffused too completely to be seen. From the outer streamline pattern it can be estimated that separation is occurring at about 70% chord point.

Fig. 3e shows conditions just past the point of maximum lift (determined in these tests by the streamline displacement). The profile is at an angle of attack of 16^{o} and as can be seen transition is very near the leading edge. (The seeming laminar separation ahead of the

transition point is produced by the photographic angle - the streamline was actually never attached to the surface). As indicated, the growth of the turbulent boundary layer is very rapid and separation occurs at approximately 50% chord point. In Fig. 3f the angle of attack of the profile has been increased to 20° and the upper surface aft of the 3 to 5% chord point is completely separated.

The force and moment characteristics of a profile subjected to trailing edge stall demonstrate smooth and continuous variations from zero lift to a point well beyond the stall. The aerodynamic characteristics of the NACA 63_3-018 are shown in Fig. 4. The break in the pitching moment curve shown for this profile is very unusual. Almost invariably trailing-edge stalling profiles reveal a smooth pitching moment stall.

Careful smoke and tuft tests conducted on a similar thick profile ($15\% \frac{t}{c}$) indicated that separation began at the trailing edge at an angle of attack corresponding to that at which the slope of the lift curve began to fall off (8° in this case), and moved forward steadily until at maximum lift the entire rear half of the profile was in a region of separated flow. Beyond the point of maximum lift, the separation point continued to move forward at a rate roughly equal to that prior to the stall for two or three degrees at which time its motion accelerated rapidly and separation occurred at the leading edge. On thicker profiles it is not uncommon for the rate of separation point movement to remain constant after the stall until the upper surface is completely separated.

The pressure distributions shown in Fig. 5 give a considerable clue as to the flow mechanisms effecting the flow over such a profile. An increase in the peak pressures continues for several degrees after the stall. The pressure recovery over the after portion of the profile is continuous to

an angle of between 6^{o} and 12^{o} after which there is a distinct flattening of the pressure distribution curve indicating the relatively constant pressure of a separation region. It will be noted that this flat portion of the curve extends forward with increasing angle of attack, actually covering about one half of the profile at the stall.

A pressure survey of the 15% thick airfoil confirmed the smoke and tuft investigations that trailing-edge separation initiated at 8^{o}. Further confirmation was found through the use of a boundary layer survey which indicated that a value of 2.6 of the boundary layer shape parameter

$$H = \frac{\text{displacement thickness}}{\text{momentum thickness}} = \frac{\delta^{*}}{\theta}$$

was achieved at the trailing edge at an angle of 8^{o}. Refs. 11 and 12 have shown that this value is indicative that turbulent boundary layer separation has occurred.

One of the interesting bits of information that can be gleaned from pressure distribution studies results from plotting the readings of individual pressure taps against the angle of attack. In many cases, the curves of the pressure variation in the region of the nose display a slight discontinuity. This is caused by a slight "bubble" of separation containing a relatively constant pressure. Given a sufficient number of curves, a rough approximation of the magnitude and location of the bubble can often be made. The appearance of this bubble is, of course, a function of the Reynolds Number, the initial turbulence of the flow, the thickness, and the radius of nose curvature, but an examination of existing data indicates that it exists at higher Reynolds Numbers and thickness ratios than was previously realized.

Since this "bubble" of separation has relatively significant effects even upon thick profiles that exhibit predominantly trailing edge separation and forms the major contribution to the phenomena of leading-edge and thin airfoil stalls, some discussion of its nature is required.

Unfortunately, far too little is known of this flow phenomenon and its mechanism remains obscure. It is known that the laminar boundary layer cannot ordinarily exist for long in a region of adverse pressure gradient, and if sufficient disturbances are lacking to cause premature transition to the turbulent regime, the extent of the laminar region will be limited by separation. Although this phenomenon is generally referred to as laminar separation, the term laminar applies to the condition of the boundary layer at the point of separation and not necessarily to the flow within or bounding the separated area. As can be seen from the high speed photographs shown in Fig. 6, the flow leaves the surface in the laminar state, continues in this manner for some distance, undergoes transition and finally reattaches to the surface in a turbulent state. A result of this turbulent reattachment is that the turbulent boundary layer at a given point downstream of the reattachment point is thicker than would be the case without the separation. Thus even the turbulent boundary layer's tendency to separate is increased.

It is extremely difficult to examine the flow within small separation "bubbles" of this nature, but smoke flow studies give an indication of a forward transport of mass along the profile surface between the separation point and the point of turbulent reattachment. This is a circulatory flow, but seems different from a vortex formation in that the velocities do not increase toward the core. Rather, the turbulent air within the

bubble demonstrates characteristics more commonly associated with a solid core type of motion although the separated region is generally oblong rather than circular.

Von Doenhoff (Ref. 13) has speculated that there is a simple relationship between the length of the separated laminar flow prior to transition and the Reynolds Number based on the local velocity outside of the boundary layer at separation and the distance between the points of separation and the beginning of transition. According to this hypothesis, assuming a constant value of this Reynolds Number, any increase in local velocity, whether due to increased angle of attack or increased free-stream velocity, would produce a decrease in the distance from separation to transition, and hence the extent of the bubble. Smoke tunnel studies and the boundary layer investigations of Refs. 14 and 15 have shown that this is an over-simplification and that the suggested Reynolds Number of 50,000 can vary between 30,000 to 60,000 for different angles of attack of the same profile, but for thin profiles at the higher angles it seems like a useful hypothesis.

The theoretical studies made to date of these boundary layer phenomena are not of much use to the designer in predicting maximum lift of such profiles, or even in predicting the type of flow that will exist at stall. Potential flow theories allow the calculation of pressure distribution provided the effects of the boundary layer flow are small. Viscous theories permit the calculation of some forms of boundary layer flow provided that the pressure distribution is known. Thus a combination of these theories and empirical boundary layer data can be used to predict the point of laminar separation, transition and turbulent separation at

low and moderate angles of attack, but as Abbott and von Doenhoff (Ref. 8) have indicated, none of the wing characteristics can be calculated with confidence if the flow is separated over an appreciable part of the surface.

General boundary layer studies so far conducted shed much light on the mechanism of the flow phenomena encountered. These studies have shown that transition takes place at a value of Reynolds Number that is dependent upon the magnitude of the disturbances to the boundary layer. There is a Reynolds Number (approximately 2,300 for pipe flow, for example) below which all disturbances are damped out by the effects of viscosity. As the Reynolds Number is increased beyond this value some types of disturbances are amplified and will eventually cause transitions. Further increase of the Reynolds Number causes amplification to occur for a greater variety of disturbances and increase the rate of amplification. Under these circumstances transition can be delayed to high values of Reynolds Number only by reducing all disturbances such as stream turbulence, unsteadiness, surface waviness and roughness to a minimum, or by the application of power in the form of suction arranged to control the growth of the boundary layer.

The mechansim of transition is still very imperfectly understood, but smoke flow studies such as those shown in Fig. 7 have added considerably to the qualitative understanding of the phenomena. As can be seen, the laminar boundary layer defined by the smoke stream begins to develop a wave-like motion of increasing amplitude as it moves downstream. Actual transition occurs when the boundary layer flow rolls up into discrete vortices that proceed for a short distance downstream before dissolving into a field of fairly uniform turbulence. It is probable that the disturbances within the laminar layer that produce the wave motion are

vortex-like in nature but it is not until the discrete vortices are formed that there is a significant change in boundary layer depth and velocity profile. These studies show that this point is not fixed, and moves back and forth over a limited area, thus accounting for the so-called "transition region".

Applying this information to the case of the thick profile near stall, one arrives at the conclusion that the laminar separation will occur if flow conditions are such that transition does not occur before the separation point. The likelihood of this being the case decreases with increasing Reynolds Number, but it must be pointed out that with low atmospheric turbulence and a smooth section laminar separation has been detected on an 18% thick section at a Reynolds Number of 5.8×10^6 (Ref. 10) and it is probable that it is a lot more common than was once supposed, particularly when some form of circulation or trailing-edge boundary layer control is applied.

3.1c Leading-Edge Stall

Leading-edge stall is a type of flow that was of little interest until after World War II. when in order to avoid compressibility difficulties aircraft began using thinner and thinner wing sections as well as heavy sweep. Although, as previously pointed out, it is impossible to assign a given type of stall to a specific airfoil, one can generalize to the extent of saying, that under normal flight conditions this type of stall is typical of sections of moderate thickness, i.e. those ranging from 9% to 15% thick.

A fairly high Reynolds Number example of leading edge stall is furnished by the characteristics of an NACA 63_1-012 profile taken from

Ref. 10. As can be seen from Fig. 8 the force and moment characteristics of this profile demonstrate abrupt discontinuities when the angle of attack for maximum lift is exceeded. The lift curve shows little or no curvature near maximum lift and the break in the curve at stall is sharp. Actually the buffeting after the stall was so severe that the tunnel dynamic pressure had to be reduced to obtain safe operation.

A study of the pressure distributions of this profile (not included here but shown in detail in Ref. 10) indicated a continual increase in the peak negative pressures at the profile nose up to the stall at which point they suddenly collapsed, and the static pressure along the chord became more or less constant as in a separated region.

Tuft and liquid film studies of this profile indicated that with the exception of a very small bubble at the leading-edge which formed at a low angle and persisted up to the stall, the flow was steady over the upper surface until the stall, at which point separation apparently occurred simultaneously over the entire profile. Under certain conditions (profile configuration, Reynolds Number, etc) such profiles remain completely separated after the stall while in other instances a turbulent reattachment takes place aft of the leading edge and the stalled profile demonstrates the characteristics of having a large circulatory flow over its leading edge. The center of this region of circulatory flow moves rearwards with increasing angle of attack, finally resulting in complete separation.

This turbulent reattachment has the effect of producing a second lift curve peak after the primary stall. This peak never achieves the same lift values of the primary stall, but the fall-off of lift is more gradual after its formation than after the sudden leading-edge separation at the maximum lift point. In this characteristic, as will be seen later, the

flow closely resembles the thin airfoil stall discussed in the next section.

Although the exact mechanism of leading-edge stall remains obscure, it is apparent that it results from a flow condition at the leading edge that, like trailing-edge separation, is initiated long before maximum lift is achieved. Since measurements have shown this leading-edge separation to be located downstream of the pressure peak, it would seem, as von Doenhoff has summarized, that the laminar boundary layer passes around the leading edge, through the pressure peak and separates, the flow continuing away from the surface along a path approximately tangent to the surface at the point of separation. Transition occurs and the expansion of the turbulent motion spreads at such an angle relative to the path of tangency of the separated laminar flow that the flow quickly reattaches to the surface as a turbulent boundary layer.

An increase in the angle of attack will move the point of minimum pressure nearer the leading edge causing the laminar separation within the adverse pressure gradient to occur sooner. Simultaneously, transition is accomplished earlier due to the instabilities caused by the increased adverse pressure gradient. Ordinarily this effect would cause a more rapid turbulent attachment, but since these flow phenomena are occurring in a region of increasing airfoil surface curvature, a certain equilibrium is achieved, the earlier transition compensating for increasing separation angle. This process continues until the angle of attack has been increased to such an extent that the separation point has moved to a region of profile curvature of such magnitude that the transition point is so located that the growth of turbulence can no longer achieve reattachment--thus limiting the maximum lift.

As a function of profile shape and local Reynolds Number, it is quite possible that the equilibrium discussed above may be lost and yet not yield immediate complete flow breakaway. Many profiles exhibit this equilibrium at low angles of attack, but there is found an angle where this previously small, constant size bubble proceeds to grow. As the angle of attack is permitted to increase further, the bubble increases in extent toward the trailing-edge until a stall occurs that is a modification of the abrupt leading edge stall of the type defined by McCullough and Gault and tends to resemble the thin airfoil stall which is characterized by the formation of a large leading-edge separation even at a low angle of attack. An example of such a separation-stall pattern is shown in the smoke flow photographs of Fig. 9.

Fig. 9a shows the profile at a zero angle of attack and clearly shows the long laminar run of the flow on the upper surface, transition, indicated by the thickening of the upper streamline, not occurring until the flow very nearly reaches the 80% chord point. When the angle is increased to 4^{o} as in Fig. 9b, it can be seen that, although transition has moved forward, the flow appears smoothly attached to the entire surface (probably a leading-edge type small bubble exists here, but the smoke flow does not reveal it). When angle of attack is allowed to increase to 8^{o}, a leading edge separation of the type shown in Fig. 9c occurs. Examination of the outer streamline pattern indicates that no trailing-edge separation is present. Fig. 9d shows the profile at a point just past its maximum lift. It will be seen that the leading-edge bubble has grown as predicted and that a very slight separation at the trailing edge can be detected. Fig. 9e illustrates the flow that results when the angle of attack is increased well beyond the stall, the flow

being completely separated from the upper surface.

As indicated by the pressure distributions of Fig. 10, the formation of the region of leading edge (thin-airfoil type) separation reduces the values of the peak negative pressures obtained at the leading edge by a considerable amount, replacing them by the region of relatively constant pressure typical of a separation. Fig. 11 shows how the formation of this separation bubble affects the force and moment characteristics of the profile. Although all the characteristics are noticeably affected, the lift curve is of most interest. It will be noticed that, when the thin-airfoil type of bubble forms, a step appears in this curve and the slope lessens an appreciable amount. It will be noted that the stall is gentle and gradual, reminiscent in shape (but not in C_l values) of the stall of a thick profile with a large leading-edge radius.

It may be expected that reductions in free-stream Reynolds Number would tend to increase the stability of the laminar boundary layer, thereby increasing the length of separated laminar flow before transition. It would thus be quite possible for free-stream Reynolds Number reductions to cause increased magnitude of the leading-edge bubble and convert stall type of a given profile from that of thin-airfoil. For this reason, and since the characteristics of the leading-edge stall and the thin airfoil type of stall are so different, profiles subject to these flow mechanisms should demonstrate relatively large and significant Reynolds Number effects. This is confirmed by investigations of the type reported in Refs. 81 and 84. In the latter Dike has suggested the formulation of a similarity parameter which would relate the stall performance of a thick

profile at a low Reynolds Number to that of a thinner profile at a higher. No attempt has been made to carry this concept past a qualitative statement and it is dubious that any rigorous quantitative procedure can readily be developed.

3 1d Thin-Airfoil Stall

As has been indicated in the previous section, thin-airfoil stall is generally associated with very thin sharp-nosed profiles. It differs from leading-edge stall primarily in the fact that separation region appears at the leading edge at very low angles of attack and grows larger with increasing angles, maximum lift generally being achieved when the angle is such that the point of flow reattachment is located approximately at the trailing edge. For a typical leading-edge stall the separation is small and grows only very slowly up to the stall at which point separation occurs very rapidly.

A diamond-shaped profile is shown in Fig. 12 to demonstrate the major characteristics of this type of flow. As can be seen, a separation appears at the leading-edge almost as soon as the angle of attack is changed. This separation represents the flow's viscous adjustment to boundary conditions. Since the theoretically infinite velocity (resulting from the infinitely sharp leading edge) is impossible, a bubbie must form as soon as there is movement of the forward stagnation point. The mechansim of the reattachment and of the flow within the separated region is only imperfectly understood.

One of the reasons for the difficulties involved in understanding the mechansim of the separation is that measurements have shown the existence of a vortex within the separation region, both by the presence

of a strong reversed flow and the shape of the static pressure profiles. This vortex presents difficulties since experiments conducted within the Subsonic Aerodynamics Laboratory strongly suggest that some axial velocity is necessary for any true vortex motion to exist. Thus it is probable that the vortex observed and measured in two-dimensional tunnels is in fact a three-dimensional phenomenon with trailing vortices extending downstream in the wall boundary layer. The interpretation of measurements thus becomes very difficult.

Boundary layer profiles measured at the point of reattachment show neither a typical laminar nor a typical turbulent shape, but tufts indicate a very rough flow just downstream of the reattachment point that gradually becomes smoother as the trailing edge is approached. This may again be an indication of the three-dimensionality of the flow. For moderate angles of attack, fully developed turbulent boundary layer profiles have been measured at the trailing edge.

When the reattachment point reaches the trailing edge, the primary stall is obtained and the lift gradually decreases with increases of angle of attack, until a flow condition is reached that causes the lift again to increase to a second peak value, which is generally higher than the first. Since the second rise seems to fall into a region in which vortex streets have been measured in the wakes of flat plates, Ref. 16, it would appear that the rise was simply due to the vertical component of the resultant force acting on a separated flat plate.

The force and moment characteristics of the double wedge investigated by McCullough and Gault are shown in Fig. 13, the pressure distribution in Fig. 14. It will be seen that the lift curve is linear

and that the stall characteristics are gentle. The pitching moment curve shows a definite tendency to cut back soon after separation initiates. This tendency appears to be a characteristic of profiles stalling in this manner and can also be seen for the 64A006 profile, Fig. 11. The pressure distributions exhibit very low pressure peaks and illustrate, by the increasing extent of the regions of constant pressure on the upper surface, the growth of the separation region from the leading-edge.

3.1e Empirical Stall Studies

As previously indicated, it is well known that the maximum lift attainable by a profile is a function of Reynolds Number, thickness, thickness distribution, and camber. Further, it would seem intuitively obvious that any effect of these parameters on maximum lift may be directly attributed to their relationship with the manner in which separation initiates and grows and the type of stall which eventually limits the airfoil's lifting capacity. The question thus arises as to what the effect of these parameters is upon separation and stall type and, knowing this, what insight can be achieved leading toward a better understanding of maximum lift phenomena.

The only means currently available to investigators of this problem is an approach based upon experimental data and involving for the most part the rather unsophisticated technique of trend-hunting. Refs. 9, 10, 22, 23, and 24 present experimental lift curves for a large number of profiles and form the basis for the following study. Only airfoils with relatively smooth surface conditions will be considered, and Mach Number effects have been assumed to be negligible. (Available information indicates that this assumption should be quite valid both for the data

utilized in this section and for full scale aircraft in landing or take-off configuration).

In Figs. 16a and b, plots of maximum lift vs. Reynolds Number for various thicknesses and thickness distributions are given. For purposes of clarity, only symmetrical profiles have been considered here except in the case of the "230" series. General trends readily observed are:

(1) Increasing Reynolds Number generally yields increased maximum lift coefficient, the thinner profiles being less susceptible to this effect than the thicker ones.

(2) Increasing thickness generally yields increased maximum lift coefficient except at low Reynolds Numbers, where a profile of approximately 12% thickness often appears to be capable of lift coefficient values in excess of those attainable even with thicker profiles.

(3) Maximum lift coefficient would seem to be less for profiles having the point of maximum thickness fairly far aft on the chord line.

(4) Increased camber increases maximum lift.

(5) At extremely low Reynolds Numbers, there would appear to be a tendency for the maximum lift coefficient of all profiles to approach a relatively constant low value ($C_{l_{max}} = .8$).

Perhaps somewhat more revealing are the crossplots of the above curves shown in Fig. 17. The "00" series of profiles has not been considered here because of insufficient data in the high thickness range and because its curve shape characteristics where known seem very similar to those of the 63, 64, and 65 series shown. In its place, the maximum

lifting potential of a series of profiles characterized by a sharp nose (and maximum thickness at 50% chord) has been presented. The double-wedge would be a typical example of this type of airfoil. It is of some interest that there is every indication that "sharp-nose" profiles have maximum lifting characteristics which are quite independent of Reynolds Number. "Sharp-nose" points plotted in Fig. 17 were obtained from references 10 and 78. The "round-nose profiles", at all Reynolds Numbers, reveal similar curve shapes. As thickness is increased, maximum lift is increased until a thickness of approximately 12% is attained. There occurs here a rather sharp change in slope, and as thickness is increased further the curve becomes closely linear. In this high thickness regime, increased thickness seems either to increase or decrease maximum lifting potential-depending upon Reynolds Number and thickness distribution. The "sharp-nose" profiles, in range of available data, appear to reverse the general thickness effect. Here, increased thickness yields slightly decreasing maximum lift. An item of possible significance is that all the profiles considered seem to show a tendency toward achieving closely the same maximum lift coefficient at a thickness of approximately 4%. This trend is very similar to that mentioned previously as an effect achieved through taking profiles of any thickness to a very low Reynolds Number, and this lift value again is $C_{l_{max}} = .8$.

Knowing now the qualitative and quantitative effect of the various parameters on maximum lift, it would be expected that, if the variation of stall pattern with these parameters could be approximated, considerable insight into a physical understanding of the meaning of the curves of Fig. 17 could be gained. To accomplish this, the shapes of the buffet and

stall regions of the lift curves of numerous symmetrical profiles were studied. The results of this study are shown in Fig. 18 for symmetrical 63, 64, 65, and 00 series airfoils. The three types of stall have been divided here into four separation-stall patterns:

(A) Stall due to trailing-edge separation. This regime is also intended to include that borderline case where separation occurs both at the leading-edge and trailing-edge, the limiting phenomena being, however, the trailing-edge type (relatively gentle buffet and stall).

(B) Stall due to leading-edge type separation. Some trailing-edge separation also possible (relatively sharp fall-off in lift at stall).

(C) Stall due to thin-airfoil type separation, possible leading-edge type separation at lower angles of attack (gentle buffet and stall).

(D) Stall due to thin-airfoil type separation. Thin-airfoil type separation initiating at angles of attack very close to zero (gentle buffet and stall).

Types A and D may be so identified, even though their stall shapes are similar, through consideration of general maximum lift level and the separating sharp stall region. The range of type C was established through the aid of Ref. 10 and it would seem possible to establish further this region by a study of maximum lift level.

Fig. 18 reveals the range of thickness and Reynolds Number, for the various thickness distributions, through which the separation-stall pattern is of each of the types above. As these curves have been defined

by data points lying between lines, their accuracy is limited by the data points available. The profiles investigated were of five thicknesses, each at from three to seven different Reynolds Number (see Figs. 16a and 16b). It may be noted that as expected, an increase in Reynolds Number for a profile of given thickness will increase its tendency away from the thin-airfoil stall and toward trailing-edge stall. Increasing R.N. from a very small value to a high value will, for the thick profiles, change stall type from D to C to D to A. Very thin profiles would seem to require a very high Reynolds Number in order to achieve trailing-edge stall, if, indeed, trailing-edge stall can ever (without control) be achieved. Increasing thickness has the same effect as increasing Reynolds Number, stall type changing from D to C to B to A. At very small Reynolds Numbers, trailing edge stall can only be achieved for very thick profiles -- perhaps not until the profile approximates a circle, where definition of stall type essentially falls down. Moving the point of maximum thickness rearward appears to increase the R.N. (const. thickness) or thickness (const. R.N.) at which the separation-stall pattern moves from one type to the next. It should be understood that smooth transition between stall-type regions and smooth variation in degree within each region can be expected. For example, a profile showing trailing-edge stall characteristics is, near the leading-edge stall-type region (B), considerably affected by leading-edge type separation. Increasing R.N. or thickness, thus moving the profile characteristics further from region B, will decrease any effects of leading-edge phenomena until reasonably pure trailing-edge separation is present. Likewise, in region C, as a profile's characteristics move from D toward B, the transition from leading-edge type separation to thin

airfoil type separation will occur at a higher and higher angle of attack until region B is entered and actual stall occurs as the result of leading-edge type separation.

Considering Fig. 17 together with Fig. 18, it now seems possible to correlate the shape of the maximum lift vs. thickness curve (Fig. 17) with the changing pattern (with thickness) of stall type. It appears that the curve can be broken down into five portions of characteristic shape. These five portions may be found from use of Fig. 18 to correspond to the four separation-stall types plus a fifth which is indicative of trailing-edge stall essentially unhampered by leading-edge effects.

Pure thin airfoil stall seems to create a relatively constant maximum lift coefficient, $C_{l_{max}} = .8$, in a thickness range of approximately 4% to 6%, and is defined by region D, Fig. 17. For a profile thickness of about 4%, at these Reynolds Numbers, the "round-nose" profiles appear to acquire characteristics very closely the same as those of "sharp-nose" sections. Note how an extrapolation of the "round-nose" curves from a thickness of 6% to that of 4% must closely approximate the maximum lift obtained here by the "sharp-nose" profile. The fall-off in maximum lift with increased thickness for the "sharp-nose" airfoils, which apparently stall in a pure thin-airfoil manner for any practical thickness and Reynold's Number, is probably explained by the increased boundary layer thickness over the aft portion of the profile at all angles of attack due to the effect of increased thickness increasing the trailing-edge angle. In that, in the low thickness range, both "round-nose" and "sharp-nose" profiles stall by the same phenomena, it might be expected that region "D" would show some increase in $C_{l_{max}}$ as thickness is decreased below that of 4-6% and that the

curves for both profile types would closely coincide. (This equalizing effect of the pure thin-airfoil stall serves to explain the phenomena mentioned previously regarding all profiles at low Reynolds Number). It would further seem logical that for Reynolds Numbers higher than those shown this coincidence would occur at a lower thickness and slightly higher maximum lift level. (Assuming the "sharp-nose" curve is relatively independent of Reynolds Number, and the effect of increased Reynolds Number is to raise the "round-nose" curves - at a R.N. of twenty million, maximum lift coefficient for 6% profiles seems to be around .95).

Portion C of the maximum lift vs. thickness curve would appear to be indicative of a stall occurring as the thin-airfoil type, but with separation of the leading-edge type occurring in the low angle-of-attack region. Increasing maximum lift with thickness (at Reynolds Number) is without doubt due to the effect of increased thickness delaying to higher angles of attack the transition from leading-edge separation type to thin-airfoil separation type. This portion of the curve is characterized by a slope increasing with thickness. Increases in Reynolds Number would appear to raise maximum lift in this range, while moving the point of maximum thickness aft will lower maximum lift.

Portion B of the maximum lift vs. thickness curve can be found to define that region where stall is due to leading-edge type separation (although a secondary stall of the thin-airfoil type may well occur in the lower portions of B). This part of the curve is characterized by lift at stall increasing with thickness, but with slope now decreasing. The lift increase is apparently due to the increased leading-edge radius created

by increased thickness, thus allowing the profile to go to higher angles of attack prior to flow breakaway. The decreased slope could well be due to partial trailing-edge separation occurring prior to final leading-edge stall -- for, in this range of lift coefficient, trailing-edge separation can well be present. Increases in Reynolds Number and changes in chordwise location of maximum thickness have the same effect on maximum lift in this region as in portion C.

Trailing-edge stall appears to initiate in region A, which may be defined as the curved region immediately aft of the point of maximum curvature. There would appear to be considerable effect from leading-edge separation present here and stall, though distinctly not of the leading-edge type, is somewhat sharper than the usual trailing-edge stall. The greater the Reynolds Number, the lower the lift level of this portion of the curve and the sooner this portion occurs along the thickness scale.

Portion Z, a relatively linear segment of the curve in the high thickness regime, is thought to define existence of quite pure trailing-edge stall, the leading-edge now having little or no effect on $C_{l_{max}}$ (very little, if any, leading-edge separation being present at angles of attack prior to trailing-edge stall). This segment of the curve will yield decreased lift with increased thickness at low Reynolds Numbers. However, as Reynolds Number is increased the slope of this portion decreases and finally increased lift is achieved with increased thickness. This change in slope with Reynolds Number would appear to be less rapid for profiles of further aft point of maximum thickness.

It has thus been shown that a study of separation-stall phenomena offers a logical means of understanding the relationship between a

symmetrical profile's thickness, thickness distribution, and Reynolds Number and the maximum lift attainable with that profile. This is particularly true in the case of nose-stalling profiles. Variations in Reynolds Number and nose radius and shape (thickness and thickness distribution) may quite logically be correlated with variations in maximum lift potentiality through consideration of the effects of these parameters on the type of nose separation, the change in magnitude and type of separation with angle of attack, and the kind of stall ultimately created by this nose separation - abrupt or gradual. Although the phenomena of trailing-edge separation and stall have long been recognized, the effect of profile shape and Reynolds Number on the maximum lift of profiles with this characteristic is not so readily subject to physical understanding and interpretation.

The curves presented in Figs., 17 and 18 serve to explain physically the variation in profile maximum lift through relating separation-stall pattern to the parameters of thickness, thickness distribution and Reynolds Number, and, of course, may also be used to predict maximum lift for the series shown. However these parameters are obviously not sufficiently definitive to allow prediction of maximum lift for <u>any</u> profile. Considering any given smooth, symmetrical airfoil of known separation- stall characteristics, it would seem reasonable that Reynolds Number and one or more geometric parameters should completely define maximum lift coefficient.

The first problem encountered in any approach of this nature is that of finding parameters which suitably define separation-stall type. In the case of nose stall (lines D-C and C-B of Fig. 18), the simple parameter of

leading-edge radius would appear to be somewhat better than that of profile thickness. Particularly, line D-C, when plotted against leading-edge radius rather than thickness, yields closely a single line independent of thickness distribution and even independent of small values of camber. As thickness (radius) is increased at Reynolds Number, leading-edge radius loses its significance, no longer being superior to thickness as parameter. It is unfortunate that these curves, because of insufficient data, could not be drawn sufficiently accurate as to permit more extensive empirical parameter study. It might be mentioned that Reynolds Number based upon the leading-edge radius could well have merit as a term of physical significance in the nose stalling configuration. However, development of any best parameter or parameters to hold for all degrees and variations of nose stall would seem very difficult until more is learned regarding the action of the boundary layer in adverse pressure gradients and regions of sharp curvature. The situation appears even more nebulous for trailing-edge stalling airfoils. Certainly the quite different separation pattern alters the emphasis on the geometric parameters useful for nose-stalling profiles while adding new terms such as trailing- edge angle, etc.

Were it possible to uncover parameters uniquely suited for prediction of separation-stall characteristics, the next step would be to apply these to the prediction of maximum lift coefficient. It is found here that leading-edge radius is no longer even closely definitive in the nose-stalling regime, yielding as wide a variation between the different thickness-distribution series as the parameter of profile thickness. Use of other simple parameters indicative of leading-edge angle proved no more

successful. One cause of this is that, when lift level is being considered, lift curve slope as effected by trailing-edge angle comes into importance even in the thin profile configuration. This effect is very noticeable in the case of the "sharp-nose" profiles. Here again, the trailing-edge stalling airfoil presents a problem as great as, or greater than, that of the nose stalling type.

Certainly the determination of exacting parameters for maximum lift prediction is a problem which can hardly be solved with current empirical data or existing theory. It is obvious that no one geometric parameter, and probably no one set of parameters, will fit both the leading-edge and trailing-edge stalling cases. Further, when cambered profiles or profiles in a turbulent free stream and/or with surface roughness (or discontinuities) are considered, considerable complexity is added. The three parameters used in this section, free-stream Reynolds Number, profile thickness, and profile thickness distribution, appear as applicable to the total symmetrical profile picture, considering both trailing-edge and leading-edge stalling profiles, as any known at this time. For this reason, and because Reynolds Number and thickness seem to yield an unusually good physical picture of the relationship between "round-nose" and "sharp-nose" airfoils, these parameters were selected for use throughout this portion of the report.

To this point very little has been stated concerning the cambered profile. Fig. 19 demonstrates the effect of increasing the amount of camber on 64 - series profiles. It will be noted that increased camber raises maximum lift coefficient throughout the thickness range.

Investigation into the separation-stall pattern (as a function of thickness and Reynolds Number for various degrees of camber applied to this and several other series of profiles) revealed that the interpretation of curve shape presented previously in the symmetrical profile case still very closely holds, correlation being perfect for the 63, 64, and 65 cambered series while the 230 series yields what is seemingly leading-edge type stall somewhat beyond what is thought to be the point of maximum curvature. The reason for this discrepancy is currently not known. It was further noted that although thin-airfoil stall gives way to leading-edge type separation at approximately the same thickness (independent of camber), increased camber allowed trailing-edge stall to become the limiting phenomenon for thinner and thinner airfoils. This can be seen by the reader, if he will accept the curve-shape principle, from study of the curve shapes, Fig. 19. A discussion of the possible significance of this and other observations regarding the cambered profile may be found in the following section.

3.1f Possible Significance of Empirical Stall Studies -- B.L.C. Concepts

At this point it would be well to discuss briefly the effects upon a profile of the application of either circulation control or boundary layer control.

These two terms have unfortunately been given a wide variety of definitions, depending upon whether the individual proposing such definitions were interested primarily in the basic function of the control itself, its overall effects, or its effects upon only a portion of the wing on profile. Invariably, however, considered in the most rudimentary sense,

circulation control involves the increase of lift at angle of attack, and boundary layer control (B.L.C.) is concerned with extending the base profile lift curve.

For purposes of this discussion (and basing definitions upon increment in lift attainable over and above that of the base profile), circulation control will be defined as that control which, through increasing effective camber, increases the lift coefficient of a profile even at an angle of attack where the profile suffers no separation or unusually thickened boundary layer (i.e.: even where the profile itself is obtaining a lift predictable by potential theory). Boundary layer control would then be that control which, through its ability to energize the boundary layer or otherwise delay or prevent separation, increases the lift coefficient of a profile only at those angles of attack where separation or a very thick boundary layer exists on the base profile. The lift attainable through such a system would, by implication, be limited by the profile's theoretical characteristics. Using these definitions, circulation control has its basis in increasing the profile's theoretical lifting capabilities while B.L.C. permits the profile to realize at least partially its own otherwise unfulfilled theoretical potentialities.

Application of circulation control normally reveals a shift of profile lift curve to the left, showing increased lift at all angles until the base profile angle for maximum lift is approached. The trailing-edge flap would be an example of a circulation control. A profile with B.L.C. generally retains the angle of zero lift of the base profile, maintains a lift curve slope close to theoretical, and achieves maximum lift at angles

of attack and thus lift coefficients in excess of those attainable by the base profile.

Any definitions for these two terms must be applied with caution and possible implications considered. Certainly all definitions depend upon what is considered to be controlled. For instance, were the definitions given here with respect to a trailing-edge flap rather than the base profile, the use of a control to assist the trailing-edge flap toward achieving its theoretical potential in effectiveness must be considered as B.L.C. (with respect to the flap). However, with respect to the base profile such a system is normally circulation control as it increases the effective camber of the overall configuration. Another possible source of difficulty is that angle of attack is itself a matter of definition. A flapped configuration may have an angle of attack based on a trailing-edge flap definition, a leading-edge flap definition, or a cambered profile definition. As the base profile (flap undeflected) has angle of attack defined in the same way in all cases, the value of circulation control due to flap deflection is very violently a function of angle of attack definition. If confusing elements such as these are kept in mind, the application of any sound definition for the boundary layer and circulation control terms is greatly facilitated.

Although in many instances both circulation control and boundary layer control (as well as other lift increasing effects) are brought into play through the use of a single controlling system, it is quite possible to have a "pure" boundary layer control (i.e.: no circulation control). The remainder of this section will be concerned with just such a system

and the implications which can be gleaned from the previous section regarding its possible capabilities. Further discussion of circulation controls may be found in Section 3.2.

As defined here, boundary layer control enables a profile to approach its theoretical lifting potentialities but not to exceed them. Hence, at low angles of attack, where due to lack of separation the profile is closely achieving its theoretical potential, the lift curve of the controlled profile closely coincides with that of the uncontrolled. When separation initiates on the base profile, the two curves will diverge, the controlled configuration maintaining a slope closely equal to that which would be theoretically predictable for the profile shape in question. The controlled profile curve follows this slope to an angle of attack which can be considerably greater than that at which the base profile stalls. The maximum lift coefficient achieved by a profile with B.L.C. can thus be much higher than that possible with the base profile.

Although a few systems can control leading-edge or trailing-edge separation with closely equal facility (complete-chord upper-surface suction, for instance), most boundary layer control systems are designed primarily to delay or prevent separation at either the leading-edge or the trailing-edge of a profile. A control located at the leading-edge would in all probability be selected for use with the thin profile which is characterized by leading-edge (or thin-airfoil) separation. A trailing-edge control would doubtless be used with trailing-edge stalling thick profiles. Although some leading-edge boundary layer control systems can also partially control trailing-edge separation, this must generally be considered a minor effect demanding of large amounts of power. Trailing-

edge B.L.C. can seemingly be of no assistance at all in controlling any leading-edge separation. It would thus seem that, for purposes of simplification, B.L.C. can here be treated as pure B.L.C. (both leading-edge and trailing-edge separation controlled, no circulation control), pure leading-edge B.L.C. (leading-edge separation controlled, no control of trailing-edge separation, no circulation control), or pure trailing-edge B.L.C. (trailing-edge separation controlled, no control of leading-edge separation, no circulation control). The pure B.L.C. system as defined can cover such systems as complete-chord upper-surface suction as well as the combination of leading-edge and trailing-edge systems located on the same (no circulation control) profile.

Considering the pure boundary layer control system, where both leading-edge and trailing-edge controls are present, the maximum lift possible with such a system can be approximated by potential theory. The lift coefficient for a profile as given by thin airfoil theory is:

$$C_l = 2\pi \sin\alpha$$

Lift coefficient can be seen to reach a maximum value of 2π (or 6.28) when $\sin\alpha$ is maximum ($\alpha = 90^\circ$). Modifications of this equation to consider the effect of profile thickness yield results such as the following for normal airfoils:

$$C_l = 2\pi \left[1 + \frac{1}{3\sqrt{3}} \left(\frac{t}{c} \right)_{MAX} \right] \sin\alpha$$

As the term added here is quite small, it can safely be stated that the

usual uncambered profile, completely controlled, has a maximum lift coefficient of close to 6.28 at an angle of attack of 90°. Certainly a great deal of control power would be necessary to achieve this, but this value does represent the maximum amount of lift which can possibly be attained by a profile with a pure (both leading-edge and trailing-edge) boundary layer control system.

A considerably more difficult problem is that of approximating the maximum lift attainable through use of either a pure leading-edge or pure trailing-edge boundary layer control. There is here, for reasons later described, no recourse to potential theory, only empirical data being available upon which to base any study. This is indeed unfortunate as the vast majority of B.L.C. applications more closely approximate the pure leading-edge or trailing-edge case than the pure (overall) B.L.C. system.

Intuitively, it would seem obvious that, even if the type of stall (leading-edge or trailing-edge) characteristic of a given profile is prevented at all angles, the profile can still experience stall of the other type if angle of attack is increased sufficiently. For instance, a pure trailing-edge B.L.C. can probably be powered sufficiently to prevent trailing-edge separation at any angle of attack, but, when the profile reaches an angle of attack where leading-edge separation initiates, stall will soon occur from the leading-edge. The reverse pattern would be expected in the case of a pure leading-edge system applied to a normally leading-edge stalling profile.

Experimental evidence seems to back up the speculation above. Fig. 20 demonstrates the appearance of typical lift curves of a thin profile with

a leading-edge control and a thick profile with a trailing-edge control. These curves represent a slightly idealized case as the two controls have been assumed to be pure B.L.C. devices. However, experimental data from actual systems which approach this idealized case reveal the same general characteristics and stall shapes.

The thin profile, without control, is seen from Fig. 20A to stall from the leading-edge. With a small amount of control, but not enough to achieve an angle of attack where trailing-edge separation initiates, this curve would be expected to extend slightly upward and stall (not shown) in closely the same manner. Thus the B.L.C. has served to delay the occurrence of stall, but has not prevented leading-edge separation. The addition of further control power would extend this curve to an angle of attack where stall is influenced by trailing-edge separation, giving a mixed type of stall as shown. Were the leading-edge control now made capable of delaying any leading-edge separation to an angle beyond that where trailing-edge stall occurs, it could be said to have prevented leading-edge separation, and, in the case of the pure system shown, the occurrence of trailing-edge stall would establish the maximum lift coefficient that this profile with B.L.C. could achieve, regardless of control power. It will be noted that leading-edge B.L.C. does little to increase the slope over that of the base thin profile as this leading-edge stalling profile yields a slope already very close to theoretical.

Fig. 20B reveals the same general pattern as Fig. 20A. Complete control of trailing-edge separation can be said to occur at that control power where the profile stalls completely from the leading-edge. Lesser

control powers, even though final stall occurs from the leading-edge, permit sufficient trailing-edge separation prior to stall to reveal a mixed (and lower lift) separation-stall pattern. It may be noted here that, unlike the case in Fig. 20A, the use of trailing-edge B.L.C. on a trailing-edge stalling profile can be expected to give some lift increment even in the relatively low angle of attack range. This is due to the fact that trailing-edge stall is normally preceeded by a rapidly thickening turbulent boundary layer and a rather long buffet (separation) regime.

The previous paragraphs have served to introduce the concept that the maximum lift attainable by a profile with either a pure leading-edge B.L.C. device or a pure trailing-edge B.L.C. device is most probably established by the lift coefficient at which there occurs pure trailing-edge or pure leading-edge stall respectively. ("Pure" stall would be that which occurs at one of the separation-prone regions with no separation occurring simultaneously at the other separation-prone region). A necessary corollary to this would be that a pure leading-edge B.L.C. system would yield no lift increment when applied to a pure trailing-edge stalling profile, nor would a pure trailing-edge boundary layer control help at all when applied to a pure leading-edge stalling profile.

The apparent complete dependence upon viscous phenomena of the lift limitations here imposed reveals why the prediction of lifting potentiality with most forms of B.L.C. cannot be approached through potential theory. Boundary layer theory is also unable to predict maximum possible lift with such devices, and hence recourse must be made to empirical data.

Considering still the pure leading-edge B.L.C. system and the pure trailing-edge B.L.C. system, it has been found that the empirical stall studies discussed previously can be of some assistance in determining the possibility of predicting the maximum lift attainable through the use of either device.

Looking now at the plot of $C_{l_{max}}$ vs. profile thickness (Fig. 17) for any profile series at a constant Reynolds Number, it would be of some value to inspect the probable changes made in this curve if the restriction were applied that profiles in this series could not separate from the leading-edge. In other words, what might be the appearance of this curve if all profiles must stall in a "pure" trailing-edge manner? One segment of the true (no control) curve already satisfies this restriction. This is the closely linear, thick profile portion, labeled "Z". Assuming that the slope of this portion of the curve is indicative of the effect of profile thickness on the maximum lift of pure trailing-edge stalling airfoils of the given series and Reynolds Number, it would seem that this linear segment might be extrapolated to lower thicknesses. Segment "Z" and its extrapolation would thus, based on the assumption above, define the appearance of this curve for the profile series which is not permitted any leading-edge separation and therefore would form the locus of maximum lifts attainable for a profile of this series and Reynolds Number with "pure" leading-edge B.L.C. (complete control stall, Fig. 20A).

Suppose now that the profile series in question, rather than restricted to pure trailing-edge stall, is restricted to pure leading-edge stall. The region of the true $C_{l_{max}}$ vs. t/c curve which most closely

satisfies this restriction is the lowest portion of segment "B", Fig. 17. In this region, trailing-edge separation, if present at all, is of minor importance. Assuming, as in the case above, that the slope of this portion of the curve is indicative of the effect of profile thickness on the maximum lift of pure leading-edge stalling airfoils, extrapolation of this segment of the true curve to higher thicknesses could yield a curve indicative of the maximum lift characteristics of profiles (of the given series at the given R.N.) stalling in the pure leading-edge manner. This extrapolation would then define the maximum lift attainable for a profile with pure trailing-edge B.L.C. (complete control stall, Fig. 20B).

These extrapolations are shown in Fig. 21A. It will be noted that linear extrapolations have been used. This is a reflection of a rather strict interpretation of the assumption given in the previous two paragraphs. That is, that not only are the slopes of the pure portions of the true curve indicative of the effect of profile thickness on the maximum lift of pure stalling profiles, but that there are no secondary thickness effects. Experimental data from tests conducted using closely pure leading-edge and trailing-edge B.L.C. systems (discussed in section 3.3) reveal rather good agreement with results obtained from use of these extrapolations, particularly above a profile thickness of approximately 6%. It thus seems that the assumption above has a good deal of validity and that even the linear interpretation has sufficient merit for use in prediction studies.

Consideration of the effects of well-forward camber on a profile's maximum lift characteristics provides some demonstration of the possibilities of the linear extrapolation method. Comparing the cambered profile

with its base symmetrical counterpart, it would be expected that cambering (considered as a control system) would provide both circulation control and B.L.C. with respect to the symmetrical profile. With a small amount of camber located fairly well forward it would be thought that the primary B.L.C. would be at the leading-edge, although the camber could also induce some premature trailing-edge separation or stall (negative trailing-edge B.L.C.). This system is, of course, anything but "pure". Its correlation with the linear extrapolation method is, however, quite possible.

Studies were made of the maximum lift characteristics, as given in Ref. 9, of 63, 64, and 65 series profiles with and without small amounts of forward camber and at three Reynolds Numbers. The plot of $C_{l_{max}}$ vs. profile thickness for the 64 series is shown in Fig. 19. This plot and those for the 63 and 65 series revealed the following: (1) The stall-type significance of the cambered profile curve shape is analogous to that for the symmetrical profile - Fig. 17. (2) In the thickness range where the base symmetrical profile stalls in a pure trailing-edge manner, cambering raises the lift-level of the $C_{l_{max}}$ vs. t/c curve but does not effectively alter its slope. (3) The pure trailing-edge stall segment of the cambered profile curve extends to a profile thickness at least as low as is the case with the base symmetrical profile, in many cases lower. (4) The trailing-edge (not necessarily pure) stall segment of the cambered profile curve extends to lower profile thicknesses the greater the camber. The regions of maximum curvature for the cambered profile curves appear to lie closely on the linear extrapolation of the base symmetrical profile's

pure trailing-edge stall line. Stall points above this extrapolation were found, with very few exceptions, to be of the trailing-edge type, while those below were leading-edge. (5) The cambered profile demonstrates very nearly the same Reynolds Number and thickness distribution effects as its base symmetrical profile. If symmetrical profiles of different thickness distributions have different pure trailing-edge stall slopes, identically cambered versions of these profiles yield closely the same slope difference. (6)$\Delta C_{l_{max}}$ due to camber is greater for thicknesses less than that defining maximum curvature for the base symmetrical profile curve.

The above observations should not be expected to hold for profiles with large amounts of camber or with camber located relatively far aft. They do hold quite well, however, for the "normally" cambered profile (small amount of camber located fairly well forward). Fig. 21B demonstrates some of the characteristics mentioned above.

The relatively constant positive lift increment due to camber in the high thickness regime must be attributed to circulation control as any leading-edge B.L.C. effect will be zero in this thickness range. The question now arises as to what portion of the lift increment at lower thicknesses can be allocated to circulation control. It is generally conceded that any positive circulation control, in the absence of leading-edge B.L.C. must increase the tendency of a profile to stall from the leading-edge. Thus a trailing-edge stalling profile, given circulation control, can stall from the leading-edge at a premature angle of attack and lift coefficient. A leading-edge stalling profile will stall even sooner when under the influence of a positive circulation control. This means, for purposes of this discussion, that a circulation control of given

effectiveness ($\Delta C_{l_{\alpha=0}}$) can never yield a $\Delta C_{l_{max}}$ greater than that which it achieves in the thick profile case. The term, $\Delta C_{l_{\alpha=0}}$, may be shown experimentally to be independent of thickness in the cambered case being considered. The creation of leading-edge boundary layer control through cambering is thus evident as camber creates even greater $\Delta C_{l_{max}}$ for the leading-edge stalling profiles than for the trailing-edge stalling airfoils. Also, it must be remembered that camber allows the profile to go to very low thicknesses and still not stall from the leading-edge.

Assuming, conservatively, that circulation control is independent of thickness and equal to $\Delta C_{l_{max}}$ for the thick profile regime, it may be subtracted out at all thicknesses. After this has been accomplished only the leading-edge B.L.C. effect of camber remains. Correlation with the linear extrapolation method as applied to the base symmetric profile is readily seen. The fall-off in maximum lift from the linear extrapolation line as thickness is decreased is explained by the fact that a given amount of camber is less effective in delaying leading-edge separation the thinner the profile.

The probable negative trailing-edge B.L.C. mentioned previously has been disregarded in the analysis above. Its effects are certainly quite small and consideration of the problem will reveal that although its effects can change the situation quantitatively it cannot be altered qualitatively. Division in this manner of the effect of any complex system (which is not achieving complete control) into its leading-edge B.L.C., trailing-edge B.L.C., and circulation control elements is certainly

most difficult and often highly misleading. One reason for this is that circulation control lacks reasonable definition and all too often becomes entangled with trailing-edge B.L.C. It is somewhat easier to assume one of the boundary layer controls to either be of negligible effect or group it with circulation control. Luckily, many systems are amenable to such an approach.

Many rather interesting features regarding the limitations and likely characteristics of systems approaching the pure leading-edge or pure trailing-edge B.L.C. cases may be derived from consideration of the implications of the linear extrapolation method. This method indicates that the limiting maximum lift attainable with such systems is very much a function of profile thickness, profile thickness distribution, and Reynolds Number.

A pure leading-edge B.L.C. system may be expected to yield zero $\Delta C_{l_{max}}$ (with respect to the base profile) at all thicknesses <u>above</u> that at which pure trailing-edge stall occurs on the base profile. This thickness where $\Delta C_{l_{max}}$ goes to zero may be expected to decrease with increased Reynolds Number and increase if the point of maximum thickness is moved aft on the profile (note trends shown in Figs. 17 and 18). A pure trailing-edge B.L.C. system will yield zero $\Delta C_{l_{max}}$ at all thicknesses <u>below</u> that at which pure leading-edge stall occurs on the base profile. Again, this limiting thickness will be smaller the greater the Reynolds Number and greater the more aft the point of maximum thickness is located on the profile. (Figs. 17 and 18).

Based upon the linear extrapolation method and study of Fig. 17, the pure leading-edge B.L.C. (complete control) will initiate gains at thicknesses less than that described above and would be expected to create greater $\Delta C_{l_{max}}$ the thinner the profile. For a given thickness, $\Delta C_{l_{max}}$ probably would be greater the less the Reynolds Number. Also, movement of the point of maximum thickness rearward on the profile seems to generally increase $\Delta C_{l_{max}}$ for given thickness. The pure trailing-edge B.L.C. (complete control) will create greater $\Delta C_{l_{max}}$ the thicker the profile. For a given thickness, $\Delta C_{l_{max}}$ will now generally be smaller the smaller the Reynolds Number. The effect of movement of the point of maximum thickness aft is also opposite to the effect shown for the pure leading-edge B.L.C. system, the aftward movement of this point generally reducing the $\Delta C_{l_{max}}$ for a given thickness. Figs. 22 through 25 demonstrate the application of the linear extrapolation method to symmetrical profiles of the 63, 64, and 65 series at Reynolds Numbers from 3×10^6 to 9×10^6.

The preceeding observations as well as Figs. 22 to 25 are based upon study of the general curve shapes of Figs. 17 and 18 and the slopes of the "pure" stalling regions shown in Fig. 17. As these data are comprised of only three profile series at three Reynolds Numbers, there is, of course, the possibility that these trends may not hold for all Reynolds Numbers and profile series. It is felt, however, that the trends are realistic in the range of data considered, and are not the result of reading too much into somewhat scattered empirical data. Confirmation of this is found in the cambered profile studies, the cambered profile characteristics

following the same trends established by the pure trailing-edge stalling portion of the corresponding base profile curve. Hence, it would be erroneous to disregard Reynolds Number, or even thickness distribution, in applying this method.

In applying the linear extrapolation method, it is first necessary to obtain data for the profile in question so as to enable at least the plotting of that portion of the $C_{l_{max}}$ vs. t/c curve from which the linear extrapolation is to be made. It is also necessary that this data be at the Reynolds Number of interest. The $C_{l_{max}}$ attainable with a pure leading-edge B.L.C. will be defined by the linear extrapolation of the pure trailing-edge stall portion of this curve. The $C_{l_{max}}$ attainable with a pure trailing-edge B.L.C. will be defined by the linear extrapolation of the pure leading- edge stall portion of the curve (a line drawn tangent to the point on the curve where slope is maximum). It must be remembered that this method predicts the <u>maximum possible</u> lift coefficient achieved through use of such systems and says nothing about the amount of control necessary to achieve this complete control.

The degree of deflection, blowing, suction, etc. which is necessary to achieve complete control is a function not only of Reynolds Number, profile thickness, and profile thickness distribution, but of the control geometry, location, and overall efficiency. The ability of any given B.L.C. system to achieve complete control, the extent to which it approaches a "pure" control, and the system's partial control characteristics will be subjects covered in Section 3.3.

As was mentioned previously, the division of any complex control into its elements is highly difficult. Let us now, however, consider a system with a fixed circulation control such as a trailing-edge flap of given deflection. If sufficient data is available for this system as applied to profiles of a given series at a given Reynolds Number, it is possible to plot a $C_{l_{max}}$ vs. t/c curve similar to that of Fig. 17. Indications are that the addition of controls does not alter the curve shape significance as given in Fig. 17. Hence it seems logical that the linear extrapolation method may be used with profiles with circulation control as well as with the base profile so long as the $C_{l_{max}}$ vs. t/c curve for that profile series with the given circulation control is known.

It further seems that if the $C_{l_{max}}$ vs. t/c curve for a profile series with a fixed amount of trailing-edge B.L.C. were known, the linear extrapolation method would indicate the limiting lift attainable through the addition of a pure leading-edge B.L.C. system to this trailing-edge system of known characteristics. The same could be said for the addition of a pure trailing-edge system to a leading-edge system of known characteristics. In fact, it appears that the limit lift attainable through the addition of either pure system to any existing system for which a $C_{l_{max}}$ vs. t/c curve may be obtained can be found through application of the linear extrapolation method. The problem here is, of course, the determination of the characteristics of the system prior to the addition of the pure system. Empirical data seems the only good source for such information.

Although much of the data shown in this summary report appear to justify the use of an approach such as the linear extrapolation method,

true establishment of its validity and shortcomings must await further investigation. If verification is achieved, it is possible that through study of the inter-relationships among the $C_{l_{max}}$ vs. t/c curves for large numbers of profiles throughout a wide Reynolds Number range, this method could become a more wieldy and quite useful tool.

3.1g Conclusions and Summary

All forms of stall result from a separation of the boundary layer and this separation may occur in either the turbulent or the laminar region. Although it is difficult to assign a given type of stall to a given profile, thicker profiles with large leading-edge curvature generally demonstrate trailing-edge stall which progresses from a turbulent separation while thinner profiles with smaller leading-edge radii generally produce a stall resulting from laminar separation at the leading edge.

Separation of the boundary layer can give rise to three different general types of stall:

(1) Trailing-edge stall (preceded by movement of the turbulent separation point forward from the trailing-edge with increasing angle of attack.)

(2) Leading-edge stall (abrupt flow separation near the leading-edge -- generally without subsequent reattachment.)

(3) Thin-airfoil stall (preceded by flow separation at the leading-edge with reattachment at a point which moves progressively rearward with increasing angle of attack.)

These three general stall types above occur as the result of the three possible separation types:

(1) Trailing-edge separation (turbulent separation point moving forward from the trailing-edge with increased angle of attack.)

(2) Leading-edge separation (laminar separation bubble occurring at the leading-edge, its extent being invariant with angle of attack until abrupt flow breakaway occurs.)

(3) Thin-airfoil separation (laminar separation bubble occurring at the leading-edge, increasing in chordwise extent with increased angle of attack.)

Although the three separation types can be said to give rise to the three corresponding stall types, it quite often occurs that two or more of the separation types can be present prior to profile stall. In fact, there are at least six separation-stall patterns possible:

(1) Stall proceded only by trailing-edge type separation --no laminar separation prior to stall.

(2) Stall due to trailing-edge type separation but with laminar separation present at angles of attack prior to stall.

(3) Stall due to leading-edge type separation but with trailing-edge separation present at angles of attack prior to stall.

(4) Stall due to leading-edge type separation -- no trailing-edge separation prior to stall.

(5) Stall due to thin-airfoil type separation, the laminar bubble at low angles of attack being of the leading-edge type -- no trailing-edge separation.

(6) Stall due to thin-airfoil type separation with no leading-edge type separation or trailing-edge separation occurring prior to stall.

There probably exists still more combinations such as stall due to thin-airfoil type separation with trailing-edge separation existing prior to stall and vice versa. Certainly it is often impossible to ascertain which separation actually triggered the stall. Just to complicate the issue, with both leading-edge and thin-airfoil stalling profiles, a secondary stall resembling the thin-airfoil type will occasionally occur. Although leading-edge or thin-airfoil separation can occur on the same profile under the same free-stream conditions, it is impossible by definition for both leading-edge and thin-airfoil separation to coexist (at the same α).

The separation-stall type for a given profile depends upon the profile thickness, thickness distribution, and Reynolds Number. For a given Reynolds Number and profile series it is possible to correlate separation-stall type with the shape of the maximum lift coefficient vs. profile thickness curve. Fig. 17 indicates that with decreasing thickness separation-stall type moves from the pure trailing-edge to the pure thin-airfoil (from 1 to 6 above). It is interesting to note how seldom there occurs only one separation type at angles of attack prior to profile stall and how much difference stall type and separation mixtures can make in profile maximum lift.

The effect of Reynolds Number on the normal profile's separation-stall characteristics is demonstrated in Fig. 18. It can be seen that decreasing Reynolds Number for a given profile is essentially the equivalent of decreasing its thickness at a constant Reynolds Number. As all "sharp-nosed" profiles such as the double wedge must stall in a thin-

airfoil manner, there is no noticeable Reynolds Number effect on such profiles.

Although the material presented in this section of the report clearly shows the trends which can be expected in the stalling characteristics and maximum lift coefficients attainable with variations in the thickness, thickness distribution, and Reynolds Number of a profile, no rigorous means of predicting these characteristics of <u>any</u> given profile are available. A study of these trends, however, casts a great deal of light on the possibilities of predicting the maximum lift attainable through the use of boundary layer controls.

It is felt that linear extrapolations from the pure trailing-edge and pure leading-edge stalling portions of the $C_{l_{max}}$ vs. t/c curve for the given profile series can closely define the limit maximum lift attainable through the use of a large number of boundary layer controls. This approach further seems logical even for use with profiles with circulation control. Although much of the data presented in later sections appear to demonstrate the validity of such an approach, true verification of its usefulness must await further investigation.

3.2 THE EFFECT OF TRAILING-EDGE DEVICES

3.2a General Discussion

The quest for shorter take-off and landing distances and better lifting characteristics in general has been going on since long before the Wright brothers' flight. Between the First World War and the present time this problem has become increasingly important and has presented ever greater difficulty in solution as aircraft have reached

for faster and faster maximum speeds. As high speed (and high wing loading) capabilities are completely at odds with the short take-off and landing concept, engineers have added to the aircraft configuration those high lift "devices" which might be used to achieve lift increases when such extra lift is desirable while creating as little adverse effect as possible when high lift is not necessary. While the word "device" has, by training, a rather ugly connotation among aerodynamicists, it must be admitted that only such controls which can be termed "devices" have to this date successfully approached a general solution to the high speed vs. short take-off and landing problem. The helicopter has so far proven itself limited in speed and range. The V.T.O.L. aircraft is still in its infancy and its maximum speed and range characteristics remain a question mark, while the integrated jet aircraft with a combined propulsive and lifting system is currently little more than a twinkle in the researcher's eye. Of course, these approaches have a great deal of potentiality, but they cannot in the very near future be expected to yield a real solution to this current and growing conflict.

The devices which will be considered in this report may be classified as (1) trailing-edge controls and (2) leading-edge controls. It is the purpose of this section to explore the high lift producing effects of those types of devices that endeavor to influence the circulation about the profile by means of effecting a change in flow conditions at the trailing-edge. Into this category are grouped all the traditional types of flap; the plain flap, the split flap, the slotted flap, etc. and, in addition, those relatively new devices that employ flow singularities either to improve

the effectiveness of a deflected flap or to influence the potential flow directly. Those controls which, although located near the trailing-edge, operate primarily as boundary layer rather than circulation controls are discussed in the section covering leading-edge devices (3.3).

An attempt is made to examine the flow mechanisms involved with each trailing-edge device so that its operation may be better understood. In addition, so far as is possible, summaries of the performance of these devices have been prepared and techniques of estimating section force and moment coefficients have been suggested. Only two-dimensional characteristics are discussed in this section, smooth profile surface conditions are assumed, and compressibility effects have been assumed to be negligible. These two assumptions were necessitated by the data available but should not invalidate the applicability of the information contained herein to the realistic, full-scale case, particularly if use of such information is limited to preliminary design purposes.

"Circulation" may be obtained in several ways, perhaps the simplest form of circulation being the "Magnus effect" created by a spinning cylinder or sphere. This effect, dependent upon viscosity for its operation, is demonstrated in Fig. 26. The smoke lines are seen to increase in both upwash and downwash when the cylinder is caused to rotate rapidly in a clockwise direction. Such a streamline pattern is indicative of a circulation being developed and generating an upward-directed lifting force. Circulation is, of course, applied to a wing profile in a much different manner. From potential flow considerations it becomes obvious that the location of the trailing-edge stagnation point has a determining

effect upon the lift generation of a profile. Looked at in its simplest terms, if the trailing-edge stagnation point can be located in such a way that the flow path from the forward stagnation point over the upper surface is maximized and the path between the forward and trailing-edge stagnation points on the lower surface is minimized, the largest value of circulation (and thus the largest lift increment at a constant angle of attack) will be obtained. This is, in effect, what is attempted by giving a profile camber. The cambered profile has circulation control with respect to its symmetrical counterpart by virtue of the reorientation caused in the relative location of the leading-edge and trailing-edge stagnation points.

Thin airfoil theory demonstrates that any given degree of camber will create a greater circulation lift if located near the trailing-edge rather than the profile leading-edge. This would indicate that the use of a large amount of camber applied to the trailing-edge of the profile could be very useful as a high-lift circulation mechanism, the one major problem being the poor high speed characteristics of such a configuration. The trailing-edge flap solves this problem, being a <u>variable</u> camber circulation control located at the trailing-edge where it can be most effective.

Of the almost infinite variety of trailing-edge flaps which have been tested, the types that have been most widely used are the plain flap, the split flap, the single slotted flap, of which the Fowler flap is a special example, and the double slotted flap. These flap types are shown in Fig. 27 while Fig. 28 demonstrates the airflow over the various flapped configurations at a constant small angle of attack. Note that the trailing-edge flap, like the spinning cylinder, yields a marked increase in upwash as compared

with the uncontrolled profile. This (if the two configurations are at the same angle of attack as is the case here) is indicative of the achievement of lift increase through increased circulation.

The plain and split flaps can be seen to create an effective stagnation area behind and beneath the flap hinge but, due to separation, cannot, at this deflection angle, force the formation of a stagnation point at the flap trailing-edge. As this amounts to a loss in potential circulation, the double-slotted and double flaps were devised. Such flaps allow higher-pressure lower surface air to bleed onto the flap upper surface, thus energizing the "dead" air in the flap's boundary layer, delaying separation, and increasing circulation through permitting the flap to more closely achieve potential flow. The Fowler flap yields additional lift benefits through extending the chord of the profile.

Fig. 29 demonstrates the effect of the several flap types upon the profile lift curve. Note that the gain in lift occurs as a shift of the entire lift curve to the left. This is a characteristic of circulation control as opposed to boundary layer control. However, boundary layer control with respect to the flap, as occurs with the slotted types, may be seen to create additional circulation control with respect to the base profile.

Official willingness to permit increases in landing-strip length and carrier size as well as catapult and arresting gear improvements for some time enabled such trailing-edge devices as discussed above to adequately contain the take-off and landing problem within reasonable bounds. However, the high speed aircraft with very large wing loadings developed in the last several years has forced a decision between the provision of even greater

landing and take-off room or the utilization of more powerful aircraft-borne controls. The latter would seem for several obvious reasons to be the more logical approach.

The devices already discussed have circulation lifts which are severely limited by flow separation, the turbulent boundary layer being unable to remain attached because of the severe adverse pressure gradients encountered along the deflected flap's upper surface. It would seem feasible then that, if this separation could be prevented and the stagnation point fixed to the flap trailing-edge, potential flow could be approximated and large circulation increases could be achieved. This thinking has led, in the past few years, to fairly intensive studies of powered flaps -- flaps utilizing blowing or suction to prevent any possible flow separation over the flap. Such research has indicated that the use of power will not only cause lift increases through energizing the flap's boundary layer but can achieve further increases due to jet reaction or effective chord extension. Additionally, it has been found that blowing or suction at the trailing-edge can, if properly designed, yield large lift increments even in the absence of a flap. Some typical powered trailing-edge devices are shown in Fig. 30.

It might be mentioned that there are two parameters which are generally used to relate the slot (or porous area) flow characteristics of a powered control to the resultant degree of boundary layer and/or circulation control provided; assuming of course a fixed profile geometry, angle of attack, location and alignment of powered device, and free stream condition. These parameters are the "flow quantity coefficient", C_Q, and the "flow momentum

coefficient", C_μ , used in the cases of suction and blowing respectively.

C_Q is a non-dimensional parameter expressing the volume flow through the control slot or porous area. This term came into being through the original theoretical suction-slot work where the slot was replaced by a sink with strength proportional to volume flow. When the suction is operating primarily on the potential flow (as could be the case with trailing-edge suction, for instance), C_Q has been found to be a unique flow parameter. Although its validity is not so clear when the system is operating mainly to control the boundary layer, no more appropriate parameter has yet been derived. The flow quantity coefficient may be defined:

$$C_Q = \frac{Q}{V_o S} \qquad (3.2a1)$$

where: Q = control volume flow - ft^3/sec
V_o = infinite free stream vel. - ft/sec
S = wing area - ft^2

The flow momentum coefficient, C_μ , was devised after theoretical and experimental work had revealed that a term based on volume flow alone was not suitable for the directed jet situation. The blowing jet cannot be simulated by a source, but acts rather like a sink distributed along a thin membrane. The basis for the parameter, C_μ , is the thrust of the jet at the slot. Here again, it is found that where the operation is primarily that of altering the potential flow pattern this term is closely unique, but it becomes less rigorous where boundary layer control is the major effect. (In practice, C_μ yields good correlation for trailing-edge systems. Its value for use with leading-edge systems has, however, not yet been fully established.) C_μ is defined where the jet thrust

has been non-dimensionalized as follows:

$$C_\mu = \frac{\frac{\omega}{g} V_j}{\frac{1}{2}\rho_o V_o^2 S} \qquad (3.2a2)$$

where: V_j = jet velocity at slot - ft/sec
ω = mass flow through slot - lb/sec

$\frac{\omega}{g} V_j$ = jet thrust at slot - lbs

ρ_o = free stream density - slugs/ft^3

This may be put in terms of C_Q;

$$C_\mu = 2 C_Q \left(\frac{V_j}{V_o}\right)\left(\frac{\rho_j}{\rho_o}\right) = 2 C_Q^2 \left(\frac{S}{S_j}\right)\left(\frac{\rho_j}{\rho_o}\right) \qquad (3.2a3)$$

where: ρ_j = density of jet at slot - slugs/ft^3

S_j = slot area - ft^2

Normally the density ratio may be assumed $\cong 1$ (except where near-sonic, sonic, or supersonic blowing is achieved).

Some investigators feel that, where the blowing slot is located well forward from the trailing-edge, it is more convenient and just as realistic to use the ratio of jet velocity at the slot to infinite free stream velocity, V_j/V_o, rather than C_μ. Available test results of forward located blowing slots shed little light as to which of these two parameters is preferable. Velocity ratio may be related to C_Q as follows:

$$\frac{V_j}{V_o} = \left(\frac{S}{S_j}\right) C_Q \qquad (3.2a4)$$

Maximum possible C_Q for a given free stream velocity occurs when sonic conditions are encountered at the slot or point of minimum area in

the duct. Any increases in suction power beyond that corresponding to such an occurance would be expected to be of little value. The blowing parameter, C_μ, however, may be made to increase, because of the density term, even after the establishment of choked conditions. Expansion slots can be used to permit even further increases in C_μ. It is understood that unpublished results of tests at these very high C_μ's indicate its continued acceptability as a definitive parameter.

The selection of a blowing or suction system of course depends very much on the requirements of the specific aircraft. Disregarding any profile pressure distribution effects, suction at the trailing-edge generally necessitates smaller pressure ratios to create the same lift increment as the blowing system, which, however, can be designed, through the use of narrow slots, to require as low or lower mass flows. The properties of the blowing jet indicate that such a system is necessary to acquire very large ΔC_ℓ's without the extensive use of flaps. Losses in the blowing slot are much less than the corresponding losses would be in a suction slot. Further, the jet engine may be bled in a rather simple manner to provide blowing while its application to a suction system is considerably more difficult. Although most of the rather over-generalized statements above would seem to favor the use of blowing, there are certainly many configurations for which suction (or combined suction and blowing) might be the preferable system. It cannot be stressed too strongly that the selection of a system is almost completely dependent upon the particular application -- the performance needs of the aircraft, structural considerations, etc.

Generally speaking, the trailing-edge device creates lift increases through its ability to provide circulation control. Many systems also provide an element of boundary layer control (with respect to the profile, the flap, or both), while some can create effective or geometrical chord extension. Additional increments can be obtained with blowing systems through jet thrust effects.

It was shown in Section 3.1 that a completely controlled (B.L.C.) symmetrical profile had a limit possible $C_{l_{max}}$ of 6.28 at an angle of attack of 90^{o}. This was determined through potential flow considerations. It might then be thought that such a profile with circulation control, providing no chord extension or jet reaction effects but yielding sufficient boundary layer control to simulate potential flow, would be limited at 90^{o} and at a lift coefficient of 6.28 plus the value of the circulation increment taken, say, at $\alpha = 0^{o}$. Hazen, in reference 61c, indicates that this would not be the case. Electrolytic plotting tank studies of a profile with various split flap arrangements show an inviscid fall-off in circulation effect as angle of attack is increased from zero. Fig. 31 demonstrates the results of these studies. It will be noted that maximum lift becomes constant for the greater values of circulation control at angles of attack around 20^{o} and at a lift coefficient of around 7.0.

Thus, although thin airfoil theory appears capable of accurately predicting the ΔC_l at $\alpha = 0^{o}$ for profiles with a given circulation control and complete boundary layer control, the maximum possible lift coefficient attainable with extremely large values of circulation will, for such a system, possibly be not much greater than the 6.28 given for the base

symmetrical profile. Again, jet reaction and chord extension effects can invalidate this estimate, permitting the attainment of much larger maximum lifts.

3.2b Effects of Circulation Control upon Leading-Edge Stall

It is often assumed that the increase in profile maximum lift coefficient due to the addition of a trailing-edge circulation control is equal to the increase in lift at zero angle of attack. This assumption is based on the many lift curves shown in texts, most of which indicate a constant stall angle independent of flap deflection. The testing and use of very thin airfoil sections and controlled flaps in recent years has shown that, although it is valid for very thick profiles with standard flap types, such an assumption can be highly erroneous for these more modern systems.

While trailing-edge circulation controls can be used to advantage in conjunction with thin airfoils, their usefulness is often severely limited due to a circulation-induced tendency toward premature leading-edge separation. Increased circulation means an increased upwash at the leading-edge and thus an increased "effective" angle of attack. As occurrence of leading-edge separation is, for a given Reynolds Number, a function of effective angle of attack, it is obvious that such separation must occur at an earlier geometric angle the greater the circulation. This effect can be further aggravated in the three-dimensional case, some configurations achieving no increases in maximum lift whatsoever through the use of such circulation controls. Fig. 32A demonstrates a typical pattern of premature stall on a thin airfoil. Note that leading-edge stall can develop beyond a

certain value of circulation even though the base profile stalls from the trailing-edge.

A lesser known phenomenon is that sometimes noticeable with the powered form of trailing-edge circulation device. It appears that, if the suction or blowing is of sufficient strength and in such a location that a portion of the profile forward of the hinge line may be effected, not only is the flap controlled, but the aft portion of the profile as well is given a modicum of trailing-edge boundary layer control. Some slotted flap data indicates that this system also can provide trailing-edge B.L.C. with respect to the profile as well as with respect to the flap. The general effect of such a phenomenon is to extend the flapped profile lift curve to higher angles of attack than that for the base uncontrolled airfoil. This extension of the lift curve would be expected to be of greater magnitude the stronger the control power. An example of such a situation is shown in Fig. 32B, where the profile has been assumed sufficiently thick that there is no counter-effect from the tendency shown in Fig. 32A. Although there is sufficient available data to verify the trends attributed here to the trailing-edge boundary layer control effect, and the existence of such an effect seems logical in a manner consistant with existing experimental information, not enough data is available to permit any attempts to predict its effects quantitatively.

There appear to be five possible variations in $\alpha_{C_{l_{max}}}$ which can take place with increased circulation: (1) For the very thick profile, itself stalling trailing-edge and equipped with an unpowered circulation device, $\alpha_{C_{l_{max}}}$ may be assumed to be invariant with circulation

control. $\Delta C_{l_{max}}$ may thus be estimated to be closely equal to $\Delta C_{l_{\alpha=0}}$ (2) If the base profile still experiences trailing-edge stall but is somewhat thinner, the application of circulation control can, at some circulation value, alter stall type to leading-edge, the angle of attack for maximum lift decreasing as circulation is increased beyond this value. There can here be expected a corresponding fall-off in $\Delta C_{l_{max}}$ as compared with $\Delta C_{l_{\alpha=0}}$. (3) Profiles stalling from the leading-edge would be expected to stall at a lower angle of attack as circulation is increased from zero. Again, $\Delta C_{l_{max}}$ will be less than $\Delta C_{l_{\alpha=0}}$. Indications are that stall can be altered from the leading-edge type to the thin airfoil type given sufficient circulation. Of course, the profile normally stalling in a thin-airfoil manner would be thought to stall in the same manner given circulation control. Such a configuration would be expected to show the same general characteristics with increased circulation as the leading-edge stalling configuration. (4) For the very thick, trailing-edge stalling profile equipped with a circulation control capable of also affecting boundary layer control, $\alpha C_{l_{max}}$ may increase with increased circulation yielding $\Delta C_{l_{max}}$ greater than the corresponding $\Delta C_{l_{\alpha=0}}$. (5) The relatively thick profile showing a trailing-edge or predominately trailing-edge stall may when equipped with a powered circulation device yeild an $\alpha C_{l_{max}}$ variation as (2) or (4) above or perhaps as a combination of the two depending upon the profile thickness compared with the degree of circulation and boundary layer control.

As is the case with the base profile, a profile with circulation control need not stall in a pure leading-edge, pure trailing-edge, or pure thin-airfoil manner but often will yield separations of two or more of these types prior to final stall. The three major stall types are shown in Fig. 33. These are much like the comparable stall patterns for the base profile, although the thin airfoil stall shows a tendency to "cut-back" and achieves a greater $\Delta C_{l_{max}}$ than does a configuration of equal circulation control which stalls in the leading-edge manner. Additionally, trailing-edge stall often seems somewhat sharper than would be expected with the base profile, apparently due to the rapid unloading of the flap. For this reason, and because there is very little data at high thicknesses for flapped profiles, it is quite difficult to correlate stall type with the shape of the $C_{l_{max}}$ vs. t/c curve as was done with the base profile in Section 3.1.

Fig. 34 shows the $C_{l_{max}}$ vs. t/c curve for a base profile series and the same profile series with a given amount of circulation control, such as a given flap deflection. Both are at the same Reynolds Number and no trailing-edge B.L.C. is present, i.e. the circulation comes from an unpowered or effectively unpowered trailing-edge device. Although, as mentioned above, stall type variation regarding the configuration provided with circulation is difficult to analyze, available information indicates that the curve-shape principles shown in Section 3.1 for the base profile should apply equally to the profile with circulation. It is interesting to note that the little existing data available at high thicknesses indicates that the profile with circulation stalls in a "pure"

trailing-edge manner for thicknesses greater than that defined by the linear extrapolation of the base profile pure leading-edge stall region. The reason for this is not immediately discernable and coincidence possibly may be a factor. At thicknesses greater than that defined by this base profile linear extrapolation, the $\Delta C_{l_{max}}$ provided by the trailing-edge device would be expected to be equal to $\Delta C_{l_{\alpha = 0}}$, as both base profile and profile with circulation have a "pure" trailing-edge stall pattern. For lower thicknesses, leading-edge separation can be present at stall and $\Delta C_{l_{max}}$ will be less than $\Delta C_{l_{\alpha = 0}}$. As thickness is constantly decreased, from that for "pure" trailing-edge stall, premature trailing-edge separation will be encountered (induced by the formation of a leading-edge bubble), then premature leading-edge stall (with trailing-edge separation present prior to final stall), "pure" leading-edge stall, and finally thin airfoil stall. Correspondingly, $\Delta C_{l_{max}}$ is seen to reduce as thickness is thusly decreased, assume a rather constant comparatively low value, and then increase when thin-airfoil type stall is initiated. In this regime of increased $\Delta C_{l_{max}}$, a profile normally stalling in a leading-edge manner may stall thin-airfoil when circulation has been applied.

Fig. 35 shows the same profile and profile plus trailing-edge circulation control, only now trailing-edge B.L.C. is present. As shown in Section 3.1, trailing-edge B.L.C. is thought to be limited by the pure leading-edge stall extrapolation. In the case of circulation such an extrapolation should be made from the leading-edge stall region of the

profile plus circulation curve. Of course, ideal trailing-edge B.L.C. as defined by this line is seldom attained and a given value of C_Q or C_μ would be expected to cause an increase in $C_{l_{max}}$ initiating at a thickness corresponding to that where final stall involves some trailing-edge separation, this increase becoming greater in magnitude with further increases in thickness. As can be seen from Fig. 35, $\Delta C_{l_{max}}$ under such conditions may be greater or less than $\Delta C_{l_{\alpha = 0}}$ depending upon the profile thickness, amount of circulation control, and degree of trailing-edge B.L.C.; Reynolds Number variations and variations in profile thickness distribution would also be expected to be most important. There should be no effect of trailing-edge B.L.C. when the profile with circulation stalls without the occurrence of trailing-edge separation. In the thickness range effected by such B.L.C., increases in control power will cause stall to tend more toward the leading-edge type, constantly decreasing the effect of trailing-edge separation.

The approximate effect of circulation control upon stall type is shown in Fig. 36. This plot was determined empirically from a rather small amount of data for configurations the majority of which involved 64 series profiles. For this reason these curves should not be considered rigorously applicable to the general case. The line separating the leading-edge and trailing-edge regions closely follows the linear extrapolation of the 64 series base profile "pure" leading-edge stall segment but only "pure" trailing-edge stall appears to occur to the right of this line. Linear extrapolation concepts would indicate that, even for 64 series profiles, the prediction given here may be pessimistic, the line shown being perhaps

at too low a slope, particularly at high circulation values. Also it would be thought that forward camber increases, increases in Reynolds Number beyond 9×10^6, and any forward movement of the point of maximum profile thickness from 40% would increase the slope of these curves somewhat and move them slightly to the left.

Fig. 37 is based upon empirical studies and predicts, for profiles without trailing-edge B.L.C., the expected variation of $\Delta C_{l_{max}}$ with $\Delta C_{l_{\alpha=0}}$ for profiles of the 64 series at a Reynolds Number of approximately 6×10^6. Increment in maximum lift is assumed to be equal to $\Delta C_{l_{\alpha=0}}$ at values of circulation ($\Delta C_{l_{\alpha=0}}$) shown for the given thickness by the trailing-edge stall line of Fig. 36. It will be noted that increased circulation will cause an increased percentage drop in $\Delta C_{l_{max}}$ as compared with $\Delta C_{l_{\alpha=0}}$. Decreased thickness will decrease $\Delta C_{l_{max}}$ for a given $\Delta C_{l_{\alpha=0}}$, at least until thin-airfoil stall is encountered ($t/c \cong 6\%-9\%$) where it will increase to a small extent. Increased Reynolds Number, forward camber, or the moving forward of the point of maximum thickness will increase the $\Delta C_{l_{\alpha=0}}$ at which divergence of the curves from the $\Delta C_{l_{max}} = \Delta C_{l_{\alpha=0}}$ line will occur. Such variations will also rotate the constant-thickness curves somewhat upward from their indicated positions. Although scattered experimental data showed violent disagreement with this plot, by far the large mass of data fell in quite well, independent of Reynolds Number, profile shape, or type of trailing-edge circulation.

The assumption that $\Delta C_{l_{\alpha = 0}}$, or amount of circulation, is the important parameter effecting premature leading-edge separation for a configuration of given thickness seems to be quite valid. Of course, variations in flap extent, etc., do change the pressure distribution for a given circulation and hence alter the effect of circulation on stall to some degree, but such secondary effects are relatively insignificant.

Unfortunately, it appears impossible with existing data to predict any correction to Fig. 37 for configurations which have the added advantage of providing trailing-edge B.L.C. In a Reynolds Number range of 3-9 x 10^6 it is doubtful that trailing-edge B.L.C. can provide any additional lift benefits for profiles of thicknesses beneath the order of 12%. Increased circulation control, if arrived at because of increased control power, would be expected to provide greater and greater B.L.C., while increased circulation due to flap deflection would probably yield a B.L.C. effect which is independent of circulation, being dependent only upon control power. As stated previously, thicker profiles will profit more from a given quantity of B.L.C. (given C_μ or C_Q). Fig. 38 demonstrates the probable trends of a correction term to Fig. 37 to take trailing-edge B.L.C. into consideration. This figure is strictly schematic, the curves shown being, for purposes of clarity, on a greatly amplified vertical scale as compared with those of Fig. 37. The assumption has been made here that an effect of increased circulation is to increase the t/c below which pure leading-edge separation initiates. It is quite possible, however, that for a given thickness the effect of increased B.L.C. with increased circulation could far outweigh any pure circulation effects. Reynolds Number would also certainly be important

here, as it is with all questions concerning stall phenomena.

It must be remembered that this discussion has to this point been limited to systems with circulation control and possibly B.L.C. and has not touched upon systems which additionally have chord extension or jet reaction effects. Disregarding the inherent slope change, chord extension would normally act as a circulation control, the relationship between $\Delta C_{l_{max}}$ and $\Delta C_{l_{\alpha = 0}}$ being closely predictable by methods described above. In the case of jet reaction, however, an increment to $\Delta C_{l_{max}}$ is achieved which is independent of circulation control as such and is a function of jet thrust and direction. In that momentum effects cannot alter the profile pressure distribution, such effects cannot contribute toward circulation or premature leading-edge stall. For this reason, stall angle may be said to be completely independent of jet reaction so long as the vertical component of that reaction is not sufficiently large to maintain lift even though the airflow over the upper surface is separated.

3.2c Trailing-Edge Suction

The first of the lift-increasing trailing-edge devices that will be examined is the application of slot suction at the trailing-edge of the profile. It was elected to investigate this relatively new flow control system before the more familiar flaps because, by its use, it is possible to alter the lift of the base profile without changing profile geometry. The major portion of this section will deal with what might be called "standard" trailing-edge suction, while a discussion of a modification to this system, the so-called "suction-vortex" profile or wing, has also been included. Drawings of these two control types are shown in Fig. 39.

A typical curve demonstrating the increase in lift created through increasing suction quantity for a profile equipped with trailing-edge suction is shown in Fig. 40.

It will be noted that this curve can be divided into three portions of characteristic shape: a rapidly rising portion as suction quantity is increased from zero (segment A), a leveling-off region (B), and a comparatively slow rising portion in the higher suction quantity regime (C).

Studies conducted at Princeton University have given some indication of the flow mechanisms which create such a characteristic curve. Fig. 41 summarizes the flow regimes possible with the trailing-edge suction system.

The first rapid rise in the curve of Fig. 40 may be attributed to the effect of suction reducing the "dead water" or stagnant region existing behind the suction slot at the rear of the profile. This stagnant region may be expected to be of greater extent, and hence the suction quantity required to create a given percentage reduction would be greater, the thicker the profile, the higher the angle of attack, or the more blunt the trailing-edge. When suction quantity is increased to a value corresponding to that defining the very uppermost portion of this segment of the curve, the stagnant region is essentially eliminated. It is replaced by two separate trailing-edge stagnation points, a true stagnation point on the profile upper-surface aft of the suction slot and the usual ideal stagnation point satisfying the Kutta condition at the profile trailing-edge. Upper surface air divides at the true stagnation point, that forward of this point being drawn into the slot and that aft flowing to the trailing-edge in the usual manner. The lift rise shown in segment "A" may be attributed to the increase

in effective camber created by the reduction in trailing-edge turbulence and the establishment of the upper-surface stagnation point, these effects causing the upper-surface flow field to bend downward as compared with the profile without this trailing-edge control.

Level-off portion "B" appears to initiate immediately after the upper-surface stagnation point has stabilized. Although the flow here is difficult to analyze, this condition seems to be reached when the suction quantity is sufficient to draw off all of the upper-surface boundary layer air but very little air from outside that boundary layer. Throughout portion B the additional suction apparently is used to thin this upper surface boundary layer through increasing its energy. There is seemingly no change in stagnation point location, the lift remaining essentially constant.

Segment "C" initiates when the upper-surface boundary layer to all intents and purposes is eliminated. This is the so-called steady state condition where the lift variation is in accordance with potential theory. This theory predicts that the lift increment due to a sink located on the upper-surface of a profile is:

$$\Delta C_\ell = 2 C_Q \cot \frac{\beta}{2} \qquad (3.2c1)$$

where, as shown in Fig. 42, β is the angle between the trailing-edge (Kutta condition) stagnation point and the sink when the profile is mapped conformally to a circle of unit radius. It will be noted that for a given configuration this portion of the lift curve would be expected to be linear. The lift rise here may be attributed to increased suction quantity (operating now on the upper-surface potential flow field) forcing the

upper-surface stagnation point further aft on the profile, thus creating greater and more effective camber.

If the suction quantity is increased sufficiently, this steady state condition can be caused to break down either by producing a free-stream stagnation point at the rear of the profile or by inducing a separation at the airfoil's leading-edge. If the suction quantity is great enough to move the upper-surface stagnation point beyond the airfoil's trailing-edge, air from the profile's lower surface will be drawn into the slot. This of course acts to spoil the circulation and causes the lift increment due to suction to decrease. The drawing of air from both the upper and lower surfaces creates a free-stream stagnation point which, although unstable for lower suction values, can seemingly be stabilized with large amounts of suction. If the configuration is such that sufficient circulation (see Section 3.2b) is created prior to the formation of the free-stream stagnation point, the lift will be limited by a lift-decreasing laminar separation from the profile leading-edge.

Fig. 43 demonstrates a series of pressure distributions obtained from an NACA 23015 profile modified as shown in Fig. 39a. As suction is initiated and flow quantities are still rather small, the major pressure distribution changes occur in the immediate neighborhood of the suction slot and the rear of the profile. This is rather typical of the effect of a boundary layer control and shows this relatively low suction quantity to be below that where potential flow is approximated. It is interesting to note that, for profiles with radically curved upper-surfaces, B.L.C. can cause what is in effect a circulation control, especially if the curvature and B.L.C.

are located well aft. Once the separated area about the trailing-edge slot has been completely removed by suction, the change in circulation results from non-viscous considerations. Here, rather than achieving simply a local distribution change, the pressure distribution about the entire profile, including the leading-edge pressure peak, undergoes modification.

Fig. 44 illustrates some typical force and moment data obtained with an NACA 23015 airfoil utilizing a trailing-edge suction slot (Fig. 39a and Ref. 36). It will be seen that the largest lift increments at low and moderate angles of attack occur in the range of suction flow coefficients below approximately .01. This is the range, for this configuration at least, in which the lift increment is due primarily to the effec of suction on the stagnation region and the boundary layer. As indicated by the curves, this lift gain is not constant with angle of attack, but decreases as the boundary layer thickens with increased angle, thereby causing the profile to display a considerable reduction in lift curve slope. Above this C_Q value, the lift increment for a given suction quantity becomes independent of angle of attack, indicating that the lift increase throughout the angle of attack range is due primarily to the effect of suction on the potential flow.

Profile drag is sharply reduced with increases of suction up to a suction coefficient of slightly greater than .01, at which point it has nearly vanished. The initial reduction of profile drag is caused by the action of suction in reducing the extent of the stagnant region. As suction is increased, the profile drag will diminish and the drag curve may be expected to remain relatively level to greater angles of attack. When the suction quantity is sufficient to

eliminate the stagnant region, the drag will become essentially independent of further increases in suction quantity and closely independent of angle of attack until stall. It is at this C_Q value that the profile drag is made up almost entirely of friction drag. Only when potential flow is achieved will there be no profile drag rise prior to stall. Note that the unusually high no-suction drag shown in Fig. 44 can be attributed to the rather blunt trailing-edge of the profile used for these studies.

It must be pointed out that, with such a system, the total two-dimensional drag is made up not only of the profile drag discussed above but also must contain a term indicative of the momentum drag. This drag is caused by the jet of air rushing through the slot in a forward direction and can be evaluated as:

$$D_M = \Delta M = \rho Q \omega_i - \rho Q \omega_o \tag{3.2c2}$$

(assuming zero velocity in the chordwise direction within the wing)

The momentum drag coefficient may then be expressed:

$$\therefore C_{d_M} = \frac{\rho Q \omega_o}{\frac{1}{2}\rho S \omega_o^2} = \frac{2Q}{S\omega_o} = 2C_Q \tag{3.2c3}$$

The total two-dimensional drag for such a system is thus:

$$C_d = C_{d_o} + 2C_Q \tag{3.2c4}$$

The necessary addition of momentum drag causes total two-dimensional drag to generally increase with increased C_Q. For this reason, trailing-edge suction as discussed here should not be considered for use as a low-drag

system. Of course, if the suction is turned again and ejected downstream the momentum drag term can be made to closely vanish, its level depending upon the internal friction within the system.

Increased suction creates increasingly negative (nose down) pitching moments as is generally the case with trailing-edge devices. The pitching moment characteristics are considerably more erratic in the low suction range, $dC_M/d\alpha$ becoming unstable for low suction quantities and then strongly stable as suction is increased. This again is an indication of the change in the action of the suction from primarily affecting the boundary layer to influencing the potential flow.

Equation 3.2c1 is indicative of the very important fact that the closer the suction slot is to the trailing-edge the greater should be the potential-flow lift increment due to a given suction quantity. This trend is limited, however, by the occurrence of the free stream stagnation point with resultant flow around the trailing-edge from the lower surface. The point at which this is apt to happen is a function of the angle of attack, suction quantity, and slot location itself and hence it is extremely difficult to find any one optimum slot location. Certainly, a profile with a slot exactly at the trailing-edge would not be expected to increase lift in the potential flow regime.

The trailing-edge suction system using a blunt trailing-edge profile with overhanging lower lip (Fig. 39a) would exhibit closely the same slope characteristics in the potential flow range of suction quantities as a more standard profile with a suction slot cut in its upper surface at the same location. There could well be differences, however, between these

two trailing-edge configurations in the lower C_Q range and in order of magnitude in the potential flow regime. The sharp trailing-edge profile (of little or no physical camber) would probably achieve closely potential flow at a lower C_Q than would be the case with a profile such as shown in Fig. 39a. However, potential flow will be attained at a low lift level as compared with the airfoil with radical upper-surface trailing-edge camber (Fig. 39a). Thus, the slope predicted by equation 3.2c1, although being identical for profiles with the same slot location, will initiate at a lower ΔC_l, so that the ΔC_l achieved even in the theoretical segment of the curve would be expected to be lower for profiles with less curvature at the rear portion of the upper surface. Unfortunately, existing knowledge of boundary layers aft of sharp curvatures is quite limited, and there is currently no possible means of predicting the effects of trailing-edge configuration changes on the lift attainable in the low suction quantity (B.L.C.) regime and, because of this, it is impossible at the present to accurately predict ΔC_l in the potential flow regime. Because of the B.L.C. effect in the low C_Q regime, effects of Reynolds Number and profile thickness may well determine the C_Q necessary for potential flow.

In the potential flow range of C_Q's, trailing-edge shape, Reynolds Number, and profile thickness can be expected to be of negligible importance. It thus would seem that equation 3.2c1 could be used to predict the slope of the ΔC_l vs. C_Q curve for any profile with any suction quantity in this regime. Tests indicate that for suction quantity coefficients in excess of approximately .01 - .015 the flow will normally

satisfy this equation regardless of trailing-edge shape so long as that suction is well aft (>90%c). The equation can break down once flow proceeds into the slot from the lower surface. It appears that this condition can occur at C_Q's as low as .02 for a slot located at 98.5%c but will not occur until $C_Q > .06$ for slots at 95%c. Thus bringing the slot closer to the trailing-edge, while increasing the ΔC_l for a given C_Q, will reduce the optimum C_Q. The sharper the trailing-edge the less will be the opportunity to prematurely affect the lower surface air and hence the higher will be the optimum C_Q.

Although the increment of lift coefficient to be expected from influencing the potential field can be expressed by the simple relation

$$\Delta C_l = 2 C_Q \cot \frac{\beta}{2} \qquad (3.2c1)$$

it is no simple matter to determine the proper value of β to be employed for a slot located at a given point on a given profile. Ringleb (Ref. 37) has developed a technique for making this computation, but it is felt to be too cumbersome for practical usage. Further, as mentioned previously, the B.L.C. segment of the ΔC_l vs. C_Q curve is almost impossible to predict for a given trailing-edge shape and, because this portion of the curve determines the lift level of the potential flow segment, the ΔC_l at any C_Q is, at the present state of the art, quite unpredictable.

Fig. 45 shows an empirical curve of $\frac{\Delta C_l}{C_Q}$ vs. slot location, a/c, which has been determined from the Princeton data, some work of Regenscheit's, and some unpublished N.A.C.A. data. This curve is felt to define this effect (both in the B.L.C. and potential flow regimes) as accurately as is

possible at present. Needless to say, for the reasons above, this accuracy is highly limited.

On the basis of the aforementioned data, the technique of estimating the ΔC_l (at any α prior to stall) yielded by trailing-edge suction may be reduced to the following steps:

1. From the lift characteristics of the basic profile obtain the slope of the lift curve.
2. From Fig. 45 determine the appropriate value of $\Delta C_l/C_Q$ for the a/c employed. (There is no data available for values of a/c over .99).
3. Multiply $\Delta C_l/C_Q$ by the selected design C_Q determined on the basis of pumping power available. (Remember that induction of lower surface air can spoil lift if C_Q is not compatible with a/c. $C_Q \cong .06$ is considered to be about maximum with a trailing-edge suction slot. If a/c is as large as 99%, $C_Q \cong .02$ will probably cause spoiling.)
4. The new lift curve can now be obtained by plotting at each value of α, the quantity $C_{l_b} + \left(\frac{\Delta C_\ell}{C_Q}\right) C_Q$ where C_{l_b} is the value of the lift coefficient of the basic profile at that angle of attack.

Little can be said regarding the stall characteristics of such a configuration as it provides trailing-edge boundary layer control in conjunction with circulation control. Because of this, stall characteristics will vary not only with profile thickness, degree of circulation and thickness distribution but with Reynolds Number and trailing-edge shape.

For thin profiles, $\Delta C_{l_{max}}$ should be lower than $\Delta C_{l_{\alpha=0}}$, while for thick profiles, $\Delta C_{l_{max}}$ may be larger than $\Delta C_{l_{\alpha=0}}$. Section 3.2b discusses the trends of interest concerning stall characteristics as affected by trailing-edge circulation controls and may provide sufficiently accurate data to permit a quantitative estimate of the stall characteristics of the design in question.

No simple method can be developed to predict the reduction of profile drag due to trailing-edge suction but experimental evidence suggests that a very rough estimate can be obtained by use of Fig. 46. The results presented by this graph neglect variations in slot shape and location, as well as angle of attack variation. It must be remembered that total two-dimensional drag is equal to profile drag plus momentum drag as shown in equation 3.2c4. The use of Fig. 46 for the determination of the profile drag term is suggested, in view of the variables above which have been neglected, only because it is anticipated that the momentum drag term will generally be much greater in magnitude. Further, in actual application, the induced drag should be of more interest than profile drag in the range of lift coefficients under consideration.

The available pitching moment data is very meager and confusing. However, in order to allow the designer to make some estimate of the amount of control required for trim, Fig. 47 has been prepared from cross plots of the available information. The results obtained in the region below $C_Q = .01$ were so erratic that only the definite trend of increasing nose-down moment could be established and, as a result, Fig.47 is not extended to these suction values.

One modification of trailing-edge suction that deserves some comment, although it shall probably never be employed in the form in which it was first developed, is the use of a snow cornice-like shape in which the application of suction generates and stabilizes a captive vortex. This effect was first discovered on a small model investigated during the course of trailing-edge suction experiments being conducted in the Princeton University Subsonic Aerodynamics Laboratory. No extensive experimental program has been conducted and mention is made of the system only because it represents an interesting variation of the basic trailing-edge suction configuration.

Fig. 39b shows the profile that was investigated. The pressure distributions for $\alpha = -1.6^{\circ}$ are shown in Fig. 48. Without suction, it can be seen that the entire after portion of the profile back of the cornice-like shape is separated and demonstrates the usual almost constant pressure. The application of suction rather drastically changes the situation affecting the circulation over the entire profile and particularly within the cornice or, as it has become known, "the cusp". Several things are worthy of note. The first is the reduction of pressure within the cusp demonstrating the presence of a weak vortex. It will be noted that directly downstream of this point a stagnation point is indicated. This was not measured by the pressure taps, but was indicated by tufts. The very high peak of low pressure aft of this point was measured at the lip of the suction slot. One other note-worthy effect is demonstrated by the pressure taps at the trailing-edge indicating the presence of considerable flow about the sharp trailing-edge into the suction slot.

Increases of suction up to a value of C_Q of approximately .025 demonstrate a slowly continuing increase in circulation and in the strength of the trapped vortex. Throughout this phase the quantity of flow around the trailing-edge steadily increases. With suction values greater than this, the change of circulation is greatly accelerated and the strength of the trapped vortex increases rapidly. It is interesting that the flow about the trailing-edge almost totally ceases as the trapped vortex strength is further allowed to increase.

A plot of the lift coefficient vs. suction quantity for this profile is given in Fig. 49. The abrupt increase in lift is evident as is the leveling out of the curve above values of C_Q = .05.

The particular profile investigated in these tests demonstrated decreasing values of maximum lift when the angle of attack was increased to values much greater than 2^o owing to a leading-edge separation. As will be seen in a later section, practical application of this device has been made to a suction flap system.

3.2d Trailing-Edge Blowing

Another device which can yield substantial changes in the lift coefficient of a profile without in any major way altering the profile geometry involves the use of a blowing jet at the trailing-edge. As currently conceived, this device employs relatively large quantities of fluid in the jet compared with more familiar trailing-edge systems. Since a large percentage of the lifting force of such a control is derived from the momentum of the jet, the "jet flap", as it is sometimes called, must be evaluated with an eye to the combination of its lifting and

propulsive merits. The jet flap is a relatively new device of some potentiality and is currently being studied by a large number of investigators. This device is worthy of such study not only by virtue of its apparent merits as a thrusting and high-lift control system but also because it provides an interesting example of the action of a blowing jet which, when used in combination with a deflected flap, comprises a circulation control system of already major importance.

Probably the most significant development in the aircraft field in the last ten years has been the rapid progress made in the design and application of the turbo-jet engine. Comparatively speaking, a small, compact, and light device, it has supplied to aircraft the power to achieve supersonic speeds and extremely high altitudes. However, as is well known, its relatively constant thrust is undesirable at low speeds and its efficiency during the take-off maneuver suffers in comparison with the high thrust producing capabilities of the "constant horsepower" reciprocating engine-propeller combination. Due to the jet aircraft's inherently clean design and the lack, as yet, of any suitable thrust reversing mechanism to correspond to reverse pitch propellers, its landing characteristics suffer as well. Thus means have been sought to employ the available jet thrust more efficiently at the low speeds associated with landing and take-off.

The most obvious way of using this jet thrust for assisting lift is to direct it immediately downward to utilize its momentum as a direct lifting force. Indeed several current aircraft, with configurations permitting high angle of attack take-off, do this to a certain extent.

It has been found, however, that, if the jet is ducted into a wing and ejected in a sheet downward along the span from the trailing-edge, it can induce a lift force which, even at low forward velocities, is well above the vertical jet momentum component. The capabilities of such an arrangement, considered two-dimensionally, will be the subject of this section of the report. As most of the test data available is for the case with no heat addition, only that simplified case will be considered here. Certainly, the expelling of high-pressure but unburnt gases constitutes a very effective control in its own right.

A trailing-edge blowing jet directed at some angle downward from the profile chord line may be expected to increase the lift of that profile through (1) the vertical component of the jet reaction and (2) the increased circulation created by the jet. The latter effect arises from two phenomena characteristic of the blowing jet. These are "jet entrainment" and the "chord extension" effect. It has been found that a blowing jet located in a moving or still free stream will induce such free stream air and entrain it. Fig. 50 demonstrates this effect. It can be seen that the blowing jet being emitted from the trailing-edge of the two-dimensional blunt body is pulling in the free stream smoke lines causing an effective stream tube contraction and eliminating any separation aft of the body. As is demonstrated through comparing Figs. 50a and 50b, increases in jet velocity cause this effect to become more noticeable. Thus the jet acts much like a distributed sink and as such serves to energize not only boundary layer air but also that from the free stream. It is of some interest to note that entrainment does not arise by virtue

of any low pressure within the jet but is caused simply by a mixing process. Tests run at Princeton University appear to indicate that no entrainment is possible where the jet boundary is in a laminar state. A jet, however, can apparently only be in such a state for a very short distance after it leaves the ejecting nozzle.

If the jet were now initially directed at same angle to the free stream, it is only logical that it must bend along its length and eventually become parallel to that free stream. The necessary curvature of a jet directed at an angle to the free stream creates what has become known as the "chord extension" effect. This curvature, of course, creates a centrifugal force and, as such curvature occurs in the steady state condition, there must be some balancing force. Analytical studies have indicated that the balancing force is a pressure discontinuity across the jet and supported by the jet. Seemingly then, there is a necessary coexistence between jet curvature and pressure discontinuity across the jet. In that the jet thus acts as a fluid membrane supporting a pressure discontinuity, the end effect may be thought of as that of extending the base profile chord, creating an effective stagnation point aft and below the profile trailing-edge. It should be remembered that there is no such thing as a definite or true trailing-edge stagnation point with such a system, the profile simply acting as if such a stagnation point had been relocated.

Fig. 51 shows a profile at zero angle of attack with and without blowing. The jet is directed from the model trailing-edge parallel to the profile chord line and hence parallel to the free stream. As this

is the case, there is nothing to force a bend in the jet and it would be expected that no lift increase could be achieved through chord extension. The smoke photos verify this, the streamlines maintaining the same orientation with the profile both with and without blowing.

The same configuration has been brought to an angle of attack of 4° in Fig. 52. Here, the jet is at a small angle to the free stream. Streamline analysis of these photographs reveals that the blowing jet has increased the lift on the profile to a greater degree than could be attributable to angle of attack effects. This lift gain is, of course, small as the angle of attack is still quite small. As angle of attack is increased, it would be expected that lift increase due to the jet effects would be correspondingly greater.

Fig. 53 shows the model at zero angle of attack but with the jet at several deflection settings. It might be mentioned that although the photographs make the profile appear to have a sharp trailing-edge it is actually somewhat rounded and the blowing slot is located very close to the trailing-edge. Note the streamline indication of greatly increased lift with increased jet deflection. Fig. 54 shows the same effect at a higher angle of attack. As smoke lines cannot be affected by momentum considerations, the lift increase shown must be attributed to increased circulation. The trailing-edge jet with an initial deflection to the chord line has become known as the "jet flap" for, indeed, through its chord extension abilities, it yields results which can be closely simulated by a trailing-edge flap of finite length and at the same deflection angle.

Dividing the circulation effects of the "jet flap" into its chord extension and jet entrainment elements might be academically desirable, but seems impossible. Variation of lift with jet deflection and with angle of attack at zero deflection indicate that the majority of the circulation lift created through trailing-edge blowing would be impossible if there were no such thing as chord extension. Were there no such effect, jet entrainment could possibly, under certain conditions, cause circulation lift increases but not of the type and magnitude characteristic of the jet flap. Jet entrainment can exist without chord extension, as is the case in Fig. 50, and presumably chord extension could, in the absence of viscosity, do its job without jet entrainment. However, in the practical case, the jet entrainment phenomena would seem a necessity at any time that the profile or jet are at sufficient angle to the free stream to induce a tendency toward separation above and aft of the jet. It is speculated that separation would spoil the balance between the pressure discontinuity across the jet and the jet curvature, causing the jet to straighten out and the chord-extension effect to be at least severely diminished. Blowing studies (not on the jet flap) conducted by the Subsonic Aerodynamics Laboratory have revealed the apparent attraction a separation region has for a blowing jet. As might be expected, such a situation often leads to oscillating of the jet between its original position and the now off-again on-again separation region.

Thus it would seem possible to say that the chord extension effect is the major cause of the circulation lift increase attained through use of the jet flap. The ability of the jet to entrain outside air, however,

creates a boundary layer control effect which permits the chord extension phenomena to exist even at high jet deflections.

Based upon the foregoing discussion, it would appear that logical parameters to be used in the development of an equation for the lift increment created by trailing-edge blowing would be the jet momentum and direction. As the ultimate result created through chord extension seems to depend upon jet angle with the free stream ($\alpha + \theta'$), this will be considered the deflection angle of importance. The blowing jet cannot be represented by a source for reasons of its directionality. Thus there is no basis for the use of the flow quantity coefficient, C_Q, as the major strength parameter influencing circulation. Experience and theory has shown that the blowing jet's aerodynamic properties are better related to the flow momentum coefficient, C_μ . For this reason it is almost invariably used as an expression relating the energy of a jet to the resultant change in circulation about a profile. It will be noted that:

(1) α = profile angle of attack

(2) θ' = initial (immediately after the slot) jet orientation with the profile chord line

(3) $(\alpha+\theta')$ = initial jet orientation with the free stream

(4) $C_\mu = \dfrac{\text{Jet thrust at slot}}{q_o S} = \dfrac{\omega/g\, V_j}{\frac{1}{2}\rho_o V_o^2 S}$

where: ω = mass flow through slot - lb/sec
V_j = jet velocity at the slot
V_o = free stream velocity
S = wing area
g = gravitational constant
ρ_o = free stream density - slugs/ft^3

As mentioned previously, the change in lift caused by the trailing-edge jet may be divided into that created by the vertical reaction component at the jet and that created by virtue of the jet's ability to alter the circulation about the profile. Let us now consider the first of these terms.

The jet reaction effect upon lift is, quite simply, that component at the jet thrust acting in a direction normal to the free stream. The term, C_μ , is a non-dimensional parameter indicative of the jet thrust and may be considered to be a thrust coefficient. As the jet angle from the free stream direction is defined by $\alpha + \theta'$, it is obvious that the increment in lift coefficient created through jet reaction may be given by:

$$\Delta C_{\ell_R} = C_\mu \sin(\alpha + \theta') \qquad (3.2d1)$$

The above equation may be found to be merely an expression of Newton's Law. If $\alpha + \theta'$ are positive, i.e. the jet is directed downward from the direction of the infinite free stream, the lift increment will be positive.

Determination of an expression for the circulation term presents a somewhat more difficult problem. It would seem intuitively, however, that this term could be related to some function of C_μ and the jet orientation angle with the free stream. The simplest relation, determined theoretically, and the one which has, to this time, proven most accurate is:

$$\Delta C_{\ell_C} = f(C_\mu)\sin(\alpha + \theta') \qquad (3.2d2)$$

The expression, $f(C_\mu)$ has been related to C_μ by Dr. Malavard and his associates in France (Ref. 42). Based on previous theory, this relationship was arrived at from a consideration of the jet as a fluid membrane with unchanged momentum assumed along the jet. The linearized theory used assumed thin sections and small angles. Final quantitative data, determined from tests in the electrolytic plotting tank and making use of the thin membrane analogy, are presented in Fig. 55a. It must be remembered that this analysis deals with ideal flow and considers only chord extension. It cannot consider changes in jet entrainment characteristics or possible alterations to the chord extension effect due to viscosity. Of course, the ability of the jet to entrain is assumed in the method. "Chord extension" theory is dealt with at some length in Refs. 41 and 42.

Willauer points out in Ref. 44 that if $f(C_\mu)$ is plotted against $\sqrt{C_\mu}$ rather than C_μ, the results of Malavard's studies appear closely linear, the slope, Fig. 55b, being approximately 3.18. Therefore it can be said that:

$$f(C_\mu) \cong K\sqrt{C_\mu} \qquad (3.2d3)$$

where $K \cong 3.18$ using the Malavard data.

The circulation term may thus be altered to:

$$\Delta C_{\ell_C} = K\sqrt{C_\mu}\,\sin(\alpha+\theta') \qquad (3.2d4)$$

Adding the expressions for the contributions of jet reaction and circulation, the equation indicative of the total lift increment created by trailing-edge blowing will be

$$\Delta C_{\ell_{TOT}} = \Delta C_{\ell_C} + \Delta C_{\ell_R}$$

where: ΔC_{l_c} = lift increment due to circulation effects

ΔC_{l_R} = lift increment due to jet reaction

or

$$\Delta C_{\ell_{TOT}} = K\sqrt{C_\mu}\sin(\alpha+\theta') + C_\mu \sin(\alpha+\theta') \tag{3.2d5}$$

The lift coefficient for the jet flap equipped profile (with base lift curve slope of 2π units/radian) will thus become:

$$C_{\ell_{TOT}} = 2\pi\sin\alpha + K\sqrt{C_\mu}\sin(\alpha+\theta') + C_\mu \sin(\alpha+\theta') \tag{3.2d6}$$

The three partial derivatives of equation 3.2d6 are:

$$\frac{\partial C_\ell}{\partial \alpha} = \frac{2\pi}{57.3} + \frac{K\sqrt{C_\mu}}{57.3}\cos(\alpha+\theta') + \frac{C_\mu}{57.3}\cos(\alpha+\theta') \tag{3.2d7}$$

$$\frac{\partial C_\ell}{\partial \theta} = \frac{K\sqrt{C_\mu}}{57.3}\cos(\alpha+\theta') + \frac{C_\mu}{57.3}\cos(\alpha+\theta') \tag{3.2d8}$$

$$\frac{\partial C_\ell}{\partial C_\mu} = \sin(\alpha+\theta') + \frac{K}{2\sqrt{C_\mu}}\sin(\alpha+\theta') \tag{3.2d9}$$

where angles are expressed in degrees and slopes per degree.

Figs. 56 through 63 show plots of various aspects of equation 3.2d6. The constant, K, has been assumed equal to 3.18. Fig. 56 shows the increase in lift due to jet reaction as well as due to circulation effect plotted against $\alpha + \theta'$. The circulation effect may be seen to be many times the magnitude of the reaction term in this C_μ range. However, as lift increment varies here as the square root of momentum coefficient, increasing C_μ yields a fall-off in the effectiveness of the

circulation term as compared with the reaction term. From equation 3.2d5, it would be expected that the circulation term would exceed the reaction term until a C_μ of greater than ten is achieved. If a jet orientation angle of 90° with the free stream could be attained, this equation indicates that lift increment would here reach a maximum for a given C_μ. Fig. 57 indicates the predicted total lift increase attained through increases in initial jet orientation up to that of 90°. Note that the ratio of total lift increment to C_μ would be expected to become smaller the greater the C_μ.

Figs. 58 and 59 reveal the predicted lift coefficient achieved by an ideal profile with trailing-edge blowing under various conditions of α, θ' and C_μ. Fig. 58 considers only the circulation term while Fig. 59 demonstrates total lift coefficient. It will be noted that with $\theta' = 0^\circ$, the effect of blowing is to increase the slope of the lift curve as a function of C_μ, maintaining $\alpha_{o.L.}$. The effects of increasing θ' are much the same as would be the case with deflecting a finite geometric flap, the entire lift curve shifting to the left. This theory, however, unlike that for the finite flap as given by thin-airfoil theory, shows a predicted fall-off in slope with increased jet deflection. This is particularly noticeable where θ' becomes equal to 90°. At angles of attack above 8 to 14 degrees a θ' of 75° is shown to be superior to that of 90°. This slope fall-off is due to the establishment of $\alpha + \theta'$ as the orientation angle of importance rather than simply θ'. It is readily seen from these plots that, as would be expected, increased C_μ increases the effectiveness of variations in θ'. This is also shown in

the cross-plots presented in Figs. 60 and 61. Note that the effect of increased C_μ is not only to increase the lift level at a given θ', but also to increase lift curve slope.

The special case where θ' is equal to zero is plotted in Fig. 62. The near linearity of these curves results from the low orientation angles achieved here, the angle itself very nearly equaling its sine. As would be expected from the previous discussion of chord extension, lift increment goes to zero when initial jet orientation angle (here equal to α) goes to zero. It is of some interest that physical extensions to the symmetrical profile chord would also create curves of this type, yielding no increase in lift at the base profile $\alpha_{o.L.}$ and increased slope with increased chord extension. Basing lift coefficient upon the original chord, the effect of physical chord extension would be:

$$\Delta C_\ell = \frac{C_E}{C} C_{\ell_{\text{BASE PROFILE}}} \qquad (3.2d10)$$

where C_E/C is the ratio of the extended part of the chord to the base chord.

This may be equated to equation 3.2d4 for the $\theta' = 0$ case, resulting in the expression:

$$\frac{C_E}{C} = \frac{K\sqrt{C_\mu}}{2\pi} \cong \frac{1}{2}\sqrt{C_\mu} \qquad (3.2d11)$$

Thus the equivalent chord extension created through blowing directly aft ($\theta' = 0$) may be determined. It should be pointed out that although equivalence in results may be attained, the two phenomena are entirely different and generally must be thought of as such. The equation above

indicates an effective chord extension which is independent of α . This is somewhat surprising in view of the actual physical situation which would seem intuitively to be expected to yield a chord extension effect increasing with angle of attack. Further, the concept of chord extension loses much of its meaning at $\alpha = 0^\circ$. Here the uncurved jet will not sustain a pressure differential while likewise the equivalent chord extension will not, in the real, symmetrical profile case, be required to carry a pressure differential. The questions here are strictly academic (and perhaps semantic): can chord extension be said to exist with the uncurved jet?-and, what might be the effect of camber?

The lift increase due to circulation may be considered to be made up of two parts --that due to angle of attack changes where $\theta' = 0$ and that due to variations in jet angle, θ' .

$$\Delta C_{\ell c} = \Delta C_{\ell c_{\theta'}} + \Delta C_{\ell c_{\theta'=0}} \qquad (3.2d12)$$

where:

$$\Delta C_{\ell c_{\theta'}} = K\sqrt{C_\mu}\left[\sin(\alpha+\theta') - \sin\alpha\right] \qquad (3.2d13)$$

Fig. 63 shows plots of the above equation. The decrease in $\Delta C_{l_{c_{\theta'}}}$ with increased α , is of particular interest in the light of chord extension equivalence. Application of thin airfoil theory to the flapped case reveals no correlation between these curves and any given value of geometric chord extension assuming the same α and $\theta'(\delta_F)$. Certainly thin airfoil theory cannot predict any lift curve slope change with θ' as is the case with this theory. Thus it may be reaffirmed that although

the concept of the existence of an equivalent finite flap is of some aid in considering the general picture, it may well, at least at the present state of the art, act as a confusing element when it is desired to study the situation in some detail.

The rather meager amount of available experimental data on jet flap characteristics indicates that the theory as given in equation 3.2d5 comes very close to giving an accurate quantitative picture in the angle of attack regime prior to the occurrence of separation. Figs. 64a, b, c, and d compare theory as given in equations 3.2d5 and 3.2d6 with the experimental results of Poisson-Quinton and Jousserandot as given in Ref. 38.

It can be seen from Fig. 64a that, for C_μ's less than 0.5, theory and experimental data will agree almost exactly if variation of the actual base profile curve from its own theoretical potential is taken into account. Note that if the difference between the theoretical base profile curve and the experimental is subtracted from the controlled profile's theoretical curves for the lower C_μ values, the result will lie very closely upon the curve defined by the experimental points for the given C_μ. Further experimental work, conducted in England and described by Davidson in Ref. 43, yielded results which appear to be as close to theory as those of Ref. 38.

Fig. 64b indicates the same very good correlation up to a $\theta' \cong 60^\circ$. Here again, divergence from theory is closely equal to that divergence attributable to the viscous characteristics of the base profile. This correlation is, of course, only good prior to separation. The effects of separation become obvious here at $\alpha \cong 12^\circ$ for the $\theta' = 33^\circ$ case and at

$\alpha \cong 8^{\circ}$ for $\theta' = 63^{\circ}$. Although separation will be discussed in some detail further along in this discussion, it is interesting to note the very flat "stall" characteristics of this system. Due to jet entrainment effects, trailing-edge separation is thought to be impossible with the trailing-edge blowing jet of reasonably high C_μ . The large circulation control created by this device, however, can induce highly premature leading-edge separation. If the jet momentum flow is sufficiently great this separation seemingly cannot completely break away from the profile, the jet entrainment forcing reattachment at the trailing-edge at least until very high angles of attack are attained. This, plus a jet reaction effect which would be expected to increase with α so long as jet directionality remains constant, causes the jet flapped profile's "stall" to be very gentle.

The variance from theory for C_μ 's greater than 0.5 is again shown in Fig. 64c. Such divergence becomes more marked as C_μ is increased or as θ' is increased. For a C_μ of 1.00 relatively extensive divergence initiates at a jet deflection of 55°, while such divergence occurs at 50° for a C_μ of 1.50. It is possible that this fairly large divergence seen with increasing θ' can be attributed to leading-edge separation phenomena.

Fig. 64d demonstrates excellent agreement at low C_μ 's, while Fig. 64e indicates good correlation in the variation of lift curve slope with C_μ . Again, variation of the base profile characteristics with the theoretical seems the major cause for any disagreement between theoretical and experimental. Data contained in Refs. 43 and 44 also show very good agreement with the theoretical curve of Fig. 64e.

The experimental data shown would seem to indicate that the theory (equation 3.2d5) holds very well at C_μ 's below 0.5, jet deflection angles up to 60°, and angles of attack prior to the definite occurrence of leading-edge separation. There is always the possibility that all variance from this theory is due to separation effects. This possibility lacks verification as the angle of attack corresponding to occurrence of separation for such a configuration is very difficult to detect from force test data, and, unfortunately no data is currently available for a profile fitted with both a jet flap and a leading-edge boundary layer control. In general, it can be said that available experimental data shows unusual agreement with theory. Such correlation is all the more remarkable considering the necessary assumptions upon which the theory is based.

The excellent verification of theory indicates that jet entrainment, while seemingly of no importance in the establishment of lift variations, serves to quite perfectly control the boundary layer so that the chord extension effect may be fully realized. This appears to be true even at low C_μ 's where, with the blowing slot located on the lower surface at 97% chord, it would be possible that slight trailing-edge turbulence could spoil the chord extension effect. Whether jet entrainment would maintain theory at very small C_μ 's and/or with the blowing slot located well forward on the lower surface is a point still in question. It might be added that the circulation portions of the experimental results verify the existence of lift curve slope fall-off with increased θ' . This, again, demonstrates the fallacy of establishing any given flapped profile in viscous or inviscid medium as an equivalent to the airfoil with jet flap.

Some possible jet flap configurations are shown in Fig. 65. Fig. 65a demonstrates the fixed-deflection flap used in the tunnel tests described by Poisson-Quinton and Jousserandot in Ref. 38. The achievement of variable deflection at a far aft chordwise location would probably necessitate the use of a trailing-edge cylinder, as shown in Figs. 65b and c, which could be rotated to the desired angle in flight. The device shown in Fig. 65c would make use of what is known as the "Coanda" effect (Refs. 156 and 157). This effect is based upon the observation that a blowing jet ejected tangentially to a curved surface will tend to follow that surface rather than break away and continue in its original direction. The occurrence of such a flow phenomenon would be expected to be a function of degree of curvature, jet velocity, free stream velocity, the initial deflection of the jet with respect to the free stream, and, probably, the viscous conditions of the flow. In any event, fairing the rotable cylinder to a point, as shown in Fig. 65c would force a discontinuation of the "Coanda" effect and the jet would travel into the free stream in the direction defined by the deflection angle of the cylinder's discontinuity.

Fig. 66 shows the various blowing slot configurations used in obtaining the experimental data given in Ref. 38. It is of some interest to note that the design jet deflection angle, θ , is seldom actually attained. The actual initial jet deflection angle, θ' , is almost always somewhat less and sometimes considerably less than the design deflections. Note that the deflection loss here seems to be greater the greater the deflection, the greater the slot width, and the further aft the slot location. The difference between θ and θ' would seemingly

be a matter of slot design. Use of a blowing passage which contracts efficiently to a small, sharp-edge slot probably would yield optimum θ'/θ for the fixed-deflection jet flap, while it is possible that the variable deflection device using the "Coanda" effect could achieve a better detlection ratio than other systems as slot design here becomes less critical.

The values of θ' shown in Fig. 66 were obtained under conditions of zero free stream velocity. Correlation of "wind-on" tests with theory indicate that θ' does not vary significantly with velocity. It would thus seem that the actual jet deflection could be attained for any system through static tests. As slot design can be a large factor, it is recommended that such an evaluation of true jet angle be made prior to final testing of any new jet flap system. Of course, the dynamic effects may become important under certain conditions and with certain systems.

A trailing-edge blowing parameter of some interest is the lifting efficiency, "E". This term is defined as the ratio of the increase in lift due to circulation to the increase in lift due to jet reaction, and represents a measure of the gain achieved through utilizing a jet in a sheet aft of a wing as compared with simply directing it downward. For any given angle of attack, lifting efficiency may be expressed as follows:

$$E = \frac{f(C_\mu)\sin(\alpha+\theta)}{C_\mu \sin(\alpha+\theta)} = \frac{f(C_\mu)}{C_\mu} \cong \frac{K\sqrt{C_\mu}}{C_\mu} \qquad (3.2d14)$$

This equation is plotted in Fig. 67 along with experimental data from Ref. 38 for the zero angle of attack case. Very good agreement between

theory and experiment will be noted along with the trend toward lower "E" with increased C_μ . Assuming the value of "K" to hold constant even for high blowing coefficients, the lifting efficiency will fall below 1.0 at a C_μ of 10.

The correlation of theory with experiment regardless of slot width (using θ' as orientational parameter) and location justifies use of the blowing momentum coefficient, C_μ , as the major blowing parameter. Because of this invariance with slot width it can be said that, even though both the circulation effect ($K\sqrt{C_\mu}$) and the ratio of jet velocity to free stream velocity (V_j / V_o) are directly proportional to $\sqrt{C_\mu}$, the increment in circulation lift coefficient yielded by the jet flap cannot be equated to V_j / V_o except for a given slot width:

$$\frac{V_j}{V_o} = \sqrt{\frac{c}{2c_j}(C_\mu)} \tag{3.2d15}$$

$$\Delta C_{\ell_c} \cong K\sqrt{C_\mu}\sin(\alpha+\theta') \cong K\left(\frac{V_j}{V_o}\right)\sqrt{\frac{2c_j}{c}}\sin(\alpha+\theta') \tag{3.2d16}$$

where: C_j = slot width

C = profile chord

Similarly, if circulation increase in lift coefficient is proportional to $\sqrt{C_\mu}$, it may be equated to C_Q for a given slot width:

$$C_Q = \sqrt{\frac{c_j}{2C}(C_\mu)} \tag{3.2d17}$$

$$\Delta C_{\ell_c} \cong K\sqrt{C_\mu}\sin(\alpha+\theta') \cong K(C_q)\sqrt{\frac{2c}{c_j}}\sin(\alpha+\theta') \qquad (3.2d18)$$

Assuming a constant slot width, θ', and α, the lift increased due to circulation effects may be shown in terms of jet velocity to be:

$$\Delta L_c = \Delta C_{\ell_c} \frac{1}{2}\rho V_o^2 S$$

$$\Delta C_{\ell_c} \cong K' \frac{V_j}{V_o}$$

$$\Delta L_c \cong K' V_j \frac{1}{2}\rho V_o S \qquad (3.2d19)$$

In terms of blowing quantity, Q, this expression becomes:

$$\Delta L_c \cong K'' Q \frac{1}{2}\rho V_o \qquad (3.2d20)$$

Disregarding three-dimensional effects, it can thus be said that, for a given blowing quantity, the lift increment created through circulation on a jet flapped wing of given configuration and angle of attack varies directly as the flight speed. The jet reaction effect would be felt to be independent of velocity, while the base wing lift varies as the velocity squared. The lift increase caused by the jet reaction and jet-induced circulation initiates at zero airplane velocity at a level slightly greater than the jet reaction lift and, as velocity is increased, increases directly with that velocity. This, of course, assumes constant Q, constant θ', a given slot width, and no trim changes in angle of attack.

Smoke tunnel tests conducted in the Subsonic Aerodynamics Laboratory's 2" x 36" tunnel demonstrated the distinct possibility of severe ground-

effect problems with this type of configuration. Impingement of the jet upon the bottom wall appeared to cause strong flow changes along with possible flow instabilities. Experiments conducted along these same lines and described in Ref. 43 revealed some loss in lift but apparently did not show the powerful and variable flow changes observed during the Princeton tests. The major difference between these two tests seems to have been that of partial lower surface flow blockage (Princeton) as opposed to no blockage (Ref. 43). Distance above the ground, C_μ , θ' , α , free stream velocity, and perhaps profile thickness could be important parameters in this problem. It is hoped that the ground effect phenomenon will receive more consideration prior to the serious design of a jet flapped aircraft.

In the case of trailing-edge blowing it is necessary to speak of separation rather than stall. Because of the trailing-edge B.L.C. effect inherent in this design (jet at the trailing-edge), generally only leading-edge separation would be expected. Observations made in the few published experimental investigations of this device indicate that once this leading-edge separation works back to the trailing-edge it will not break away, the jet entraining the air about the separated region and thus preventing it from completely detaching. Such complete detachment, however, might well be possible at low C_μ's and/or high angles of attack. What effect leading-edge stall type (leading-edge or thin-airfoil) might have upon the separation characteristics of this system is not known.

For the reasons above, the "stall" pattern observed with tested jet flaps is a leveling-off of circulation lift, no true stall being present.

If jet reaction effects are considered, lift would still increase with angle of attack even after fairly complete upper surface separation. There would, of course, be expected to exist an angle where the jet could no longer contain the separation bubble, and stall (lift fall-off) would occur.

As increases in jet deflection angle or C_μ both serve to increase circulation, such increases would further the likelihood of separation at a given angle of attack. Again, as was the case with the trailing-edge suction system, $C_{l_{max}}$ (or the occurrence of rapid fall-off in lift curve slope) is very difficult to accurately predict primarily because the device provides trailing-edge B.L.C. Rough estimations may be made, however, from the information contained in Section 3.2b. Outside of the separated regime, the lifting characteristics of the jet flapped profile may be obtained through using the theoretical values as determined from equations 3.2d5 or 3.2d6, or the corresponding figures. "K" may be assumed equal to 3.18. Experimental data indicates that theory for such a configuration is at least as accurate as that for the base profile. Possible areas for divergence from theory are: (1) at high C_μ 's, where the value of "K" may change, (2) at high Θ' 's, where the value of "K" may change, (3) for configurations with blowing slots well forward on the lower surface, (4) for configurations in ground effect, and (5) for separated configurations. The first two of these areas of possible divergence await further testing, although it is understood that unpublished N.A.C.A. work indicates that "K" maintains its value ($\cong$ 3) to quite high C_μ 's and Θ' 's.

It would be thought that the further forward the blowing slot was located on the lower surface, the less likely would be the achievement of potential flow and the desired chord extension at a given C_μ. This is due to the fact that jet entrainment from the upper surface would be more difficult the further forward the slot. For a slot at a given location, full entrainment would be more likely if the profile trailing-edge were rounded rather than sharp. Ref. 38 indicates that theoretical values can be achieved even at low C_μ's with a slot located at 90% chord and a rounded trailing-edge. The use of theory to predict lift for configurations with slots much further forward than this is not recommended -- particularly when at low C_μ's and high α's. The possibility of aiding such a configuration through adding trailing-edge suction, however, should not be overlooked.

The drag increment created through the use of a jet flap would normally be expected to be negative, or actually a thrust. The thrust attainable through jet reaction effects may be shown to be:

$$\Delta C_{d_R} = C_\mu \cos(\theta' + \alpha) \qquad (3.2d21)$$

Entrainment created by the blowing jet has been shown with a minimum of C_μ to be capable of preventing any profile separation for θ''s up to 90°. Thus it would be expected that profile drag (discounting jet reaction) would always be equal to friction drag, i.e. essentially independent of angle of attack. Fig. 68 shows the profile drags for various C_μ and θ' as given in Ref. 38 compared with the results attainable through applying equation (3.2d21). It can be seen that at this angle of

attack ($\alpha = 0^\circ$) and for $\theta' < 40^\circ$ the correlation is very good, with the total thrust exceeding the reaction thrust by a quantity of the order of magnitude of the friction drag. At θ' 's greater than 40° the total thrust exceeds the reaction thrust by an amount which increases with increasing θ' and increasing C_μ . Davidson (Ref. 43) points out that this effect is probably due to the increased circulation which causes an acceleration of the air about the profile leading-edge and thus (in the absence of separation) a suction at that location. Davidson further indicates that a suction drag may be expected at the trailing-edge due to the local acceleration of the air by the jet entrainment action. The magnitude of this jet drag, according to tests made in England, will be equal to 5% to 6 % of the gross thrust. Ref. 43, however, indicates that if systems employing gases at elevated temperatures are employed, jet drag will cease to be a "problem" and may indeed become a rather large thrust term.

This writer has not had the opportunity to follow up the statement made by Davidson that gross thrust may be shown by theory to be equal to the total jet reaction and is independent of jet deflection. If this were the case, then all variation from $C_d = C_\mu$ must be allocated to friction drag plus "jet drag".

For the present it would seem that the drag (thrust) increment provided by trailing-edge blowing of unheated air can be approximated by use of equation (3.2d21). Thrust may be expected to increase beyond this predicted value at high θ' 's or high C_μ 's. The greater the magnitude of C_μ , θ' , or α , the larger would be the increase in thrust over such a prediction. Of course, if separation is encountered,

such an estimate will be invalidated.

Fig. 69 gives a very approximate estimate of the expected pitching moment coefficients created through trailing-edge blowing. This curve, which was determined empirically from data contained Ref. 38, should be applied for constant angle of attack and the lift coefficient shown is intended to include both circulation lift and reaction lift. It is of interest that θ' does not seem to be a significant factor in determining the ratio, $\Delta C_{m_{c/4}} / \Delta C_{\ell}{}_{\text{BLOWING}}$. The trailing-edge jet's reaction can be shown to theoretically yield a value for this ratio of -1.33, independent of C_{μ}. Unfortunately, the nature of this ratio does not permit true separation of the circulation and reaction effects and thus the remaining portion cannot necessarily be attributed to circulation lift. The jet reaction's influence upon pitching moment can be reduced if the jet is moved forward on the lower surface and negated if the jet reaction is brought to act through the quarter-chord point. Of course, moving the nozzle to such a location will not be expected to assist the large negative pitching moment created by circulation lift unless spoiling occurs -- in which case the system is operating inefficiently. Thus, no matter where the "trailing-edge" blowing is located, the high nose-down pitching moments characteristic of any trailing-edge high-lift device must be expected.

3.2e Applicability of Potential Theory-Trailing-Edge Flaps

As was the case with the trailing-edge suction and trailing-edge blowing configurations, theoretical considerations are of no small value as an aid in predicting the aerodynamic characteristics of trailing-edge flaps. Potential theory can be expected to closely predict such characteristics for any profile with circulation, providing separation does not exist. Therefore, for the profile with unpowered flap, potential considerations should be valuable for deflection angles below approximately 15^{o} (in which range flap separation is normally of small extent) and at angles of attack prior to those at which separation of the leading-edge or trailing-edge type can initiate. In the absence of jet reaction effects and chord extension and at angles of attack below that for leading-edge stall, the ideal circulation lift given by theory should quite rigorously define the change in lift possible due to a given deflection of the flap which is provided with boundary layer control in the form of a blowing or suction system.

The simplest means of determining the inviscid aerodynamic characteristics of a profile; flapped or unflapped, is through the use of the thin airfoil theory, an approximate theory conceived by Glauert (Ref. 46) and based on the potential flow over a profile of zero thickness. This concept has been described in numerous texts including Refs. 4 and 5. A summary of the results yielded by application of the methods involved in this theory to the general case of the profile (mean line) with any camber is given below:

(a) $$\frac{dC_{\ell}}{d\alpha} = \frac{2\pi}{57.3} \qquad (\alpha \text{ in degrees})$$

(b) $\alpha_{o.L.} = \frac{-57.3}{\pi}\int_0^{\pi} \frac{dy}{dx}(\cos\theta - 1)\, d\theta$ (α in degrees)

(c) $C_\ell = \frac{2\pi\alpha}{57.3} + 2\int_0^{\pi} \frac{dy}{dx}(\cos\theta - 1)\, d\theta$ (α in degrees)

(d) $C_{M.A.C.} = \frac{1}{2}\int_0^{\pi} \frac{dy}{dx}(\cos 2\theta - \cos\theta)\, d\theta$

(e) Location of a.c. = .25c' aft of leading-edge regardless of camber

where: c' = chord based on straight line distance from leading-edge to trailing-edge
x = distance of any point on mean line from leading-edge measured parallel to direction of c'.
y = distance of any point on mean line from c' measured perpendicular to c'

$\theta = \cos^{-1}\left(1 - \frac{2x}{c'}\right)$ by definition

For the case of the symmetrical profile, these parameters reduce to:

(a) $\frac{dC_\ell}{d\alpha} = \frac{2\pi}{57.3}$

(b) $\alpha_{o.L.} = 0$

(c) $C_\ell = \frac{2\pi\alpha}{57.3}$

(d) $C_{M.A.C.} = 0$

(e) Location of a.c. = .25c'

The plain flapped profile when viewed as a special case of the previously considered cambered profile may quite readily be analyzed on the basis of thin airfoil theory. It might be mentioned that, because the effects of base airfoil camber on the increment of lift due to a deflected flap are felt to be small (particularly considering the limitations of the system), lifting

capabilities of the airfoil with flap may generally be determined as an increment of lift over that of a base symmetrical profile - even though the airfoil under consideration is cambered. This increment could then be added to the lift for the profile (without flap) of the given base camber. Treatment in this manner avoids the necessity of writing the equation of the mean line for the cambered profile plus flap, the only "cambering" now to be considered being the singularity at the flap hinge-line.

In that the airfoil with plain flap is to be analyzed as a special case of the cambered profile theory, the definition of profile chord (c'--linear distance from leading-edge to trailing-edge) must remain unaltered. Classical treatment of thin airfoil theory assumes that c' is always equal to c, the chord of the profile with no flap deflection, regardless of deflection angle. Obviously, as shown in Fig. 70, this assumption becomes rather poor at high values of deflection. Knowlton suggests that a more rigorous treatment, making use of true c' at all flap angles, would yield added accuracy in the comparatively high deflection regime and thus be more realistic for application to the case of the flap with controls sufficiently powerful to permit operation at high deflection angles. Based on the general thin-airfoil formulae and the geometry given in Fig. 70, this more rigorous analysis yields the results shown below. Both the trailing-edge and leading-edge flap (which differs from the trailing-edge flap only by way of angle of attack definition) have been considered, while the base profile has been assumed to be symmetrical for reasons described previously.

(a) $$\frac{dc_\ell}{d\alpha} = \frac{2\pi}{57.3}\,\frac{c'}{c}$$

(b) $$\Delta\alpha_{o.L.} \text{ due to flap} = \frac{57.3}{2\pi}\left\{2\pi\left[\tan^{-1}\left(\frac{h}{1-E}\right)+\frac{h}{E}\right]+\left[\frac{h}{E(1-E)}\left(2\sin\theta_h-2\theta_h\right)\right]\right\}-57.3(P)^*$$

(c) $$\Delta C_\ell \text{ due to flap} = \left\{2\pi\left[\tan^{-1}\left(\frac{h}{1-E}\right)+\frac{h}{E}\right]-2\pi P^*+\left[\frac{h}{E(1-E)}\left(2\sin\theta_h-2\theta_h\right)\right]\right\}\left[\frac{\sqrt{\bar{OA}^2+\bar{AT}^2+2\bar{OA}\,\bar{AT}\cos\eta}}{C}\right]$$

(d) $$C_{M.A.C.} = \left[\sin\theta_h(\cos\theta_h-1)\right]\left[\frac{h}{2E(1-E)}\right]\left[\frac{\sqrt{\bar{OA}^2+\bar{AT}^2+2\bar{OA}\,\bar{AT}\cos\eta}}{C}\right]$$

(e) Location of a.c. = .25c' (must be geometrically transferred to mean line)

where: η = flap deflection in radians

$\theta_h = \cos^{-1}\left(1-\frac{2\chi_h}{c'}\right)$ (angle in radians)

χ_h = distance along c' line from leading-edge to flap hinge line

$$c' = \sqrt{\bar{OA}^2+\bar{AT}^2+2\bar{OA}\,\bar{AT}\cos\bar{\eta}}$$

$(P)^* = 0$ for case of trailing-edge flap

$(P)^* = \eta$ for case of leading-edge flap

If flap angles are assumed to be small, the preceding formulae reduce to the results of the classical treatment where $c \cong c'$ and $\eta \cong \frac{h}{E(1-E)}$.

(a) $$\frac{dC_\ell}{d\alpha} = \frac{L\pi}{57.3}$$

(b) $$\Delta\alpha_{o.L.} \text{ due to flap} = \frac{57.3}{\pi}\left[\sin\theta_h-\theta_h+Q^*\right]\eta$$

(c) $$\Delta C_\ell \text{ due to flap} = 2\left[\sin\theta_h-\theta_h+Q^*\right]\eta$$

(d) $$C_{MAC} = \eta\left[\frac{1}{2}\sin\Theta_h(\cos\Theta_h - 1)\right]$$

(e) Location of a.c. = .25c

where: $Q^* = \pi$ for case of trailing-edge flap

$Q^* = 0$ for case of leading-edge flap

A theoretical approach which permits consideration of profile thickness and thickness distribution effects has, largely through the efforts of Theodorsen (Ref. 47), grown out of the basic concepts of thin-airfoil theory. This type of analysis utilizes conformal transformation methods and has become known as the "thick-airfoil theory". Reference 4 treats this theory at some length as do several others. Certainly use of this method of analysis rather than the thin-airfoil theory will yield more rigorous results, particularly (under unseparated conditions) for very thick profiles. However, thick-airfoil theory can be lengthy and tedious in application, and, for this reason, the somewhat less accurate thin-airfoil theory is often used even when a theory considering thickness would be preferable.

Perhaps the method for determining theoretical characteristics of profiles which provides the greatest accuracy for a minimum of labor is the experimental approach made possible with the development of the electrolytic plotting tank. This device, through its ability to establish analogy between electrical potential and aerodynamic potential, enables the testing in a pseudo-inviscid medium of a model of any profile. The plotting tank thus may almost be considered an inviscid wind tunnel. In that the analogy established satisfies LaPlace's equation directly, no accuracy-spoiling assumptions (such as are necessary in the thick-airfoil theory) are involved. However,

inaccuracies do arise here from the same sources as would be the case in the wind tunnel, such factors as boundary conditions, sensitivity of measurement, and caution in handling the equipment becoming important.

It is generally felt, among those familiar with both, that a soundly designed plotting tank handled by an experienced operator can produce results which are more accurate than those obtained through using the much more time consuming methods of the thick airfoil theory. (Of course, advancements in electronic computer techniques may one day prove the mathmetical approach to be the more convenient). The electrolytic plotting tank is discussed at length in Ref. 27. In addition, much information may be found in the publications of Malavard. Unfortunately, many of these have not yet been translated from the French. A photograph of the Princeton University version of this device is shown in Fig. 71 and is described in Ref. 246. A rather interesting comparison of the streamline patterns about a flapped profile as obtained in the plotting tank and as obtained, under the influence of B.L.C., in the smoke tunnel is given in Ref. 248.

There are thus three basic methods for determining the theoretical characteristics of any profile or profile with flap. The method selected for use is dependent upon the degree of accuracy required, the amount the airfoil differs from the slightly cambered, zero-thickness profile, and the availability of a plotting tank and/or mathematicians. Thin-airfoil theory works very well for the profile with plain flap while the plotting tank gives what appears to be good results for the more complex configurations such as the split or slotted flap. If large viscous effects are present under the real flow conditions, all three methods seem equally poor. The

regime of applicability of theoretical concepts to the real fluid case must normally be determined through correlation of the theoretical and experimental results. Once this has been accomplished, it is possible to obtain empirical factors with which to modify the theoretical relations. An example of this type of approach may be found in Ref. 78 where the real fluid pressure distributions for a sharp-edged profile with leading-edge and trailing-edge flaps are derived from both ideal and viscous relationships.

Shown plotted in Figs. 72 and 73 are applications of thin-airfoil theory to the trailing-edge flap, leading-edge flap and cambered profile cases. Figure 72 shows the lift increments theoretically predictable through use of both the classical and the more rigorous applications of the thin-airfoil analysis. The high values theoretically attainable with flap of practical chord extent indicate the potentiality of trailing-edge flaps which are permitted closely theoretical characteristics through the use of suction or blowing. Figure 73 indicates the effect of angle of attack definition upon profile characteristics as a function of flap hinge location. It is here obvious that, as would be expected, the lift increment will differ by a fixed large amount depending on whether the flap is of the leading-edge flap type or the trailing-edge, even though the two configurations are geometrically identical. The cambered profile curves shown indicate an increase in lift as point of maximum camber is moved aft from the nose. The ultimate decrease in lift increment as this point is brought near the trailing-edge occurs because degree of camber varies as point of maximum camber is moved. (These curves are based on constant flap deflection). It can be readily demonstrated, however, that moving a given

degree of camber aft of a profile will cause the lift-increasing effects of the camber to become greater until the trailing-edge is encountered. Figure 73 also illustrates the inaccuracies brought about at high deflections by the assumptions of the classical method as opposed to the more rigorous treatment. Of course, with near 90° deflection even the rigorous treatment may be somewhat in error due to inaccuracies inherent in the thin-airfoil theory itself.

3.2f Unpowered Trailing-edge Flaps

This section deals with conventional uncontrolled flaps, by which is meant a flap without any form of powered control (i.e.: blowing or suction). Although the discussion presented herein is not intended to delve deeply into the detail design of such devices, it is hoped that sufficient information is included to form a basis for intelligent preliminary design proceedings. Literature available on unpowered trailing-edge flaps is most voluminous and the reader interested in more detail is referred to the numerous references in the bibliography. (Refs. 3 and 45 are of unusual bibliographic interest, while Ref. 45 constitutes a very fine summary of the characteristics of unpowered trailing-edge devices).

The trailing-edge flap makes use of the camber principle to effect a change in flow conditions at the profile trailing-edge and hence alter the circulation about that profile. From potential flow considerations it becomes obvious that the location of the trailing-edge stagnation point has a determining effect upon the lift generation of a profile. Looked at in its simplest terms, if the trailing-edge stagnation point can be located in such a way that the flow path from the forward stagnation point over the upper surface is maximized and the path between the forward and trailing-edge stagnation

points on the lower surface is minimized, the largest value of circulation (and thus the largest lift increment at a given angle of attack) will be attained. This, in effect, is what is attempted by giving a profile camber. The cambered profile has circulation control with respect to its symmetrical counterpart by virtue of the reorientation caused in the relative location of the leading-edge and trailing-edge stagnation points. Thin-airfoil theory demonstrates that any given degree of camber will create a greater circulation lift if located near the trailing-edge rather than the profile leading-edge. This would indicate that the use of a large amount of camber applied to the trailing-edge of the profile could be very useful as a high-lift circulation mechanism, the one major problem being the poor high speed characteristics of such a configuration. The trailing-edge flap solves this problem, inasmuch as it is a variable camber circulation control located at the trailing-edge where it can be most effective.

The forms of trailing-edge flaps which are most commonly in use are the plain flap, the split flap, the single slotted flap, of which the Fowler flap is a special example, and the double slotted flap. These flaps are shown in Fig. 27 and the discussion within this section will be limited to these types.

Figure 28 demonstrates the airflow over the various flapped configurations at a constant small angle of attack. Note that all forms of the trailing-edge flap yield a marked increase in upwash as compared with the uncontrolled profile. This (if the two configurations are at the same angle of attack, as is the case here) is indicative of the achievement of lift increase through increased circulation. The plain and split flaps can

be seen to create an effective stagnation area behind and beneath the flap hinge, but, due to separation, cannot, at this deflection angle, force formation of a stagnation point at the flap trailing-edge. As this amounts to a loss in potential circulation, the slotted and double slotted flaps were devised. Such flaps allow higher-pressure lower surface air to bleed onto the flap upper surface, thus energizing the "dead" air in the flap's boundary layer, delaying separation, and increasing circulation through permitting the flap more closely to achieve potential flow. The Fowler flap yields additional lift benefits through extending the effective chord of the profile.

Figure 29 compares the various flap types at a given flap deflection. These typical curves indicate that lift-increasing capabilities become greater as flap type is changed from plain to split to slotted. Note also that lift gain occurs as a shift of the entire lift curve to the left. This is a characteristic of circulation control as opposed to boundary layer control. However, boundary layer control with respect to the flap, as occurs with the slotted types, is the major reason the slotted flaps demonstrate greater circulation than the unslotted.

Typical variation of the lift curve with flap deflection is shown in Fig. 74. Flap effectiveness can be seen to decrease at a relatively slow rate as deflection is increased. This can be attributed to the growth of the separated region aft of the flap with increasing deflection. Because of this characteristic separation aft of deflected flaps, few "unpowered" flaps are able to approximate theoretical (thin airfoil) predictions for values of flap deflection in excess of 5^{o} - 10^{o}. Although the addition of slots

aids this situation considerably, even the slotted flaps can be shown to fall far short of the theoretical values for deflections greater than 15°.

Unpowered trailing-edge flaps generally reveal either a constant stall angle or a stall angle decreasing with increased flap deflection. Thus, for the usual case, $\Delta C_{l_{max}}$ due to flap deflection will be, at best, equal to $\Delta C_{l_{\alpha=0}}$ (degree of circulation), and will normally be less than this term. Indications are that only very efficiently designed slotted flaps show any tendency to produce the "trailing-edge B.L.C." effect mentioned in Section 3.2b, which permits $\Delta C_{l_{max}}$ to increase beyond $\Delta C_{l_{\alpha=0}}$.

Figure 75 shows the typical variation of chordwise pressure distribution with plain flap deflection for a profile at a given angle of attack. Plain flap deflection may be seen to create a second pressure peak at the flap hinge line. This pressure peak increases in magnitude as flap deflection is increased until the adverse pressure gradient over the flap upper-surface becomes sufficient to create turbulent separation at the flap trailing-edge with a resultant decrease in flap effectiveness. Of course, laminar separation would never be expected to occur from the flap hinge-line unless the profile were at a large negative angle of attack.

The occurrence of turbulent separation over the flap is to a certain extent dependent upon the entire pressure distribution on the profile upper surface, as well as the hinge-line pressure peak. Figure 75 reveals that the majority of lift increase due to flap deflection is reflected in the increased negative level of the pressure distribution over the profile upper surface rather than in the hinge-line pressure peak. In fact, it is the increased level of the leading-edge pressure peak which causes the flapped profile to have a greater tendency to stall from the leading-edge than would be the

case with the profile without a deflected flap. If stall reverts to the leading-edge type, stall angle will decrease and $\Delta C_{l_{max}}$ due to flap deflection will become less than $\Delta C_{l_{\alpha=0}}$, as described previously. It appears that the uncontrolled flap (with the possible exception of the slotted types) has little effect upon profile trailing-edge stall. That is, so long as leading-edge separation does not occur, stall angle for the flapped profile is closely equal to that for the unflapped profile, with $\Delta C_{l_{max}}$ approximately equal to $\Delta C_{l_{\alpha=0}}$. Section 3.2b attempts to consider in as thorough a manner as possible the variation of $\Delta C_{l_{max}}$ with $\Delta C_{l_{\alpha=0}}$ for flapped profiles. For this reason, this section will concern itself only with degree of circulation, $\Delta C_{l_{\alpha=0}}$.

Although the flap will not separate so readily, pressure distributions for slotted and double slotted flaps will have very nearly the same appearance as that shown in Fig. 75. Because of the B.L.C. effect of such slots, the slotted flap will reveal at the higher deflection settings, a greater "hinge-line" pressure peak and more negative overall upper-surface pressure distribution than would the plain flap at the same deflection. Tendency toward leading-edge stall would thus be greater. The split flap pressure distributions will differ from that for the plain flap in that the second pressure peak here occurs at the profile trailing-edge. Thus, even though the split flap is moved to a more forward location, the pressure peak must still occur at the same position, and no improvement in pitching moment can be attained except through permitting lift to decrease. The large nose-down pitching moment created by any trailing-edge circulation control is a problem for which there is no real solution.

Degree of circulation, which may be defined as lift increase at a given angle of attack, has more meaning at an angle of attack where little separation exists on the profile. For this reason, $\Delta C_{l\,\alpha=0}$ will be used here as a measure of circulation. It is obvious that this term can vary with flap deflection and it has been pointed out that it can vary with flap type. Further, it is possible that flap chordwise extent, profile shape, and Reynolds Number may affect $\Delta C_{l\,\alpha=0}$. For the plain flap case, the "gap", or distance between the flap leading-edge and the trailing-edge of the fixed portion of the profile, may influence circulation. Obviously, the slot configuration, for the case of the slotted flap, should be important in regard to the extent of flap B.L.C., and thus would be thought to affect profile circulation.

Figure 76 shows circulation lift increment due to a 20%c split flap deflected 60° as a function of profile thickness. It can be seen that increased thickness causes an increase in $\Delta C_{l\,\alpha=0}$, but that, for a given profile series, the effect of a thickness increase from that of t/c = 6% to t/c = 22% is to increase $\Delta C_{l\,\alpha=0}$ by only approximately .15. The effect of variations in profile series does not show the uniformity of the thickness effect. However, observations of the characteristics of the symmetrical series presented as well as numerous other symmetrical and cambered series reveal a maximum variation in $\Delta C_{l\,\alpha=0}$ due to profile shape to be, again, approximately .15. The spread of observed results is indicated in Fig. 76. As the influence of profile thickness and thickness distribution is only of the order of 10% of $\Delta C_{l\,\alpha=0}$, such effects may normally be neglected. Although little data are available, Reynolds

Number effects seem to be of closely the same order of magnitude as the effects of thickness and thickness distribution. It is possible that the slotted flap represents an exception to this statement, the slot or slots being particularly susceptible to Reynolds Number variations. Unfortunately, the small amount of data available for slotted flaps at various Reynolds Numbers, with other parameters maintained constant, does not permit any predictions regarding this effect. In general, however, it should be possible to state that the effects upon $\Delta C_l \; _{\alpha=0}$ of thickness, thickness distribution, and Reynolds Number may be neglected, particularly for preliminary design purposes.

The plain trailing-edge flap is formed, as may be seen in Fig. 27, by hinging the rearmost portion of the airfoil about a point within the contour. A downward, or positive, flap deflection effectively increases the camber of the wing section. Although it is possible to apply thin-airfoil theory to the plain flap case, such a method may be made to correlate with experimental data only for very small flap deflections. Thus empirical means have been utilized in attempting to predict the characteristics of the plain flap as well as the split and slotted flaps.

In addition to the variables of flap deflection and flap chordwise extent, a parameter which could influence $\Delta C_l \; _{\alpha=0}$ for the plain flap case is that of gap size. Through permitting air to leak to the low pressure on the upper surface through a gap between the airfoil and flap, the flap characteristics may be altered. Figure 77 demonstrates typical effects of gap size upon $\Delta C_l \; _{\alpha=0}$. It will be noted that circulation lift falls off with increases in gap size and, for a $\delta_F = 15^\circ$, can reduce $\Delta C_l \; _{\alpha=0}$ by approximately .2 if gap size is of the

order of 1% chord. Very poorly designed gaps can yield even greater lift losses. It would be thought, however, that a gap which can keep these losses to under $\Delta C_l = .1$ can readily be designed. Also, proper sealing can remove all effects of gap width.

Figure 78 attempts to predict circulation lift, $\Delta C_{l_{\alpha=0}}$ on the basis of the fundamental design parameters, flap-chord ratio and the angle at which the flap is deflected. Theoretical curves, based upon the more rigorous interpretation of the thin-airfoil theory are included with the empirical curves, which have been plotted on the basis of all experimental results available to the authors. It will be observed that the plain flap has characteristics which fall far below the theoretical for deflections greater than 10°. As would be expected, however, increases in flap deflection increases $\Delta C_{l_{\alpha=0}}$ at least until $\delta_F \cong 60^\circ$ where an optimum appears to have been reached. Also, theory does predict the proper trend of the flap extent effect, flaps of greater chord producing greater $\Delta C_{l_{\alpha=0}}$. There is without doubt an optimum flap length as well as an optimum deflection. The meager amount of existing data indicates that the optimum plain flap has a chordwise extent of approximately 40% c, although it is possible that this value may vary somewhat for different profiles under different free stream conditions.

The empirical curves of Fig. 78 should hold quite well for plain flaps of small gap width under any free-stream conditions and for any profile. Unusually wide or poorly designed gaps may lower the curves by amounts up to about $\Delta C_l = .3$ at $\delta_F = 60^\circ$, while the use of sealed gaps may raise the curves by a $\Delta C_l = .1$ at $\delta_F = 60^\circ$. These values

may be seen to be of approximately the same magnitude as the possible error due to profile and free-stream variations.

Perhaps even simpler than the plain flap from the mechanical point of view is the split trailing-edge flap (Fig. 27) which is generally formed by deflecting the aft portion of the lower surfaces about a hinge point on this surface at the forward edge of the deflected portion. Like the plain flap, the split flap derives its increased lifting power from an increase in effective camber. Some variations of the split flap have been employed, such as the "zap" type flap, which employs a movable hinge line to increase the effective wing area as the flap is deflected. As with the plain flap configuration, the more important design parameters affecting the aerodynamic characteristics of the profile with split flap are those with basis in theory, flap-chord ratio and flap deflection.

Figure 79 presents the results of an empirical study of the effects of split flap deflection upon circulation. Again, as with Fig. 78, theoretical curves (based on the plain flap) have been included for purposes of comparison. The same trends as were noticeable with the plain flap may be observed here. It will be noted, comparing Figs. 78 and 79, that, in the high deflection regime, the split flap achieves considerably more lift increase than the plain flap. However, for δ_F's of less than 20^o, the two flap types have closely identical characteristics. Although the reason for the superiority of the split flap in the high deflection region is not clear, if may be found that over the upper rear surface of the airfoil there are no abrupt breaks or changes in surface curvature as there are over the plain flap. Thus the flow will tend to remain unseparated to the trailing-edge and permit the

effective stagnation region to be at a lower position aft of the trailing-edge than would be the case with the plain flap. Optimum flap deflection for the split flap seems to be approximately 75°, while optimum flap chord appears to be about 40% c. Figure 79 is based upon results of investigations using split flaps which, when retracted, have trailing-edges which coincide with the profile trailing-edges. Although this is the usual case, several configurations have been designed where flap length bears no unique relationship to flap hinge position. The curves of Fig. 79 cannot be expected to hold good for use with such systems.

If information on an extensible split flap is desired, a rough approximation - as to its characteristics may be made through redefining its chord length, estimating its coefficients as a normal split flap based on the new chord length, and then scaling the coefficients so that they are based on the original chord length. In cases where a large flap is moved back close to the trailing-edge, it may prove somewhat more accurate to treat the extensible split flap as a plain flap on the extended chord length.

The term "slotted flap" covers a vast variety of flap configurations which range from a simple hinged flap with a slot directly forward to devices of great mechanical complexity which are more like multiple slotted, extensible wings. Here only the more important configurations will be covered, with the two main classes being divided into "single-slotted" flaps and "double-slotted" flaps (Fig. 27).

Slotted flaps permit increases in $\Delta C_{l_{\alpha=0}}$ in three ways: by increasing effective camber as do the plain and split flaps, by boundary layer control on the flap upper surface created by the air ducted through the

slot or slots, and by increasing the length of the airfoil chord as a trailing-edge extension. The first two of these effects may be seen to increase profile circulation and are present with any reasonably designed slotted flap. The third effect need not be designed into the configuration, but, mostly for reasons of physical necessity, may be found present on the majority of designs.

Temporarily disregarding chord-extension, the slotted flap achieves circulation gains over the plain flap in the following manner: with the plain flap, the turbulent boundary layer, upon passing over the flap hinge position, thickens and the flow next to the flap surface loses much of its energy and rapidly begins to display the reverse flow characteristic of a separated region; on the other hand, the slotted flap, by virtue of its geometry, directs a jet of relatively high energy air into the boundary layer immediately adjacent to the flap surface -- thereby re-energizing this layer and delaying separation. Thus a properly designed slotted flap can be expected to permit greater flap deflections before separation proceeds to produce marked fall-offs in flap effectiveness. For this reason, degree of circulation ($\Delta C_{l\ \alpha=o}$) can be considerably greater for the slotted flap than for either the plain or split flap of like chord and deflection.

A typical <u>single slotted flap</u> configuration is shown in Fig. 80A. It will be seen that chord extension can be expressed by:

$$\text{chord extension} = C_a - \gamma_f + \frac{C_f}{C} - 1$$

where: C_a and γ_f are in %c/100
and: C = profile chord with flap undeflected.

Since lift coefficients are based on the original chord length it is obvious, and checked in practice, that, barring other changes, the longer the effective chord the higher will be the lift coefficient for a given angle of attack. In general, however, design chord extension is so small that this effect is nearly lost alongside the more powerful effects of camber and boundary layer control of the flap.

The major physical parameters affecting the aerodynamic efficiency of the single slotted flap are flap size, flap deflection, the chordwise location of the slot lip, and the slot shape. The slot shape, in turn, is controlled by the combination of slot-entry shape, slot-lip shape, and the position of the flap with respect to the slot lip. All of these parameters except flap size and deflection affect the boundary-layer-control action of the slot. Fig. 80B shows typical slot-entry configurations, while Fig. 80C presents two typical flap nose configurations. The possible effects upon lift of slot entry configuration and flap position are indicated in Fig. 81. The sensitivity of maximum lift coefficient to small changes in flap position and the variation of optimum flap position with changes in slot entry shape are here clearly demonstrated.

It is obvious that prediction of the effects of slot shape and location upon $\Delta C_{l\ \alpha=0}$ is extremely difficult. In addition to the many important geometric parameters mentioned above and their possible cross-effects, it is thought that Reynolds Number can create changes in B.L.C. capability due to possible alterations in slot characteristics with scale. Further, the size and shape of the flap and slot are often dependent upon the original airfoil section as well as upon mechanical feasibility. Thus the flap that appears

best on any given airfoil may not be optimum on another. Also, from the point of view of both the structural and shape limitations, it is often impractical to build a wing duplicating the best wind-tunnel model.

It would seem that the optimum flap location and slot shape can be determined only by laborious experimental trial and error, and to a large extent this is, indeed, true. However, a general rule can be used as an aid in designing the flap location and slot shape. This is that the flap should form a converging passage with the slot entry and slot lip so that no separation can occur within the slot nozzle. It is also important that at the exit the flow be directed so that it flows smoothly tangent to the flap upper surface.

With the exception of stating the above rule, no attempt will be made here to predict the variation in $\Delta C_{l\,\alpha=0}$ due to alterations in slot shape and flap position. In lieu of such a prediction, the table of Fig. 82 is presented so as to give some indication of what might be expected of various slot configurations when applied to several different profiles. (Flap nose shape and slot entry configuration are denoted by letters corresponding to those for the shapes given in Figs. 80B and 80C.) Although lift coefficients are given here as $C_{l_{max}}$, general trends in $C_{l\,\alpha=0}$ can be inferred--particularly for the case of various slot configurations applied to one given profile.

Double-slotted flaps are similar to the single slotted variety with the exception of an additional turning vane located ahead of the flap. In this way, a double nozzle is provided giving a greater boundary layer control effect and greater turning power. The important design parameters are the same as with single slotted flaps except that the position and angle of the turn vane must, of course, be considered.

Figure 83 demonstrates the typical double-slotted flap configuration in both the retracted and extended position. It will be noted that for the double-slotted configuration it is quite standard to provide a slot-entry skirt on the profile lower surface. Indeed, many single slotted flaps utilize such a device. The slot-entry skirt is provided primarily to reduce drag when the flap is in a retracted position, and has, in general, been found to continue to maintain a minimum drag even after the flap has been extended. Increases in skirt extent aft do, however, produce lift decrements compared with the no-skirt case. The values of deflection and magnitude of skirt extent at which this lift decrement may become large seems to depend upon the geometry of the overall configuration and hence there is no means currently available through which prediction could be attempted.

Contours of maximum lift attainable as a function of slot shape is shown for both upper and lower slots of a double-slotted-flapped profile in Fig. 84. As with the single slotted flap, it can be seen that lift increment is extremely sensitive to slight variations in slot shape. This extreme sensitivity, the short supply of methodical data, and the ever present possibility of large Reynolds Number effects upon slot characteristics prevent attempts to indicate the effects upon profile lift of the numerous geometric variables inherent in the double-slotted flap design. Figure 85 has thus been presented as a partial summary of results achieved to date.

Figure 86 has been drawn up to provide some means of predicting the lifting characteristics of the single-slotted and double-slotted flaps. These curves have been faired from highly scattered data and thus are of value only for very preliminary design purposes. Detail flap geometry was

found to alter $\Delta C_{l\,\alpha=0}$ as much as a 20%c change in flap chord ratio. It was therefore decided to plot these curves for an "average" flap design--not too bad, but still not optimum. In this way, a 30%c slotted flap, for instance, can, if very well designed, have characteristics corresponding to the 40%c curve. On the other hand, a poorly designed slotted flap of this chord extent will yield lifting characteristics closely similar to those shown for the 20%c flap. Through consideration of this observed spread due to slot shape variations, etc., it is hoped that the designer may get some additional feeling for the importance of such "details" within the framework of the overall picture.

It will be noted from Fig. 86 that the boundary layer control provided through the use of slots enables the flap to much more closely achieve its theoretical potentialities. Also, the double-slotted flap is, on the average, considerably superior to the single-slotted, particularly in the high-deflection regime. As with the plain and split flaps, a C_F/C of approximately 40% seems nearly optimum, while deflections of greater than 75° may well be practical. It should be remembered that the chord extension normally found with slotted flaps has already been included in these curves. This is usually a very small effect for the case of the single-slotted flap and seldom is the chord extended by more than 10%-15% through deflection of double-slotted flaps. Undoubtedly, larger vanes and larger flaps with greater extensions would give greater lift coefficients based upon the original chord length, but this soon becomes ridiculous from the points of view of practical construction and trimming the large nose-down pitching moment.

Comparison of Figs. 78, 79, and 86 indicates that even when its design is considerably far from optimum the single-slotted flap may be expected to yield greater lift increases than the plain or split flap. Thus flap selection is seen to be a matter of overall aerodynamic efficiency versus space, weight, and complexity limitations. As is well known, slotted flaps have generally been considered practical only for large aircraft, but here their superiority to the other forms of "unpowered" flap is undenied.

The typical effect of flap deflection upon profile drag is demonstrated in Fig. 87. It will be noted that while the profile with undeflected flap gives minimum drag in the low lift-coefficient range, minimum drag is attained with some finite deflection in the high-lift regime. As lift coefficient is increased, greater and greater deflections are required for minimum drag. It may further be seen from this plot that increased flap deflection, at angles of attack well below stall, provides an increment to profile drag which is closely a linear function of deflection angle. It is thus felt that the effects of trailing-edge flaps upon profile drag can best be described and compared through use of two concepts: (1) change in profile drag coefficient at constant angle of attack, $\alpha = 0^{\circ}$ for instance, and (2) the minimum drag envelop polar, plotting minimum drag coefficient, regardless of flap deflection necessary, vs. section lift coefficient.

Figure 88 compares the envelop minimum drag polars of a profile with a plain and split flap. All other variables are identical. It can be seen that, for lifts greater than that attainable with the base profile alone, the split flap will show lesser drag for a given lift. This is, of course, simply a reflection of the split flap's apparent ability to achieve greater deflections than the plain flap without creating excessive flap separation.

The effects of flap type and profile thickness on increment in profile drag due to flap deflection at $\alpha = 0^{o}$ are shown in Fig. 89. Profile thickness may be seen to have a relatively large effect upon constant α profile drag, at least on the basis of these split flap tests. Figure 89B indicates that, although the split and plain flaps yield closely the same drag increment with deflection, the slotted flap can be designed to operate with only 2/3 the drag increment created by the other flap types. The effect of flap chordwise extent is also demonstrated here, flaps of greater extent yielding greater drag by virtue of the more extensive separation region created.

Figure 90 demonstrates the effect of profile thickness and Reynolds Number upon the minimum-drag envelop polars. There would appear to be little effect from either thickness variation or scale, the thicker profile yielding slightly higher drags for a given lift and increases in Reynolds Number permitting some drag reduction.

Available indications are thus that flap type and possible flap extent can alter the minimum-drag envelop polar to a greater degree than could any effects of Reynolds Number and profile thickness. Generally, the latter two could be considered negligible. Flap deflection cannot enter in by virtue of the definition of the minimum-drag envelop polar. In the case of drag increment at zero angle of attack, flap deflection will become a variable as will profile thickness. Flap type and flap extent will also affect drag, although Reynolds Number changes probably will have only an insignificant effect.

Figures 91, 92, and 93 attempt to predict as closely as possible the drag characteristics of plain, split, and slotted flaps as functions of the variables which seem of greatest importance. The $\Delta C_{d_{o}}{}_{\alpha=0}$ curves are based upon results for a relatively thick profile (t/c $\cong$ 20%). Figure 89 may be used to correct the curves to other thicknesses, although the accuracy of these plots may not justify such a rigorous procedure. It may be seen that the plain and split flaps have very nearly the same characteristics while the slotted flap would be expected to provide lesser drag increments at $\alpha = 0^{o}$. The envelop minimum drag polars, which are perhaps of greater practical interest, were obtained from information contained in Ref. 45. The variation of minimum drag with flap chord ratio is normally small, but may become important for high deflections and large lift coefficients. It will be noted that flap type also makes little difference upon the envelop minimum drag polar in the low lift range. However, the slotted flap delays the sharp upward swing of the polar to greater lift coefficients than is the case with the other two flap types. It should be pointed out that the drag increment given in these plots is the increment beyond that for the profile with flap undeflected--not an increment beyond the base profile drag. Thus the slotted flap may reveal comparatively higher drag increment (with respect to the base profile) than are indicated because of its normally poor drag characteristics when undeflected.

Pitching moments created through the deflection of plain, split, and slotted flaps are predicted in Figs. 94, 95, and 96. The ratio of pitching moment coefficient to lift increment caused by the deflection of a plain

flap can be shown by thin airfoil theory to be dependent only upon flap-chord ratio. Experimental data given in Fig. 94 indicate that the theoretical relationship is actually closely obtained. The split flap, Fig. 95, yields pitching moment increments which are rather further from the thin airfoil prediction than the plain flap results. This discrepancy is without doubt due in the main to the fact that the airfoil with split flap deflected creates a configuration which is quite different from the theoretical (which is at least approximated by the plain flap). The slotted and double slotted flaps can be seen from Fig. 96 to create pitching moments somewhat in excess of those for the split and plain flaps. For the prediction of slotted-flap pitching moments, flap-chord ratio and airfoil chord must be redefined on the basis of total chord with flap extended. The same may be said for the case of the extensible split flap. The presentation of Figs. 94, 95, and 96 assumes that dC_m/dC_L about a given point on the profile is equal to zero and that flap deflection changes only C_{mac}. These assumptions are felt to be sufficiently close to the truth to make these figures useful as preliminary design tools.

3.2g Powered Trailing-Edge Flaps

The search for higher and higher values of lift has led to the application of power in the form of suction or blowing to the flow passing over deflected flaps in order to overcome the separations produced by the larger deflection angles. These applications, as shown by Fig. 97, have ranged all the way from controlling the turbulent boundary layer over the entire profile to concentrated suction and blowing slots in the region of the flap leading edge. Since control of the entire profile is really a

combination of a leading and trailing edge control system, it will not be treated in this section, attention being concentrated only on those systems which apply power in the region of the flap.

A distinction must be drawn between the use of suction or blowing for the purpose of flap lift augmentation. The use of suction produces the results demonstrated in Fig. 98. As indicated by Ringleb (Ref. 71) the purpose of the suction slot (or region, in the case of perforated or porous suction systems) is to remove a sufficient amount of low energy boundary layer air to permit the flow to make the turn at the flap leading edge and to remain attached up to the trailing edge, thereby achieving the lift values indicated by potential theory. As demonstrated in Section 3.2C, the location of a sink on the upper surface will in itself produce a lift increment, but this tends to become negligibly small as its location is moved forward. Since most of the systems of practical interest will have the suction located from 20% to 30% of the chord forward of the trailing edge, except at extremely high values of suction coefficient, the sink effect can be completely neglected.

A blowing flap can, however, achieve appreciable lift increases in several ways. First of all, by adding energy to the boundary layer, flap attachment and the resulting lift increment can be obtained. In addition, the flow leaving the trailing edge has a residual momentum and produces a direct thrust-lift component. Finally, as explained in Section 3.2d, the blowing jet due to this residual momentum, possesses a stiffness, resisting turning by the free stream and hence supporting a pressure differential, thereby acting as a flap chord extention. These two effects couple to

produce an appreciable lift increase with increasing blowing quantity even after flow attachment as demonstrated by Fig. 99.

The above discussion has been limited to the cases of plain or slotted flaps. It must be pointed out that although these are by far the most common types of powered systems, other arrangements have been tested. Typical of these is the combination of trailing edge suction with a split flap. This arrangement was tried since it was felt that the addition of the split flap would enable the location of the trailing edge slot to be moved further aft on the profile by reducing the amount of overhang of the lower slot lip required, perhaps even to the extent of permitting the slot to be located on the under surface of the profile trailing edge, thus inducing flow from the upper surface around the trailing edge and creating very high values of lift. These hopes were based on the fact that, theoretically at least, the trailing edge stagnation point is located at the trailing edge of the flap and that the region between the deflected flap and the trailing edge of the profile was occupied by a stagnation region which could be readily influenced if the flow from the upper surface were directed downward with sufficient energy.

A model was tested at Princeton (Refs. 61 and 70) equipped with a trailing edge slot with a variable lower surface adjustable in such a manner that either an over- or under- hang could be achieved, depending upon whether it was desired to lead the flow from the upper or lower surface. As was anticipated, it was found that the optimum slot location was different from that of the unflapped profile, the over-hang being roughly only one-half as large, but the best slot location remained on the upper

surface of the profile and except for the optimum slot shape, the effects of trailing edge suction and flap were not additive. Figure 100 illustrates typical results with this optimum trailing edge.

It will be noted that at the lower values of flap deflection and suction, a favorable increase of lift increment is experienced, but this effect decreases with increasing flap deflection, diminishing until at $\delta_f = 60^\circ$ the effect of flap and suction are merely additive. Varying the point of flap attachment to the profile had no significant effect upon these results, although it seems reasonable to assume that in the flapped case, as with the plain profile carrying the slot aft, making it smaller, and going to higher powers, would produce higher lift increments. But these tests were not carried out.

The explanation of the behavior of this system could at once be seen from the smoke tunnel. When the split flap was deflected slightly, the flow left its trailing edge smoothly, and trailing edge suction permitted a streamline from the upper surface to stagnate on its trailing edge producing a considerable change in lift. However, as the split flap deflection was increased, vortices began to be shed from its sharp trailing edge and the resulting flow disturbances broke down the flow established by the trailing edge suction. The problem could thus be resolved to one of flow instability.

On the basis of these findings, it was decided to investigate the possible use of a blowing jet issuing over the deflected flap. The decision to utilize such a system was greatly influenced by previous smoke tunnel studies of the nature of blowing jets, in which two outstanding properties

of such jets had become clear. The first of these was the tendency for the low pressure region produced by the velocity of the jet to influence the external flow field in a manner similar to a line of distributed sinks, and the second was the ability of the blowing sheet to seemingly extend the chord of the deflected flap.

A series of investigations resulted in the configuration shown in Fig. 101. Test results with this configuration have been extremely promising, but there are so few data existing that it is impossible at this time to develop any method by which intelligent predictions of the performance of this or any similar system may be made. The scarcity of available information makes it essentially impossible to predict the lift increment to be obtained from a controlled flap system with any degree of accuracy and although the following information is offered as an indication of trends and of gross effects it cannot in any sense be considered as design information.

In the case of suction flaps, a considerable variation in the performance of the various proposed schemes of control occurs in the lower ranges of suction coefficient. This variation arises from the varying effectiveness of the suction configurations in attaching the flow to the deflected flap. Once the flow is attached most of the systems demonstrate similar relationships between ΔC_ℓ and C_Q (namely a slightly increasing lift due primarily to the sink effect). One exception to this generality is the case of distributed suction which if intelligently applied over the entire profile can produce and maintain attached flow for very low values of power and suction. Since such a system is sensitive to clogging

with ice, rain and dust, there has been considerable opposition to its use although Raspet and others claim to have demonstrated that these problems can be overcome.

If one excepts the distributed suction case, the most efficient form of suction slot is the cusp or "trapped vortex" arrangement similar to that shown in Fig. 102. A summary of the available information about such a system is presented in Fig. 103. In general it would appear that below a suction coefficient of .025 experimental data about the particular system under consideration must be obtained while above this value the theoretical methods proposed by Ringleb (Ref. 71) can be used.

Blowing systems have, in the past, found more favor than suction arrangements, primarily for two reasons. The first is the simplicity with which such an arrangement can be applied, particularly if the application is being made to a jet aircraft with bleed air readily available from its compressor and the second is the fact that the additional lift increment available from the combination of the jet momentum and jet flap effects is much greater than that to be expected from the sink effect of a suction system.

Helmbold in a Fairchild Aircraft intercompany report entitled the Theory of the Finite-Span Blowing Wing has proposed the following expression for the two-dimensional lift of a blowing airfoil system.

$$\Delta C_\ell = C_E \sin\delta_{te} + 2\pi\sin\alpha + f(C_E)\sin\delta_{te} \qquad (3.2g1)$$

where the angle δ_{te} is defined in Fig. 104. The coefficient C_E is defined as

$$C_E = 2\frac{(V_j^2 - V^2)}{V^2}\frac{h}{c} \qquad (3.2g2)$$

where V_j = jet velocity

V = the free stream velocity

h = jet sheet thickness

c = airfoil chord

In equation (3.2g1) the first term represents the contribution from the direct momentum effects of the jet, the second term the contribution of angle of attack and the third term the lift induced by the lifting vorticity of the jet sheet (jet-induced lift). The function $f(C_E)$ has been computed for a flat plate at zero angle of attack with the jet leaving the trailing edge under a small deflection to be approximately $f(C_E) = \pi\sqrt{C_E}$. It has been found that this value is satisfactory for preliminary design purposes.

It must be pointed out that the above equation should be based on conditions not at the blowing slot, but at the trailing edge of the flap. Little information about the losses over the flap is currently available, but Fig. 105 shows a typical experimental result.

Once the lift increment at zero angle of attack of such a powered flap system is estimated, the rest of the airfoil characteristics can be estimated by the methods outlined in the other sections of this report.

3.3 THE EFFECT OF LEADING-EDGE DEVICES

3.3a General Discussion

Increased emphasis on high speed aircraft in recent years has led to the use of thinner and thinner wings -- wings characterized by leading-edge or the so-called thin airfoil stall as described in Section 3.1

of this report. Necessarily, these high speed profiles yield stall at quite low angles of attack and hence achieve low maximum lift coefficients. This, in addition to the low aspect ratio and high wing loading typical of this type of aircraft, has created increasingly greater minimum flying speeds and hence much longer take-off and landing runs. The problem thus presented is one of shortening take-off and landing distance while maintaining very closely the same high speed characteristics.

Convertaplanes and V.T.O.L. aircraft represent partial solutions of current interest. However, at present, these are intended as special-mission machines of an experimental nature, and cannot now be considered truly competitive with the more conventional high speed aircraft. Such techniques as drogue chute landings and the use of high α take-offs to achieve some lifting thrust are of rather limited application. It is felt that a solution of more general application to the speed range problem (increased lift coefficient can also be utilized to increase high speed by allowing wing area reduction) lies in the use of lift-increasing controls existing as integral parts of the wing but of such a nature as not to materially damage the aircraft's high speed performance.

Although trailing-edge flaps can be used to advantage on thin airfoils, their usefulness is somewhat limited due to the tendency toward premature leading-edge separation induced by a trailing-edge circulation control. This is particularly true in the three-dimensional case, some configurations achieving zero or even negative changes in maximum lift due to deflection of trailing-edge flaps. Additionally, trailing-edge flaps are, on many designs, severely limited in possible span extent and cannot be utilized at

all in the case of the tailless aircraft which generally requires up-elevon for low-speed trim. Further, the severe nose-down moment created by the trailing-edge flap is often considered excessive.

Many investigators believe that the use of controls located at or near the profile's leading edge represents the most logical approach to increasing the lift capabilities of the leading-edge-stalling thin airfoil. Certainly, the potentiality of such a device in improving the efficiency of the thin airfoil's trailing-edge control is undeniable. In addition, many forms of the leading-edge type of control appear to yield benefits for even the thicker profiles. It is therefore the purpose of the following pages to describe the aerodynamic characteristics of several leading-edge controls and to attempt wherever possible to develop semi-empirical relations for use in preliminary performance prediction. While granting that planform optimizations can well be utilized to improve lift and that the three-dimensional situation can be considerably different from the two, only two-dimensional characteristics will be considered. In this way, many confusing variables will be eliminated and the controls may be analyzed and compared more readily. Also, although such devices appear to have certain advantages in the upper region of the aircraft's speed range, the lower-speed phenomena will be emphasized throughout this section.

The two-dimensional aerodynamic characteristics of the following leading-edge controls will be discussed:

(1) Leading-edge flaps

(2) Leading-edge boundary layer control devices

References treating the above subjects are listed in the bibliography. Information presented is based upon these references as well as the experience of the Subsonic Aerodynamics Group, Princeton University, in the field of leading-edge controls.

In many areas where experimental data was limited or non-existent, it was felt advisable to resort to some "calculated" speculation so as to perhaps indicate the direction future testing might take as well as to attempt to give some idea regarding expected trends. The thinking of Section 3.1f was used extensively in these more speculative regimes.

Before proceeding, it is well to point out that most leading-edge controls operate by one or both of two principles:

(1) Altering the profile geometrically so as to eliminate or alleviate the characteristic leading-edge pressure peak normally creating separation.

(2) Eliminating or delaying separation aft of this pressure peak through energizing the boundary layer.

Certain controls have the additional characteristics of increasing circulation, delaying trailing-edge separation, or increasing wing area.

3.3b Leading-Edge Flaps

Leading-edge flaps received significant attention only after thin wing research was well advanced and it had become obvious that a low speed control could be of great advantage in combination with this increasingly important wing type. Like many other forms of boundary layer control, most of the initial developmental work was done in Germany during the Second World War.

The physical feature of the high speed (thin, usually uncambered) profile acting as the most serious deterent to its maximum lifting capabilities is the relatively sharp leading-edge which allows the forward stagnation point to move only a short distance beneath the profile before creating a negative pressure peak of sufficient magnitude to initiate laminar separation at this sharp leading-edge. Therefore, maximum lift is achieved at rather low angles of attack and is consequently limited to comparatively low values.

The leading-edge flap provides a means of redistributing the pressure over the profile in such a way as to eliminate the pressure peak normally leading to premature stall, while closely maintaining, through increased effective camber, the lift capacity of the original profile at all angles of attack. Airfoil stall would then be determined by phenomena characteristic of higher angles of attack and higher lift such as trailing-edge separation.

Several forms of leading-edge flap type control have undergone testing and limited full-scale usage. These are shown in Fig. 106 and are:

(1) The "droop snoot"

(2) The contoured (articulated) leading-edge flap

(3) Flap hinged about the leading-edge radius (Krüger flap)

(4) The N.A.C.A. upper-surface leading-edge flap

(5) The N.A.C.A. lower-surface leading-edge flap.

The "droop snoot" (Fig. 106a) might be defined as a contoured leading-edge flap of fixed deflection or it could be thought of as simply positive camber applied to the most forward portion of the profile. In many instances this configuration has found favor for use with high speed aircraft by virtue of its tendency toward low profile drag at cruise. However, as

nose deflection angle must generally be much greater for optimum take-off than for minimum profile drag at cruise, the variable deflection nose flap is considerably more effective than the "droop snoot" in increasing the aircraft's speed range -- although only at the cost of increased mechanical complexity. The aerodynamic properties of the "droop snoot" are, of course, very similar to those of the contoured leading-edge flap to be considered in the following paragraphs.

The contoured leading-edge flap, also known as the articulated leading-edge flap, is shown in Fig. 106b. The entire nose of the profile is hinged (usually at the lower surface) in such a manner that the leading-edge may be deflected downward to any desired angle within the physical limitations of the configuration. Normally, this flap is fitted with an arc-shaped trailing-edge, with center at the hinge line, so as to maintain rubbing contact, at all values of nose flap deflection, with the skirt on the upper surface of the fixed portion of the profile.

The contoured flap might be said to accomplish the delay or elimination of leading-edge separation by essentially "chasing" the profile's forward stagnation point as it attempts, with increasing angle of attack, to move further beneath the airfoil's nose.

Because of the increase in effective camber due to nose flap deflection, this stagnation point must be located further forward on the lower surface (and thus closer to the profile nose) than would be the case for the base profile at the same angle of attack. Thus, for small nose flap deflections, the stagnation point does not reach such a location as to create separation until a higher angle of attack is attained, and leading-edge stall is therefore

delayed. For greater deflections, the stagnation point can, even at high angles of attack, be located extremely close to the leading-edge or actually on the flap upper surface. If this is the case, leading-edge stall may not occur, the lift now being limited either by trailing-edge stall or flow breakaway from the rather sharp curvature which has been created above the flap hinge line.

Fig. 107 represents an attempt to graphically illustrate the foregoing discussion. As flap deflection is increased, the angle of attack at which the stagnation point moves from the upper to the lower surface also increases. Stall angle and stall type depend very much upon this variation. If the angle of attack at which the stagnation point has moved sufficiently beneath the nose to induce leading-edge stall is below that angle of attack where trailing-edge separation can trigger stall, stall will be of the leading-edge type. If now, flap deflection is increased so that trailing-edge separation becomes extensive prior to that angle of attack where the stagnation point achieves its maximum distance beneath the profile, trailing-edge stall may well occur. In this range of flap deflections, it seems that a flow separation is possible from the upper surface of the flap hinge location. The occurrence of trailing-edge separation, hinge-line separation, or both is a function of a great many things and the prediction of stall type in this deflection regime can be quite difficult.

The fall-off in angle of attack for maximum lift at high deflection values shown in Fig. 107 may be attributed to the occurrence of laminar separation at the upper surface of the hinge region. This high-deflection phenomenon is caused by the inability of the leading-edge stagnation point

to move sufficiently beneath the profile nose to induce turbulent flow at the hinge station prior to the initiation of a laminar breakaway or development of a large bubble at this station.

Fig. 108A demonstrates the effect of increasing flap deflection on a profile at such an angle of attack that it is stalled in its $c_N = 0$ condition. Deflecting the flap 10° does not bring about stall recovery. Fifteen degrees deflection, however, establishes flow reattachment. As deflection is further increased, the hinge-line pressure peak builds up while the leading edge peak decreases in magnitude. At 35° there is no longer any leading-edge peak. This is indicative of the stagnation point being approximately on the leading-edge. It would be expected that further increases in nose flap angle would probably generate laminar separation at the hinge-line and a return to the stalled condition at this angle of attack.

The effect of variations in angle of attack upon the pressure distributions of a profile with leading-edge flap deflection 30° is shown in Fig. 108B. The undersurface may be seen to be partially stalled at $\alpha \cong 2°$. At an angle of attack of 6°, the forward stagnation point is still on the profile uppersurface, the separation region being nearly eliminated however. At $\alpha = 12°$ the stagnation point has moved to the leading-edge. Note also the increase in magnitude of the hingeline pressure peak with increased angle of attack.

Smoke photographs, taken in the Princeton University 2" by 36" smoke tunnel, of a 64-010 airfoil with and without contoured leading-edge flap are shown in Fig. 109. The growth of the leading-edge bubble is evident for the unflapped profile. Final stall occurring here was of the thin

airfoil type. The deflection of the leading-edge flap eliminated the leading-edge bubble at all angles of attack. Separation occurs in this case as a combination of trailing-edge separation and the growth of a laminar (thin airfoil type) bubble aft of the upper surface hinge-line area. It will be noted that the leading-edge flap has served to delay profile stall. While the base profile has completely stalled at 18^{o}, the flapped profile is only partially separated at $\alpha = 20^{o}$. Note the steeper smoke line approach angle, indicative of greater lift, evidenced by the latter as compared with the 18^{o} base profile.

Prior to discussing the contour-flapped profile's characteristics at and near stall, it might be well to consider the effects of this leading-edge control upon the lift curve. Fig. 110 shows curves of sectional lift coefficient vs. angle of attack for a typical thin profile with various deflections of its contoured leading-edge flap. The major effect which can be seen here is that maximum lift is increased almost entirely by virtue of stall angle increases. This phenomenon, which is typical of the "boundary layer" control (as opposed to the "circulation" control), is significant in that it points out that such a control may be limited in its practical applicability by considerations of aircraft geometry and visibility. Of course, when applied to variable incidence wings or wings with trailing-edge controls, this limitation would probably cease to exist.

Observing Fig. 110, it can further be seen that deflection of the contoured flap increases both angle of attack for zero lift and lift-curve slope in the low angle of attack range. Thin profiles with deflected nose flap also yield a characteristic fall-off of slope with increasing angle of

attack, much the same as the slope change associated with the thin profile itself.

Considering a given angle of attack in the base profile range of angles, as nose deflection is increased, the upper surface leading-edge pressure peak will become less negative and finally be forced positive. Simultaneously, a new pressure peak will be formed at the flap hinge-line which will become increasingly negative as deflection is increased. Unfortunately, (for the case of lift at low α) the rate of change of the hinge-line pressure peak with nose flap deflection would seem to be less than that for the leading-edge peak, thus creating a situation of decreased lift at α with increased flap deflection. Added to this is the spoiling effect leading-edge flap deflection has upon the lower surface, causing loss of lift in the low α regime, particularly at high deflections. For these reasons, angle of zero lift is made more positive the greater the deflection. Although this would at first seem contrary to the expected effect on this parameter of what is essentially camber, it must be remembered that angle of attack for a profile with leading-edge flap is based upon the base airfoil's chord line while the identical cambered profile has an angle of attack defined by a chord line drawn from the trailing-edge to the drooped leading-edge. Were the definition changed here to that for a cambered profile, one would see at least for the smaller nose deflections where undersurface spoiling is not severe, the usual effect of increasing camber producing decreasing angle of zero lift.

The higher slope, in the low α range, created by increased leading-edge flap deflection may be attributed primarily to the favorable effect on

undersurface spoiling of increasing angle of attack, this effect quite logically being greater the greater the deflection. It is possible that, in addition to these viscous phenomena, there is an overall inviscid contribution leading to increasing slopes with the larger flap deflections. As thin airfoil theory cannot predict such slope changes, tests were conducted in the Princeton University electrolytic plotting tank facility. These tests failed, however, due to point-scatter, to either confirm or deny the existence of this slope change in potential flow.

As has been mentioned, there is a certain non-linearity in the lift curves with flap deflected. Slope fall-off, at any given deflection, is greater for the thinner profiles -- curves for a 12% airfoil being closely linear. A profile with given flap deflection will yield a lift curve decreasing in slope only very slightly until an angle of attack is reached which would seem to closely coincide with that angle at which the stagnation point has moved somewhat beneath the flap nose producing a tendency toward upper surface leading-edge separation (and elimination of lower surface separation). From this point on, the slope generally is seen to decrease at an accelerated rate until stall occurs. Rapid slope fall-off thus may be expected sooner the less the flap deflection. Thicker profiles yield practically no high-α slope fall-off until immediately prior to stall, probably because of the existence of the leading-edge type bubble in separation rather than the more powerful thin-airfoil type. It might be pointed out that the relatively thin profile with no flap deflection also retains a nearly constant slope until thin-airfoil type separation is initiated, at which point fall-off takes place. This, of course, can occur

at very low angles of attack for the profiles of sharper leading-edge.

It is possible with this type configuration for buffet and stall to occur at the lower end of the lift curve (due to fairly complete undersurface separation) even at positive angles of attack. However, this would seem to take place only with unusually high values of leading-edge flap deflection ($S_N \cong 45^o$).

Fig. 111 and 112 represent an attempt to establish empirical relationships for use in predicting the change in angle of zero lift and low α lift curve slope due to flap deflection as functions of profile thickness and leading-edge flap chord. These curves have been obtained from experimental data contained in Refs. 74 through 85 and demonstrate (1) the effect on $\alpha_{o.L.}$ and slope of nose deflection and profile thickness for profiles with leading-edge flap chord equal to approximately 15% profile chord and (2) the effect of altering flap chordwise extent from that of 15%. Some mention might be made here regarding how the slopes shown in Fig. 112 were measured. These slopes were taken from available lift curves for this type of configuration through use of a secant slope between $C_l = 0$ and $C_l = .6$. This procedure seemed to yield as good or better correlation between profiles as any other method of slope measurement on this rather non-linear lift curve. Maximum variation of the curve from the secant line in this range was only $\Delta\alpha \cong .1$ (curve lying to the left of the secant line). This maximum variation occurred for the thinner profiles. The thicker airfoils reveal very closely a linear curve in this regime, coincident with the secant line.

It will be noted from these empirical curves that, for a given flap deflection greater than zero, increases in profile thickness will lower the angle of zero lift and lessen the lift curve slope. This thickness effect is greater the larger the flap deflection and can be attributed in the main to the relative insensitivity of the thicker profiles to undersurface separation. It can also be seen that, apparently due largely to an alteration in rate of change with nose deflection of upper surface pressure distribution as well as the longer region of adverse pressure gradient created on the lower surface, the effect of increase in leading-edge flap chord is to increase both angle of zero lift and slope. In the case of $\alpha_{o.L.}$, this effect is greater for the larger nose flap deflections, while slope change due to change in flap chord would seem for all practical purposes relatively independent of deflection.

Indications are that, with reasonable cleanliness of leading-edge flap installation, there should be no significant difference in lift curve prior to stall between the base (no-flap) profile and the same profile with a contoured L.E. flap at zero degrees deflection. Therefore, the increments given in Figs. 111 and 112 can very validly be added to the values of angle of attack for zero lift and lift curve slope as obtained for the no-flap profile so long as that profile is symmetrical (these empirical curves were obtained from data gathered from tests utilizing symmetrical airfoils only). It is believed that the curves can still be used with slightly cambered profiles without going beyond the original order of accuracy. However, radical camber would without doubt invalidate the predictions as shown.

Comparing data contained in Refs. 83 and 84, it appears that the effect of increasing Reynolds Number from approximately one million to six million is, for the 10% thick profiles described, to decrease $\alpha_{o.L.}$ by about 0.1^{o} while increasing slope by an amount in the order of .002. This surprisingly small change would seem to indicate that any effect of Reynolds Number variation (at least within the landing and take-off regime) could be considered to be relatively negligible alongside the effects of profiie thickness and nose-flap deflection. Because of this experimental data and the fact that separation type becomes comparatively independent of Reynolds Number in the higher Reynolds Number range (see Fig. 123), it was decided that Reynolds Number effects could be neglected in the presentation of these prediction plots.

The empirical curves shown for change in angle of zero lift and slope change due to deflection of the 15% chord flap have been "paint-brushed" so as to permit a means of indicating the influence of base profile thickness distribution upon these parameters. It can in general be said that those configurations with sharper leading-edges (double-wedge, etc.) will yield values lying along the lower boundary of the $\alpha_{o.L.}$ "paint-brush" curves and along the upper boundary in the case of the slope change plot. Conversely, values of change in angle of zero lift and change in slope due to flap deflection for profiles with larger nose radii (64 series, etc.) may be found along the upper boundary of the given $\alpha_{o.L.}$ curve or the lower boundary of the slope change curve.

The ability of potential theory to predict the $\alpha_{o.L.}$ characteristics of this type of configuration is demonstrated by the theoretical curves

shown in Fig. 111. These curves are based on thin airfoil theory and represent an application of the treatment given by Abzug in Ref. 74. Although it is clear that thin airfoil theory will reveal the general trends as regards to the effects of nose flap deflection and flap chord extent on $\alpha_{o.L.}$, its ability to quantitatively predict would seem to fall down for the thinner profiles and at the higher flap deflections. This is without doubt due in the main to the occurrence in the real flow of low-angle-of-attack separation regions which are more extensive the thinner the profile or the greater the flap deflection. Use of thick airfoil theory or electrolytic tank methods would thus probably be of mostly academic interest and of little aid in reasonably accurate prediction studies.

As has been stated previously, thin airfoil theory cannot predict constant - δ_N slope change, and plotting tank tests failed to either confirm or deny the existance in the ideal fluid of any effect upon slope of variations in flap deflection. Here again, it is thought that inviscid effects would be negligible compared with the viscous.

Variations in flap extent from that of 15% c create changes in $\alpha_{o.L.}$ as shown in Fig. 111b. The only empirical curves available are those for a 4.23% thick double-wedge profile (Ref. 76) and hence secondary thickness effects cannot be defined. Based on the previous discussion, it is felt that thicker profiles will demonstrate characteristics closer to the theoretical curves shown. Therefore it is recommended that the empirical curves be used for profiles of approximately 4% thickness, the theoretical curves for 12% profiles, and interpolated values for airfoils of intermediate thickness. Indications are that Reynolds Number effects can

be assumed to be comparatively negligible.

Observation of a large number of leading-edge flap lift curves indicates that, unlike the $\alpha_{o.L.}$ case, the slope change due to variations in flap chordwise extent (Fig. 112b) is quite independent of flap deflection. In fact, the entire secondary slope-change effect (flap extent) may well be considered to be negligible compared with that shown in Fig. 112a.

Figure 111 may be used to predict $\alpha_{o.L.}$ as follows:

$$\alpha_{o.L.} = \alpha_{o.L._o} + \Delta_1\alpha_{o.L.} + \Delta_2\alpha_{o.L.}$$

where: $\alpha_{o.L.}$ = angle of attack for zero lift at the given leading-edge flap deflection, δ_N.

$\alpha_{o.L._o}$ = base profile angle of attack for zero lift (zero for symmetrical profiles)

$\Delta_1\alpha_{o.L.}$ = is as determined from Fig. 111a.

$\Delta_2\alpha_{o.L.}$ = is as determined from Fig. 111b.

Profiles with sharp leading-edges (double-wedge, etc.) will yield values lying along the lower boundary of the "paint-brush" curves (Fig. 111a) while "round-nose" profiles will lie along the upper boundaries. In Fig. 111b, the empirical curve may be considered valid for 4% profiles, the theoretical for 12% profiles. The $\Delta_2\alpha_{o.L.}$ for intermediate profiles may be estimated through interpolation.

Fig. 112 may be used to predict $dC_l/d\alpha$ in the range of lift coefficients from zero to 0.6:

$$a = a_o + \Delta_1 a + \Delta_2 a$$

where: a = lift curve slope with given leading-edge flap deflection, δ_N.

a_o = base profile lift curve slope

$\Delta_1 a$ = is as determined from Fig. 112a

$\Delta_2 a$ = is as determined from Fig. 112b

Profiles with sharp leading-edges will yield values along the upper boundary of the "paint-brush" curves (Fig. 112a), while profiles with rounded leading-edges will have values lying along the lower boundaries. The predicted slope should be applied as a secant slope from $C_l = 0$ to $C_l = .6$ (as shown in Fig. 112c).

The above procedures should yield closely accurate results for symmetrical and slightly cambered profiles at Reynolds Numbers in the landing and take-off range.

As has been stated previously, the contoured leading-edge flap permits increases on the thin profile's maximum lift coefficient through re-distributing the pressure over the profile in such a way as to delay or eliminate the leading-edge pressure peak which normally induces stall. Airfoil stall would then be determined by phenomena characteristic of higher angles of attack and higher lift such as trailing-edge separation. Also, the upper-surface pressure redistribution creates a second pressure peak immediately above the flap hinge line which in some instances can initiate separation prior to the occurrence of trailing-edge flow detachment. Thus separation can occur from the profile leading-edge, the upper-surface hinge line curvature, or the profile trailing-edge, with final stall being the result of any or all of these possible separations depending upon the flapped profile's shape and free stream and local flow conditions.

The foregoing paragraphs discussed that portion of the lift curve below the buffet regime. The following paragraphs will attempt to analyze the upper

portion of the lift curve, the separation and stall types, and possible means of $C_{l_{max}}$ prediction.

The leading-edge flap may be considered to be primarily a boundary layer control. That is in the main, it achieves an increase in $C_{l_{max}}$ over and above the base profile through extending the lift curve rather than through shifting the curve to the left. This is brought about by virtue of its ability to delay or eliminate leading-edge separation.

Section 3.1 describes the phenomena of the "thin-airfoil" and "leading-edge" separations. The occurrence of separation from the profile's leading-edge was shown to be more likely the smaller the Reynolds Number, the thinner the profile, or the more aft the location of maximum profile thickness.

The latter two criteria are essentially a measure of leading-edge sharpness. It could thus be said that, if the primary usefulness of the leading-edge flap lies in its ability to delay or prevent leading-edge separation, such a flap would be of little aid to profiles of a shape and in a Reynolds Number range where such a separation would not occur.

Considering airfoils which normally yield leading-edge separation prior to stall, let us deflect the flap a given amount, δ_N . Here it would seem logical that, as nose sharpness and Reynolds Number determine the likelihood of leading-edge separation (for a given δ_N) those contour-flapped profiles of greater thickness and/or greater Reynolds Number would be less apt to reveal such separation. (Of course, increases in δ_N for any configuration will diminish the effects of leading-edge separation so long as such phenomena exits.) Assuming for the present that hinge-

line separation cannot occur and therefore that maximum possible lift for this type configuration is determined by the occurrence of what ought be called "pure" trailing-edge stall, optimum δ_N (here temporarily defined as the smallest possible deflection needed to entirely prevent leading-edge separation) would thus be expected to be greater for those profiles which are thinner and/or at lower Reynolds Numbers.

Separation may be initiated at the curved portion of the upper surface immediately above the contoured flap's hinge and this separation can well define maximum lift for the profile. Separation here will be of the laminar type. The laminar separation may occur as either the thin-airfoil or leading-edge variety, as described in Section 3.1. Laminar separation from the hinge-line curvature would seem more likely the greater the flap deflection, the smaller the hinge-line radius of curvature (thinner the profile) and, perhaps, the smaller the flap extent. Such separation depends upon the existence of laminar flow in the hinge-line area and thus cannot occur if the forward stagnation point is sufficiently beneath the leading-edge to permit a leading-edge separation bubble. Therefore, if laminar separation from this point is to be introduced, the configuration must be such that sufficient curvature to cause hinge-line separation is present prior to the movement of the stagnation point to a position which would initiate leading-edge separation.

For the thicker profiles at the higher Reynolds Numbers laminar hinge-line separation appears to normally occur through the formation of a leading-edge type of bubble. This bubble shows no tendency to break away prior to the occurrence of the relieving bubble at the flap leading-edge until quite

high flap deflections are attained ($\delta_N \cong 35^o$-45^o). Thinner profiles and profiles at very low Reynolds Numbers demonstrate a thin-airfoil type of separation at the hinge-line curvature. Even at δ_N's of 20^o to 30^o this bubble can become rather extensive prior to the formation of the nose bubble. Here again, for high deflection values, complete hinge-line flow breakaway may be expected before turbulent flow is established over the flap. The persistance at the hinge-line of either the leading-edge type or thin-airfoil type of bubble to angles of attack beyond that corresponding to the movement of the stagnation point beneath the nose depends upon the stagnation point location, Reynolds Number, and nose radius. It seems sometimes possible to have such a hinge-line separation even though the stagnation point is on the lower surface, so long as there is no separation at the nose and the pressure gradient between the stagnation point and the hinge curvature is predominatly favorable. References 83 and 84 infer the possibility of a turbulent flow breakaway from the hinge-line curvature. In these reports, stall at certain δ_N's was thought to occur from the hinge-line, but the lift pattern does not appear to be compatible with the expected trends of laminar separation. Therefore it would be possible that stall here was the result of a "turbulent breakaway". Unfortunately, data is not available to truly deny or verify such a concept. A phenomenon of this nature would, however, seem improbable because of the relatively gradual curvature involved and the well known "sticking" power of a thin turbulent layer.

It would be well to mention the importance of hinge location normal to the chord and of maintaining a relatively clean flap-wing juncture. It

stands to reason that a flap hinged at the profile lower surface would create a greater radius of curvature than one hinged at the chord line. Such a flap could therefore be expected to reduce the possibilities of hinge-curvature separation. Tests conducted at Princeton University and described in Ref. 84 indicated that any relatively minor surface discontinuities in this area of curvature can cause very premature separation. Although this factor would not be expected to be so critical at higher Reynolds Numbers and is thus not felt to be a practical deterent, it is a point to be borne in mind.

If hinge-line stall and leading-edge stall are prevented for the profile with a leading-edge flap, separation moving forward from the airfoil's trailing-edge will limit the lift of such a configuration. Trailing-edge separation occurs prematurely if a separation bubble is present at the leading-edge or hinge-line area. Of the two it appears that hinge-line separation can cause a greater thickening of the trailing-edge turbulent layer and hence should have more effect upon the trailing-edge stall characteristics.

The majority of profiles with contoured leading-edge flaps exhibit stalls at most c_{N}'s which are the result of separations at more than one of the separation-prone areas. For this reason, stall type is very difficult to determine from the results of force tests and, in the absence of pressure distribution studies or boundary layer surveys, much confusion can exist as to the flow pecularities which are present. It is regretable that so little information regarding actual separation patterns with such a configuration is available as the leading-edge flapped profile offers an

excellent opportunity for the study of separation interaction effects.

Figs. 113 through 116 demonstrate the maximum lift characteristics of six profiles with contoured leading-edge flaps. All of these models have a flap extent of approximately 15%c. and are at a Reynolds Number of closely 6×10^6. Three profiles are of the "round-nose" type (64 series, etc.) while three have "sharp" leading-edges (double-wedge, etc.). The data plotted in these figures have been obtained from the wind tunnel investigations described in Refs. 75, 78, 81, 83, and 85.

The angle of attack for maximum lift and maximum lift coefficient are plotted as functions of nose flap deflection in Figs. 113 and 114. It may be seen that, although they represent as great a thickness range, the "sharp-nose" profiles have very similar characteristics, whereas the profiles with more rounded leading-edges display very little similarity with each other. Fig. 113 reveals a definite pattern of increasing $\alpha_{C_{\ell MAX}}$ with increased δ_N, but shows varying trends with profile thickness. Flap deflection for greatest $\alpha_{C_{\ell MAX}}$ appears to be 30° for the sharp-nosed profile configurations, but varies and is less definite in the case of the configuration with rounded leading-edges. Fig. 114 indicates a consistent variation with thickness for the sharp nosed profiles, but no overall trend can be seen for the airfoils with more rounded leading-edges. Optimum δ_N is (from the $C_{l_{max}}$ plot) however approximately 30° for all the configurations considered.

Figs. 115 and 116 plot the increment in $\alpha_{C_{\ell MAX}}$ and lift coefficient created by nose flap deflection over and above that attainable by the profile with flap at zero deflection. The same curve-shape

characteristics are discernible here as in Figs. 113 and 114. Obviously, these curves must be studied with an eye to separation-stall phenomenon in order to give them any meaning.

Let us first attempt to analyze the characteristics of the sharp-nosed profile with leading-edge flap. Base airfoils of this shape characteristically yield leading-edge stall of the thin airfoil type, the bubble initiating at angles of attack very close to zero. Observing Fig. 116, it can be seen that lift increment increases closely linearly with flap deflection up to a $\delta_N \cong 25^\circ$. In this range, it would be expected that leading-edge separation (thin airfoil) is the only major viscous effect existing. Ref. 77 describes tuft and boundary layer surveys which verify such a statement for a flapped configuration with a 4.23% double-wedge base profile. The same report demonstrates that the angle of attack where the stagnation point goes beneath the leading edge varies almost linearly with δ_N. Data from Ref. 77 also indicates that, regardless of δ_N, there exists a closely constant increment between the angle of attack at which the stagnation point moves beneath the nose and the angle of attack where the leading-edge separation has grown sufficiently to cause stall ($\alpha_{c_{\ell MAX}}$). This may be seen to provide the reason for the linearity of the $\Delta\alpha_{c_{\ell MAX}}$ and $\Delta c_{\ell MAX}$ curves in the pure leading-edge stalling regime.

In this range of nose flap deflections there exists in the sharp-nosed case a minor trend indicative of higher $\Delta c_{\ell MAX}$ for a given δ_N as profile thickness is increased. This could not be explained by any leading-edge differences as all of these profiles have the same "sharp" nose. The following might, however, be a valid explanation for this trend.

It will be noted from Fig. 114 that the thicker base profile has the lower Cl_{max}. The cause of this is the reduced lift curve slope created by the thickened turbulent boundary layer which has been established by the relatively large trailing-edge angle. At a given δ_N, the thicker sharp-nosed profile still finds itself at a lower lift level than its thinner counterpart as the thin airfoil bubble is increasing in extent. The lower lift level acts in the same way upon the leading-edge bubble as decreasing circulation control, serving to delay the bubble's growth and leading to a greater $\Delta C_{\ell_{MAX}}$ and $\Delta \alpha_{C_{\ell_{MAX}}}$ for the thicker profiles.

From $\delta_N \cong 25^\circ$ to $\delta_N \cong 30^\circ$-35°, the $\Delta C_{\ell_{MAX}}$ curve, Fig. 116, diverges from the linear in the sharp leading-edge case and decreasing slope is noted until maximum $\Delta C_{\ell_{MAX}}$ is attained at 30°-35°. Indications are that no hinge-line separation is present in this range at stall, although these phenomena may exist at lower angles of attack for these and lesser δ_N's. Apparently stall here is still from the profile leading-edge but, prior to stall, trailing-edge separation is also seen to be present in a small amount. This premature trailing-edge separation has been induced by the leading-edge bubble which acts to turbulize the flow over the trailing-edge to an extent far in excess of that which would exist with no leading-edge bubble. It is interesting to note that the lift level for occurrence of this combined stall pattern is closely equal to that at which the thicker, round-nosed base profile also starts developing a combination stall.

For flap deflections in excess of 35° stall occurs abruptly from the hinge-line curvature or it is possible that what is seen is actually separation from the trailing-edge due to the influence of a large hinge-

line bubble. In either case, the laminar hinge-line bubble, which, at these δ_N's, is able to grow to an extent which precipitates stall prior to the formation of the neutralizing leading-edge bubble, is the major culprit. Maximum lift falls off quite violently here due to the necessarily lower $\alpha_{C_{\ell MAX}}$ as well as the higher $\alpha_{o.L.}$ as compared with the 30° deflection case.

The "rounded" leading-edge profiles demonstrate characteristics with increasing flap deflection which are somewhat less uniform. The initial rise of the $\Delta C_{\ell MAX}$ curve (Fig. 116) is not linear but shows a definite tendency to constantly decrease in slope. Further, thickness effects seem larger and less uniform.

The curve of $\Delta\alpha_{C_{\ell MAX}}$ vs. δ_N (Fig. 115) indicates that for these configurations the initial increase in angle of attack for maximum lift is relatively independent of thickness and of the same order of magnitude as that for the thicker sharp-nosed configuration. In this region, where leading-edge separation is the major limiting factor, $C_{l_{max}}$ (Fig. 114) is a function of the distance beneath the leading-edge that the stagnation point can travel prior to inducing leading-edge separation. At a given small δ_N, leading-edge separation would thus be expected to occur at a later angle of attack the thicker the profile. The 64A010 and 63$_1$012 are suspected of having a primary separation of the leading-edge variety up to flap deflection values, which while not rigorously noted in the references, appear to be approximately 15° and 5° respectively. The fall-off in $\Delta\alpha_{C_{\ell MAX}}$ for the 65A006 at deflection values greater than 15° is difficult to explain but may well be due to discontinuity-induced premature hinge-line separation

which can, in turn, induce premature trailing-edge stall. The curves shown in Ref. 85 infer that stall at all δ_N's to 25° is of the relatively gentle variety. It is possible that leading-edge stall of the thin airfoil type is the limiting factor for the 65A006 configuration to approximately 15° and that highly premature trailing-edge stall takes over after this point.

Fig. 116 reveals, within the δ_N range for leading-edge stall, closely the same slope for the 64A010 and 63$_1$012 configurations, this slope being greater than that for the 65A006 configuration. This slope change may at least in part be a characteristic of the leading-edge type bubble growth as opposed to the thin-airfoil bubble growth. Another possible cause could be the relative prematurity of base profile stall, due to flap addition. The 65A006, which should demonstrate the thin-airfoil type of leading-edge bubble, shows a slope in this range closely identical with those for the sharp leading-edged configurations.

The slope fall-off in this range of flap deflections for the 64A010 configuration (as seen in Fig. 116) is brought about by the high lift level which permits the leading-edge bubble to induce premature trailing-edge separation, a separation type which is very much a function of lift level. This effect is greater the greater the lift level and, consequently, is greater the larger the δ_N. Such a decrease in slope in this regime would probably be discernible for the 63$_1$012 configuration were more data points available.

Ref. 83 indicates that, for the 64A010 configuration at δ_N's in excess of 15°, separation initiates from the hinge-line. It may be that what is

seen here is actually premature and rapid trailing-edge separation induced by a hinge-line bubble of the leading-edge type. Between 5° and 30° the 63$_1$012 system reveals relatively flat $\Delta C_{\ell MAX}$ and $\Delta \alpha_{o.L.}$ curves indicative of the attainment of optimum flap deflection. No hinge-line separation was noticed and it is quite probable that none occurred. It is felt that premature trailing-edge separation induced by the presence of a forward laminar bubble was here the cause of final stall--at least between 10° and 30° δ_N . The slight rise in lift at 30° could possibly indicate that trailing-edge separation occurred at this point uninfluenced by any leading-edge separation.

The optimum δ_N (based upon the $C_{l_{max}}$ curves) for all round-nosed configurations, as was the case with the sharp-nosed, seems to be approximately 30°. The 65A006 indicates a leveling off at 30° where stall seems to be due to thin airfoil type separation at the hinge-line, possibly with trailing-edge separation present and influencing.

The lift decrease of flap deflections in excess of 30° may be attributed to laminar breakaway from the hinge-line. The lift increase which follows this fall off for the 65A006 and 64A010 could be explained by the secondary stall patterns (initiated in this case from the hinge-line) discussed in Section 3.1.

Figure 117 demonstrates the general trends of the leading-edge flapped configuration's maximum lifting capabilities as a function of thickness. It will be noted that only "pure" stall from each of the three separation-prone regions has been considered. Although angle of attack has been used as the ordinate for these curves, lift coefficient would be expected to follow the same general patterns.

For the case of "pure" leading-edge stall (Fig. 117A) it is necessary to consider the "sharp" leading-edged configuration separately from the "rounded". This is because the leading-edge bubble forms at an α relatively independent of thickness for the sharp profiles, while rounding the leading-edge delays this bubble formation to a later angle of attack (later the greater the leading-edge radius of curvature). For thin airfoil type separation, it can be inferred from Ref. 77 that the angle of attack where the bubble initiates will vary linearly with δ_N and that there is a closely constant increment at all δ_N's between this angle and that for thin-airfoil stall. These observations would be expected to also hold nearly true for configurations with a characteristic leading-edge type of separation and stall.

The decrease in $\alpha C_{\ell_{MAX}}$ (and thus $C_{l_{max}}$) with increased profile thickness for the sharp-nosed configurations is not truly inherent in the "pure" leading-edge stall but rather represents an effect of the thickened trailing-edge turbulent boundary layer as previously described. The increased slope of the $\alpha C_{\ell_{MAX}}$ curves with increasing thickness is also created by this effect. Were there no trailing-edge effect here, there, in all probability, would be no effect of thickness upon $\alpha C_{\ell_{MAX}}$.

Occurrence of leading-edge or thin airfoil stall on the rounded leading-edged configurations is a definite function of leading-edge radius and thickness. In any event, increased thickness (or leading-edge radius) will cause an increase in the angle of attack at which the significant bubble forms. The maximum $\alpha C_{\ell_{MAX}}$ or $C_{l_{max}}$ appears also to be a function of nose radius (or profile thickness), increasing with increased thickness as

well as with δ_N . Although variance with leading-edge stall type cannot be ascertained from available data, it can be said that the $\alpha C_{\ell_{MAX}}$ (and $C_{l_{max}}$) of the round-nosed configuration would, from the empirical data, be expected to always be as great as or greater than that attainable with any sharp nosed profile. The same can indeed be said for $\triangle C_{l_{max}}$ due to the flap with respect to the base profile.

For the case of pure hinge-line stall, qualitative variation would be thought to take the form shown in Fig. 117B. The separation phenomena here can either be of the leading-edge or thin-airfoil type. Stall type might be quite important with regard to persistence of separation, and it is unfortunate that so little research has been conducted along these lines. Because of increased hinge-line radius of curvature, increased thickness should decrease the likelihood of separation and, using the concept of a separation-to-stall increment relatively independent of thickness (as indicated in the leading-edge stall case) $\alpha C_{\ell_{MAX}}$ and $C_{l_{max}}$ should be greater the greater the profile thickness. It might be pointed out that, although thickness distribution can be important here, the sharpness or lack of same at the profile leading-edge can have no effect.

Pure trailing-edge stall, as shown in Fig. 117C, makes the assumption that the "linear extrapolation method" of Section 3.1 is valid. The Reynolds Number has here been assumed to be such that there is no effect of thickness upon the "pure" trailing-edge stall extrapolation. This would not be expected to hold true for all Reynolds Numbers but would seem proper for purposes of this demonstration. The increase in angle of attack for the initiation of separation and for the occurrence of $C_{l_{max}}$ is based upon the

expected effect of increased camber. The circulation increase due to increased camber will not be nearly so great as that which would be predicted theoretically because of the counteracting B.L.C. effect, increasing camber increasing the likelihood of trailing-edge separation. Studies of cambered profiles and the previously discussed test results indicate that this inefficiency should limit the slope of this curve to values considerably less than the slope for the pure leading-edge stall curves.

The "pure" curves shown in Fig. 117, of course, will seldom occur over any large range of δ_N . As flap deflection is increased on a profile normally stalling from the leading-edge, separation will soon cease to occur from that point and jump to the area of hinge-line curvature, the trailing-edge, or both. However, such "pure" curves permit the qualitative build-up of the total leading-edge flap picture. Fig. 118A shows the variation in $\alpha C_{\ell_{MAX}}$ which would be expected from a very thin profile with a contoured leading-edge flap. It will be noted that the resultant separation-stall pattern combines leading-edge with hinge-line separations. A round-nosed profile has been assumed, but the $\alpha C_{\ell_{MAX}}$ variation would hold as well for a sharp airfoil.

Fig. 118A demonstrates the important probability that leading-edge stall can persist only to that δ_N where hinge-line <u>stall</u> occurs very slightly prior to the initiation of leading-edge <u>separation</u>. An assumption here, which is felt to be valid, is that no hinge-line stall may occur in the presence of a leading-edge bubble. This assumption is, of course, based upon the belief that laminar flow at the hinge-line is necessary for stall to occur at this point. A further assumption is that a leading-edge bubble is

necessary to establish turbulent flow at the hinge-line curvature. The latter is felt to generally be true or so closely true that possible variation is insignificant. The thick line of Fig. 118A represents the $\alpha C_{\ell_{MAX}}$ vs δ_N for this configuration and offers an indication of the maximum lift variation. Note the separation regions into which the picture can be divided and that hinge-line <u>separation</u> can well be present even at δ_N's less than 30° for angles of attack prior to stall. Trailing-edge separation has been assumed to not enter into this semi-hypothetical situation. Whether a profile can ever actually be sufficiently thin for this to be the case is a matter for conjecture. The 4.23% double-wedge described in Ref. 77 did show some effect of what was probably premature trailing-edge separation.

The case of combined leading-edge and trailing-edge stall is illustrated in Fig. 118B. This infers a hinge-line curvature which is controlled (by suction, for instance) or may be taken to simply demonstrate such a combined effect at δ_N's less than that necessary for hinge-line stall. As indicated in this curve, <u>pure</u> leading-edge stall can only persist to an angle which is slightly beneath that for the occurrence of pure trailing-edge separation. This is due to the leading-edge bubble inducing premature trailing-edge separation which, in turn, although relieving the leading-edge bubble to some extent, creates a lift curve slope fall-off that diminishes the lifting potential of the leading-edge stalling profile. For this reason, there will occur here a fall-off in slope of the $\alpha C_{\ell_{MAX}}$ (and $C_{l_{max}}$) vs δ_N curve. As δ_N is increased, stall can alter from premature leading-edge to premature trailing-edge. Only after the leading-edge separation line (not shown) crosses the trailing-edge stall line can pure trailing-edge stall occur.

Fig. 118C illustrates the case of combined trailing-edge and hinge-line stall occurring, in sequence, as δ_N is increased. Such a pattern may be expected in the case of very thick profiles. Obviously such a combination, without a preceeding leading-edge stall, represents a rather inefficient system, increases in δ_N serving to increase lift only by the camber effect. For such a trailing-edge stalling profile, a trailing-edge control would doubtless be of more value. It will be noted that upon the initiation of the hinge-line bubble trailing-edge stall becomes premature, increasingly so until stall is actually of the hinge-line type.

In Fig. 119, profile thickness is allowed to increase from 119A to 119D. It should be remembered that these curves are based to a large extent upon the speculation and calculated guesses of the preceeding pages. Correlation, however, between the results of this technique and the small amount of existing experimental data is good. The plots shown here are combination patterns similar to those of Fig. 118A, unlabeled in this case so as to avoid unnecessary crowding. The curves drawn with large dashes represent initiation of pure separation. The undashed curves indicate pure stall, while the heavy line shown $\propto C_{\ell_{MAX}}$, not considering instantaneous separation mixtures. The short-dashed curves represent $\propto C_{\ell_{MAX}}$ considering such mixtures. The straight lines of lower slope indicate trailing-edge separation and stall and, in agreement with a previous assumption, have locations invarient with profile thickness. Hinge-line and leading-edge stall curves are permitted to move vertically as thickness is increased and the hinge-line stall and leading-edge separation lines are assumed to cross at the same δ_N in all cases. There may at this point be a dissenting opinion to the effect that the assumption of invariance with thickness of the

locations of the pure trailing-edge stall and separation curves is erroneous. Certainly, this is true. In the Reynolds Number range of $3\text{-}9\times10^6$, it can be seen from Fig. 17 that, accepting the linear extrapolation method, thickness can become quite important. However, in this range, the effect of thickness is, other than at that Reynolds Number where there is closely no effect, to decrease Cl_{max} with increased thickness. Thus, for these Reynolds Numbers, at least, the pure leading-edge stall and pure trailing-edge stall curves must move into each other with increased thickness and hence Fig. 119 will not be altered schematically by the selection of any other Reynolds Number in this low-speed regime.

Fig. 119A illustrates the expected stall pattern for a configuration with thickness slightly greater than that whose expected pattern is shown in Fig. 118A. The only difference between these two patterns is that, for the profile of Fig. 119A, the trailing-edge separation line is, prior to hinge-line stall, sufficiently close to the trailing-edge stall line to induce premature leading-edge separation. This progression is typical of the sharp nosed profiles (of any thickness) due to the inherently low lift level of their leading-edge stall line. Of course, were this a sharp-nosed profile, the leading-edge separation line would go through the origin of the axes. Fig. 119B demonstrates the effect of increasing the thickness slightly beyond that shown in Fig. 119A. Here, the trailing-edge and leading-edge lines having moved closer together, progression is from premature leading-edge stall to premature trailing-edge stall, with the final limitation, as usual, being the advent of complete stall from the hinge-line. It will be noted that this thickness is somewhat greater than that for Fig. 118B.

As mentioned previously, leading-edge stall will become premature at an angle somewhat less than that required for pure trailing-edge separation. This premature leading-edge stall is likely to change to premature trailing-edge stall at the σ_N where the pure leading-edge stall line crosses the pure trailing-edge stall line. It would further be expected that, where premature leading-edge stall exists, the angle of attack for such an occurrence would diverge with increasing σ_N from the pure leading-edge stall line, while, where premature trailing-edge stall exists, the occurrence angle (short-dashed line) would approach the pure trailing-edge stall line as deflection is increased.

A pattern characteristic of even higher thicknesses is shown in Fig. 119C. Here, premature trailing-edge stall takes over at a considerably lower deflection value than in the previous case. The 63$_1$-012 configuration has apparent characteristics closely identical with those shown here.

Fitting the 64A010 results into this scheme of things seems somewhat difficult. Although test observations indicated a hinge-line stall at σ_N's where lift was still increasing, the laminar requirement here imposed and the expected degree-of-curvature effect would infer the impossibility of this. It is quite possible that what was seen here was premature trailing-edge stall created either by leading-edge separation (with hinge-line separation at low angles of attack) or by hinge-line separation. To be in keeping with the stall pattern summarized in Fig. 119, the former would be most likely. However, the thickness distribution change between the 63$_1$-012 and the 64A010 could, for such small thickness changes, permit some deviation in a stall-pattern progression such as that shown in Fig. 119 which assumes constant

optimum δ_N (thus inferring constant nose radius to hinge-line radius ratio or constant thickness distribution).

Fig. 119D shows a very thick profile's stall progression. Such a profile reveals a trailing-edge stall (though somewhat premature) even for zero nose flap deflection. The factor permitting lift increases here is simply the increased camber provided by deflecting the flap. When hinge-line separation is encountered, this stall becomes more and more premature until δ_N's are reached where stall occurs directly from the hinge-line. It will be noted that optimum δ_N may be greater here than in the thinner-profile cases. In all cases, the leading-edge separation and pure hinge-line stall line have been assumed to cross (normally creating an optimum) at a constant δ_N. In the case of Fig. 119D, trailing-edge stall occurs, at this δ_N, previous to leading-edge stall, allowing a greater optimum.

The curves of Fig. 119 indicate increasing $\alpha C_{\ell_{MAX}}$ (at optimum δ_N) as thickness is increased. This would probably be true for the case where pure trailing-edge stall is independent of thickness, but would not necessarily hold for Reynolds Numbers where the level of the pure trailing-edge stall line decreases (or increases) with increasing thickness. It can, however, be reasoned that maximum lift (or $\alpha C_{\ell_{MAX}}$) at optimum δ_N will increase with thickness until trailing-edge stall is approximated. For most Reynolds Numbers between 3×10^6 and 9×10^6, there will here occur a fall-off in maximum attainable lift with further increases in t/c until a relatively constant level or a level slightly increasing with thickness is attained, the latter effect being due to the probable achievement of greater δ_N's prior to hinge-line stall with a resultant increase in permitable camber.

It should be remembered, in evaluating Fig. 119, that a change in leading-edge stall type, with increasing thickness, from thin-airfoil to leading-edge will seemingly increase the slope of the pure leading-edge curves, at least if they are taken to represent lift rather than angle. Although this creates a quantitative difference, it does not establish any alterations in the qualitative interpretation.

Any quantitative prediction of maximum lift attainable by profiles fitted with a contoured leading-edge flap must currently be based upon the rather meager available test data and a reasoning process as just given. The numerous important aerodynamic and geometric variables effecting the lifting characteristics of this type of configuration make such a procedure extremely difficult and the resulting prediction subject to some quantitative doubt. It has been decided, however, to attempt to consider all of the major variables so that, even though the accuracy may not be necessarily enhanced, the probable trends due to alteration of these variables can be more readily visualized.

Let us first consider the leading-edge flapped configuration at a constant Reynolds Number and fixed chordwise flap hinge location. The important variables in such a case are the profile thickness and thickness distribution, as well as hinge location (normal to the chord line), and the possible presence of hinge-line roughness or discontinuities. Even disregarding the latter two variables as parameters which may readily be altered or negated in design, prediction is complicated by the many flow changes created by thickness and thickness distribution variations. Maximum lift values in the leading-edge stall regime may be altered by leading-edge

stall type and the degree of prematurity of that stall. Methods must also be found to define the existence of trailing-edge stall and its complicating secondary effect, trailing-edge stall prematurity. The "camber effect" must be predicted. Occurrence of hinge-line separation and stall depends upon just about all of the effects above.

So as to be able to achieve as reasonable a basis as possible for the prediction of $\Delta C_{l_{max}}$ for the constant Reynolds Number, constant C_N/C case, this prediction will first be made for the R.N. $\cong 6 \times 10^6$, $C_N/C \cong 15\%$ conditions where the majority of experimental data are to be found.

Available experimental results indicate the optimum flap deflection is 30° throughout the thickness and thickness distribution range considered. As indicated by Fig. 119D, however, further thickness increases might well serve to increase optimum δ_N. Unfortunately, prediction of optimum δ_N throughout the complete thickness range seems impossible, but it would appear safe to say that, for profiles which in their base condition stall from the leading-edge, optimum δ_N will be approximately 30°. The δ_N for lift fall-off, created by hinge-line stall, will be approximately 35°.

As shown in the previous discussion, trailing-edge stall can, for the thicker profiles, become predominant at δ_N's less than that optimum defined by hinge-line stall. It thus becomes important to define the $C_{l_{max}}$ or $\Delta C_{l_{max}}$ where trailing-edge stall can occur. The linear extrapolation method, as described in Section 3.1 offers the best means known to this author toward this prediction. Fig. 120 shows $C_{l_{max}}$ plotted against t/c for the various leading-edge flapped configurations at the Reynolds Number and C_N/C in question. The close agreement, for the round-nosed profiles,

with the linear extrapolation method is readily discernable. The 64A010 configuration correlates almost exactly with such a method. However, it must be remembered that there exist two effects which would alter the application of the linear extrapolation method which is intended to indicate where the given profile will stall in a pure trailing-edge manner, $\delta_N = 0°$. These are the camber effect, which would indicate that trailing-edge stall, at any δ_N larger than zero, will occur at a greater $C_{l_{max}}$ than that predicted by the base profile linear extrapolation (see Section 3.1f), and trailing-edge stall prematurity caused by a forward bubble, which serves to reduce maximum lift beneath that predicted by the linear extrapolation method. The very good agreement of the 64A010 configuration at a δ_N of 30° with the linear extrapolation must be a coincidence, created by the near equality of two counteracting effects. However, a general qualitative verification of the linear extrapolation method, considering both the 64A010 and the 63$_1$012, is indicated.

Fig. 116 indicates that when the manner of leading-edge stall reverts, through decreased thickness, from the leading-edge type to the thin airfoil type, the slope of the $\Delta C_{l_{max}}$ vs δ_N curve in the leading-edge stalling regime should decrease. It is suspected that the degree of decrease is not truly so great as is indicated in this figure. The reason for this is that prematurity of <u>base</u> profile stall appears to become more excessive the greater the profile thickness. This prematurity, as indicated in Fig. 120, is apparently caused by the detrimental effect of the profile-flap juncture; that is, the profile with leading-edge flap at zero δ_N will have a lower $C_{l_{max}}$ than the same profile with no contoured leading-edge

flap. The sharp-nosed curves given in Fig. 120 show for base profile characteristics only the $\delta_N = 0^o$ case, with no information being available for the no-leading-edge-flap configurations. Obviously, in order to keep the thicker round-nosed curves and the sharp nosed curves on the same basis, knowledge of the sharp-nosed base profile curves would be necessary. In the absence of this data, it is not possible to rigorously ascertain a correction to the slope variation indicated in Fig. 116. The subtraction of the base profile prematurity may be shown to yield a $\Delta C_{l_{max}}$ vs δ_N curve stall with a higher slope than the unaltered sharp-nosed profiles, indicating that slope change with increasing thickness (or with a change in leading-edge stall type) is valid. Further, such a procedure does not alter the fact that the thicker round-nosed configurations show a slope fall-off ($C_{l_{max}}$ vs δ_N) while the sharp-nosed profiles do not in the leading-edge stall regime.

In order to predict $\Delta C_{l_{max}}$ vs δ_N , it is necessary to establish a standard for the base profile $C_{l_{max}}$. In the case of the round-nosed profiles, which often encounter closely pure trailing-edge stall, it is almost necessary, so as to be consistent with the linear extrapolation predictions, to take this as the base profile $C_{l_{max}}$ where there is <u>no</u> leading-edge flap. These values, for various profiles are shown in Figs. 16 and 17. In that such values are not available for the sharp-nosed profiles, the $C_{l_{max}}$'s shown in Fig. 17 being for a $\delta_N = 0^o$ case, the $\Delta C_{l_{max}}$ for these configurations will be based, in the prediction curve to be discussed in the following paragraphs, upon the base profile $C_{l_{max}}$ when $\delta_N = 0^o$ (Fig. 17). This will not disrupt use of the linear extrapolation method as such sharp-

nosed profiles can seemingly never act at a lift level where pure trailing-edge stall is approached. The rising solid lines of Fig. 121A predict the variation in the $\Delta C_{l_{max}}$ vs δ_N curve in the leading-edge stall regime neglecting the possible occurrence of closely pure trailing-edge stall. The curve for the leading-edge type stalling profiles was obtained from the 64A010 and 63$_1$012 characteristics at least temporarily limiting the application of this curve to R.N. $\cong 6 \times 10^6$, $C_N/C \cong 15\%$, corrected to take premature base profile stall into consideration and considering, insofar as possible, only leading-edge stall prematurity (not trailing-edge stall prematurity). The thin-airfoil stall curve is an uncorrected repeat of the sharp-leading-edge curve of Fig. 116. Stall type may be ascertained from Fig. 18 and those base profiles which show a mixed leading-edge separation-stall pattern (type "B", Fig. 18) can be assumed to have characteristics which lie between the two lines. It might be mentioned that the thin-airfoil stalling 65A006 has characteristics which fall nearly upon the sharp-nose characteristics, both before and after the base $C_{l_{max}}$ correction is applied. Thickness and thickness distribution effects on the slope fall-off for the leading-edge stall type configurations have been assumed to be negligeable, an enforced assumption which may or may not be realistic in relation to the variation shown.

Optimum δ_N, or the maximum $\Delta C_{l_{max}}$, is assumed to occur at 30°, except with very thick profiles. It is possible, if the profile is sufficiently thick, that the flapped configuration's characteristics will have the leading-edge curves prior to the attainment, along the leading-edge stall line, of such an optimum. This would be due to the initiation of

closely pure trailing-edge stall. The $\Delta C_{l_{max}}$ for pure trailing-edge stall may be approximated by adding to the increment predicted by the linear extrapolation method that increment due to effective camber. As previously stated, the camber increment will, based upon combered profile studies, be considerably less than would be predicted through thin airfoil theory. A "guestimate" of the approximate effect of increasing δ_N on a pure trailing-edge stalling profile of C_N/C = 15% is given in Fig. 121 C. The $\Delta C_{l_{max}}$ for the base profile, to which the camber effect must be added, can be considered to be independent of flap extent and may be obtained from Fig. 24 or from the "linear extrapolation" of the profile series in question at the given Reynolds Number (6×10^6, in this case). Fig. 121B demonstrates the appearance of the no-camber $\Delta C_{l_{max}}$ required for attainment of pure trailing-edge stall with 64 series configurations at a Reynolds Number of 6×10^6. The nearly horizontal dashed lines of Fig. 121A represent the sum of these two terms for 64 series profiles at this Reynolds Number and C_N/C = 15%.

For any configuration at this Reynolds Number and of this flap extent, the $\Delta C_{l_{max}}$ variation may be assumed to ride up the leading-edge stall or thin-airfoil stall line (dependent upon base profile stall characteristics) until either the pure trailing-edge stall line is encountered or a δ_N of 30° is attained. For the 64 series configuration it can be seen that the former would be expected to occur for thicknesses greater than approximately 10% while the latter would probably occur for thickness under 10%. If the trailing-edge stall line is not encountered prior to 30°, this value of δ_N indicates the maximum $\Delta C_{l_{max}}$ attainable. If trailing-edge

stall is encountered, $\Delta C_{l_{max}}$ variation follows this curve to optimum δ_N, which might, for the greater thickness, be larger than 30^o. It will be noted that for the 64 series configuration (R.N. = 6×10^6) all configurations of t/c $\geq$ 14% will be expected to have closely the same characteristics, dependent only upon the camber effect. Of course, it is possible that the hinge-line cut-off δ_N may vary, creating greater optimum δ_N's and thus greater $\Delta C_{l_{max}}$'s for very thick profiles as compared with that for the 14% t/c.

It has been noted that for the 64A010 configuration the prematurity of stall created by a forward separation apparently completely discounts any camber effect, $\Delta C_{l_{max}}$ compared with the no-flap profile being approximately .45 from the experimental data. Such prematurity of trailing-edge stall may be expected to decrease the level of the pure trailing-edge stall line by an amount which is greater the thinner the profile. For instance, the 12% profile shown here probably, because of its thickness, has little prematurity of trailing-edge stall and hence a level more readily amenable to such a method of prediction.

The leading-edge and hinge-line stall lines (undashed) of Fig. 12IA should be valid for configurations at Reynolds Numbers close to 6×10^6 and with C_N/C = 15%. These curves have been assumed to be essentially independent of profile series. The trailing-edge stall line is, however, a function of profile series. Variation from a given profile series is felt definitely to effect the trailing-edge stall lines much more than the leading-edge, although, in the final analysis, trailing-edge stall prematurity may in some cases completely cloud the effect of profile series.

In the same way, using two curves to take into account differences in leading-edge stall type might well, for prediction purposes, be splitting hairs. This is particularly true if variations due to leading-edge stall prematurity are larger than expected. A poorly designed flap-wing juncture or, to a lesser extent, location of the hinge at any point other than the lower surface (assumed in this analysis) could also alter the situation considerably. Thus, Fig. 121A does not purport to yield extremely accurate data but does reveal the expected trends and, it is thought, gives as close a prediction as is possible considering the dearth of systematic experimental work.

Fig. 121A demonstrates the nature of the constant Reynolds Number, constant C_N/C case, and attempts to predict $\Delta\ C_{l_{max}}$ attainable when R.N. $\cong 6 \times 10^6$ and $C_N/C \cong 15\%$. It says nothing, however, concerning the effects of Reynolds Number or flap extent variations. Reynolds Numbers effects would be expected to be quite important with regard to the characteristics of any control with the basic function of delaying or eliminating leading-edge separation. Decreasing Reynolds Number, from Section 3.1, would be expected to have the same general effects as decreasing profile thickness or leading-edge radius. Stall would tend away from the leading-edge type and toward the thin-airfoil. Due to the variable Reynolds Number effects upon trailing-edge stall implied by the linear extrapolation method, however, stall-pattern progression could not be expected to be the same as shown, for the case of thickness, in Fig. 119.

Figs. 122 and 123 present the totality of information available for profiles with contoured leading-edge flaps tested throughout a series of

Reynolds Numbers. Deflected flap data for the sharp leading-edged profiles of Fig. 122 and the 65A006 (Fig. 123) covers only the case of combined leading-edge and trailing-edge flap deflections. However, in that the base profile as well as the flap-deflected data shows a near invariance with Reynolds Number for these thin-airfoil type stalling configurations, it should be safe to say that Reynolds Number effects upon the sharp-nosed configuration are negligible for all values of leading-edge flap deflection.

The 64A010 configuration shows characteristics which vary considerably with Reynolds Number. The $\Delta C_{l_{max}}$, whether based upon the $\delta_N = 0^o$ case or the no-flap (dashed line) case, demonstrates variations nearly as large as $C_{l_{max}}$ variations, particularly at high deflection values. Possible Reynolds Number effects upon the leading-edge stall line of Fig. 121 are extremely clouded, again because of the apparent prematurity of base profile stall, as well as the lack of base (no flap) data for the lower Reynolds Numbers. Basing $\Delta C_{l_{max}}$ upon the no-flap profile (dashed line Fig. 122), correlation at all but the higher Reynolds Numbers with the R.N. $\cong 6 \times 10^6$ curve of Fig. 121 seems reasonably good. The same can be said for the low Reynolds Number data given in Ref. 84. It would thus be thought that, for prediction purposes, the thin-airfoil and leading-edge lines of Fig. 121 can be taken to hold good for all Reynolds Numbers. The very small amount of data upon which this assumption is based should, however, be borne in mind, and exacting accuracy should not be expected.

The fall-off in $\Delta C_{l_{max}}$, even at low values of δ_N, at the higher Reynolds Numbers is felt to be attributable to the advent of trailing-edge stall. Fig. 123 compares the variation of the $C_{l_{max}}$ required for trailing-

edge stall, as obtained from the linear extrapolation method (64 series) with Reynolds Number and the $C_{l_{max}}$ attainable at a $\delta_N' = 30^\circ$ for the 64A010 also vs Reynolds Number. There appears here to be an unusually good correlation. As stated previously, such correlation is, to a certain extent, happenstance because the linear extrapolation method as used does not consider either camber effect or the reverse trend of stall prematurity due to leading-edge separation. However, some corroboration of the linear extrapolation method is seen in such a curve.

Fig. 125 demonstrates the effect of Reynolds Number upon trailing-edge stall, from the linear extrapolation method, for 63 and 65 series profiles as compared with the data points available for the 63|012 and 65A006 configurations at $\delta_N = 30^\circ$. The 63|012 has a greater than predicted value due to the camber effect and relative absence of any stall prematurity while the 65A006 attains a much lower lift because, due to its thinness, it cannot approach the pure trailing-edge stall condition.

For the 64A010 configuration at all Reynolds Numbers, it can be seen that, as the linear extrapolation method correlates almost exactly, the camber effect must be opposed by a closely equal effect of stall prematurity. This counteracting effect must be considered in applying the trailing-edge stalling curves, at the Reynolds Number in question, as shown in Fig. 121. Unfortunately, all that can be said regarding this phenomenon is that trailing-edge stall prematurity can reduce the $\Delta C_{l_{max}}$ for trailing-edge stall by as much as 0.1. Also, stall prematurity will be most severe for profiles of lesser thickness, reducing to zero for the thicker profiles which show the least $\Delta C_{l_{max}}$ attainable.

Although the $C_{l_{max}}$ with flap at the lower Reynolds Numbers appears to fall-off (Fig. 124), this is not felt to be true of $\Delta C_{l_{max}}$, assuming a rapidly decreasing (with Reynolds Number) base profile $C_{l_{max}}$ in this regime. There is an indication that, at this low Reynolds Number, optimum δ_N can increase beyond 30°. The mechanism by which this is accomplished is not understood, and, in fact, very low Reynolds Number work done at Princeton showed no such tendency.

The important indication obtained from the Reynolds Number studies is that increasing the Reynolds Number of round-nosed profiles can decrease the $\Delta C_{l_{max}}$ attainable through the use of the contoured leading-edge flap. Section 3.1 (Fig.s 22 to 25) demonstrate that, according to the linear extrapolation method, increasing Reynolds Number decreases the thickness for which lift increment due to the prevention of leading-edge stall goes to zero. For such thicknesses and greater, the only $\Delta C_{l_{max}}$ attainable will be that due to camber effect, which is of negligible value. Thus low speed wind tunnel tests should not be expected to yield accurate flight prediction for leading-edge flapped configurations of 8% to 14% thickness. Relatively thin sharp-nosed configurations and round-nosed configurations under 6% in thickness would however be thought to be amenable to such an approach so long as flight Reynolds Number is under approximately 15×10^6.

The effect of chordwise flap extent has only been treated in one reference using only one profile and Reynolds Number and, as a consequence, little can be said regarding the many cross effects. Fig. 126 demonstrates the results of the studies described in Ref. 76. It will be noted that, for this configuration, increases in flap chordwise extent serves to increase $\Delta C_{l_{max}}$.

This effect is more pronounced the greater the flap deflection until a deflection of greater than 20° is obtained, after which this secondary effect diminishes.

The major cause for this trend is felt to be "camber effect". Theoretical considerations show that camber is more effective as it is moved aft from the profile nose; and, it must be remembered, that a portion, though only a portion, of the lift increase caused by a leading-edge flap, even in the leading-edge stalling regime, can be attributed to camber. (See the camber studies of Section 3.1). Of course, full theoretical circulation cannot be achieved due to the adverse effect of camber on trailing-edge stall. However, a comparison between the data given in Fig. 126 and the camber effect estimated in Fig. 121C reveals a correlation in keeping with the expected effect of moving the point of maximum camber aft.

The fall-off where δ_N is increased beyond 20° is difficult to explain, but is probably phenomena created through premature trailing-edge separation, such prematurity initiating either through a leading-edge bubble, the adverse effect of camber, or both. Optimum δ_N holds at slightly greater than 30° for all flap extents tested.

If the effect of flap extent can indeed be attributed to the camber effect or circulation, it would be expected that the curves of Fig. 126 will closely hold at all Reynolds Numbers and for all thicknesses. In the absence of additional data such must be assumed, at least for δ_N's up to 20°.

The leading-edge flap would become the equivalent of a trailing-edge flap if the hinge-line were moved sufficiently aft. Here optimum δ_N (or, in this case, δ_F) can increase to greater than 60° and, judging from

test data, $\Delta C_{l_{max}}$ will be greater at all profile thicknesses and Reynolds Numbers than could be possible with the usual leading-edge flap. This superiority in lifting capability shown by the trailing-edge flap is considerably greater for profile thicknesses where the base profile stalls from the trailing-edge. Although the trailing-edge flap looks, on the surface, to be the "best leading-edge flap", it must be remembered that there is such a thing as pitching moment, and, further, that a leading-edge flap can be of considerable value in conjunction with a trailing-edge circulation control.

For prediction purposes, it would seem reasonable to use Fig. 126 additively with Fig. 121A in the leading-edge stalling regime. For trailing-edge stall, it is possible that the values shown in Fig. 126 for δ_N's greater than 20° are misleadingly low.

Little could be gained, in predicting Reynolds Number effect and the effect of flap extent, to become as deeply involved as in the presentation of the thickness effect. The apparent flow mechanisms were outlined for the thickness effect on the basis of logic and a reasonable amount of experimental data. Here, consideration of all the many variables would, in the rather shocking absence of experimental data, only lead to undue rationalization.

Fig. 127 shows the $\Delta C_{l_{max}}$ attainable through use of contoured leading-edge flaps. In contrast to Fig. 121, this plot considers probable C_N/C effects and the estimated effects of Reynolds Number. Fig. 127 is intended to serve either of two purposes; (1) to indicate the trends which might be of importance in pre-design investigations and, (2) to predict as closely as possible, under the limitations of existing knowledge, the

$\Delta C_{l_{max}}$ attainable for a given configuration under given free-stream conditions. Because of this dual purpose, these curves infer a greater accuracy than is probably the case. The many conflicting phenomena involved and the low magnitudes of $\Delta C_{l_{max}}$ which must be dealt with make truly accurate prediction impossible, but do permit evaluation of the trends.

The $\Delta C_{l_{max}}$ shown for this figure is based upon the characteristics of the no-flap base profile. Such characteristics may be found from Fig. 16 and 17, Refs. 9, 21, 22, 23, or 24, or from tunnel tests. If it is desired to use $\delta_N = 0^o$ as a base, the difference in base profile $C_{l_{max}}$ between these two cases should, if large, be taken into account.

Although taking base profile stall type into consideration for the prediction of the leading-edge stall line probably exceeds the accuracy of Fig. 127 when it is used for prediction purposes, this information may be estimated from Fig. 18. The effect of C_N/C may be determined from Fig. 126. The leading-edge stall line may then be defined.

The trailing-edge stall line may be defined through use of the linear extrapolation method. The $\Delta C_{l_{max}}$ predicted by this method is given vs thickness for various Reynolds Numbers and profile series in Figs. 24 and 25. To the quantity obtained here, values must be added for the camber effect and subtracted for the effect of trailing-edge stall prematurity. The camber effect has been estimated in Fig. 127B through cambered profile considerations and the information of Fig. 126. Rather arbitrarily, and based only upon the limited experimental information available, the effect of trailing-edge stall prematurity is assumed to reduce $\Delta C_{l_{max}}$, as estimated from the linear-extrapolation method plus the camber effect, by

0.10 at a δ_N of 30° where the previously estimated $\Delta C_{l_{max}}$ is greater than 0.40. If the previous $\Delta C_{l_{max}}$ is less than 0.40, there is assumed to be no stall prematurity. After adding the linear extrapolation result, the camber effect, and the prematurity effect, this trailing-edge stall curve may be superimposed upon the previously defined leading-edge stall line. If the trailing-edge stall line crosses the leading-edge line, it, the trailing-edge line, will establish $\Delta C_{l_{max}}$ for δ_N's greater than that at cross-over and less than that for hinge-line stall.

Hinge-line stall (or rather, optimum δ_N) occurs along the $\delta_N = 30°$ line except for the thicker trailing-edge stalling profiles which may have characteristics continuing out along the trailing-edge stall line to flap deflections as great as 45°.

Although many of the effects here considered may be disregarded for normal prediction work, the general trends due to the advent of trailing-edge stall are felt to be quite important and should not be neglected.

Fig. 106 illustrates three additional types of leading-edge flap: the Krüger flap, the N.A.C.A. upper-surface leading-edge flap, and the N.A.C.A. lower-surface leading-edge flap. These three controls may be described as "extensible" leading-edge flaps, as each provides a means of increasing wing area while flap deflection is taking place. Their relationship to the "contoured" leading-edge flap is thus somewhat analogous to that of the Fowler flap to the plain trailing-edge flap.

The three extensible leading-edge flaps differ in the manner in which flap deflection and the resulting chord extension is brought about. The Krüger flap, provides a flap hinge at the profile leading-edge, the flap

upper-surface being of a camber indentical to that of the portion of the profile lower-surface into which it must retract when not in use. The N.A.C.A. lower-surface flap operates in a manner similar to the Kruger flap, but here the flap hinge, rather than being at the profile leading-edge, is located somewhat beneath the profile's nose on the lower surface. As opposed to the hinged geometry of the other two flaps, the N.A.C.A. upper-surface leading-edge flap provides a sliding flap, which, when not in use, forms the profile nose and the most forward portion of the profile upper-surface. While the Krüger and lower-surface flaps provide for nearly 180° of flap deflection, the upper-surface flap is pretty much limited to one deflection value for any one extension setting, this deflection being a function of the radius of curvature provided for the sliding action. Of course, for a given thin profile, this system permits only slight chord extension for high deflection values or very limited deflection for large values of chord extension. It will be noted that all the extensible flaps shown in Fig. 106 are provided with a bulb-like leading-edge as the majority of tests described in the literature make use of this device. Extensible leading-edge flaps are treated in Refs. 72, 88, 91, 92, and 93. Fig. 128 demonstrates the notation which will be used to describe extensible flap geometry in this report.

The characteristics of the extensible flap should differ from contour-flap characteristics by virtue of the chord extension and also because the flap leading-edge radius no longer need be identical to that for the base profile. Thus it would be expected that the extensible flap could be designed to produce greater lift increments and also, because of the forward

chord extension, to create a more favorable pitching moment situation. The general flow mechanisms discussed for the contoured flap configuration should still hold, however, for the extensible versions.

Fig. 129 shows test results of $\Delta C_{l_{max}}$ vs flap deflection for five configurations utilizing extensible leading-edge flaps. All three extensible flap types are represented here and flap extent is .10c for each case. Reynolds Number and flap bulb size are, however, variable. It should be here pointed out that the selected notation reveals for the hinges flaps a δ_N of closely 180° when the flap is in the retracted position. Hence, for the lower-surface and Krüger flaps, increasing deflection with the retracted position as base will decrease δ_N from 180° until, at zero degrees, the flap is extended directly forward from the profile leading-edge. Because of under-surface spoiling and a resultant negative effective camber, $C_{l_{max}}$ can be seen from this figure to actually decrease for such flap types until $\delta_N \cong 90°$. As the flap is further deflected (decreasing δ_N) maximum lift proceeds to increase, and only at nominal δ_N's beneath 70° does such a flap become a lift increasing device with respect to the base profile. Between $\delta_N = 0°$ and $\delta_N = 70°$ it would be thought that these configurations would have the same general characteristics and show the same separation-stall phenomena as the contoured flap. Unfortunately, no data exists for either the Krüger or lower-surface flaps at δ_N's of less than 40°. Stall is suspected, for the configurations shown, to be of the laminar type and to occur from the <u>base</u> profile leading-edge for all δ_N's greater than approximately 50°. In that this type of stall corresponds physically to the hinge-line stall which finally limits $\Delta C_{l_{max}}$ for

contour-flapped configurations, Fig. 129 gives some insight into the trends which contour-flap maximum lift would take if δ_N were permitted to increase beyond the values considered in that discussion. The initial lift loss achieved in deflecting the hinged type of extensible flap may be an important consideration in determining the feasibility of applying such a system.

The apparent optimum δ_N for the cases shown in Fig. 129 is between 45° and 60°. It is felt that this comparitively large optimum deflection may be somewhat misleading, probably being an effect of low Reynolds Number at least for the Krüger flap cases. For the configuration with the lower-surface flap this large apparent optimum deflection value is difficult to explain, the effect of the profile overhang being almost impossible to analyze with such limited experimental data. The probable explanation in this case is that the stall shown is actually a secondary stall, with no data taken at sufficiently low δ_N's to define the primary stall.

The lower surface flap would be expected to reveal an early primary stall, and lift increases through deflection of this device should be quite small. The reason for these effects is the overhanging profile nose which will cause very early separation compared with the other flap types under discussion. Fig. 129 reveals considerably more potentiality for the upper-surface flap than for the lower surface. Here there is no sharp break at the upper portion of the flap and the flow is not forced through nearly so large an adverse pressure gradient.

Available data for configurations fitted with the Krüger flap indicate that it is as effective as the upper-surface flap. This should certainly be

the case, as these two flaps differ only in mechanical operation and cannot be distinguished aerodynamically. It will be noted that, with the 2315 BIS profile, the Krüger flap yields a greater $\Delta C_{l_{max}}$ where the D/C = .024 than where D/C = .008. This is felt to be indicative of leading-edge (or thin-airfoil) stall being the limiting phenomena at all δ_N's prior to the advent of hinge-line stall. Certainly, bulb size would create such an effect if this were the case, while, if trailing-edge stall governed lifting capabilities at the lower δ_N's , such an effect would not be expected.

Trailing-edge stall is possibly present at low δ_N's for the "changed" Mustang configuration. The thick section and higher Reynolds Number would be capable of creating this stall type and the comparatively low maximum $\Delta C_{l_{max}}$ in combination with a fairly large bulb would indicate the possibility of such separation phenomena. Of course, the rapid lift fall-off shown in decreasing δ_N beneath the apparent optimum would seem to weaken this interpretation.

Fig. 130 demonstrates the effect of flap extent and bulb size (D/C) upon the lift increasing capabilities of the 2315B IS profile. An increase in c_N/c results in a larger lift loss in the high δ_N range while seemingly lowering the optimum δ_N . Increases in c_N/c at constant D/C yield an increase in $\Delta C_{l_{max}}$ at the apparent optimum δ_N , while increased D/C also increases $\Delta C_{l_{max}}$, most noticeably at the apparent optimum flap deflection. Fig. 131 demonstrates the latter trends somewhat more clearly. It can be seen here, however, that, when D/C is greater than $\cong$ .04, $\Delta C_{l_{max}}$ may level or fall-off. Again, this increase in lifting potential with increases in D/C may be attributed to the effect of the

larger bulb size permitting the forward stagnation point to move further around the bulb prior to initiation of separation. C_N/C effect may be seen to be in keeping with the order of magnitude described for the contoured flap (high δ_N) and thus may be attributed to the increase in effective camber created by moving the hinge line proportionately aft. Of course the increase in chord created by such chord extensions has some additional and additive effect.

Krüger (Ref. 88) plotted the data available to him and produced the curve of Fig. 132. Although, to the extent that it indicates the ineffectiveness of such a device for use with thick profiles, this plot does show a realistic trend, it does not maintain a constant D/C and permits rather large Reynolds Number variation. Plotting additional data on the same graph, as has been done in Fig. 132, shows Krüger's curve to be an oversimplification. In fact, had he chosen a D/C of other than .024 for the 2315 BIS profile (see Fig. 131), his curve would have been altered considerably. It is strongly felt that D/C, C_N/C , and Reynolds Number as well as profile thickness and shape are important variables and must be considered in any prediction of the extensible flap's effectiveness in increasing maximum lift beyond that attainable by the base profile.

Although little data exists, it is possible to at least qualitatively predict the effects of the several variables in the range from $\delta_N = 0^o$ to δ_N = optimum. Beyond this, ie., in the range where the Krüger type of flap operates when being deflected, it must suffice to say that maximum lift will be decreased beneath that for the base profile, this effect being greater the greater the flap extent. Only immediately prior to the attainment of optimum δ_N will the lift increment become positive.

The extensible flap case differs from that of the contour flap's by virtue of (1) the extension of the physical chord and (2) the possibility, with extensible flaps, of placing almost any sized bulb on the flap leading-edge, thus making the flap leading-edge radius capable of being considerably different from the profile leading-edge radius. Because of this latter variable, the approach here, for qualitatively predicting the $\Delta C_{l_{max}}$ created by any leading-edge flap in the low δ_N range, will be based upon the concept of an equivalent profile, this profile being that which is produced if the flap is permitted to be deflected to a position where $\delta_N = 0^o$; that is, where the flap leading-edge lies upon the base profile's chord line.

This equivalent profile will be of considerably different section, the characteristics of which are not readily ascertainable without resorting to experimentation. However, if only leading-edge stall is considered, it may be possible, from such a concept, to demonstrate the low-deflection trends in $\Delta C_{l_{max}}$. It will be assumed for the time being that no trailing-edge stall may occur and that leading-edge radius may replace profile thickness and thickness distribution in determining leading-edge stall characteristics. Were this the case, it might be said that when the bulb diameter is made closely equal to the diameter of the base profile leading-edge, the maximum lift coefficients of the two profiles-base and equivalent-would be closely equal. If lift coefficient were based on the base profile chord, the equivalent profile with $\frac{D}{C+C_N} \simeq \frac{2r}{C}$ (see Fig. 128) would yield a $\Delta C_{l_{max}}$ equal to the chord extension effect:

$$\Delta C_{\ell_{MAX}} = C_{\ell_{MAX}} \times C_N/C$$

It might be observed that base profile stall prematurity should not enter into this problem as the base and equivalent profiles would experience closely equal difficulties along this line. The concept of equivalence of radii here presented is highly qualitative, taking profile shape completely out of the picture.

Using this concept as a datum for the $\sigma_N = 0^o$ case, it is obvious, considering the mechanism of leading-edge stall, that increases in D/C beyond that equal to 2r/c will increase $\Delta C_{l_{max}}$ while decreases in D/C will decrease $\Delta C_{l_{max}}$. There of course might come a time where increases in D/C can do no further good, but this would be thought to be a matter involving the occurrence of trailing-edge stall which is currently being neglected. Whether, at $\sigma_N = 0^o$, $\Delta C_{l_{max}}$ (with respect to the base profile) becomes negative is a matter of profile leading-edge radius and shape, D/C, and C_N/C. However it is quite possible with sufficiently low D/C for this to occur.

It is thus obvious that increases in base profile thickness can cause severe diminishing in the $\Delta C_{l_{max}}$ provided by a bulb of fixed D/C even where $\sigma_N = 0^o$. Reference 85 treats the effects of leading-edge bulbs upon profile lifting characteristics and it is interesting to note that such bulbs even at zero flap deflection, can be as effective as a contoured leading-edge flap in increasing the profile's maximum lift. This is not surprising considering the primary function of both devices is to delay or prevent leading-edge stall.

Still assuming that trailing-edge separation will not occur, it is of some interest to speculate upon the appearance of the $\Delta C_{l_{max}}$ vs δ_N curve for the extensible flap case when δ_N is between zero and optimum. Although the origin ($\delta_N = 0^o$) of such a curve will depend upon C_N/C, D/C, and base profile thickness, it is felt that its slope will depend for the most part only on C_N/C. This effect will cause increased slope with increased C_N/C by virtue of the greater circulation provided and will not include chord extension as this has been already accounted for at $\delta_N = 0^o$. For this reason, the slope of the $\Delta C_{l_{max}}$ vs δ_N curve may be estimated from the contoured flap work. Fig. 133 illustrates the probable appearance of the low - δ_N portion of the $\Delta C_{l_{max}}$ vs deflection curve for such flaps, based upon this discussion.

The occurrence of trailing-edge stall and the effects of trailing-edge separation on the leading-edge stall pattern discussed above is somewhat difficult to predict. This is because trailing-edge stall characteristics will be altered by the chord extension and the bulb. The "equivalent" profile thus may have considerably different characteristics than the base, and its linear extrapolation is difficult to ascertain. From information included in Ref. 85, it may be inferred that the combination of a very large D/C and a small C_N/C will alter profile shape so as to raise the lift level of the linear extrapolation. Also, such a flap can change the stall pattern for the $\delta_N = 0^o$ case from leading-edge to trailing-edge. Of course, the extensible flap with a D/C small in comparison with the diameter of the base profile's leading-edge and with a large C_N/C would probably lower the lift level of the linear extrapolation and, if applied to a trailing-edge

stalling profile, could alter the $\delta_N = 0^o$ stall type to leading-edge. Therefore the trailing-edge stall pattern should be established for the equivalent profile rather than the base. This would probably be best done through comparing the equivalent profile (discounting the under-surface cutout) with known profile series in an attempt to find correspondence of the term D/C divided by $2\left[\frac{t}{c+c_N}\right]$, with the term, r/c divided by $(t/c_{max})^2$ and point of maximum thickness. The corresponding profile series' linear extrapolation would then be used to determine the occurrence of trailing-edge stall. It can also be seen that the profile which most nearly corresponds to the equivalent profile may be used to determine the equivalent profiles' $C_{l_{max}}$ at zero δ_N. The $\Delta C_{l_{max}}$, with respect to the base profile, for the $\delta_N = 0^o$ case may thus be obtained after correction is made for chord extension. Of course, data for a profile series of which the equivalent profile could be a member may very likely not exist and the assumption of no effect of under-surface cutout will be somewhat invalid for many bulb sizes unless the bulb is made to fair, in a reasonably flat curve, into the flap lower-surface. However, such an approach as presented here seems currently the only way to semi-quantitatively indicate the suspected trends.

For quantitative prediction, the following procedure is suggested for the estimation of $\Delta C_{l_{max}}$ due to extensible flaps.

(1) Determine the $D/C/(t/c_{max})^2$ and point of max. t/c for the equivalent profile (the new profile with $\delta_N = 0^o$ - flap straight forward)

(2) Find a profile and profile series of known characteristics or estimate (through interpolation) such characteristics ($C_{l_{max}}$ vs t/c) where:

(a) $\frac{r/c}{(t/c)_{MAX}} \cong \frac{D/c}{2\left[\frac{t}{c+c_N}\right]_{equiv.\ profile}}$ (for series and profile)

(b) $t/c \cong \frac{t}{(c+c_N)_{equiv.\ profile}}$ (for profile)

(c) Point of max t/c $\cong$ Point of max t/c for equiv. profile

(Use of sharp leading-edge, 00 series, and 63 series data for interpolation purposes may be helpful - Point of max. thickness should not be too important in step 3 so long as stall is of the leading-edge type)

(3) Estimate the corresponding profile's $C_{l_{max}}$ at the given Reynolds Number. Assume $C_{l_{max}}$ of the equivalent profile to be the same. Find the $\Delta C_{l_{max}}$ given by the flap at $\delta_N = 0^o$ by the formula:

$$\Delta C_{l_{MAX}} = \left(C_{l_{MAX.\ \substack{equiv \\ profile}}} \times \frac{C_N + C}{C} \right) - C_{l_{MAX.\ \substack{base \\ profile}}}$$

(4) Knowing $C_N/(C_N + C)$, determine $\Delta C_{l_{max}}$ due to δ_N for leading-edge (or thin airfoil) stall from the leading-edge stall curve of Fig. 127. (Remember $C_N/(C_N + C)$ should be used as C_N/C in this step)

(5) Ascertain the linear extrapolation $\Delta C_{l_{max}}$ for trailing-edge stall from information, at the given Reynolds Number, obtained from the profile series which most closely conforms geometrically to the equivalent profile (use $t/c = \frac{t}{c+c_N}$ for equiv. profile).

(6) Determine the effect of δ_N by procedure outlined in Fig. 127.

(7) Add $\Delta C_{l_{max}}$ for $\delta_N = 0^o$ (step 3) and that for the δ_N effect (step 6). Use hinge-line cut-off shown in Fig. 127.

Again, as was the case with the contoured flap predictions, the tedious method seems unjustified considering its probable inaccuracies, but does, it is thought, provide a means of ascertaining the more pertinent probable

alterations in characteristics created by changes in configuration and free stream conditions.

Although only optimums are given, Fig. 131 and 132 may be seen to qualitatively verify the trends indicated in the foregoing discussion at least as regards the effect of C_N/C and D/C. Fig. 131 illustrates, however, that, for the practical case, Fig. 133 exaggerates the effect of D/C as compared with the C_N/C effect.

Thus increased D/C and C_N/C seem to generally increase $\Delta C_{l_{max}}$ attainable through the use of extensible flaps. There should be no reason to provide D/C $< \frac{2r}{c}$, although too large a D/C may actually be deleterious regarding the advent of trailing-edge stall as well as being geometrically impractical. Excessive C_N/C may also create premature trailing-edge stall and would in most cases be impractical. D/C's of up to 6% should normally prove helpful (especially with fairing aft of the bulb-see Ref. 85) while C_N/C's to at least 15% would seem advantageous. A given relatively large D/C will provide greater $\Delta C_{l_{max}}$ for thinner profiles, the leading-edge, and probably the trailing-edge, stall being delayed compared with the base profile. For the thick, trailing-edge stalling base profile the only gains are through some trailing-edge stall delay, the camber effect and chord extension. It might be pointed out that, for a leading-edge stalling base profile, increases in D/C beyond that $\simeq \frac{2r}{c}$ should delay both leading-edge and trailing-edge stall in such a way that trailing-edge stall initiates at a lower δ_N the greater the D/C, until it finally occurs at $\delta_N = 0^o$. The concept of increased leading-edge radius delaying trailing-edge stall is a calculated speculation based upon limited

profile studies and the results of Ref. 85. This concept is certainly not without its limitations and probably when D/C is increased to the order of t/c_{max} it will no longer hold good because of the long adverse pressure gradient established at any positive angle of attack. The effect of Reynolds Number increases upon $\Delta C_{l_{max}}$ should, as with the contoured flap, decrease the $\Delta C_{l_{max}}$ attainable for leading-edge stalling profiles. Also, the range of profile thicknesses where such a flap is really worthwhile (the leading-edge stalling regime) is reduced with increased Reynolds Number in exactly the same degree as was the contoured flap case. If a profile is already stalling from the trailing-edge, a trailing-edge control (not necessarily <u>at</u> the trailing-edge) must be installed. Only the, when leading-edge stall is established, will the leading-edge flap be of real use for such thick profiles.

In that the extensible flap provides a means of altering leading-edge radius and gives increased chord extent in addition to the deflection effect, it would seem logical that it could provide greater $\Delta C_{l_{max}}$ than the contoured flap. This should be especially true for the thinner profiles where increases in D/C might well be able to prevent nearly all leading-edge stall and provide $\Delta C_{l_{max}}$'s close to that predicted by the linear extrapolation method. For thicker profiles the chord extension and trailing-edge stall delay will give lift a boost. <u>Very</u> thin profiles may not achieve the $\Delta C_{l_{max}}$'s of the profiles with intermediate t/c due to probable ineffectiveness of permittable increases in D/C. The Krüger and upper surface flaps should be more effective than the lower surface flap as it initiates considerable trouble from the hinge-line. Only where $\delta_N \rightarrow 0^\circ$

will it be comparable with the other two types.

Considering the angle of attack for zero lift and lift curve slope for extensible flaps, it is felt that Fig. 111 and 112 will closely retain their accuracy, although the base profile lift curve slope should be raised by an amount, C_N/C.

3.3c Leading-Edge Boundary Layer Control Devices

The leading-edge flap has been shown to delay leading-edge separation by altering the profile geometry in such a manner as to alleviate the pressure peak which would normally cause premature flow detachment. It has been found that separation may also be delayed by energizing the boundary layer, the separation producing pressure peak being permitted to attain what would otherwise (no energy addition) be a stall-inducing magnitude. There, thus, are two methods by which the leading-edge separation can be delayed or prevented:

(1) by reducing the magnitude of the pressure peak and the resultant adverse pressure gradient, or,

(2) by energizing the boundary layer so that it may remain attached even under the influence of large adverse gradients.

This second method, as was the case with powered trailing edge flaps, can be achieved by either blowing or suction and may as in the case of hinge-line control for nose flaps, be used in conjunction with the first method. It is obvious that any "natural" method such as directing high pressure lower-surface air into the upper-surface boundary layer (a slot or slat system) can, at best, be of only limited effectiveness. For this reason, powered systems have been investigated as a means of attacking the problem of leading-edge

separation control. This section will consider the effectiveness of both the "natural" systems and the powered arrangements.

Considerable investigation has been made since the late 1930's, particularly by the NACA, of the value of leading-edge slats and slots as high lift devices. They are used as a boundary layer device to increase maximum lift and lift-drag ratio at high lifts, and to improve lateral stability and control at high angles of attack by delaying stall over the outer portions of the wings and ailerons.

By definition, a slat creates a slot, or gap, between the trailing-edge of the slat and the leading-edge of the wing. Thus, when one is discussing a fixed slat, the configuration is the same as a wing slot and vice-versa, but obviously with a fixed slat one must use the leading-edge of the slat in determining the chord length in order to avoid misinterpretation of the lift coefficient definition.

Whether a leading edge flap or a slat is superior is a question that may not be totally answered by aerodynamic reasons, but by mechanical problems which will not be dealt with here. Often for a small slat it has been found to be used most effectively in a position which makes it practically a leading-edge flap. With the larger slats it is likely that a good amount of the so-called increase in maximum lift coefficient can be traced not only to increased efficiency of the system due to boundary layer control but also to an effective increase in the wing area forward in much the same way that a Fowler flap or certain double slotted flaps extend the effective wing area to the rear. It is obvious that, aerodynamically, a device that thus increases the wing area forward during crucial periods of flight when high

lift is required will be very desirable, since as well as obtaining more lift by itself, it should tend to give nose up moments at the same time that flaps at the trailing-edge are in all probability being extended and deflected to give severe nose down moments. However, the mechanical difficulties of extending large heavy slats could be as great as extending trailing-edge flaps without nearly the same increase in lift coefficient as obtained with trailing-edge flaps, especially of the double slotted type. Just where the "break-even" point is from design to design will have to be determined by the aerodynamicist and mechanical engineer working together.

The arguments for a fixed slat (or slot) would seem quite small on modern wings if a proper wing section and airplane design have been used. However, it might be useful over part of the span to "fix" undesirable stalling characteristics, particularly on relatively low speed aircraft when it is not desired to pay the weight penalty necessary to make the slat movable. The "automatic slat" i.e., the slot which automatically extends when a certain leading-edge pressure distribution corresponding to a given lift coefficient is achieved is an idea which at certain times may represent a suitable compromise having both advantages and disadvantages, but usually sacrificing a bit aerodynamically to obtain better operation.

The British have conducted wind tunnel tests, most of them on thick cambered airfoil sections with considerable upper surface curvature towards the leading-edge, Ref. 105 with slat chords of 10%, 20% and 30%. The lift coefficient measurements were made at Reynolds Numbers of 0.62×10^6 to 0.94×10^6, and occasionally with a 60° split flap. The latter had no effect due to an increase of the Reynolds Number from 0.62×10^6 to $0.94 \times$

10^6, but with the flap closed an increase in $C_{l_{max}}$ resulted with increasing Reynolds Number.

The best forward extension was found to be 15.3% chord for the 20% chord slat and 23% chord for the 30% chord slat. In contrast, however, as the forward extension of the 10% chord slat was reduced, an additional region of high $C_{l_{max}}$ appeared at a forward extension of 3% chord. This occurred at large values of the slat dip and with small gaps. The gap became zero and the highest $C_{l_{max}}$ for this slat was given when it acted as a nose flap ($C_{l_{max}}$ = 1.335). It appears that on a symmetrical thin wing there is a big advantage in using the small chord slat as a turned-down nose to give the equivalent of camber. However, this moves the no-lift angle to a more positive value, decreasing the lift at a given pre-stall incidence. To get a good slot shape on the flatter wing surface with the larger slats, the slat must be at a shallower angle than with more cambered sections, making the forward extension greater.

Generally, it seemed that a split flap with a 10% slat extended yielded greater $\Delta C_{l_{max}}$ than with the same flap and slats of larger chord. On the EQ 1040 profile a small gap increase (about 0.5% wing chord) was indicated when the flap was used. (Which does not seem to agree with NACA results below.) Unless we are to question the data, this would seem to be an excellent indication of how sensitive slats are to wing design and slat design not to mention Reynolds Number effects on the slot.

As a first approximation the following "rule-of-thumb" rules for slot design are given (Ref. 105):

(1) Slat chord: 12 1/2 per cent wing chord for wing thickness ratios up to 10 per cent and equal to the thickness ratio plus 2 1/2 per cent for wings of greater thickness.

(2) Forward Extension: at least 60 per cent slat chord.

(3) Dip: 25 per cent of forward extension.

(4) Gap: 2.4 per cent wing chord for wing thickness ratios up to 6 per cent increasing by 0.3 per cent for every 2 per cent increase in wing thickness.

(5) W (defined in Fig. 134): 2 per cent wing chord, increasing slightly for thick wings.

In experiments at Langley Field (Ref. 104) optimum slat positions, with split flaps deflected at 60°, were determined at a Reynolds Number of 2.0×10^6. Tests were run at Reynolds Numbers between 2.0×10^6 and 9.0×10^6 with a 14% chord leading-edge slat and a 20% chord split trailing-edge flap. It was found that the increase in $C_{l_{max}}$ caused by the slat and flap was approximately equal to the sum of the increments produced individually. Extension of the leading-edge or an increase in Reynolds Number with slats caused the stall to become more gradual. Extension of the flap caused the aerodynamic center to move forward to a point approximately equal to the quarter-chord point of the extended chord. Deflection of the split flap on a 641-212 airfoil section changed optimum slat location so that a smaller slot was required between the slat trailing edge and the main part of the airfoil section. This latter result is exactly the opposite of the British findings indicated above, but seems to agree with other NACA results below.

Considerably earlier tests had been made at Langley (Ref. 96) on a NACA 23012 airfoil with fixed wing slot (or fixed slat depending upon definition). It was found that the slat chord and slot gap and width are the only slat parameters which will appreciably affect $C_{l_{max}}$ and section angle of attack at $C_{l_{max}}$. A slat chord of about 15% was found to be the optimum, and a slot gap of about 3% or 4% chord the optimum, the larger number with a smaller flap deflection.

In more recent investigations at Ames Aeronautical Laboratory (Ref. 83) which like the other referenced studies in this section were made in a two-dimensional wind tunnel, tests were conducted with an NACA 64A010 airfoil equipped with various combinations of a leading-edge slat, leading edge flap, split flap, and a double-slotted flap. Optimum slat positions were ascertained for a Reynolds Number of 6.0×10^6 for the model with no trailing-edge flap and with two trailing-edge flaps deflected. Section lift and pitching-moment characteristics of the various model combinations were determined for Reynolds Numbers of 2.0×10^6, 4.0×10^6, 6.0×10^6, and 7.0×10^6. The results of these investigations showed that the average increment in $C_{l_{max}}$ for the leading-edge slat was 0.83 and for the leading-edge flap 0.66; combined with a trailing-edge device their effect was approximately equal to the increments produced separately. Deflection of either of these leading-edge devices moved the aerodynamic center forward. In the case of the slat this movement was to approximately the quarter point of the extended chord. Finally, it was again found that trailing-edge flaps seemed to move the optimum slat positions so as to reduce the gap, but it is to be noted that this airfoil was also of the NACA 64 series.

In other Ames Tests(Ref. 106)at Mach numbers ranging between 0.25 and 0.85 with Reynolds Numbers from 3.4×10^6 to 8.1×10^6, slat positions were investigated on an NACA 64A010 airfoil: (1) with the slat leading-edge extended forward along the airfoil chord line and (2) with the slat extended forward and displaced below the chord line. Although the results indicated that over the entire Mach number range the airfoil with the slat retracted was somewhat dynamically superior to any of the other airfoil arrangements for section lift coefficients up to 0.60, it is generally true that at the lower Mach numbers the greatest $C_{l_{max}}$ and largest lift-drag ratios at high angles of attack were obtained with the slat extended forward but with its nose displaced below the extended chord line of the airfoil. For section lift coefficients above 0.80 and for the widest range of Mach numbers, the most effective position is with the nose of the slat in the extended chord line of the airfoil. This increase at higher angles of attack can be explained primarily by the increased loading carried by the slat and the forward part of the airfoil, and by the greater pressure recovery on the upper surface of the airfoil. The energizing effect of the boundary layer on the airfoil surface, often attributed to the air stream flowing through the slot, seemed here to be only of secondary importance in evaluating slat performance.

A very rough approximation, accredited to Young, (Ref. 170) is that for standard slats

$$\Delta C_{l_{MAX}} \approx \frac{10}{3} \times \frac{\text{SLAT CHORD}}{\text{WING CHORD}}$$

This seems to hold for thick wings with or without trailing-edge flaps with slats between 15% and 30% at a Reynolds Number of about 3.0×10^6. For

medium thickness wings (about 10% - 15%) it seems that slightly lower increments may be expected. For thin wings it may be possible to have higher increments, although trailing-edge flaps may not be completely additive.

Since the above two-dimensional results are always applied on three-dimensional wings, where the conditions may be quite different from two-dimensional a few tests on three-dimensional effects will be very briefly summarized (Ref. 170).

The Germans found quite early that although on an unswept wing the slat should cover the whole span and be sealed at the wing-body junction, part span slats used at the tip may often be effective to delay stall on a swept-back wing.

Tests have been made at varying Reynolds Numbers on the use of 20% full span slats on wings with sweep-back angles between 32° and 35°, aspect ratios near 6, taper ratios near 0.5, and a symmetrical wing section 12% thick at the root and 10% at the tips. It was found that the maximum lift coefficient increased as the Reynolds Number became larger. However, increasing the slat chord by more than 20% of the wing chord gave only small gains. At Reynolds Numbers between 2×10^6 and 6×10^6 the $\Delta C_{l_{max}}$ seemed to be about 0.5.

Other tests on a 35° swept-back wing indicated a $\Delta C_{l_{max}}$ due to slats on the outer half of the wing to be 0.24 while full span slats gave $\Delta C_{l_{max}}$ 0.48. The half span slats combined with half span split flap on the inboard section gave 0.51 in maximum lift coefficient while full span flaps combined with full span slots gave about 1.02 in $C_{l_{max}}$.

There seem to be no exact experimental results on sweep-back angles greater than 35°, but it was determined that slats continued beneficial effects at angles greater than 45°, although there appear to be no gains at a 60° angle. However the slats seemed slightly inferior to leading-edge flaps on swept wings.

From the foregoing it would appear that the following conclusions could be drawn:

1. Combined use of slats and a trailing edge device normally give a $C_{l_{max}}$ approximately equal to the sum of the increments produced individually.
2. A deflected extended slat moves the aerodynamic center forward to approximately the quarter point of the extended chord. (In other words, a nose up pitching moment would occur about the original quarter chord point).

Although the unpowered devices, represented by the leading-edge flaps discussed in the previous section as well as by the slats just examined, can combat leading-edge separations successfully over a range of lift cofficients. When the value of airfoil circulation achieves the levels made potentially possible by the use of powered trailing-edge systems, still more powerful devices are required. For this reason considerable effort and interest has recently been expended on the study of arrangements utilizing suction and blowing. The analysis of the behavior of such systems is dealt with in the remainder of this section.

Suction at any chordwise location may be said to act primarily to remove, at this location, the lower regions of the profile's boundary layer.

The layer is thus made thin, with all velocities within the newly formed layer becoming greater than the velocities existing at corresponding distances from the profile surface prior to the application of suction. The new layer should initiate at a chordwise station somewhat forward of the point or region where suction is applied and extend to the profile's trailing-edge. Of course, the more aft the point of interest as compared with the suction location the less will be the difference between the old and new boundary layers, the suction simply freshening the boundary layer and then permitting it to run its natural course.

Depending upon the quantity of suction and the condition of the boundary layer at the point of application, the removal of surface air through suction can: (1) prevent laminar or turbulent separation by altering the velocity profile at what would normally be the point of separation, (2) thin the laminar layer and thus move the transition point to a more aft location, (3) recreate laminar flow from an already turbulent layer, and/or (4) alter potential flow by removing not only the entire boundary layer but external air as well, thus creating a true stagnation point aft of the sink.

The first three effects above are based upon suction's ability to thin the laminar or turbulent layer and may be classified as the possible contributions of such a system to boundary layer control while the fourth falls within the domain of circulation control. Effects (1) and (2) both have considerable bearing upon the field of high-lift flow control, item (1) for obvious reasons and item (2) because it infers that trailing-edge stall may be delayed by suction at even a well-forward location. Likewise, effects (1) and (2) are of great interest as a means of minimizing

profile drag. Prevention of separation is necessary to maintain pressure drag at a minimum and any elongation of the laminar run serves to reduce friction drag. Because of the large suction quantities involved, the third effect is of practical interest only in conjunction with item (4). The latter effect requires large suction quantities and its use as a high-lift device has been shown to be feasible only when the suction is applied very near the profile's trailing-edge. Such a system is discussed in some detail in Section 3.2c of this report.

The following pages will deal with suction as a high-lift boundary layer control with emphasis upon the ability of suction to prevent leading-edge (laminar) separation, but also considering the possibilities of applying such control to the turbulent type of separation. Those systems which have been developed to delay leading-edge separation comprise two general types: (1) leading-edge slot suction and (2) leading-edge area suction. The first involves a single open slot running spanwise and located very close to the wing leading-edge. The second replaces the slot with a porous medium which generally is designed to have greater chordwise extent than is the case with the slot.

Solution to the problem of turbulent separation at the profile trailing-edge has been approached through the application of several suction arrangements. These can loosely be divided into: (1) midchord type suction, involving a slot or several slots located somewhere between the 10% and 80% chord positions; (2) distributed upper-surface suction, utilizing a large number of slots or perforations, or a large area of porous material. (Generally, porosity is extended aft to the trailing-edge while quite often

the extent of suction is brought forward as far as the leading-edge, making this a dual type of systems, providing efficient control of both laminar and turbulent separation and (3) trailing-edge suction, which can yield circulation control in addition to trailing-edge B.L.C. An academically interesting configuration which could perhaps be considered a form of trailing-edge suction, Griffith type suction, is the only version of the trailing-edge system which will be touched upon here, the better known types having been discussed previously. Additionally, there has been some research done on combined leading-edge and midchord suction. It is to a large extent because of the promise shown by such combinations that the decision was made to include within this "leading-edge" section those systems which operate primarily upon the turbulent rather than the laminar layer. Fig. 135 shows the five major systems described.

In attempting to apply suction for the purpose of preventing or delaying leading-edge stall, it would first be desirable to determine some optimum location for the slot or porous area. This optimum will here be defined as that location which provides stall delay with a minimum of suction quantity. So as to negate the complicating parameter of slot width, only the extremely narrow slot will be considered in the following qualitative discussion. This discussion will use several assumptions which are based only upon limited experimental observations and, although the assumptions seem logical, they may thus be subject to some doubt. The first of these is that the narrow slot delays leading-edge stall most efficiently if its location is directly beneath the position where the leading-edge of the laminar-bubble would exist if no control were used. A second assumption is therefore necessitated which

would yield some feeling for the position of the leading-edge bubble under no-control conditions. It has here been assumed that the laminar bubble will form at the point of maximum adverse pressure gradient when the angle of attack is such that this gradient achieves some critical value. Further, the bubble will break away and the profile will stall when the maximum adverse pressure gradient has reached some other critical value. The initial (α just equal to that necessary for stall) break away point should coincide with the position where this second critical value is achieved on the profile. It should be mentioned that the locations where these two critical values are attained, as well as the values themselves bear no known relationship to each other and each without doubt will vary with profile shape and changes in viscous condition.

Using the assumptions above, one likely position for the narrow slot would be at that point where the adverse pressure gradient would, without suction, become sufficient to permit formation of the laminar bubble. Such a location could readily be determined experimentally. However, as angle of attack is increased beyond that corresponding to base profile initial bubble formation, the maximum adverse pressure gradient will increase and, at least in the case of "leading-edge" type separation, its location as well as that of the bubble will move forward. Although, to the best of this writer's knowledge, no motion of the point of initiation of the "thin-airfoil" type of bubble has been observed, forward transport of the "leading-edge"type of bubble has been found to be as great as 1% chord between bubble initiation and final stall. Therefore, at an angle of attack corresponding to break-away, the suction slot (in optimum position to prevent low-α bubble

initiation) will likely be too far aft for most efficient operation. This would suggest placing the slot at that chordwise location where the maximum adverse pressure gradient exists immediately prior to stall. This location could be determined experimentally and it seems obvious that such a location is superior to that discussed previously if increase in maximum lift is desired. If, then, this slot location is selected, the profile, with suction, will be able to achieve angles of attack considerably greater than would be attainable with the base profile. (Always assuming, of course, that leading-edge stall limits base profile lift.) As angle of attack is permitted through suction to further increase in this range, maximum adverse pressure gradient will increase beyond that normally triggering base profile stall and its location would appear to continue to move forward. While maximum adverse pressure gradient moves forward with increased angle of attack, theoretical and experimental investigations reveal that, as angle of attack is increased beyond that for base profile stall, the value of pressure gradient equal to that necessary for base profile stall moves aft. Under the previous assumptions, it thus seems that leading-edge stall may initiate in the high-lift regime not only at the point of maximum adverse pressure gradient, but anywhere between the point of maximum adverse pressure gradient and the more aft point where adverse pressure gradient has the critical value necessary for base profile leading-edge stall. (In fact, there may be an area forward of the maximum adverse pressure gradient location which will have a gradient greater than base-profile critical. This area will normally be infinitesimal as the locations for maximum gradient and pressure peak will usually closely coincide for large lifts on relatively thin profiles.)

It can be seen that, even for a given profile, there is no definite optimum "narrow" slot location for the prevention of leading-edge separation. Increased lift increment yields an increasingly divergent chordwise distance through which separation may initiate. If a slot could only exercise control at a point directly above, no "narrow" suction slot would be capable of producing more than very small lift gains. Of course, suction controls the flow before as well as aft of the slot. It can contain a bubble or retard its formation forward of the slot and can retard separation behind. Although little is known of the comparative efficiency of suction when the flow wants to separate upstream or downstream, it would be thought that such a slot would be more efficient when located near the upstream boundary of the separation-prone area both because, for the usual profile, this represents the most separation-sensitive region and because, if a bubble should form upstream of the slot, the suction will be forced to operate on a power-consuming turbulent or turbulizing boundary layer. For this reason, it is suggested that the narrow suction slot would delay leading-edge separation most efficiently if placed beneath the point of maximum adverse pressure gradient(where separation is <u>most</u> likely), permitting its downstream separation-preventing characteristics to take care of the region aft where the gradient is still somewhat greater than that for base profile stall.

The proper location for such a slot now becomes, for a given profile, a matter of the degree of maximum lift increase desired. The relatively aft position corresponding to the base profile break away point will probably be optimum for very small lift gains, while a well forward position will be most efficient for large lift increases. The best solution for maximum

efficiency in the use of suction to delay leading-edge stall might, therefore be for the relatively narrow slot case, a slot moving forward in such a way that it is always in the most favorable position as lift is increased.

In that the variably located "narrow" slot is highly impractical and considering the possibility that control very slightly ahead of or behind the point of probable flow detachment would not be excessively disadvantageous, investigators have attempted, rather than chasing the optimum location forward as angle of attack increased, to make judicious compromises. Slot location and chordwise extent of the slot or porous area have been varied and optimum locations have been found which generally lie in the range of expected travel of the "narrow" slot optimum discussed above. Variations in chordwise suction velocity distribution have been studied in an attempt to reduce the waste created by finite suction chordwise extent. Without such suction distribution, the slot or porous area with width can produce excessive suction velocity at locations which, although near the optimum suction position for the achievement of a given lift, are, at this lift, considerably less than optimum. The problem of determining optimum suction location and distribution under varying free stream and lift conditions seems extremely difficult in solution and investigations to this point have merely scratched the surface.

Fig. 136 shows a typical curve of $\Delta C_{l_{max}}$ vs suction quantity, C_Q, for a profile with leading-edge suction. The vast majority of experimental results available demonstrated this characteristic shape. As suction quantity is initially increased from zero, the lift increment increases at a very rapid rate. At a lift level which appears to be closely related to the base profile's trailing-edge stall line as predicted by the linear

extrapolation method (Section 3.1f), the curve bends and eventually becomes flat or of very low slope. A study of stall points revealed that all suction profiles investigated show leading-edge stall in the range of lifts where the curve has its initial steep slope, mixed stall (leading-edge and trailing-edge separation present at time of break away) where the curve bends, and trailing-edge stall for the relatively flat upper portion of the curve. Fig. 136A thus demonstrates two facts: (1) leading- edge suction will generally not only delay leading-edge separation but, to a lesser extent, also may delay trailing-edge separation, and (2) the linear extrapolation method could be of assistance in at least qualitatively predicting the approximate ultimate lift economically feasible with leading-edge suction.

The ability of leading-edge suction to delay trailing-edge separation explains why, in some cases, suction which would seem too far aft for efficient leading-edge control has been regarded as being of optimum location. A slot location which allows trailing-edge control in addition to effective leading-edge control will enable the profile to achieve greater maximum lifts than would be the case were no trailing-edge control provided. This is obviously because the profile's ultimate maximum lift is no longer limited by natural trailing-edge stall but is now limited only by the suction system's capabilities as a trailing-edge stall deterrent. Of course, using such a slot location, some slope decrease would be expected in the leading-edge stall portion of this curve as power is being expended here to control the trailing-edge unnecessarily. The concept of optimum leading-edge suction location is thus further confused by the trailing-edge B.L.C. phenomena. It can, however, be repeated that, to a large extent, optimum suction location is a function of the desired lift level as well as profile shape. Leading-edge

suction operates in the general case as a combined leading-edge and trailing-edge control. Luckily, however, such a system is primarily a leading-edge control, which means that certain of its behavioral trends may be deduced through use of the linear extrapolation method and predictions of maximum ecomonic lift for such a system, based on this method, should yield results which may be accepted with approximately as much faith as the engineer is able to place in the method itself.

Taken as a pure leading-edge control, leading-edge suction would be expected, from the linear extrapolation method, to have characteristics as shown in Fig. 137A. The linear extrapolation of the "pure" trailing-edge stall line defines the ultimate maximum lift attainable with such a control. As suction quantity is increased the partial control characteristics will be approximately as shown. (Complete control is said to occur when C_Q is of a value which permits stall for the given profile to be of the "pure" trailing-edge variety.) Fig. 137B demonstrates the typical characteristics of a pure trailing-edge control. Here, the linear extrapolation of the "pure" leading-edge stall line will define ultimate maximum lift attainable. Fig. 137c takes the liberty of combining A and B in an attempt to qualitatively indicate the probable action of the typical leading-edge suction system as a function of profile thickness. It will be noted that the trailing-edge separation delaying capabilities of such a system have been assumed to be quite minor as compared with its abilities to delay leading-edge separation. This assumption is, of course, realistic for the case being considered and infers that, given sufficient C_Q, trailing-edge stall will finally limit the effectiveness of the system--if there is any final limit with such a

combined system. Such an inference permits the plotting of Fig. 137c without regard for any pure leading-edge stall extrapolations. That is, the trailing-edge stall extrapolations ultimately govern the very high lift characteristics of the $C_{l_{max}}$ vs t/c curve. In addition to the assumption of relatively small trailing-edge B.L.C., Fig. 137c uses the assumption that the slopes of the trailing-edge stall portions of the curves with boundary layer control are approximately equal to that for the trailing-edge stall portion of the no-control curve. This effect appears experimentally to be reasonably valid for profiles with trailing-edge B.L.C. The fairing of Fig. 137c is in accordance with these two assumptions together with the findings of the cambered profile studies (Section 3.1g) which also dealt with what might be called a "mixed" system. As can be seen from the figure, increases in C_Q would be expected to be considerably more beneficial for the thin, leading-edge stalling profiles than for thick, trailing-edge stalling profiles which are assisted only by virtue of the leading-edge suction's rather poor ability to delay trailing-edge separation and stall. Considering only the leading-edge stalling profiles, those which are thicker will experience mixed stall and finally trailing-edge stall at lesser C_Q's and lower $\Delta C_{l_{max}}$'s than the very thin airfoils. Thus, these thicker profiles are limited, for practical values of C_Q, to lower maximum lift increments. It should be pointed out that the curve shape significance given to the base profile $C_{l_{max}}$ vs t/c curve in Fig. 17 should apply for any given value of C_Q. Therefore, the expected stall pattern can be traced as a qualitative function of C_Q and t/c in Fig. 137c.

Taking any given t/c in the base profile leading-edge stalling regime and mentally cross-plotting Fig. 137c for $C_{l_{max}}$ vs C_Q, it can be seen that a characteristic curve of the shape of that shown in Fig. 136 will be obtained. This series to correlate the characteristic curve shape with concepts of the linear extrapolation method, and thus permits a means of visualizing the changes in magnitude which can be expected in the $\Delta C_{l_{max}}$ vs C_Q curve with alterations in profile thickness. Trailing-edge stall and the resultant leveling of the curve of Fig. 136 occurs at a lift level greater than that predicted through the "pure" trailing-edge stall line's linear extrapolation by an amount which may be thought of as equal to the trailing-edge B.L.C. effect of this C_Q. The slope of this relatively pure trailing-edge portion of the $\Delta C_{l_{max}}$ vs C_Q curve depends upon the variation of trailing-edge B.L.C. with suction quantity. Unfortunately, as the degree of trailing-edge control is a probable function of Reynolds Numbers as well as the location and flow characteristics of the suction system, quantitative predictions as to the value of this slope are extremely difficult. The same can be said for any predictions regarding the slope and slope variation of the leading-edge stall portion of Fig. 136. The magnitude of trailing-edge control, of leading-edge control, and their relationship to each other depends upon such things as slot location and width or porous extent, chordwise suction velocity distribution, the effect of free stream velocity upon suction velocity distribution, and, of course, profile shape and suction quantity. For profiles with leading-edge suction systems which are found to yield little trailing-edge control, however, the linear extrapolation method should yield quite accurate ultimate maximum lift predictions.

Remember that the apparent usefulness of such a treatment infers that a strong Reynolds Number effect should be expected upon the maximum lift of profiles with leading-edge suction as well as large variations in ultimate maximum lift due to changes in profile shape. Also it should be remembered that the linear extrapolation method attempts to predict "complete control" characteristics and cannot quantitatively predict "partial control"; i.e., variation of maximum lift with C_Q. Although this method will not treat the effects of trailing-edge stall delay, indications are that it can still be of some usefulness even in this general case.

Available experimental data dealing with leading-edge slot suction (Fig. 135A) are extremely limited. McCullough and Gault, however, in Refs. 123 and 124, present results of tunnel tests on a 63_1-012 airfoil with single leading-edge slots of varying widths and locations. Their findings are summarized in Figs. 138, 139, and 140 of this report.

Fig. 138 shows a summary of the maximum lift characteristics of all powered configurations tested during the investigation reported in Ref. 123. It will first be noted that the addition of the slot reduces the maximum lift coefficient under no-suction conditions by approximately .25 as compared with the base, unslotted airfoil, indicating that some minimum suction quantity is necessary simple to reëstablish base profile characteristics. With only one exception, these curves clearly demonstrate the shape previously indicated in Fig. 137A, with the C_Q corresponding to rapid loss in slope being between .0015 and .0025. Maximum lift coefficient which was attained ranged from approximately 1.6 to 1.8, representing lift increases beyond maximum for the base profile of from $\Delta C_{l_{max}} \cong .20$ to $\Delta C_{l_{max}} \cong .45$.

Fig. 23 indicates that a $C_{l_{max}} \cong 1.48$ would, based upon the linear extrapolation method, yield pure trailing-edge stall for this profile at a Reynolds Number of 5.8×10^6. This value can be seen to be considerably less than the lifts attained by the great majority of the configurations shown in Fig. 138. Assuming the validity of the application of the linear extrapolation method to the leading-edge suction system as discussed previously, the indication here is that the majority of the slot configurations shown realize much of their effectiveness through controlling trailing-edge separation. This is not indicated for the two slots located directly at the profile leading-edge. Neither of these configurations achieves in this C_Q range lift even as great as that predicted by the linear extrapolation method. A study of stall patterns reveals that the 63$_1$-012 profile with a small amount of suction shows separation from the trailing-edge at a lift level considerably lower than that predicted by the linear extrapolation method. It is thus felt that combined leading-edge and trailing-edge separation is creating final stall even in the low C_Q range. In fact, the base profile itself should, from Fig. 17, show a mixed type of stall. Boundary layer surveys made for one slot configuration in the high C_Q regime indicate trailing-edge separation at angles of attack well below stall. Applying the approximate increment usually found between the lift coefficient for initiation of trailing-edge separation and that for stall, there is a definite indication of the existence of relatively "pure" trailing-edge stall in this range. The stall-type interpretation given to the curve shape (Fig. 136) therefore would appear, from this meager information, to hold for the 63$_1$-012 configuration in the high C_Q, low slope portion of the curve. Of course, the initial rise

is, in this case, characterized by mixed stall rather than the leading-edge type.

Figs. 139 and 140 demonstrate the effect of slot width and location upon the maximum lift attainable in the C_Q range investigated. It can be seen from Fig. 139 that for the narrower slots (.2%-.4% chord) the optimum location for the slot leading-edge is at approximately .5% chord. For wider slots, however, the optimum slot location appears to move aft. Fig. 140 is a cross-plot of Fig. 139 extrapolated on the basis of results shown in Ref. 124 of tests conducted with this profile utilizing a relatively wide slot (1.4% chord). Here, it is noted that optimum slot width increases with increasing suction quantity. For the .5% slot leading-edge location, the .6% chord slot appears optimum for C_Q's $\cong$ .0015 while a slot of 1.0% width seems best for C_Q's of approximately .0040. This trend serves to demonstrate that optimum suction slot location and width depends to a very large extent upon the desired maximum lift level.

Liquid film studies indicate that the laminar (leading-edge type) bubble extends, immediately prior to stall for this particular base profile, between the .2% and .5% chord locations. The systems which seem optimum here, however, all utilize suction slots which have leading-edges <u>downstream</u> of this region. This would seem to demonstrate that the optimum widths and locations shown in Figs. 139 and 140 are considerably aft of the expected optimum for the prevention of leading-edge separation and must represent near-optimums for the mixed or trailing-edge separation cases, certain configurations being superior in the high-lift trailing-edge stall region, and others being better where stall is of the mixed variety. (It will be noted that at lift levels

where stall appears to be of the mixed variety, a considerably different slot configuration seems optimum than is the case where lift level is in the relatively "pure" trailing-edge stall range).

It might be pointed out that for maximum lifts up to levels somewhat beneath that indicated by the linear extrapolation method the optimum slot would for the general profile likely be very closely that which is best for the delay of pure leading-edge stall. This statement would certainly hold true where base profile stall is of the pure leading-edge type. Where separation at stall is of the mixed variety, but with final stall occurring from the leading-edge, it is felt to still be valid as there would seem to be little sense in robbing the leading-edge slot of its most efficient product, delay of leading-edge separation, in order to inefficiently delay a separation type which never culminates in stall. For base profiles which have maximum lift only slightly beneath that given by linear extrapolation and whose stalls occur from the trailing-edge (but prematurily by virtue of the existence of a leading-edge bubble) the optimum leading-edge slot would probably move back to a position where it can more effectively delay trailing-edge separation while taking only small losses in its efficiency with respect to leading-edge stall delay. The lift level at which the optimum slot for leading-edge stall delay is felt to give way to that optimum for mixed stall could be represented by the point of maximum curvature of the curves of Fig. 137A.(assuming the curve shape interpretation of Fig. 17 to be correct). It can be seen that this point of optimum slot change is proportionately extremely close to the linear extrapolation line for all profiles except those which have no-control characteristics which place them near this point of maximum curvature on the

no-control (base profile) curve of Fig. 137A. It is admitted that this stall-type criterion for changing slot location as a function of desired lift level has been developed intuitively and seems, in ways, somewhat arbitrary and difficult to apply. Optimum slot position does not jump from one place to another as lift level changes but probably undergoes a rather constant displacement. The "jump" change, however, seems the only practical way of approaching the problem. In application, it should usually be possible to assume that, for most profiles, the linear extrapolation line represents the lift level beyond which the slot must be moved aft to the "mixed stall" optimum for most efficient operation. This would create proportionately large errors only for those profiles which, in their no-control condition, suffer mixed stall.

There can therefore be said to be three separate regions of maximum lift which necessitate at least three optimum slots--slot selection being a matter of desired maximum lift. Inspection of Figs. 138, 139, and 140 gives some idea of the different slots required for greatest efficiency in the several lift regimes for the case of the 63$_1$-012 configuration. For lifts up to the mixed (trailing-edge) stall lift level, the thinner slot located directly on the profile nose indeed seems the best of the configurations tested. This is more obvious (Fig. 138)when it is recalled that closely half of the suction quantity is here being wasted on the lower surface. Other leading-edge suction tests have indicated that extending suction to the lower surface serves only to add to the necessary suction quantity. The wider nose-centered slot is highly inefficient because it not only throws away power over a large

portion of the under surface, but also extends to a prohibitive length on the upper surface. It will be noted that, as the 631-012 itself stalls in a mixed manner, very little lift increase could be achieved through use of the optimum slot for leading-edge stall control. Again, it would generally be expected that, for most profiles, the linear extrapolation could be used to define the lift where the leading-edge stall optimum slot location ceases to be optimum for the profile. The invalidity of this method for use with profiles which show a good deal of trailing-edge separation prior to base-profile stall is demonstrated by these tests which not only show the nose-centered slots losing efficiency at a lift level considerably under the linear extrapolation lift level, but indicate that slots initiating at locations from .3% to .4%c become rapidly interior, even in this relatively low lift regime, to those at intermediate (.5%c-.7%c) positions.

For lift levels in the portion of the stall curve where stall seems of the trailing-edge type but with leading-edge separation present and influencing, those slots with leading-edges in the region from .5%c to .7%c appear optimum. Intermediate slot widths (.4%c to .6%c) seem best but slot location is seen to be the dominant factor.

Fig. 138 reveals that the most efficient slot for the attainment of very high lifts is the wide, comparatively aft slot. The more aft the slot extends the greater is the achievable lift, but only at the premium of considerably additional C_Q. For this profile, a .8%c wide slot with its leading-edge at the .38%c station will attain a $C_{l_{max}}$ of 1.8 at a C_Q of .004. A 1.4%c slot with its leading-edge at the same location can achieve a $C_{l_{max}}$ of 2.0 at a C_Q of .007 (Ref. 124).

Again, dividing optimum slot configurations for the attainment of lifts in excess of what is approximately linear extrapolation lift into a "mixed" stall optimum and a "pure trailing-edge stall" optimum is arbitrary, there without doubt being a smooth variation in optimum slot configuration with lift level desired. This, however, represents the simplest method of presentation.

From a comparison of the characteristics of the medium lift level ("mixed stall") optimum slot and the high lift level ("trailing-edge stall") optimum in the leading-edge stalling, low lift level regime, it is obvious that, while the trailing-edge stall optimum delays trailing-edge stall most efficiently, the mixed stall optimum delays leading-edge stall more readily. The comparatively high initial slope of the $C_{l_{max}}$ vs C_Q curve for the optimum "mixed-stall" configuration falls off and crosses the curve of the optimum "trailing-edge stall" configuration at a lift level considerably greater than that given by linear extrapolation and at a comparatively high C_Q. By comparison, the more forward located optimum "leading-edge stall" configuration will yield the highest initial slope but its lift-increasing abilities deteriorate at a lift level somewhat below that given by the linear extrapolation method. These observations, although far from yielding a complete picture, give some insight into the operation of leading-edge suction upon trailing-edge separation. Firstly, within the range tested, the more aft the suction is applied, the greater will be the trailing-edge control. Also, the more aft the suction is applied, the less efficient will it be in delaying leading-edge separation. A third observation is that suction extending no more aft than that point where the optimum slot for leading-edge stall delay would be

located could be expected to do little or no good for trailing-edge stall delay.

Thus, for the achievement of lifts in the trailing-edge stall regime, a compromise must be reached whereby suction may be applied as far aft as possible while still sufficiently forward to assure reasonable leading-edge control. "Reasonable" leading-edge control would be thought to mean not only control of leading-edge separation, but preservation of laminar flow to the slot. It would be expected that, were the flow turbulent at the slot (by virtue of a laminar bubble and/or large adverse pressure gradients), excessive C_Q would be required for a given amount of trailing-edge control. The most aft location at which the leading-edge of the slot for optimum trailing-edge control may be efficiently located is difficult to derive from the data, but indications are that it is only slightly (.1%c-.2%c) aft of the point where the base profile experiences laminar break away (approximately .5%c). It further seems that initiating the slot much further forward than such a location will result in increased high-lift suction quantity requirements because of the increased width required and the greater external pressures opposed. Optimum location of the slot trailing-edge for the attainment of very high lifts is difficult to predict. It could be guessed, however, that there would be little value in extending the slot any further aft than that chordwise region where the external pressure peak ceases, to all extents and purposes, to exist. Extension of the slot aft of this most sensitive region would, in the absence of controlled suction quantity distribution, probably create excessive C_Q requirements.

By relating the optimum slot locations obtained for the 63_1-012 configuration to the location of the laminar bubble for base profile stall, it may be possible to qualitatively indicate the variation in suction slot optimum position with stall regime, or lift level, for the general case. It has already been suggested that, in the general case, for the attainment of lifts in the leading-edge stall regime, or the portion of the mixed-stall regime lying beneath the pure trailing-edge stall line (as predicted by the linear extrapolation method), the slot would best be located before or under the position where the laminar bubble exists immediately prior to base profile stall.

In the portion of the stall curve where stall seems of the trailing-edge type but with leading-edge separation present and influencing, these slots with leading-edges in the region from .5%c to .7%c appear optimum. Intermediate slot widths (.4%c to .6%c) seem best but slot location is seen to be the dominant factor. This upper portion of the mixed stall regime is difficult to analyze in that slot configurations which, by location, would be thought to handle leading-edge separation well and trailing-edge separation poorly can at some C_Q be as efficient as slots which control trailing-edge separation comparatively better than leading-edge. However, if the slot is quite efficient in dealing with trailing-edge stall the mixed stall region extends to higher lifts and greater C_Q's than would be the case had the slot a configuration not so amenable to trailing-edge control. Thus, in the plot of $C_{l_{max}}$ vs C_Q, the low initial slope and high level-off lift coefficient is characteristic of a leading-edge slot with good trailing-edge control capabilities (at the necessary expense of leading-edge control) while the

high initial slope and low level-off lift coefficient is characteristic of a slot with good leading-edge control capabilities. The next paragraph will show that, for the model under consideration at least, the slot which efficiently controls trailing-edge separation is of considerably different configuration than the well forward, narrow slot which seems most suitable for leading-edge control.

Fig. 138 reveals that the most efficient slot for the high-lift, relatively flat (trailing-edge stall) portion of the curve is the very wide, comparatively aft slot. The more aft the slot extends the greater will be the achievable lift, but, of course, only at the premium of additional C_Q. In order to maintain C_Q at a minimum in the lower lift range, it seems best to initiate the slot sufficiently forward to permit at least reasonable efficiency in controlling leading-edge separation. Thus certain compromises between slot width and slot initiation point must be made and the lower lift sacrifices must be considered if very high lift is desired. For this profile, a .8%c wide slot with its leading-edge at the .38%c station will attain a $C_{l_{max}}$ of 1.8 at a C_Q of .004. A 1.4%c slot with its leading-edge at the same location can achieve a $C_{l_{max}}$ of 2.0 at a C_Q of .007 (Ref. 124). Beyond these respective suction quantities, which indicate the initiation of the pure trailing-edge stall regimes, the lift curves are relatively flat. Unfortunately, there seems no reasonable way currently available to predict the effect of further C_Q increases upon pure trailing-edge stall delay for slots at these forward locations.

By relating the optimum slot locations obtained for the 631-012 configuration to the location of the laminar bubble for base profile stall, it

may be possible to qualitatively indicate the variation in suction slot optimum position with stall regime or lift level for the general case. It has already been suggested that, in the general case, for the attainment of lifts in the leading-edge stall regime or the portion of the mixed stall regime lying beneath the pure trailing-edge stall line (as predicted by the linear extrapolation method) the slot would best be located before or under the position where the laminar bubble exists immediately prior to base profile stall. In most cases such a position would be forward of the .5% chord station. As has been indicated, the slot should not normally extend beyond the profile leading-edge. This would indicate that the slot should be placed somewhere between the profile leading-edge and the .5% location. The 63_1-012 studies serve to demonstrate approximate bubble position but represent an exception to the linear extrapolation criterion above. The slot which is in optimum position for leading-edge stall delay will be, for profiles which stall in their uncontrolled condition with a large amount of trailing-edge separation present, too far forward for greatest efficiency unless only a very small lift gain is desired. In this case, such a slot is optimum only to lift levels considerably less than that given by the trailing-edge linear extrapolation. The point where this location is no longer optimum is probably very close to the lift where final stall is of the trailing-edge (but mixed) type.

For the trailing-edge stall portion of the mixed-stall regime, relatively wide slots (.4-.6%c) initiating immediately aft of the location of the bubble (base profile stall) should yield better results than more forward or aft slots. So as to efficiently attain lifts in the high lift region governed by

the pure trailing-edge stall portion of the $C_{l_{max}}$ vs C_Q curve, the wide slot (.8-2.0%c) extending aft from approximately the base-profile-stall bubble location is recommended. The chordwise location at which the laminar bubble exists immediately prior to base profile stall will, of course, vary with profile shape, the thinner profiles probably yielding a more forward position.

Of course, trailing-edge stalling profiles, whether the separation is mixed or pure, may benefit more from midchord or trailing-edge suction, with the now relatively unimportant leading-edge bubble being neglected or very inefficiently delayed. If the base profile stalls from the leading-edge, however, the slot locations above, although based upon only one series of tests, for one profile at one Reynolds Number, should be valid. Certainly, more tests would be of considerable value in better defining the picture.

One major parameter which has been mentioned but not discussed in connection with this investigation is the effect of the chordwise distribution of velocity into the slot. In that the leading-edge suction slot is generally located in a region of external adverse pressure gradient, the slot should experience a chordwise suction velocity distribution which yields a suction velocity increasing as the station of interest is moved from slot leading-edge to slot trailing-edge. The suction velocity gradient depends for a given C_Q, of course, upon slot location and slot width as well as free-stream velocity. This gradient is, in addition to general slot location, probably the most important variable effecting the aerodynamic efficiency of a leading-edge suction slot. In that suction velocity distribution may change with free-stream velocity, it is expected that variations in forward velocity can somewhat modify optimum slot location for any of the three flow

regimes considered, but possibly not beyond the limits of the locations recommended here. This should be considered in further investigations. Comparing the probable qualitative suction velocity distributions against the experimentally determined optimum slot location indicates that for best control of trailing-edge separation at a given lift (for the leading-edge slot case), there should exist some minimum suction velocity at some location considerably aft of the laminar bubble point. The slot must, however, extend forward sufficiently to provide reasonable suction velocity at a point where growth or detachment of this bubble may be controlled. Any velocity distribution which gives an excess of velocity at the trailing-edge of such a slot and/or too little velocity near the laminar bubble position will be less than optimum. The optimum slot locations for the other two flow regimes may be analyzed from the point of view of suction velocity distribution in a similar highly qualitative manner. Unfortunately, just what suction velocity or velocity distribution is needed at what location or throughout which area is still a question mark necessitating rather basic research in order to achieve any solid answer.

In that any given airfoil can normally have only one leading-edge slot and not one for each of the previously described three flow regimes it may pass through, it becomes necessary to ascertain which slot would be best for which airfoil. The criterion here would probably be the greatest $\Delta C_{l_{max}}$ for the least C_Q. It is suggested that for thin airfoils which necessitate a very high $\Delta C_{l_{max}}$ in order to reach the $C_{l_{max}}$ value predicted by linear extrapolation, the more forward slot would probably be selected as the best optimum. For thicker profiles which still stall from

the leading-edge without control, the location which is optimum for attaining lifts in the upper portion of the mixed-stall regime is suggested, although if excess C_Q is available, it would be wise to use the wide trailing-edge control type of slot. The optimum slot location for profiles which normally stall from the trailing-edge, but in a mixed manner, is difficult to predict. Although for low lift levels the slot last suggested might be best, it could well be that a slot located as far aft as the 10% chord position might be best for very high lifts. Such a slot could control the now comparatively ineffectual leading-edge bubble and much more effectively actuate the boundary layer over the trailing-edge. For thick profiles which in base condition stall from the trailing-edge in a pure manner, it would, in the single slot case, probably be better to leave the leading-edge entirely and use a slot considerably further aft. This would certainly be the case for the very thick profile ($t/c \cong 24\%$).

It must be borne in mind that the optimum slots suggested here are based upon optimum aerodynamic efficiency and do not necessarily represent optimums from the point of view of power required. Although the latter would certainly be a superior criterion, lack of test information and individuality of systems in this respect makes such a consideration beyond the scope of this report. It may be pointed out, however, that for a given C_Q, power required depends upon the magnitude of the external pressure distribution assummed over the slot opening and thus depends upon profile shape, free-stream velocity, and slot location and width. Obviously, this places the leading-edge slot in a rather bad position power-wise as compared with slots located well aft of the leading-edge pressure peak. Also,

considering only leading-edge slots, power considerations may alter the optimum slot location, possibly tending to move such locations somewhat aft.

Ref. 123 indicates no change in lift curve slope through leading-edge suction until angles of attack immediately below that for base profile stall are attained. It is thought that this would only be true for base profiles stalling from the leading-edge with the leading-edge type of bubble preceding such stall. In such a case, the base profile itself maintains a nearly theoretical slope which is the maximum slope attainable even with extremely large C_Q's. This author can find no case where leading-edge suction can create circulation control at the profile nose. It might be mentioned, however, that leading-edge blowing utilizing very high momentum coefficients appears to be capable of producing such an effect. For profiles yielding leading-edge separation of the thin-airfoil type, leading-edge suction will probably increase the slope of the lift curve for angles of attack greater than that at which the bubble forms on the base profile. This is due to the characteristic fall-off in slope of the base airfoil's lift curve in this range.

For the usual profile, leading-edge suction should not produce any change in angle of attack for zero lift, such a change, in view of the lack of circulation control, only becoming possible with thick, cambered profiles which show a very thick or partially detached boundary layer over the trailing-edge even at zero angle of attack. Here suction, through controlling the trailing-edge, may affect changes in $\alpha_{o.L.}$.

It is of some interest to note from Ref. 123 that not until an angle of attack of approximately 5^o did the suction proceed to thin the turbulent boundary layer. At lower angles, the slot was seen to actually cause

premature turbulence. Another interesting point brought out in this reference is that some lift increment may be attributed to the fact that the pressure felt at the slot will be the internal pressure, which will always be more negative than would be indicated by use of the external pressure distribution. However, it is shown that a slot of .75%c width and a C_Q of .0065 will yield a lift increment due to this effect of only $\Delta C_{l_{max}} = +.05$. As the majority of practical slots will normally be smaller and operating at lesser C_Q's, it would seem that this effect can generally be neglected.

The only other literature available dealing with leading-edge slot suction describes investigations conducted in England and in Germany in the late and middle forties. The British suction work was performed using two special airfoils, the "Glauert" suction profile and the "Lighthill" suction profile. Tests of these thin airfoils are described in Refs. 120 and 121 and the results are summarized in Fig. 141A. It will be noted that both profiles demonstrate $C_{l_{max}}$ vs C_Q slopes which are lower than any found in the experiments described in Ref. 123 (previously discussed). This relative inefficiency is probably the result of poor slot location. The sharp-nosed "Glauert" profile has a very small slot located at approximately the .7%c location. It is proposed that this slot is too far aft for proper control of leading-edge separation. Fig. 141A seems to indicate that widening the slot will increase maximum lift, but, as only one point is given for this wide-slot condition, this cannot be said with certainty. On the other hand, the "Lighthill" profile has a slot located at the airfoil leading-edge, which would logically seem to be optimum for such sharp-nosed profiles. It is felt that the problem here is excessive slot width as well as the wasteful

extension of the slot to the lower surface. Thus it appears that although these two configurations have characteristics that can be faired to one curve, they quite likely suffer from different forms of the same disease--non-optimum slot location.

The German investigations were involved with the determination of optimum slot location for profiles of various thicknesses. Some of the results of this early work of Walz were reproduced by Thomson in Ref. 170 and are again reproduced here in Fig. 141B. In that, according to Thomson, the original work did not indicate slot width, much of the value of this curve is lost. Also, as the desired maximum lift seems important with regard to optimum slot location, this curve should probably really be a family of curves in C_Q. It is thus recommended that Fig. 141B would best be approached with more than a little caution. Although the trend shown here is felt to be correct, the magnitude and the use of a single curve could be misleading.

One of the major problems of leading-edge slot suction appears to be the provision of sufficient suction velocity at the optimum chordwise location without simultaneously creating excessive suction quantity at other chordwise locations within the range of the finite slot. The external pressure peak under which the slot must operate creates this problem by producing a distribution of suction velocity into the slot which characteristically shows suction velocity increasing rapidly from slot leading-edge to slot trailing-edge. The problem is made more complex by the forward movement and increased magnitude of this pressure peak with increasing angle of attack. This, for the most properly located slot, will generally induce rapid increases in the

suction velocity gradient along with forward movement of the optimum suction location. A situation of this nature, which establishes an inherent incompatibility of slot location and width required and suction velocity distribution required, is obviously wasteful of suction quantity because the majority of the suction flow is moving aft while the point where it is needed is moving forward.

One means which has been developed to alleviate this condition is the use of porous suction over the leading-edge portion of the wing. This type of system, often referred to as area suction, provides a certain amount of suction flow resistivity which acts to lessen the suction velocity gradient for a given C_Q or, through permitting resistivity to increase from the leading-edge of the porous area to the trailing-edge, may even permit suction velocities actually decreasing in the aft direction. It has generally been found that properly designed area suction can attain a given $\Delta C_{l_{max}}$ for a lower C_Q than would be possible with an optimum suction slot. It should be recalled, however, that increased resistivity means increased power for a given C_Q. Therefore the smaller suction quantity necessitated by area suction as compared to slot suction may be outweighed by an increased power requirement. Although it is felt that area suction can be designed to require less power than leading-edge slot suction, insufficient data is available to rigidly establish this point.

Various materials have been tested for use as porous media. These include perforated metal sheet, sintered metal, ceramics, wood, felt, and filter paper. At test Reynolds Numbers, the most practical of these have been felt, filter paper, and sintered bronze.

The degree of resistivity of a porous material may be indicated by its "index of resistivity", τ , which is defined as the total pressure difference in inches of water required to induce a suction air velocity of one foot/sec. through a porous material of given thickness. This is measured where free stream velocity is zero so that the effect of external pressure gradient may be cancelled. Fig. 142 illustrates three general types of permeability arrangements, constant resistivity, tapered resistivity, and stepped resistivity. For the constant resistivity case, a suction velocity distribution is established which yields velocity increasing from the leading-edge of the porous area to its trailing-edge. For a given C_Q, leading-edge suction velocity increases while trailing-edge velocity correspondingly decreases as resistivity, τ , is increased. In order to achieve a relatively efficient suction velocity distribution it is thus necessary to go to high resistivities which necessarily means high suction powers to produce a given suction quantity. Because this is the case, and because the constant permeability arrangement can yield, at best, only a constant suction velocity distribution across the porous area, designers have devised tapering and/or stepping the chordwise resistivity distribution in such a way that, even for low values of τ , a constant velocity distribution or one decreasing from leading-edge to porous area trailing-edge may be readily achieved. In that such a suction velocity distribution appears desirable, it would seem that the tapered or stepped arrangement could provide closely optimum aerodynamic performance while maintaining power requirements only slightly in excess of those for leading-edge slots (which appear to be aerodynamically less efficient than porous suction in every case).

Felt readily lends itself as the porous material in the tapered permeability design, while filter paper in stepped layers seems a convenient arrangement through which to attain stepped permeability. A surface material such as perforated metal sheet must normally cover the felt to protect it from being roughened and from other possible mishaps caused by the airflow. Of course, any filter paper arrangement necessitates strong backing (perforated metal or screen) even though the filter paper may, under test conditions, be placed at the profile surface.

Refs. 116, 117, 118, and 119 describe experiments performed by the NACA in the field of leading-edge porous suction. In addition to providing information regarding the effectiveness of various permeability arrangements, these references give some indication of the optimum chordwise extent and location of leading-edge porous suction. These findings are summarized in Figs. 143 and 144.

Figs. 143 and 145 demonstrate the effects of porous suction location and extent upon the characteristics of a 10.51% profile (Refs. 117 and 118), a 64_1A212 profile (Ref. 116), and a 0006 profile (Ref. 119). With the exception of the 0006 case where such data was not available, data shown is for constant permeability conditions. It is felt that, for most realistic curve fairing, the curves should initiate ($C_Q = 0$) at the lift coefficient where the profile stalls with porous area present but sealed to prevent outflow. This is consistant with the handling of the leading-edge suction slot discussed previously.

The 10.51% profile of Fig. 143 is of a series which appears closely a cross between the "00" series and the "64" series. Although the nose has

a bluntness slightly greater than that for the 0010, general profile shape aft tends to approximate the 64-010. The base 10.51% profile appears from boundary-layer surveys to stall in a closely pure leading-edge manner, although trailing-edge separation seems imminent. Stall pattern with suction is indicated, from studies of lift-curve stall shapes, to be quite consistent with the trend indicated in Fig. 136 and an estimated linear extrapolation $C_{l_{max}}$ of 1.65 for this profile at this Reynolds Number very closely divides stalls which are predominantly leading-edge from those which are primarily of the trailing-edge type.

Fig. 143A reveals that, as might be expected on the basis of the leading-edge slot observations, optimum porous extent is primarily a function of desired lift level. The porous area extending from the leading-edge to the .75%c location looks to be the best of those tested from the point of view of leading-edge stall delay. Again, fall-off prior to the achievement of linear extrapolation lift is seen and is felt to be indicative of the mixed stall region into which this profile enters at comparatively small values of C_Q. As with the leading-edge slot, increases in chordwise porous extent serve to decrease the initial slope of maximum lift vs C_Q but increase the ultimate lift attainable. It will be noticed that, unlike the leading-edge slot case, trailing-edge BLC for a given configuration ceases to become more powerful with suction quantity increases or increase in chordwise suction extent after a given C_Q is attained. (Note the leveling-off of the curve at $C_{l_{max}} = 1.8$)). Although the reason for this effect is not obvious, it is possible that it can be attributed to the comparative insensitivity to C_Q variations in the case of porous suction with

relatively large resistivity, of the seemingly important suction velocity at the control's trailing-edge.

Fig. 143B is indicative of the large effect resistivity may have on the aerodynamic efficiency of leading-edge suction. Comparing Fig. 138, 143B and 143A cannot fail to reveal the highly beneficial effect resistivity can produce--from the aerodynamic point of view if not from that of power. It will be further noted from this figure that the apparent optimum slot configuration initiates at the .3% chord location rather than the profile leading-edge. Pressure distributions indicate that the blunt nose causes a base profile pressure peak to occur at the .6% chord location immediately prior to stall and that this peak does not move far forward of the .2% location even under high C_Q, high α conditions. Thus initiating suction this far aft will not detract from leading-edge stall prevention and without doubt diminishes the total suction flow required. On the majority of profiles, however, it would be thought that porosity should initiate at the leading-edge. Although such a location may waste a little power, it is felt that it is better to be sure of having the leading-edge bubble under efficient control than to initiate suction too far aft. The configuration with suction initiating at the .5% chord point will be seen to be inferior to that initiating at the .3% position--probably because it is too far aft to properly control the leading-edge separation. Fig. 143B also points up the fact that excessive porous area will create inefficiencies particularly in the leading-edge stalling regime, while extending porosity beneath the leading-edge can do nothing but create waste in suction quantity and power required.

The 64_1A212 characteristics summarized in Fig. 144A show the same trends regarding the effect of porosity extent as indicated for the 10.51% configuration. Although the base profile stall was of the mixed leading-edge type, stall under all powered conditions tested appeared to be of the mixed trailing-edge or pure trailing-edge type. Linear extrapolation maximum lift coefficient is here $\cong$ 1.45. The indication here is that all porous extents tested were much too wide for optimum control of leading-edge stall, and, in most cases, too wide even for best operation upon the turbulent layer. With a profile of this thickness, of course, any leading-edge suction would be expected to necessitate large C_Q's in order to attain appreciable gains in maximum lift.

Fig. 144B demonstrates the effect of porous extent upon a thin, thin-airfoil stalling profile. The data shown here is for the tapered permeability case in which no systematic data is available under constant permeability conditions. Stall here was of the pure thin-airfoil type throughout the entire lift and C_Q range investigated. Linear extrapolation maximum lift coefficient is estimated to be approximately 1.85 for this profile at test Reynolds Number. The narrowest porous area, 0%c - .5%c was here found to be optimum. This, recalling the failure of the flow to separate from the trailing-edge under any of the test conditions, serves to demonstrate the need for a very narrow, well forward porous area if only leading-edge separation is to be considered, wider areas being optimum only for the mixed or trailing-edge stall cases. It is interesting that the porous configuration which wastefully initiates on the lower surface of this profile has better characteristics than those which initiate even as far forward as .1% chord

on the upper surface. Here, the disadvantage of letting the bubble get a head start is well illustrated.

Thwaites, in Ref. 111, suggests a method, based upon theoretical considerations, which predicts the amount of area suction necessary to overcome leading-edge separation and is based upon the extrapolated pressure distributions of the base profile. The distance over which suction should be applied need extend only to the chordwise station at which the adverse velocity gradient corresponding to the desired lift level is no more severe than the maximum velocity gradient incurred on the base (no suction) profile prior to stall. This analysis is in agreement with the rather intuitive suggestions made at the beginning of this section and seems to hold well. It has been observed, however, that while theory shows this key chordwise station to generally move aft as lift is increased beyond base profile maximum, available experimental data indicates that it moves forward.

Fig. 145A attempts to demonstrate, on the basis of the two profiles for which data is available at approximately the same Reynolds Number and resistivity index, possible effects of profile thickness upon the appearance of the $C_{l_{max}}$ vs C_Q plot. Unfortunately, little can be seen here as neither configuration has what would appear to be true optimum porous extent. Thus, although it seems that the two profiles would have similar initial slopes, it is feared that this is merely a matter of coincidence and cannot be of any value as an aid in prediction. Fig. 145B indicates the type of velocity distribution which might be expected at stall under relatively high C_Q conditions when such small resistivity is utilized. For the zero resistivity, slot case, the slopes of these curves would be expected to be higher, with the

suction velocity at the leading-edge lower and that at the trailing-edge higher than with the configurations shown here.

The effect upon maximum lift characteristics of variations in resistivity for the constant permeability case is illustrated in Fig. 146. Here the effect mentioned in the preceding paragraph of increasing resistivity decreasing the value of the suction velocity gradient at a given lift level is clearly seen. Fig. 146B reveals that those configurations of greater resistivity require less suction quantity in order to achieve the lift coefficient for which the suction velocity distributions are shown (C_ℓ = 1.7). Further, indications are that the configurations of greater resistivity will show greater aerodynamic efficiency throughout the entire leading-edge and mixed stall range. It may be, however, that use of porous regions with small resistivity can effect greater potential lifts in the trailing-edge stall regime due to the comparatively large suction velocity located relatively far aft.

Fig. 147 demonstrates the distributed resistivity arrangements examined in Refs. 118 and 119. Fig. 148A demonstrates the effect upon $C_{l_{max}}$ produced by the application of tapered permeability to a 0006 airfoil which displays thin-airfoil stalling characteristics. The data shown are for a porous extent ranging from the leading-edge to 1%c, somewhat greater than would appear to be optimum from a $\Delta C_\ell / C_Q$ point of view. A comparison of the velocity distributions is shown in Fig. 148B. The linear extrapolation maximum lift coefficient (trailing-edge stall) for this profile was estimated to be 1.85. It will be seen that in the range of these tests the tapered permeability permits greater efficiency. There are no data available to prove

the point, but it would be expected that as the trailing-edge stall is approached the difference between the two arrangements would cease to exist. It is unlikely that the constant permeability case, displaying the higher suction velocities at the downstream end of the porous region, would have a discernibly greater effect upon trailing-edge stall then the tapered case for so forward a suction location. In any event, with such a small extent of porous area the effect on trailing-edge stall would not be expected to be great.

The effect of tapering the permeability in the manner illustrated by Fig. 147 upon the maximum lift characteristics of the 10.51% symmetrical profile is demonstrated by Fig. 149A. Fig. 149B illustrates the suction velocity profiles obtained with these distributions for stall at $C_{l_{max}} = 1.7$. It will be remembered that the linear extrapolation method indicated that after $C_{l_{max}} = 1.65$ this profile could be expected to stall in a very nearly pure trailing-edge manner. As can be seen from the figure, it is the velocity at the downstream end of the porous region which determines the lift level above this lift coefficient and as would be expected, it is the resistivity arrangement that achieves this velocity while maintaining a lower leading-edge flow that appears most efficient.

Figs. 150A and B are similar plots for the stepped permeability arrangements as shown in Fig. 147. The conclusions are generally the same as for the tapered case although the violent discontinuities produced in the suction velocity profiles somewhat obscure the results. For $C_l > 1.65$, i.e. the region of leading-edge or mixed stall distributions achieving relatively constant velocity profiles are most efficient. Above this lift

coefficient, when the stall becomes predominantly trailing-edge in nature, the arrangements having downstream velocities higher than the average suction velocity display markedly improved performance.

Before concluding these remarks about leading-edge area suction, some mention must be made about the effect of variations in free stream velocity. A change in free stream velocity at a constant value of suction coefficient implies a similar change in suction velocity. Depending upon the material being used to obtain the porous area this may produce a change in velocity distribution, the permeability of some substances not being linear with the pressure differential applied. Experimental evidence would seem to indicate that this is a small effect that in most cases can be ignored.

A far more influential effect of change in free stream velocity is the resultant effect that altering the Reynolds Number has upon the stall characteristics of the profile. If the porous region is located in the optimum position for control of a leading-edge type of separation, clearly a change in Reynolds Number causing the stall type to change to the mixed variety or even to the pure trailing-edge type, will greatly reduce if not totally obscure the effectiveness of the system. This same remark, of course, holds for trailing-edge separation type controls when a reduction in Reynolds Number changes the stall to the leading-edge type separation.

Moving the slot location aft on the profile would appear to be beneficial for those profiles displaying predominantly trailing-edge type separation. The results produced by such slots are illustrated by Figs. 151 and 152. Unfortunately although the slot is located at the 45% chord point in all the cases illustrated different slot widths have been utilized so direct comparison may be somewhat hazardous. It is believed, however, that definite trends can be illustrated.

The 65_2-415 profile displayed a mixed variety of stall. Mid-chord suction produced two opposite working effects. By controlling the trailing-edge separation, it produced an increase of circulation and hence an increase in local angle of attack thereby aggravating the leading-edge separation. The net result is a relatively low increase of C_l at all Reynolds Numbers. The rest of the profiles illustrated in Figs. 151 and 152 are of the trailing-edge stalling type and are markedly helped by the application of mid-chord suction. As expected, the initial application of suction produces large increments in $C_{l_{max}}$. The rate of increase in $C_{l_{max}}$ with C_Q decreases as complete control of trailing-edge separation is approached.

It appears possible for profiles with large leading-edge radii to approach their potential lift level for sufficiently large suction quantities. At such quantities, the effect of suction, although still largely a trailing-edge control produces appreciable leading-edge and sink effects. Profiles with sharper leading-edges will not achieve these lift levels being limited by the advent of leading-edge separation. It has been possible to estimate this effect with fair accuracy by use of the linear extrapolation method.

Figs. 153 and 154 present a summary of the available data. The slight effect of mid-chord suction upon the profiles demonstrating mixed stall characteristics is markedly shown as is the strong effect on those having trailing-edge separations. The effect of Reynolds Number on the initial lift increment with suction is also demonstrated. It would appear that at a Reynolds Number of 1×10^6 the thicker profiles experienced some premature separation. At 6×10^6 this effect vanished and a fully turbulent boundary layer developed well forward of the slot. Suction thus could serve from its

initiation to thin the boundary layer in order to overcome trailing-edge separation, and was not required to achieve flow attachment first.

Fig. 155 illustrates the effect of mid-chord suction as a function of thickness ratio for the camber profiles examined. The close adherence of the suction lines to the linear extrapolation leading-edge separation line is evident. Figs. 156 and 157 demonstrate this same effect by comparing the $C_{l_{max}}$ obtainable on a thin, leading-edge stalling profile as a function of slot location and suction quantity.

There are few data available concerning the effect of combining mid-chord and leading-edge suction. What few there are bear out the expected result if the leading-edge stall is avoided, trailing-edge separation suppression increases the lift level appreciably. The results of very limited tests on a 63_1-012 profile are shown in Fig. 158. In these tests it appears that the optimum distribution of suction quantity between the slots was not achieved. Fig. 159 summarizes the remaining data available from the literature.

In order to utilize a powered leading-edge control effectively the designer must first of all know the separation type to be expected at the Reynolds Number and circulation level desired. The linear extrapolation type of argument based on the known characteristics of the base profile forms the basis for this estimation. If leading-edge stall is present, care should be taken to place the slot or porous region in the most nearly optimum position in order to minimize the power required. If trailing-edge stall forms the limiting case the designer may elect to employ a mid-chord slot, although it is probable that he would use one of the more powerful and probably simpler from a structual point of view, trailing-edge systems. The increment in lift

to be expected from the application of a given suction quantity C_Q can only be estimated from existing test results of similar systems. This estimation can only be intelligently made if the separation conditions being overcome are similar in the two cases.

Having now studied the characteristics of suction systems in some detail, it is of interest to examine the effect of blowing as a turbulent boundary layer control. As has previously been explained, suction appears to be the most efficient method, both aerodynamically and powerwise, of controlling the boundary layer. Further, it offers the possibility of laminar boundary layer stabilization and resultant drag reduction. However the relatively extensive equipment and the possible requirement of auxiliary power as well as provisions for internal low pressure ducts severely limit its use on modern high density aircraft.

Blowing systems on the other hand, although wasteful of power, are simple, compact and easy to apply. Since the flow issuing from the blowing nozzle is decelerating, the pressure gradient the flow is proceeding against is adverse which means it must of necessity be turbulent, and no possibility of laminar boundary layer stabilization exists. Some of the disadvantages of blowing arrangements are compensated by the so called "jet flap" or "chord extension" effect which induces additional lift on the profile as well as the direct jet momentum components.

It must be pointed out again, however, that both of these effects depend primarily upon the residual energy remaining in the blowing jet as it leaves the trailing-edge. Since locations of blowing nozzles forward of the trailing-edge or flap hinge are required if the system is to have an

appreciable effect upon the stall characteristics of thin profiles, these compensating factors are pretty much absent and the decision to use blowing rather than suction must be based solely on mechanical complexity, reliability and weight.

Studies were conducted at Princeton on both leading and trailing-edge stalling profiles (Refs. 146, 147, 149 and 153). Blowing slots under the leading-edge, just aft of the leading-edge and at various mid-chord positions were explored. The configurations studied are shown in Fig. 160.

The initial investigation of the possibility of alleviating leading-edge separation by blowing was conducted in the smoke tunnel. The NACA 64-006 airfoil was selected for these tests. The purpose of these smoke studies was the determination of the optimum position of the blowing slot. A solid airfoil was first tested in order to study the nature of the separation. From an examination of close-up photographs of the solid section model it became apparent that at these Reynolds Numbers the leading-edge separation became quite pronounced even at low angles of attack. Noticeable separation appeared at $\alpha = 4^{\circ}$ (Fig. 161A) and rapidly increased in severity up to the stall. From the close-up at $\alpha = 6^{\circ}$ (Fig. 161B) it will be seen that the flow started to separate almost directly at the nose of the profile, reached a maximum separation distance at approximately 1.5% and finally reattached at about 4%. This test was followed by a series of studies of profiles equipped with slots at 0, 1.5, and 4% of the chord.

Strong blowing from a slot located at the 4% chord point produced a marked change in the flow field past the airfoil, the photographs revealing the tendency of the streamlines to flow toward the jet and the considerably

thicker turbulent boundary layer caused by the expansion aft of the jet nozzles. It must be noted that the flow still separated from the profile leading-edge (Fig. 162). Actually even though it had rather profound effects upon the flow field, the blowing seemed to exert only a very slight influence upon the location of the separation point as would be expected. It did, of course, exert a marked influence upon the extent and shape of the separated region, reattaching the flow just aft of the blowing slot.

From a study of the photographs it is seen that the model with the blowing slot located at 1.5% was an improvement over the 4% slot (Fig. 163). The flow separated above an angle of 8^{o}. Here again it left the airfoil at the leading-edge. The maximum separation distance was, of course, less than with the 4% location, the flow reattaching just downstream of the slot.

With the blowing slot at 0% (Fig. 164) the jet blew out along a path perpendicular to the chord lines of the section even though it was initially directed tangent to the surface. Later tests, although not defining it in detail, have shown that there is a relationship between jet size, velocity, pressure and the curvature of the surface for which the jet will stay attached to and follow the surface (Coanda effect). These tests were made well beyond the critical values and attachment was impossible. As the size of the profile is increased, the physical dimensions of the nose increases and it is possible that flow attachment could be achieved in full scale application. In no case in these small scale laboratory tests was it possible to achieve attachment to high speed profiles although the flow could be guided about the leading-edges of thicker profiles with ease.

On the basis of these preliminary smoke studies, a model employing a blowing slot at the 1.5% chord point was tested in the wind tunnel. This

position gave the smallest leading-edge separation distance, most jet induction effect on the flow pattern, and the greatest lift increment of the three positions tested. The trend seems to indicate that the optimum location is still ahead of the 1.5% chord point. The ideal location based on a given jet velocity, but not necessarily power required, would be to have the blowing slot as close to the leading-edge as possible but still keep the jet attached to the surface. (Since this is a region of high negative pressure, it is possible that such a location could be advantageous power-wise even though the duct losses caused by the restricted space available would be very high).

The results of the wind tunnel tests are shown in Fig. 165 from which it can be seen that there is an increase in maximum lift coefficient with increasing jet velocity as well as a slight increase in lift curve slope. The lift curve of the airfoil with no blowing is shown for purposes of comparison. Even though the curve of the airfoil with no blowing was not carried into the region of stall, it is apparent that the application of blowing tends to gradually flatten the lift curve prior to stall. From the smoke tunnel tests it was seen that the stall itself remains quite abrupt even with blowing. Under all conditions the stall was very violent. Because of the danger of breaking up the model before all tests were completed, it was decided not to try to obtain data past the stall.

Fig. 166A demonstrates the effect of velocity ratio upon the lift of the airfoil section. Generally speaking, increasing the velocity ratio will bring continually higher stall angles and rapidly increasing lift, as well as producing slightly increased lift for a given angle of attack (an increase arising partly from the lower static pressures induced by the jet and partly from the momentum component). The only exception to this is noted at

high angles of attack and for velocity ratios of under 3 where the lift drops off slightly as the velocity ratio is increased from zero. This is due to the disruptive effect of the low energy air issuing from the slot at less than the local velocity. Above a velocity ratio of 3 the induction effect upon the free stream air became appreciable. Since the wind tunnel equipment limited the magnitude of the velocity ratio obtainable, further smoke tunnel studies were conducted at very high jet velocities. Fig. 167 shows the strong lift increase produced by a velocity ratio of 12 as well as the effect of slot location.

A certain insight into the mechanism of the blowing jet can be obtained by studying Figs. 168, 169, and 170. Fig. 168 shows the chordwise pressure distribution of the NACA 64-006 profile modified to contain a blowing slot at the 1.5% chord point. The blowing to free stream velocity ratio is maintained equal to zero throughout the angle of attack range tested. The formation and extent of the leading-edge bubble is clearly visible as a relatively constant pressure region at the nose. Also noticeable is the lack of pressure recovery at the trailing-edge indicating a tendancy of the thickened boundary layer to separate.

Fig. 169 is a similar plot for a velocity ratio of 5.2. The effect of the blowing jet on the leading-edge is clearly visible. It is interesting to note that the pressure recovery at the trailing-edge is only slightly affected even at this relatively high velocity ratio indicating that most of the energy of the jet is dissipated before the trailing-edge is reached. At these blowing quantities it can therefore be concluded that the system is a leading-edge control that affects trailing-edge stall only slightly. Studies

have shown that what effect there is arises primarily from the alteration of the boundary layer achieved by preventing appreciable leading-edge separation. Fig. 170 is a plot of the chordwise pressure distribution at $\alpha = 7.1^{\circ}$ for velocity ratios up to 5.1. These distributions display the effectiveness of blowing in surpressing the leading-edge separation.

As the angle of attack is still further increased, leading-edge separation occurs ahead of the jet, but is reattached until final stall is reached. The smoke tunnel studies indicate that in the region of blowing velocities below VR $\cong$ 6, a mixed leading and trailing-edge separation existed, but that stall was primarily of the leading-edge variety. As the blowing jet was increased in strength, however, even though it developed increased effectiveness as a trailing-edge separation suppressor, its leading-edge effectiveness was still greater and the profile after going through a mixed stall region approached the pure trailing-edge separation case. These cases could not be approached in the wind tunnel owing to limited blowing capacity and stall was in all cases of a violent leading-edge type.

An interesting comparison to these tests is afforded by the explorations described in Refs. 146 and 147 where leading-edge blowing was applied to a relatively thick profile having a moderately large leading-edge radius. The model was a section taken from a Sikorsky S-56 blade which had a slightly modified NACA 0012 section. Unfortunately there were no pressure distribution data taken so it is not possible to directly compare the mechanisms of the two profiles.

Owing to the relatively large leading-edge radius it was possible in the case of the 0012 profile to place the blowing slot directly at the leading-edge

and in some cases actually slightly under it, the Coanda Effect being sufficient to maintain the blowing jet completely attached to the upper surface. The slot configurations are demonstrated in Fig. 171.

Fig. 172 shows typical lift curves obtained from these tests. Data points are not shown since in order to obtain the higher values of blowing to free stream velocity ratios the tunnel had to be slowed down and the results presented represent an attempt to correct all data to the same value of Reynolds Number. One will immediately note how much more effective leading-edge blowing for a given velocity ratio is in this case than for the 64-006 profile. The momentum coefficient C_μ would perhaps be a better quantity to compare, but for qualitative purposes V_j / V_o will do since the two slots were not of excessively different sizes.

The explanation for the improved efficiency of the blowing jet is related to the pressure distribution and stall characteristics of the two profiles. The 64-006 profile displayed leading-edge separations that eventually produced stall. If these separations were surpressed and the theoretical potential flow distribution achieved, a very steep adverse gradient appeared just aft of the leading-edge. This gradient was extremely destabilizing for any jet moving against it, with the result that the blowing jet thickened, rapidly dissipating most of its energy as turbulence. On the other hand, the 0012 profile at these Reynolds Numbers, stalls in a mixed manner with the trailing-edge separations being predominant. If this stall is surpressed and the angle of attack increased still further, even though the leading-edge gradient is such that it tends to produce leading-edge stall, it does not approach the severity of that experienced by the sharper nosed

profile. For this reason, the blowing jet passing over the upper surface did not dissipate its energy so rapidly, an effect visible in the smoke tunnel where the character of the jet at the trailing-edge could be clearly seen.

Fig. 173 demonstrates the variation of c_ℓ with jet velocity ratio. The increasing slope of the lines with angle of attack reflects the increased portion of c_ℓ arising from the vertical jet momentum component and the chord extension effect. There is unfortunately insufficient information to permit the determination of the stall pattern. Since the observation was made that the stall was in every case violent, it would appear that the relatively gentle pressure gradients permitted the jet to remain attached with sufficient energy to form an effective trailing-edge separation control up to the point where the jet separated, probably at the point of maximum gradient near the nose.

Ref. 149 contains a report of some additional tests conducted within the Subsonic Aerodynamics Laboratory on the stall suppression of relatively thick profiles by means of blowing jets. In this case the profile was again the 0012, but for some of the tests a modified nose was employed to avoid leading-edge separations. A series of interchangeable nozzles made it possible to test nozzle locations at the .45, .50 and .55c points. The results of investigation are shown in Figs. 174 and 175.

The results for only one slot location have been reproduced here but they serve to demonstrate the type of lift increment that could be obtained. Fig. 174 shows the variation of c_ℓ with C_Q for constant values of α. Fig. 175 is a cross plot of the data in the more conventional lift curve form. Two things will be noted from the figure, the first that the slope of the lift

curve varies with blowing quantity and secondly that blowing has a slight effect upon the stall angle.

The increasing slope of the lift curve, is as in the case of the nose blowing system, a measure of the circulation control produced primarily by the chord extension effect (as shown by a sample calculation in Ref. 149 where it is demonstrated that under the conditions $\alpha = 4^{o}$ and $C_Q = .016$ the expected momentum lift component would be .015 while the actual change was .23). The additional factors contributing to this lift increase at a given angle are, of course, the momentum component and the distributed sink effect produced by the jet passing over the after half of the profile.

Insufficient data were recorded to accurately determine the stall type under the various conditions tested, but it is probable that it was of the mixed variety with the presence of the mid-chord slot causing premature separations to occur at the slot lip. Clearly the leading-edge was sensitive, the application of trailing-edge control failing to extend the lift curve except slightly at the higher quantities where the jet induction effect reattached the leading-edge separation.

Fig. 176 is a comparison plot of the lift increments obtained at the same C_Q for the leading-edge and mid-chord slots. The tremendous advantage when applied to this airfoil enjoyed by the leading-edge system is evident. It is surprising that the slope of the mid-chord system is less than the leading-edge system as one would expect that the jet issuing from a point down to the trailing-edge would exert the stronger chord extension effect. It indeed seems to produce (presumably largely through the distributed sink effect) the larger lift increment at the low angles of attack. At the higher

angles it would appear that the increased flow induction produced by the longer extent of the leading-edge jet over-balances the strength of the mid-chord system.

Unfortunately not nearly enough is understood about the phenomena herein outlined briefly to enable the development of performance estimation techniques; however, certain general conclusions can be drawn. If the profile is of the leading-edge or thin-airfoil stalling type, the pressure gradients produced are extremely disruptive to the jet. Whether or not it is possible to get a jet far enough forward in such a profile to prevent the formation of the bubble rather than merely contain it is open to conjecture. On mixed-stalling or trailing-edge stalling profiles these gradients are much less disruptive and leading-edge jets produce excellent results. In any case irrespective of the stall type jet nozzle locations at other than the leading-edge seem to offer little or no aerodynamic advantages and should be employed only where necessary owing to structual limitations.

Since leading-edge blowing proved to be such a disappointingly inefficient method of overcoming leading-edge separations on sharp nosed profiles owing to the disruptive pressure gradients, an attempt was made to alleviate these gradients by incorporating a blowing slot with an adjustable leading-edge flap, the jet issuing from the break in the flap as indicated in Fig. 177. Both smoke tunnel and wind tunnel pressure distribution tests were conducted with this configuration and are reported in detail in Ref. 159.

The general results obtained can best be visualized by examining the smoke tunnel photographs shown in Fig. 178. The profile under consideration is a NACA 64-006 equipped with a 17.5% leading-edge flap with a tangential

blowing slot located at the break of the flap. Fig. 178A shows the profile with zero nose deflection at its angle for maximum lift $\alpha = 10^{\circ}$. When the angle of attack is increased to 12° the profile stalls abruptly from the leading-edge as demonstrated by Fig. 178B. Turning blowing on reattaches the flow as was the case with leading-edge blowing but as shown in Fig. 178C, blowing at this location merely contains the separation bubble and is extremely wasteful of effort.

The effect of nose flap deflection and blowing at the break of the flap are demonstrated in Fig. 179. Figs. 179A through 179C demonstrate the no blowing case, Figs. 179D through 179F the effect of blowing. The quantity of blowing air employed in this case was high and resulted in considerable circulation control producing a separation from the leading-edge of the nose flap which for these tests unfortunately could not be deflected past 30°. The true efficiency of the system therefore is not shown, but it is interesting that complete stall did not occur until $\alpha = 45^{\circ}$, a result that has not been obtained with any other blowing system even under the high flow conditions herein demonstrated.

One very important characteristic of the system is its ability to improve the efficiency of a trailing-edge circulation control system. This is clearly demonstrated by Fig. 180 which shows the profile equipped with a 30% plain flap which also utilizes tangential blowing. The angle of attack was maintained at 20° at which the unpowered profile was completely stalled. Applying blowing ($C_{\mu} = .07$)over the plain flap deflected 30°, failed to produce any appreciable change in the flow picture, the blowing jet near the trailing-edge being unable to produce reattachment. A similar quantity of

blowing at the break of the leading-edge flap, however, caused a profound change, unstalling the profile and producing a large increment in lift even though a leading-edge bubble existed. Applying blowing over the deflected trailing-edge flap now produced the expected lift increment.

Further insight into the functioning of this system is given by a study of Figs. 181 through 187. Fig. 181 shows the pressure distribution at several angles of attack of a NACA 65-006 profile equipped with a 17 1/2% nose flap deflected 30°. Figs. 182 is a similar plot for a nose deflection of 45°. These plots demonstrate all of the essential characteristics expected, tuft studies indicating that stall was initiating from the flap break.

Figs. 183 and 184 are similar plots with blowing applied from the break of the flap. Although the results are somewhat confused it can be seen that blowing has produced a considerable change in the pressure distribution over the leading-edge flap, the pressure peaks becoming considerably more pronounced.

To define the effect of the blowing, Figs. 185 and 186 have been prepared. Fig. 185 shows the effect of blowing at a low angle of attack ($\alpha = 6^{o}$) and a nose deflection $\delta_N = 45^{o}$. As can be seen, for the quantity of blowing applied, there is essentially no effect except directly in the region of the slot, indicating that the blowing jet lacks sufficient energy to appreciably affect the circulation of the profile other than by flow attachment (the effect of the strong adverse gradient). Fig. 186 demonstrates the same effect at a higher angle of attack ($\alpha = 20^{o}$). Here it will be seen that blowing re-establishes the pressure peak at the flap break. It will be noted that once this peak is re-established essentially doubling the amount of blowing has almost no noticeable effect. Fig. 187

summarizes the test results.

With the flap break controlled (in this case with blowing, but suction could as readily be applied) the stall becomes of the trailing-edge variety, the flow near maximum lift actually separating just downstream of the flap break. Further lift increases can thus be expected only if trailing-edge control is resorted to. The smoke tunnel demonstrated that leading-edge flap break blowing could be applied for this purpose if the jet strength was sufficiently increased. It would appear, however, that although the blowing jet is located at a region of low pressure and hence is relatively efficient quantity-wise as a local re-attachment system, very large increases in quantity (by a factor of at least 10 based on smoke tunnel studies) would be required to overcome the effect of the gradient aft of the hinge-line before appreciable trailing-edge control could be achieved.

As in the case of the leading-edge and mid-chord blowing systems, there is insufficient data available for prediction purposes. It is apparent that the droop nose is effective in reducing the magnitude of the adverse pressure gradient against which the jet must move. The effectiveness of blowing at the hinge line would thus be expected to be greater than leading-edge blowing as is observed experimentally. The more the magnitude of the adverse gradient aft of the blowing slot can be reduced the greater will be the expected effectiveness of a given blowing quantity. If it is possible to produce several such breaks in the contour of the upper surface, effectiveness approaching that of leading-edge blowing on a thick profile might be approached.

IV

THREE-DIMENSIONAL LIFTING CHARACTERISTICS OF WINGS

4.1 Flow Mechanisms of Finite Wings

4.1a Three-Dimensional Flow Phenomena

The low speed aerodynamics of wings designed for high speed flight have long presented a perplexing dilemma for the aerodynamicist. As one yields to the aerodynamic and structural requirements of very high speed flight, the low speed performance suffers accordingly with the result that landing speeds have become increasingly prohibitive in recent years. Before one can even begin to cope with this problem, a fundemental understanding of the flow mechanisms involved is essential, and it is with this subject that this section will be concerned.

Because viscous phenomena become so prominent on swept and/or low aspect ratio wings, a mathematical treatment is, at the present state of the art, decidedly inadequate. Lifting surface theory can predict the span loading characteristics over the linear lift range fairly accurately but this range is, unfortunately, small for most wings. Hence, one must rely mainly on a qualitative description of the three-dimensional flow phenomena, and, when possible, empirical generalizations which can be correlated from existing literature.

The flow mechanisms acting on a swept wing can be classified into several major effects which are: the spanwise drift of the boundary layer, the formation and growth of a leading-edge vortex, the characteristic induced angle of attack distribution, and the induced camber effect. When one considers the relationship and inter-related effects of these various phenomena acting on any given wing, it becomes immediately apparent that the resultant problem is quite complex even from a qualitative viewpoint. The

most prominant as well as least understood of these mechanisms seems to be the formation, location, and influence of the leading-edge vortex. Because this vortex may under certain conditions improve the wing's lifting characteristics and create a stable pitching moment while, under other loading conditions, separate portions of the wing and create severe pitching-up moments, a knowledge of its formation and control would be invaluable. Unfortunately, at the time of the writing of this report, existing literature provides only a cursory description of this flow phenomenon, leaving a most profitable field of research practically untouched.

It has been observed that if a bound flow, such as that in a channel, is subjected to a uniform flow perpendicular to its direction, the bound flow will roll up into a vortex. Precisely why this should happen is not at all evident, but it does nevertheless provide a clue to the presence of the leading-edge vortex observed on many swept-back wings. In two-dimensional flow, it is well established that certain thin airfoils exhibit a large bounded leading-edge separation bubble. One would naturally suppose that a leading-edge vortex would form when these sections are incorporated into a swept-back wing and subjected to the spanwise pressure gradient that arises from sweep-back. However this statement assumes more the dimensions of an intuitive feeling than a satisfactory factual explanation, and certainly leaves much to be desired. What is even more perplexing is that the vortex can form on swept wings which are not constructed of those sections which exhibit the large separation bubble.

The leading-edge vortex can be characterized as conical in cross section with the diameter of the cone increasing toward the wing tip due to the

accumulation of flow in the spanwise direction. Generally, the axis of the cone will lie somewhere in the vicinity of the wing leading-edge although it may either join the wing vortex system or be shed somewhere inboard of the tip depending upon the wings geometric parameters and aerodynamic loading.

The spanwise drift of the boundary layer can easily be explained by first considering a swept wing of infinite aspect ratio. Here, the respective chordwise pressure distributions are staggered so that on any line perpendicular to the flow direction, there exists a span wise pressure gradient tending to transport mass along the wing in the direction of sweep. At any given lift coefficient, the degree to which this outflow is established depends primarily on the sweep angle involved (Ref. 309). For a finite wing, the spanwise flow of the boundary layer results in several important effects; first, because of the absence of boundary layer on the inboard sections of the wing, stall is effectively delayed, and the sections there can obtain values of lift coefficient far in excess of their two-dimensional capabilities, and second, because the pressure gradient vanishes in the vicinity of the wing tip, the accumulation of boundary layer from the inboard sections of the wing tends to separate the tip sections more easily than the corresponding sections with normal boundary layer thicknesses.

It is well known that sweep changes the spanwise distribution of induced angle of attack, causing the load on a wing of given aspect ratio and taper ratio to be concentrated farther outboard for increasing angle of sweep. Also because the minimum induced angle of attack occurs somewhere inboard of the tips, i.e., the effective angle of attack becomes a maximum, this is the most likely location for the formation of the leading-edge vortex, particularly

for wings made of those airfoils which exhibit thin airfoil type stall.

For swept and unswept wings, the induced camber is positive at the root and negative at the tip (Ref. 309). As the induced camber becomes more positive, the center of pressure at any given spanwise station, moves aft, but no simple relation expressing this variation is known. The negative induced camber at the tip produces an adverse pressure gradient tending to promote tip separation, while the positive induced camber on the inboard sections hinders flow separation.

The influence of aspect ratio does not become predominant before the wing tip edges parallel to the free stream approach the dimensions of those edges perpendicular to this direction (Ref. 285). For these very small aspect ratios, the tip vortices moves in over the top surface of the wing and induce suction forces strong enough to alter the lift distribution of the wing. This effect is somewhat analogous to the leading-edge vortex effect over a swept or delta wing as the vortex breaks away from the leading-edge before joining the trailing vortex.

In Ref. 309, Furlong and McHugh attribute the formation of a leading-edge vortex on those wings not made of sections which exhibit thin airfoil characteristics, to the induced camber effect, saying that if this effect is great enough, a section which in two-dimensional flow exhibits trailing-edge stall, will stall from the leading-edge. Although this explanation seems quite plausible, it leaves much open to question. Even though no distinction is made between airfoils which stall from the leading-edge, i.e. leading-edge stall type or thin airfoil stall type, the implication is that a leading-edge bubble, characteristic of airfoils exhibiting leading-edge

stall, is sufficient to start a leading-edge vortex. Further, this implication is explicitly stated by H. O. Palme in Ref. 285; Palme states that the leading-edge vortex can form on wings with large sweep which are composed of airfoil sections exhibiting either thin airfoil or leading-edge stall. Although what follows has no experimental verification, it would seem reasonable that a large leading-edge separation bubble, characteristic of a two-dimensional thin airfoil stall, is needed for the formation of a leading-edge vortex. It is well known that the existence of the leading-edge vortex is much easier to predict, and takes place at relatively lower angles of sweep on wings which have sharp leading-edges, i.e., the sections have large leading-edge bubbles. Also, it is generally recognized that in two-dimensional flow, the stall type of an airfoil can be changed by adding circulation control and/or boundary layer control. For example, an airfoil which normally stalls from the trailing-edge can be made to stall from the leading-edge with the addition of a flap. Effectively, circulation control involves shifting the center of pressure aft on the airfoil, and boundary layer control prevents flow separation on the surface of the airfoil.

Then, if an airfoil section which does not exhibit a thin airfoil type stall is incorporated into a wing with a sufficient amount of sweep, the combined effects of the spanwise boundary layer drift and induced camber will precipitate a thin airfoil type leading-edge bubble on the inboard sections. The induced camber on these sections will shift the center of pressure aft while the drainage of boundary layer air will tend to prevent flow separation. It must be emphasized that this explanation is of a speculative nature, and is based solely on trends observed in current aeronautical literature.

When the cumulative effects of the various flow mechanisms operating on a swept wing are considered, one can draw several general conclusions. The inboard sections are extremely resistant to flow separation, and can obtain lift coefficients in excess of their two-dimensional capabilities because the boundary layer drift operates as a trailing-edge control to prevent flow separation, and the induced camber effect results in a rearward shift of the pressure distribution which creates a more favorable pressure gradient. Further, because of the characteristic induced angle of attack distribution operating along with the above conditions, the root sections may obtain exceedingly high angles of attack before stalling which contributes to the severe pitch-up tendency observed on many swept wings. On the other hand, the outboard sections are vulnerable to separation because of the combined influence of the induced camber effect, the characteristic induced angle of attack distribution, and the accumulation of spanwise boundary layer flow. Although premature tip separation has frequently been attributed mainly to excessive boundary layer growth recent experimental evidence seems to indicate that these sections may actually obtain their theoretical two-dimensional capabilities, i.e. according to simple sweep theory ($\cos^2 \Lambda$ law). This would seem to indicate that the span loading characteristics resulting from the typical induced angle of attack distribution are the more important factor influencing premature separation than the generally accepted excessive boundary layer explanation.

4.1b Stall Types

From Ref. 258, the basic types of stall for finite wings may be classified as follows:

I. Two-Dimensional Stall

II. Swept Wing Stall

IIa. Trailing-Edge Separation

IIb. Leading-Edge Separation

III. Low Aspect Ratio Wing Stall

IIIa. Delta Wing

IIIb. Straight Wing

Being essentially a viscous phenomenon, the stall of a finite wing is a function of all the viscous effects observed in two and three-dimensional flow plus the effects of section and plan-form parameters. Stall prediction for Type I has been fairly successful (Ref. 255) because the stall pattern is mainly two-dimensional, and the point of initial stall can be calculated from a consideration of section stall and plan-form parameters. From the discussion of the preceding section, one can surmise that, at the present state of the art, the three-dimensional viscous flow mechanisms of swept and/or low aspect ratio wings render any analytical attempt at stall prediction quite useless. In Ref. 281, an attempt was made on the basis of conventional unswept wing theory combined with simple sweep theory to predict the point of initial separation on a moderately swept wing which illustrated that mathematical methods were decidedly inadequate.

Stall types IIa and IIb, trailing-edge and leading-edge separation on swept wings, differentiate between the predominant effects of the spanwise boundary layer drift and leading-edge vortex flow. For stall Type IIa, the separation initiates on the tip trailing-edges, moving inboard and advancing forward on the chord with increasing angle of attack. Characteristic of moderately swept wings composed of fairly thick sections, this type of stall

is mainly dependent upon the spanwise boundary layer drift and induced angle of attack distribution. As mentioned at the end of the preceding section, recent investigations seem to indicate that the span loading characteristics may be the more important factor determining tip separation than the accumulation of spanwise boundary layer flow. Thus it would seem that the tip sections of such a wing do stall prematurely due to the span loading characteristics, but that the lift coefficient obtained is roughly commensurate with that which would be expected from simple sweep theory. Because of the absence of boundary layer on the inboard sections, however, these sections can still obtain lift coefficients far in excess of what would be expected two-dimensionally which indicates that the boundary layer drift remains quite influential.

Stall Type IIb is characteristic of moderate to high sweep angles and thin wing sections. After the formation of the leading-edge vortex, the outboard wing sections experience a lifting force created by the low pressure region of the vortex, and as mentioned in the preceding section, the center of pressure on sections affected by the vortex shifts aft. As the angle of attack is increased, the vortex grows in strength and eventually becomes so large and unwieldly that it partially diffuses and sheds from the wing with the result that the tip sections are left in a region of diffused vortex flow. While the outboard sections are partially stalled, the root sections are obtaining exceedingly high lift coefficients due to the drainage of boundary layer air which results in the severe pitch-up tendency observed on many swept-back wings.

The stability of swept wings appears to be a function of three parameters; sweep angle, aspect ratio, and taper ratio. It is interesting to note that an unbalance of moment areas is the more important factor with regard to stability than the occurrence and severity of tip stall (Ref. 309). From an emperical investigation, a stability boundary was determined which worked well for wings having a taper ratio of approximately one (Fig. 188); it was found, however, that a correction was needed for delta wings where the taper ratio is zero. By taking the ratio of the area aft of the quarter chord line to the total area, it was found that a value of .69 agreed well with the stability boundary for taper ratios of one, and also gave good results for taper ratios of zero (Fig. 189). Because the tip sections of highly tapered wings operate at higher values of lift coefficient relative to the root sections than those on untapered wings, tip separation occurs earlier. It will be observed that the boundary for zero taper shifts to the right, wheras if tip stall were of primary concern, it would be expected to shift to the left.

The type of swept-wing separation seems to depend primarily on angle of sweep-back and the section leading-edge radius, assuming the Reynolds Number to be held constant; Fig. 190, represents the predominant tendencies of swept wing separation at a Reynolds Number of approximately 6 million. For unstable wings, several interesting trends in the variation of pitching moment coefficient with lift coefficient can be observed. With increasing lift coefficient, the pitching moment coefficient for wings with trailing-edge separation grows progressively more positive, usually quite smoothly as more and more separation takes place. A similar, simple relationship for leading-

edge separation is not evident because, except for wings with very small leading-edge radii, it is almost always accompanied by some degree of trailing-edge separation. As the leading-edge vortex grows, it will produce a negative pitching moment because of the redistribution of chordwise loading on the outboard sections. This effect may be completely nullified, however, by the loss in lift due to trailing-edge separation. Depending upon the predominant influence acting upon the tips, the pitching moment coefficient may go either positive or negative at low lift coefficients. However, the distinctive characteristic of unstable leading-edge separation is the severe pitch-up tendency when the vortex moves inboard, and leaves the tips in a region of diffused vortex flow. The partial stalling of the tips combined with the high lift coefficients obtainable by the root sections give a powerful unstable moment which can usually be recognized quite easily.

Stall Type IIIa, delta wing stall, is mainly an extreme varient of leading-edge separation on swept-back wings. At low angles of attack, the leading-edge vortex moves in over the wing, just inboard of the tips, where it provides additional lifting forces and stable pitching moments. As the angle of attack increases, the vortex moves well inboard, partially separating from the surface, and leaves the outboard sections in a region of diffused vortex flow. Consequently, the wing loses lift and a destablizing moment develops. Thin profiles produce stronger vorticies and larger lift increases, but tip stall also happens earlier.

Stall Type IIIb, small aspect ratio, straight wing stall, usually concerns wings of large taper ratio. The section shape seems to have little influence, but the wing tips are a critical point. Along the tips is created a strong

trailing vortex which induces high suction forces in the vicinity of the top trailing-edges. Consequently, an additional lift force is created which produces a stable moment. At larger angles of attack, the vortex separates from the surface, and complete wing stall is obtained at once (Ref. 285). The stall pattern is then similar to that of a flat plate; the lift is reduced and the pitching moment is stable.

The concept of stall for wings exhibiting pronounced three-dimensional viscous effects is somewhat ambiguous, and it is advisable to clarify this term before proceeding with a discussion of finite wing lift. On conventional high aspect ratio, straight wings, stall is usually identified with wing separation and a consequent loss in lift. The point of initial separation occurs when the section at some spanwise location exceeds its maximum lift coefficient, and from this point, the separation usually grows rapidly and results in a complete deterioration of lift on the entire wing. Because of the effects of finite span, i.e. variable induced angle of attack distribution, the maximum lift coefficient of the wing is usually less than the maximum lift coefficient of the sections of which it is made (for an elliptical load distribution, both would be the same; but this is seldom realized). For swept and/or low aspect ratio wings, however, separation may occur at some spanwise station below the section maximum lift coefficient, and invariably well below the wing maximum lift coefficient. Usually when separation does occur on such a wing, either a pronounced stable or unstable trend of the moment coefficient is observed which defines the usable or available lift coefficient. Thus, the maximum lift coefficient of a swept wing can seldom be realized.

4.2 Effect of Wing and Section Parameters on Lift

4.2a General Discussion

From analytical results and statistical computations, basic trends of the various wing parameters on the lifting characteristics of finite wings can be established. An attempt will be made in this section to summarize the more important results found in existing literature, and to present these in an orderly form. It is not recommended that these curves be used for design purposes, for they will be presented mainly to show trends and, in most cases, a complete specification of all the wing parameters and test conditions will not be explicitly stated. Every effort has been made, however, to correlate only those tests made under approximately the same conditions on any one curve. Also, this section will deal entirely with plain wings. High lift devices will be considered in the next section.

The discussion that follows will primarily be concerned with the effects on the lifting capabilities of finite wings of:

a) Aspect Ratio

b) Sweep-back Angle

c) Taper Ratio

d) Aerodynamic and/or Geometric Twist

e) Section Camber

f) Section Thickness and/or Leading-edge Radius

g) Reynolds Number

It should be pointed out that the maximum lift coefficient for wings with strong three-dimensional flow phenomena is quite often not a true indication of the wings lifting capabilities. Because such a wing may demonstrate an increase in lift even after portions of the wing have stalled, it is desirable

to introduce the concept of "inflection" or "usable" lift coefficient. These terms are commonly used to define the lift coefficient of a swept wing at which large undesirable shifts in the aerodynamic center occur; because the inflection lift coefficient represents the usable amount of lift, it is of more importance to the design engineer than the maximum lift coefficient. Further, to illustrate the effects of cambered sections and/or twisted wings, the ratio of inflection lift coefficient and maximum lift coefficient is a useful parameter.

4.2b Aspect Ratio

The influence of aspect ratio on maximum lift for three basic plan-forms is shown schematically in Fig. 191, part of which was taken from Ref. 285. Accompanying these curves are the angle of attack distributions at which these maximum lift coefficients were obtained. It must be emphasized that the curves shown indicate trends only, for the degree of sweep, section type and thickness, Reynolds Number, and various other parameters must be considered for any given wing.

Because of the influence and strength of the three-dimensional viscous effects, all three plan-forms exhibit high maximum lift coefficients in the very low aspect ratio range. For straight wings the powerful tip vortex creates additional lift forces which seem to have their maximum strength for an aspect ratio of approximately one. As the aspect ratio increases, the tip vortex becomes less influential and $C_{l_{max}}$ decreases until an aspect ratio of about three is reached; with further increase in aspect ratio, the wing loading becomes more elliptical, and $C_{l_{max}}$ shows a general increase as the wing maximum lift coefficient approaches the section maximum lift coefficient.

The delta wing reaches its maximum lift coefficient at an aspect ratio of about two, where the lifting force due to the leading-edge vortex seems to be the strongest. For larger aspect ratios, the angle of sweep, and hence the strength of the leading-edge vortex, would decrease; also, if the vortex attains sufficient strength to move inboard for a wing of larger aspect ratio, a greater portion of the wing tip will lie in a region of diffused vortex flow, and hence the effectiveness of the vortex in creating lift is counteracted by the partially stalled tips. Therefore for aspect ratios larger than 2.5, the maximum lift potential of a delta wing falls off quickly.

It is interesting to note that the trend of maximum lift coefficient with increasing aspect ratio for swept wings is opposite to that displayed by straight wings, i.e. as the aspect ratio increases for swept wings, the maximum lift coefficient decreases. It has been suggested that the flow becomes increasingly two-dimensional as the aspect ratio increases, and that the maximum wing lift coefficient approaches that which would be expected from simple sweep theory. As can be observed from Fig. 192, the maximum lift coefficient of a swept wing is always greater than that which would be expected from simple sweep theory ($\cos^2\Lambda$ law) because of the various flow phenomena which have already been described in section 4.1b. When one considers the curves of the ratio of inflection lift coefficient to maximum lift coefficient versus sweep angle for various aspect ratios (Fig. 193), this simple explanation no longer seems adequate. For a given sweep angle, the ratio of inflection lift coefficient to maximum lift coefficient decreases with increasing aspect ratio, i.e. separation occurs earlier on wings of large aspect ratio. For example, on a wing with forty degrees of sweep, and

an aspect ratio of four separation seems to determine the maximum lift coefficient, while for an aspect ratio of ten, separation occurs at half the maximum lift coefficient. This would seem to indicate that the spanwise flow of the boundary layer becomes increasingly severe as the aspect ratio increases, and that the accumulation of boundary layer on the outboard sections limits these sections to very low values of lift. It has been observed that after the initial separation, the region of separated flow moves rapidly inboard with increasing wing lift coefficient. Hence, the low values of maximum wing lift coefficient for high aspect ratios can be attributed to the large regions of separation rather than any tendency toward two-dimensional flow.

Although the preceding may seem contradictory when one considers the lift increasing influence of the spanwise boundary layer flow over the inboard sections, it appears that the region of separated flow becomes so large with high aspect ratios, that the additional lift produced by the root sections cannot compensate for the loss in lift over the outboard sections; therefore, wings of a given sweep experience a loss of maximum lift coefficient with increasing aspect ratio.

4.2c Sweep-back Angle

The influence of sweep angle on the maximum lift coefficient is presented schematically in Fig. 194. As was stated in section 4.1b, the effect of sweep is to create a spanwise pressure gradient which increases in intensity as the angle of sweep increases. Therefore, for a wing which exhibits predominant trailing-edge stall, the maximum lift coefficient will decrease with increasing sweep because of the aggravating effects on the lift of the

outboard sections due to the accumulation of boundary layer. With a wing exhibiting leading-edge separation, however, a quite opposite tendency is observed, i.e. the maximum lift coefficient increases with increasing sweep. Because the leading-edge vortex creates a lifting force, the greater the strength of the vortex, the more lift produced by the wing; since the vortex strength is a function of the sweep angle, it follows that as the sweep angle is increased on any wing which exhibits leading-edge vortex formation, the maximum lift coefficient will increase.

These same trends are presented in a different form in Fig. 192; here, the ratio of the maximum lift coefficient of a wing with no sweep to the maximum lift coefficient of the same wing with varying amounts of sweep is presented for the two types of separation. It is interesting to note that the ratios for both leading-edge vortex flow present and absent exceed the ratio predicted by simple sweep theory.

From Fig. 193, one observes that for a given aspect ratio, the ratio of the inflection lift coefficient to maximum lift coefficient decreases with increasing angle of sweep. Therefore, increasing the angle of sweep on any given wing will cause separation to occur at lower wing loadings, a conclusion which is obvious from previous discussions of three-dimensional flow phenomena.

4.2d Taper Ratio

Unfortunately, little can be said concerning the effect of taper ratio without first considering the wing plan-form, aspect ratio, stall type, and various other parameters. From Fig. 191, one observes that the maximum lift coefficient for delta wings is larger than that for swept wings

of comparable aspect ratio (from one to three). For these small aspect ratios, it appears that as the taper ratio decreases, the maximum lift coefficient increases. If one assumes the presence of a leading-edge vortex, an assumption which is quite reasonable for a delta wing of an aspect ratio of two, this effect is easily explained. Because the greater part of the wing area is located inboard near the root for small taper ratios, the lifting forces created by the leading-edge vortex operate over a larger area, and hence, enable the wing to obtain high values of lift coefficient even though the tips are stalled.

On a high aspect ratio swept wing ($AR > 5$), the effect of decreasing the taper ratio is to decrease the maximum lift coefficient, while on a low aspect ratio swept wing ($AR < 4$), decreasing the taper ratio seems to increase the maximum lift coefficient. The reason for this behavior is probably an increased tendency toward tip stall in the first case, and an increase in the leading-edge vortex strength in the later case.

4.2e Aerodynamic and/or Geometric Twist

It is well known that large gains can be made on the high-speed performance of swept-back wings if the load is uniformly distributed spanwise and chordwise. In addition to these gains at high speed, study of the problem has indicated that the same qualities should significantly improve the low speed characteristics because the redistribution of spanwise loading should relieve the highly loaded tips while the redistribution of the chordwise loading should delay leading-edge separation. Consequently, almost all experimental results deal with the combination of twist and camber.

Probably the most significant effect of wing twist from the standpoint of an increase in lift, is the pronounced change in the inflection lift coefficient, i.e. that lift coefficient where flow separation seriously affects the pitching moment characteristics. From comparisons between plain and twisted wings, the ratio of inflection lift coefficient to maximum lift coefficient may range from .5 for the plain wing to .90 or .95 for the twisted wing. It must be emphasized, however, that almost every twisted wing also incorporates some degree of camber, and that the effect of twist alone cannot be isolated.

4.2f Section Thickness and/or Leading-Edge Radius

Although these parameters greatly influence the maximum lift of finite wings, their relationship to maximum lift for any given plan-form is often quite complex. For straight wings of high aspect ratio, section parameters can in the majority of cases be handled mathematically, and no difficulty arises. However, for swept and/or low aspect ratio wings, the two-dimensional characteristics of a given section combine with three-dimensional flow mechanisms to produce inter-related effects which may considerably alter the maximum lift coefficient. For example, the type of flow separation present on a swept wing appears to be mainly a function of sweep angle and leading-edge radius (Fig. 190) so that, depending upon the section leading-edge radius, a wing of a given angle of sweep may separate from either the leading or trailing-edge. Conversely, for a wing of given section and leading-edge radius, increasing the sweep angle may effectively alter the section characteristics by the application of trailing-edge circulation and/or boundary layer control (section 4.1b). Thus the wing may

stall from trailing-edge separation at moderate angles of sweep, but stall from the leading-edge at higher sweep angles.

For delta wings, the effect of profile shape is large but existing information seems inadequate to evaluate the influence of leading-edge radius or section thickness on maximum lift. Thin profiles produce stronger leading-edge vorticies but also induce earlier tip stalling tendencies. An analysis by Palme (Ref. 285) indicates no definite trend between maximum lift coefficient and section thickness; this, however, does not necessarily negate some sort of correlation, for leading-edge radius rather than section thickness appears to be the more important section parameter when dealing with the formation of a leading-edge vortex.

Profile shape exerts little influence on the aerodynamics of a very small aspect ratio straight wing because the tip vorticies have such a predominant effect on the flow field.

4.2g Camber

Because camber serves only to redistribute the chordwise loading, little information is available concerning the effects of camber alone on swept or low aspect ratio wings. As mentioned in section 4.2d almost all experimental results involving the incorporation of camber into a wing have considered it in combination with twist, and hence the direct effect of camber on maximum lift is quite obscure.

For a moderately swept wing ($\Lambda = 35^{\circ}$) with 12% sections, a study of camber indicated that the expected trim changes occurred, but the pitching moment characteristics exhibited little variation (Ref. 500). It was further postulated in this reference that the improvements on maximum lift coefficient

due to camber could be estimated from two-dimensional data. However, another NACA test of a 45° swept-back wing of aspect ratio 5.5 having increasing camber along the span (intended to prevent tip stall) indicates that the effects of the spanwise boundary layer flow were so predominant that changing the camber along the span had a secondary effect on the pitching moment characteristics (Ref. 318). But with the addition of several fences, it is interesting to note that the boundary layer flow was sufficiently restricted so that the moment characteristics were similar to what might be expected from the theoretical loading on the wing. Evidently, an increase in sweep angle from 35° to 45° was sufficient to induce a boundary layer drift of such magnitude that a prediction of the wing aerodynamic characteristics from two-dimensional data was rendered impossible, i.e. without stall control devices.

Because camber effectively reduces the leading-edge pressure peak in two-dimensional flow, one would expect that cambered sections on a swept wing would delay the onset of leading-edge flow separation to higher wing-lift coefficients. The only experimental evidence tending to corroborate this expectation combines camber with an increase in leading-edge radius (Ref. 347), and since both modifications would have a similar influence on leading-edge separation, the results are inconclusive.

4.2h Reynolds Number

Those wings which fall to either side of the boundary defined in Fig. 190 are definitely characterized by either leading-edge or trailing-edge separation. But for those wings whose geometric characteristics place them in the immediate vicinity of the boundary, separation will be influenced by both boundary layer drift and leading-edge vortex flow. For such a wing,

vortex flow may be observed at low Reynolds Numbers and low lift coefficients. However, the formation of the vortex has been observed to take place at higher values of lift coefficient when the Reynolds Number is increased. Evidently, the stall pattern of a swept wing exhibiting mixed separation, i.e. both trailing and leading-edge, may change from leading-edge at low Reynolds Numbers to trailing-edge at higher Reynolds Numbers. For this reason, the maximum lift coefficients of swept wings increase with increasing angle of sweepback at low Reynolds Numbers, and decrease with increasing sweepback at high Reynolds Numbers.

For wings which clearly exhibit leading-edge or trailing-edge separation, the variation of maximum lift coefficient with Reynolds Number is shown schematically in Fig. 195. It is interesting to note that these tendencies are very similar to the results for two-dimensional stall characteristics.

4.3 High Lift and Stall Control Devices

4.3a General Discussion

It was the primary purpose of this report to investigate high lift devices with particular emphasis on leading-edge controls, and to provide, if at all possible, some correlation between section data concerning these controls and their influence on the three-dimensional characteristics of a finite wing. From the preceding discussion of flow mechanisms and stall types of those wings which exhibit pronounced three-dimensional phenomena, it does not seem unreasonable to state, at this time, that any purely theoretical approach at predicting maximum lift, either with or without high lift devices, is inadequate. Further, while a semi-empirical or statistical study might prove of considerable use to the design engineer, it is unfortunate that even though the number of experimental investigations is

large, so too is the number of variables involved. Thus, it appears that at the present moment, empirical results based on closely similar configurations form the only adequate means of determining the high lift capabilities of a given design. Consequently, from a designer's point of view the greatest value of this section lies in the rather complete, cross indexed bibliography that follows.

Even though the complexity of the problem renders a comprehensive analysis impossible, certain general trends may be extablished, and it is with this type of material that the remainder of this section will be concerned.

4.3b Trailing-Edge Devices

From the great mass of information available concerning the application of trailing-edge high lift devices to swept and/or low aspect ratio wings, it is indeed unfortunate that no accurate and comprehensive method of predicting their lift increments can be developed. It is well known that flap effectiveness falls off quite rapidly as the angle of sweep is increased, and as one might suspect, the type of flow separation present on a given wing greatly influences the ability of a trailing-edge device to produce a lift increment, particularly at maximum lift. Further, it does not seem unreasonable to assume that the presence of a flap on a wing, expecially a wing whose geometric characteristics place it near the boundary of Fig. 190, may change or, at least, alter the type of flow separation present on the plain wing. Hence, the problem of predicting the lift increments and pitching moment characteristics of a flapped wing must include a consideration of the wing flow field as well as the more conventional parameters used in such an analysis. The discussion that follows will be for

the most part, a speculative discussion on the effect of, and effect produced by, a trailing-edge device on swept wings exhibiting either trailing-edge or leading-edge separation, or a combination of both types of separation.

For wings having predominant trailing-edge separation, it appears that the lift increment produced by an unpowered trailing-edge device is roughly that which would be expected from simple sweep theory ($\cos^2 \Lambda$ law). Also, because the difference between the linear and maximum lift increments remains approximately constant throughout the sweep range, it would seem reasonable to expect that a fairly accurate prediction of the effectiveness of a flap could be made in this case (Fig. 191). Although a Swedish investigation of high lift devices on swept wings (by H. O. Palme, Ref. 284) makes no distinction between stall types, it appears that the results of this statistical study concern mainly wings which exhibit trailing-edge separation. The data on highly swept, thin wings are widely scattered and show little correlation with the data concerning moderately swept, relatively thick wings; indeed, the author points out that the scatter of these points is probably attributable to the existence of a strong leading-edge vortex. Hence it is recommended that the results of this investigation be restricted in scope to apply only to those wings which exhibit predominantly trailing-edge separation.

For wings exhibiting pronounced leading-edge separation, the addition of a flap produces interesting and sometimes detrimental effects on the wings maximum lift capabilities. Even at zero angle of attack, the circulation control created by the flap is sufficient to initiate the leading-edge vortex with the result that the lift increment is well above that expected from simple sweep theory. From this early start, the strength of the vortex quickly

increases with increasing angle of attack, and for certain wings, a negative rather than positive lift increment may be obtained at maximum lift. The explanation for this behavior seems to be that because the vortex becomes so large at relatively low angles of attack, it is swept off the wing prematurely. Thus, even though sizeable lift increments are produced at low angles of attack, the suction forces attributable to the leading-edge vortex are not realized at maximum lift because a greater portion of the outboard sections of the wing lie in a region of diffused vortex flow than for a geometrically similar plain wing. Although this phenomenon has been observed from both wind tunnel and flight tests, existing literature sheds little light on when and under what conditions it should be expected for any given planform.

On wings whose geometric characteristics place them in the vicinity of the boundary of Fig. 190, the addition of a flap could easily change the stall pattern from trailing to leading-edge. As was discussed in section 4.1b, the application of circulation and/or boundary layer control can change the stall pattern of an airfoil section from leading-edge to thin airfoil, and the flap is, of course, primarily a circulation control device. Therefore, the effect of a flap on the inboard sections of such a wing could alter the two-dimensional stall characteristics with the resultant formation of a leading-edge vortex. This would result in a somewhat greater lift increment at zero angle of attack than would otherwise be expected, but for wings of these particular geometric characteristics, a radical change in the lift increment at maximum lift is not likely. Because this effect is marginal, the leading-edge vortex would probably not be of sufficient strength to separate

prematurely, and positive lift increments at maximum lift would be observed to rather high angles of sweep, even though the increments become quite small at the higher sweep angles (Fig. 196).

4.3c Leading-Edge Devices

Although the various devices that may be employed on the leading-edge of a finite wing usually contribute to the maximum lift capabilities of the plain wing, their most frequent application is on the outboard sections of swept-back wings in the form of a stall prevention measure. If lift can be maintained on the outboard sections until separation occurs inboard, the performance of a swept wing is greatly improved even though the maximum lift coefficient has not changed perceptibly. The most important leading-edge devices are the droop nose, the extensible flap or slat, and the chord extension. Of these three devices, only two, the droop nose and extensible flap or slat, introduce camber into the wing, and it is with these devices that this section will be concerned.

Even though the extensible flap is used quite frequently in wind tunnel tests, the actual construction and installation of this device on airplanes has proved to be extremely difficult, and hence, a slat is generally substituted. It has been assumed that the overall effects on the wing flow field due to this substitution are small, so that in the discussion that follows no distinction will be made between these devices.

Both the slat and droop nose are generally partial span devices, having their outboard ends in the vicinity of the wing tip and their inboard ends between 40% and 60% of the semispan. Even though both of these devices introduce camber into a wing their effects are often quite different because

of the chord extension qualities of the leading-edge slat. The various flow mechanisms associated with the chord extension are described in some detail in section 4.3e. Briefly, two important phenomena take place as a result of the planform discontinuity; the spanwise pressure gradient is partially unstaggered which reduces the spanwise boundary layer drift and second, a vortex, opposite in direction of rotation to the wing tip, trailing vortex, is shed from the inboard end of the device. Because of its direction of rotation, this shed vortex opposes boundary layer drift, and exerts a powerful influence on the location and strength of the leading-edge vortex. Also, because a pressure discontinuity exists at the inboard end of the slat, initial flow separation at a station inboard of the tips is encouraged. The camber of the slat, as opposed to the plain chord extension, allows the outboard sections of the wing to obtain higher angles of attack before separating.

Generally to obtain the greatest increment in lift coefficient and the maximum gain in longitudinal stability, the inboard end of the slat should be located somewhere in the vicinity of half the semispan, so that initial separation occurs just ahead of the moment center. Two factors which influence the location and the spanwise extent of this device are: 1) the formation of a leading-edge vortex and; 2) the proximity of the wings geometric characteristics to the boundary described in Fig. 190. In the first case, the optimum span is generally smaller than for the case of trailing-edge separation on a wing of similar geometrical characteristics, and for the second case, the optimum span may be quite large. Similarly, for wings which are initially stable, the greatest gains in maximum lift

coefficient are obtained when the span of the device extends well inboard.

The droop nose device enables the tip sections to reach higher lift coefficients by virtue of its increased camber effect, but because there is no chord extension, the vortex shed from the inboard end is much weaker, and may perhaps, even exhibit a reversal of the direction of rotation. Hence, the droop nose by itself is not nearly as effective a stabilizing device as the leading-edge flap or slat; however, the droop nose used in combination with a system of fences is frequently an excellent practical solution to many cases of premature separation and instability.

4.3d Powered Control Systems

Although much has been said and done concerning the application of powered boundary layer and/or circulation control systems, there are few concrete results from which general trends and conclusions can be drawn. The investigations found in existing literature apply to widely divergent planforms, attempt to improve flow conditions by a multiplicity of schemes, and generally show no continuity that might lead to a correlation of results. It has long been known that flow separation can be delayed by adding energy to the boundary layer by means of a blowing mechanism, or by removing the boundary layer entirely through suction slots. Because both of these schemes prevent flow separation, they will generally increase the wing's circulation, particularly if they are applied in conjunction with a trailing-edge device, so it is frequently impossible to classify a given system as being either a boundary layer control or circulation control device.

Numerous two-dimensional tests have shown that throughout the same lift increment range, the results produced by a blowing or suction device are

approximately the same. However the method used is primarily dependent upon the specific application, and is frequently determined by availability of a source, e.g. the jet engine is much more adaptable for blowing than suction.

Many investigations of powered boundary layer control systems have concerned wings which exhibit leading-edge separation. These experiments have shown that the most favorable slot location for controlling flow separation to be just aft of the section negative pressure peak. Being so close to the leading-edge, this position is very hard to obtain experimentally, and some investigators have consequently resorted to a porous wing leading-edge.

The spanwise extent of this control is determined by considerations similar to mechanical leading-edge devices. For initially stable wings, the control may approach full span but for unstable wings, the inboard end of the control will be located in the vicinity of half the semispan. The initial flow separation should occur just forward of the moment center, as with chord extension devices. Because this application of boundary layer control serves to improve the wing flow field, it will have the rather peculiar effect of reducing the wing maximum lift coefficient, and consequently, it assumes the dual role of a more-or-less pure boundary layer control system and stall control device.

For increasing the maximum lift potential of a wing, boundary layer control is frequently used in conjunction with a trailing-edge device. The Arado low velocity, combined suction and blowing system still leaves much to be desired but shows strong future potential. A great variety of other systems is available, and the reader is referred to the two-dimensional section of this report for further information.

4.3e Chord Extensions

Chord extensions would be expected to have a beneficial effect on the maximum lift of any finite wing simply because of the increase in wing area. However, on swept wings where the leading-edge chord extension is employed most advantageously, the device is considered primarily as a stall control device for it provides little, if any, lift increment. Because a discontinuity in planform usually results in the shedding of a streamwise vortex, the effect of a chord extension device in conjunction with the other three-dimensional phenomena that occur on a swept wing is both very interesting and profitable to consider. Since this vortex rotates in a direction opposite to that of the wing tip trailing vortex, it tends to prevent the low energy boundary layer air from the inboard sections from influencing the boundary layer on the outboard sections. Further, on wings which exhibit leading-edge vortex formation, the presence of this opposing vortex tends to alter the direction and magnitude of the leading-edge vortex, and hence the lift and pitching moment characteristics are changed considerably. The angle of attack range through which this improvement in flow over the outboard sections is realized and the manner in which the lift and pitching moment characteristics are altered seems to depend on the airfoil section of the wing, and to some extent, on the wing planform (Ref. 309). Briefly, the influence of chord extension depends upon the predominant type of flow separation involved, which is, from section 4.1a, a function of leading-edge radius and aspect ratio, (Fig. 190). A distinction seems to be evident, however, between wings with sections of sharp leading-edges and wings of small leading-edge radii, e.g. 6-series sections of small thickness ratios. For

wings which incorporate sections of very sharp leading-edges, the vortex forms at extremely low lift coefficients, and it has been observed that the vortex is quite strong at lift coefficients much lower than those at which trailing-edge separation would be expected on a wing of similar planform but constructed of sections with a large leading-edge radius. However, for swept wings whose sections have a small but finite leading-edge radius, the vortex may appear simultaneously or only slightly prior to trailing-edge separation. Hence the effect of the planform discontinuity vortex may be different for these two cases, and the discussion that follows will attempt to clarify this distinction.

The manner in which a chord extension device influences wings exhibiting leading-edge vortex formations that arise from sections with sharp leading-edges can best be explained by the pitching moment characteristics shown in Fig. 197.

Without the chord extension, i.e. plain wing, the influence of the leading-edge vortex moving in over the outboard sections causes an increase in lift, and consequently the variation of pitching moment coefficient with lift coefficient is as shown from A to B. Then, as the vortex grows in intensity and moves farther inboard leaving the tips in a region of diffused vortex flow, the decrease in lift over the outboard sections combined with the increased lift over the inboard sections, drives the pitching moment coefficient positive with increasing lift coefficient (from B to C). The hook shown in this figure, for both wings with and without a chord extension, is a result of complete flow deterioration and consequent flat plate stall.

Now with the application of a chord extension device over the outboard panels, a vortex forms as a result of the discontinuity, and experimental investigations have shown that the diffused combination of the two opposing vorticies accompanied by the low energy boundary layer air from the inboard sections is swept off the wing at some station just outboard of the inboard end of the chord extension. Obviously, for optimum results, great care must be taken when determining the spanwise extent of a chord extension device. And it is important to note that while the flow conditions over the outboard sections are improved, lift is lost, not gained, as might be expected when flow conditions are improved. This phenomenon is, of course, attributable to the absence of the leading-edge vortex over the outboard sections. It is also most important to realize that Fig. 197 indicates a trend only, and that a chord extension device does not necessarily guarantee a linear pitching moment curve but simply serves to alleviate the severe stable tendency of many thin swept wings in the low lift coefficient range. To obtain linear pitching momentum great care must be taken. It is notable that at higher lift coefficients, the predominant three-dimensional flow mechanisms of swept wings virtually eliminate the relatively minor disturbances due to the chord extension, and little change in the flow field is observed with or without a planform discontinuity.

A similar though less severe tendency is observed for wings which exhibit mixed separation, i.e. both leading and trailing-edge separation; for these wings of small but finite section leading-edge radii, the stable trend at low lift coefficients is not quite so pronounced and the unstable trend at higher lift coefficients is somewhat less violent. Thus, while the chord extension

diffuses and directs the inboard vortex as with the case of the sharp leading-edge wing, of equal importance is the influence of the chord extension vortex on the spanwise flow of the boundary layer. By obtaining a marked improvement of flow over the outboard sections with the consequent improvement of lift, the pitching up tendency characteristic of such a wing may be entirely eliminated. That is, the chord extension effect persists with great strength up to and including the maximum lift coefficient as contrasted with the first case considered.

On a wing with pure trailing-edge separation, a chord extension will improve the flow over the outboard sections by the elimination of boundary layer air over these sections, and improvements in the pitching moment and lift characteristics are as expected.

4.3f Fences

Perhaps the most obvious method of controlling swept wing flow separation, the fence or vane simply restricts the spanwise flow phenomena by providing a physical barrier to such flow. For wings exhibiting trailing-edge separation, the application of a suitable number of fences will eliminate boundary layer accumulation over the vulnerable tip sections, and hence, premature stall over these sections will be avoided. When leading-edge separation is present, the fence can be employed to redirect or diffuse the vortex so that linear pitching moment characteristics are obtained. Although restrictions to the spanwise flow mechanisms operating on a swept wing do serve to improve the pitching moment characteristics throughout the entire lift range, the induced angle of attack distribution and induced camber effect remain unchanged. Hence for the wing exhibiting trailing-edge separation, the

tip sections still separate earlier than the inboard sections with the result that the pitching moment break at the maximum lift coefficient is seldom affected by the addition of a fence; Fig. 189, based on the wing's geometry (AR & Λ) can be relied upon to indicate stability or instability at stall even for a wing with fences, i.e. that exhibits trailing-edge separation. Although much the same trend is indicated for wings exhibiting leading-edge separation, there have been instances where the addition of a fence (or fences) has changed the stability at stall. Generally, however, the addition of this type of stall control device will not change the stability characteristics of a given wing.

Even though the reasoning behind the application of a fence is quite simple, the location, size, and number of fences required to obtain the desired results is somewhat more complicated. For trailing-edge separation, the fence must be of adequate size to prevent the accumulation of boundary layer from spilling over, and hence defeating its purpose. It may be necessary to install several fences along the span, for if on a large aspect ratio wing, only one high fence was located at half the semi-span, the boundary layer accumulation outboard of this point might be sufficient to promote tip stall. Obviously a fence intended to prevent trailing-edge separation should cover the rear portion of the chord, and experimental investigations have shown that for maximum effectiveness at high lift coefficients, it should also extend well forward, perhaps to within five percent chord of the leading-edge.

For wings exhibiting leading-edge separation, it is evident that the fence should be located on the forward portion of the chord, and experience has shown that for maximum effectiveness, it should extend around the leading-edge to

the lower surface. Because so little is known about the size or formation of the leading-edge vortex, the requirements for the size or location of such a fence cannot be stated, or even intelligently guessed.

V.

BIBLIOGRAPHY

ABOUT THE BIBLIOGRAPHY

The bibliography to be found on the following pages includes not only the references directly cited in the body of this report but the large majority of literature available to the authors regarding experimental researches into the external aerodynamics of high-lift flow controls. In addition to references describing the characteristics of the various systems, much in the way of pertinent theoretical work has been included, and the more detailed reports describing relatively new and useful testing techniques in this field are given. Further, it was attempted to include reports which have unusual bibliographical value or which describe some of the lesser-understood phenomena ("Coanda effect", "chord-extension effect", etc.).

Although several references are presented which deal primarily with power requirements, low-drag suction, suction slot design, etc., this bibliography can in no way be taken to be complete in such fields, these references being given simply to provide some start for the engineer becoming interested in such matters. The bibliography is intended, however, to be as complete as is possible (within the limitations of practicality and availability) in the one region dealt with in this report -- external aerodynamics of high-lift flow controls. Because of the familiarity of such devices and the vast amount of literature at hand, only a portion of the available unpowered trailing-edge flap work has been included. Completeness, however, was regarded as a criterion for the other systems described.

It is hoped that this rather extensive bibliography may be of considerable use in indicating the scope of the work done in this area and thus facilitate the initiation of B.L.C. projects as well as prevent the duplication of

effort which seems all too common in this field.

The first 250 references deal primarily with two-dimensional phenomena while the remainder treat the three-dimensional case. Because of the unusual length of the bibliography, a subject index as well as an author index has been included for the convenience of the searcher. These indices may be found immediately after the list of references.

5.1 List of References

1. Smith, M.H., "Bibliography on Boundary Layer Control", Princeton University, The James Forrestal Research Center, Literature Search No. 6, January, 1955.

2. Smith, M.H., "Bibliography on Boundary Layer Control - Classified References", Princeton University, The James Forrestal Research Center, Literature Search No. 9, March, 1956, (Classified).

3. Brewer, J.D., "Description and Bibliography of NACA Research on Wing Controls, January, 1946 - February 1955", NACA RM 54K24, March, 1955, (Classified).

4. Pope, A., Basic Wing and Airfoil Theory, McGraw-Hill Book Company, 1951.

5. Kuethe, A.M., and Schetzer, J.D., Foundationsof Aerodynamics, Wiley, 1950.

6. Perkins, C.D., and Hage, R.E., Airplane Performance, Stability, and Control, Wiley, 1949.

7. Goldstein, S., Modern Developments in Fluid Dynamics - Vol. II, Oxford University Press, 1938.

8. Abbot, I.H. and von Doenhoff, A.E., Theory of Wing Sections, McGraw-Hill Book Company, Inc. 1949.

9. Abbot, I.H., von Doenhoff, A.E., and Stivers, L.S., Jr., "Summary of Airfoil Data", NACA Report No. 824, 1945.

10. McCullough, G.B., and Gault, D.E., "Examples of Three Representative Types of Airfoil-Section Stall at Low Speed", NACA TN 2502, 1951.

11. Von Doenhoff, A.E., and Tetervin, N., "Determination of General Relations for the Behavior of the Turbulent Boundary Layers", NACA Report No. 772, 1943.

12. Schubauer, G.B., and Klebanoff, P.S., "Investigation of Separation of the Turbulent Boundary Layer", NACA TN 2133, 1950.

13. Von Doenhoff, A.E., "A Preliminary Investigation of Boundary-Layer Transition Along a Flat Plate with Adverse Pressure Gradient", NACA TN 639, 1938.

14. Von Doenhoff, A.E., and Tetervin, N., "Investigation of the Variation of Lift Coefficient with Reynolds Number at a Moderate Angle of Attack on a Low-Drag Airfoil," NACA CB(19), November, 1942.

15. Gault, D.E., "Boundary-Layer and Stalling Characteristics of the NACA 63-009 Airfoil Section", NACA TN 1894, 1949.

16. Fage, A., and Johansen, F.C., "On the Flow of Air Behind an Inclined Flat Plate of Infinite Span", British R&M 1104, 1927.

17. Norbury, J.F., "A Simplified Model of the Incompressible Flow Past Two-Dimensional Aerofoils with a Long Bubble Type of Flow Separation", Royal Aircraft Establishment, Farnborough, Tech. Note No: Aero 2352, June, 1955.

18. Pinkerton, R.M., "Calculated and Measured Pressure Distribution over the Midspan Section of the NACA 4412 Airfoil", NACA Report No. 563, 1936.

19. Nonweiler, T., "A Resume of Maximum Lift Data for Symmetrical Wings with Various High Lift Aids", College of Aeronautica, Cranfield, CoA Note No. 5, 1954.

20. Richard, E.J., "Notes on the Stalling Properties of Wings", Journal of the Royal Aeronautical Society, November, 1946.

21. Loftin, L.K., Jr., "Theoretical and Experimental Data for a Number of NACA 6A-Series Airfoil Sections", NACA Report No. 903, 1948.

22. Loftin, L.K., Jr., and Bursnall, W.J., "The Effects of Variation in Reynolds Number Between 3.0×10^6 and 25.0×10^6 upon the Aerodynamic Characteristics of a Number of NACA 6-Series Airfoil Sections", NACA TN 1773, December, 1948.

23. Loftin, L.K., Jr., and Smith, H.A., "Aerodynamic Characteristics of 15 NACA Airfoil Sections at Seven Reynolds Numbers from $.7 \times 10^6$ to 9.0×10^6", NACA TN 1945, October, 1949.

24. Jacobs, E.N., and Sherman, A., "Airfoil Section Characteristics as Effected by Variations of the Reynolds Number. NACA Report No. 586, 1937.

25. Hazen, D.C., and Lehnert, R.F., "Smoke Flow Studies Conducted at Princeton University", Princeton University Report No. 290, 1955.

26. Knowlton, M.P., "A Theoretical Investigation on the Determination of Lift Coefficients in Two-Dimensional Smoke Tunnels", Princeton University Report No. 280, 1954.

27. Brower, W.B., Jr., "The Application of the Electrical Analogy to Two-Dimensional Problems in Aeronautics", Rensselaer Polytechnic Institute, TR AE5406, November, 1953.

28. Regenscheit, B., "On a New Application of Suction for the Increase of Lift of an Airfoil", FB 1474, 1941.

29. Goldsmith, J., "Summary of Analysis of Trailing-Edge Suction Slot", United Aircraft Corporation Inter-Company Report, 1948.

30. Goldsmith, J., "Effect of Trailing-Edge Suction and Pressure Slots", United Aircraft Corporation Report No. R-95374-3, February, 1951.

31. Ehlers, F., "On the Influence of Sinks on the Lift and Pressure Distribution of Airfoils with Suctions Slots" M.A.P. Volkenrode Ref: MAP-VG67-189T.

32. Regenscheit, B., "Test on a Wing with Suction at the Trailing-Edge", FB 1594, January, 1947.

33. Ringleb, F.O., "Theory and Application of the Flow over a Cusp", Princeton University Report No. 192, 1953.

34. Hazen, D.C., Lehnert, R.F., Sweeney, T.E., and Ringleb, F.O., "Preliminary Reports on Circulation Control by Means of Trailing-Edge Suction and the Cusp Effect", Princeton University Report No. 234, 1953.

35. Hazen, D.C., Sweeney, T.E., and Lehnert, R.F., "Circulation Control by Means of Trailing-Edge Suction (Detailed Data Report)", Princeton University Report No. 241, September, 1953.

36. Hazen, D.C., Sweeney, T.E., Lehnert, R.F., and Ringleb, F.O., "Circulation Control by Means of Trailing-Edge Suction (Final Report)", Princeton University Report No. 239, August, 1953.

37. Ringleb, F.O., "Flow Control by Generation of Standing Vortices and the Cusp Effect", Princeton University Report No. 317, 1955.

38. Poisson-Quinton, PH., et Jousserandot, P., "Hypersustention et Pilotage des Avions par Controle de Circulation", Association Technique Maritime et Aeronautique, Paris, Session 1955 (Translated by C. Boehler of Fairchild Aircraft, July, 1955 as "High Lift and Control of Airplanes by Control of Circulation").

39. Jousserandot, P., "Synthese sur des Essais Systematiques d'Hypercirculation par soufflage au Bord de Fuite d'un Profile en Incompressible", Conference Technique du 17 Decembre, 1954, a L' O.N.E.R.A.

40. United Aircraft Corporation Inter-Company Correspondence from Mr. J. Goldsmith to Mr. J. G. Lee of Nov. 22, 1948. (Outline of Tentative Test Program for Tests of High Lift Devices).

41. Helmbold, H.B., "On the Lift of a Blowing Wing in a Parallel Stream", University of Wichita Engineering Study No. 110, August, 1953.

42. Malavard, L., "Contribution to the Theoretical Study of Blowing at the Trailing Edge of a Wing Section", December 31, 1954 (Translated by L. W. Sheridan of Fairchild Aircraft, July, 1955).

43. Davidson, I.M., "Jet Flap Development - A Report of a Lecture Given Oct. 20, 1955 to the R.Ae. S.," Flight, October 21, and 28, 1955.

44. Willauer, W.R., "Two-Dimensional Smoke Tunnel Investigations of the Jet Flap", Princeton University Report No. 341, March 1956 (Proprietary).

45. Cahill, J.F., "Summary of Section Data on Trailing-Edge High Lift Devices", NACA Report No. 938, 1949.

46. Glauert, H., "A Theory of Thin Airfoils", British R&M 910, 1924.

47. Theodorsen, T., "Theory of Wing Sections of Arbitrary Shape", NACA Report 411, 1932.

48. Keune, F., "Lift on a Bent, Flat Plate", NACA TM 1340, 1955.

49. Cahill, J.F., "Two-Dimensional Wind-Tunnel Investigation of Four Types of High-Lift Flap on an NACA 65-210 Airfoil Section", NACA TN 1191, 1947.

50. Spearman, M.L., "Wind-Tunnel Investigation of an NACA 0009 Airfoil with 0.25 and 0.50 Airfoil-Chord Plain Flaps Tested Independently and in Combination", NACA TN 1517, March, 1948.

51. Wenzinger, C.J., "Wind-Tunnel Investigation of Ordinary and Split Flaps on Airfoils of Different Profile", NACA Report 554, 1936.

52. Wenzinger, C.J., and Harris, T.A., "Wind-Tunnel Investigation of NACA 23012, 23021, and 23030 Airfoils with Various Sizes of Split Flaps," NACA Report No. 668, 1939.

53. Weick, F.E., and Harris, T.A., "The Aerodynamic Characteristics of a Model Wing having a Split Flap Deflected Downward and Moved to the Rear", NACA TN 422, 1932.

54. Holtzclaw, R.W., and Weisman, Y., "Wind-Tunnel Investigation of the Effects of Slot Shape and Flap Location on the Characteristics of a Low-Drag Airfoil Equipped with a 0.25 Chord Slotted Flap", NACA WR A-80, 1944.

55. Wenzinger, C.J., and Harris, T.A., "Wind-Tunnel Investigation of an NACA 23012 Airfoil with Various Arrangements of Slotted Flaps," NACA Report No. 664, 1939.

56. Lowry, J.B., "Wind-Tunnel Investigation of an NACA 23012 Airfoil with Several Arrangements of Slotted Flaps with Extended Lips", NACA TN 808, 1941.

57. Cahill, J.F., and Racisz, S.F., "Wind-Tunnel Investigation of Seven Thin NACA Airfoil Sections to Determine Optimum Double-Slotted Flap Configurations", NACA TN 1545, 1948.

58. Riebe, J.M., "A Correlation of Two-Dimensional Data on Lift Coefficient Available with Blowing-, Suction-, Slotted-, and Plain-Flap High-Lift Devices", NACA RM L55D29a, October, 1955 (Classified).

59. Williams, J., "An Analysis of Aerodynamic Data on Blowing Over Trailing-Edge Flaps for Increasing Lift", NPL/Aero/209, A.R.C. 17,814, September, 1954.

60. Harkleroad, E.L., and Murphy, R.D., "Two-Dimensional Wind-Tunnel Tests of a model of an F9F-5 Airplane Wing Section Using a High-Speed Jet Blowing over the Flap - Part I:- Test of a 6-Foot Chord Model", David Taylor Model Basin, Aero. Report 845, May, 1953. (Classified)

61. David Taylor Model Basin Symposium on Boundary-Layer-Control Systems: "A Compilation of the Papers Presented September 8-9, 1954," Aero. Report 876 (Classified)
(a) Murphy, R.D. (D.T.M.B.), "Effects of High-Speed B.L.C. on Section Characteristics of a Moderately Thick Airfoil", pp. 9-46.
(b) Wallace, R.E. (University of Wichita), "Systematic Two-Dimensional Test on an NACA 23015 Airfoil with Single-Slotted Flap and Circulation Control", pp. 169-244.
(c) Hazen, D.C. (Princeton University), "Preliminary Evaluation of Circulation Control Systems Utilizing Split Flaps", pp. 273-332.
(d) De los Santos, S.T. (D.T.M.B.), "Tangential Blowing on the Surface of an Airfoil as a Boundary-Value Problem", pp. 247-271.

62. Razak, K., "Boundary Layer Control by Blowing - A Method of Increasing Flap Effectiveness", University of Wichita, Eng'g Study No. 139, September, 1954 (Classified).

63. Wallace, R.E., Stalter, J.L., and Bondie, R.J., "A Two-Dimensional Experimental Investigation of Single-Slotted-Flap Position on a NACA 23015 Airfoil Section with Circulation Control", University of Wichita, Aero. Report No. 152, August, 1954 (Classified).

64. Wallace, R.E., Stalter, J.L., and Yarnell, W.L., "An Experimental Study of the Pressure Distribution on an NACA 23015 Airfoil Section with a Single-Slotted Flap as Influenced by Circulation Control", University of Wichita, Aero. Report No. 153, August 1954 (Classified).

65. Hazen, D.C., and Sweeney, T.E. (Princeton University) "A Proposed Circulation Control System for C-119 Aircraft", Consultational Report, Fairchild Aircraft, 1953, (Classified and Proprietary).

66. Nunemaker, J.J. and Fisher, J.W., "Two-Dimensional Wind-Tunnel Investigation of Boundary-Layer Control by Blowing on an NACA 23015 Airfoil", University of Wichita, Eng'g Report No. 023, April 1950.

67. Hazen, D.C., and Lehnert, R.F., "Smoke Tunnel Investigation of a Circulation Control System Utilizing Blowing over a Deflected Fowler Flap", Princeton University Report No. 256, 1953, (Classified).

68. Hazen, D. C., "Preliminary Evaluation of Circulation Control Systems Utilizing Split Flaps", Princeton University Report No. 278, September, 1954, (Classified)

69. Regenscheit, B., and Schrenk, H., "Tests on Boundary Layer of Flapped Aerofoils of Various Camber and Camber Position", (Translated from ZWB Forschungsbericht No. 1061), Gt. Britain Ministry of Supply Volherrode Reports and Translations No. 484, ATI 74,440, June, 1947.

70. Hazen, D.C., Lehnert, R.F., Dike, D.J. and Knowlton, M.P., "Circulation Control by Means of Trailing-Edge Suction Applied to Profiles with Split Flaps", Princeton University Report No. 315, (To be published).

71. Ringleb, F.O., "Investigation of Suction Flaps", Princeton University Report No. 304, 1955.

72. Krüger, W., and Walz, A., "Aerodynamic Coefficients of the Aerofoils", Ministry of Aircraft Production, Voelkerode, No. MAP-VG243-943T.

73. Jacobs, E.N., Pinkerton, R.M., and Greenberg, H., "Tests of Related Forward Camber Airfoils in the Variable-Density Wind-Tunnel", NACA Report No. 610, 1937.

74. Abzug, N.J., "Estimation of the Lift and Moment Parameters of Leading-Edge Flaps", Journal of Aeronautical Sciences, September, 1955.

75. Rose, L.M., and Altman, J.M., "Low-Speed Experimental Investigation of a Thin, Faired, Double-Wedge Airfoil Section with Nose and Trailing Edge Flaps", NACA TN 1934, August, 1949.

76. Rose, L.M., and Altman, J.M., "Low-Speed Investigation of a Thin, Faired, Double-Wedge Airfoil Section with Nose Flaps of Various Chords", NACA TN 2018, Feb., 1950.

77. Rose, L.M., and Altman, J.M., "Low-Speed Investigation of the Stalling of a Thin, Faired, Double-Wedge Airfoil with Nose Flap", NACA TN 2172, August, 1950.

78. Cahill, J.R., Underwood, W.J., Nuber, R.F., and Cheesman, C.A., "Aerodynamic Forces and Loadings on Symmetrical Circular-Arc Airfoils with Plain Leading-Edge and Plain Trailing-Edge Flaps", NACA Report No. 1146, 1953.

79. Underwood, W.J., and Nuber, R.J., "Two-Dimensional Wind-Tunnel Investigation at High Reynolds Numbers of Two Symmetrical Circular Arc Airfoil Sections with High-Lift Devices", NACA RM L6K22, March, 1947.

80. Underwood, W.J., and Nuber, R.J., "Aerodynamic Load Measurements of Leading-Edge and Trailing-Edge Plain Flaps on a 6% Thick Symmetrical Circular-Arc Airfoil Section", NACA RM L7H04, October, 1947.

81. Nuber, R.J., and Gottlieb, S.M., "Two-Dimensional Wind-Tunnel Investigation at High Reynolds Number of an NACA 65A006 Airfoil with High-Lift Devices", NACA RM L7K06, February, 1948.

82. Humphreys, M.D., "Transonic Aerodynamic Characteristics of an NACA 64A006 Airfoil Section with 15% Chord Leading-Edge Flap", NACA TM L53G23, September, 1953.

83. Kelly, J.A., and Hayter, N.F., "Lift and Pitching Moment at Low Speeds of the NACA 64A010 Airfoil Section Equipped with Various Combinations of a Leading-Edge Slat, Leading-Edge Flap, Split Flap, and Double-Slotted Flap", NACA TN 3007, September, 1953.

84. Dike, D.J., "A Low Speed Wind-Tunnel Investigation of a 64-010 Airfoil Section with Nose Flap and Split Trailing-Edge Flap", Princeton University Report No. 301, July, 1955.

85. Kelly, J.A., "Effects of Modifications to the Leading-Edge Region on the Stalling Characteristics of the NACA 63_1-012 Airfoil Section, NACA TN 2228, November, 1950.

86. Nonweiler, T., "Flaps, Slots, and Other High Lift Aids", Aircraft Engineering, September, 1955.

87. Marshall, W.S.D., Levacic, I., Young, A.D., and Powter, G.J., "Low-Speed Wind Tunnel Tests of a High-Lift Supersonic Wing", British R&M No. 2365, 1950.

88. Fullmer, F.F., Jr., "Two-Dimensional Wind-Tunnel Investigation of the NACA 64_1-012 Airfoil Equipped with Two Types of Leading-Edge Flap", NACA TN 1277, May, 1947.

89. Bidwell, J.M., and Cahill, J.F., "Survey of Two-Dimensional Data on Pitching-Moment Changes Near Maximum Lift Caused by Deflection of High-Lift Devices", NACA RM L9J03, December, 1949.

90. Lemme, H.A., (Translation) "Force and Pressure-Distribution Measurements on a Rectangular Wing with Double-Hinge Nose", NACA TM 1117, 1947.

91. Kruger, W., (Translation) "Wind-Tunnel Investigations on a Changed Mustang Profile with Nose Flap", NACA TM 1177, September, 1947.

92. Kruger, W., (Translation) "Systematic Wind-Tunnel Measurements on a Laminar Wing with Nose Flap", NACA TM 1119, April, 1947.

93. Riegels, F., (Translation) "Russian Laminar Flow Airfoils, 3RD Part: Measurements on the Profile No. 2315 BIS with AVA-Nose Flap", NACA TM 1127, September, 1947.

94. Betz, A., (Gottingen), "Theory of the Slotted Wing", NACA TN 100, June, 1922.

95. Sherman, A., and Harris, T.A., "The Effects of Equal-Pressure Fixed Slots on the Characteristics of a Clark Y Airfoil", NACA TN 507, October, 1934.

96. Bamber, M.J., "Wind-Tunnel Tests of Several Forms of Fixed Wing Slot in Combination with a Slotted Flap on an NACA 23012 Airfoil", NACA TN 702, April, 1939.

97. Wenzinger, C.J., and Rogallo, F.M., "Resumé of Air-Load Data on Slats and Flaps", NACA TN 690, March, 1939.

98. Gauvain, W.E., "Wind-Tunnel Tests of a Clark Y Wing with 'Maxwell' Leading-Edge Slots", NACA TN 598, April, 1937.

99. Lowry, J.G., and McKee, J.W., "Wind-Tunnel Investigation of an NACA 23012 Airfoil with a 30-Percent-Chord Maxwell Slat and with Trailing-Edge Flaps", NACA WR L-693, June, 1941.

100. Gillis, C.L., and McKee, J.W., "Wind-Tunnel Investigation of an NACA 23012 Airfoil with an 18.05-Percent-Chord Maxwell Slat and with Trailing-Edge Flaps", NACA WR L-574, October, 1941.

101. Weick, F.E., and Platt, R.C., "Wind-Tunnel Tests on Model Wing with Fowler Flap and Specially Developed Leading-Edge Slot", NACA TN 459, May, 1933.

102. Jacobs, E.N., "Pressure Distribution on a Slotted R.A.F. 31 Airfoil in the Variable Density Wind Tunnel", NACA TN 308, June, 1929.

103. Schuldenfrei, M.J., "Wind-Tunnel Investigation of an NACA 23012 Airfoil with a Handley Page Slat and Two Flap Arrangements", NACA WR L261, February, 1942.

104. Gottlieb, S.M., "Two-Dimensional Wind-Tunnel Investigation of Two NACA 6-Series Airfoils with Leading-Edge Slats", NACA RM L8K22, January, 1949.

105. Moss, G.F., "Systematic Wind-Tunnel Tests with Slats on a 10 Percent Thick Symmetrical Wing Section CEQ 1040 Profile" British R&M 2705, October, 1948.

106. Axelson, J.A., and Stevens, G.L., "Investigation of a Slat in Several Different Positions on an NACA 64A010 Airfoil for a Wide Range of Subsonic Mach Numbers", NACA TN 3129, March, 1954.

107. Lemme, H.G., (Translation) "Force and Pressure-Distribution Measurements on a Rectangular Wing with a Slotted Droop Nose and with Either Plain and Split Flaps in Combination or a Slotted Flap", NACA TM 1108, March, 1947.

108. Bamber, M.J., "Wind-Tunnel Tests on an Airfoil Equipped with a Split Flap and Slot", NACA TN 324, October, 1929.

109. Watson, W.J., "Note on the Effect of Boundary-Layer Suction on Separation", British R&M 2538, May 1947.

110. Lighthill, M.J., "A Theoretical Discussion of Wings with Leading-Edge Suction", British R&M 2162, May, 1945.

111. Thwaites, B., "A Theoretical Discussion of High-Lift Aerofoils With Leading-Edge Porous Suction", British R&M 2242, July, 1946.

112. Von Doenhoff, A.E., and Loftin, L.K., Jr., "Present Status of Research on Boundary Layer Control", J.A.S., Vol. 16 N. 12, December, 1949.

113. Lew, H.G., and Mathiew, R.D., "Boundary Layer Control by Porous Suction", Pennsylvania State University Technical Report No. 3, June, 1954.

114. Gregory, N., Walker, W.S., and Devereux, A.N., "Wind-Tunnel Tests on the 30 Percent Symmetrical Griffith Aerofoil with Distributed Suction over the Nose", British R&M 2647, June, 1948.

115. Pankhurst, R.C., Raymer, W.G., and Devereux, A.N., "Wind-Tunnel Tests of the Stalling Properties of an 8 Percent Thick Symmetrical Section with Nose Suction Through a Porous Surface", British R&M 2666, June, 1948.

116. Nuber, R.J., and Needham, J.R., Jr., "Exploratory Wind-Tunnel Investigation of the Effectiveness of Area Suction in Eliminating Leading-Edge Separation over an NACA 64_1A212 Airfoil", NACA TN 1741, November, 1948.

117. Dannenberg, R.E., and Weiberg, J.A., "Section Characteristics of a 10.5-Percent-Thick Airfoil with Area Suction as Affected by Chordwise Distribution of Permeability", NACA TN 2847, December, 1952.

118. Dannenberg, R.E., and Weiberg, J.A., "Effect of Type of Porous Surface and Suction Velocity Distribution on the Characteristics of a 10.5-Percent-Thick Airfoil with Area Suction", NACA TN 3093, December, 1953.

119. Weiberg, J.A., and Dannenberg, R.E., "Section Characteristics of an NACA 0006 Airfoil with Area Suction Near the Leading-Edge", NACA TN 3285, September, 1954.

120. Cheers, F., Raymer, W.G., and Douglas, O., "Tests on a 'Lighthill' Nose-Suction Aerofoil in the N.P.L. 4-Ft. No. 2 Wind-Tunnel", British R&M 2355, April, 1947.

121. Cheers, F., and Douglas, O., "Tests on a 'Glauert' Nose-Suction Aerofoil in the N.P.L. 4-Ft. No. 2 Wind Tunnel", British R&M 2356, April, 1947.

122. Williams, J., "Some Investigations on Thin Nose-Suction Aerofoils, Parts I and II", British R&M 2693, April, 1950.

123. McCullough, G.B., and Gault, D.E., "An Experimental Investigation of an NACA 63_1-012 Airfoil Section with Leading-Edge Suction Slots", NACA TN 1683, August, 1948.

124. McCullough, G.B., and Gault, D.E., "An Experimental Investigation of the NACA 63_1-012 Airfoil Section with Leading-Edge and Midchord Suction Slots", NACA TN 2041, February, 1950.

125. Racisz, S.F., "Experimental Investigation of the Effectiveness of Various Suction-Slot Arrangements as a Means for Increasing the Maximum Lift of the NACA 65_3-018 Airfoil Section", NACA RM L50A10, March, 1950.

126. Quinn, J.H., Jr., "Wind-Tunnel Investigation of Boundary Layer Control by Suction on the NACA 65_3-418, a = 1.0 Airfoil Section with a 0.29-Airfoil-Chord Double Slotted Flap", NACA TN 1071, June, 1946.

127. Quinn, J.H., Jr., "Tests of the NACA 64_1A212 Airfoil Section with a Slat, a Double Slotted Flap, and Boundary Layer Control by Suction", NACA TN 1293, May, 1947.

128. Quinn, J.H., Jr., "Wind-Tunnel Investigation of the NACA 65_4-421 Airfoil Section with a Double Slotted Flap and Boundary-Layer Control by Suction", NACA TN 1395, July, 1947.

129. Racisz, S.F., and Quinn, J.H., Jr., "Wind-Tunnel Investigation of Boundary-Layer Control by Suction on NACA 65_5-424 Airfoil with Double Slotted Flap", NACA TN 1631, June, 1948.

130. Horton, E.A., Racisz, S.F., and Paradiso, N.J., "Investigation of Boundary-Layer Control to Improve the Lift and Drag Characteristics of the NACA 65_2-415 Airfoil Section with Double Slotted and Plain Flaps", NACA TN 2149, August, 1950.

131. Horton, E.A., Racisz, S.F., and Paradiso, N.J., "Investigation of NACA 64,2-432 and 64,3-440 Airfoil Sections with Boundary-Layer Control and an Analytical Study of Their Possible Applications", NACA TN 2405, July, 1951.

132. Cocke, B.W., Fink, M.P., and Gottlieb, S.M., "The Aerodynamic Characteristics of an Aspect-Ratio-20 Wing Having Thick Airfoil Sections and Employing Boundary-Layer Control by Suction", NACA TN 2980, August, 1953.

133. Walkowicz, Major T.F., "Boundary-Layer Control Work in Japan", Air Technical Intelligence Review No. F-IR-132-RE, March, 1947.

134. Richards, E.J., Walker, W.S., and Greening, J.R., "Tests of a Griffith Aerofoil in the 13 ft. x 9 ft. Wind Tunnel", British R&M 2148, March, 1944.

135. Glauert, M.B., "The Design of Suction Aerofoils with a Very Large C_L - Range", British R&M 2111, November, 1945.

136. Richards, E.J., Walker, W.S., and Taylor, C.R., "Wing-Tunnel Tests on a 30 Percent Suction Wing", British R&M 2149, July, 1945.

137. Gregory, N., and Walker, W.S., "Further Wind-Tunnel Tests on a 30 Percent Symmetrical Suction Aerofoil with a Movable Flap", British R&M 2287, July, 1946.

138. Preston, J.M., Gregory, N., and Rawcliffe, A.G., "The Theoretical Estimation of Power Requirements for Slot-Suction Aerofoils, with Numberical Results for Two Thick Griffith Type Sections", British R&M 2577, November, 1946.

139. Pearcey, H.H., and Rogers, E.W.E., "The Effect of Compressibility on the Performance of a Griffith Aerofoil", Britich R&M 2511, November, 1946.

140. Glauert, M.B., Walker, W.S., Raymer, W.G., and Gregory, N., "Wing-Tunnel Tests on a Thick Suction Aerofoil with a Single Slot", British R&M 2645, October, 1948.

141. Gregory, N., Pankhurst, R.C., and Walker, W.S., "Wind-Tunnel Tests on the Prevention of Boundary-Layer Separation Distributed Suction at the Rear of a Thick Aerofoil", British R&M 2788, October, 1950.

142. Hunter, P.A., and Johnson, H.I., "A Flight Investigation of the Practical Problems Associated with Porous-Leading-Edge Suction", NACA TN 3062, February, 1954.

143. McCullough, G.B., and Gambucci, B.J., "Boundary-Layer Measurements on Several Porous Materials with Suction Applied", NACA RM A52D01b, June, 1952.

144. Rawcliffe, A.G., "Suction-Slot Ducting Design", British R&M 2580, April, 1947.

145. Raspet, A., Cornish, J.J., III, and Bryant, G.D., (Mississippi State College) "Delay of the Stall by Suction Through Distributed Perforations", Paper Presented by Dr. Raspet at the 24th Annual Meeting of the Institute of the Aeronautical Sciences, January 23-26, 1956.

146. Dike, D.J., and Vadas, M.M., "A Wind-Tunnel Investigation of a Sikorsky S-56 Blade Section Fitted with the Griswold Leading Edge Blowing Slot", Princeton University Report No. 283, December, 1954, (Proprietary).

147. Lehnert, F.F., "A Smoke Tunnel Investigation of a Sikorsky S-56 Blade Section Fitted with the Griswold Leading-Edge Blowing Slot", Princeton University Report No. 285, 1955, (Proprietary).

148. Cornish, J.J., "A Preliminary Investigation of the Effects of a Blowing Slot Near the Leading Edge of an Airfoil", Mississippi State College, Research Note No. 1, April, 1954, (Classified).

149. Mamrol, F.E., Jr., "Wind-Tunnel Tests on Airfoils with Blowing Slot Circulation Control", Inter-Company Piasecki Helicopter Corporation, June, 1954.

150. Poisson-Quinton, Ph., Mousserandot, P., et Chevallier, J.P., "Recherches Theoretiques et Experimentals sur le Mecanisme et l'Application du Controle de la Couche Limite", September, 1947. (Translated by the Aerophysics Department of Mississippi State College as "Theoretical And Experimental Researches on the Mechanisms and the Application of Boundary Layer Control").

151. Gregory, N., Walker, W.S., and Raymer, W.G., "Wind-Tunnel Tests on the 30 Percent Symmetrical Griffith Aerofoil with Ejection of Air at the Slots", British R&M 2475, November, 1946.

152. Preston, J.H., Walker, W.S., and Taylor, C.R., "The Effect on Drag of the Ejection of Air from Backward-Facing Slots on a 16.2 Percent Griffith Aerofoil", British R&M 2108, 1946.

153. Schwartz, G.W., "Investigation of Leading Edge Blowing on a Thin Profile", Princeton University Report No. 312, 1956 (Classified).

154. Sweeney, T.E., "Preliminary Full Scale Measurements of Jet Spoiler Performance on the L-21 Airplane", Princeton University Report No. 291, 1955.

155. Powell, D.G., "Full Scale Pressure Distribution Investigation of a Jet Spoiler on the L-21 Airplane", Princeton University Report No. 308, 1955.

156. Metral, A.R., "On the Phenomenon Concerning the Deviation of Fluid Veins and their Application-Coanda Effect", AAF, Wright Field TR F-TR-823-RE.

157. Voedisch, A., "Analytical Investigation of the Coanda Effect", AAF, Wright Field, TR F-TR-2155-ND.

158. Schweir, W. (Translation) "Lift Increase by Blowing Out Air, Tests on Airfoil of 12 Percent Thickness, Using Various Types of Flap", NACA TM 1148, June 1947.

159. Lehnert, R.F., Dike, D.J., and Chauncey, W.E., "An Investigation of a Leading-Edge Flapped Thin Profile Utilizing Blowing at the Flap-Break", Princeton University Report No. 342, January, 1957.

160. Thwaites, B., "The Production of Lift Independently of Incidence", Journal of the Royal Aeronautical Society, Vol. 52, n. 445, January, 1948.

161. Jarros, T.A., and Recant, I.G., "Wind-Tunnel Investigation of NACA 23012, 23021, and 23030 Airfoils Equipped with 40-Percent-Chord Double Slotted Flaps", NACA Report No. 723, 1941.

162. Visconti, F., "Investigation of an Approximately 0.178-Chord-Thick NACA 6-Series-Type Airfoil Section Equipped with Sealed Internally Balanced 0.20-Chord Ailerons and with a 0.05-Chord Tab", NACA TN 1590, May, 1948.

163. Holtzclaw, R.W., and Dods, J.B., Jr., "Wind-Tunnel Investigation of Drooped Ailerons on a 16-Percent-Thick Low-Drag Airfoil", NACA TN 1386, August, 1947.

164. Racisz, S.F., and Cahill, J.F., "Wind-Tunnel Investigation of Effects of Forward Movements of Transition on Section Characteristics of a Low-Drag Airfoil with a 0.24-Chord Sealed Plain Aileron", NACA TN 1582, May, 1948.

165. Stevenson, D.B., and Adler, A.A., "High-Speed Wind-Tunnel Tests of an NACA 0009-64 Airfoil Having a 33.4-Percent-Chord Flap with an Overhang 20.1 Percent of the Flap Chord", NACA TN 1417, September, 1947.

166. Brewer, J.D., and Queijo, M.J., "Wind-Tunnel Investigation of the Effect of Tab Balance on Tab and Control-Surface Characteristics", NACA TN 1403, August, 1947.

167. Luoma, A.A., "An Investigation of the Section Characteristics of Plain Unsealed Ailerons on an NACA 66, 1-115 Airfoil Section in the Langley 8-Foot High-Speed Tunnel", NACA TN 1596, January, 1949.

168. Braslow, A.L., "Two-Dimensional Wind-Tunnel Investigation of a 10.7-Percent-Thick Symmetrical Tail Section with a 0.40 Airfoil-Chord Control Surface and a 0.20 Control-Surface-Chord Tab", NACA TN 1228, June, 1947.

169. Quinn, J.H., Jr., "Drag Tests of an NACA $65_{(215)}$-114, a = 1.0 Practical-Construction Airfoil Section Equipped with a 0.295-Airfoil-Chord Slotted Flap", N.A.C.A. T.N. 1236, April, 1917.

170. Thomson, K.D., "A Review of Leading-Edge High Lift Devices", Aero. Research Laboratories, Australia, Report A-77, June, 1951.

171. Hunton, L.W., and James, H.A., "Use of Two-Dimensional Data in Estimating Loads on a 45° Sweptback Wing with Slats and Partial-Span Flaps", NACA TN 3040, November, 1953.

172. Wenzinger, C.J., "Wind Tunnel Tests of a Clark Y Wing Having Split Flaps with Gaps", NACA TN 650, May, 1938.

173. Harris, T.A., "Wind-Tunnel Investigation of an NACA 23012 Airfoil with Two Arrangements of a Wide-Chord Slotted Flap", NACA TN 715, June, 1939.

174. Pinkerton, R.M., "Analytical Determination of the Load on a Trailing Edge Flap", NACA TN 353, October, 1930.

175. Brewer, J.D., and Polhamus, J.F., "Wind-Tunnel Investigation of the Boundary Layer on an NACA 0009 Airfoil Having 0.25- and 0.50-Airfoil Chord Plain Sealed Flaps", NACA TN 1574, April, 1948.

176. Braslow, A.L., "Two-Dimensional Wind-Tunnel Investigation of Sealed 0.22-Airfoil-Chord Internally Balanced Ailerons of Different Contour on an NACA $65_{(112)}$-213 Airfoil", NACA TN 1099, July, 1946.

177. Braslow, A.L., "Two-Dimensional Wind-Tunnel Investigation of Low-Drag Vertical-Tail, Horizontal-Tail, and Wing Sections Equipped with Sealed Internally Balanced Control Surfaces", NACA TN 1048, April, 1946.

178. Cheers, F., Walker, W.S., and Taylor, C.R., "Two-Dimensional Tests on a 15% Thick Symmetrical Roof-Top Aerofoil with 20% Plain Flap in the National Physical Laboratory 13 ft. x 9 ft. Wind Tunnel", British R. & M. 2412, June, 1946.

179. Braslow, A.L. and Visconti, F., "Two-Dimensional Wind-Tunnel Investigation of Two NACA 7-Series Type Airfoils Equipped with a Slot-Tip Aileron, Trailing-Edge Frise Aileron, and a Double Slotted Flap", NACA, RM L9B23, March, 1949.

180. Fischel, J., and Riebe, J.M., "Wind-Tunnel Investigation of an NACA 23021 Airfoil with a 0.32-Airfoil-Chord Double Slotted Flap", NACA WR L-7, October, 1944.

181. Riebe, J.M., and Church, O., "Wind-Tunnel Investigation of Control-Surface Characteristics: XXI-Medium and Large Aerodynamic Balances of Two Nose Shapes and a Plain Overhang Used with a 0.40-Airfoil-Chord Flap on an NACA 0009 Airfoil", NACA WR L-175, March, 1945.

182. Purser, P.E., Fischel, J., and Riebe, J.M., "Wind-Tunnel Investigation of an NACA 23012 Airfoil with a 0.30-Airfoil-Chord Double Slotted Flap", NACA WR L-469, December, 1943.

183. Cahill, J.F., "Aerodynamic Data for a Wing Section of the Republic XF-12 Airplane Equipped with a Double Slotted Flap", NACA WR L-544, January, 1946.

184. Nuber, R.J., and Rice, F.J., Jr., "Lift Tests of a 0.1536c Thick Douglas Airfoil Section of NACA 7-Series Type Equipped with a Lateral-Control Device for Use with a Full-Span Double-Slotted Flap on the C-74 Airplane", NACA WR L-641, March, 1945.

185. Purser, P.E., and Johnson, H.S., "Effects of Trailing-Edge Modifications on Pitching Characteristics of Airfoils", NACA WR L-664, September, 1944.

186. Bogdonoff, S.M., "Wind-Tunnel Investigation of a Low-Drag Airfoil Section with a Double Slotted Flap", NACA WR L-697, September, 1943.

187. Wenzinger, C.J., and Gauvain, W.E., "Wind-Tunnel Investigations of an NACA 23012 Airfoil with a Slotted Flap and Three Types of Auxiliary Flap", NACA No. 679, 1939.

188. Fullmer, F.F., Jr., "Wind-Tunnel Investigation of NACA 66(215)-216, 66, 1-212, and 65$_1$-212 Airfoils with 0.20-Airfoil-Chord Split Flaps", NACA WR L-140, July, 1944.

189. Wenzinger, C.J., and Harris, T.A., "Wind-Tunnel Investigation of an NACA 23021 Airfoil with Various Arrangements of Slotted Flaps", NACA Report No. 677, 1939.

190. Wenzinger, C.J., "Pressure Distribution over an NACA 23012 Airfoil with an NACA 23012 External-Airfoil Flap", NACA Report No. 614, 1938.

191. Jones, R., Bell, A.H., and Smyth, E., "Tests on Aerofoil Flaps in the Compressed Air Tunnel", British R. & M. 1636, November, 1934.

192. Williams, D.H., Bell, A.H., and Smyth, E., "Tests on a 16% Handley-Page Aerofoil with 20% Slotted Flap in the Compressed Air Tunnel", British R. & M. 1854, August, 1938.

193. Williams, D.H., and Brown, A.F., "Experiments on an NACA 23021 Aerofoil with a 15 Per Cent Handley Page Slotted Flap in the Compressed Air Tunnel", British R. & M. 2305, October, 1939

194. Jones, R., "Tests in the Compressed Air Tunnel on the Aerofoils NACA 0015 and NACA 0030 with and without Split Flap and on other Aerofoils of Various Thicknesses with a Split Flap", British R. & M. 2584, June, 1940.

195. Stevenson, D.B., and Byrne, R.W., "High-Speed Wind-Tunnel Tests of an NACA 16-009 Airfoil having a 32.9-Percent-Chord Flap with an Overhang 20.7 Percent of the Flap Chord", N.A.C.A., T.N. 1406, August, 1947.

196. Sears, R.I., "Wind-Tunnel Data on the Aerodynamic Characteristics of Airplane Control Surfaces", N.A.C.A. W.R. L-663, December, 1943.

197. Williams, D.H., and Brown, A.F., "Experiments on a Small-Chord Flap on a Clark YH Aerofoil in the Compressed Air Tunnel", British R. & M. 1681, May, 1935.

198. Bryant, L.W., Halliday, A.S., and Batson, A.S., "Two-Dimensional Control Characteristics", British R. & M. 2730, April, 1950.

199. Abbot, I.H., and Greenberg, H., "Tests in the Variable-Density Wind Tunnel of the NACA 23012 Airfoil with Plain and Split Flaps", N.A.C.A. Report No. 661, 1939.

200. Allen, H. J. "Calculation of the Chordwise Load Distribution over Airfoil Sections with Plain, Split, or Serially Hinged Trailing-Edge Flaps", N.A.C.A. Report No. 634, 1938.

201. Wenzinger, C.J., and Delano, J.B., "Pressure Distribution over an NACA 23012 Airfoil with a Slotted and a Plain Flap" N.A.C.A., Report No. 633, 1938.

202. Clark, K.W., and Kirkby, F.W., "Wind Tunnel Tests of the Characteristics of Wing Flaps and their Wakes", British R. & M. 1698, August, 1935.

203. Dods, J.B., Jr., and Watson, E.C., "The Effects of Blowing over Various Trailing-Edge Flaps on an NACA 0006 Airfoil Section, Comparisons with Various Types of Flaps on other Airfoil Sections, and an Analysis of Flow and Power Relationships for Blowing Systems", N.A.C.A. R.M. A56C01, June, 1956 (Classified).

204. Hazen, D.C., and Lehnert, R.F., "Smoke Tunnel Investigation of a Flap Configuration Developed by Chase Aircraft Co.", Princeton University Report No. 245. (Classified).

205. Richardson, D., "Wind Tunnel Tests of a 17% Thick Airfoil with BLC by Suction, Part II", Chase Aircraft Co. Report No. 17-185, August, 1953, (Classified).

206. Seredinsky, V., "Wind-Tunnel Tests of a 17% Thick Airfoil with BLC by Suction, Part I", Chase Aircraft Co. Report No. 17-184, June, 1953, (Classified).

207. Recant, I.G., "Wind-Tunnel Investigation of an NACA 23030 Airfoil with Various Arrangements of Slotted Flaps", N.A.C.A. T.N. 755, March, 1940.

208. Freeman, H.B., "Boundary-Layer-Control Tests of Two Wings in the Langley Propellor-Research Tunnel", N.A.C.A., T.N. 1007, January, 1946.

209. Dannenberg, R.E., and Weiberg, J.A., "Exploratory Investigation of an Airfoil with Area Suction Applied to a Porous, Round Trailing Edge Fitted with a Lift-Control Vane", N.A.C.A. T.N. 3498, April, 1955.

210. Harris, T.A., and Lowry, J.G., "Pressure Distribution over an NACA 23012 Airfoil with a Fixed Slot and a Slotted Flap", N.A.C.A. Report No. 732, 1942.

211. Heughan, D.M., "An Experimental Study of a Symmetrical Aerofoil with a Rear Suction Slot and a Retractable Flap", Great Britain Aeronautical Research Council Technical Report 15790, April, 1953.

212. Chaplin, H.R., "Preliminary Investigation of a B.L.C. Device for Delaying Leading-Edge Stall on Thin, Sharp Wings", David Taylor Model Basin, Aero. Report 907, August, 1956 (Classified).

213. Maskell, M.A., "Pressure Distributions Illustrating Flow Reattachment Behind a Forward Mounted Flap", British C.P. No. 211 (Tech. Note No. Aero. 2295), March, 1954.

214. Murphy, R.D., and Barnard, G.A., "Two-Dimensional Wind Tunnel Tests of a Model of an F9F-5 Airplane Wing Section Using a High-Speed Jet Blowing over the Flap - Part II: Tests of a 1.35 - Foot Chord Model", David Taylor Model Basin, Aero. Report 845, April, 1955. (Classified)

215. Silverstein, A., Katzoff, S., and Bullivant, W.K., "Downwash and Wake Behind Plain and Flapped Airfoils", NACA Report No. 651, 1939.

216. Betz, A., "New Results in Influencing Lift of Wings" (translated by F. Wagner), University of Wichita, Eng'gr. Study No. 083, September, 1952.

217. Razak, V.L. and Ten Eyck, V.C., "Two-Dimensional Wind-Tunnel Investigation of Boundary-Layer Control by Suction on an NACA 23015 Airfoil with a Single-Slotted Flap", University of Wichita, Aerodynamic Report 058, June, 1952.

218. Lee, G.H., "High Maximum Lift", The Aeroplane, October 30, 1953.

219. Young, A.D., "The Aerodynamic Characteristics of Flaps", British R&M 2622, February, 1947.

220. Reid, E.G. and Bamber, J.J., "Preliminary Investigation on Boundary Layer Control by Means of Suction and Pressure with the U.S.A. 27 Airfoil", N.A.C.A., T.N. 286, May, 1928.

221. Lighthill, J.J., "A New Method of Two-Dimensional Aerodynamic Design", British R&M 2112, April, 1945.

222. Seewald, F., "Increasing Lift by Releasing Compressed Air on Suction Side of Airfoil", N.A.C.A. T.M. 441, December, 1947.

223. Jacobs, E.N., Ward, K.E., and Pinkerton, R.M., "The Characteristics of 78 Related Airfoil Sections from Tests in the Variable-Density Wind Tunnel", N.A.C.A. Report No. 460, 1933.

224. Bamber, M. J., "Wind Tunnel Tests on Airfoil Boundary Layer Control Using a Backward-Opening Slot", N.A.C.A. Report No. 385, 1931.

225. Quinn, J.H., Jr., "Tests of the NACA 65_3-018 Airfoil Section with Boundary-Layer Control by Suction", N.A.C.A. W.R. L-209, October, 1944.

226. Pfenninger, W., "Experiments on a Laminar Suction Airfoil of 17 Per Cent Thickness", Journal of the Aeronautical Sciences, April, 1949.

227. Dickinson, H.B., "Flight and Tunnel Test Research on Boundary-Layer Control", Journal of the Aeronautical Sciences, April, 1949.

228. Spence, D.A., "Prediction of the Characteristics of Two-Dimensional Airfoils", Journal of the Aeronautical Sciences, September, 1954.

229. Schrenk, O., "Experiments with a Wing Model from which the Boundary is Removed by Suction", N.A.C.A. T.M. 534, October, 1929.

230. Schrenk, O., "Experiments with a Wing from which the Boundary Layer is Removed by Suction", N.A.C.A. T.M. 634, August, 1931.

231. Woods, L. C., "The Two-Dimensional Subsonic Flow of an Inviscid Fluid about an Aerofoil of Arbitrary Shape", British R&M 2811, November, 1950.

232. Preston, J.H., "The Calculation of Lift Taking Account of the Boundary Layer", British R. & M. 2725, November, 1949.

233. Preston, J.H., "The Approximate Calculation of the Lift of Symmetrical Aerofoils Taking Account of the Boundary Layer with Application to Control Problems", British R. & M. 1996, May, 1943.

234. Preston, J.H. and Sweeting, N.E., "The Experimental Determination of the Boundary Layer and Wake Characteristics of a Simple Joukowski Aerofoil, with Particular Reference to the Trailing Edge Region", British R. & M. 1998, March, 1943.

235. Preston, J.H., Sweeting, N.E., and Cox, D.K., "The Experimental Determination of the Boundary Layer and Wake Characteristics of a Piercy 12/40 Aerofoil, with Particular Reference to the Trailing Edge Region", British R. & M. 2013, February, 1945.

236. Seddon, J., and Haverty, L., "Some Tests on the Spread of Velocity in a Cold Jet Discharging with Excess Pressure from a Sonic Exit into Still Air", Royal Aircraft Establishment, Farnsborough, Tech. Note No. Aero. 2400, November, 1955.

237. Smith, A.M.O., and Roberts, H.E., "The Jet Airplane Utilizing Boundary Layer Air for Propulsion", Journal of the Aeronautical Sciences, Vol. 14, No. 2, February, 1947.

238. Stratford, B.S., "Early Thoughts on the Jet Flap", The Aeronautical Quarterly, February, 1956.

239. Stratford, B.S., "Mixing and the Jet Flap", The Aeronautical Quarterly, May, 1956.

240. Cornish, J.J., III, "Prevention of Turbulent Separation Through a Perforated Surface", Mississippi State College, Research Report No. 7, October, 1953.

241. Lee, J.M., "A Review of Air-Flow Visualization by Means of Mist, Smoke, and Dust", David Taylor Model Basin, Aero. Report 883, October, 1955.

242. Attinello, J.S., "Wing Lift Augmentation Methods for the Improvement of the Low Speed Performance of High Speed Aircraft", preprint #512 of paper presented before the SAE Anniversary Aeronautic Meeting, New York, N. Y., April 18 - 21, 1955.

243. Attinello, J.S., "Flow Control - The Integration of Power Plant and Airframe for Future Aircraft", Bureau of Aeronautics, Research Division Report No. DR-1745, April, 1955.

244. Attinello, J.S., "Boundary-Layer Control and Supercirculation", Aeronautical Engineering Review, September, 1953.

245. Dike, D.J., "A Study of the Possibilities of Empirically Predicting Maximum Lift for Profiles with Boundary Layer Controls", Princeton University Report No. 359, January, 1957.

246. McCabe, W.L., "The Development of the Princeton University Analog Plotting Tank Facility", Princeton University Report No. 316, August, 1955.

247. Sweeney, T.E., and Lehnert, R.F., "Two-Dimensional Characteristics of T.E.S.A.B.O.F. System Applied to N.A.C.A. 64010 Profile", Princeton University Report No. 330, 1955.

248. Cincotta, T.A., "A Method for Optimizing Two-Dimensional Airfoils", Princeton University Report No. 355, May, 1956.

249. Malavard, L., Poisson-Quinton, Ph., and Jousserandot, P., "Theoretical and Experimental Investigations of Circulation Control", (Translated by T. M. Berthoff and D. C. Hazen of Princeton University). Released in U.S.A. as Princeton University Report No. 358, July, 1956.

250. Schlichting, H., Boundary Layer Theory, McGraw-Hill Book Co., 1955.

251. Main-Smith, J.D., "Chemical Solids as Diffusible Coating Films for Visual Indications of Boundary-Layer Transition in Air and Water", British R&M 2755, February, 1950.

252. Lambourne, N.C., and Pusey, P.S., "Some Visual Observations of the Flow over a Swept-Back Wing in a Water Tunnel with Particular Reference to High Incidences", British C.P. No. 192, May, 1954.

253. Katzoff, S., and Silverstein, A., "Design Charts for Predicting Downwash Angles and Wake Characteristics behind Plain and Flapped Wings", N.A.C.A. Report No. 648, 1939.

254. DeYoung, J., "Theoretical Symmetric Span Loading Due to Flap Deflection for Wings of Arbitrary Plan Form at Subsonic Speeds", N.A.C.A. Report No. 1071, 1952.

255. Anderson, R.F., "Determination of the Characteristics of Tapered Wings", N.A.C.A. Report No. 572, 1940.

256. Polhamus, E.C., "A Simple Method of Estimating the Subsonic Lift and Damping in Roll of Sweptback Wings", N.A.C.A. T.N. No. 1862, April 1949.

257. DeYoung, J., "Theoretical Additional Span Loading Characteristics of Wings with Arbitrary Sweep, Aspect Ratio, and Taper Ratio", N.A.C.A. T.N. No. 1491, December 1947.

258. Mutterperl, W., "The Calculation of Span Load Distributions on Swept-Back Wings", N.A.C.A. T.N. No. 834, December, 1941.

259. McCormack, G.M. and Cook, W.L., "Effects of Boundary-Layer Control on the Longitudinal Characteristics of a 45° Swept-Forward Wing-Fuselage Combination", N.A.C.A. R.M. A9K02a, February 2, 1950.

260. Lange, R.H., "Maximum-Lift Characteristics of a Wing with the Leading-Edge Sweepback Decreasing from 45° at the Root to 20° at the Tip at Reynolds Numbers from 2.4×10^6 to 6.0×10^6", N.A.C.A. R.M. L50A04a, July 6, 1950.

261. Weissinger, J., "The List Distribution of Swept-Back Wings", N.A.C.A. T.M. No. 1120, March 1947.

262. Toll, T.A., and Queijo, M.J., "Approximate Relations and Charts for Low-Speed Stability Derivatives of Swept Wings", N.A.C.A. T.N. No. 1581, May 1948.

263. Woods, R.L., and Spooner, S. H., "Effects of High-Lift and Stall-Control Devices, Fuselage, and Horizontal Tail on a Wing Swept Back 42° at the Leading Edge and Having Symmetrical Circular-ARC Airfoil Sections at a Reynolds Number of 6.9×10^6", N.A.C.A. R.M. No. L9B11, April 20, 1949.

264. Salmi, R.J., "Effects of Leading-Edge Devices and Trailing-Edge Flaps on Longitudinal Characteristics of Two 47.7° Sweptback Wings of Aspect Ratios 5.1 and 6.0 at a Reynolds Number of 6.0×10^6", N.A.C.A. R.M. L50F20, August 30, 1950.

265. Cahill, J.F., and Gottlieb, S.M., "Low-Speed Aerodynamic Characteristics of a Series of Swept Wings Having NACA 65A006 Airfoil Section (Revised)", N.A.C.A. R.M. L50F16, October 17, 1950.

266. Kelly, M.W., "Low-Speed Aerodynamic Characteristics of a Large-Scale 60° Swept-Back Wing with High Lift Devices", N.A.C.A. R.M. A52A14a, March 3, 1952.

267. Harper, J.J., "Investigation at Low Speed of 45° and 60° Sweptback, Tapered, Low-Drag Wings Equipped with Various Types of Full-Span, Trailing-Edge Flaps", N.A.C.A. T.N. 2468, October, 1951.

268. McCormack, G.M., and Stevens, V.I., Jr., "An Investigation of the Low-Speed Stability and Control Characteristics of Swept-Forward and Swept-Back Wings in the Ames 40- By 80- Foot Wind Tunnel", N.A.C.A. R.M. No. A6K15, June 10, 1947.

269. Wick, B.H., and Graham, D., "Exploratory Investigation of the Effect of Skewed Plain Nose Flaps on the Low-Speed Characteristics of a Large-Scale Triangular-Wing-Fuselage Model", N.A.C.A. R.M. A9K22, January 12, 1950.

270. Barnett, U.R., Jr., and Lange, R.H., "Low-Speed Pressure-Distribution Measurements at a Reynolds Number of 3.5×10^6 on a Wing with Leading-Edge Sweepback Decreasing from 45° at the Root to 20° at the Tip", N.A.C.A. R.M. L50A23a, July 7, 1950.

271. Pearson, H.A., "Span Load Distribution for Tapered Wings with Partial-Span Flaps", N.A.C.A. Report No. 585, 1937.

272. DeYoung, J., and Harper, C.W., "Theoretical Symmetric Span Loading at Subsonic Speeds for Wings Having Arbitrary Plan Form", N.A.C.A. Report No. 921, 1948.

273. Pasamanick, J., and Sellers, T.B., "Low-Speed Investigation of Leading-Edge and Trailing-Edge Flaps on a 47.5° Sweptback Wing of Aspect Ratio 3.4 at a Reynolds Number of 4.4×10^6", N.A.C.A. R.M. L50E02, June 12, 1950.

274. Foster, G.V., and Griner, R.F., "Low-Speed Longitudinal Characteristics of a Circular-ARC 52° Sweptback Wing of Aspect Ratio 2.84 with and without Leading-Edge and Trailing-Edge Flaps at Reynolds Numbers from 1.6×10^6 to 9.7×10^6", N.A.C.A. R.M. L50F16a, August 11, 1950.

275. Johnson, H.S., and Hagerman, J.R., "Wind-Tunnel Investigation at Low Speed of a 45° Sweptback Untapered Semispan Wing of Aspect Ratio 1.59 Equipped with Various 25-Percent-Chord Plain Flaps", N.A.C.A. T.N. 2169, August 1950.

276. Hoggard, H.P., Jr., and McKinney, E.G., "Wind-Tunnel Investigation of Control-Surface Characteristics of Plain and Balanced Flaps with Several Trailing-Edge Angles on an NACA 0009 Tapered Semispan Wing", N.A.C.A. T.N. No. 1248, April, 1947.

277. Letko, W., and Goodman, A., "Preliminary Wind-Tunnel Investigation at Low Speed of Stability and Control Characteristics of Swept-Back Wings", N.A.C.A. T.N. No. 1046, April, 1946.

278. Fischel, J., and Vogler, R.D., "High-Lift and Lateral Control Characteristics of an NACA 65_2-215 Semispan Wing Equipped with Plug and Retractable Ailerons and a Full-Span Slotted Flap", N.A.C.A. T.N. No. 1872, April 1949.

279. Johnson, H.S., and Hagerman, J.R., "Wind-Tunnel Investigation at Low Speed of an Unswept Untapered Semispan Wing of Aspect Ratio 3.13 Equipped with Various 25-Percent-Chord Plain Flaps", N.A.C.A. T.N. 2080, April, 1950.

280. Ashkenas, H., and Riddell, F.R., "Investigation of the Turbulent Boundary Layer on a Yawed Flat Plate", N.A.C.A. T.N. 3383, April, 1955.

281. Maki, R.L., "The Use of Two-Dimensional Section Data to Estimate the Low-Speed Wing Lift Coefficient at which Section Stall First Appears on a Swept Wing", N.A.C.A. R.M. A51E15, July 27, 1951.

282. Hollingdale, S.H., "Aerodynamic Characteristics of Tapered Wings with Flaps and Slots", British R. & M. No. 1774, October 30, 1936.

283. Irving, H.B., Batson, A.S., Warsap, J.H., and Gummer, H.J., "Some Aerodynamic Characteristics of Tapered Wings Fitted with Flaps of Various Spans", British R. & M. No. 1796, February 27, 1937.

284. Palme, H.O., "Summary of Wind Tunnel Data for High-Lift Devices on Swept Wings", Sweden, SAAB T.N. 16, April 20, 1953.

285. Palme, H.O., "Summary of Stalling Characteristics and Maximum Lift of Wings of Low Speeds", SAAB T.N. 15, April 10, 1953.

286. Irving, H.B., and Batson, A.S., "A Comparison of Aileron Control on Tapered Wings with Straight Leading Edge and Straight Trailing Edge", British R. & M. No. 183, May 6, 1938.

287. Cohen, J. and Fraser, S/L H.P., "Flight Tests of a Falcon Fitted with an Irving Flap", British R. & M. No. 1863, September 5, 1938.

288. Gates, S.B., "Note on Effects of Landing Flaps on Stability and Control", British R. & M. No. 1732, May 25, 1935.

289. Gates, S.B., "Split Flaps and Other Devices for Facilitating Landing", British R. & M. No. 1659, April 1934.

290. Hartley, J.H. and Curtis, W.H., "Note on Wind Tunnel Tests on a Parasol Monoplane with Zap and Split Flaps", British R. & M. No. 1728, May 11, 1936.

291. Williams, D.H., Brown, A.F., and Smyth, L., "Tests of Aerofoils R.A.F. 69 and R.A.F. 89, with and without Split Flaps, in the Compressed Air Tunnel", British R. & M. No. 1717, May 25, 1936.

292. Serby, J.E. and Squire, H.B., "Full Scale Tests of Slots and Flaps on a Heinkel He.64 with Special Reference to Landing", British R. & M. No. 1713, November 5, 1935.

293. Jones, E.T., Cohen, J., and Hufton, P.A., "Full Scale Lift, Drag and Landing Measurements of a Monoplane fitted with a Zap Flap", British R. & M. No. 1741, May 1, 1936.

294. Furlong, C.C., "Exploratory Investigation of Leading-Edge Chord-Extensions to Improve the Longitudinal Stability Characteristics of Two 52° Sweptback Wings", N.A.C.A. R.M. L50A30, March 10, 1950.

295. Demele, F.A. and Sutton F.B., "The Effects of Increasing the Leading-Edge Radius and Adding Forward Camber on the Aerodynamic Characteristics of a Wing with 35° of Sweepback", N.A.C.A. R.M. A50K28a, February 9, 1951.

296. Lange, R.H., Cocke, B.W., Jr., and Proterra, A.J., "Preliminary Full-Scale Investigation of a 1/3 -Scale Model of a Convertible-Type Airplane", N.A.C.A. R.M. L9C29, June 7, 1949.

297. James, H.A., "Low-Speed Aerodynamic Characteristics of a Large-Scale 45° Swept-Back Wing with Partial-Span Slats, Double-Slotted Flaps, and Ailerons", N.A.C.A. R.M. A52B19, April 28, 1952.

298. Purser, P.E. and Spearman, M.L., "Wing-Tunnel Tests at Low Speed of Swept and Yawed Wings having Various Plan Forms", N.A.C.A. R.M. No. L7D23, May 22, 1947.

299. Martina, A.P. and Deters, O.J., "Maximum Lift and Longitudinal Stability Characteristics at Reynolds Numbers up to 7.8 x 10^6 of a 35° Sweptforward Wing Equipped with High-Lift and Stall-Control Devices, Fuselage, and Horizontal Tail", N.A.C.A. R.M. L9H18a, February 9, 1950.

300. Queijo, M.J. and Lichtenstein, J.H., "The Effects of High-Lift Devices on the Low-Speed Stability Characteristics of a Tapered 37.5° Sweptback Wing of Aspect Ratio 3 in Straight and Rolling Flow", N.A.C.A. R.M. No. L8I03, November 9, 1948.

301. Croom, D.R., "Characteristics of Flap-Type Spoiler Ailerons at Various Locations on a 60° Delta Wing with a Double Slotted Flap", N.A.C.A. R.M. L52J24, December 18, 1952.

302. Spooner, S.H. and Mollenberg, E.F., "Positioning Investigation of Single Slotted Flaps on a 47.7° Sweptback Wing at Reynolds Numbers of 4.0×10^6 and 6.0×10^6", N.A.C.A. R.M. L50H29, October 9, 1950.

303. Conner, D.W. and Neely, R.H., "Effects of a Fuselage and Various High-Lift and Stall-Control Flaps on Aerodynamic Characteristics in Pitch of an NACA 64-Series 40° Swept-Back Wing", N.A.C.A. R.M. No. L6L27, May 26, 1947.

304. Foster, G.V. and Fitzpatrick, J.E., "Longitudinal-Stability Investigation of High-Lift and Stall-Control Devices on a 52° Sweptback Wing with and without Fuselage and Horizontal Tail at a Reynolds Number of 6.8×10^6", N.A.C.A. R.M. No. L8I08, December 20, 1948.

305. Barnett, U.R., Jr. and Lipson, S., "Effects of Several High-Lift and Stall-Control Devices on the Aerodynamic Characteristics of a Semispan 49° Sweptback Wing", N.A.C.A. R.M. L52D17a, September 15, 1952.

306. Razak, K., Razak, V., and Bondie, R.J., "Wind-Tunnel Investigation of a Method of Boundary-Layer Control as Applied to a Reflection-Plane Model at Full-Scale Reynolds Number", University of Wichita, Report No. 032, June, 1951.

307. Wallace, R.E., Bondie, R.J., Jr., and Stalter, J.L., "Wind-Tunnel Tests of a Swept-Wing Semispan Model with Circulation Control", University of Wichita, Report No. 101, August 1953.

308. Anderson, S.B., Matteson, F.H., and Van Dyke, R.D., Jr., "A Flight Investigation of the Effect of Leading-Edge Camber on the Aerodynamic Characteristics of a Swept-Wing Airplane", N.A.C.A. R.M. A52L16a, February, 1953, (Classified).

309. Furlong, G.C. and McHugh, J.G., "A Summary and Analysis of the Low-Speed Longitudinal Characteristics of Swept Wings at High Reynolds Number", N.A.C.A. R.M. L52D16, August, 1952, (Classified)

310. Griner, R.F. and Foster, G.V., "Low-Speed Longitudinal and Wake Air-Flow Characteristics at a Reynolds Number of 6.0×10^6 of a 52° Sweptback Wing Equipped with Various Spans of Leading-Edge and Trailing-Edge Flaps, a Fuselage, and a Horizontal Tail at Various Vertical Positions", N.A.C.A. R.M. L50K29, February, 1951. (Classified).

CONFIDENTIAL

311. Cahill, J.F. and Nuber, R.J., "Aerodynamic Load Measurements over a Leading-Edge Slat on a 40° Sweptback Wing at Mach Numbers from 0.10 to 0.91", N.A.C.A. R.M. L52G18a, September, 1952. (Classified).

312. Heitmeyer, J.C., "Effect of Nose Shape and Trailing-Edge Bluntness on the Aerodynamic Characteristics of an Unswept Wing of Aspect Ratio 3.1, Taper Ratio 0.4, and 3-Percent Thickness", N.A.C.A. R.M. A54A04, Mary, 1954. (Classified).

313. Kelly, M.W. and Tolhurst, W.H., Jr., "The Use of Area Suction to Increase the Effectiveness of a Trailing-Edge Flap on a Triangular Wing of Aspect Ratio 2", N.A.C.A. R.M. A54A25, April, 1954. (Classified).

314. Heitmeyer, J. C., "Effect of a Leading-Edge Flap upon the Lift, Drag, and Pitching Moment of an Airplane Employing a Thin, Unswept Wing", N.A.C.A. R.M. A54B16, October, 1954. (Classified).

315. Matteson, F.H. and Van Dyke, R.D., Jr., "Flight Investigation of the Effects of a Partial-Span Leading-Edge Chord Extension on the Aerodynamic Characteristics of a 35° Swept-Wing Fighter Airplane", N.A.C.A. R.M. A54B26, April, 1954. (Classified).

316. Heitmeyer, J.C. and Hightower, R.C., "Lift, Drag, and Pitching Moment of Low-Aspect-Ratio Wings at Subsonic and Supersonic Speeds-Plane Triangular Wing of Aspect Ratio 4 with 3-Percent-Thick Rounded Nose Section", N.A.C.A. R.M. A51F21, August, 1951. (Classified).

317. Foster, G.V., Mollenberg, E.F., and Woods, R.L., "Low-Speed Longitudinal Characteristics of an Unswept Hexagonal Win with and without a Fuselage and a Horizontal Tail Located at Various Positions at Reynolds Numbers from 2.8×10^6 to 7.6×10^6", N.A.C.A. R.M. L52L11b, February, 1953. (Classified).

318. Cleary, J.W. and Boddy, L.E., "Wind-Tunnel Investigation of a 45° Sweptback Wing having a Symmetrical Root and a Highly Cambered Tip, Including the Effects of Fences and Lateral Controls", N.A.C.A. R.M. A53121, November, 1953. (Classified).

319. Yates, E.C., Jr., "Low-Speed Wind-Tunnel Investigation of Leading-Edge Porous Suction on a 4-Percent-Thick 60° Delta Wing", N.A.C.A. R.M. L54L21, March, 1955.

CONFIDENTIAL

320. Selan, R. and Bandettini, A., "The Effects of Leading-Edge Extensions, a Trailing-Edge Extension, and a Fence on the Static Longitudinal Stability of a Wing-Fuselage-Tail Combination having a Wing with 35° of Sweepback and an Aspect Ratio of 4.5", N.A.C.A. R.M. A53E12, August, 1953. (Classified).

321. de los Santos, S.T., Chaplin, H.R., and Harkleroad, E.L., "Correlation of Wind-Tunnel Measurements on the Basis of Blowing Momentum Required to Produce Theoretical Flap Effectiveness on Airplane Models Equipped with Boundary-Layer-Control Devices", David Taylor Model Basin, Aero. Report 891, December, 1955. (Classified).

322. Whittle, E.F., Jr., and Lipson, S., "Effect on the Low-Speed Aerodynamic Characteristics of a 49° Sweptback Wing having an Aspect Ratio of 3.78 of Blowing Air over the Trailing-Edge Flap and Aileron", N.A.C.A. R.M. L54C05, April, 1954.

323. Blackaby, J. R., "Wind-Tunnel Investigation at Low Speed of a Wing having 63° Sweepback and a Drooped Tip", N.A.C.A. R.M. A55B14, April, 1955. (Classified).

324. Cook, W.L., Griffin, R.N., Jr., and McCormack, G.M., "The Use of Area Suction for the Purposes of Delaying Separation of Air Flow at the Leading Edge of a 63° Swept-Back Wing", N.A.C.A. R.M. A50H09, November, 1950. (Classified).

325. Cook, W.L., Holzhouser, C.A., and Kelly, M.W., "The Use of Area Suction for the Purpose of Improving Trailing-Edge Effectiveness on a 35° Sweptback Wing", N.A.C.A. R.M. A53E06, July, 1953. (Classified).

326. Weil, J., Sleeman, W.C., Jr., and Byrnes, A.L., Jr., "Investigation of the Effects of Wing and Tail Modifications on the Low-Speed Stability Characteristics of a Model having a Thin 40° Swept Wing of Aspect Ratio 3.5", N.A.C.A. R.M. L53C09, April, 1953. (Classified).

327. Concro, P.A., "Low-Speed Aileron Effectiveness as Determined by Force Tests and Visual-Flow Observations on a 52° Sweptback Wing with and without Chord-Extension", N.A.C.A. R.M. L53B26, April, 1953. (Classified).

328. Pasamanick, J. and Scallion, W.I., "The Effects of Suction through Porous Leading-Edge Surfaces on the Aerodynamic Characteristics of a 47.5° Sweptback Wing-Fuselage Combination at a Reynolds Number of 4.4×10^6", N.A.C.A. R.M. L51K15, March, 1952. (Classified).

329. Maki, R.L. and Embry, U.R., "Effects of High-Lift Devices and Horizontal-Tail Location on the Low-Speed Characteristics of a Large-Scale 45° Swept-Wing Airplane Configuration", N.A.C.A. R.M. A54E10, August, 1954. (Classified).

330. Holzhauser, C.A. and Martin, R.K., "The Use of a Leading-Edge Area-Suction Flap to Delay Separation of Air Flow from the Leading Edge of a 35° Sweptback Wing", N.A.C.A. R.M. A53J26, December, 1953. (Classified).

331. Bursnall, W.J., "Experimental Investigation of the Effects of Vortex Generators on the Maximum Lift of a 6-Percent-Thick Symmetrical Circular-Arc Airfoil Section", N.A.C.A. R.M. L52G24, October, 1952. (Classified).

332. West, F.E., Jr. and Henderson, J.H., "Relationship of Flow over a 45° Sweptback Wing with and without Leading-Edge Chord-Extension to Longitudinal Stability Characteristics at Mach Numbers from 0.60 to 1.03", N.A.C.A. R.M. L53H18b, October, 1953. (Classified).

333. West, F.E., Jr., Liner, C., and Martz, C.S., "Effect of Leading-Edge Chord-Extensions on the Aerodynamic Characteristics of a 45° Sweptback Wing-Fuselage Combination at Mach Numbers of 0.40 to 1.03", N.A.C.A. R.M. L53B02, April, 1953. (Classified).

334. David Taylor Model Basin Symposium on Boundary-Layer-Control Systems: "A Compilation of the Papers Presented September 8-9, 1954", Aero. Report 876. (Classified).

(a). Harkleroad, E.L., (D.T.M.B.), "Application of High-Speed Blowing BLC to a Straight-Wing Navy Fighter Aircraft", pp. 47-72.

(b). Fretwell, J.L. LCDR. (USN), "Carrier Aspects of BLC", pp. 73-88.

(c). Barnard, G.A. (D.T.M.B.), "Application of High-Speed Blowing BLC to Two Swept Wing Navy Fighter Aircraft", pp. 89-102.

335. Croom, D.R., "A Low-Speed Investigation of a Thin 60° Delta Wing Equipped with a Double Slotted Flap to Determine the Chordwise Pressure Distribution and the Effect of Vane Size:, N.A.C.A. R.M. L54L03a, March, 1955. (Classified).

336. James, H.A. and Hunton, L.W., "Estimation of Incremental Pitching Moments due to Trailing-Edge Flaps on Swept and Triangular Wings", N.A.C.A. R.M. A55D07, June, 1955. (Classified).

337. Cook, W.L., Griffin, R.N., Jr., and Hickey, D.H., "A Preliminary Investigation of the use of Circulation Control to Increase the Lift of a 45° Sweptback Wing by Suction Through Trailing-Edge Slots", N.A.C.A. R.M. A54I2I, December, 1954. (Classified)

338. Goldsmith, J., "Factors Influencing the Design of Full-Scale and Model High Lift Wings which Utilize Boundary Layer Control", Northrop Aircraft Report No. NAI-54-672, October, 1954. (Classified).

339. Razak, K., Razak, V., Wagner, F., and Wallace, R.E., "Experimental Development and Tests of a High-Lift, Circulation-Control Wing", University of Wichita, Aerodynamic Report No. 097, May, 1953. (Classified).

340. Holford, J.F. and Dee, F.W., "Low Speed Tunnel Tests of some Split Flap Arrangements on a 9% t/c Rectangular Wing", Royal Aircraft Establishment, Technical Note: No. Aero. 2312, July, 1954. (Classified)

341. Bartlett, G.E. and Vidal, R.J., "Experimental Investigation of Influence of Edge Shape on the Aerodynamic Characteristics of Low-Aspect-Ratio Wings at Low Speeds", Cornell Aeronautical Laboratory, Report No. CAL-62, June, 1954.

342. Fisher, J.W., Gertsen, W.M., Wise, W.D., Walter, H.L., Little, H.H., and McGuckin, M., "Flight Tests Results on the Use of High Lift Boundary Layer Control Applied to a Modified Liaison Airplane", Cessna Aircraft Co., Report No. 1339-7, March, 1956.

343. Visconti, F. and Anderson, R., "The Effect of a Supercirculation System on the Lift and Flying Qualities of an F9F-4 Aircraft", Grumman Aircraft Engineering Corporation, Report No. FT79-0-1c.8.

344. Anderson, A.E., "An Investigation at Low Speed of a Large-Scale Triangular Wing of Aspect Ratio Two.- I. Characteristics of a Wing having a Double-Wedge Airfoil Section with Maximum Thickness at 20-Percent Chord", N.A.C.A. R.M. No. A7F06, November 13, 1947.

345. Graham, D., "Chordwise and Spanwise Loadings Measured at Low Speeds on a Large Triangular Wing having an Aspect Ratio of 2 and a Thin, Subsonic-Type Airfoil Section", N.A.C.A. R.M. A50A04a, March 13, 1950.

346. Hunton, L.W., "Effects of Twist and Camber on the Low-Speed Characteristics of a Large-Scale 45° Swept-Back Wing", N.A.C.A. R.M. A50A10, March 20, 1950.

347. James, H.A. and Dew, J.K., "Effects of Double-Slotted Flaps and Leading-Edge Modifications on the Low-Speed Characteristics of a Large-Scale 45° Swept-Back Wing with and without Camber and Twist", N.A.C.A. R.M. A51D18, July 23, 1951.

348. Whitcomb, R.T., "An Investigation of the Effects of Sweep on the Characteristics of a High-Aspect-Ratio Wing in the Langley 8-Foot High-Speed Tunnel", N.A.C.A. R.M. No. L6J01a, February 14, 1947.

349. Neely, R.H. and Conner, D.W., "Aerodynamic Characteristics of a 42° Swept-Back Wing with Aspect Ratio 4 and NACA 64$_1$-112 Airfoil Sections at Reynolds Numbers from 1,700,000 to 9,500,000", N.A.C.A. R.M. No. L7D14, May 23, 1947.

350. Johnson, H.I., "Measurements of Aerodynamic Characteristics of a 35° Sweptback NACA 65-009 Airfoil Model with 1/4-Chord Plain Flap by the NACA Wing-Flow Method", N.A.C.A. R.M. No. L7F13, August 5, 1947.

351. Bielat, R.P. and Cahn, M.S., "An Investigation of the Characteristics of an Unswept Wing of Aspect Ratio 4.01 in the Langley 8-Foot High-Speed Tunnel", N.A.C.A. R.M. L9H23, November 8, 1949

352. Pasamanick, J. and Sellers, T.B., "Full-Scale Investigation of Boundary-Layer Control by Suction through Leading-Edge Slots On a Wing-Fuselage Configuration having 17.5° Leading-Edge Sweep with and without Flaps", N.A.C.A. R.M. L50B15, April 5, 1950.

353. Freeman, H.B., "Boundary-Layer-Control Tests of Two Wings in the Langley Propeller-Research Tunnel", N.A.C.A. T.N. No. 1007, January 1946.

354. MacLeod, R.G., "A Preliminary Low-Speed Wind-Tunnel Investigation of a Thin Delta Wing Equipped with a Double and a Single Slotted Flap", N.A.C.A. R.M. L51J26, January 15, 1952.

355. Pratt, G.L. and Shields, E.R., "Low-Speed Longitudinal Characteristics of a 45° Sweptback Wing of Aspect Ratio 8 with High-Lift and Stall-Control Devices at Reynolds Numbers from 1,500,000 to 4,800,000", N.A.C.A. R.M. L51J04, February 28, 1952.

356. Harper, J.J., "Wind-Tunnel Investigation of Effects of Various Aerodynamic Balance Shapes and Sweepback on Control-Surface Characteristics of Semispan Tail Surfaces with NACA 0009, 0015, 66-009, 66(215)-014, and Circular-ARC Airfoil Sections", N.A.C.A. T.N. 2495, October 1951.

357. Fitzpatrick, J.E. and Schneider, W.C., "Effects of Mach Number Variation between 0.07 and 0.34 and Reynolds Number Variation between 0.97 x 10^6 on the Maximum Lift Coefficient of a Wing of NACA 64-210 Airfoil Sections", N.A.C.A. T.N. 2753, August 1952.

358. Lange, R.H., "Langley Full-Scale-Tunnel Investigation of the Maximum-Lift and Stalling Characteristics of a Trapezoidal Wing of Aspect Ratio 4 with Circular-ARC Airfoil Sections", N.A.C.A. T.N. 2823, November, 1952.

359. Cocke, B.W., Jr., Fink, M.P., and Gottlieb, S.M., "The Aerodynamic Characteristics of an Aspect-Ratio-20 Wing having Thick Airfoil Sections and Employing Boundary-Layer Control by Suction", N.A.C.A. T.N. 2980, August 1953.

360. Crandall, S.M., "Lifting-Surface-Theory Results for Thin Elliptic Wings of Aspect Ratio 3 with Chordwise Loadings Corresponding to 0.5-Chord Plain Flap and to Parabolic-Arc Camber", N.A.C.A. T.N. No. 1064, May 1946.

361. Conner, D.W., "Effect of Reflex Camber on the Aerodynamic Characteristics of a Highly Tapered Moderately Swept-Back Wing at Reynolds Numbers up to 8,000,000", N.A.C.A. T.N. No. 1212, March 1947.

362. Poisson-Quinton, P., "On the Mechanism and Application of Boundary Layer Control to Airplanes", O.N.E.R.A.

363. Maggin, B. and Bennett, C.V., "Flight Tests of an Airplane Model with a 42° Swept-Back Wing in the Langley Free-Flight Tunnel", N.A.C.A. T.N. No. 1287, May 1947.

364. Racisz, S.F. and Paradiso, N.J., "Wind-Tunnel Investigation at High and Low Subsonic Mach Numbers of a Thin Sweptback Wing having an Airfoil Section designed for High Maximum Lift", N.A.C.A. R.M. L51L04, February 26, 1952.

365. Fischel, J. and O'Hare, W.M., "Low-Speed Investigation of Deflectable Wing-Tip Elevators on a Low-Aspect-Ratio Untapered 45° Sweptback Semispan Wing with and without an End Plate", N.A.C.A. R.M. L50D19, June 1, 1950.

366. Kemp, W.B., Jr., Becht, R.E., and Few, A.G., Jr., "Investigation of the Low-Speed Aerodynamic Characteristics of a Variable-Sweep Airplane Model with a Twisted and Cambered Wing", N.A.C.A. R.M. L51K22, February 1, 1952.

367. Pasamanick, J. and Sellers, T.B., "Low-Speed Investigation of the Effect of Several Flap and Spoiler Ailerons on the Lateral Characteristics of a 47.5° Sweptback-Wing-Fuselage Combination at a Reynolds Number of 4.4×10^6", N.A.C.A. R.M. L50J20, December 8, 1950.

368. Nelson, W.H. and Erickson, A.L., "The Effect of Aspect Ratio on the Subsonic Aerodynamic Characteristics of Wings with NACA 65-210 Sections", N.A.C.A. R.M. A9K18, February 3, 1950.

369. Van Dorn, N.H. and DeYoung, J., "A Comparison of Three Theoretical Methods of Calculating Span Load Distribution on Swept Wings", N.A.C.A. T.N. No. 1476, November 1947.

370. Neely, R.H., Bollech, T.V., Westrick, G.C., and Graham, R.R., "Experimental and Calculated Characteristics of Several NACA 44-Series Wings with Aspect Ratios of 8, 10, and 12 and Taper Ratios of 2.5 and 3.5", N.A.C.A. T.N. No. 1270, May 1947.

371. Letko, W. and Feigenbaum, D., "Wind-Tunnel Investigation of Split Trailing-Edge Lift and Trim Flaps on a Tapered Wing with 23° Sweepback", N.A.C.A. T.N. No. 1352, July 1947.

372. Anderson, R.F., "The Aerodynamic Characteristics of Three Tapered Airfoils Tested in the Variable Density Wind Tunnel", N.A.C.A. T.N. No. 367, February, 1931.

373. Brown, C.E. and Michael, W.H., Jr., "On Slender Delta Wings with Leading-Edge Separation", N.A.C.A. T.N. 3430, April 1955.

374. DeYoung, J. and Barling, W.H., Jr., "Prediction of Downwash behind Swept-Wing Airplanes at Subsonic Speed", N.A.C.A. T.N. 3346, January 1955.

375. Polhamus, E.C., "A Note on the Drag due to Lift of Rectangular Wings of Low Aspect Ratio", N.A.C.A. T.N. 3324, January 1955.

376. McCormack, G.M. and Cook, W.L., "A Study of Stall Phenomena on a 45° Swept-Forward Wing", N.A.C.A. T.N. No. 1797, January 1949.

377. Murray, H.E., "Comparison with Experiment of Several Methods of Predicting the Lift of Wings in Subsonic Compressible Flow", N.A.C.A. T.N. No. 1739, October 1948.

378. Sjoberg, S.A. and Reeder, J.P., "Flight Measurements of the Longitudinal Stability, Stalling, and Lift Characteristics of an Airplane having a 35° Sweptback Wing without Slots and with 40-Percent-Span Slots and a Comparison with Wind-Tunnel Data", N.A.C.A. T.N. No. 1679, August 1948.

379. Bollech, T.V., "Experimental and Calculated Characteristics of Several High-Aspect-Ratio Tapered Wings Incorporating NACA 44-Series, 230-Series, and Low-Drag 64-Series Airfoil Sections", N.A.C.A. T.N. No. 1677, September 1948.

380. Wick, B.H., "Chordwise and Spanwise Loadings Measured at Low Speed on a Triangular Wing having an Aspect Ratio of Two and an NACA 0012 Airfoil Section", N.A.C.A. T.N. No. 1650, June 1948.

381. Weick, F.E. and Sanders, R., "Wind-Tunnel Tests of a Hall High-Lift Wing", N.A.C.A. T.N. No. 417, May, 1932.

382. Weick, F.E. and Platt, R.C., "Wind-Tunnel Tests of the Fowler Variable-Area Wing", N.A.C.A. T.N. No. 419, May, 1932.

383. Weick, F.E. and Scudder, N.F., "The Effect on Lift, Drag, and Spinning Characteristics of Sharp Leading Edges on Airplane Wings", N.A.C.A. T.N. No. 447, February, 1933.

384. Wenzinger, C.J., "The Effects of Full-Span and Partial-Span Split Flaps on the Aerodynamic Characteristics of a Tapered Wing", N.A.C.A. T.N. No. 505, September 1934.

385. Parsons, J.F. and Silverstein, A., "Full-Scale Load Distribution on a Tapered Wing with Split Flaps of Various Spans", N.A.C.A. T.N. No. 591, February 1937.

386. Wenzinger, C.J. and Ames, M.B., Jr., "Wind-Tunnel Investigation of Rectangular and Tapered N.A.C.A. 23012 Wings with Plain Ailerons and Full-Span Split Flaps", N.A.C.A. T.N. No. 661, August 1938.

387. House, R.O., "The Effects of Partial-Span Plain Flaps on the Aerodynamic Characteristics of a Rectangular and a Tapered Clark Y Wing", N.A.C.A. T.N. No. 663, September, 1938.

388. Anderson, R.F., "A Comparison of Several Tapered Wings Designed to Avoid Tip Stalling", N.A.C.A. T.N. No. 713, June 1939.

389. House, R.O., "The Effects of Partial-Span Slotted Flaps on the Aerodynamic Characteristics of a Rectangular and a Tapered N.A.C.A. 23012 Wing", N.A.C.A. T.N. No. 719, July 1939.

390. Sherman, A., "A Simple Method of Obtaining Span Load Distributions", N.A.C.A. T.N. No. 732, October 1939.

391. Furlong, G.C. and Fitzpatrick, J.E., "Effects of Mach Number up to 0.34 and Reynolds Number up to 8×10^6 on the Maximum Lift Coefficient of a Wing of NACA 66-Series Airfoil Sections", N.A.C.A. T.N. 2251, December 1950.

392. DeYoung, J., "Theoretical Symmetric Span Loading Due to Flap Deflection for Wings of Arbitrary Plan Form at Subsonic Speeds", N.A.C.A. T.N. 2278, January 1951.

393. Sivells, J.C. and Westrick, G.C., "Method for Calculating Lift Distributions for Unswept Wings with Flaps or Ailerons by Use of Nonlinear Section Lift Data", N.A.C.A. T.N. 2283, January 1951.

394. Lipson, S. and Barnett, U.R., Jr., "Force and Pressure Investigation at Large Scale of a 49° Sweptback Semispan Wing having NACA 65A006 Sections and Equipped with Various Slat Arrangements", N.A.C.A. R.M. L51K26, January 29, 1952.

395. Weinig, F., "Lift and Drag of Wings with Small Span", (Translation) N.A.C. T.M. No. 1151, August 1947.

396. Jones, G.W., Jr., "Investigation of the Effects of Variations in the Reynolds Number between 0.4×10^6 and 3.0×10^6 on the Low-Speed Aerodynamic Characteristics of Three Low-Aspect-Ratio Symmetrical Wings with Rectangular Plan Forms", N.A.C.A. R.M. L52G18, September 22, 1952.

397. Whittle, E.F., Jr., and Lipson, S., "Low-Speed, Large-Scale Investigation of Aerodynamic Characteristics of a Semi-span Wing with a Fowler Flap in Combination with a Plain Flap, Slats, and Fences", N.A.C.A. R.M. L53D09, June 5, 1953.

398. Kelly, H.N., "The Calculated and Experimental Loads and Moments Produced by Split Flaps of Various Spans and Spanwise Locations on a 45° Sweptback Wing of Aspect Ratio 8", N.A.C.A. R.M. L53F12, September 4, 1953.

399. Cohen, D., "A Method for Determining the Camber and Twist of a Surface to Support a given Distribution of Lift, with Applications to the Load over a Sweptback Wing", N.A.C.A. Report No. 826, 1945.

400. Sivells, J.C. and Westrick, G.C., "Method for Calculating Lift Distributions for Unswept Wings with Flaps or Ailerons by use of Nonlinear Section Lift Data", N.A.C.A. Report 1090, 1952.

401. Lange/Wacke, "Test Report on Three- and Six-Component Measurements on a Series of Tapered Wings of Small Aspect Ratio (Partial Report: Elliptic Wing)" (Translation), N.A.C.A. T.M. No. 1146, June 1947.

402. Thiel, A. and Weissinger, J., "Pressure-Distribution Measurements on a Straight and on a 35° Swept-Back Tapered Wing", N.A.C.A. T.M. No. 1126, January 1947.

403. Göthert and Röber, "Systematic Investigations of the Effects of Plan Form and Gap between the Fixed Surface and Control Surface on Simple Flapped Wings", N.A.C.A. T.M. No. 1206, May 1949.

404. Lange/Wacke, "Test Report on Three- and Six-Component Measurements on a Series of Tapered Wings of Small Aspect Ratio (Partial Report: Trapezoidal Wing)" (Translation), N.A.C.A. T.M. No. 1225, May 1949.

405. Haus, F., "The Use of Slots for Increasing the Lift of Airplane Wings", N.A.C.A. T.M. No. 635, August, 1931.

406. Stuper, "Flight Experimences and Tests on Two Airplanes with Suction Slots", (Translation), N.A.C.A. T.M. 1232, January 1950.

407. Lippisch, A., "Method for the Determination of the Spanwise Lift Distribution", N.A.C.A. T.M. No. 778, October 1935.

408. Ruden, P., "Experiments on a Slotted Wing", N.A.C.A. T.M. No. 890, March 1939.

409. Schmieden, C., "Flow Around Wings Accompanied by Separation of Vortices", N.A.C.A. T.M. No. 961, December 1940.

410. Thiel, G. and Weissinger, F. (Translation), "Six-Component Measurements on a Straight and a 35° Swept-Back Trapezoidal Wing with and without Split Flap", N.A.C.A. T.M. No. 1107, June 1947.

411. Lemme, H.A. (Translation), "Force and Pressure-Distribution Measurements on a Rectangular Wing with Double-Hinged Nose", N.A.C.A. T.M. No. 1117, March 1947.

412. Katzoff, S. and Finn, R.S., "Note on the Interpretation of Wake-Survey Data and Its Use in the Estimation of Induced Drag due to Irregularities", N.A.C.A. MR, January 1944.

413. Rogallo, F.M and Schuldenfrei, M., "Wind-Tunnel Investigation of a Plain and a Slot-Lip Aileron on a Wing with a Full-Span Flap Consisting of an Inboard Fowler and an Outboard Slotted Flap", N.A.C.A. A.R.R. June 1941.

414. Neely, R.H., "Wind-Tunnel Tests of Two Tapered Wings with Straight Trailing Edges and with Constant-Chord Center Sections of Different Spans", N.A.C.A. A.R.R. March 1943.

415. Fairbanks, R.W. and Alexander, S.R., "Wind-Tunnel Tests of Two Tapere Wings with Straight Leading Edges and with Constant-Chord Center Sections of Different Spans", N.A.C.A. A.R.R. No. 3J28, October, 1943.

416. Harris, T.A. and Purser, P.E., "Wind-Tunnel Investigation of Plain Ailerons for a Wing with a Full-Span Flap Consisting of an Inboard Fowler and an Outboard Retractable Split Flap", N.A.C.A. A.C.R. March 1941.

417. Jacobs, E.N., "Tapered Wings, Tip Stalling, and Preliminary Results from Tests of the Stall-Control Flap" N.A.C.A., A.C.R. November, 1937.

418. Harmon, S.M., "Additional Design Charts Relating to the Stalling of Tapered Wings", N.A.C.A. A.R.R. January 1943.

419. Cohen, D., "Theoretical Distribution of Load over a Swept-Back Wing", N.A.C.A. A.R.R. October 1942.

420. Neely, R.H. and Foster, G.V., "Wind-Tunnel Investigation of an NACA 66-Series 16-Percent-Thick Low-Drag Tapered Wing with Fowler and Split Flaps", N.A.C.A. A.C.R. No. L5F28, January 1946.

421. Zalovcik, J.A., "Flight Investigation of Boundary-Layer and Profile-Drag Characteristics of Smooth Wing Sections of a P-47D Airplane", N.A.C.A. A.C.R. No. L5H11a, October 1945.

422. Krüger, W. (Translation), "Calculations and Experimental Investigations on the Feed-Power Requirement of Airplanes with Boundary-Layer Control", N.A.C.A. T.M. No. 1167, September 1947.

423. Hunton, L.W., "Effects of Finite Span on the Section Characteristics of Two 45° Swept-Back Wings of Aspect Ratio 6", N.A.C.A. R.M. A52A10, March 17, 1952.

424. Rebuffet, P. and Poisson-Quinton, P. (Translation), "Investigations of the Boundary-Layer Control on a Full Scale Swept Wing with Air Bled off from the Turbojet", N.A.C.A. T.M. 1331, April, 1952.

425. Bray, R.S. and Innis, R.C., "Flight Tests of a Leading-Edge Area Suction on a Fighter-Type Airplane with a 35° Sweptback Wing", N.A.C.A. R.M. A55C07, June 9, 1955.

426. Wallace, R.E., "The Experimental Investigation of a Swept-Wing Research Model Boundary Layer", University of Wichita, Aero. Report No. 092, January 1953.

427. Hancock, G.J., "Method for the Determination of the Pressure Distribution over a Finite Thin Wing at a Steady Low Speed", British C.P. No. 128, September 2, 1952.

428. Carner, H.C., "Swept-Wing Loading. A Critical Comparison of Four Subsonic Vortex Sheet Theories", British C.P. No. 102, October 11, 1951.

429. Young, A.D., and Hufton, P.A., "Note on the Lift and Profile Drag Effects of Split and Slotted Flaps", British R. & M. No. 2545, September 1941.

430. Dickson, R., "Comparison of Two Methods of Calculating Aerodynamic Loading on an Aerofoil with Large Sweepback and Small Aspect Ratio", British R. & M. No. 2353, June, 1946.

431. Falkner, V.M., "Calculated Loadings due to Incidence of a Number of Straight and Swept-Back Wings", British R. & M. No. 2596, June, 1948.

432. Jousserandot, P., "Influence of Blowing over the Flaps and Ailerons of a Complete Airplane Model (MF 30) with Sweptback Wing", O.N.E.R.A., Report No. 2/95 A, April 1951.

433. Jousserandot, P., "Investigation of the Influence of Blowing on a Complete Airplane Model, ME 109", O.N.E.R.A., Report No. 1/95 A, April 1951.

434. Poisson-Quinton, P., "Idées nouvelles sur le controle de la couche limite appliqué aux ailes d'avions", Les cahiers aerodynamique, v. 1-7, November 28, 1945.

435. Jones, R.T., "Effects of Sweep-Back on Boundary Layer and Separation", N.A.C.A. Report No. 884, 1947.

436. Sivells, J.C. and Neely, R.H., "Method for Calculating Wing Characteristics by Lifting-Line Theory Using Nonlinear Section Lift Data", N.A.C.A. Report No. 865, 1947.

437. Sivells, J.C. and Spooner S.H., "Investigation in the Langley 19-Foot Pressure Tunnel of Two Wings of NACA 65-210 and 64-210 Airfoil Sections with Various Type Flaps", N.A.C.A. Report 942, 1949.

438. Jones, R.T., "Properties of Low-Aspect-Ratio Pointed Wings at Speeds Below and Above the Speed of Sound", N.A.C.A. Report No. 835.

439. Boltz, F.W. and Kolbe, C.D., "The Forces and Pressure Distribution at Subsonic Speeds on a Cambered and Twisted Wing having 45° of Sweepback, an Aspect Ratio of 3, and a Taper Ratio of 0.5", N.A.C.A. R.M. A52D22, July 18, 1952.

440. Wallace, R.E., "Preliminary Report on Wind-Tunnel Tests of the ONR Swept-Wing Research Model", University of Wichita, Aero. Report No. 062, October 1952.

441. Weick, F.E. and Sanders R., "Wind-Tunnel Tests on Combinations of a Wing with Fixed Auxiliary Airfoils having Various Chords and Profiles", N.A.C.A. Report No. 472, 1933.

442. Platt, R.C., "Aerodynamic Characteristics of Wings with Cambered External-Airfoil Flaps, Including Lateral Control with a Full-Span Flap", N.A.C.A. Report No. 541, 1935.

443. Anderson, R.F., "The Experimental and Calculated Characteristics of 22 Tapered Wings", N.A.C.A. Report No. 627, 1938.

444. Jacobs, E.N. and Rhode, R.V., "Airfoil Section Characteristics as Applied to the Prediction of Air Forces and their Distribution on Wings", N.A.C.A. Report No. 631, 1938.

445. Parker, H.F., "The Parker Variable Camber Wing", N.A.C.A. Report No. 77, 1919.

446. Scarborough, J.B., "Some Problems on the Lift and Rolling Moment of Airplane Wings", N.A.C.A. Report No. 200, 1925.

447. Salmi, R.J., "Low Speed Longitudinal Aerodynamic Characteristics of a Twisted and Cambered Wing of 45° Sweepback and Aspect Ratio 8 with and without High-Lift and Stall-Control Devices and a Fuselage at Reynolds Numbers from 1.5×10^6 to 4.8×10^6, June 11, 1952.

448. Betz, A. and J. Latz, "Reduction of Wing Left by the Drag", NACA, TM No. 681, August, 1932.

449. Lambourne, N.C. and Pusey, P.S., "Some Visual Observations of the Flow Over a Swept-back Wing in a Water Tunnel, with Particular Reference to High Incidences, British C. P. No. 192, May 31, 1954.

5.2 SUBJECT INDEX

I. Of General Interest:

Refs. #4, 5, 6, 7, 8, 72, 86, 89, 112, 113, 150, 158, 170, 218, 237, 240, 242, 243, 244, 245, 249, 250.

II. Of Unusual Bibliographic Interest:

Refs. #1, 2, 3, 113, 170, 219, 284, 285, 308.

III. Experimental Techniques:

Refs. #25, 26, 27, 42, 145, 241, 246, 251, 252.

IV. Two-Dimensional Profiles (Low Speed) with and without Flow Control:

(A) Summaries of Base Profile Characteristics:
Refs. #9, 19, 21, 22, 23, 24, 73, 198, 223.

(B) Base Profile Viscid and Inviscid Phenomena:
Refs. #10, 11, 12, 13, 14, 15, 16, 17, 20, 26, 215, 221, 228, 231, 232, 233, 234, 235, 245, 248, 250.

(C) Trailing-Edge Suction:
Refs. #28, 29, 30, 31, 32, 33, 34, 35, 36, 37, 38, 61C, 70, 150, 209, 211, 216, 249.

(D) Trailing-Edge Blowing:
Refs. #30, 38, 39, 40, 41, 42, 43, 44, 216, 238, 239, 249.

(E) "Chord Extension Effect":
Refs. #41, 42.

(F) "Coanda Effect":
Refs. #156, 157.

(G) Blowing Jets:
Refs. #61d, 236.

(H) Plain Trailing-Edge Flaps:
Refs. #50, 51, 75, 78, 79, 80, 81, 107, 130, 158, 162, 164, 165, 166, 167, 168, 174, 175, 176, 177, 178, 181, 195, 196, 197, 198, 199, 200, 201.

(I) Split Trailing-Edge Flaps:
Refs. #51, 52, 83, 84, 91, 92, 93, 98, 99, 100, 103, 104, 105, 107, 108, 172, 188, 191, 194, 199, 200, 213.

(J) Slotted Trailing-Edge Flaps:
Refs. #49, 53, 54, 55, 56, 57, 83, 87, 96, 99, 100, 103, 107, 126, 127, 128, 129, 130, 132, 158, 161, 163, 169, 171, 173, 179, 180, 181, 182, 183, 184, 186, 187, 189, 192, 201, 204, 206, 207, 210, 217.

(K) Suction Flaps (Trailing-Edge):
Refs. #61C, 68, 69, 70, 71, 112, 130, 150, 205, 206, 208, 209, 217, 243, 244, 247.

(L) Blowing Flaps (Trailing-Edge):
Refs. #38, 42, 59, 60, 16a, 61b, 62, 63, 64, 66, 68, 69, 112, 150, 158, 159, 203, 214, 243, 244, 247, 249.

(M) Flaps (Trailing-Edge) with Combined Suction and Blowing:
Refs. #61c, 216, 247, 249.

(N) Leading-Edge Flaps:
Refs. #72, 73, 74, 75, 76, 77, 78, 79, 80, 81, 82, 83, 84, 85, 87, 88, 89, 90, 91, 93, 150, 158, 159, 170, 212, 214, 243, 244.

(O) Leading-Edge Slots and Slats:
Refs. #72, 83, 87, 89, 94, 95, 96, 97, 98, 99, 100, 101, 102, 103, 104, 105, 106, 107, 108, 158, 170, 171, 210.

(P) Leading-Edge Suction:
Refs. #108, 109, 110, 111, 112, 113, 114, 115, 116, 117, 118, 119, 120, 121, 122, 123, 124, 125, 126, 127, 128, 129, 130, 131, 132, 133, 134, 135, 136, 137, 138, 139, 140, 141, 142, 143, 144, 145, 150, 170, 208, 220, 225, 226, 227, 229, 230, 240, 243, 244.

(Q) Leading-Edge Blowing:
Refs. #146, 147, 148, 149, 150, 151, 152, 153, 154, 155, 156, 157, 158, 159, 170, 208, 212, 220, 222, 224.

(R) Combined Leading-Edge Devices:
Refs. #66, 150, 158, 159, 170, 212, 243, 244.

(S) Combined Leading-Edge and Trailing-Edge Devices:
Refs. #61a, 66, 75, 78, 79, 80, 81, 83, 84, 87, 89, 91, 92, 93, 96, 97, 98 99, 100, 101, 102, 103, 104, 105, 107, 108, 112, 126, 127, 128, 129, 130, 132, 158, 159, 206, 208, 214, 217, 243, 244.

V. Three-Dimensional Wings (Low Speed) with and without Flow Control:

(A) Straight Wings:
Refs. #279, 312, 314, 340, 351, 357, 359, 360, 375, 379, 386, 396, 402.

(B) Swept-Back Wings:
Refs. #256, 257, 260, 261, 262, 263, 265, 266, 267, 268, 270, 273, 274, 275, 277, 281, 284, 294, 295, 297, 298, 300, 302, 303, 304, 307, 308, 309, 310, 311, 315, 318, 320, 322, 323, 324, 325, 326, 327, 328, 329, 330, 332, 333, 336, 337, 343, 346, 347, 348, 349, 352, 355, 356, 361, 363, 364, 365, 366, 367, 371, 374, 378, 394, 397, 398, 399, 402, 423, 424, 425, 430, 435, 439, 440, 447.

(C) Delta Wings:
Refs. #269, 301, 313, 316, 319, 335, 336, 341, 344, 345, 354, 373, 380.

(D) Swept-Forward Wings:
Refs. #259, 268, 299, 376.

(E) Trapezoidal Wings:
Refs. #276, 317, 358.

(F) Effects of Camber:
Refs. #295, 308, 318, 346, 347, 360, 361, 366, 399, 439, 447.

(G) Effects of Twist:
Refs. #346, 347, 366, 399, 447.

(H) Effects of Taper:
Refs. #255, 257, 271, 276, 282, 283, 286, 361, 371, 384, 385, 386, 388, 401 415, 417, 418, 420, 439, 443.

(I) Effects of Reynolds Number:
Refs. #260, 274, 285, 299, 302, 309, 349, 355, 357, 361, 447.

(J) Effects of Leading-Edge Radius and/or Wing Section:
Refs. #295, 312, 341, 344, 345, 356, 364, 368, 383, 391, 423.

(K) Effects of Aspect Ratio:
Refs. #262, 265, 284, 285, 298, 309, 368.

(L) Effects of Sweep:
Refs. #262, 265, 277, 285, 298, 309, 348.

(M) Trailing-Edge High Lift Devices:
Refs. #254, 263, 264, 266, 267, 271, 273, 274, 275, 276, 278, 279, 282, 283, 284, 288, 293, 297, 299, 300, 301, 302, 303, 304, 305, 308, 310, 329, 335, 336, 340, 347, 350, 354, 355, 360, 371, 384, 385, 386, 394, 397, 413, 420, 447.

(N) Leading-Edge High Lift Devices:
Refs. #263, 264, 266, 269, 273, 274, 284, 297, 299, 300, 303, 304, 305, 308, 310, 311, 314, 320, 329, 347, 355, 378, 394, 397, 398, 447.

(O) Combined Leading-Edge and Trailing-Edge Devices:
Refs. #263, 264, 266, 273, 274, 284, 297, 299, 300, 303, 304, 305, 308, 310, 320, 329, 347, 355, 394, 397, 398, 447.

(P) Boundary Layer Control:
Refs. #259, 306, 307, 313, 319, 321, 322, 324, 325, 328, 330, 334, 337, 338, 339, 342, 343, 352, 359, 362, 406, 422, 424, 425, 432.

(Q) Stall Control Devices:
Refs. #263, 299, 303, 304, 305, 318, 320, 324, 330, 331, 355, 397, 417, 447.

(R) Chord Extension:
Refs. #294, 315, 320, 327, 332, 333.

(S) Span Loading Methods:
Refs. #257, 258, 261, 272, 369, 390, 392, 400, 407, 419, 431, 436, 441.

5.3 AUTHOR INDEX
WITH CORRESPONDING REFERENCE NUMBERS

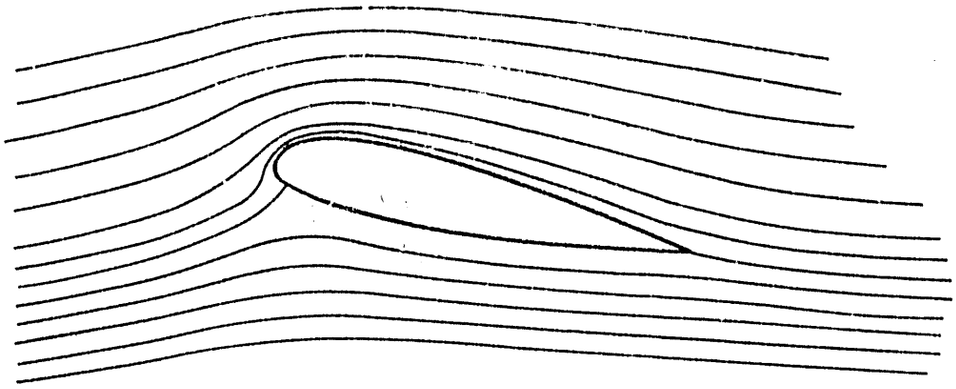

ELECTROLYTIC PLOTTING TANK DIAGRAM OF POTENTIAL FLOW ABOUT NACA 23015 PROFILE AT $\alpha = 12°$

FIG. 1

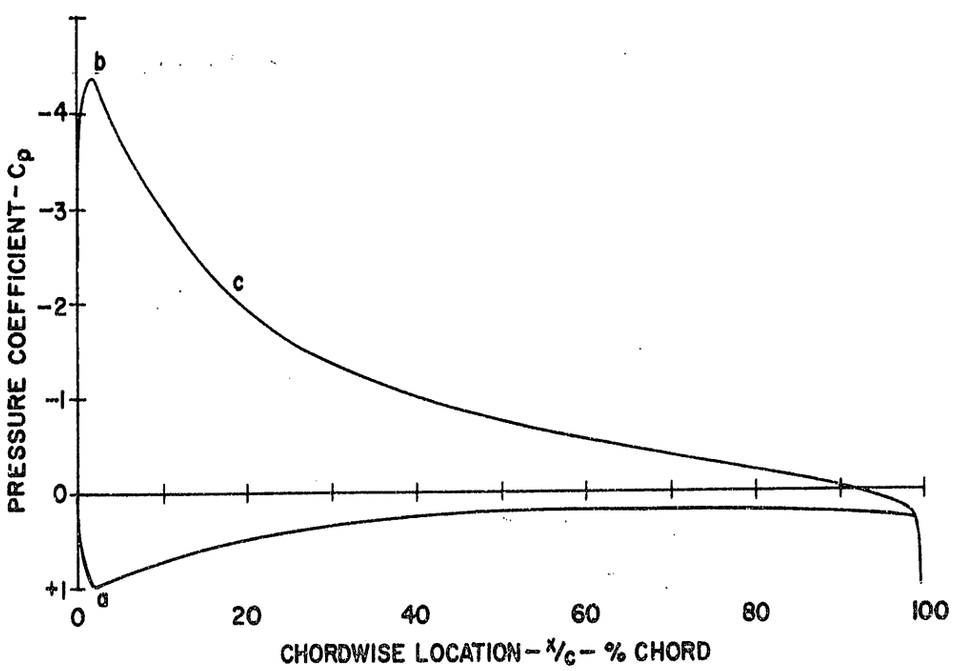

THEORETICAL PRESSURE DISTRIBUTION ABOUT NACA 23015 PROFILE AT $\alpha = 12°$

FIG. 2

THE DEVELOPMENT OF TRAILING-EDGE STALL ON AN NACA 23015

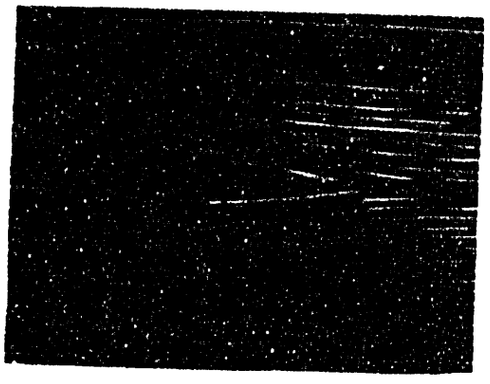

(a) $\alpha = 0°$

(b) $\alpha = 4°$

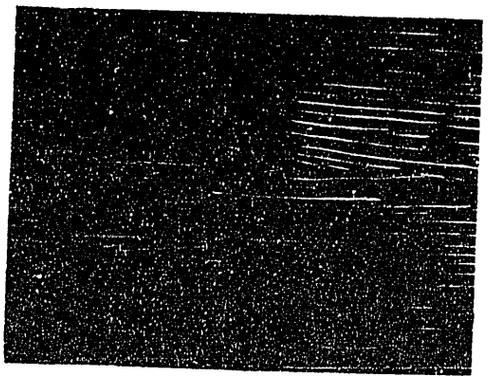

(c) $\alpha = 8°$

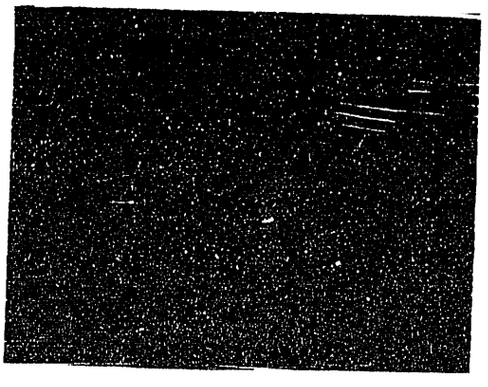

(d) $\alpha = 12°$

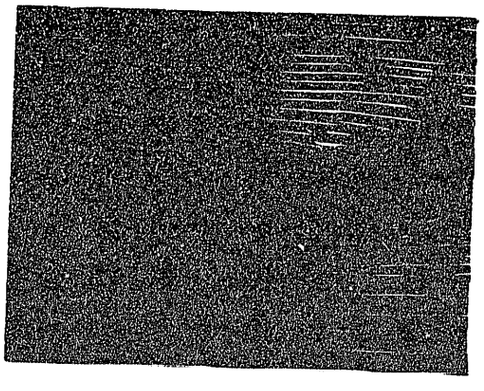

(e) $\alpha = 16°$

(f) $\alpha = 20°$

FIG. 3

LIFT, DRAG, & PITCHING MOMENT CHARACTERISTICS OF NACA 63-010

NOTE: DRAG COEFFICIENT SHOWN IS COEFF. OF PRESSURE DRAG ONLY

$R_N = 5.9 \times 10^6$

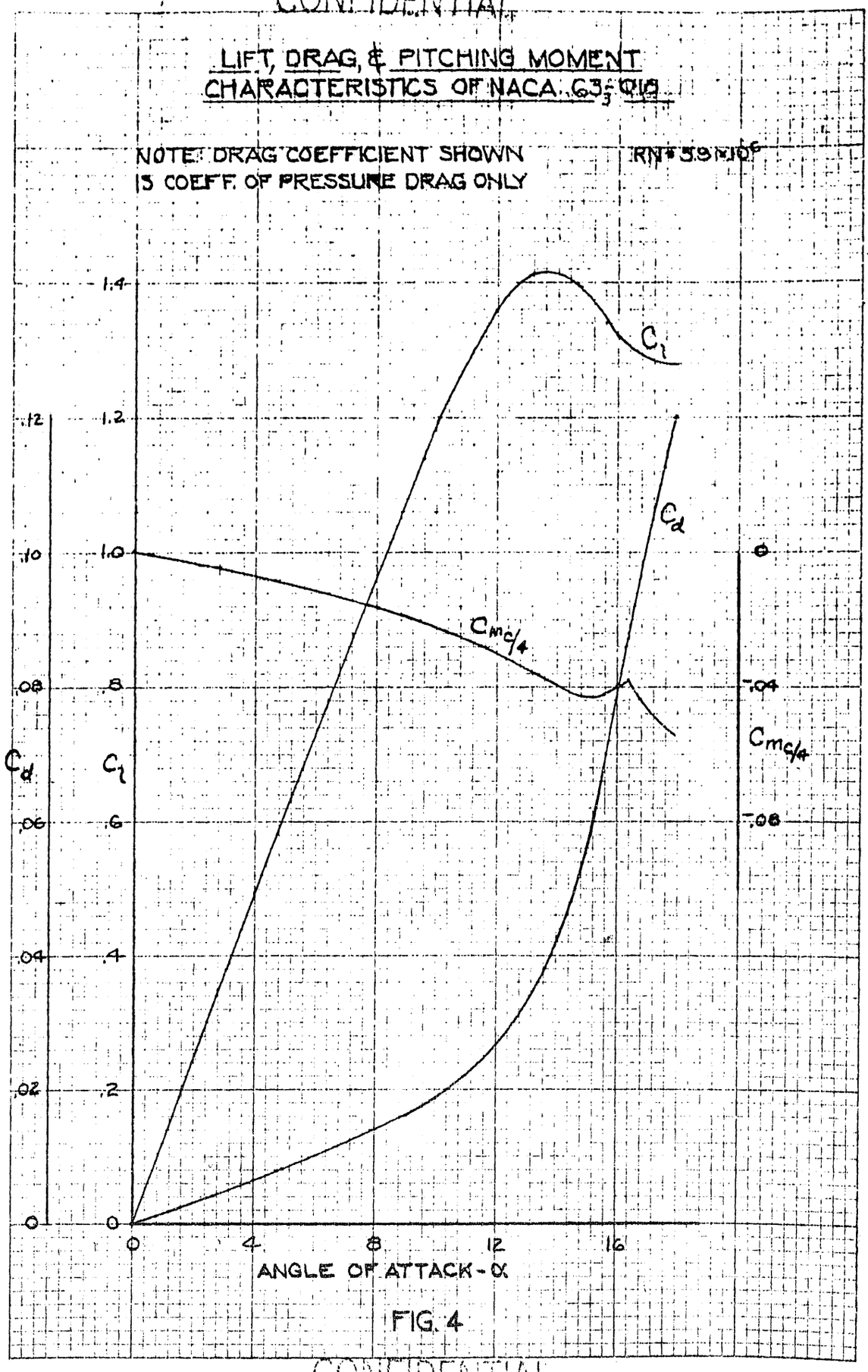

FIG. 4

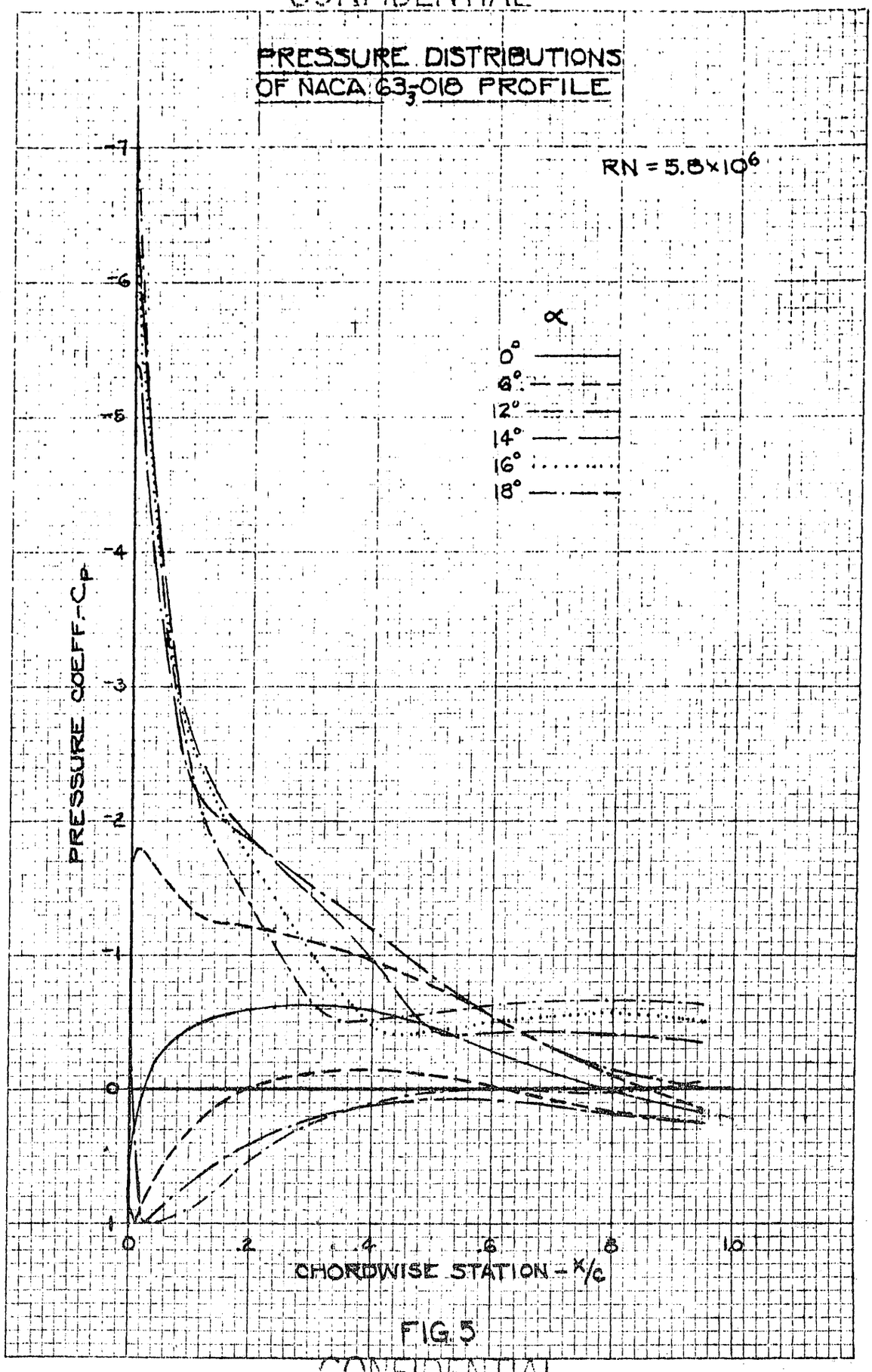

FIG. 5

DEVELOPMENT OF A LEADING-EDGE LAMINAR SEPARATION BUBBLE

FIG .6

BOUNDARY LAYER TRANSITION STUDIES

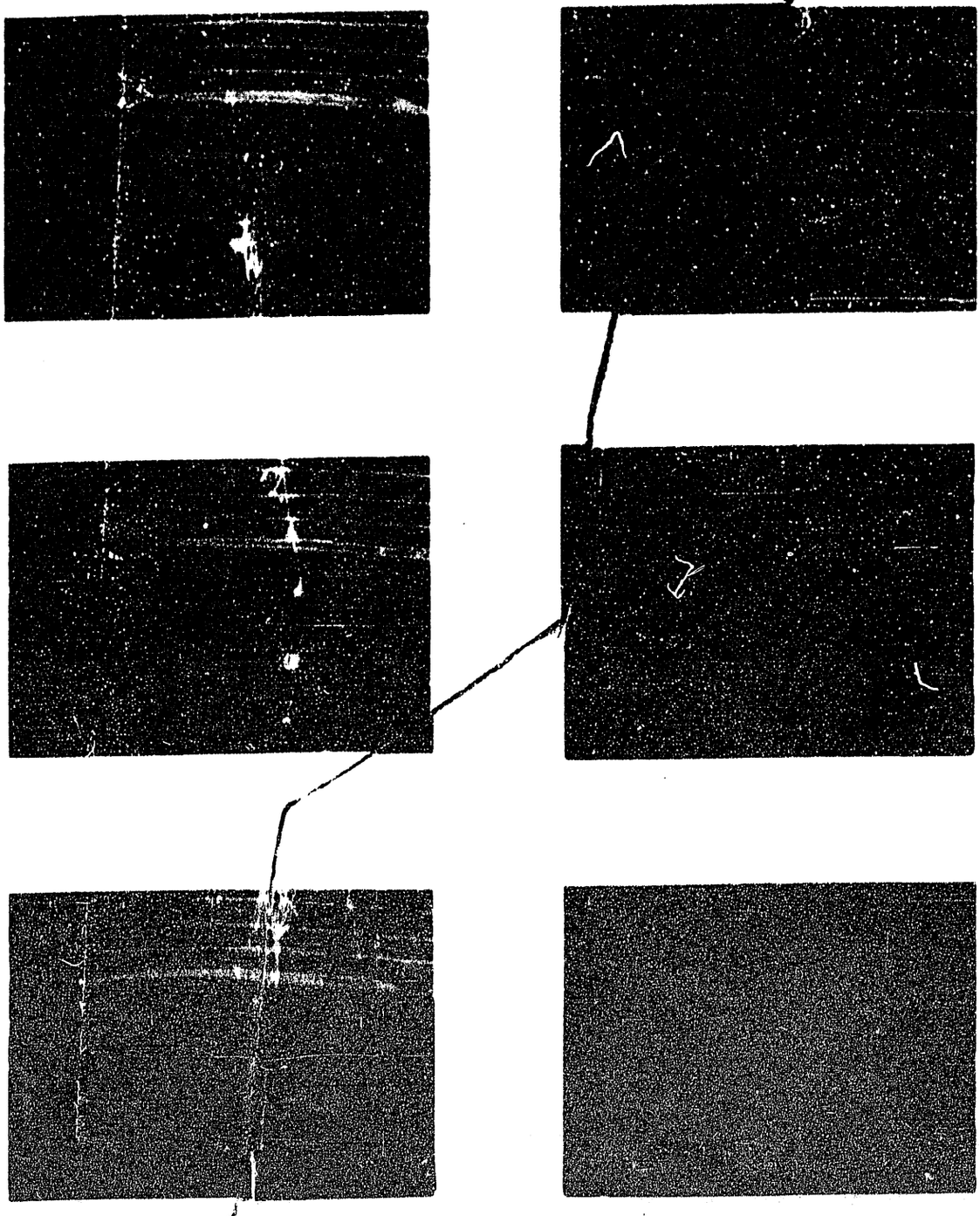

FREE STREAM SMOKE

SMOKE BLED FROM LEADING-EDGE

FIG. 7

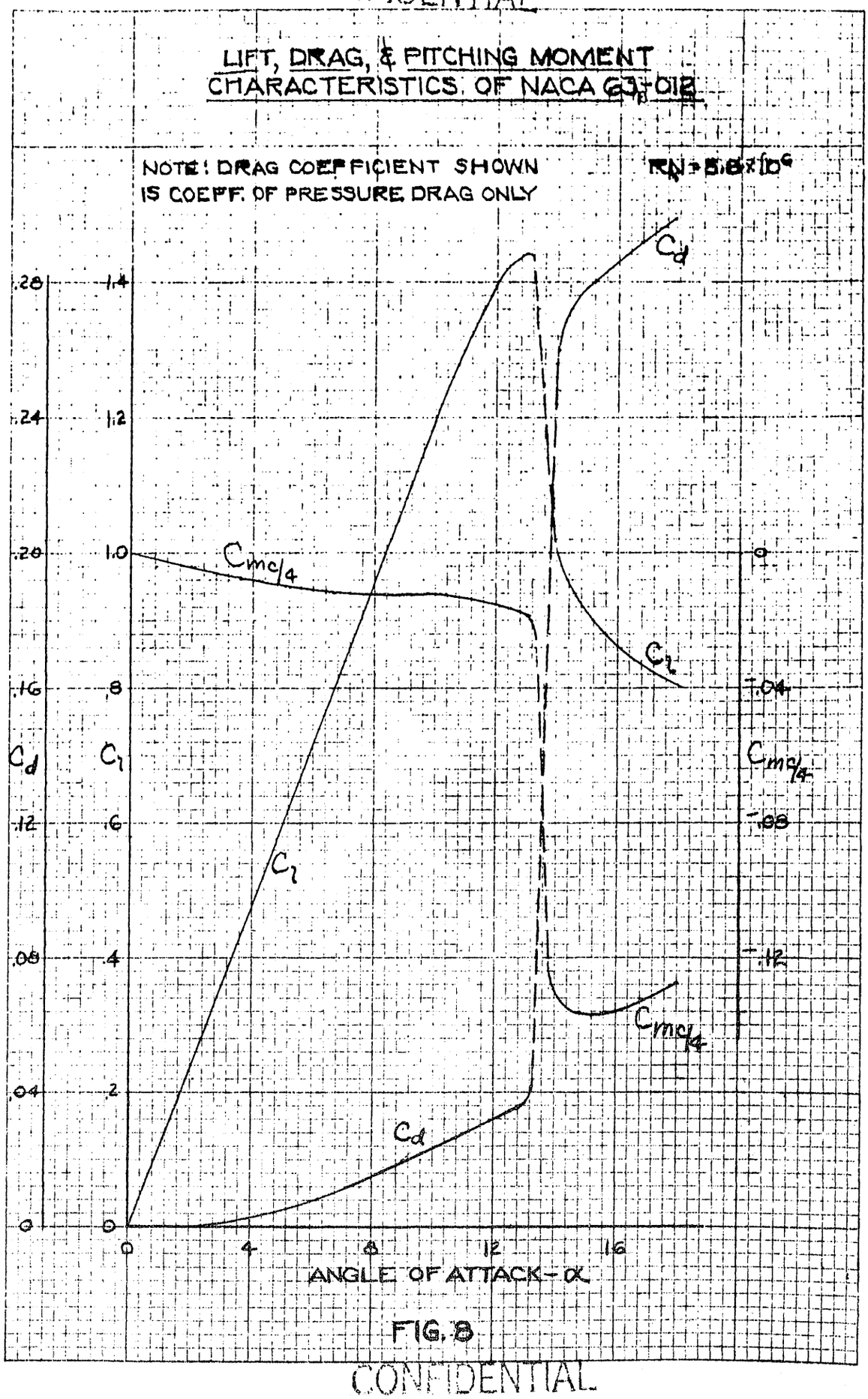

FIG. 8

STALL DEVELOPMENT ON AN NACA 64A006 PROFILE

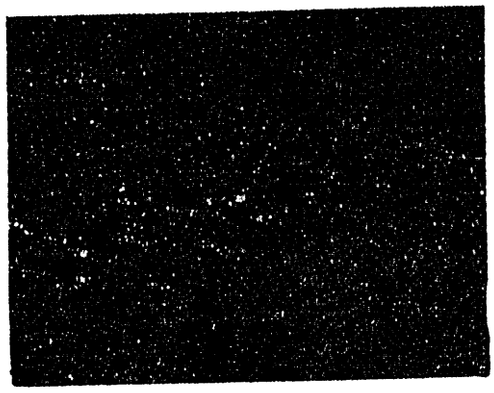

(a) $\alpha = 0°$

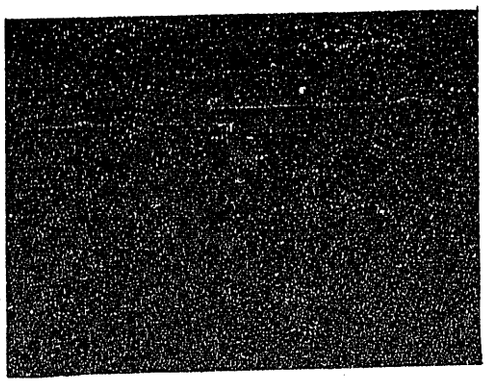

(b) $\alpha = 4°$

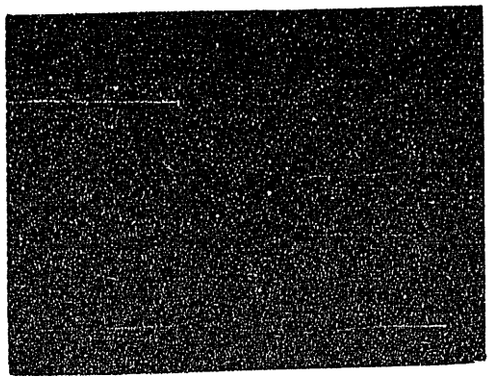

(c) $\alpha = 8°$

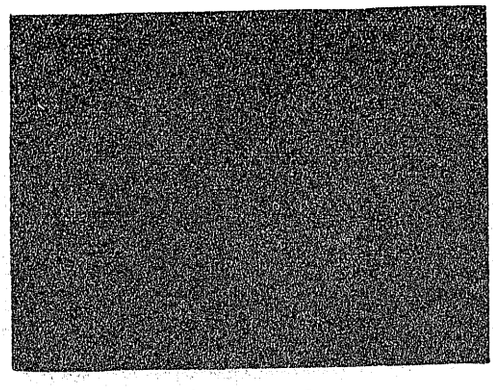

(d) $\alpha = 12°$

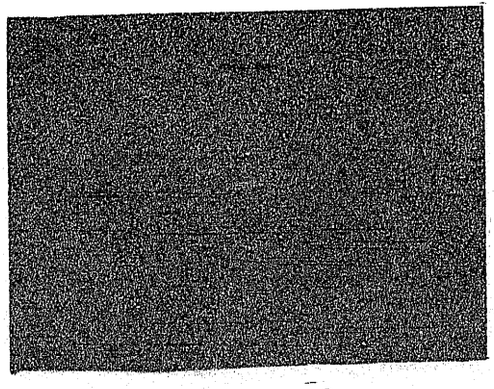

(e) $\alpha = 16°$

FIG. 9

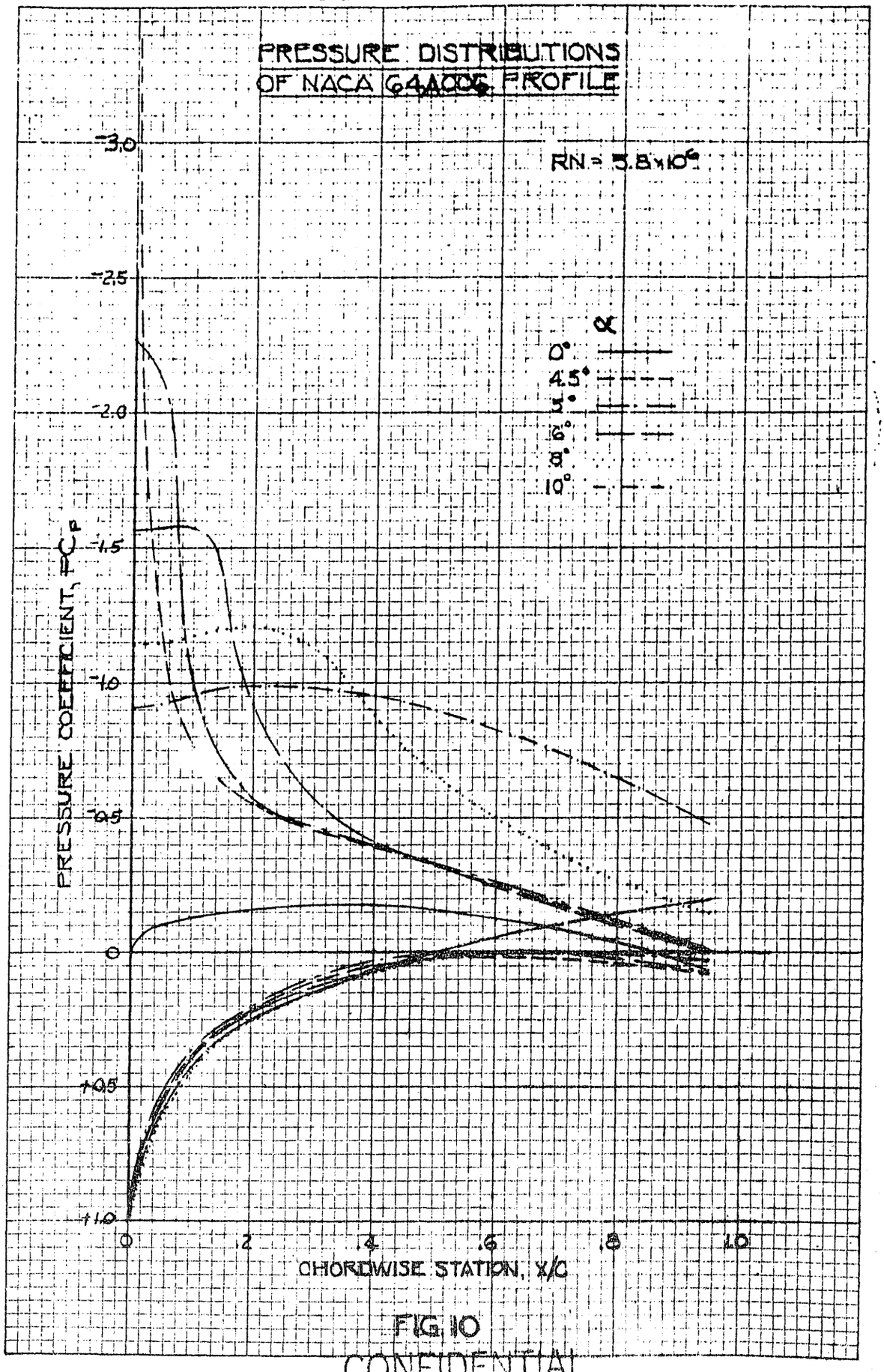

FIG. 10

CONFIDENTIAL

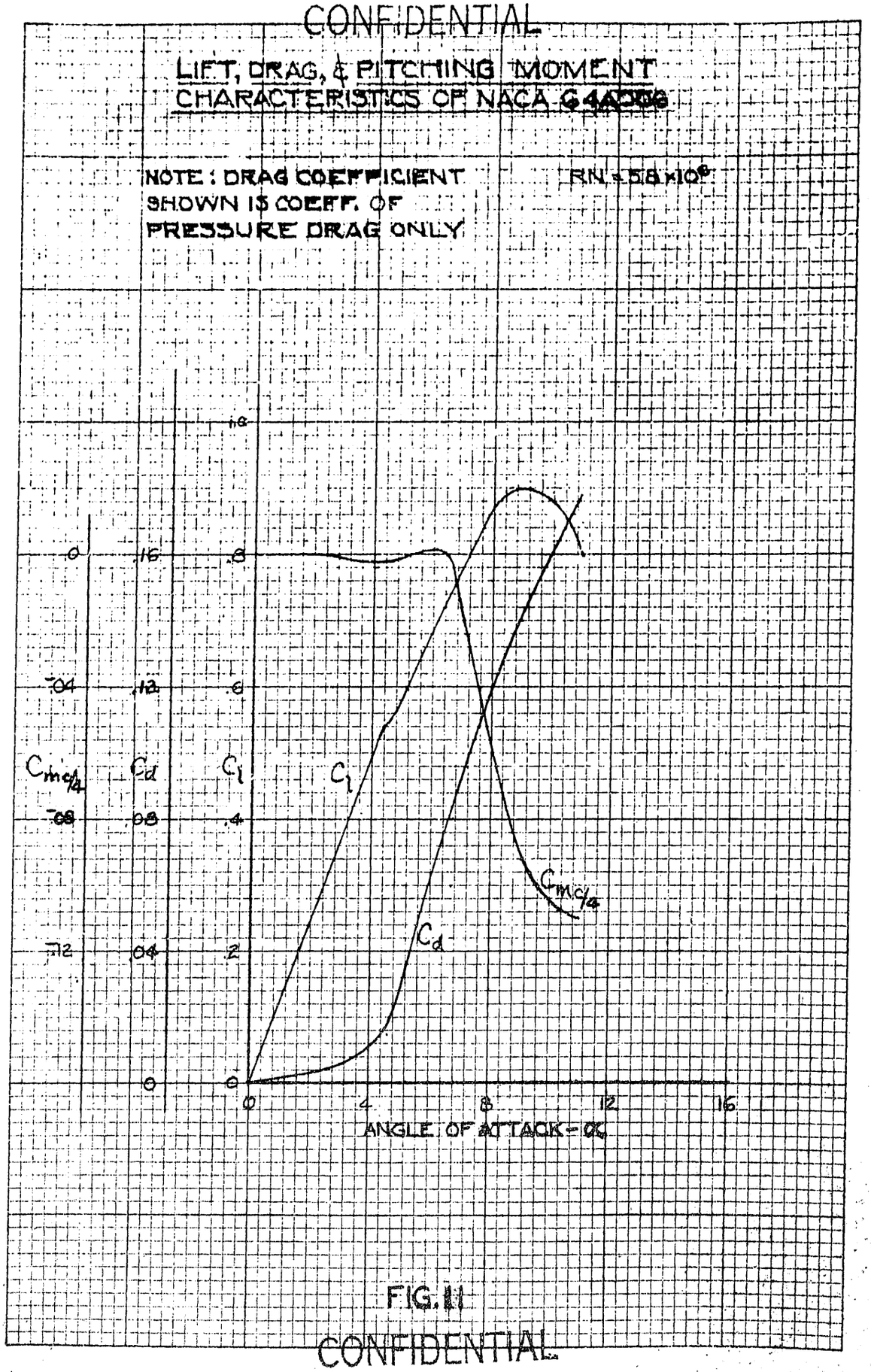

FIG. 11

CONFIDENTIAL

STALL DEVELOPMENT ON A DOUBLE-WEDGE PROFILE

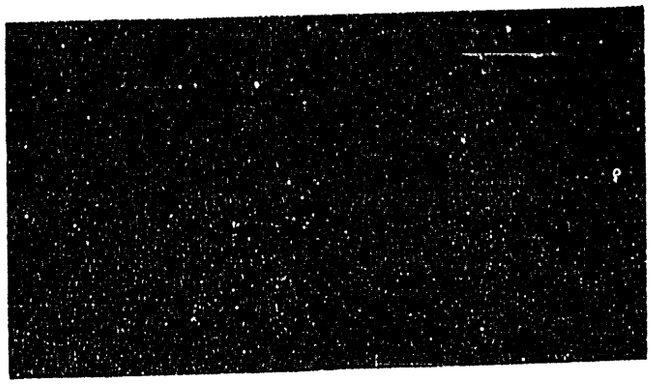

(a) $\alpha = 3°$

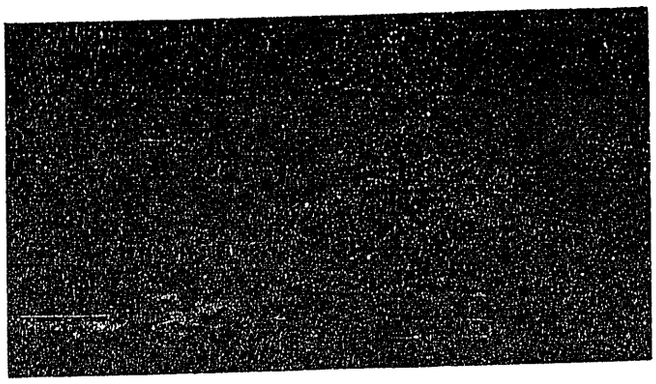

(b) $\alpha = 9°$

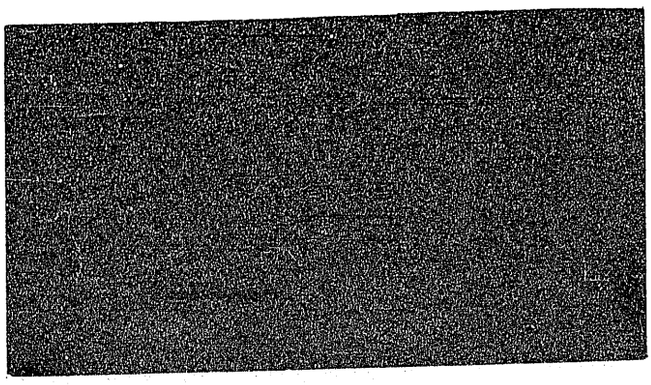

(c) $\alpha = 15°$

FIG. 12

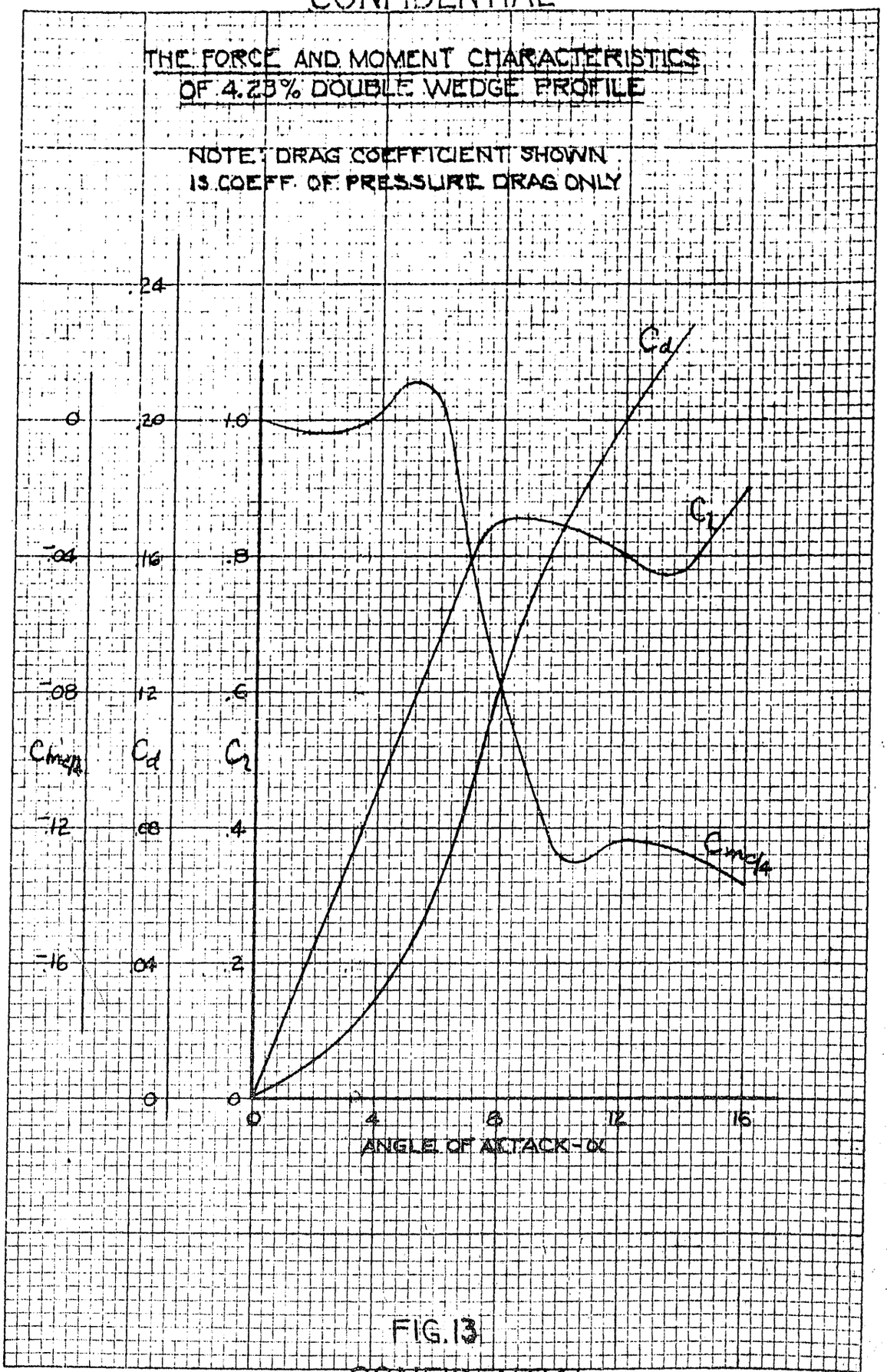

FIG. 13

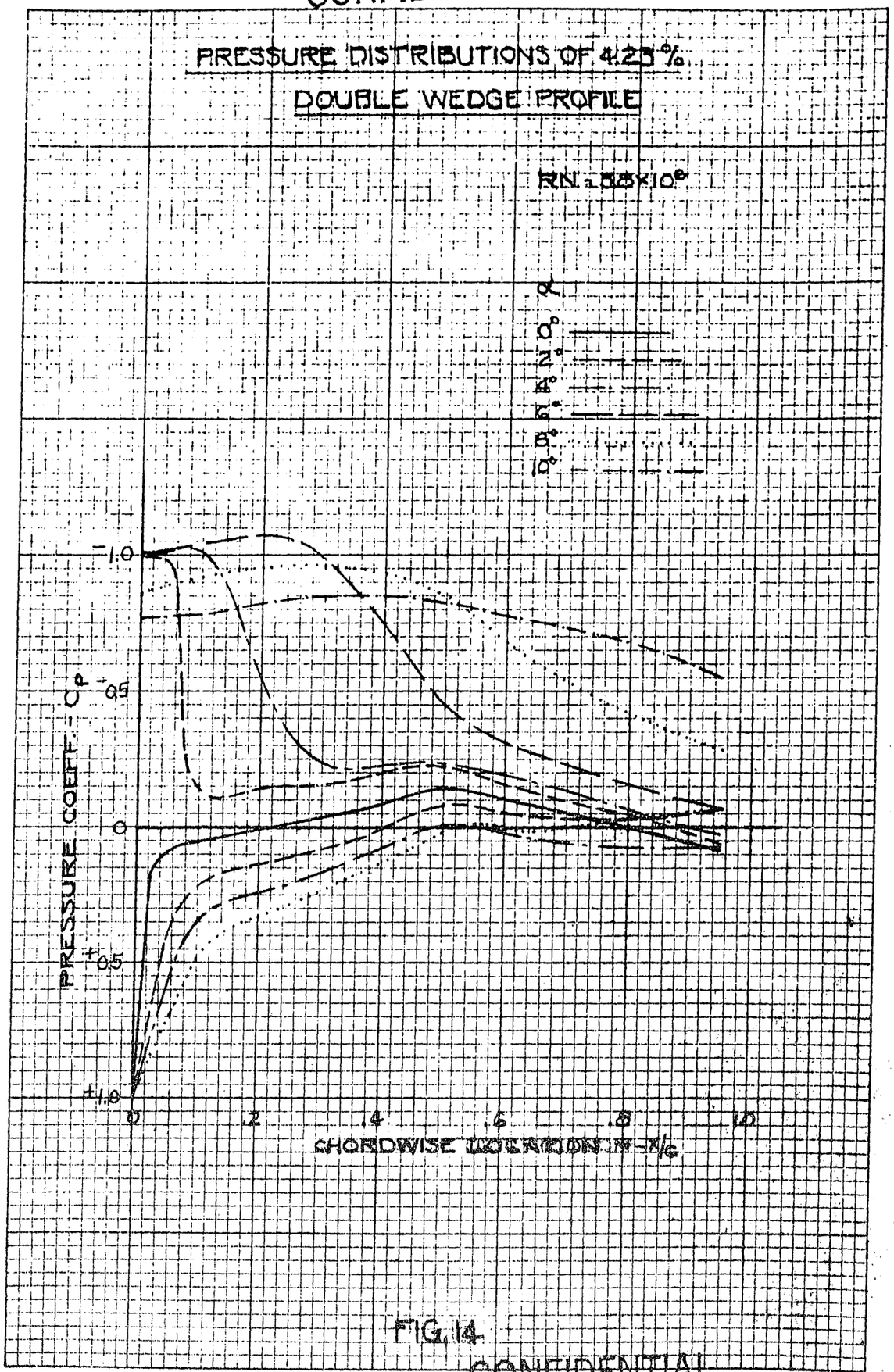

FIG. 14

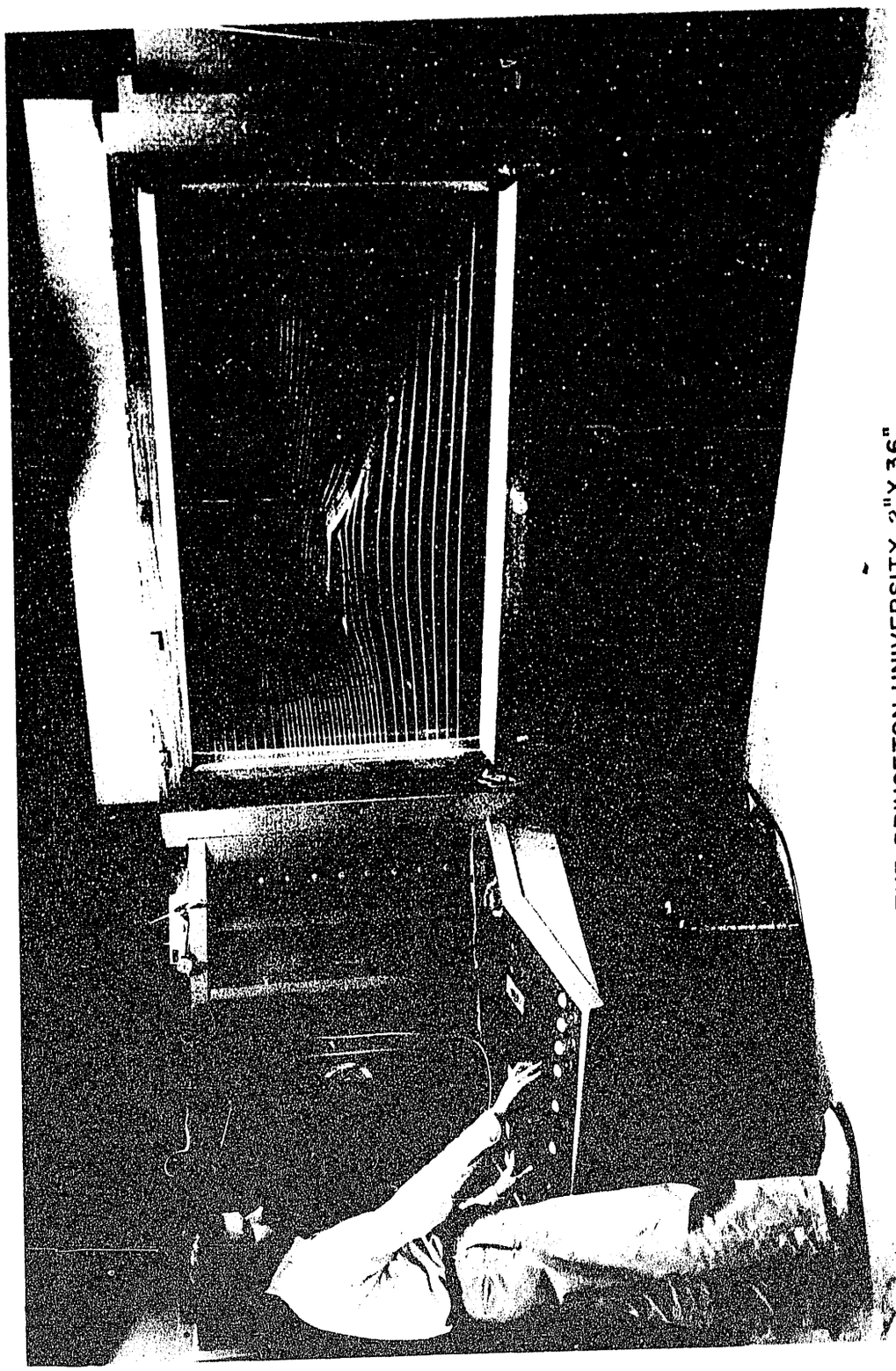

THE PRINCETON UNIVERSITY 2"X 36"
TWO-DIMENSIONAL SMOKE TUNNEL
FIGURE 15

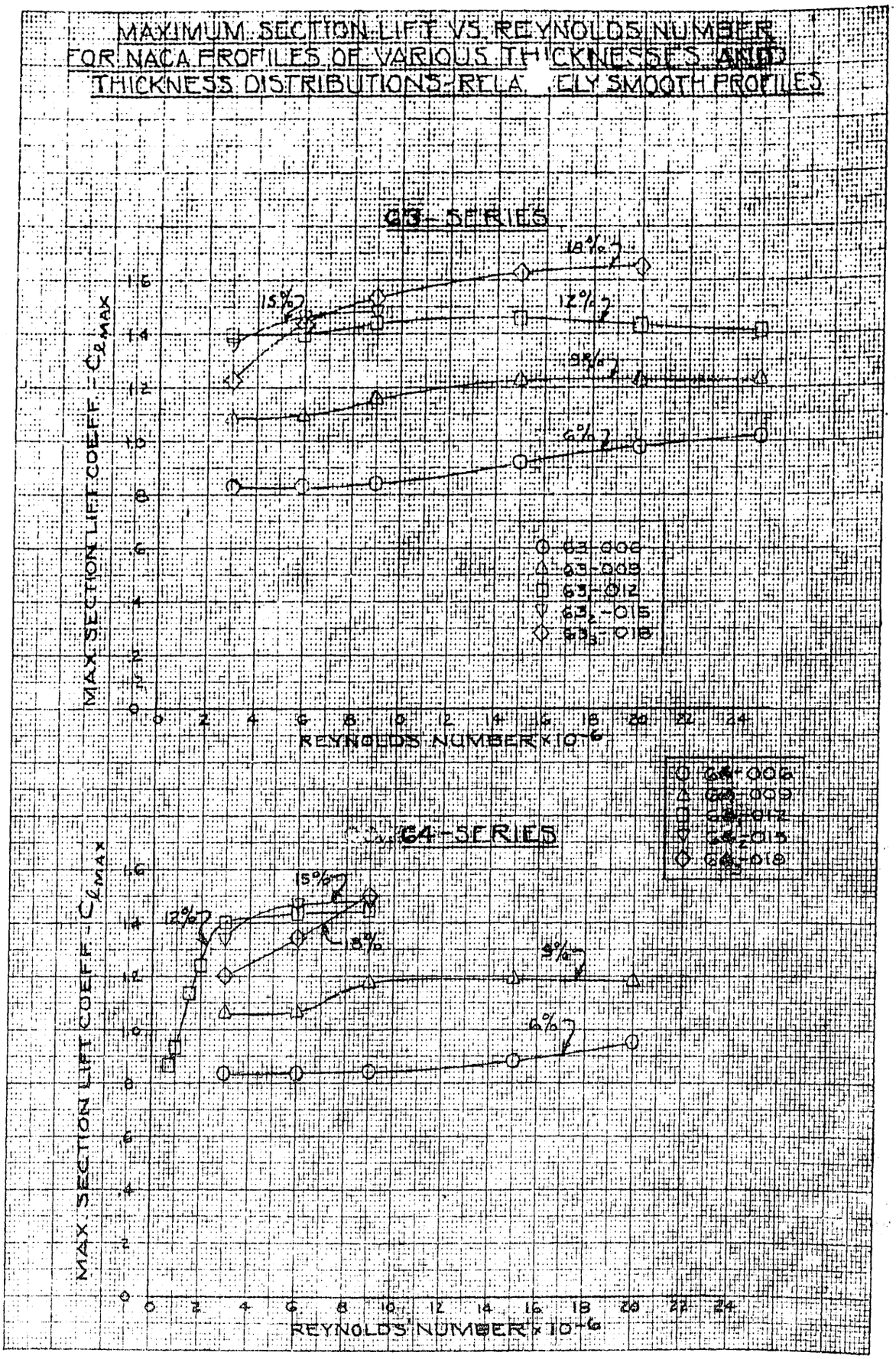
MAXIMUM SECTION LIFT VS. REYNOLDS NUMBER FOR NACA PROFILES OF VARIOUS THICKNESSES AND THICKNESS DISTRIBUTIONS - RELATIVELY SMOOTH PROFILES
63-SERIES
MAX. SECTION LIFT COEFF. - $C_{l\,MAX}$
REYNOLDS NUMBER × 10^{-6}
18%
15%
12%
9%
6%
63-006
63-009
63-012
63-015
63-018
64-SERIES
MAX. SECTION LIFT COEFF. - $C_{l\,MAX}$
REYNOLDS NUMBER × 10^{-6}
15%
12%
9%
6%
64-006
64-009
64-012
64-015
64-018

FIG. 16a

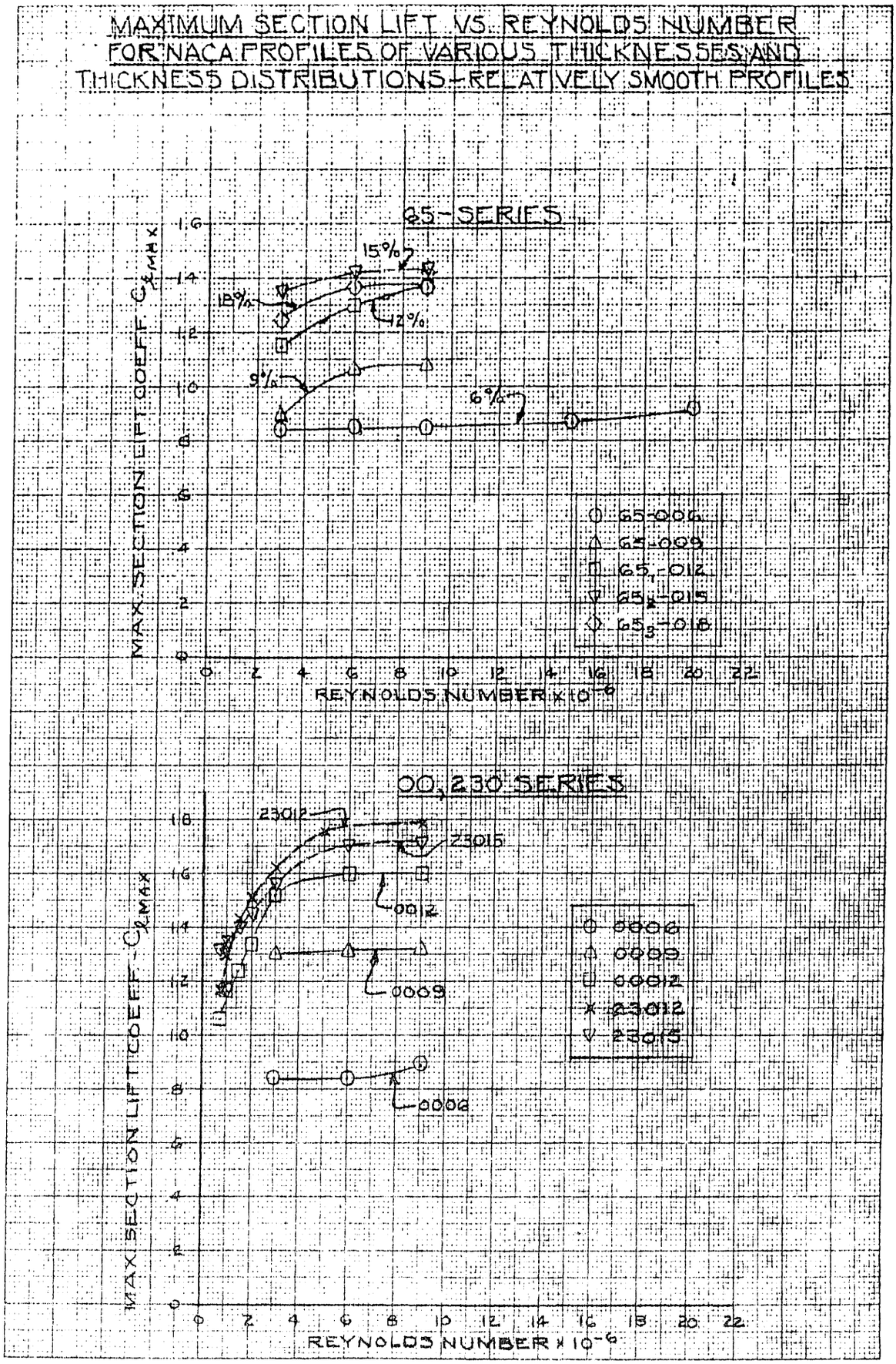
MAXIMUM SECTION LIFT VS. REYNOLDS NUMBER FOR NACA PROFILES OF VARIOUS THICKNESSES AND THICKNESS DISTRIBUTIONS - RELATIVELY SMOOTH PROFILES
65-SERIES
MAX. SECTION LIFT COEFF. $C_{l_{MAX}}$
REYNOLDS NUMBER x 10^{-6}
15%
18%
12%
9%
6%
65-006
65-009
65_1-012
65-015
65_3-018
00, 230 SERIES
MAX SECTION LIFT COEFF - $C_{l_{MAX}}$
REYNOLDS NUMBER x 10^{-6}
23012
23015
0012
0009
0006
0006
0009
00012
23012
23015

FIG. 16b

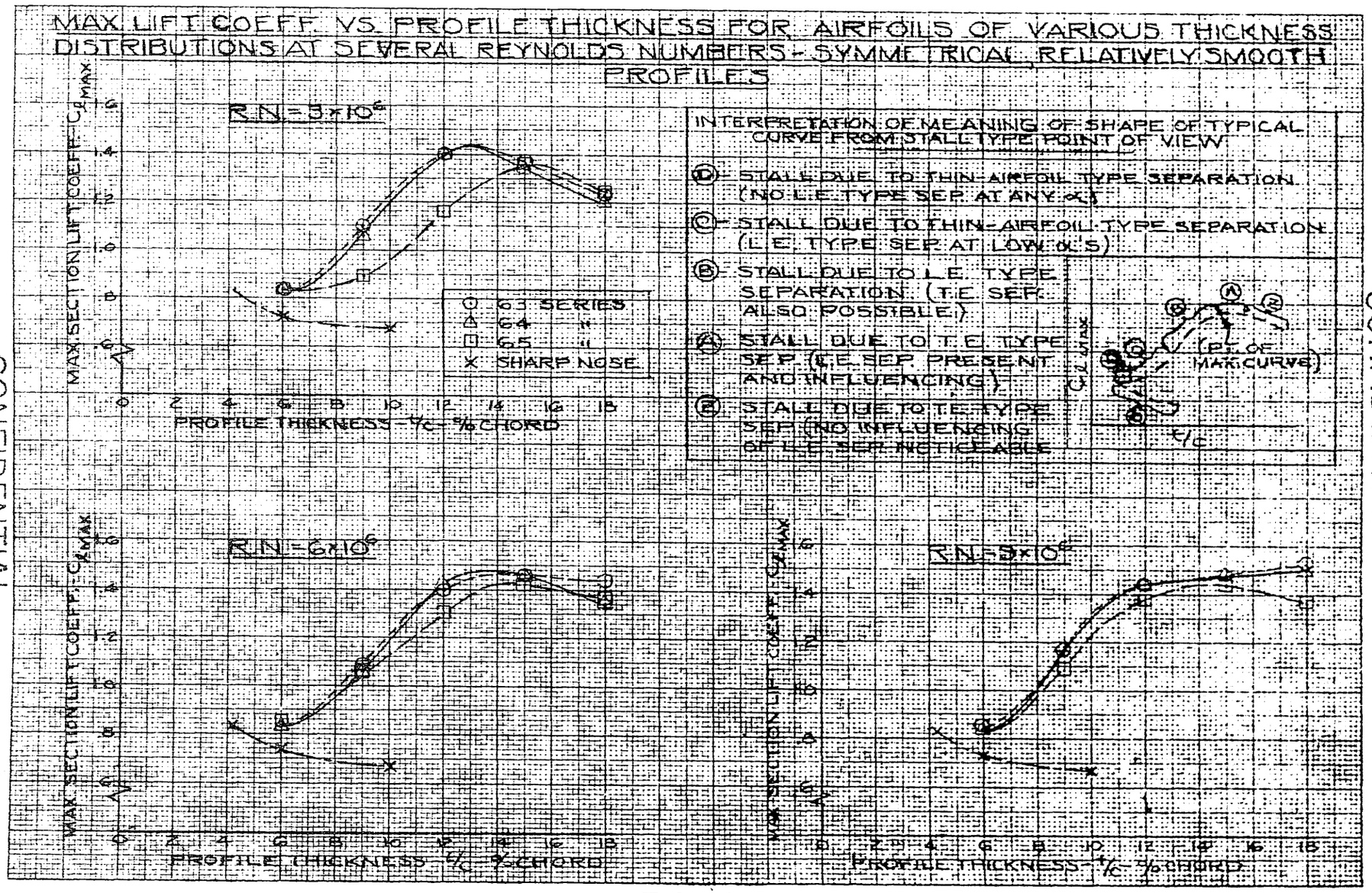

FIG. 17

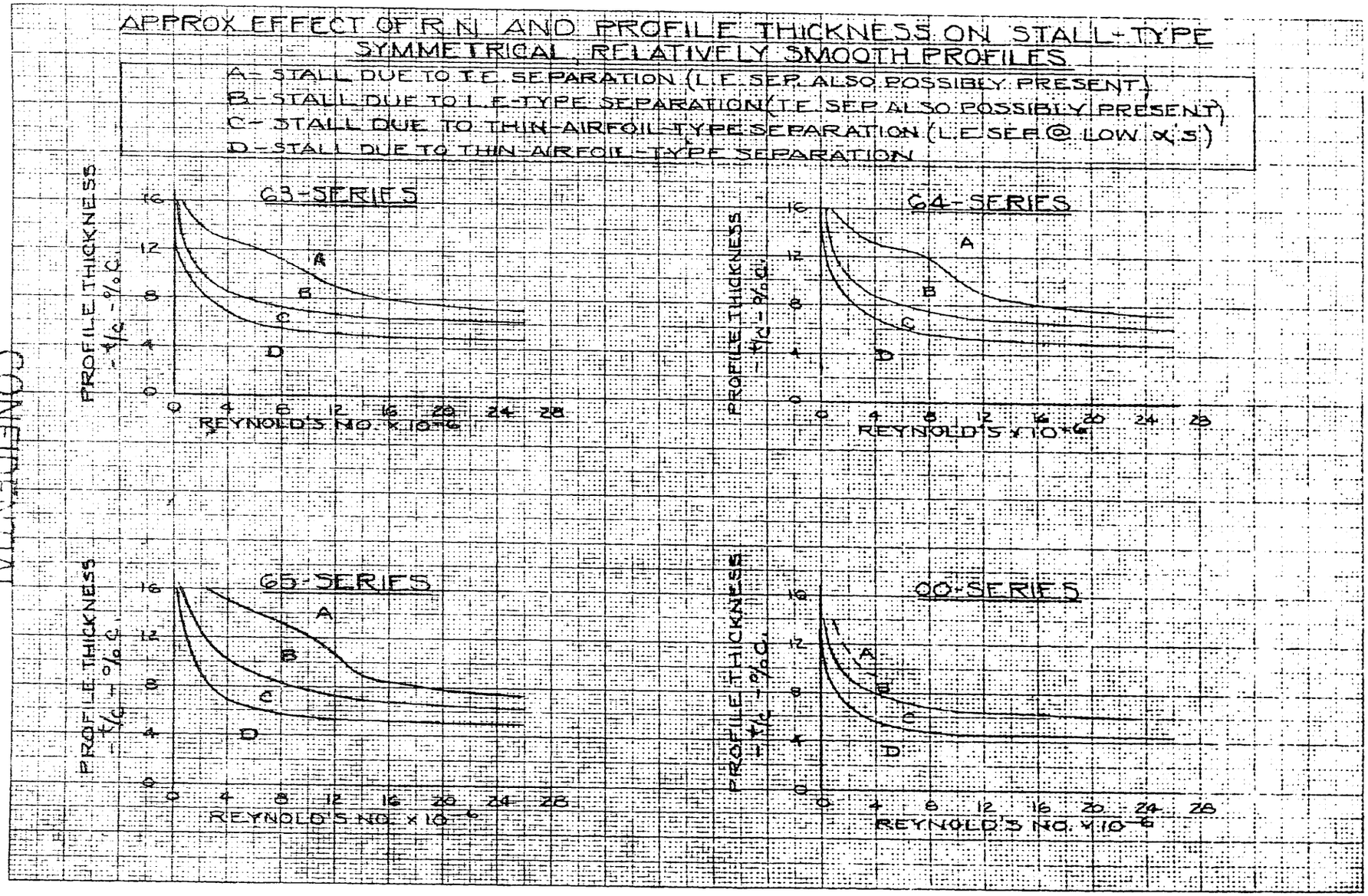

FIG. 18

MAX LIFT COEFF VS PROFILE THICKNESS FOR PROFILES OF VARIOUS DEGREES OF CAMBER AT SEVERAL REYNOLDS NUMBERS - RELATIVELY SMOOTH PROFILES

64 SERIES

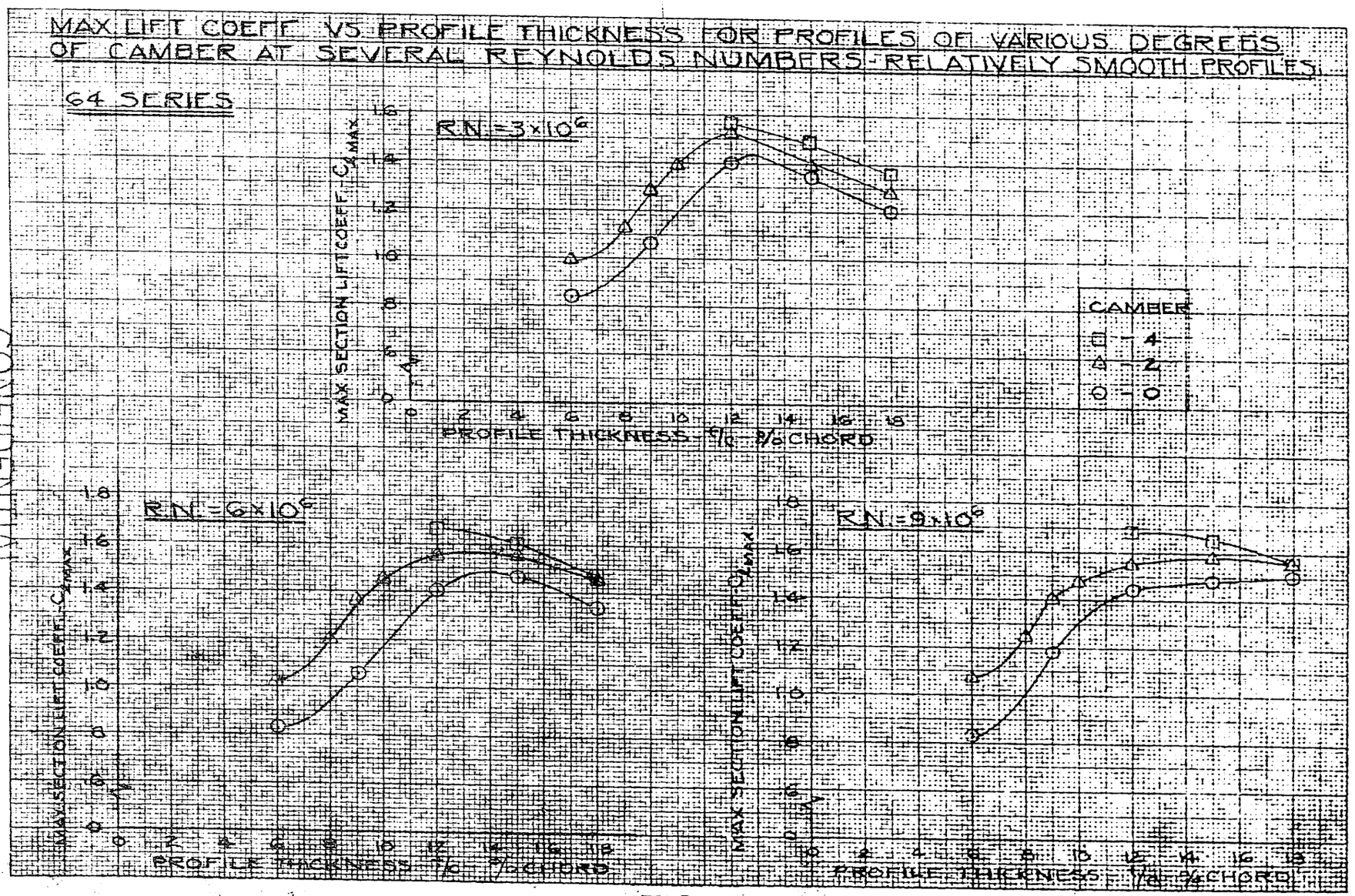

FIG. 19

APPEARANCE OF PROFILE LIFT CURVES AS INFLUENCED BY EITHER A PURE LEADING-EDGE OR A PURE TRAILING-EDGE CONTROL - NO CIRCULATION CONTROL

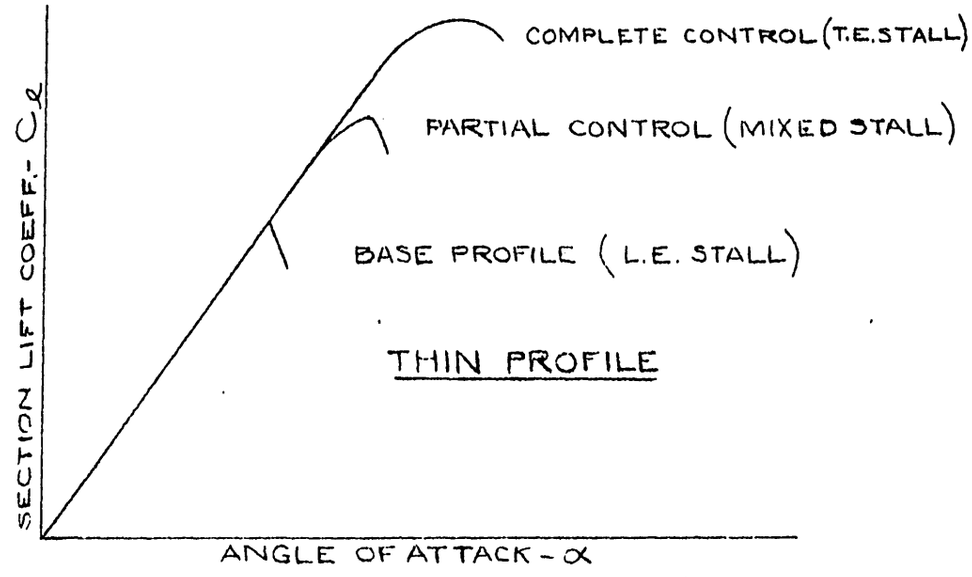

(A) LEADING-EDGE B.L.C.

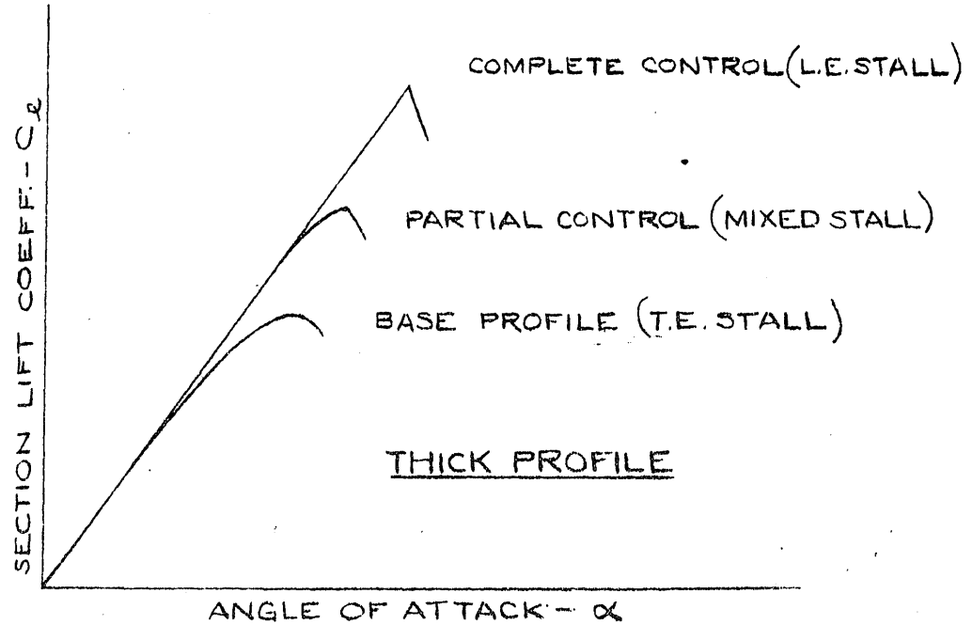

(B) TRAILING-EDGE B.L.C.

FIG. 20

DEMONSTRATION OF THE POSSIBLE SIGNIFICANCE OF THE EMPIRICAL STALL STUDIES

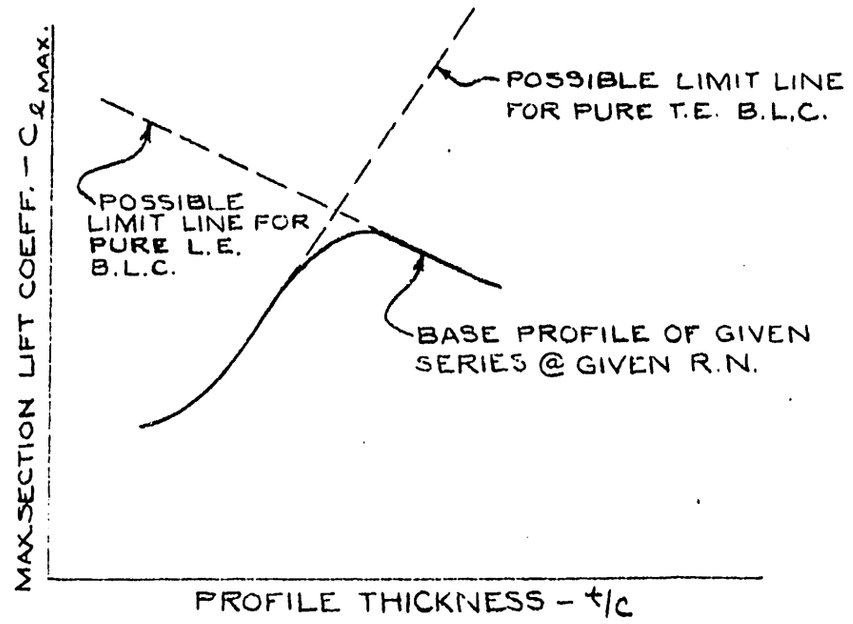

(A) LINEAR EXTRAPOLATION METHOD

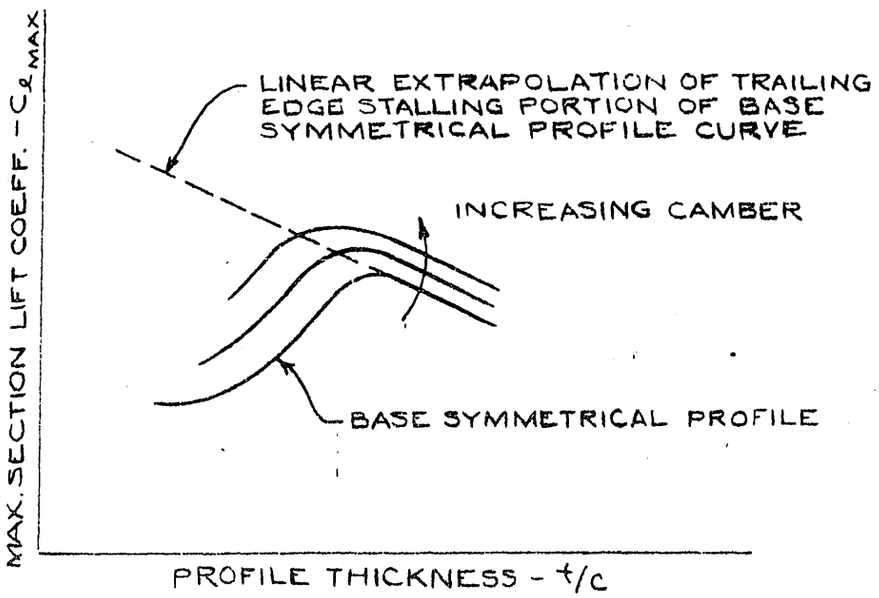

(B) EFFECT OF FORWARD CAMBER

FIG. 21

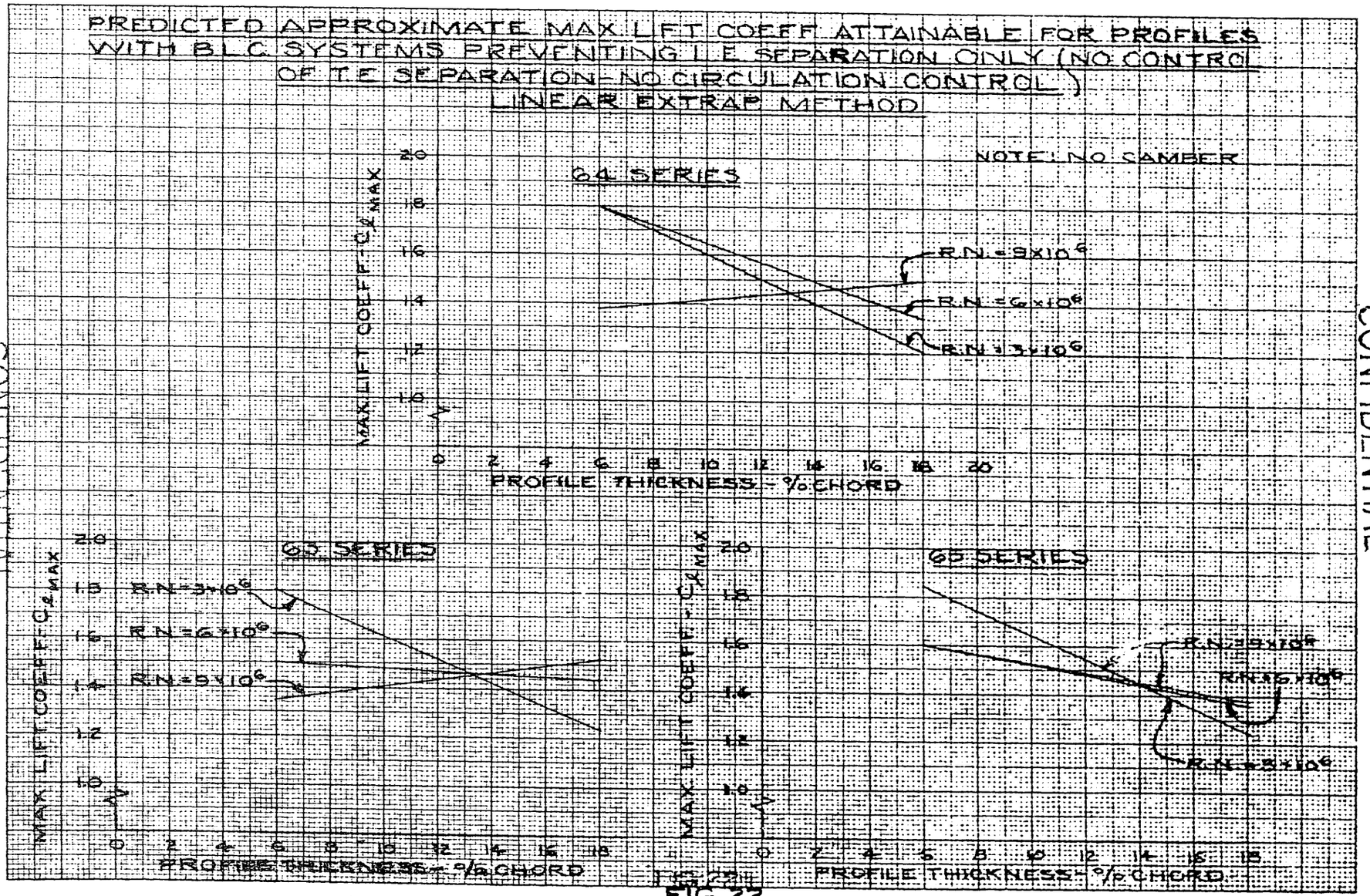

FIG. 22

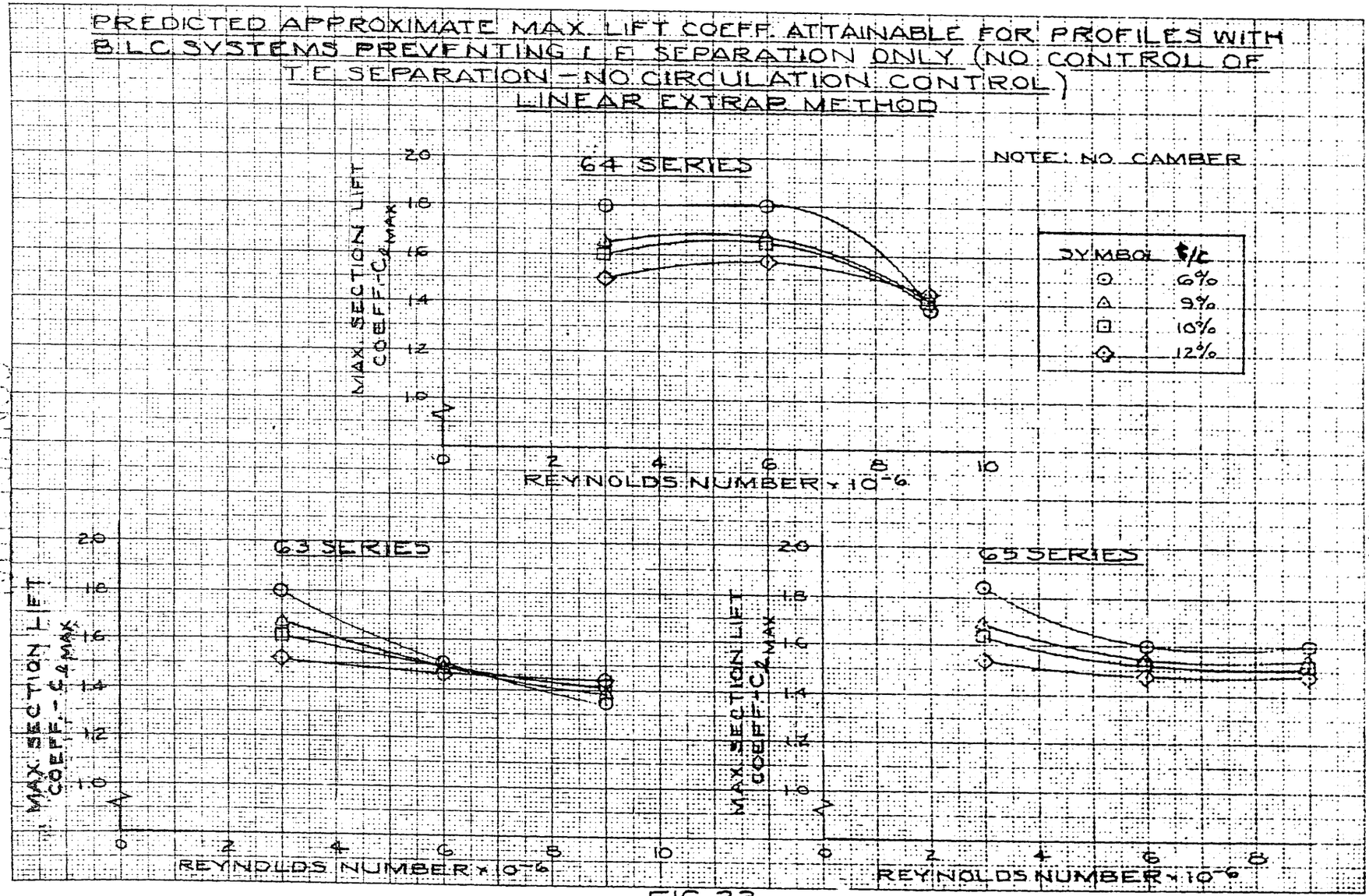
PREDICTED APPROXIMATE MAX. LIFT COEFF. ATTAINABLE FOR PROFILES WITH B.L.C. SYSTEMS PREVENTING L.E. SEPARATION ONLY (NO CONTROL OF T.E. SEPARATION – NO CIRCULATION CONTROL)
LINEAR EXTRAP METHOD
64 SERIES
NOTE: NO CAMBER
SYMBOL t/c
6%
9%
10%
12%
MAX. SECTION LIFT COEFF. - $C_{l_{MAX}}$
REYNOLDS NUMBER x 10^{-6}
63 SERIES
65 SERIES
CONFIDENTIAL

FIG. 23

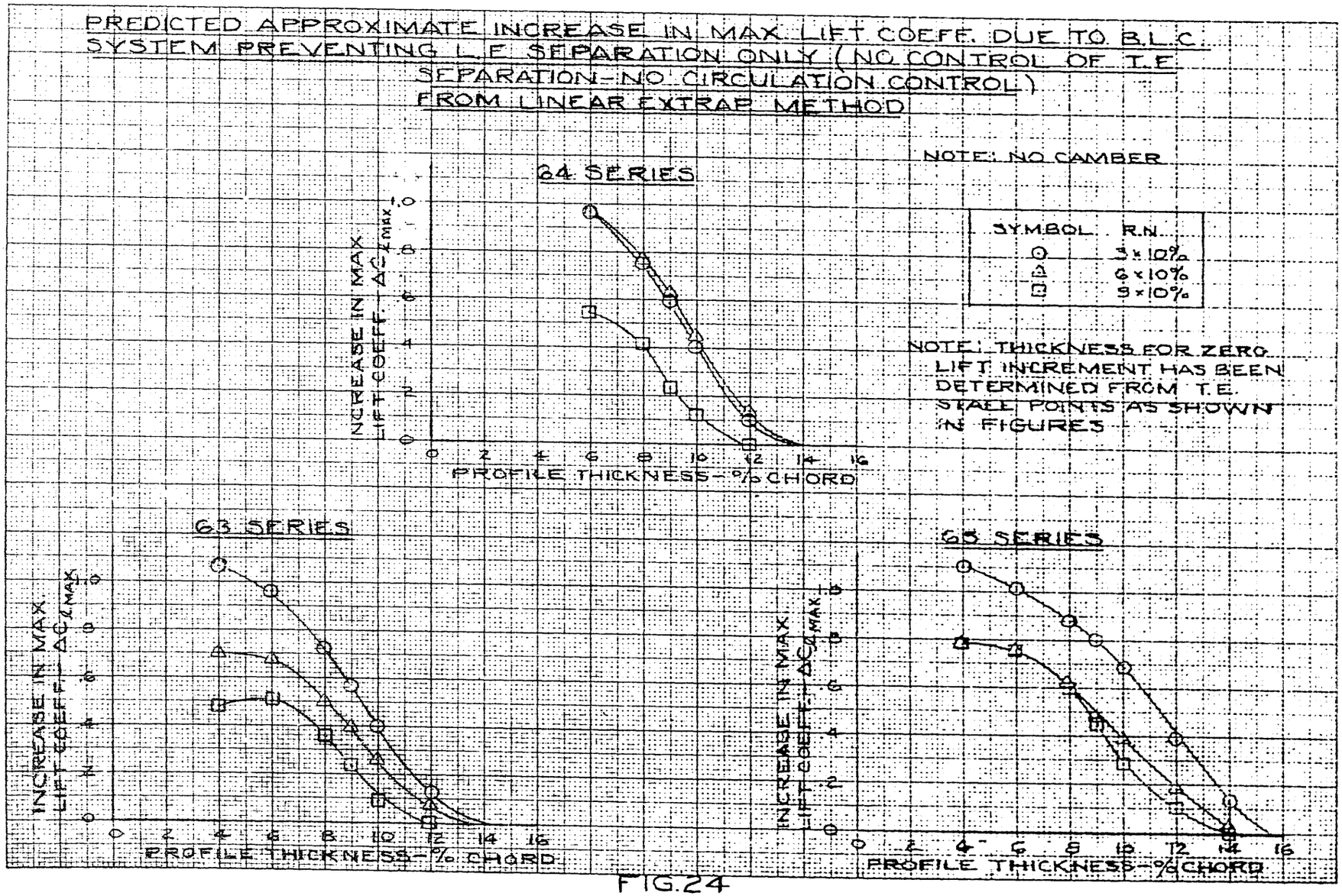

FIG. 24

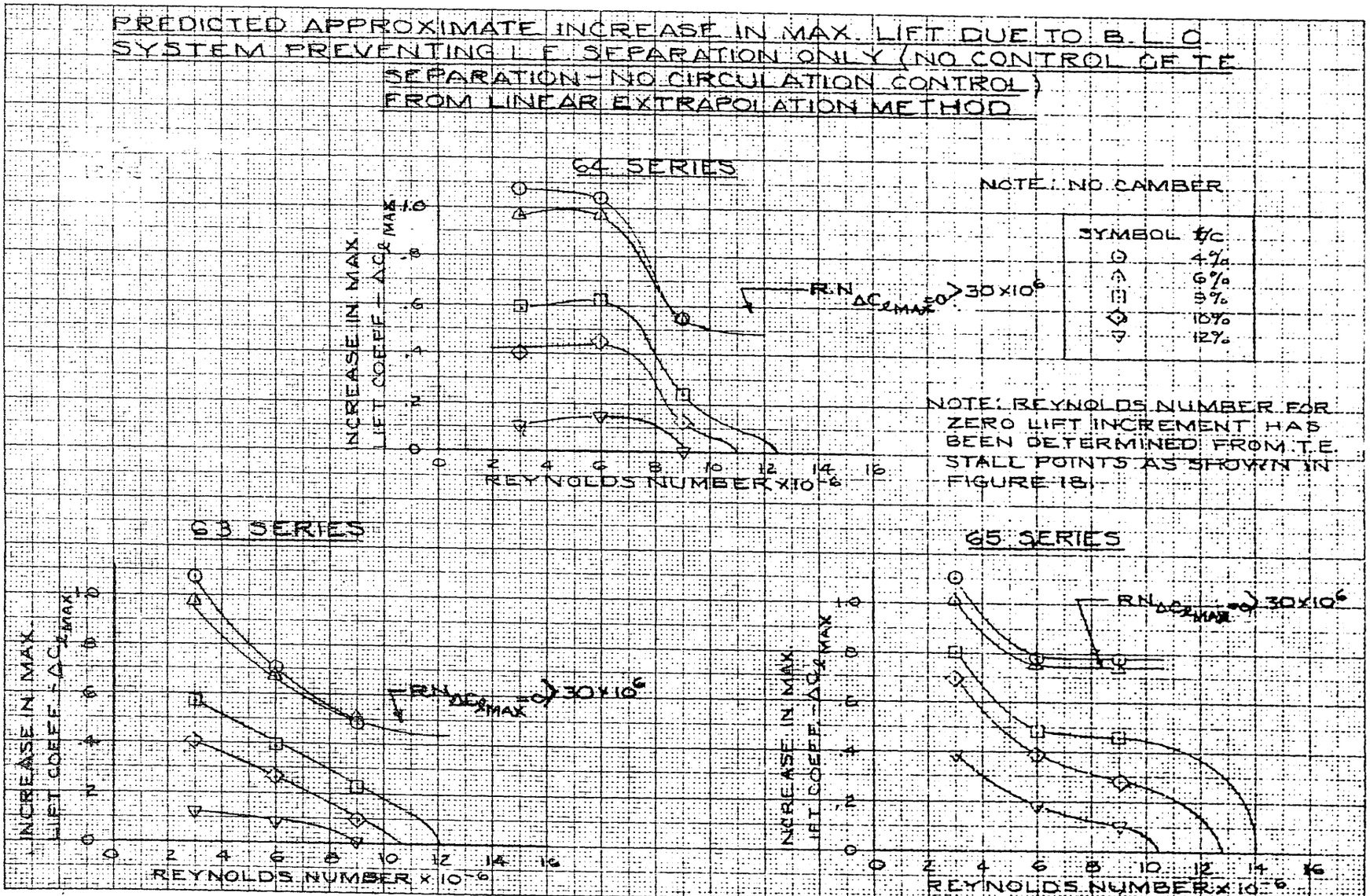

FIG. 25

CIRCULATION AS ATTAINED THROUGH ROTATING CYLINDER

(A) NO ROTATION

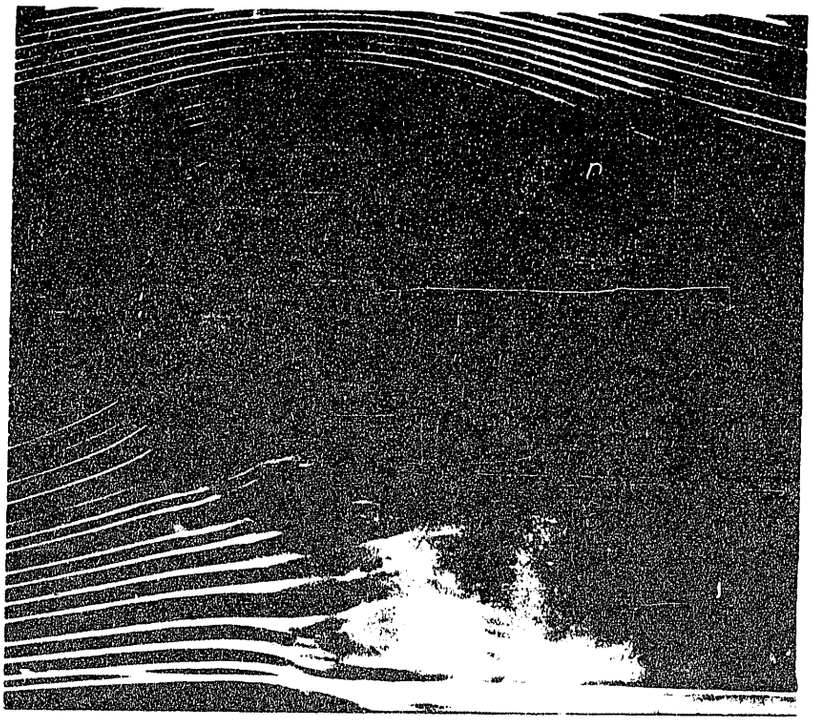

(B) ROTATING CLOCKWISE

FIG. 26

MAJOR TYPES OF TRAILING-EDGE FLAPS

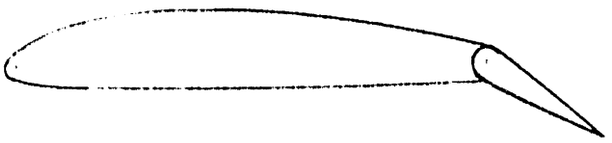

(a) PLAIN FLAP

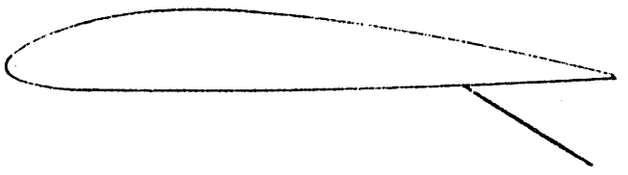

(b) SPLIT FLAP

(c) SINGLE SLOTTED FLAP

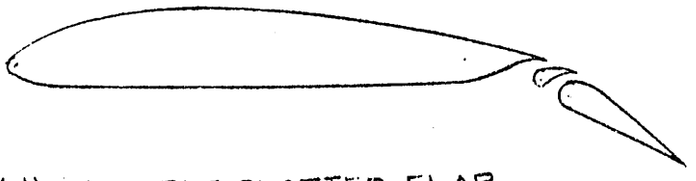

(d) DOUBLE SLOTTED FLAP

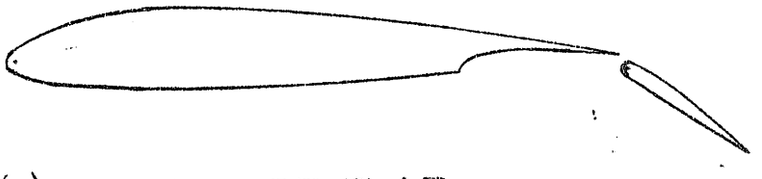

(e) FOWLER FLAP

FIG. 27

FLOW PATTERNS ABOUT PROFILES WITH TRAILING-EDGE FLAPS

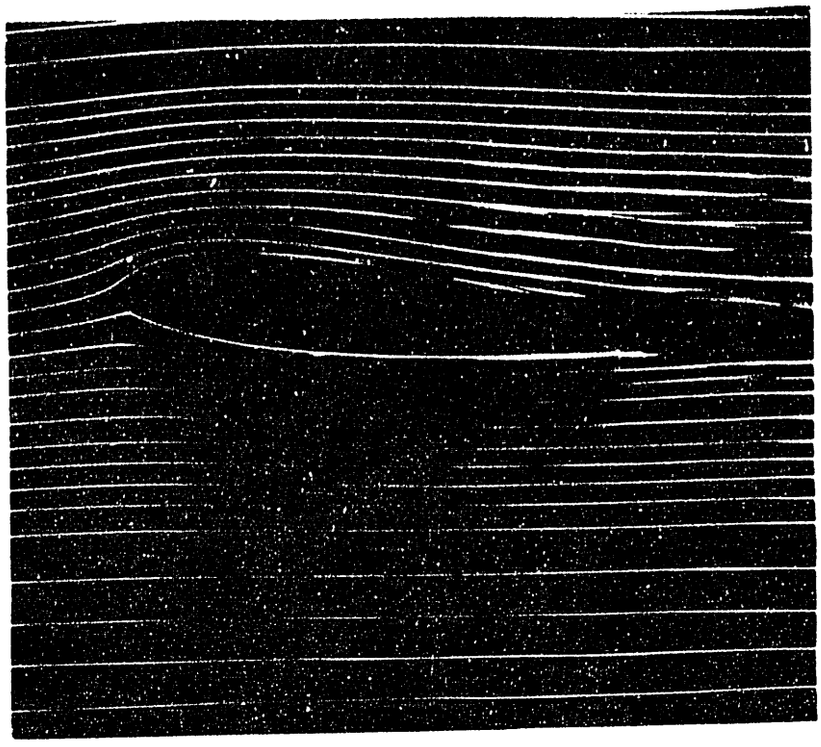

(A) BASE PROFILE

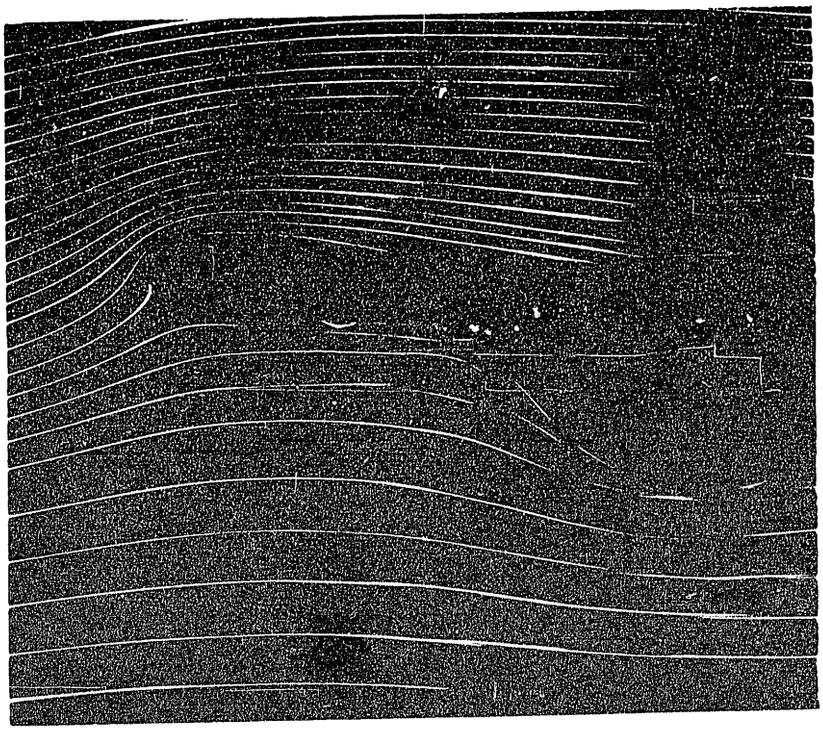

(B) PLAIN FLAP

FIG. 28

FLOW PATTERNS ABOUT PROFILES WITH TRAILING-EDGE FLAPS

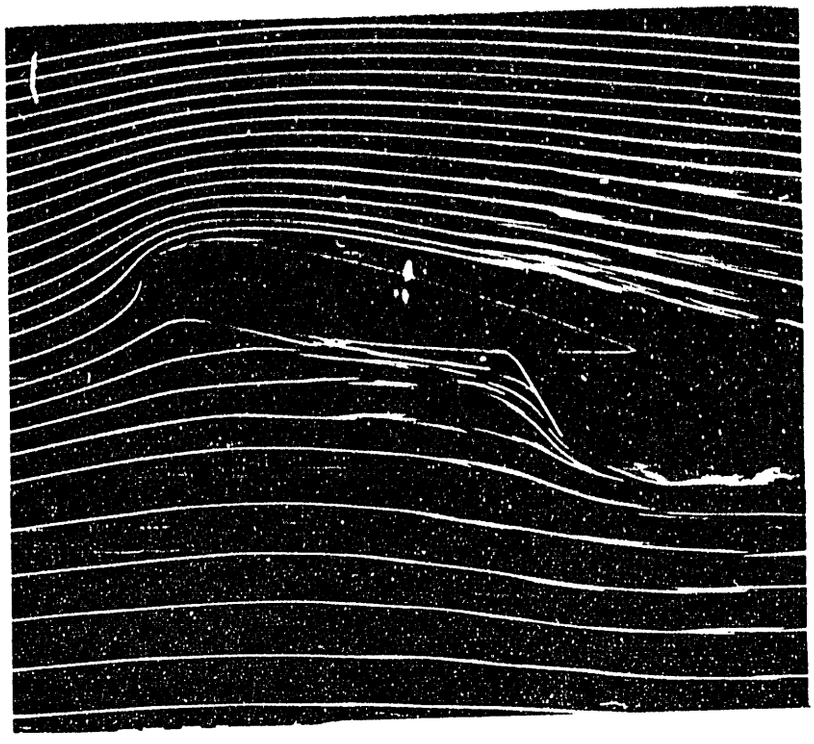

(C) SPLIT FLAP

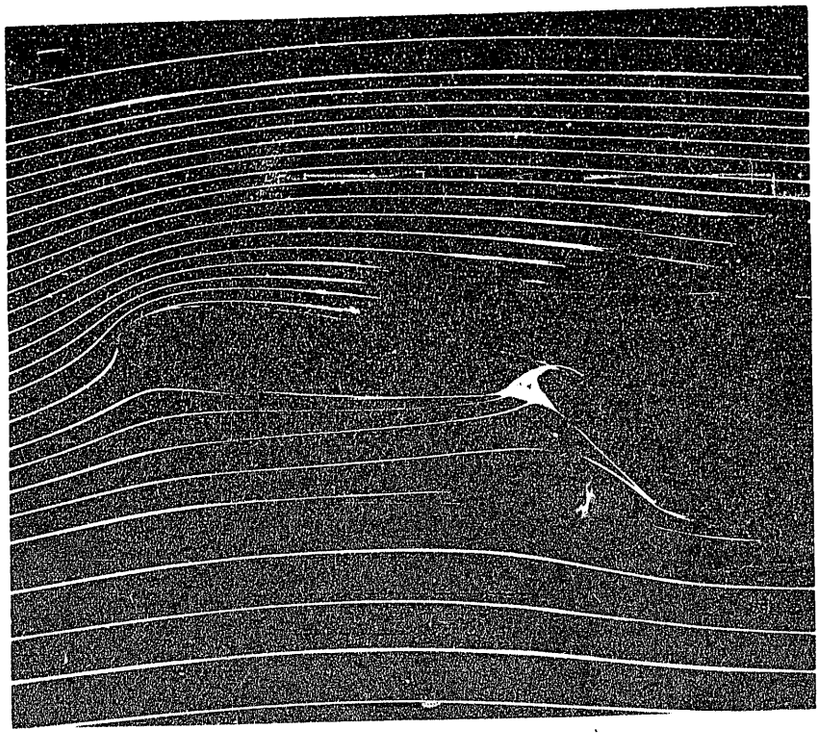

(D) SLOTTED FLAP

FIG. 28

FLOW PATTERNS ABOUT PROFILES WITH TRAILING-EDGE FLAPS

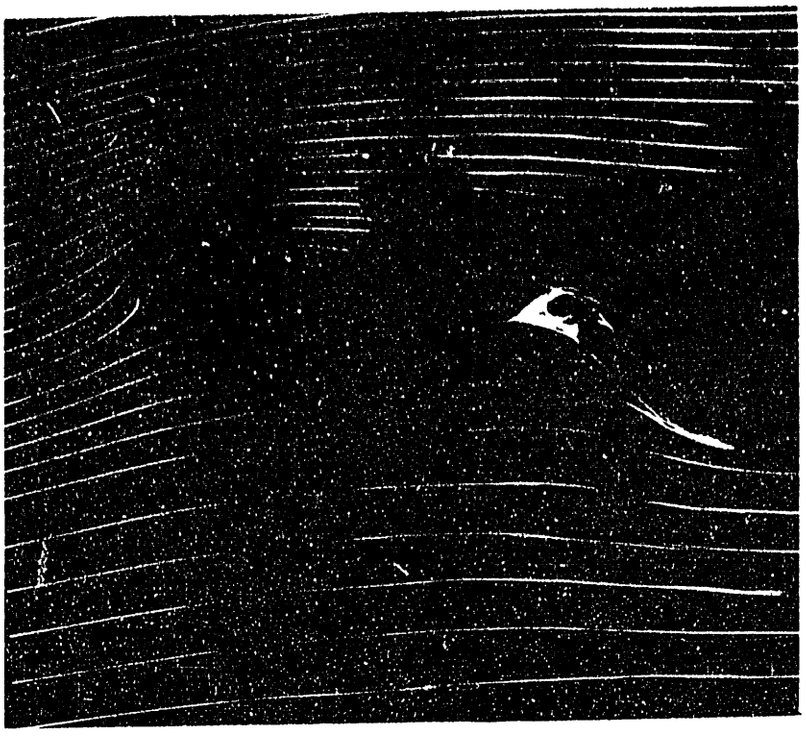

(E) DOUBLE-SLOTTED FLAP

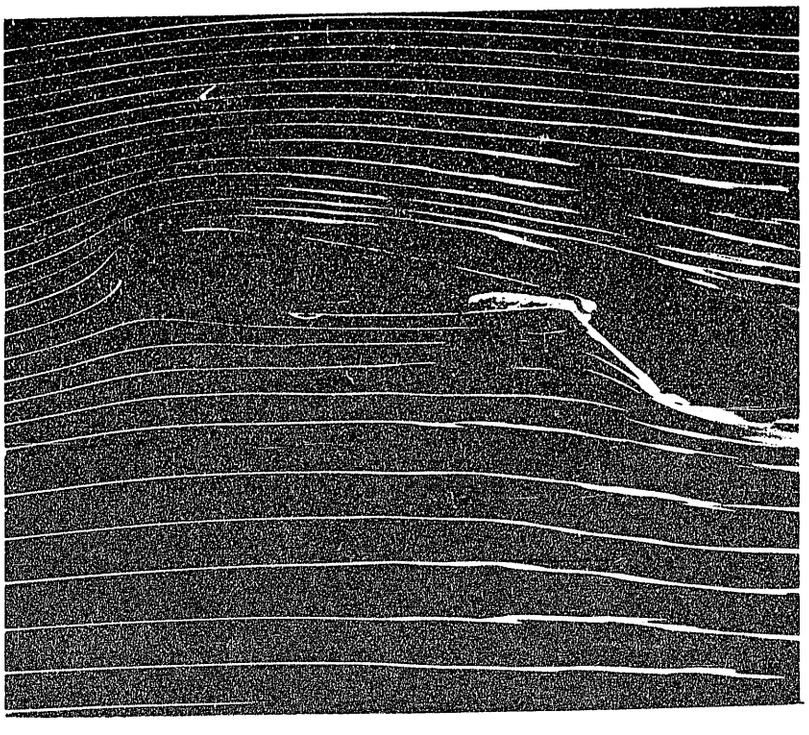

(F) FOWLER FLAP

FIG. 28

TYPICAL TWO-DIMENSIONAL LIFT CHARACTERISTICS OF PROFILES WITH TRAILING-EDGE FLAPS

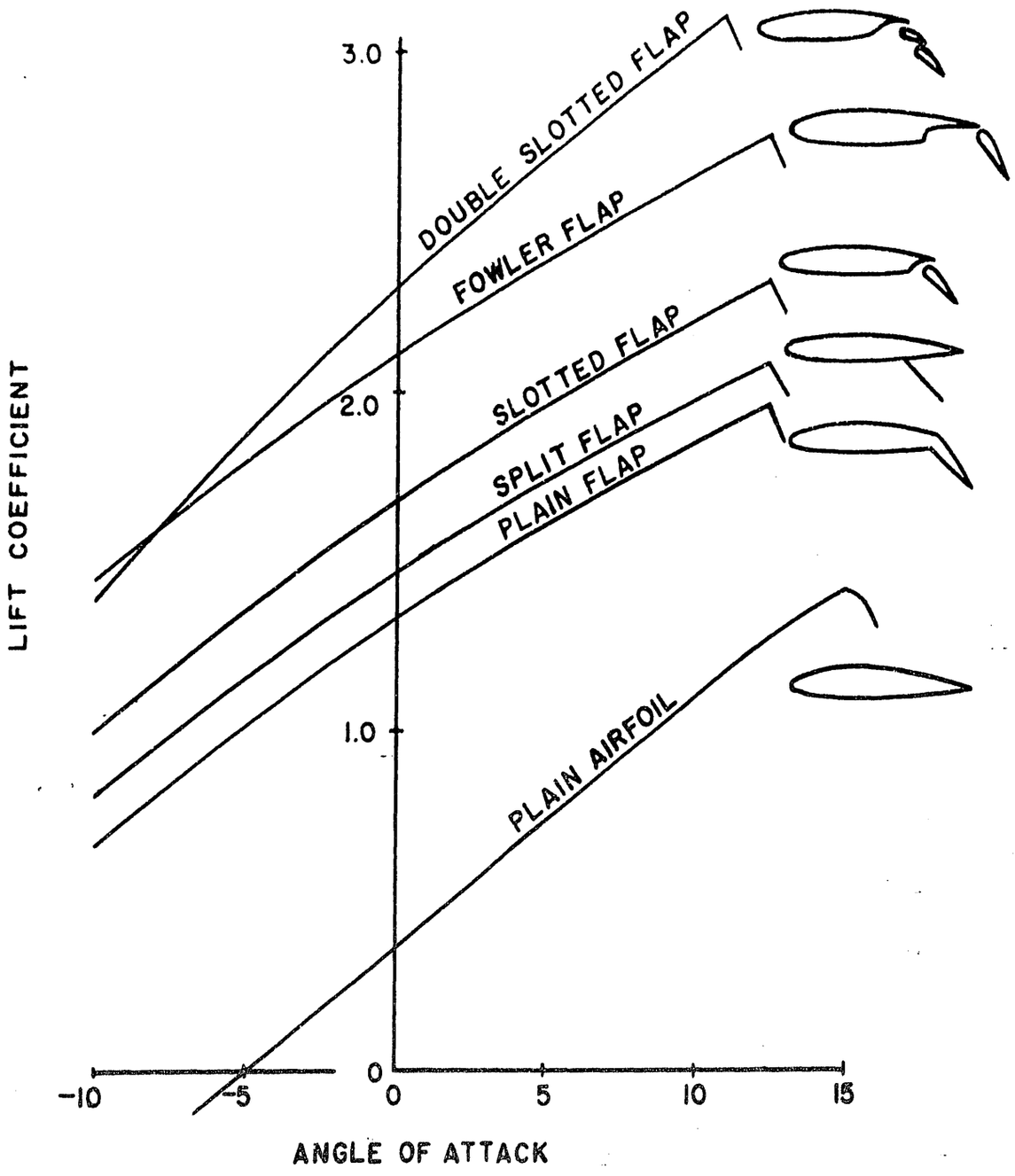

FIG. 29

CONFIDENTIAL

POWERED TRAILING-EDGE DEVICES

(A) BLOWING FLAP

(B) SUCTION FLAP

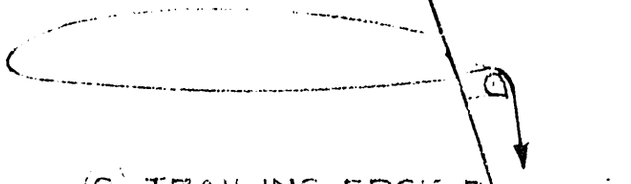

(C) TRAILING-EDGE BLOWING

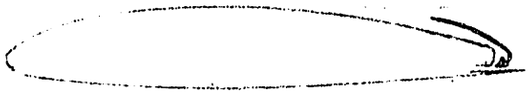

(D) TRAILING-EDGE SUCTION

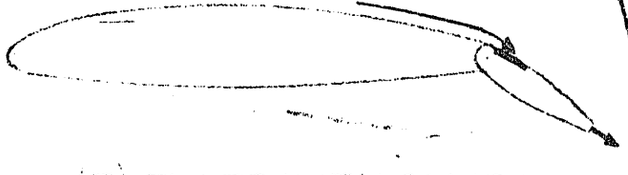

(E) FLAPS WITH COMBINED SUCTION AND BLOWING

FIG. 30 CONFIDENTIAL

THEORETICAL LIFT CURVES OF NACA 64A010 WITH SPLIT FLAP - AS OBTAINED FROM ELECTROLYTIC PLOTTING TANK

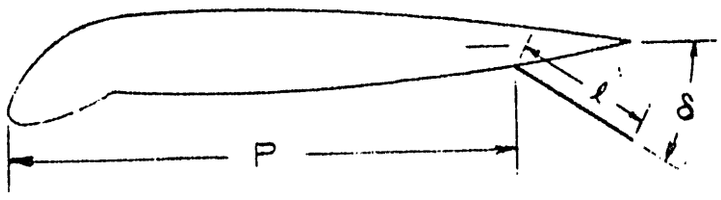

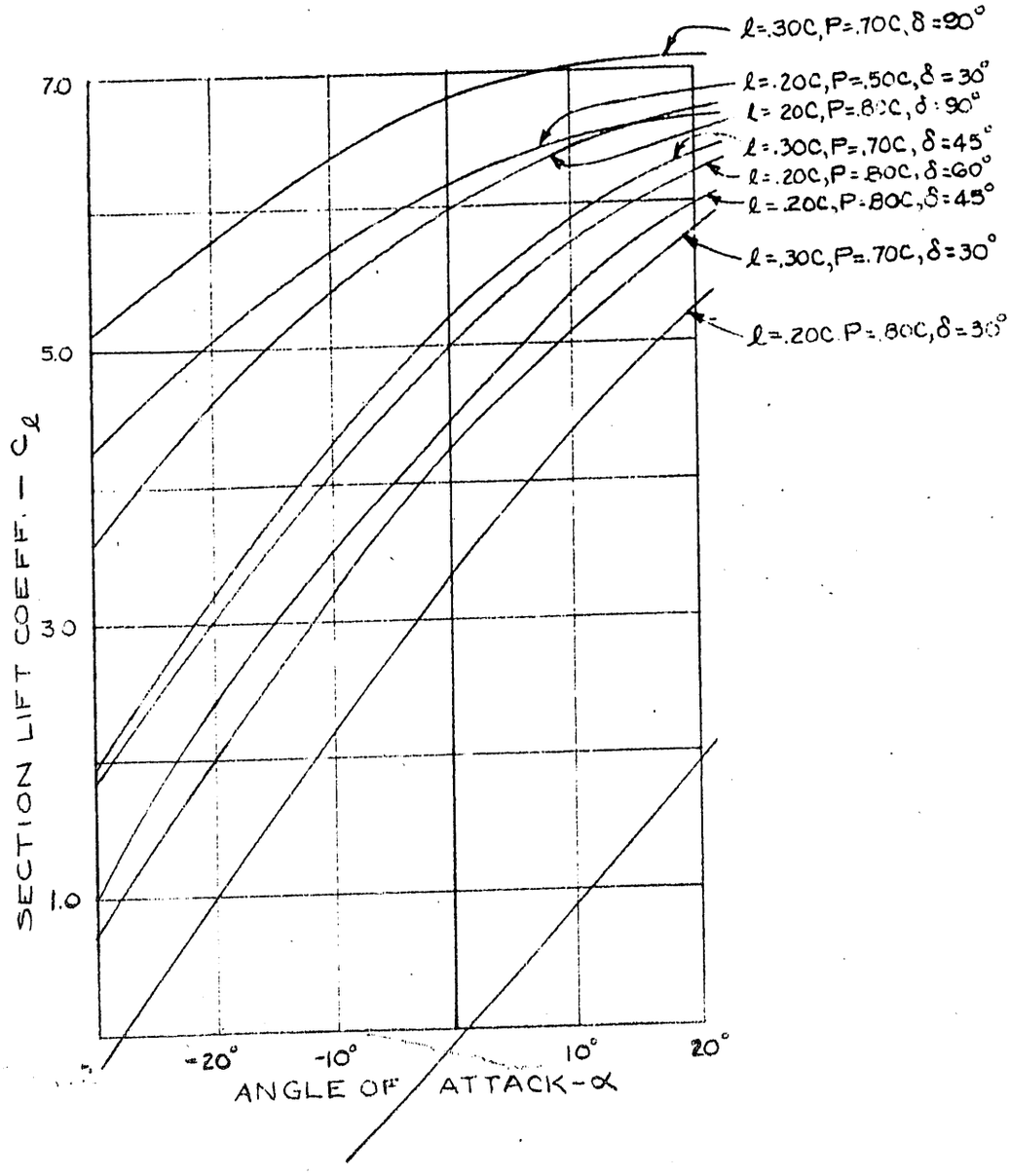

FIG. 31

EFFECT OF INCREASED TRAILING-EDGE CIRCULATION UPON STALL ANGLE

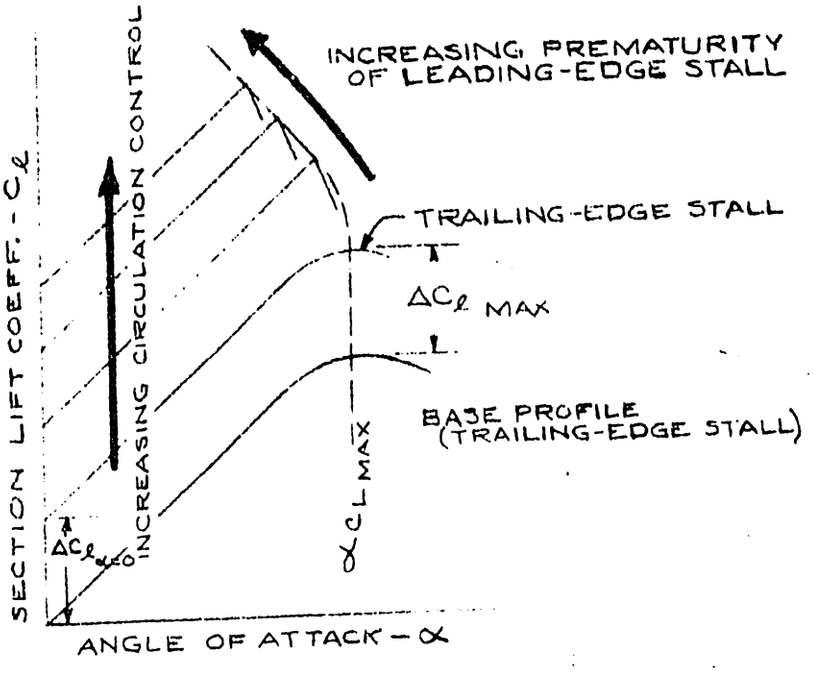

(A) RELATIVELY THIN PROFILE

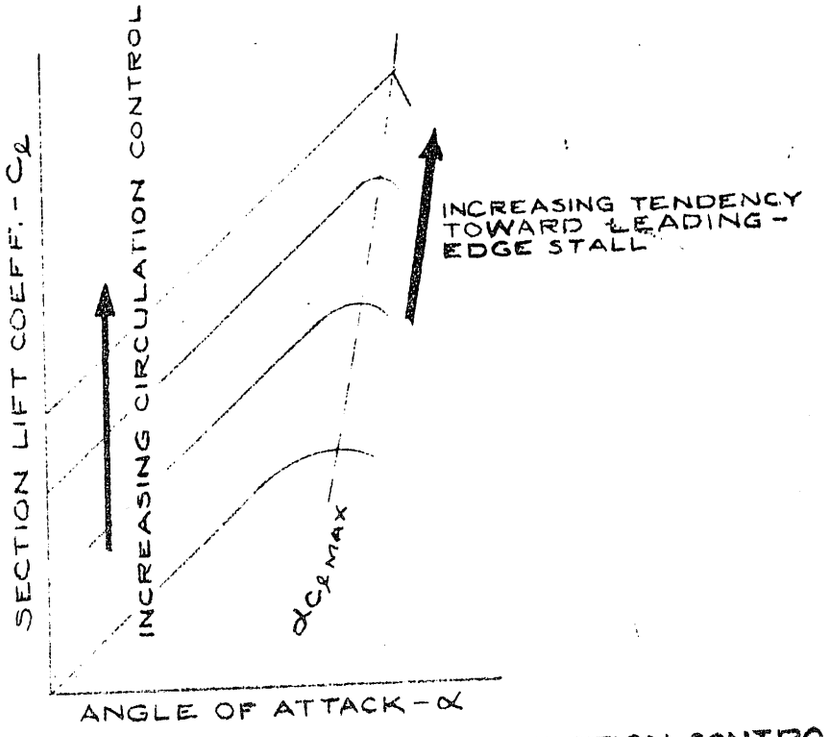

(B) THICK PROFILE WITH POWERED CIRCULATION CONTROL

FIG. 32

STALL TYPES FOR PROFILES WITH TRAILING-EDGE CIRCULATION CONTROL

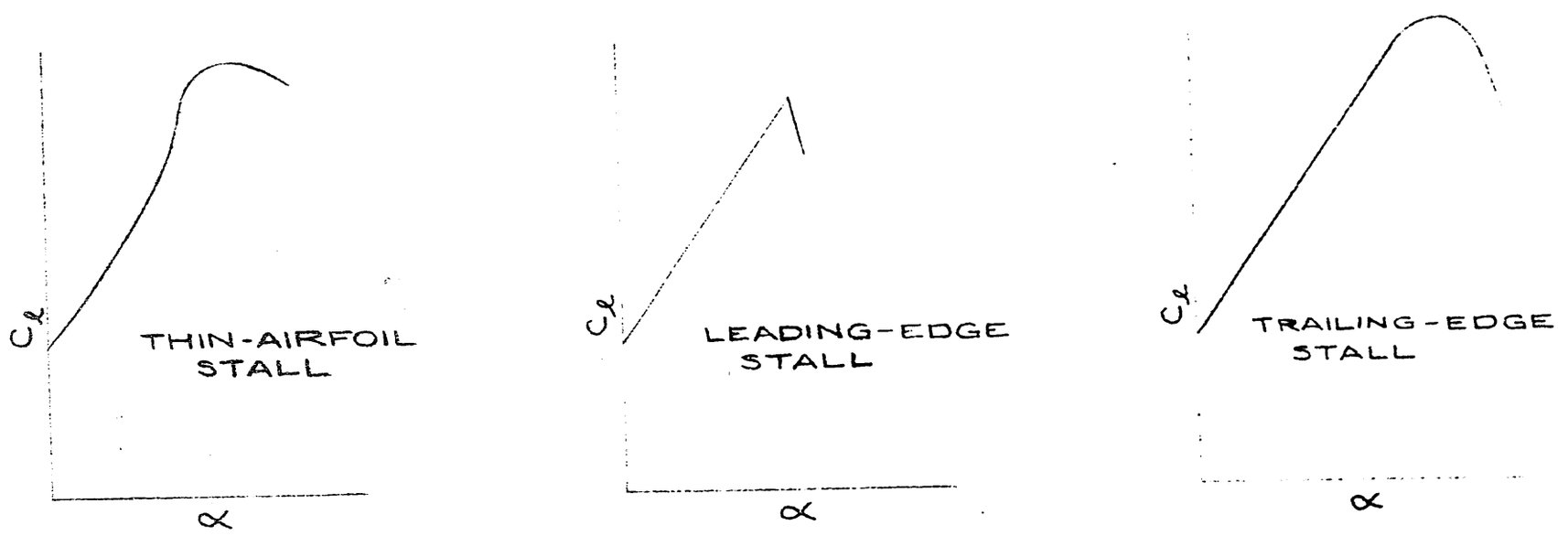

FIG. 33

VARIATION OF MAX. LIFT COEFFICIENT WITH PROFILE THICKNESS FOR AIRFOIL WITH TRAILING-EDGE CIRCULATION CONTROL

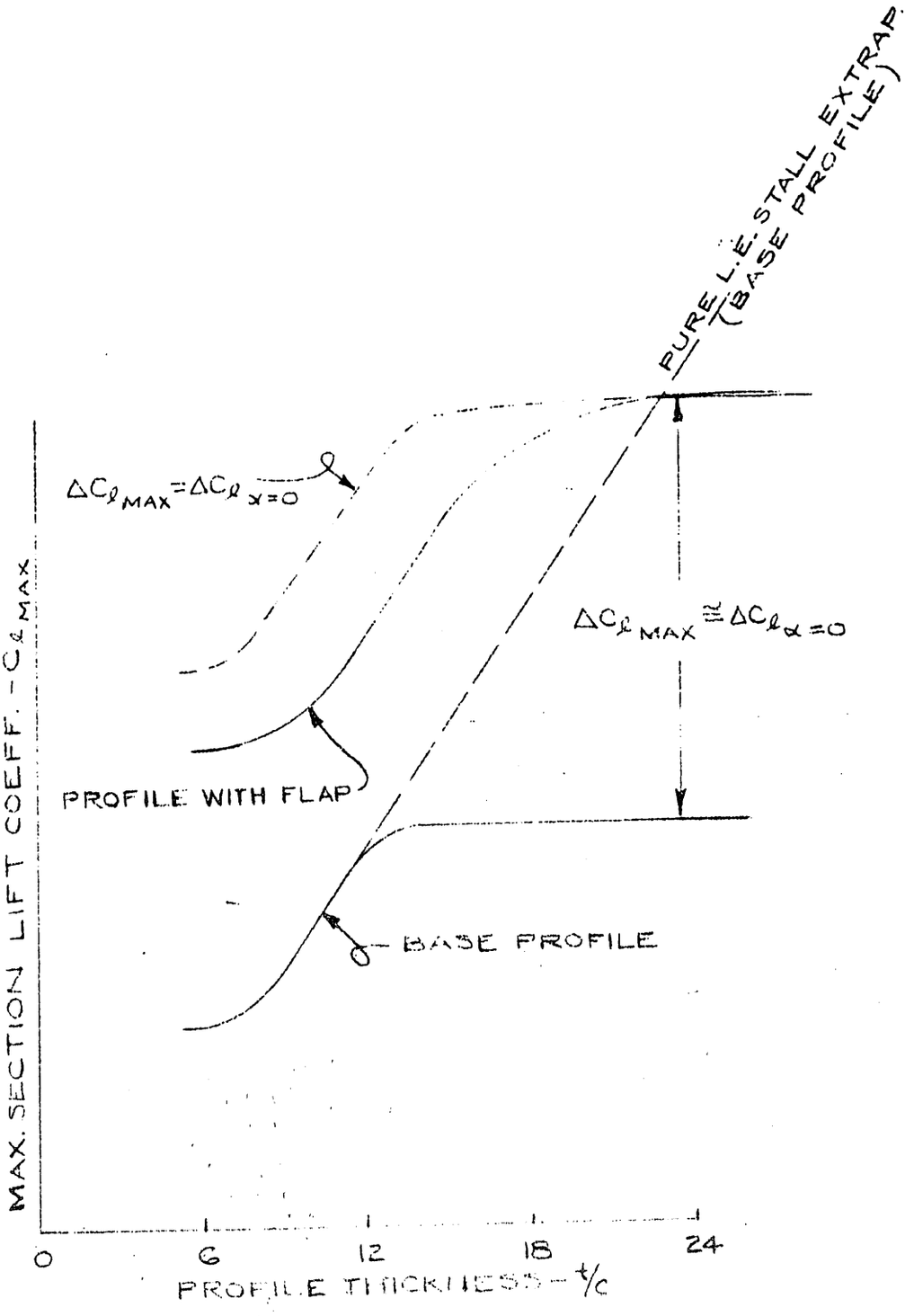

FIG 34

POSSIBLE EFFECT OF CIRCULATION CONTROL WHICH PROVIDES TRAILING-EDGE B.L.C.

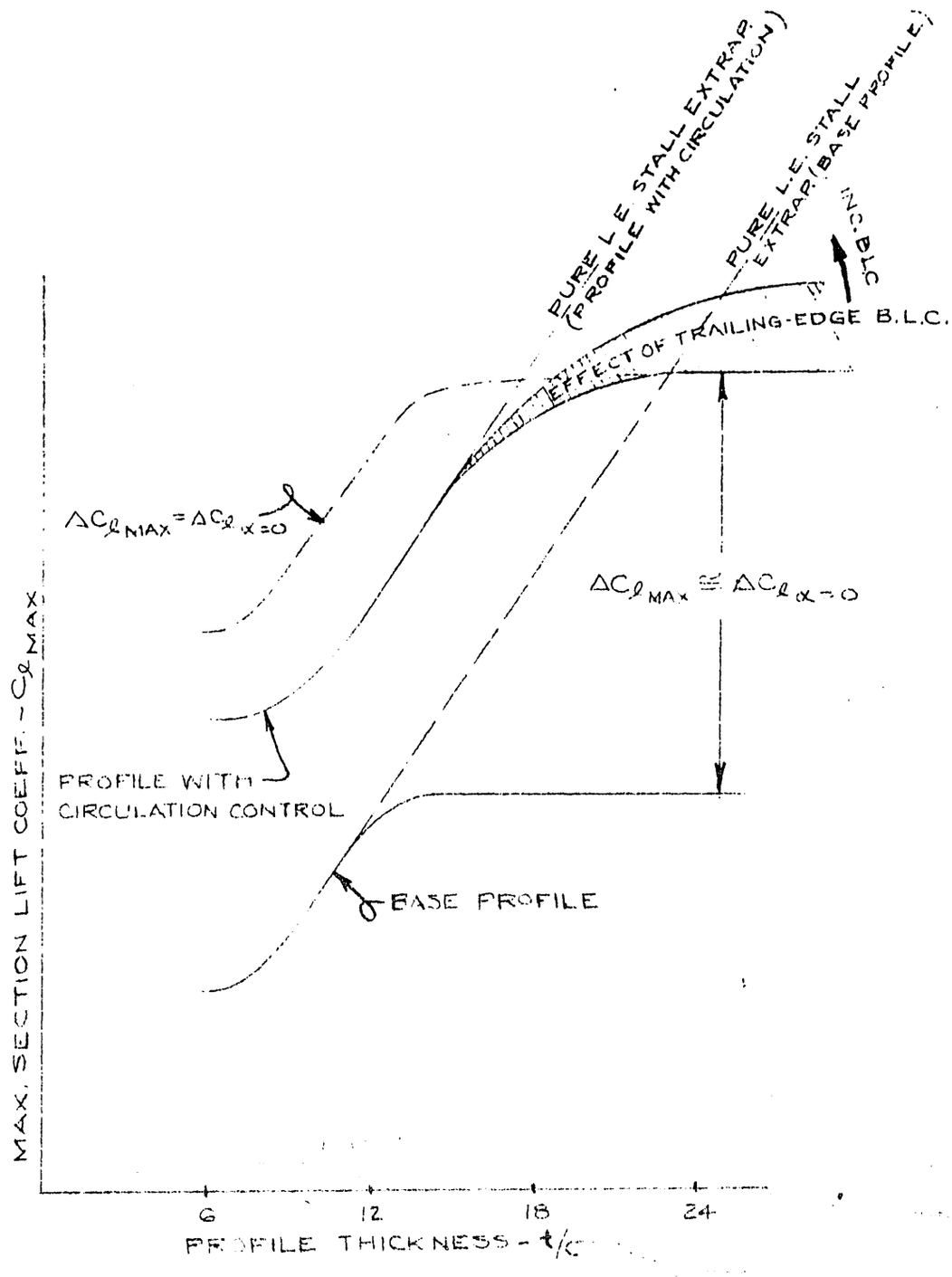

FIG. 35

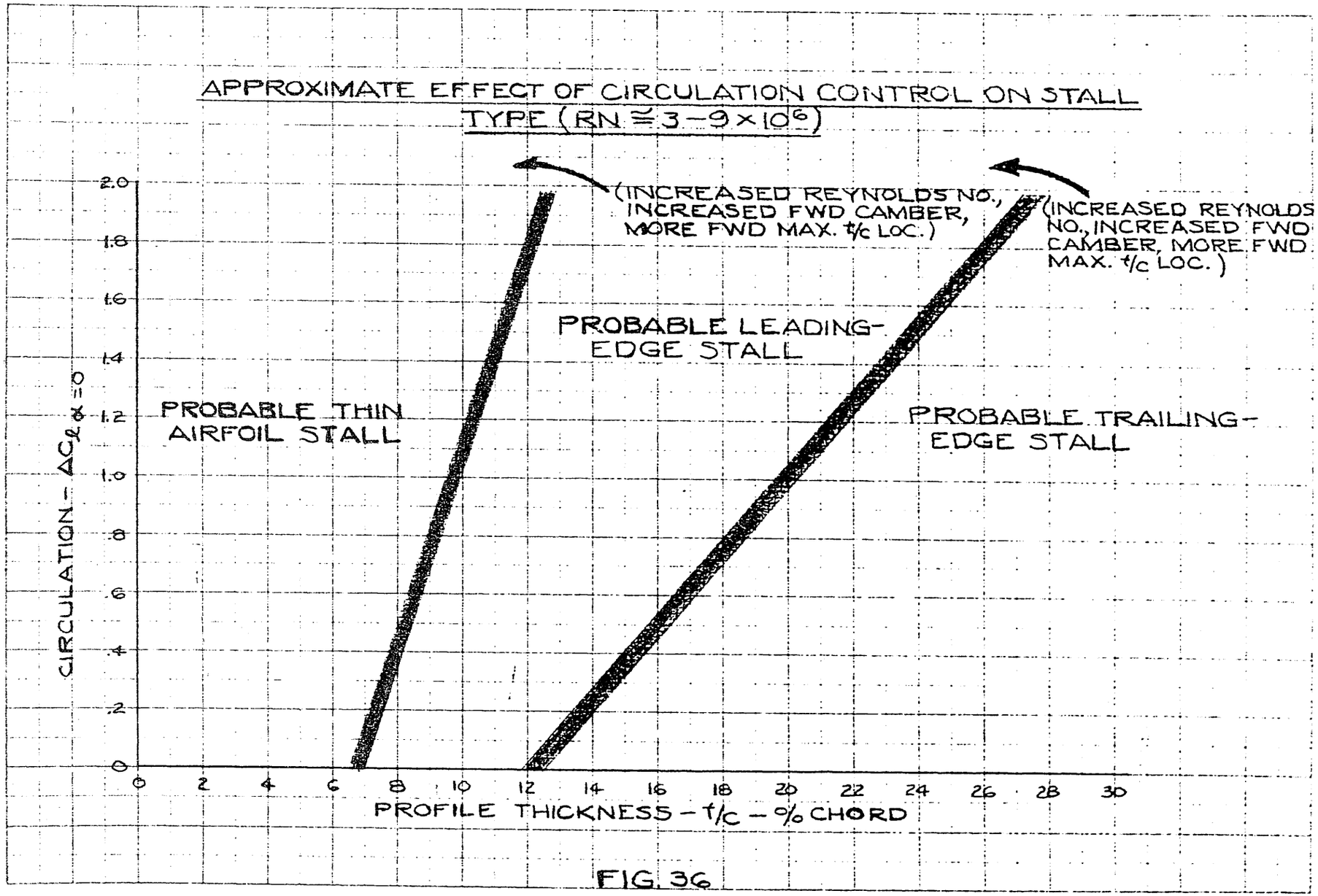
APPROXIMATE EFFECT OF CIRCULATION CONTROL ON STALL TYPE (RN ≅ 3–9 × 10⁶)
(INCREASED REYNOLDS NO., INCREASED FWD CAMBER, MORE FWD MAX. t/c LOC.)
(INCREASED REYNOLDS NO., INCREASED FWD CAMBER, MORE FWD MAX. t/c LOC.)
PROBABLE LEADING-EDGE STALL
PROBABLE THIN AIRFOIL STALL
PROBABLE TRAILING-EDGE STALL
CIRCULATION – ΔCℓ α=0
2.0
1.8
1.6
1.4
1.2
1.0
.8
.6
.4
.2
0
0 2 4 6 8 10 12 14 16 18 20 22 24 26 28 30
PROFILE THICKNESS – t/c – % CHORD

FIG. 36

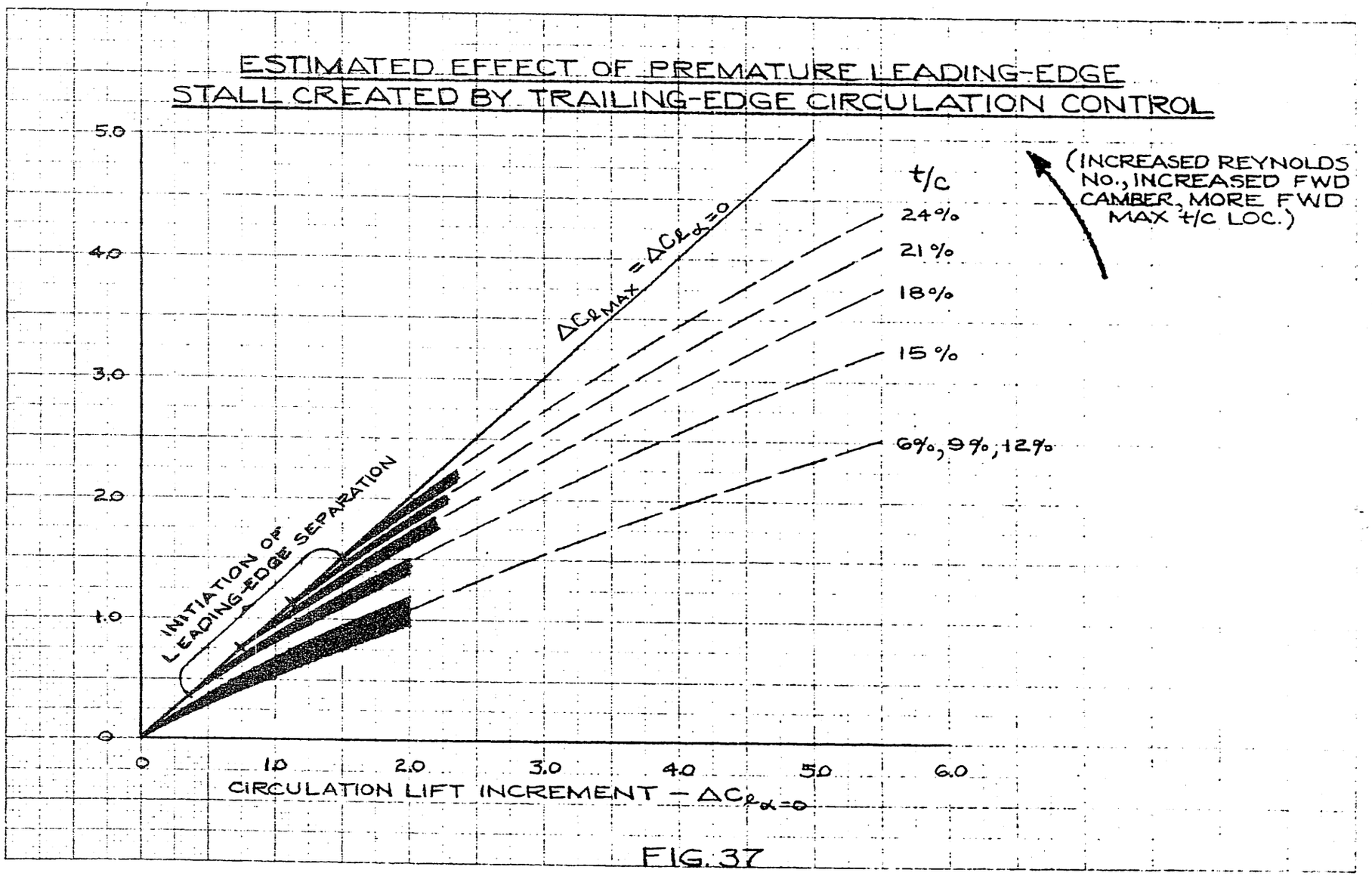
ESTIMATED EFFECT OF PREMATURE LEADING-EDGE STALL CREATED BY TRAILING-EDGE CIRCULATION CONTROL
5.0
4.0
3.0
2.0
1.0
0
t/c
24%
21%
18%
15%
6%, 9%, 12%
(INCREASED REYNOLDS NO., INCREASED FWD CAMBER, MORE FWD MAX t/c LOC.)
$\Delta C_{\ell_{MAX}} = \Delta C_{\ell_{\alpha=0}}$
INITIATION OF LEADING-EDGE SEPARATION
0
1.0
2.0
3.0
4.0
5.0
6.0
CIRCULATION LIFT INCREMENT — $\Delta C_{\ell_{\alpha=0}}$

FIG. 37

PROBABLE TREND OF INCREMENT TO $C_{l\,max}$ PROVIDED BY TRAILING-EDGE B.L.C.

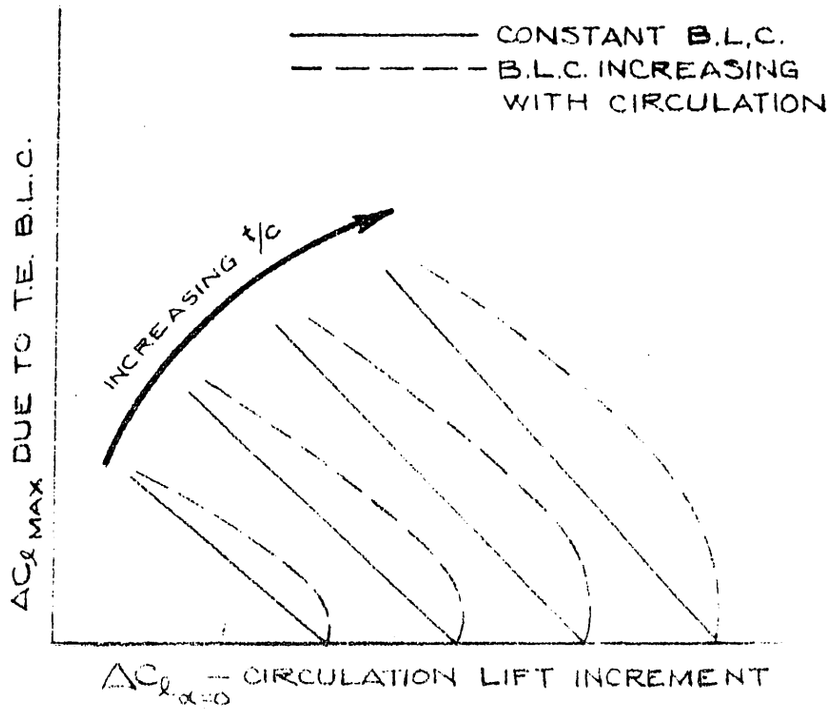

FIG. 38

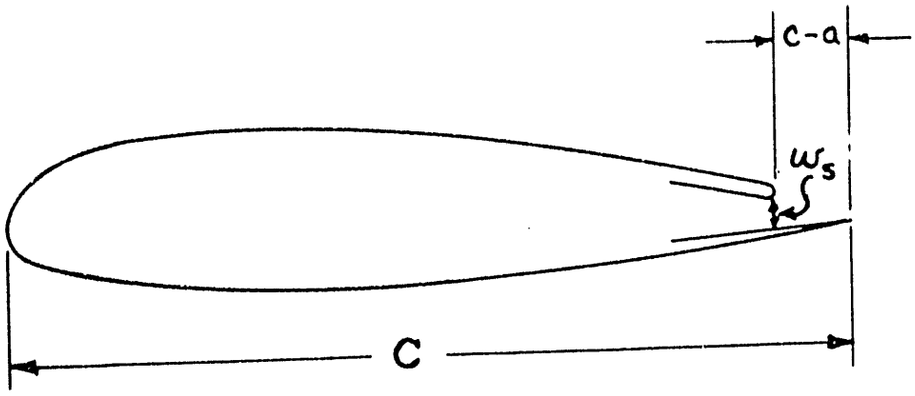

NACA 23015 PROFILE
EQUIPPED WITH TRAILING EDGE SUCTION SLOT

FIG. 39a

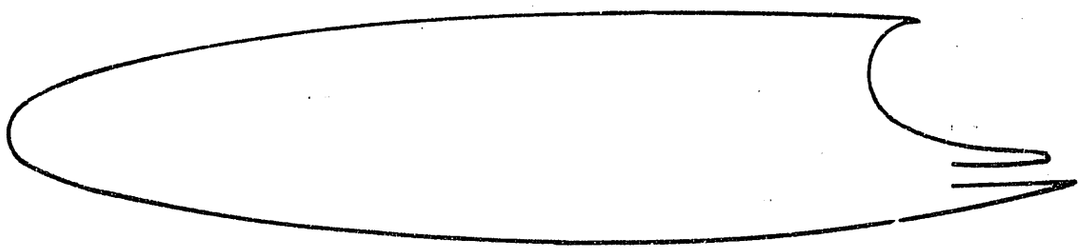

THE "SUCTION VORTEX WING"

FIG. 39b

FIG. 39

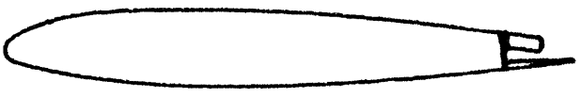

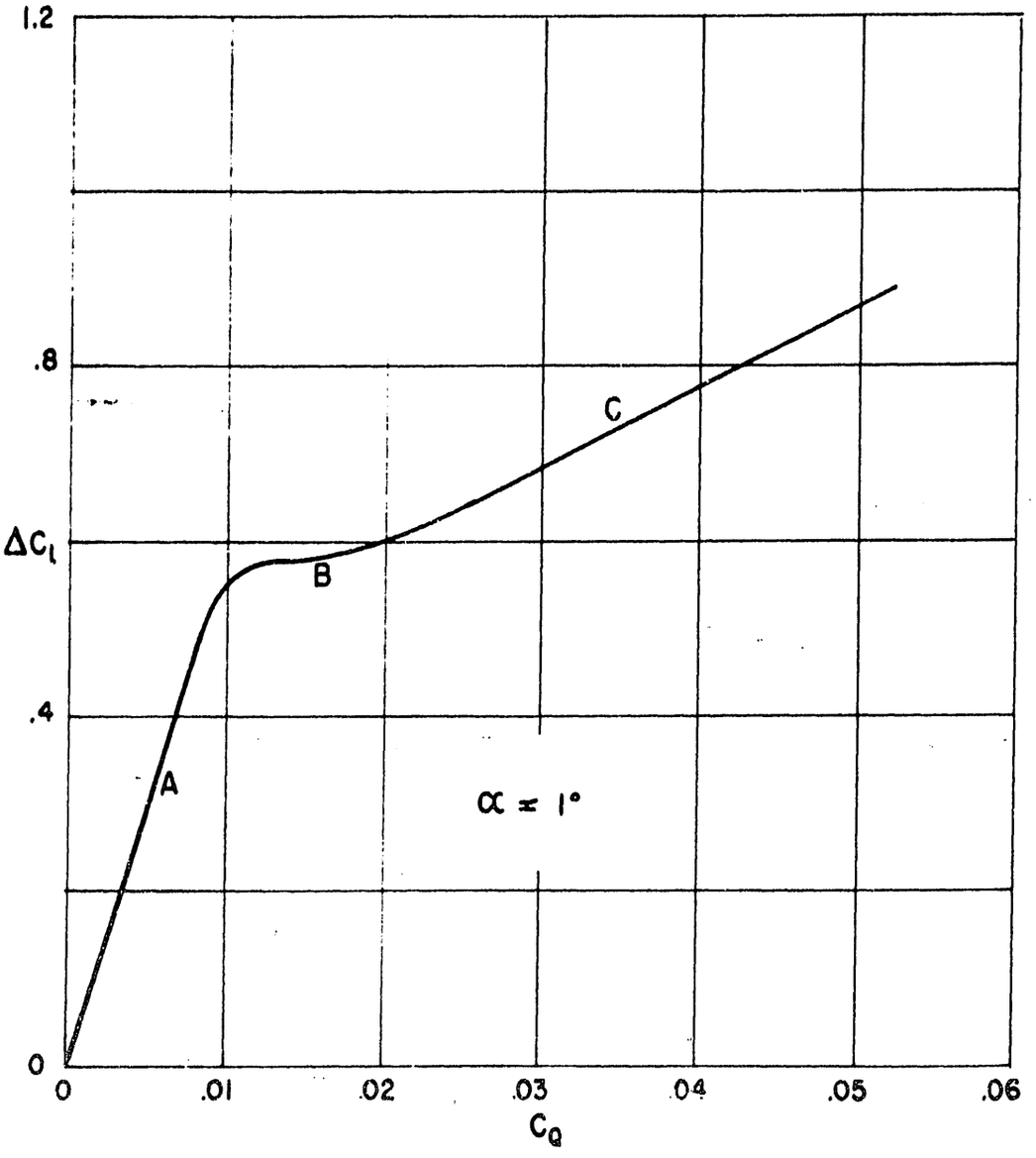

TYPICAL INCREMENTAL LIFT VARIATION
PROFILE EQUIPPED WITH
TRAILING EDGE SUCTION

FIG.40

INITIAL CONDITION- NO SUCTION

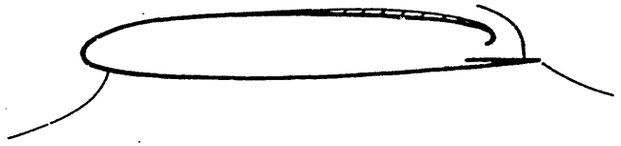

STEADY STATE CONDITION
(PART "C" OF CURVE OF FIG. 1)

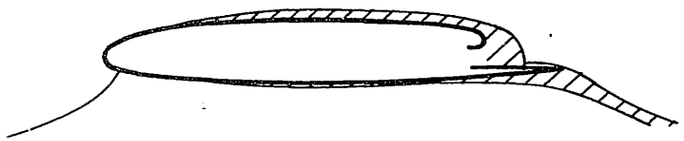

INITIAL APPLICATION OF SUCTION
(PART "A" OF CURVE OF FIG. 1)

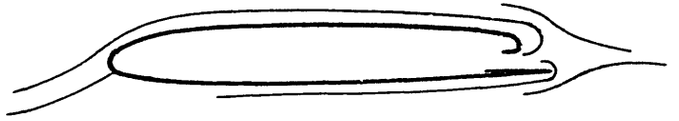

FREE STREAM STAGNATION POINT

THINING OF UPPER BOUNDARY LAYER
(PART "B" OF CURVE OF FIG. 1)

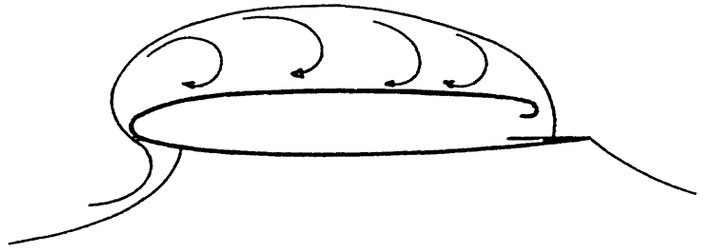

LEADING EDGE SEPARATION

TRAILING EDGE SUCTION
FLOW REGIMES
FIG. 41

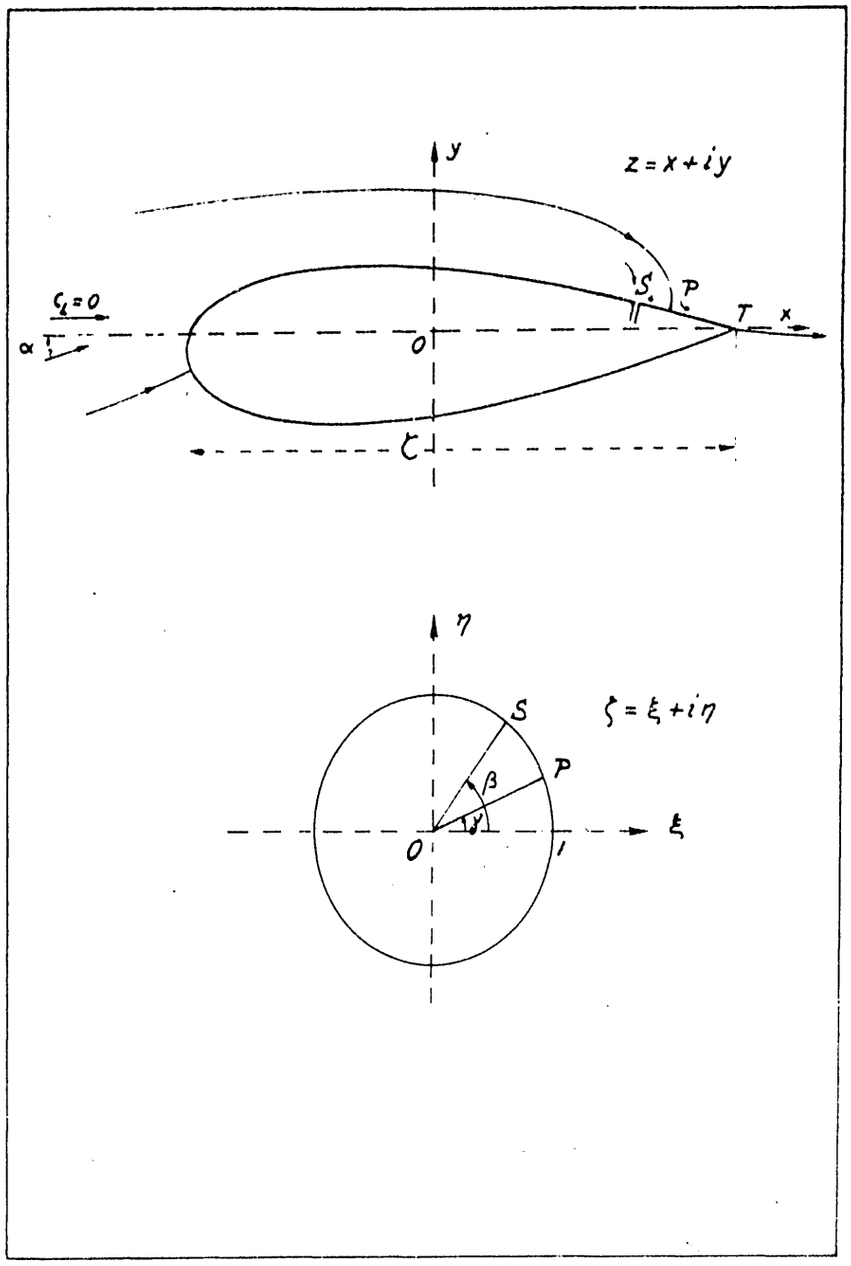

POTENTIAL FLOW CONSIDERATIONS
FOR THE CASE OF TRAILING EDGE SUCTION

FIG. 42

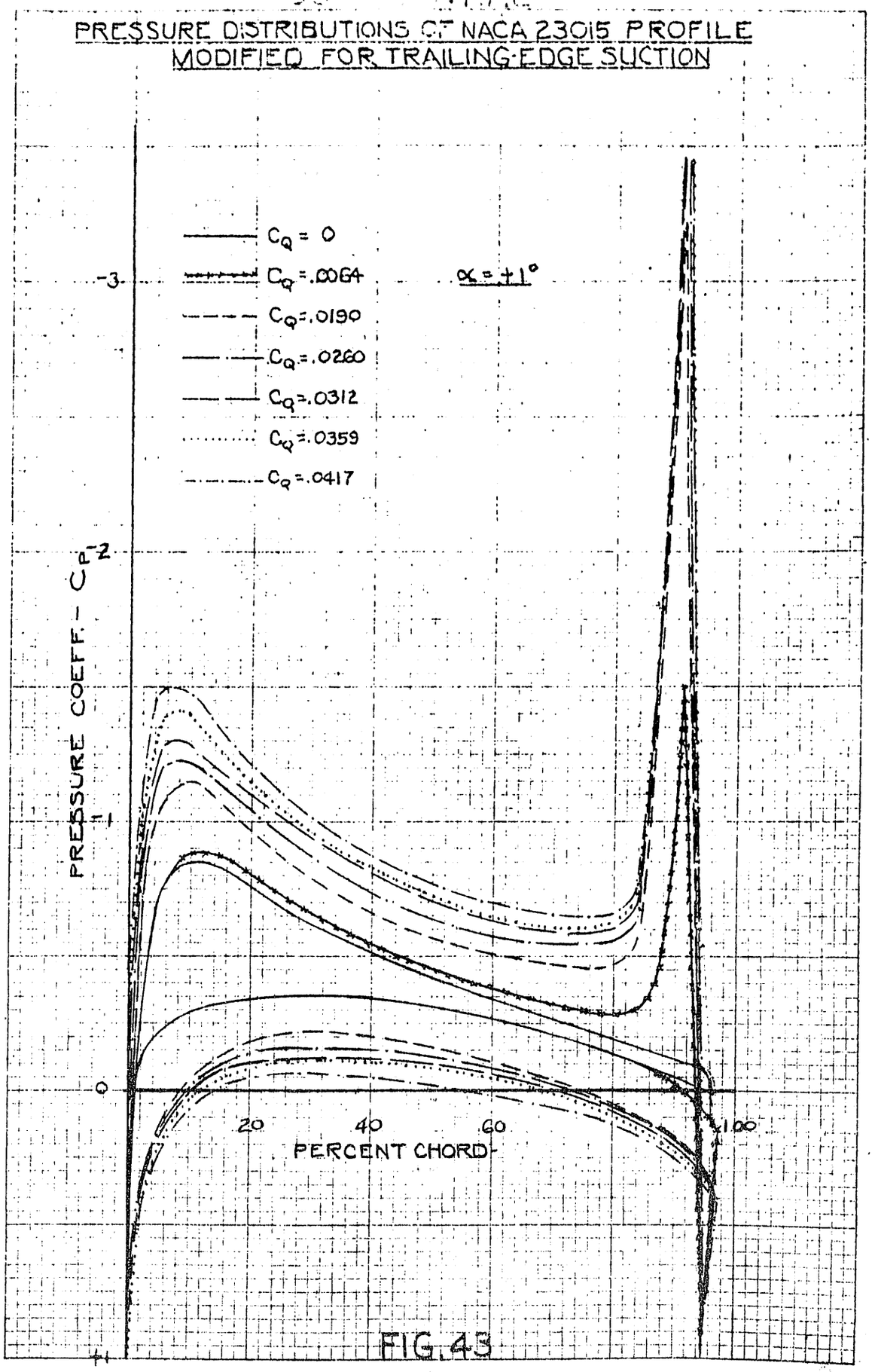

FIG. 43

FORCE AND MOMENT CHARACTERISTICS OF AN NACA 23015 PROFILE EQUIPPED WITH A TRAILING EDGE SUCTION SLOT

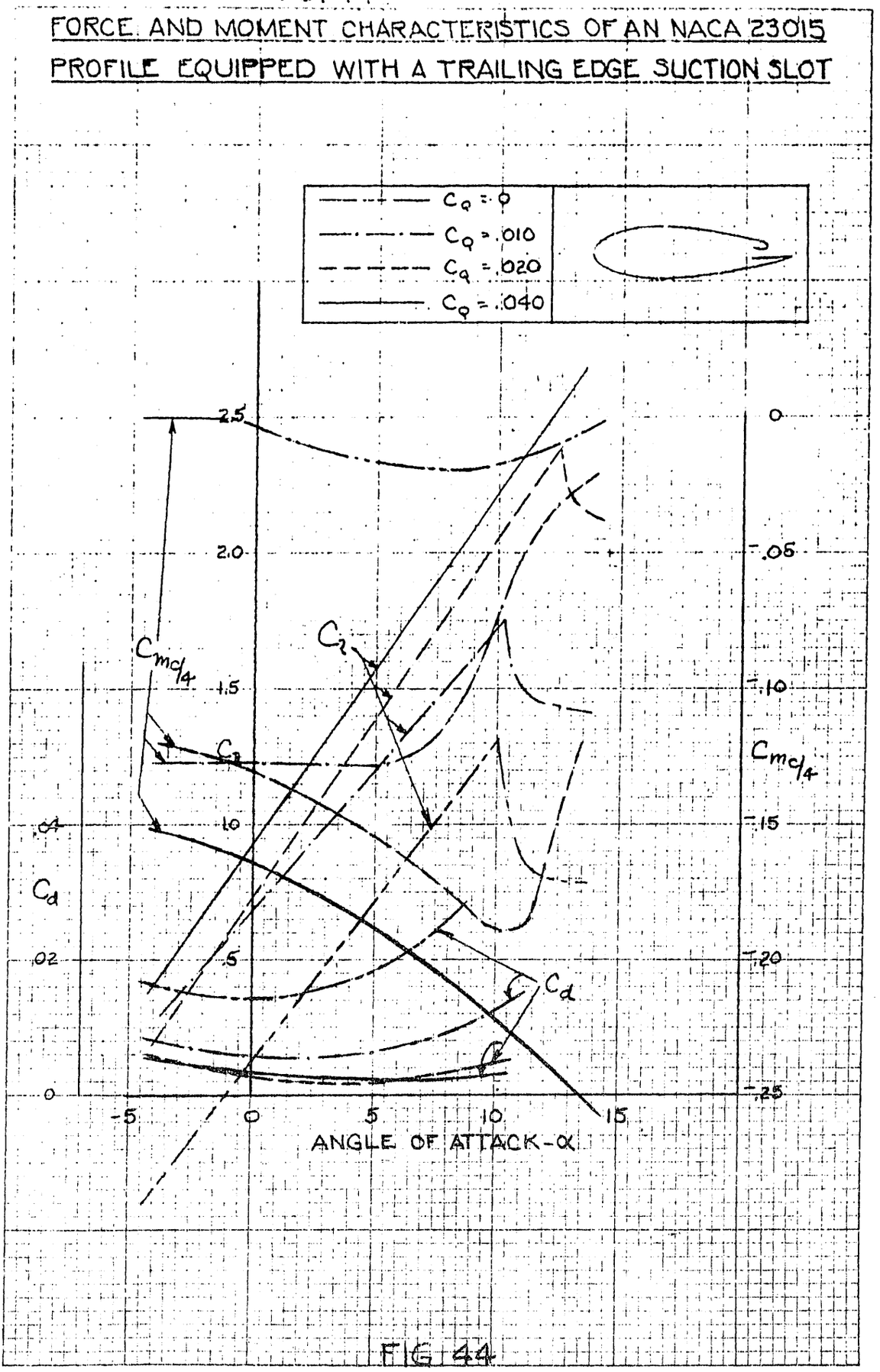

FIG 44

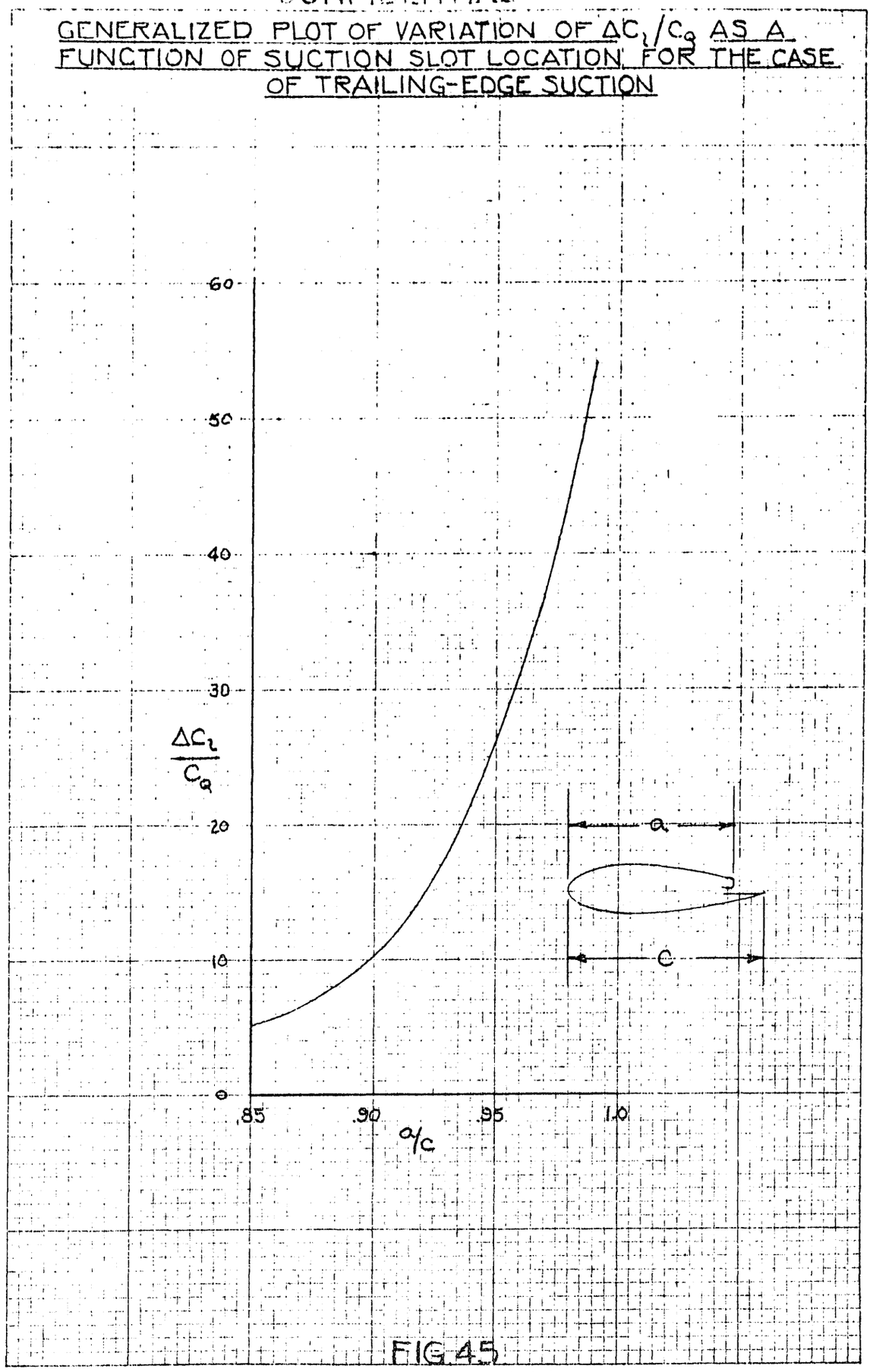

FIG 45

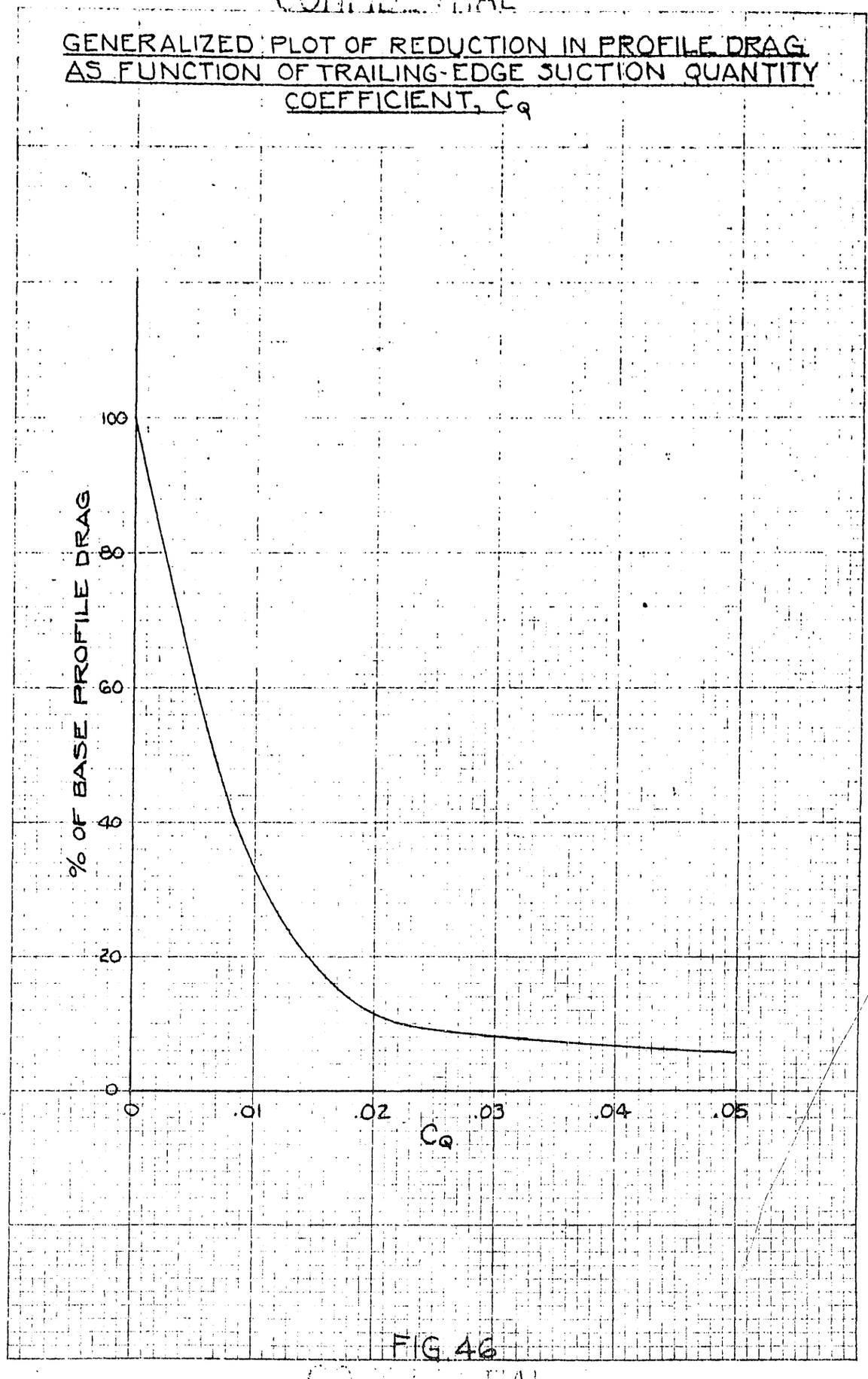

FIG 46

GENERALIZED PLOT OF CHANGE IN PITCHING MOMENT COEFFICIENT AS FUNCTION OF SLOT LOCATION, a/c, AND TRAILING-EDGE SUCTION QUANTITY COEFFICIENT, C_Q

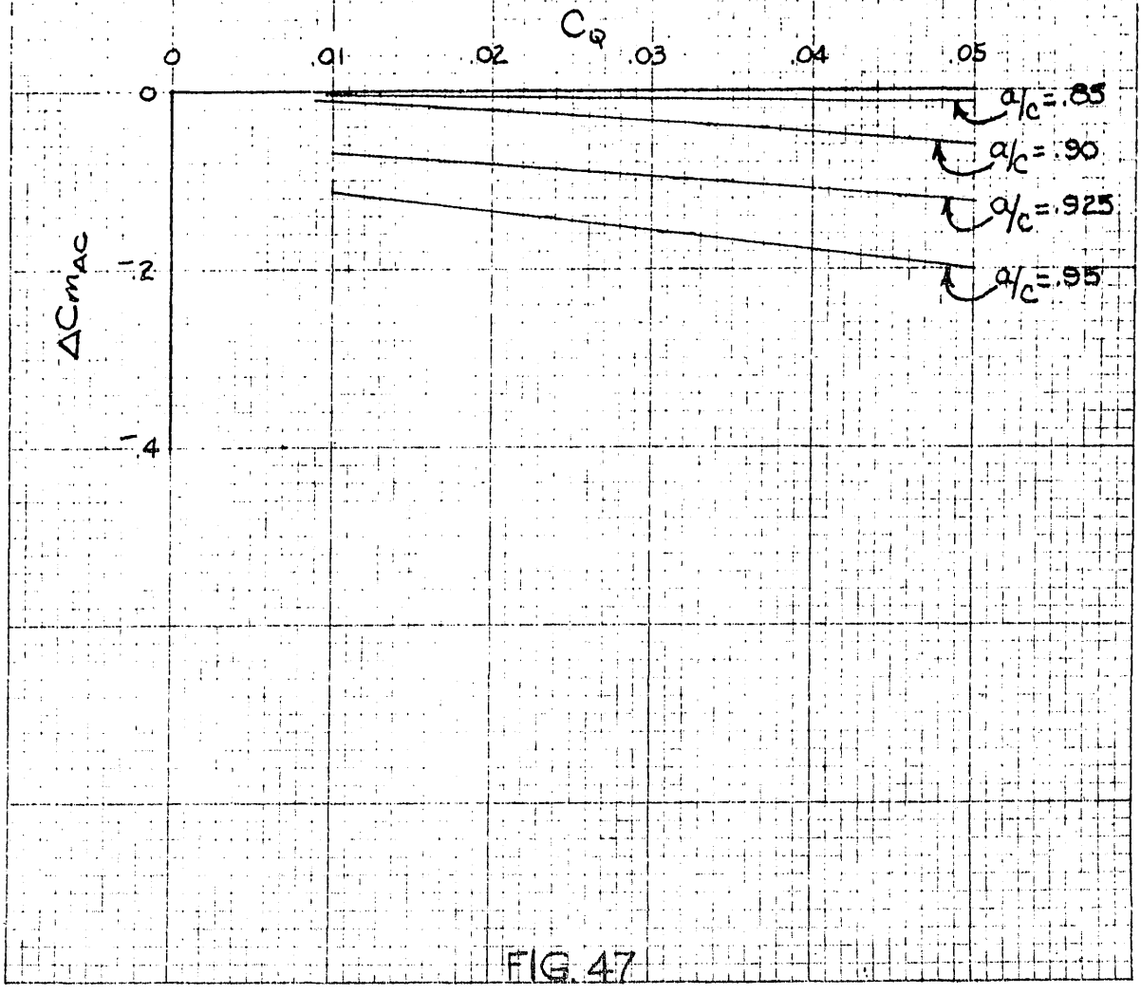

FIG. 47

PRESSURE DISTRIBUTION OF "SUCTION VORTEX WING" SECTION

$\alpha = -1.6°$ R.N. $= .725 \times 10^6$

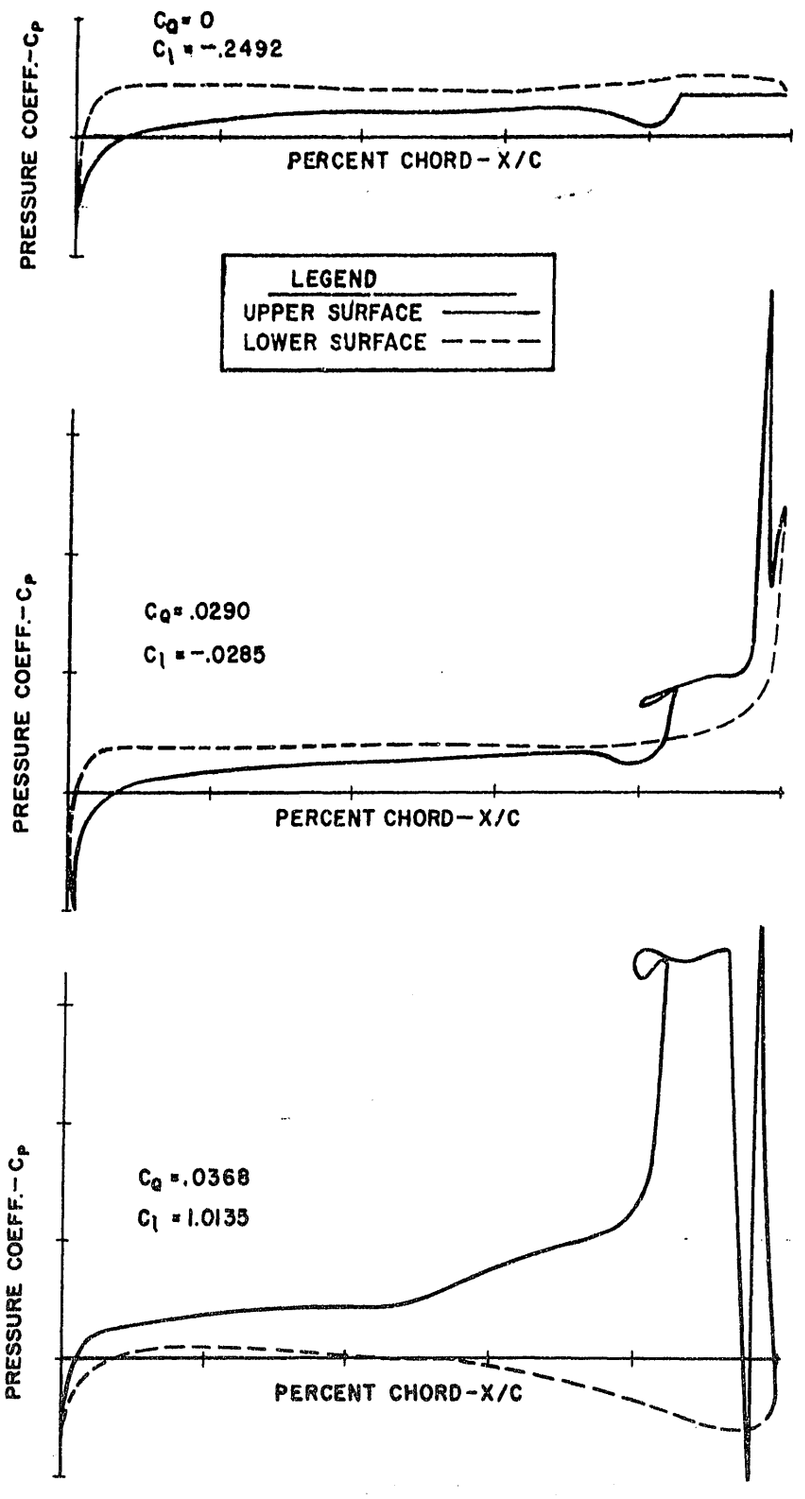

FIG. 48

CONFIDENTIAL

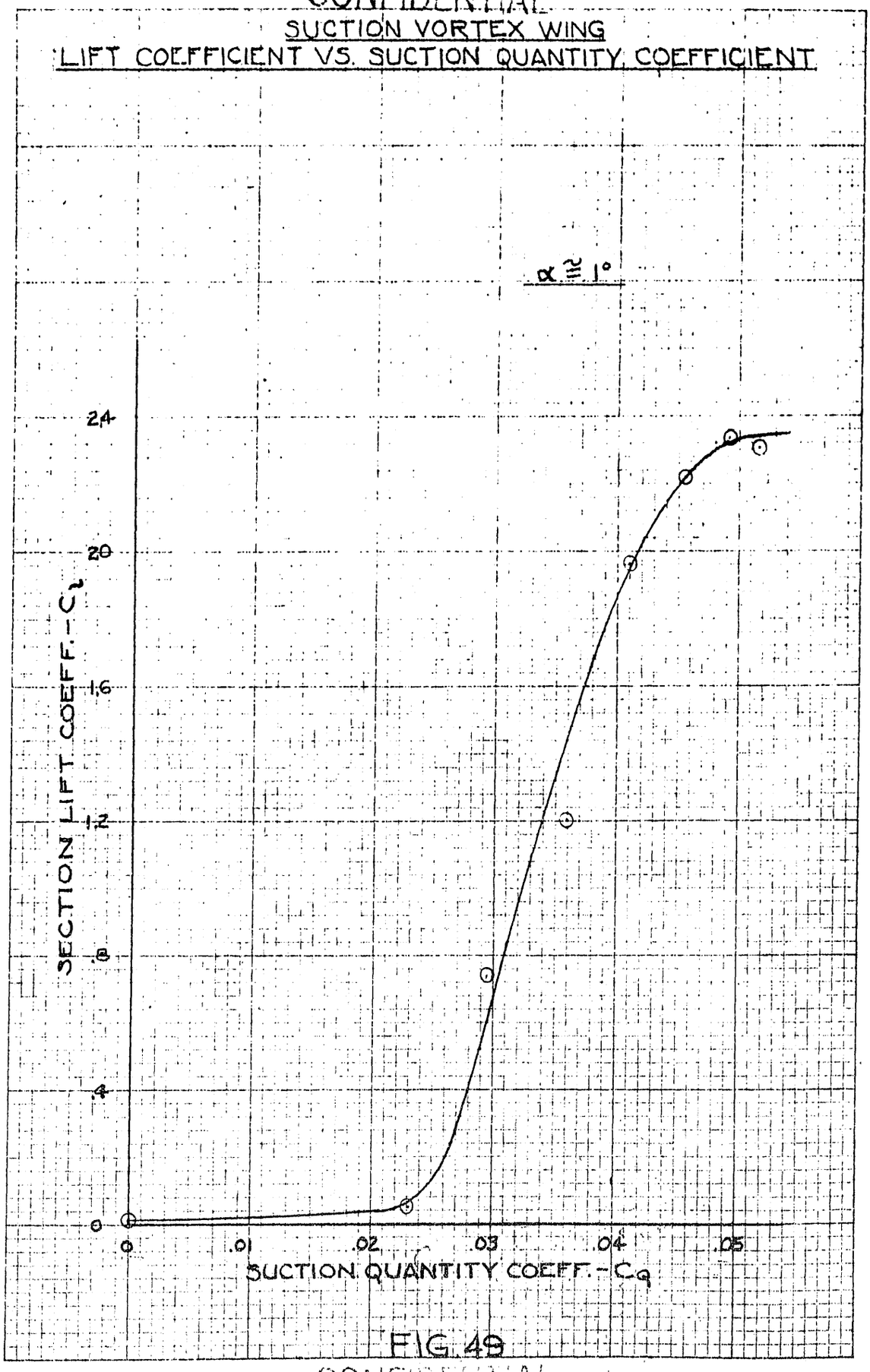

FIG. 49

CONFIDENTIAL

TRAILING-EDGE BLOWING
FREE STREAM BLOWING JET

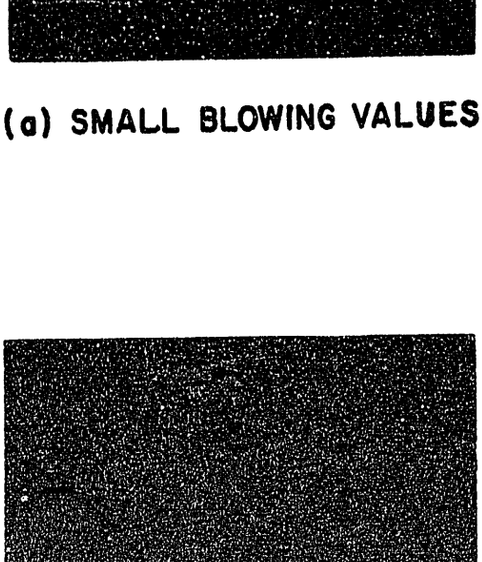

(a) SMALL BLOWING VALUES

(b) LARGE BLOWING VALUES

FIG. 50

TRAILING-EDGE BLOWING

$\alpha_c = 0°$

$\theta' = 0°$

(a) $C_\mu = 0$

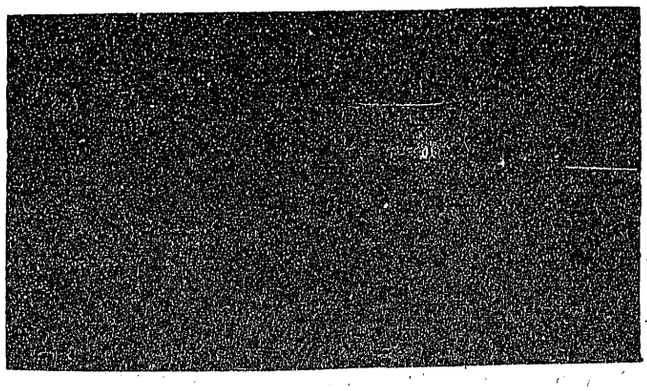

(b) $C_\mu = .669$

FIG. 51

TRAILING-EDGE BLOWING

$\alpha = 4°$

$\theta' = 0°$

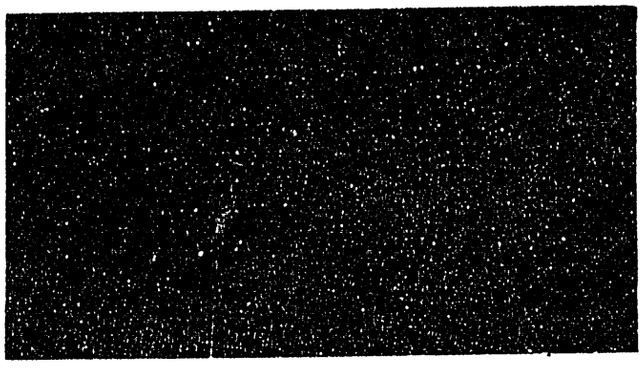

(a) $C_\mu = 0$

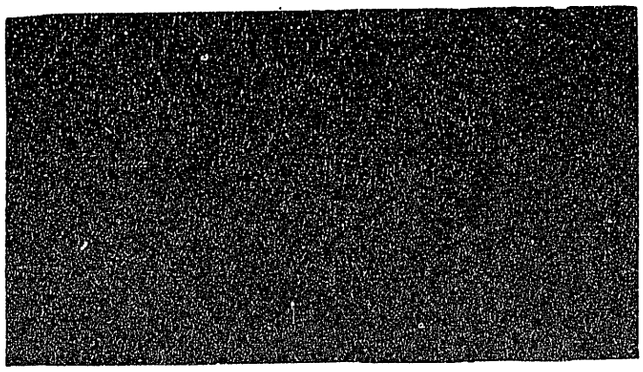

(b) $C_\mu = .669$

FIG. 52

TRAILING-EDGE BLOWING

$\alpha = 0°$

$C_\mu = .669$

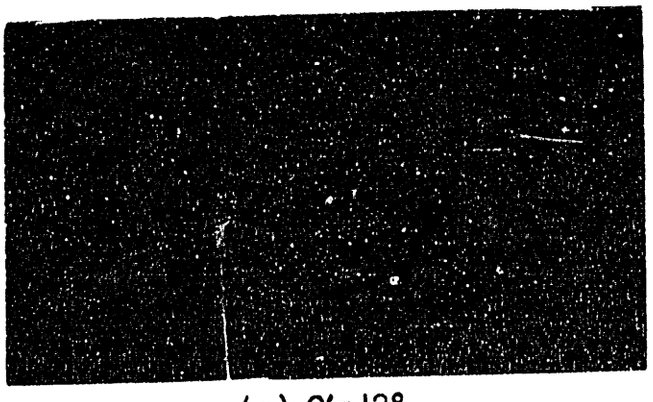

(a) $\theta' = 12°$

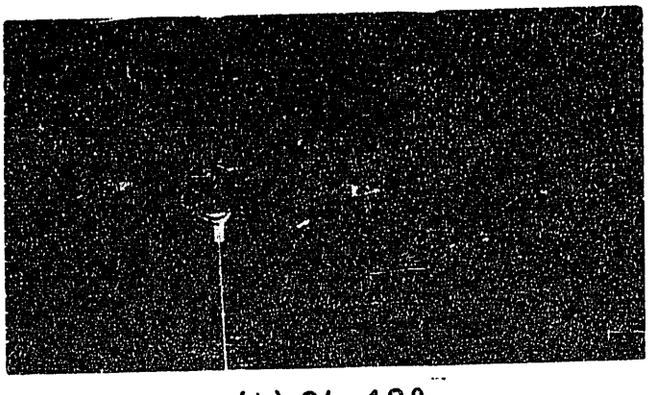

(b) $\theta' = 42°$

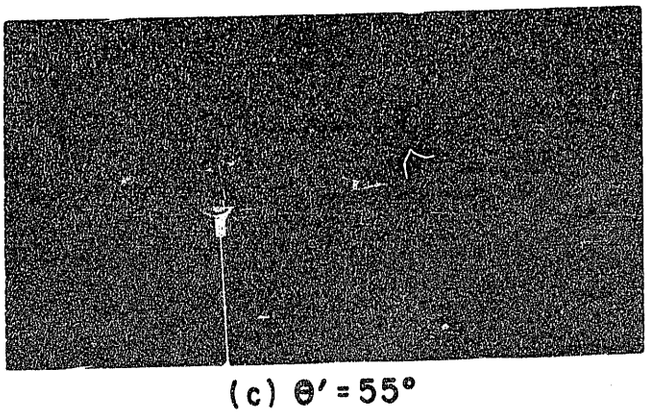

(c) $\theta' = 55°$

FIG. 53

TRAILING-EDGE BLOWING

$\alpha_c = 12°$

$C_\mu = .669$

(a) $\theta' = 0°$

(b) $\theta' = 33°$

FIG. 54

FIG 55

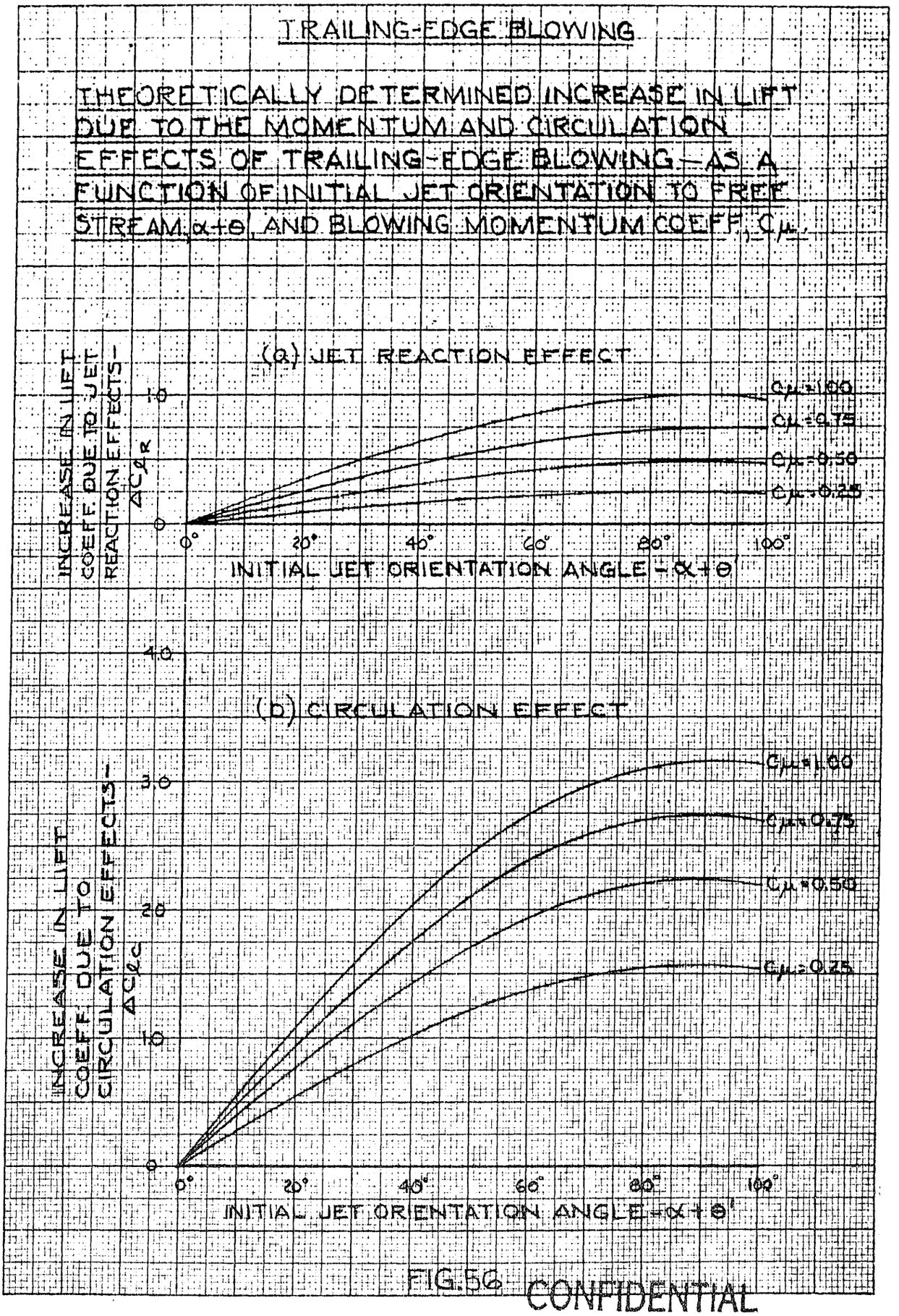
TRAILING-EDGE BLOWING
THEORETICALLY DETERMINED INCREASE IN LIFT DUE TO THE MOMENTUM AND CIRCULATION EFFECTS OF TRAILING-EDGE BLOWING — AS A FUNCTION OF INITIAL JET ORIENTATION TO FREE STREAM, α+θ, AND BLOWING MOMENTUM COEFF., Cμ
(a) JET REACTION EFFECT
INCREASE IN LIFT COEFF. DUE TO JET REACTION EFFECTS — ΔCLR
1.0
0
0°
20°
40°
60°
80°
100°
INITIAL JET ORIENTATION ANGLE - α+θ
Cμ=1.00
Cμ=0.75
Cμ=0.50
Cμ=0.25
(b) CIRCULATION EFFECT
INCREASE IN LIFT COEFF. DUE TO CIRCULATION EFFECTS — ΔCLC
4.0
3.0
2.0
1.0
0
0°
20°
40°
60°
80°
100°
INITIAL JET ORIENTATION ANGLE - α+θ
Cμ=1.00
Cμ=0.75
Cμ=0.50
Cμ=0.25

FIG. 56

TRAILING-EDGE BLOWING

THEOR-DETERMINED TOTAL INCREASE IN LIFT DUE TO TRAILING-EDGE BLOWING AS A FUNCTION OF INITIAL JET ORIENTATION TO FREE STREAM, $\alpha + \theta'$, AND BLOWING MOMENTUM COEFF., C_μ

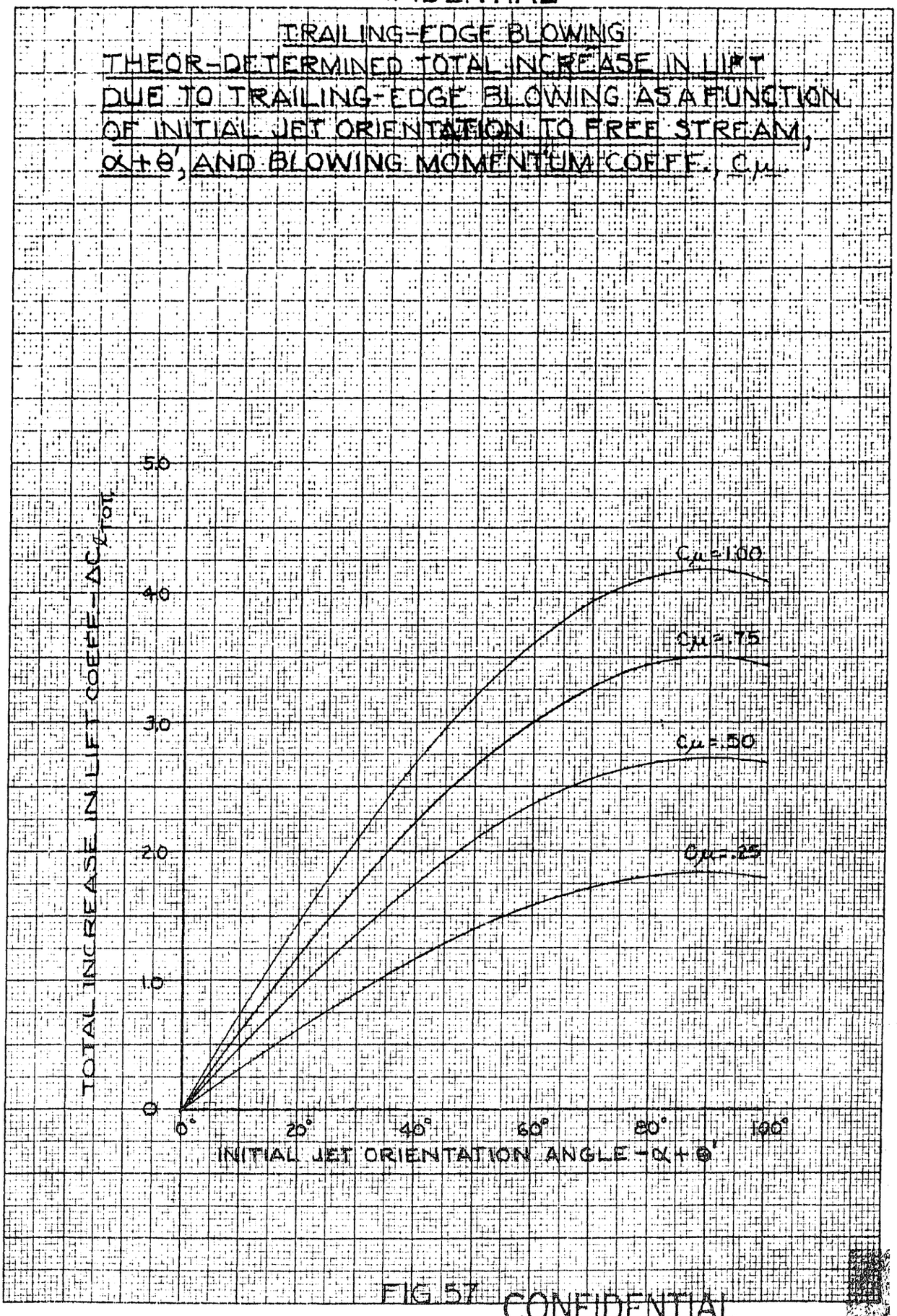

FIG 57

TRAILING-EDGE BLOWING

THEORETICALLY-DETERMINED LIFT COEFF. FOR PROFILE WITH TRAILING-EDGE BLOWING – NO JET REACTION EFFECTS CONSIDERED – AS FUNCTION OF α, θ', AND C_μ

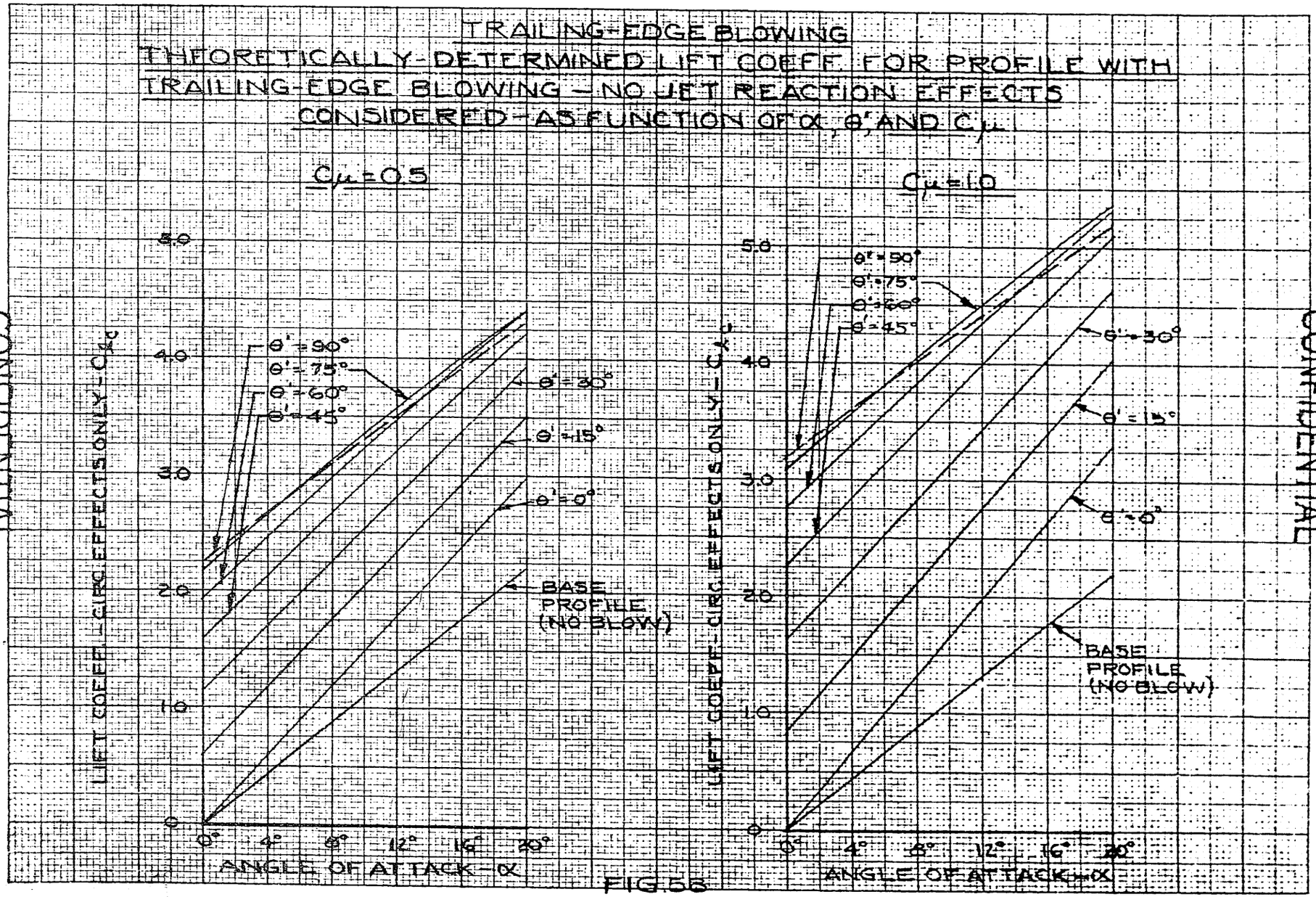

FIG 56

FIG. 5B

FIG 60

CONFIDENTIAL
THEOR. DETERMINED TOTAL LIFT COEFF. FOR PROFILE WITH
TRAILING-EDGE BLOWING - AS FUNCTION OF α, θ', AND Cμ
θ' = 30°
θ' = 60°
Cμ = 1.0
Cμ = 0.75
Cμ = 0.50
Cμ = 0.25
Cμ = 0
TOTAL LIFT COEFF - $C_{A_{tot}}$
ANGLE OF ATTACK - α
0°
4°
8°
12°
16°
20°
30°
1.0
2.0
3.0
4.0
5.0
CONFIDENTIAL

FIG. 61

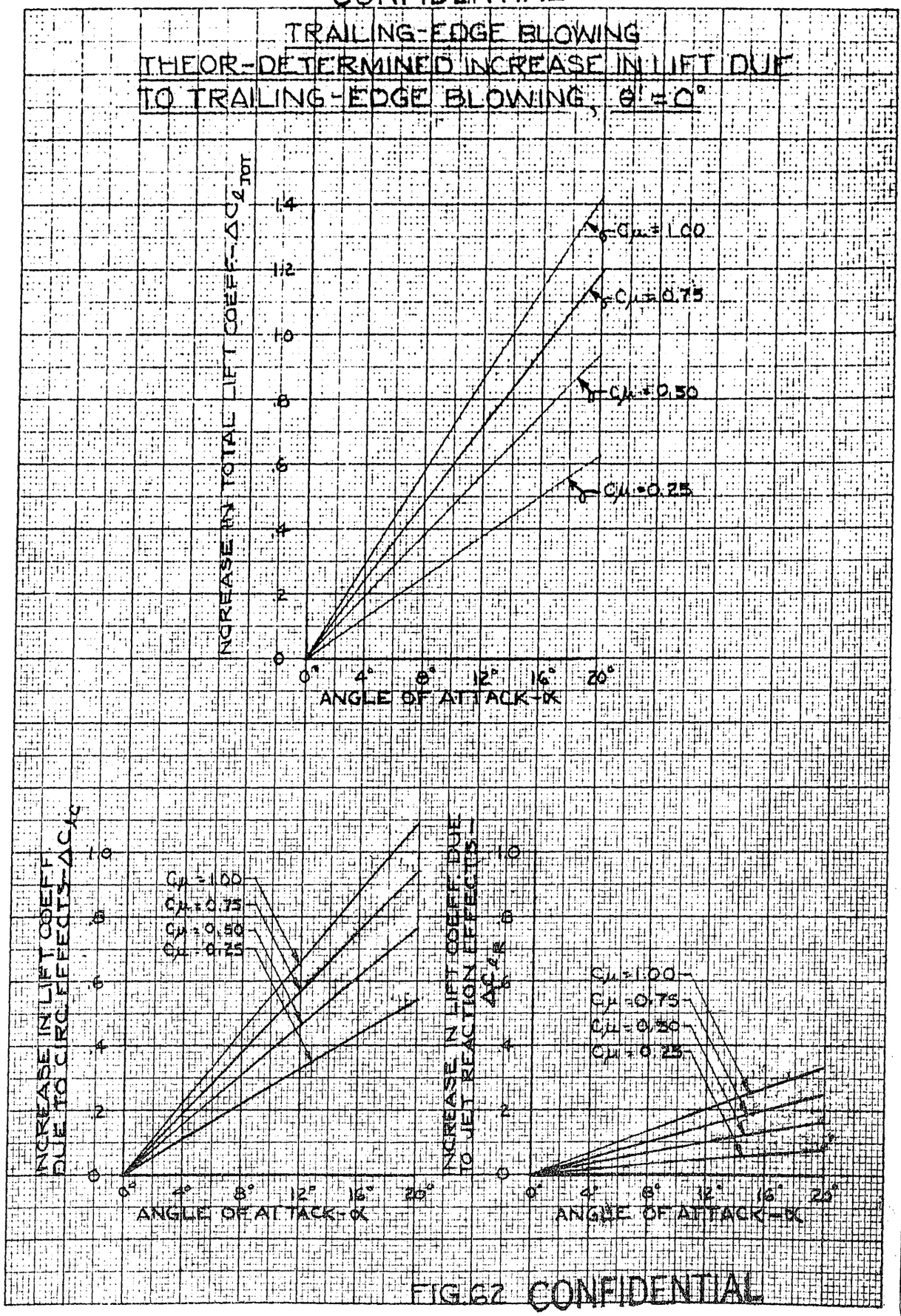
TRAILING-EDGE BLOWING
THEOR-DETERMINED INCREASE IN LIFT DUE TO TRAILING-EDGE BLOWING, δf = 0°
INCREASE IN TOTAL LIFT COEFF.-ΔCL TOT
Cμ = 1.00
Cμ = 0.75
Cμ = 0.50
Cμ = 0.25
ANGLE OF ATTACK-α
INCREASE IN LIFT COEFF. DUE TO CIRC. EFFECTS-ΔCLc
INCREASE IN LIFT COEFF. DUE TO JET REACTION EFFECTS-ΔCLJ

FIG. 62

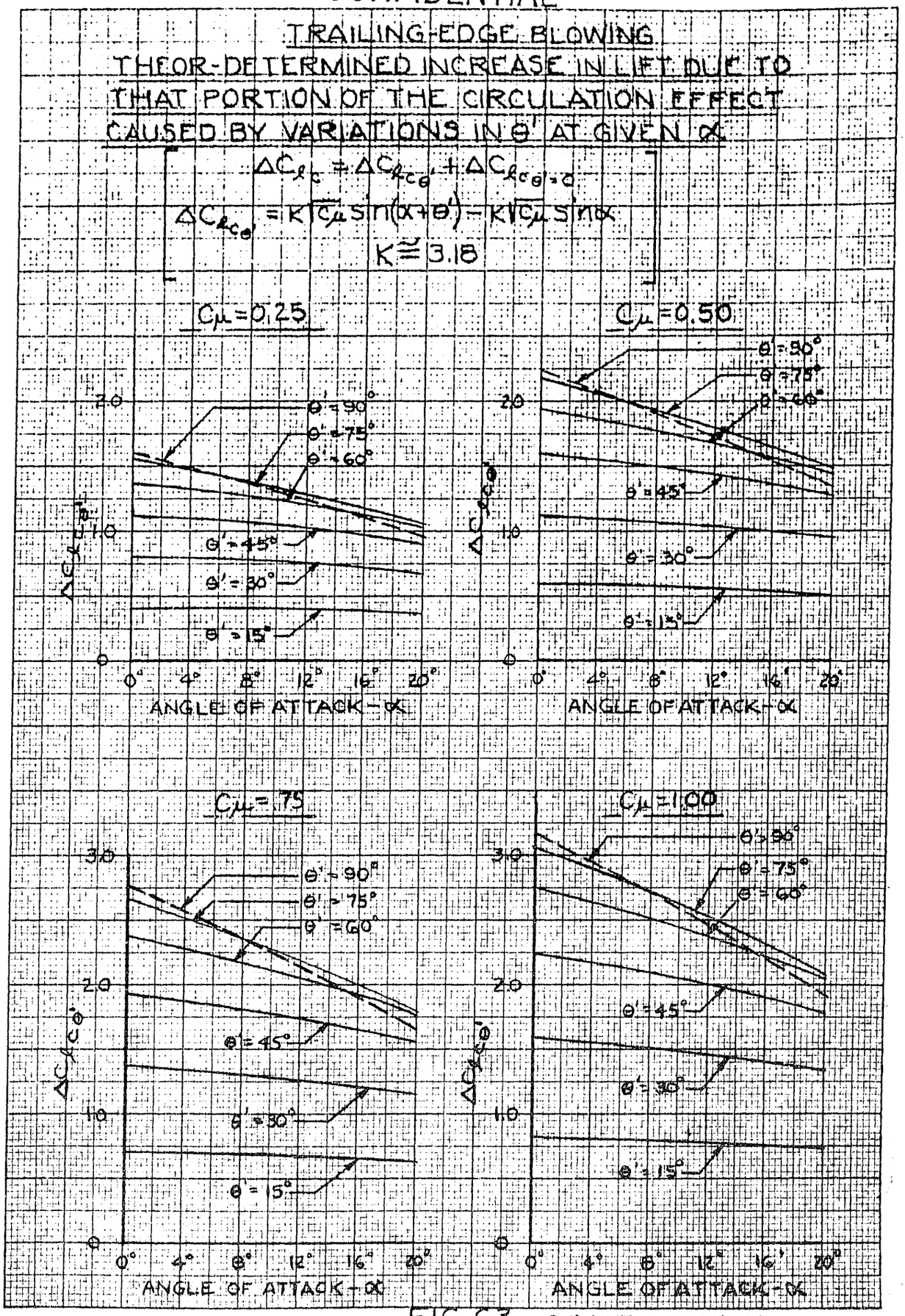
TRAILING-EDGE BLOWING
THEOR-DETERMINED INCREASE IN LIFT DUE TO THAT PORTION OF THE CIRCULATION EFFECT CAUSED BY VARIATIONS IN θ' AT GIVEN α
$\Delta C_{\ell_c} = \Delta C_{\ell_{c\theta'}} + \Delta C_{\ell_{c\theta'=0}}$
$\Delta C_{\ell_{c\theta'}} = K\sqrt{C_\mu}\sin(\alpha+\theta') - K\sqrt{C_\mu}\sin\alpha$
$K \cong 3.18$
$C_\mu = 0.25$
$C_\mu = 0.50$
$C_\mu = .75$
$C_\mu = 1.00$
θ' = 90°
θ' = 75°
θ' = 60°
θ' = 45°
θ' = 30°
θ' = 15°
$\Delta C_{\ell_{c\theta'}}$
ANGLE OF ATTACK - α
0° 4° 8° 12° 16° 20°
0 1.0 2.0 3.0

FIG. 63

TRAILING-EDGE BLOWING

COMPARISON OF THEORY WITH EXPERIMENTAL RESULTS FOR NACA 0018 ($R_N \cong 0.6 \times 10^6$) (EXPERIMENTAL RESULTS OBTAINED FROM REF. 38)

LIFT

(a) $C_{L_{TOT}}$ VS. α FOR $\theta' = 33°$ AND VARIOUS C_μ

EXPERIMENTAL
- ○ $C_\mu = 0$
- □ $C_\mu = 0.08$
- △ $C_\mu = 0.34$
- ◇ $C_\mu = 0.76$
- ▽ $C_\mu = 1.03$

THEORY

$C_\mu = 1.03$, $C_\mu = 0.76$, $C_\mu = 0.34$, $C_\mu = 0.08$, $C_\mu = 0$

TOTAL LIFT COEFF. – $C_{L_{TOT}}$

ANGLE OF ATTACK – α

(b) $C_{L_{TOT}}$ VS. α FOR $C_\mu = 0.5$ AND VARIOUS θ'

EXPERIMENTAL
- ○ $\theta' = 0°$, $C_\mu = 0$
- □ $\theta' = 0°$, $C_\mu = 0.5$
- △ $\theta' = 33°$, $C_\mu = 0.5$
- ◇ $\theta' = 65°$, $C_\mu = 0.5$

THEORY

$\theta' = 65°$, $\theta' = 33°$, $\theta' = 0°$, $C_\mu = 0.5$, $\theta' = 0°$, $C_\mu = 0$

TOTAL LIFT COEFF. – $C_{L_{TOT}}$

ANGLE OF ATTACK – α

FIG. C4 (3 of 3)

CONFIDENTIAL

CONFIDENTIAL

CONFIDENTIAL

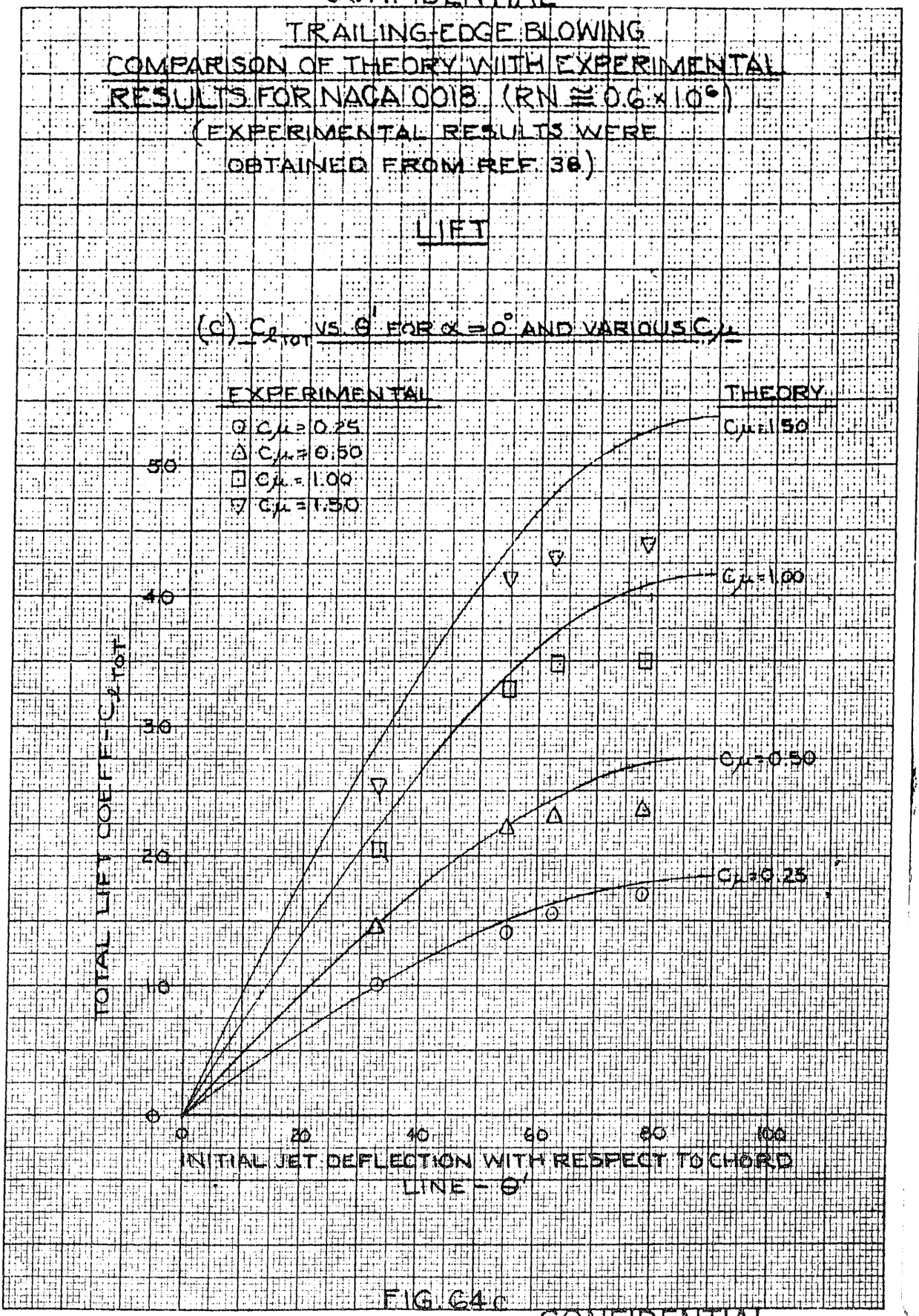

FIG. 64c

CONFIDENTIAL

TRAILING-EDGE BLOWING

COMPARISON OF THEORY WITH EXPERIMENTAL RESULTS FOR NACA 0018 ($R_N \cong 0.6 \times 10^6$)

(EXPERIMENTAL RESULTS WERE OBTAINED FROM REF. 38.)

LIFT

(a) $\Delta C_{L_{TOT}}$ VS C_μ FOR $\alpha = 0°$ AND $\theta' = 32°$

(b) $\frac{dC_L}{d\alpha}$ VS C_μ FOR $\alpha = 0°$ AND $\theta' = 32°$

FIG. 64 (a) & (b)

TRAILING-EDGE BLOWING

SOME POSSIBLE JET FLAP CONFIGURATIONS

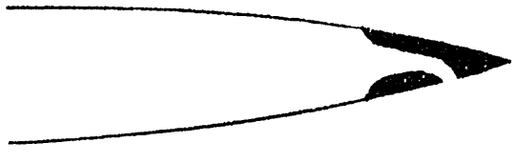

(A) FIXED DEFLECTION

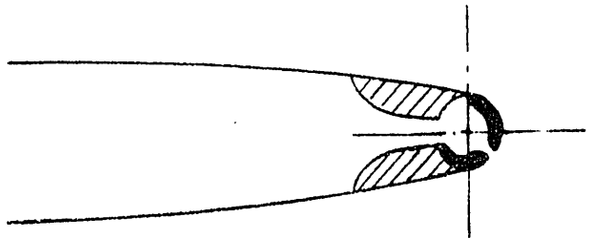

(B) VARIABLE DEFLECTION

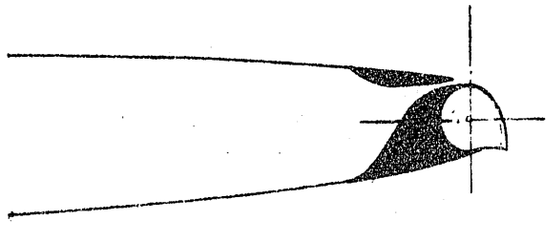

(C) VARIABLE DEFLECTION
UTILIZING "COANDA" EFFECT

FIG. 65

CONFIDENTIAL

TRAILING-EDGE BLOWING

RELATIONSHIP OF DESIGN INITIAL JET ANGLE, θ, WITH ACTUAL INITIAL JET ANGLE, θ', FOR CONFIGURATIONS TESTED IN REF. 38 (STATIC TESTS)

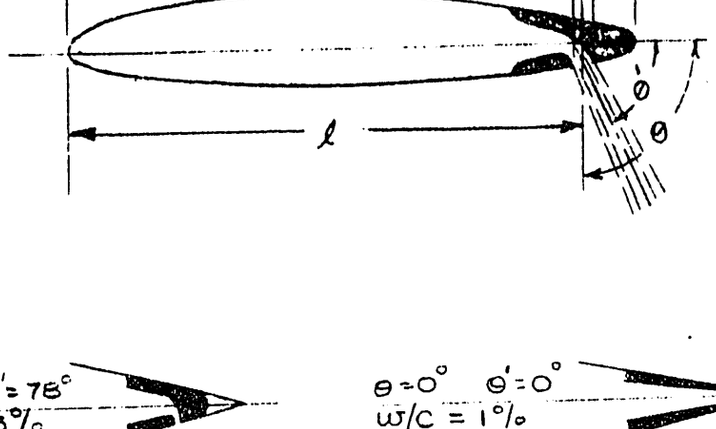

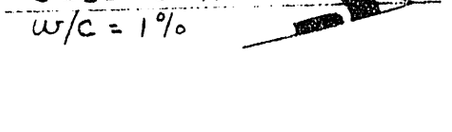

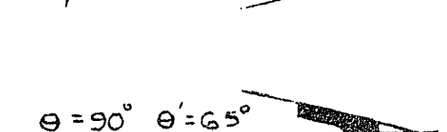

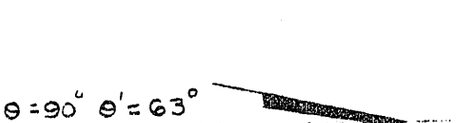

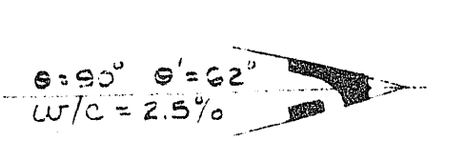

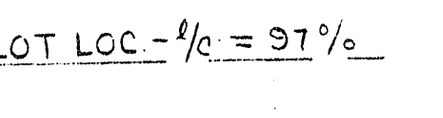

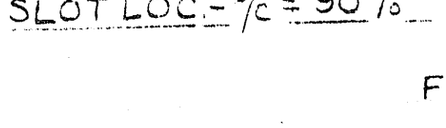

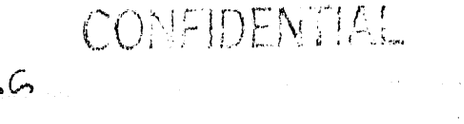

SLOT LOC. - ℓ/c = 97%

SLOT LOC. - ℓ/c = 90%

CONFIDENTIAL

FIG. 66

CONFIDENTIAL

TRAILING-EDGE BLOWING

"LIFTING EFFICIENCY"

COMPARISON OF THEORY WITH EXPERIMENTAL RESULTS FOR NACA 0018 ($R_N \cong 0.6 \times 10^6$)

(EXPERIMENTAL RESULTS WERE OBTAINED FROM REF 38.)

EXPERIMENTAL DATA

SLOT LOCATION 90% CHORD			SLOT LOCATION 97% CHORD		
SYMBOL	SLOT WIDTH % CHORD	θ' DEG.	SYMBOL	SLOT WIDTH	θ' DEG.
□	.5	78	●	.0	33
×	1.0	71	◆	.0	55
+	1.3	68	■	.0	63
○	2.0	65			
△	2.5	62			

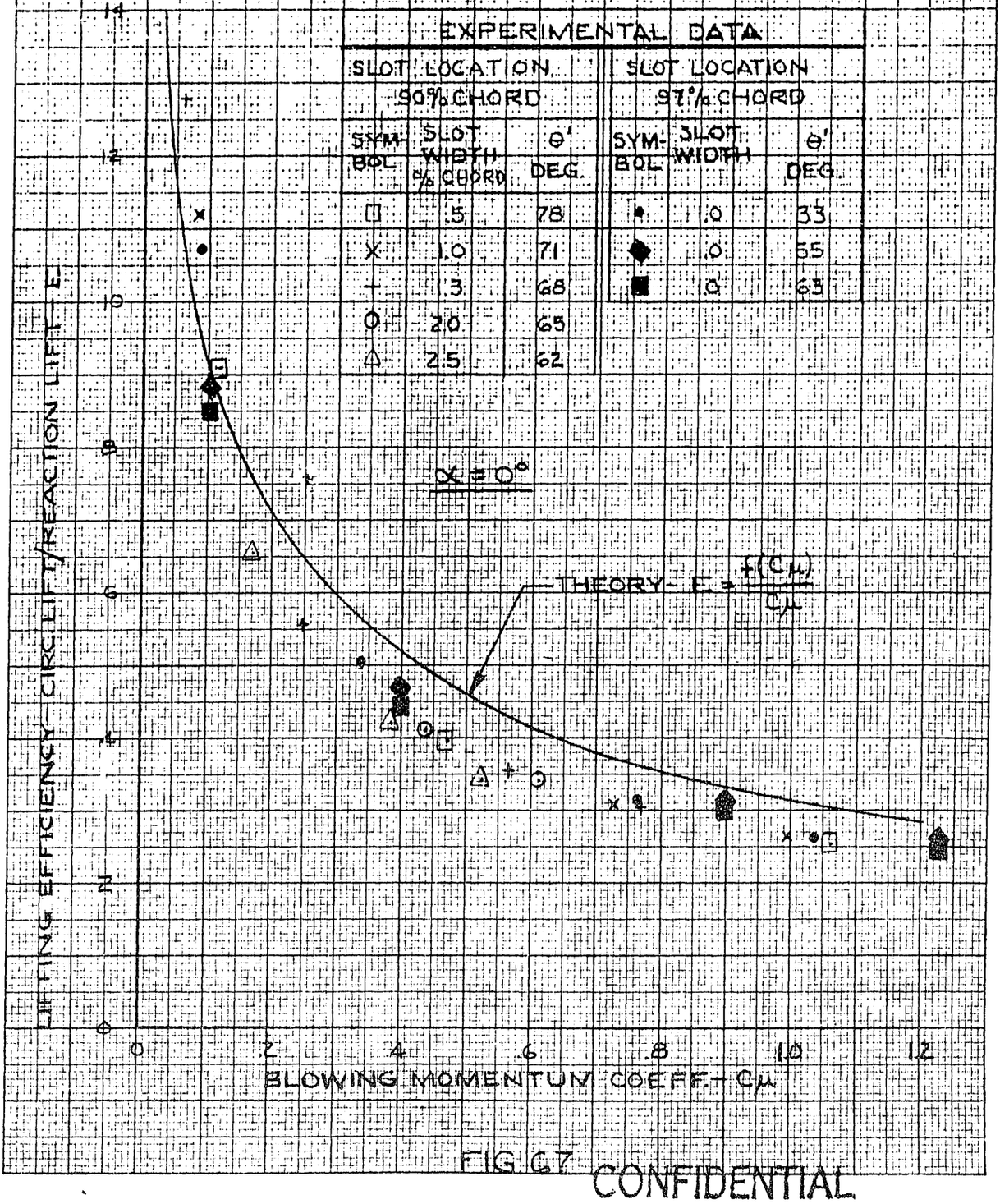

FIG 6.7

CONFIDENTIAL

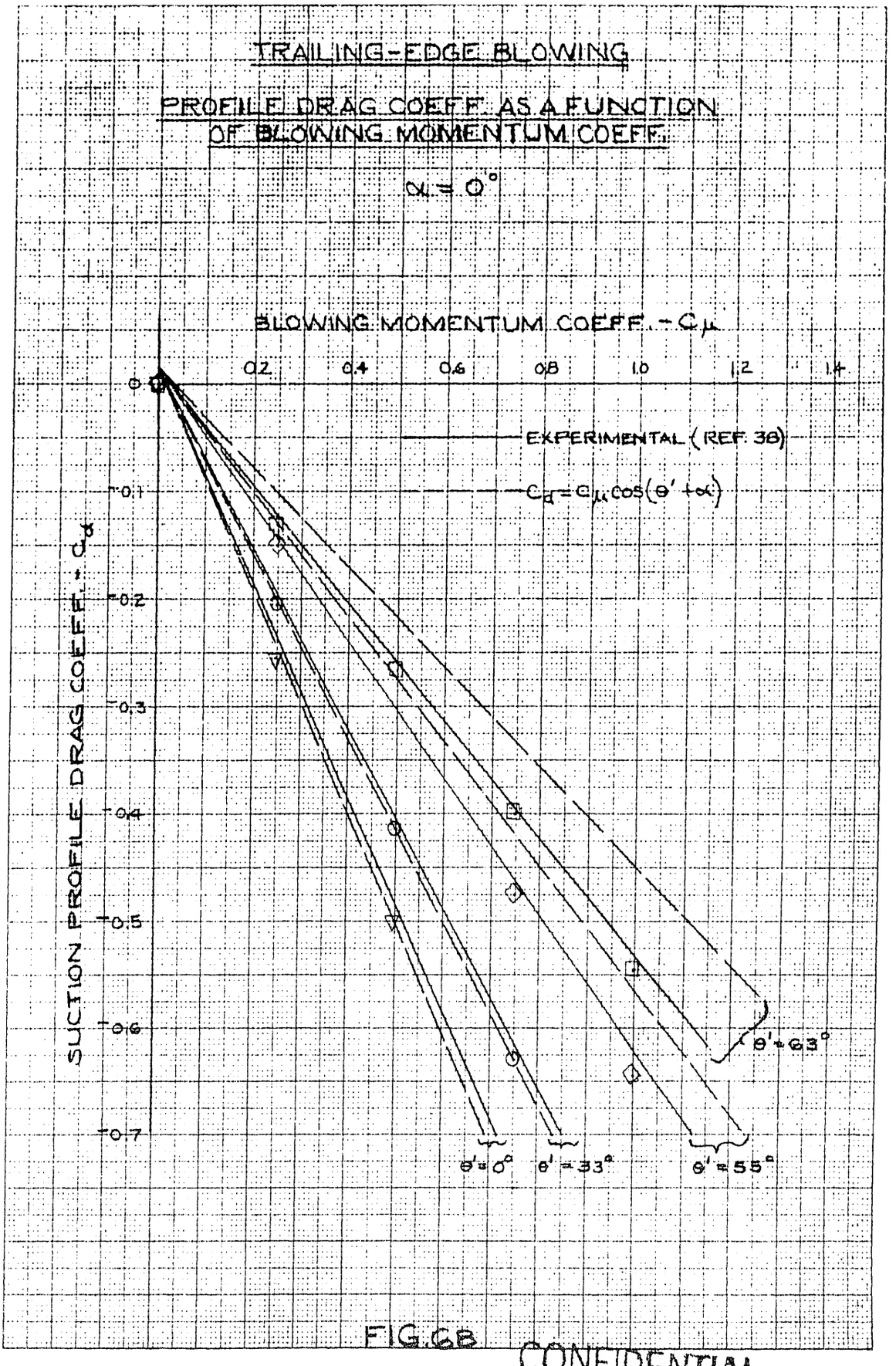

FIG. 6B

TRAILING-EDGE BLOWING
APPROXIMATE VARIATION IN PITCHING MOMENT COEFFICIENT WITH C_μ AND LIFT INCREMENT DUE TO TRAILING-EDGE BLOWING

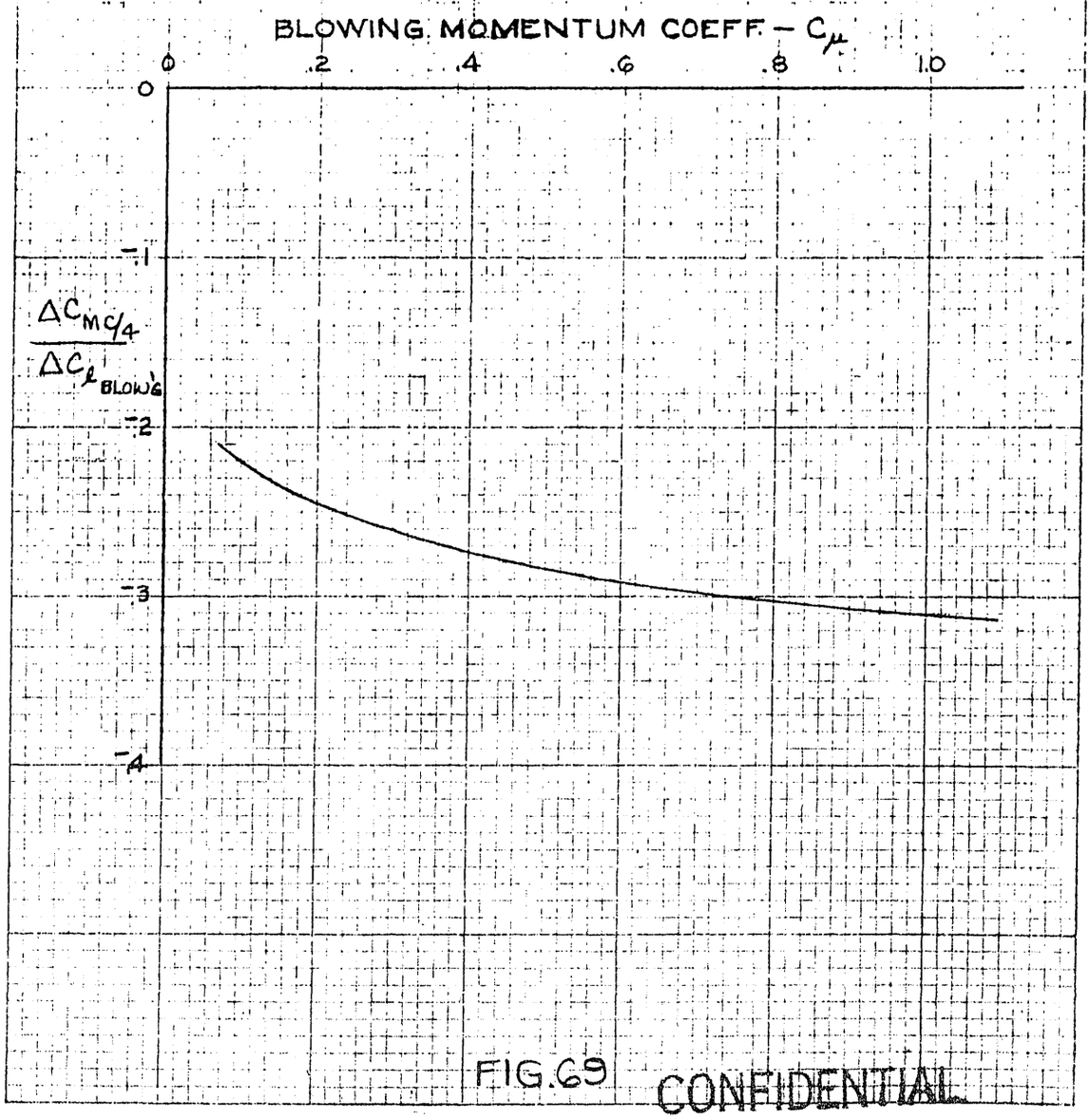

FIG. 69

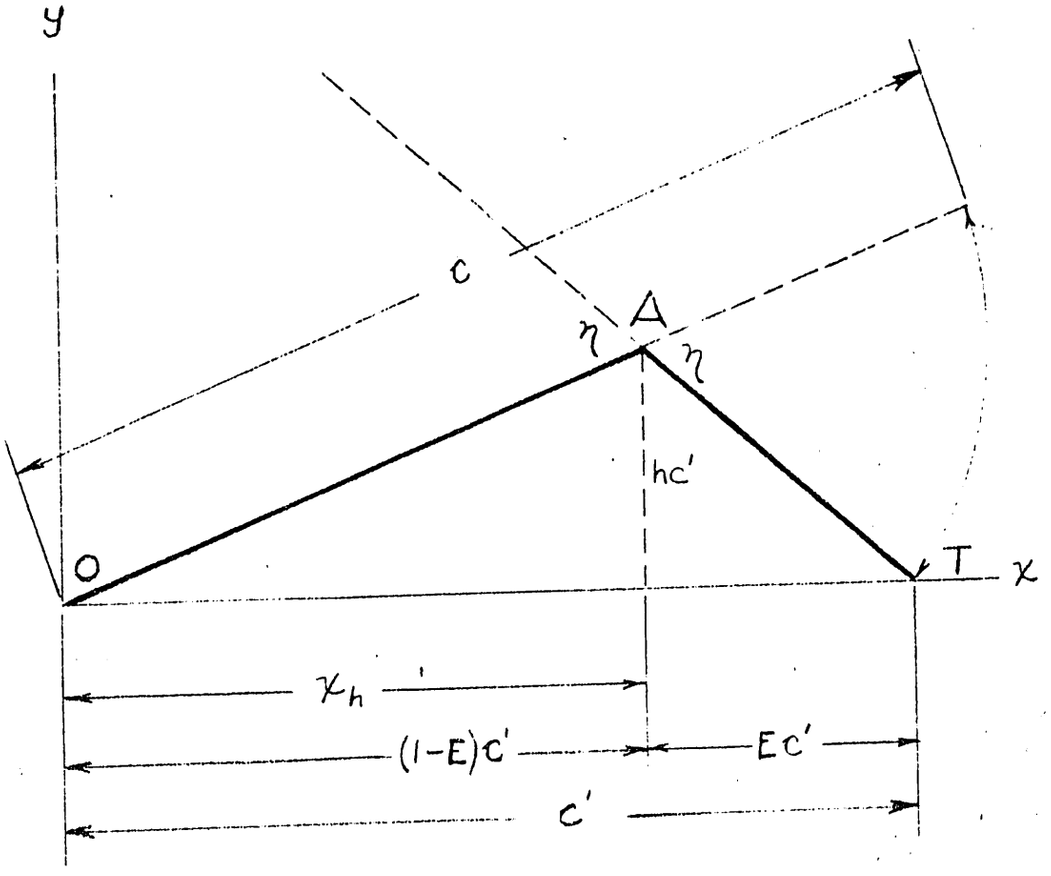

THIN AIRFOIL ANALYSIS
WHERE C' IS NOT ASSUMED = C

FIG. 70

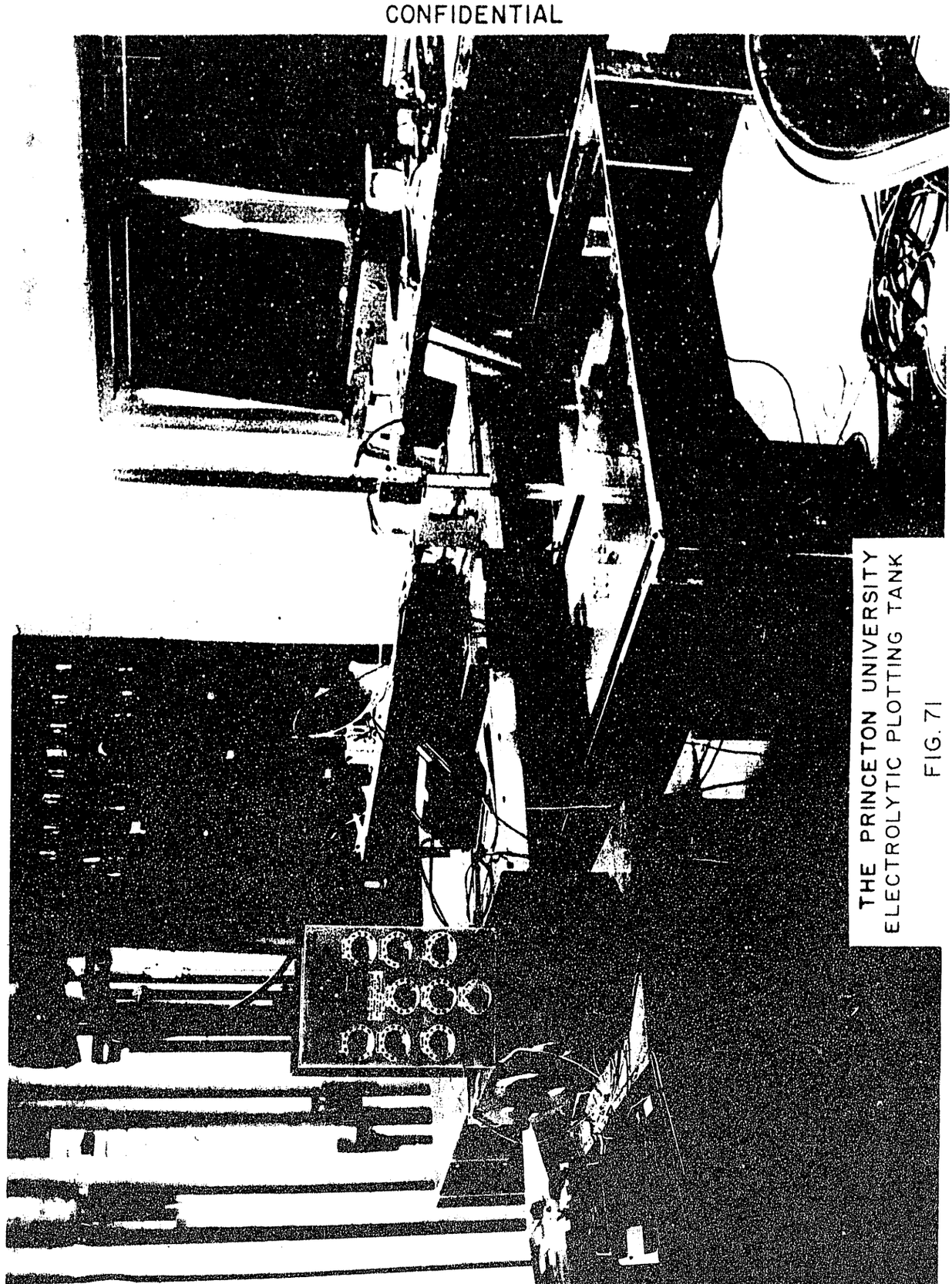

THE PRINCETON UNIVERSITY
ELECTROLYTIC PLOTTING TANK

FIG. 71

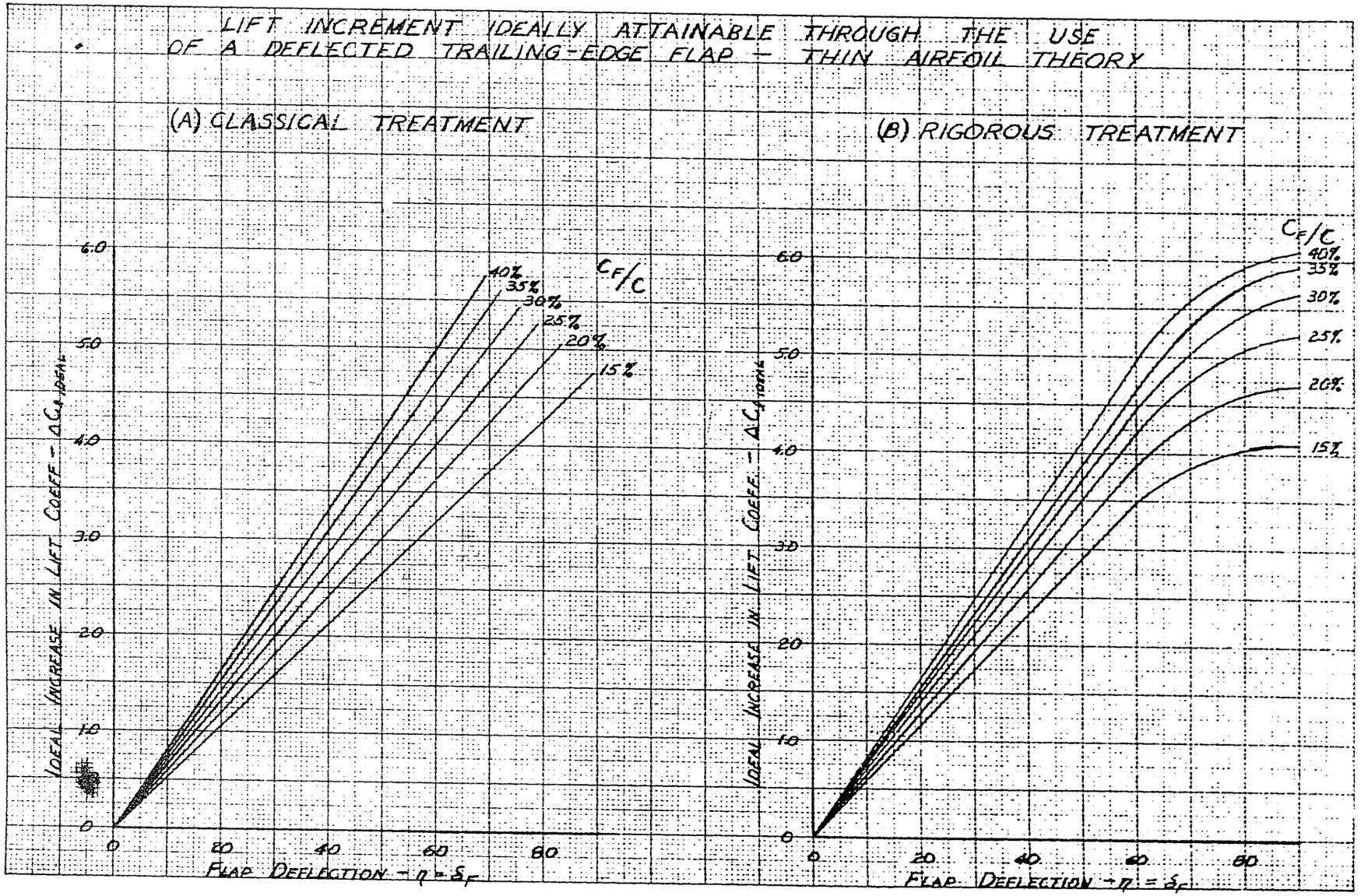

FIG. 72

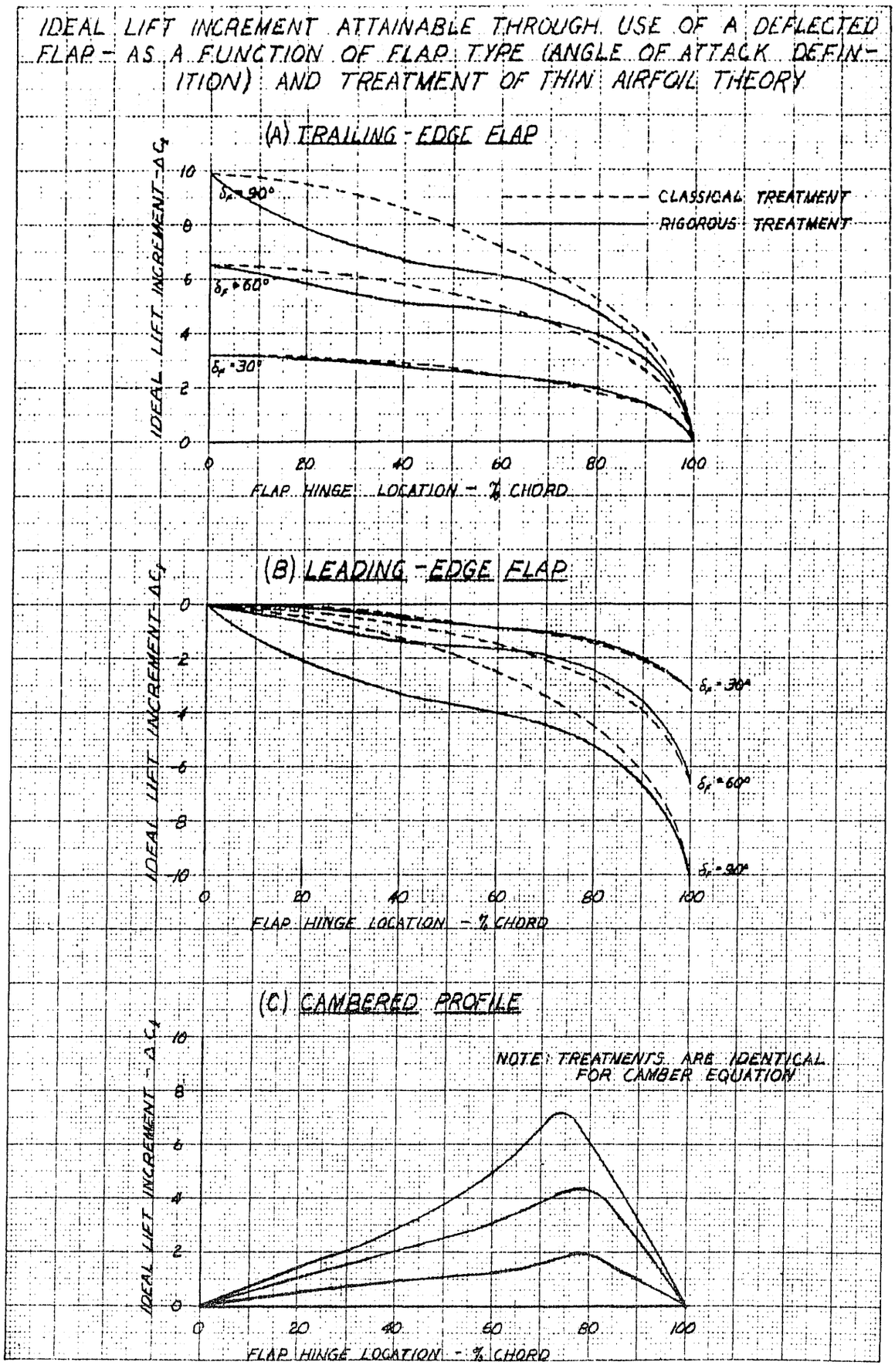

FIG. 73

TRAILING-EDGE FLAPS.
TYPICAL CURVES OF SECTION LIFT COEFF. VS. ANGLE OF ATTACK FOR PROFILES WITH TRAILING-EDGE FLAPS-VARIOUS FLAP DEFLECTIONS.

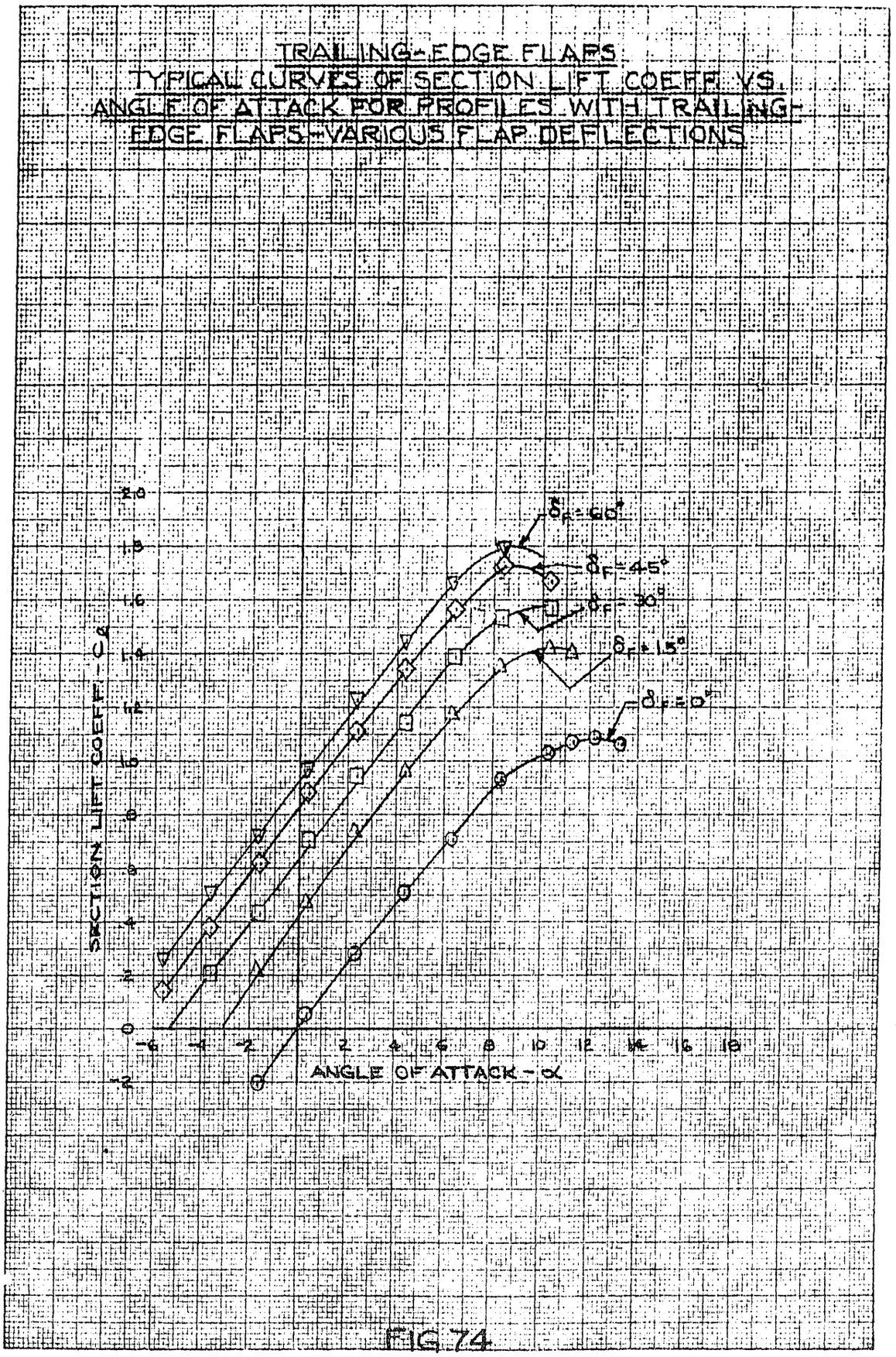

FIG 74

TRAILING EDGE FLAPS

TYPICAL VARIATION IN CHORDWISE PRESSURE DISTRIBUTION CREATED THROUGH DEFLECTION OF A TRAILING-EDGE FLAP

$\alpha = 8°$ 23012 AIRFOIL

PLAIN FLAP - $C_F/C = 20\%$

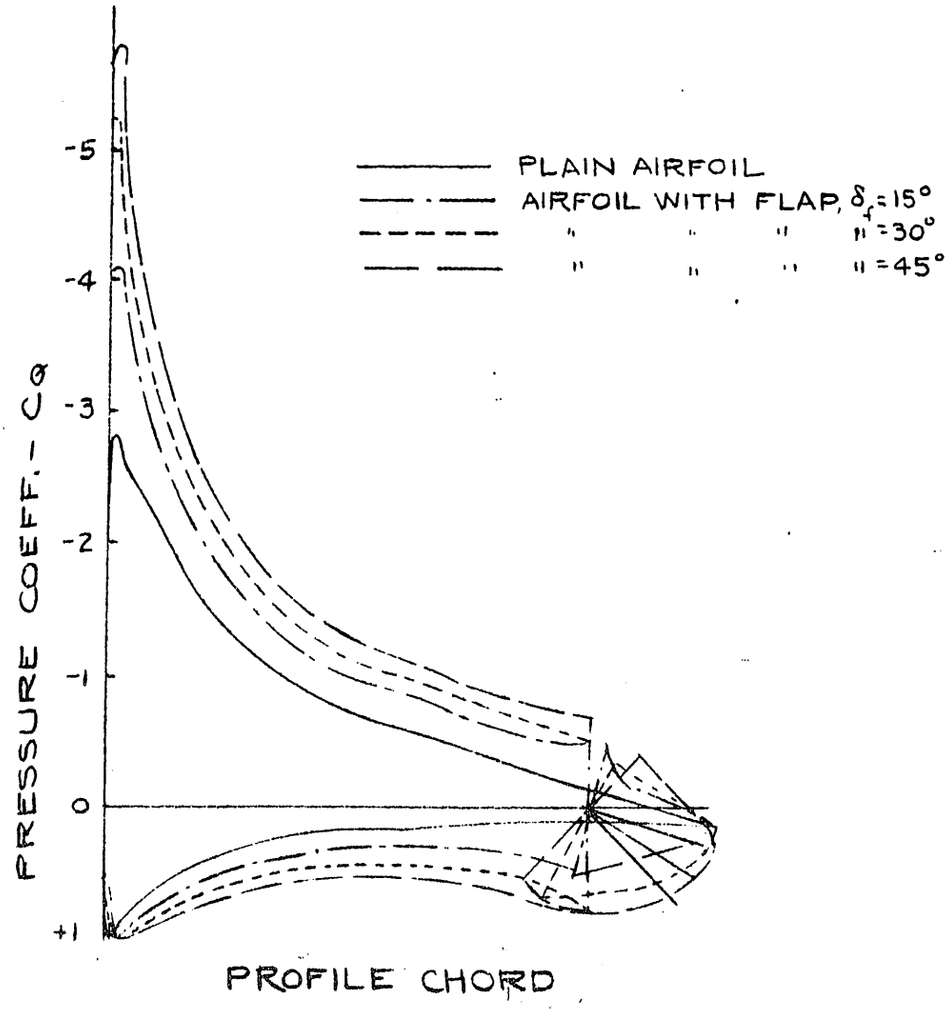

FIG. 75

TRAILING-EDGE FLAPS

EFFECTS OF PROFILE THICKNESS AND SHAPE ON CIRCULATION LIFT INCREMENT DUE TO A DEFLECTED FLAP

20% C SPLIT FLAP
R.N. = 6×10^6
$\delta_f = 60°$
SYMMETRICAL PROFILES

◇ 63 SERIES PROFILES
□ 64 SERIES PROFILES
△ 65 SERIES PROFILES

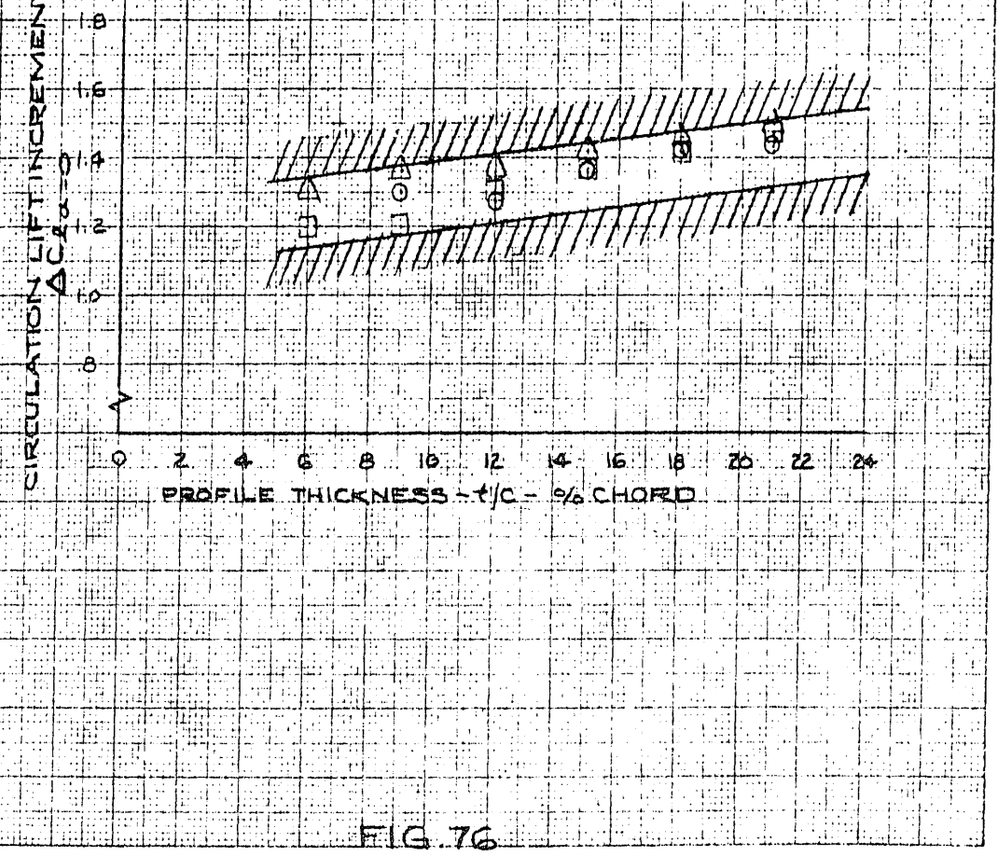

FIG. 76

PLAIN FLAP

EFFECTS OF GAP SIZE ON CIRCULATION LIFT INCREMENT DUE TO A DEFLECTED PLAIN FLAP

20% C. PLAIN FLAP
R.N. ≅ 2.8 × 10⁶
$\delta_F = 15°$
VARIOUS PROFILE

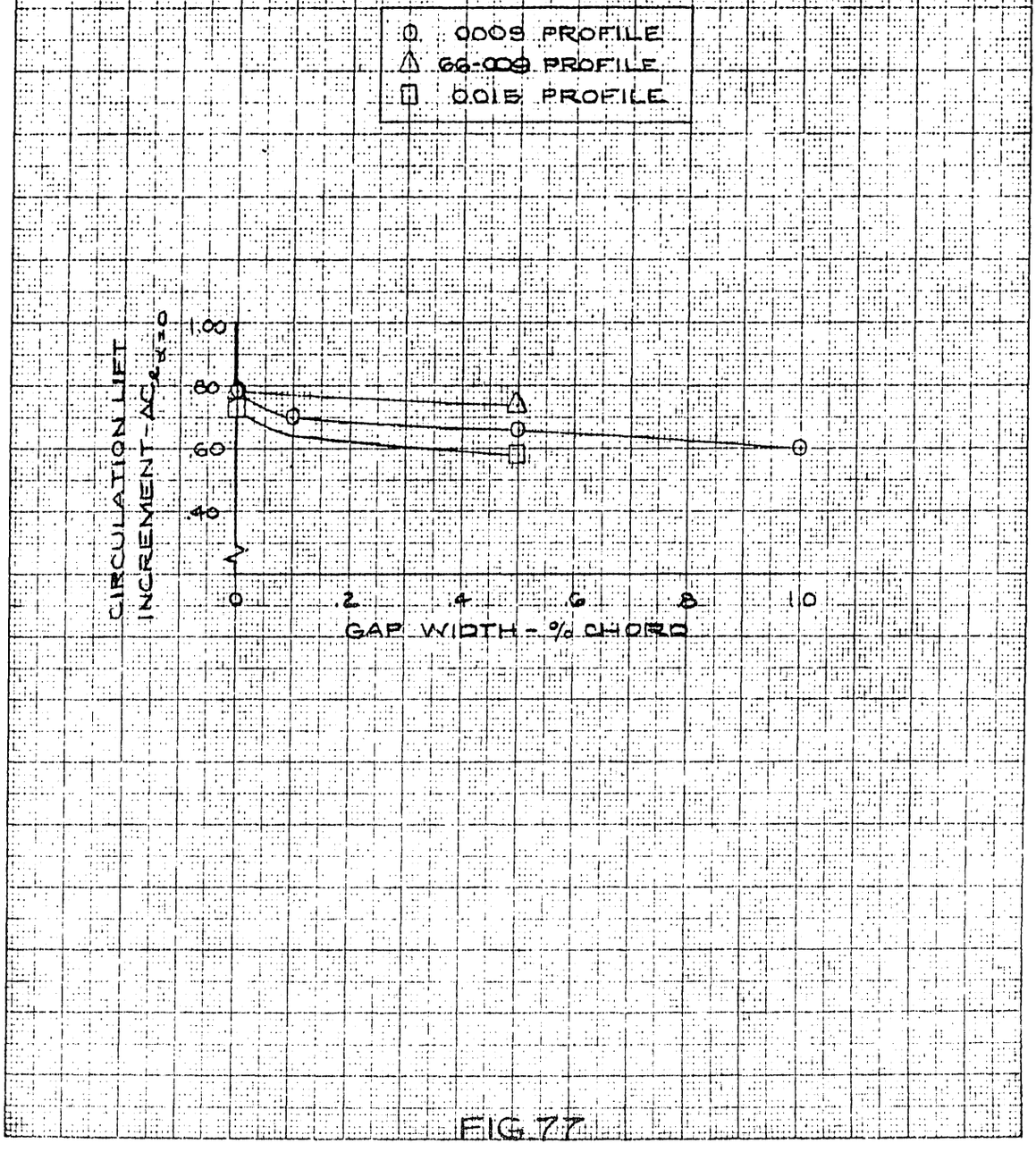

FIG. 77

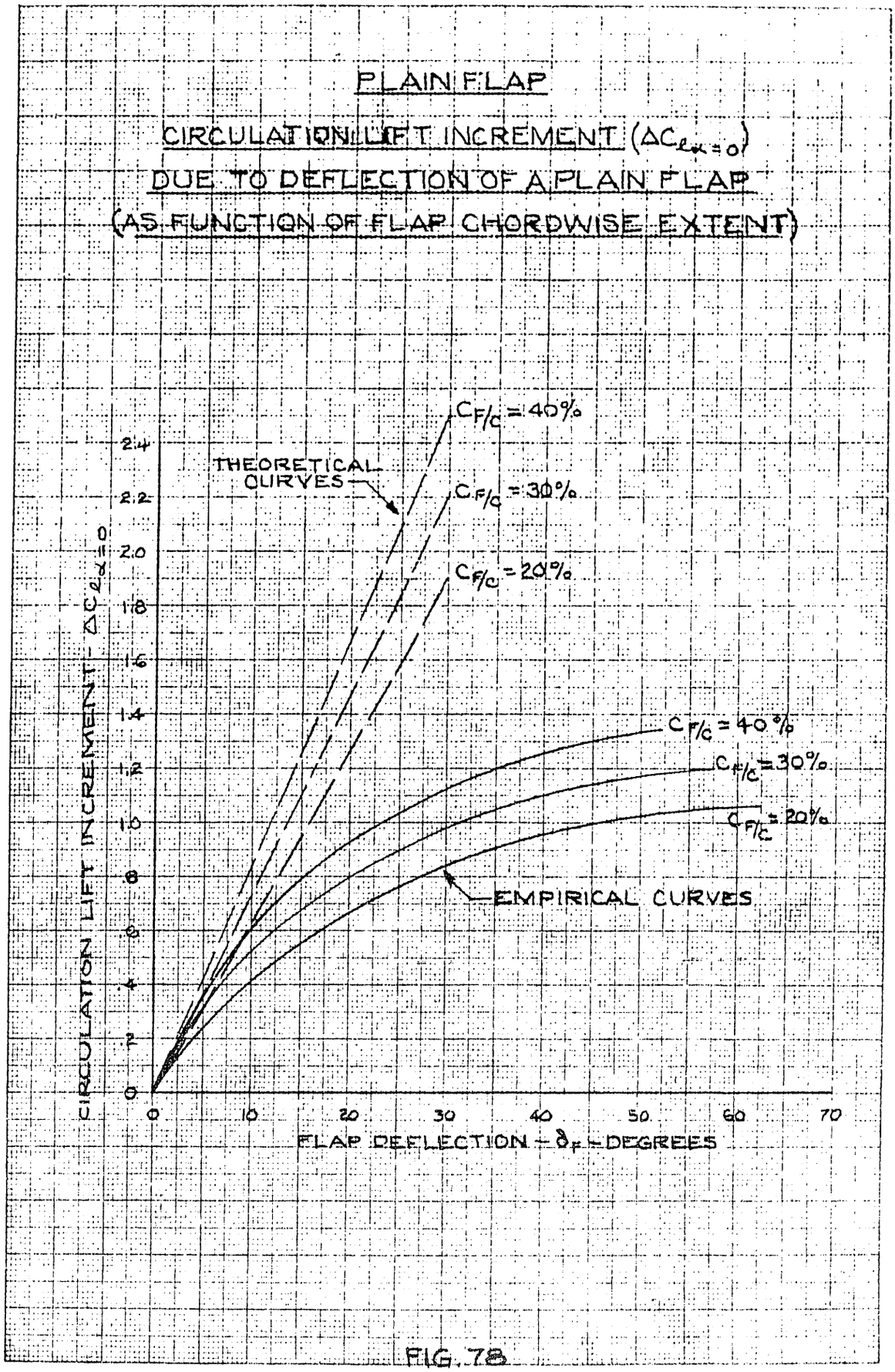

FIG. 78

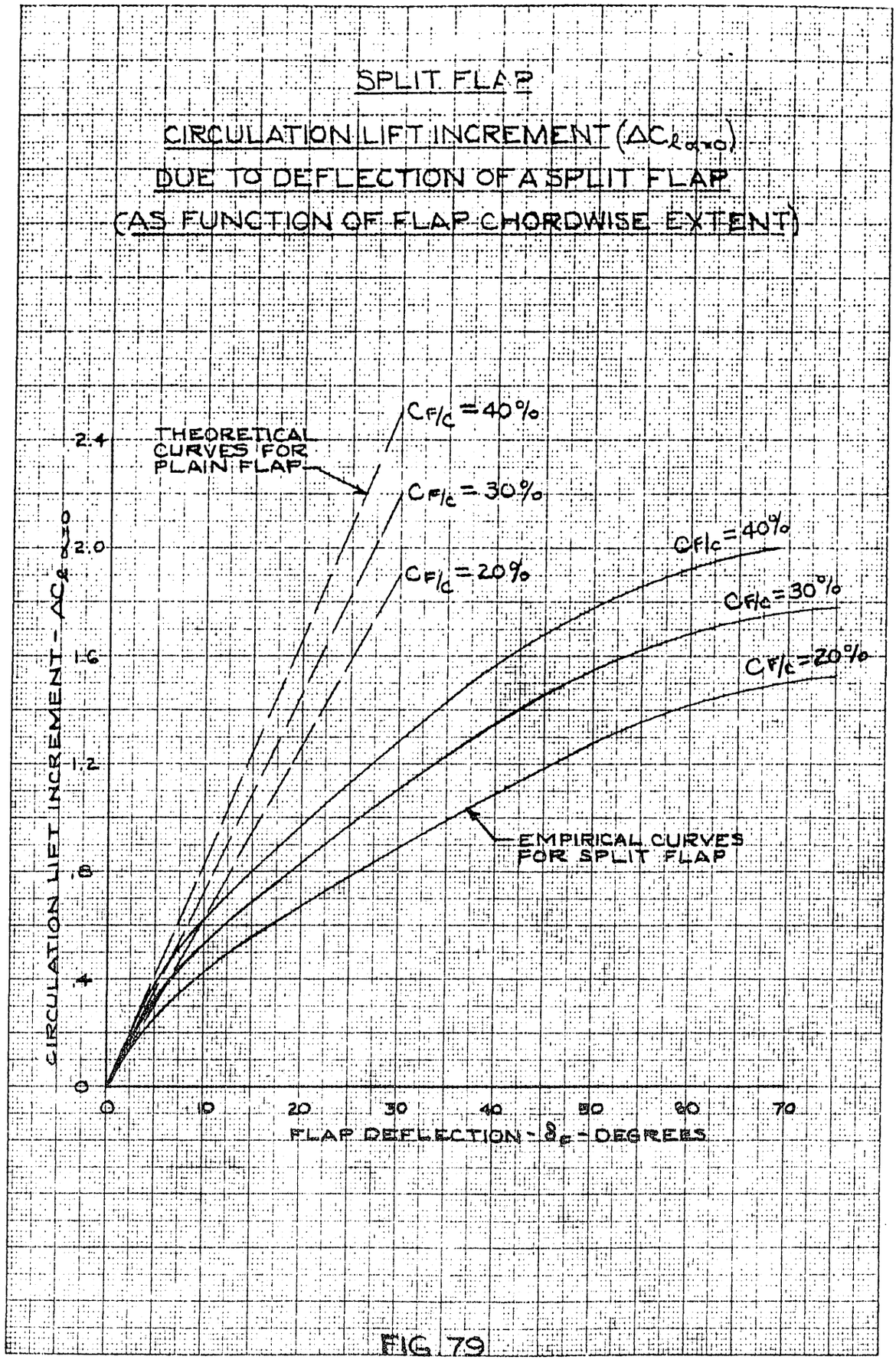

FIG. 79

SINGLE-SLOTTED FLAP

TYPICAL SINGLE-SLOTTED FLAP CONFIGURATION

(A) TYPICAL OVERALL CONFIGURATION SHOWING STANDARD DIMENSIONS

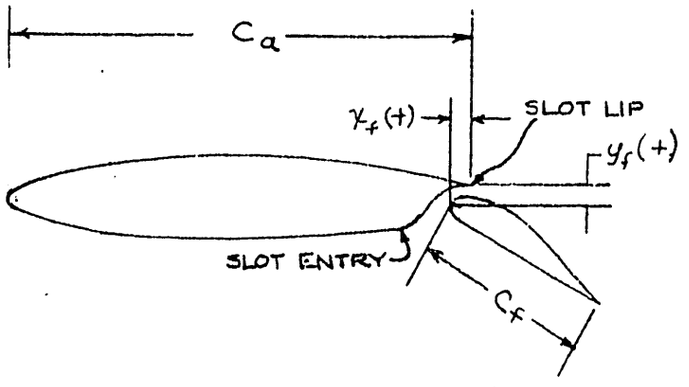

(B) TYPICAL SLOT-ENTRY CONFIGURATIONS

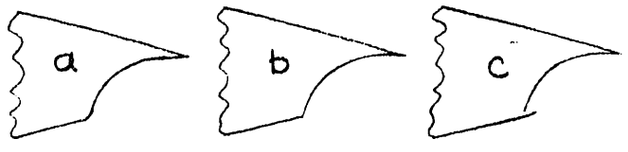

(C) TYPICAL FLAP NOSE CONFIGURATIONS

FIG. 80

CONFIDENTIAL

SINGLE-SLOTTED FLAP

CONTOURS OF FLAP POSITION FOR MAXIMUM SECTION LIFT COEFF. FOR AN AIRFOIL EQUIPPED WITH SINGLE SLOTTED FLAP - AS FUNCTION OF FLAP CONFIGURATION

66, 2-216, a=0.6 AIRFOIL $c_{F/c} = 25\%$

$\delta_F = 40^\circ$ R.N. $= 5.1 \times 10^6$

(A) SLOT ENTRY "a"

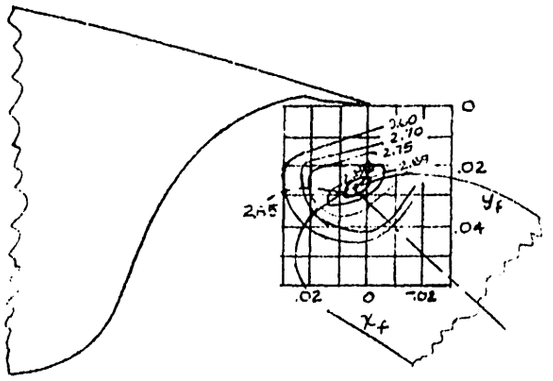

(B) SLOT ENTRY "c"

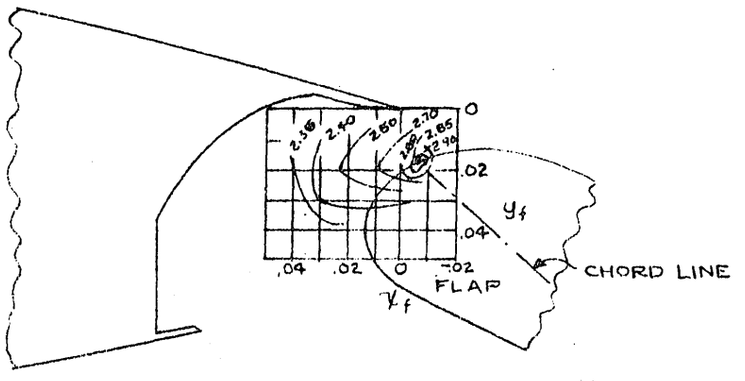

FIG. 81

SINGLE-SLOTTED FLAP

EFFECT OF FLAP CONFIGURATION UPON MAXIMUM LIFT CHARACTERISTICS OF PROFILES WITH SINGLE-SLOTTED FLAPS

AIRFOIL SECTION	c_f/c	$\frac{c_a}{c}$	SLOT-ENTRY CONFIG-URATION	FLAP NOSE SHAPE	$c_{l_{max}}$	f (deg)	$\frac{x_f}{c}$	$\frac{y_f}{c}$	R.N.
Clark Y	0.20	1.00	b	A	2.44	30	0	-0.025	0.61×10
Clark Y	.30	1.00	b	A	2.83	40	0	-.025	.61
Clark Y	.40	1.00	b	A	3.10	40	0	-.025	.61
23012	.10	.93	a	A	2.25	50	.004	.005	3.5
23012	.15	1.00	b	A	2.68	30	0	.015	3.5
23012	.25	1.00	b	A	3.22	40	0	.015	3.5
23012	.256	.800	a	B	2.76	50	.005	.018	3.5
23012	.257	.83	a	A	2.81	50	.005	.016	3.5
23012	.257	.83	a	A	2.83	40	.013	.024	3.5
23012	.267	1.00	b	A	2.90	30	0	.025	3.5
23012	.30	.90	c	A	2.92	50	.002	.010	3.5
23012	.30	.90	c	A	2.92	40	.002	.020	3.5
23012	.30	.90	c	A	2.93	30	.002	.030	3.5
23012	.30	.90	b	A	2.88	40	.002	.020	3.5
23012	.30	1.00	b	A	3.29	40	0	.015	3.5
23012	.40	.715	b	A	2.87	50	.015	.015	3.5
23012	.40	.715	a	A	2.90	50	.015	.015	3.5
23012	.15	1.00	b	A	2.59	60	0	.015	3.5
23012	.15	1.00	b	A	2.66	60	.050	.030	3.5
23012	.25	1.00	b	A	3.17	40	.025	.015	3.5
23012	.257	.827	b	B	2.69	60	0	.015	3.5
23012	.257	.827	a	B	2.74	60	0	.015	3.5
23012	.257	.827	b	A	2.71	60	.005	.020	3.5
23012	.257	.827	a	A	2.82	50	0	.025	3.5
23012	.40	.715	b	A	2.79	50	.015	.025	3.5
23012	.40	.715	a	A	2.88	50	.015	.045	3.5
23030	.257	.860	b	B	2.59	60	.025	.040	3.5

FIG. 82

CONFIDENTIAL

AIRFOIL SECTION	c_f/c	$\frac{c_a}{c}$ 100	SLOT-ENTRY CONFIG-URATION	FLAP NOSE SHAPE	$c_{l_{max}}$	f (deg)	$\frac{x_f}{c}$ 100	$\frac{y_f}{c}$ 100	R.N.
23030	.257	.860	a	B	2.68	60	-.005	.040	3.5
23030	.40	.775	b	B	2.82	50	.025	.060	3.5
23030	.40	.775	a	B	2.90	50	.025	.060	3.5
63,4-420	.25	.88	b	B	3.00	35	.018	.045	6.0
60,4-421 (approx.)	.243	.835	a	A	3.21	40	0	.027	9.0
65-210	.25	.84	c	A	2.47	45	.009	.010	6.0
65-210	.25	.90	c	A	2.48	41.3	.014	.009	6.0
65-210	.25	.975	c	A	2.45	35	.004	.020	6.0
65 A111 (approx.)	.35	.839	c	A	2.69	35	-.020	.032	9.0
65$_1$-213 (approx.)	.336	.889	c	A	2.63	40	.019	.046	9.0
65 -114	.259	.915	c	A	2.80	40	.019	.038	9.0
65,2-221 (approx.)	.263	.832	a	B	2.83	30	.025	.046	9.95
66(215)-116, a = 0.6	.25	.824	c	B	2.70	55	0	.028	6.0
66,2-116, a = 0.6	.25	.827	a	A	2.69	45	.017	.038	6.0
66,2-216, a = 0.6	.30	.90	c	A	2.92	37	0	.016	6.0
66,2-216, a = 0.6	.25	.824	a	A	2.89	40	.023	.040	5.1
66,2-216, a = 0.6	.25	.834	c	A	2.88	45	.011	.031	5.1
66,2-118	.25	.90			2.68	32.5			6.0

FIG. 82 (CON'T)

DOUBLE-SLOTTED FLAP

TYPICAL DOUBLE-SLOTTED FLAP CONFIGURATION

(A) FLAP RETRACTED CONDITION

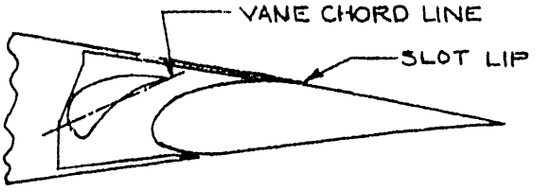

(B) FLAP DEFLECTED CONDITION, SHOWING STANDARD DIMENSIONS

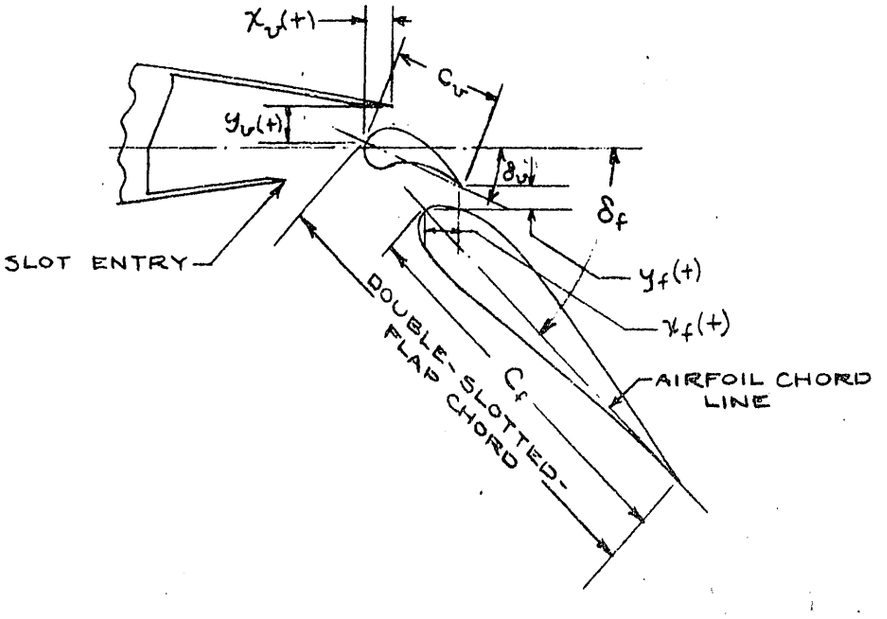

FIG. 83

DOUBLE-SLOTTED FLAP

CONTOURS OF FLAP AND VANE POSITION FOR MAXIMUM SECTION LIFT COEFF. FOR AN AIRFOIL EQUIPPED WITH DOUBLE-SLOTTED FLAP

64,-212 AIRFOIL
R.N. = 6×10^6

$c_{F/c}$ = 25%
δ_F = 50°

(A) UPPER-SLOT CONTOUR

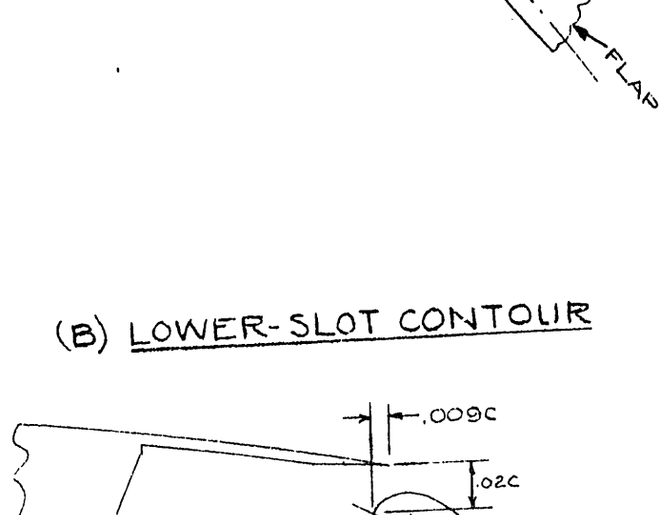

(B) LOWER-SLOT CONTOUR

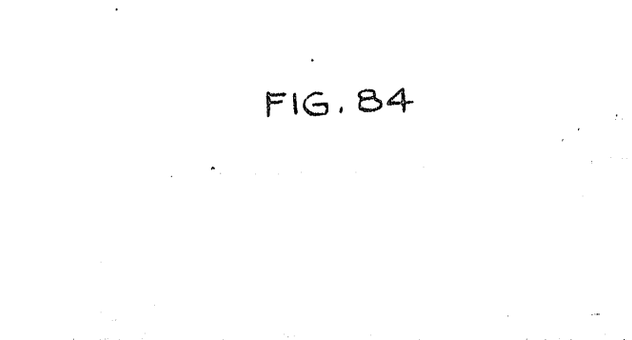

FIG. 84

DOUBLE-SLOTTED FLAP

EFFECT OF FLAP CONFIGURATION UPON MAXIMUM LIFT CHARACTERISTICS OF PROFILES WITH DOUBLE-SLOTTED FLAPS

AIRFOIL SECTION	c_f/c	c_v/c	$\frac{c_a}{c} \times 100$	$c_{l_{max}}$	f (deg)	v (deg)	$\frac{x_f}{c} \times 100$	$\frac{y_f}{c} \times 100$	$\frac{x_v}{c} \times 100$	$\frac{y_v}{c} \times 100$	R.N.
23012	0.10	0.189	0.83	2.99	70	40	0.009	0.009	0.014	0.024	3.5×10^6
23012	.257	.227	.715	3.47	70	30	.014	.012	.015	.035	3.5
23012	.257	.227	.715	3.56	60	30	.019	.024	.025	.065	3.5
23030	.257	.260	.715	3.71	80	40	.049	.050	.045	.040	3.5
23012	.257	.117	.826	3.30	60	25	-.016	-.004	-.004	.017	3.5
23021	.257	.147	.827	3.32	70	30	.017	.027	.007	.024	3.5
63-210	.25	.075	.84	2.91	50	25	.022	.024	.024	.018	6.0
63,4-421 (approx.)	.195	.083	.87	3.30	55	14	.038	.012	-.009	.016	6.0
64-208	.25	.075	.84	2.51	45	30	.015	.015	.015	.019	6.0
64-208	.25	.056	.84	2.40	50	25	.018	.014	.015	.024	6.0
64-210	.25	.075	.84	2.82	55	30	.023	.006	.012	.018	6.0
64_1-212	.25	.075	.84	3.03	50	30	.021	.020	.010	.019	6.0
64_1A212	.229	.083	.833	2.83	55	26	.044	.005	.004	.014	6.0
65-210	.25	.075	.84	2.72	50	25	.025	.011	.009	.024	6.0
65(216)-215, a = 0.8	.248	.096	.82	3.38	70	12	.024	.010	.025	.032	6.3
65_3-118	.244	.10	.864	3.35	65	23	.038	.007	.009	.025	6.0
65_3-418	.236	.106	.851	3.50	65	21	.027	.007	.012	.028	6.0
65_4-421	.236	.109	.85	3.08	51	20	.029	.017	.012	.024	2.2
66-210	.25	.075	.84	2.64	55	25	.029	.023	.012	.022	6.0
66-210	.25	.100	.84	2.72	60	25	.027	.039	.024	.021	6.0
66_2-214 (approx.)	.227	.085	.854	3.00	55	20	.044	.009	.004	.025	9.0
1410	.25	.075	.84	3.06	50	25	.026	.016	.012	.019	6.0

FIG. 85

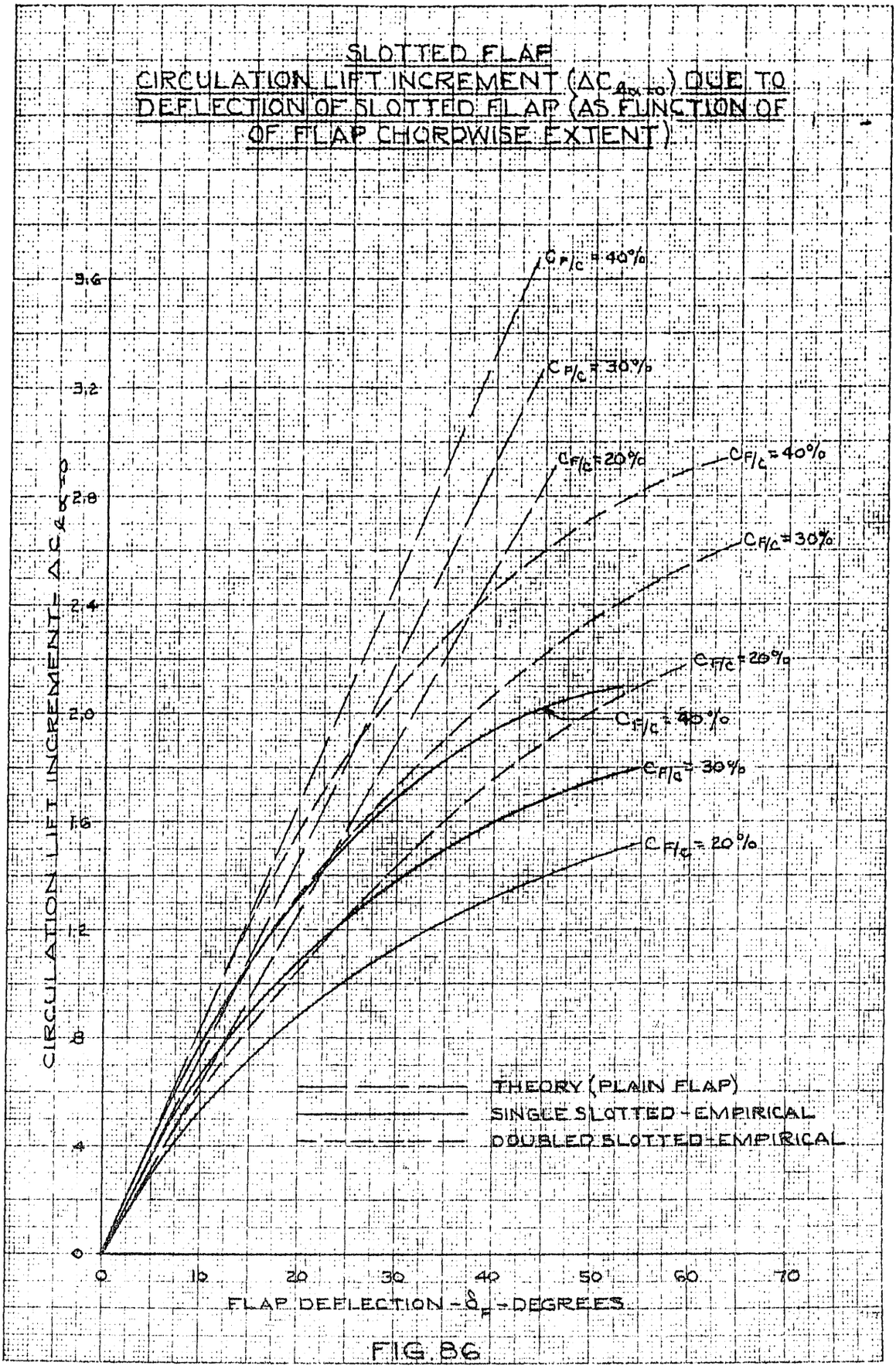

FIG. 86

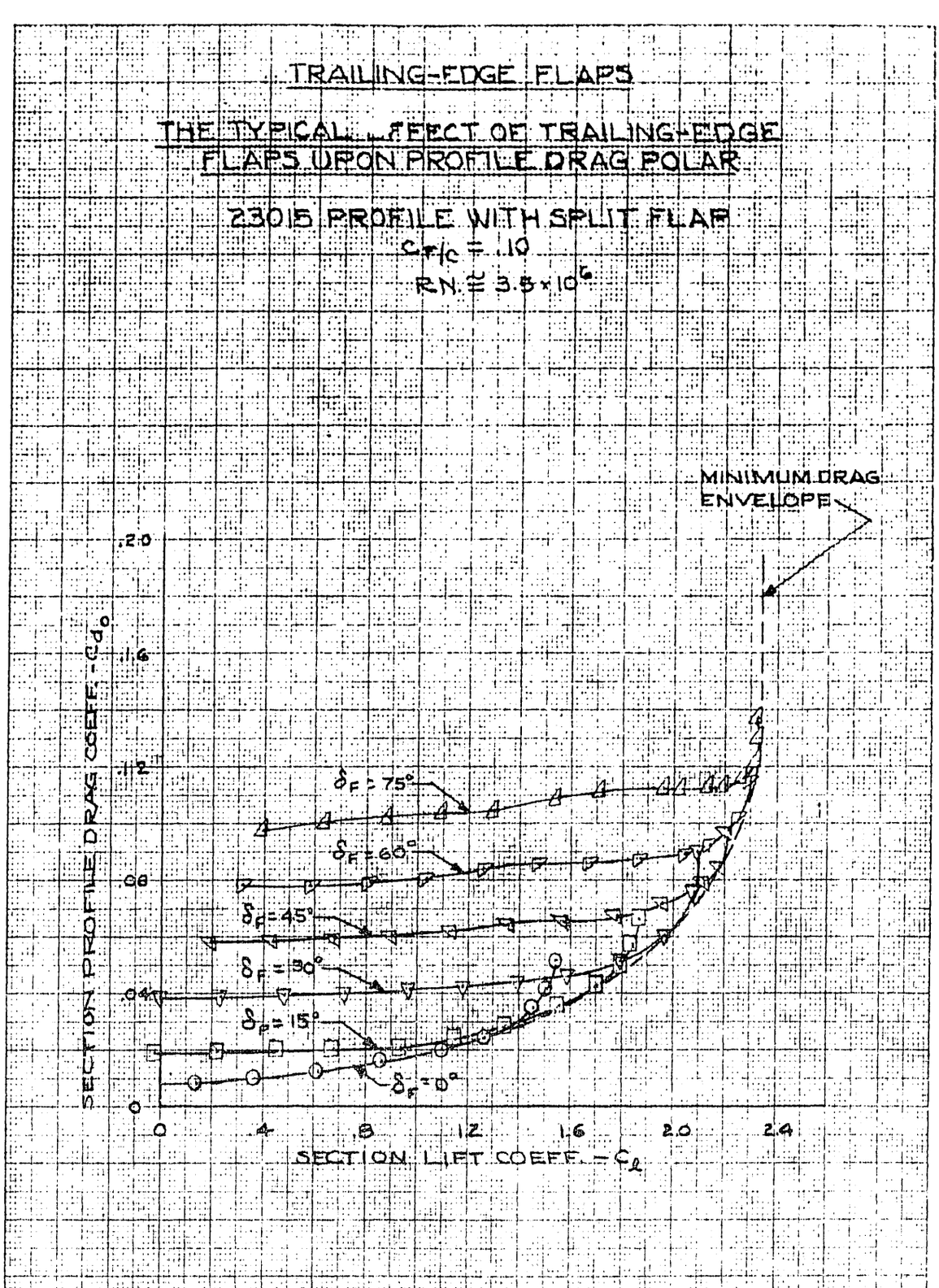

FIG. 87

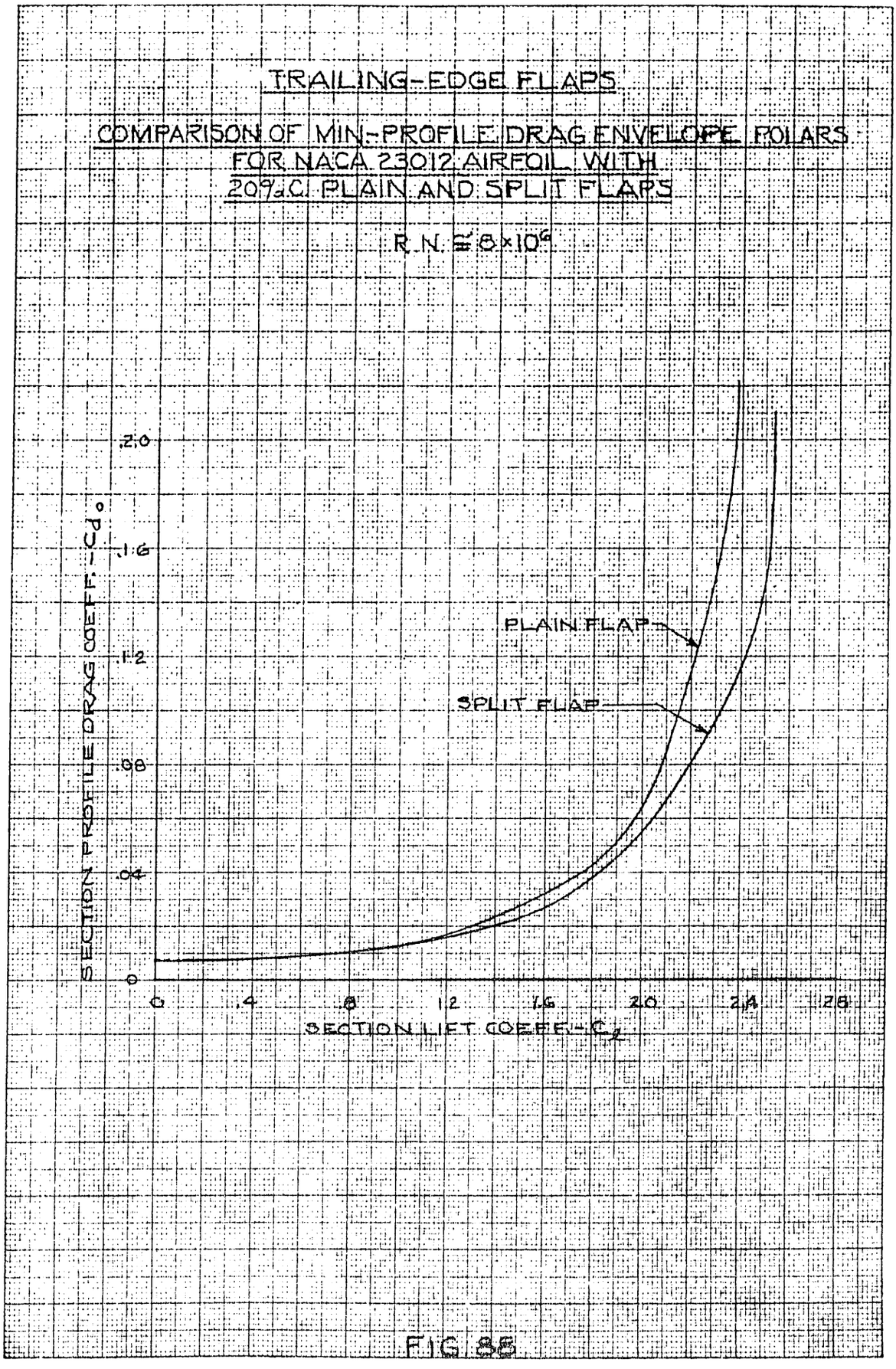

FIG. 8B

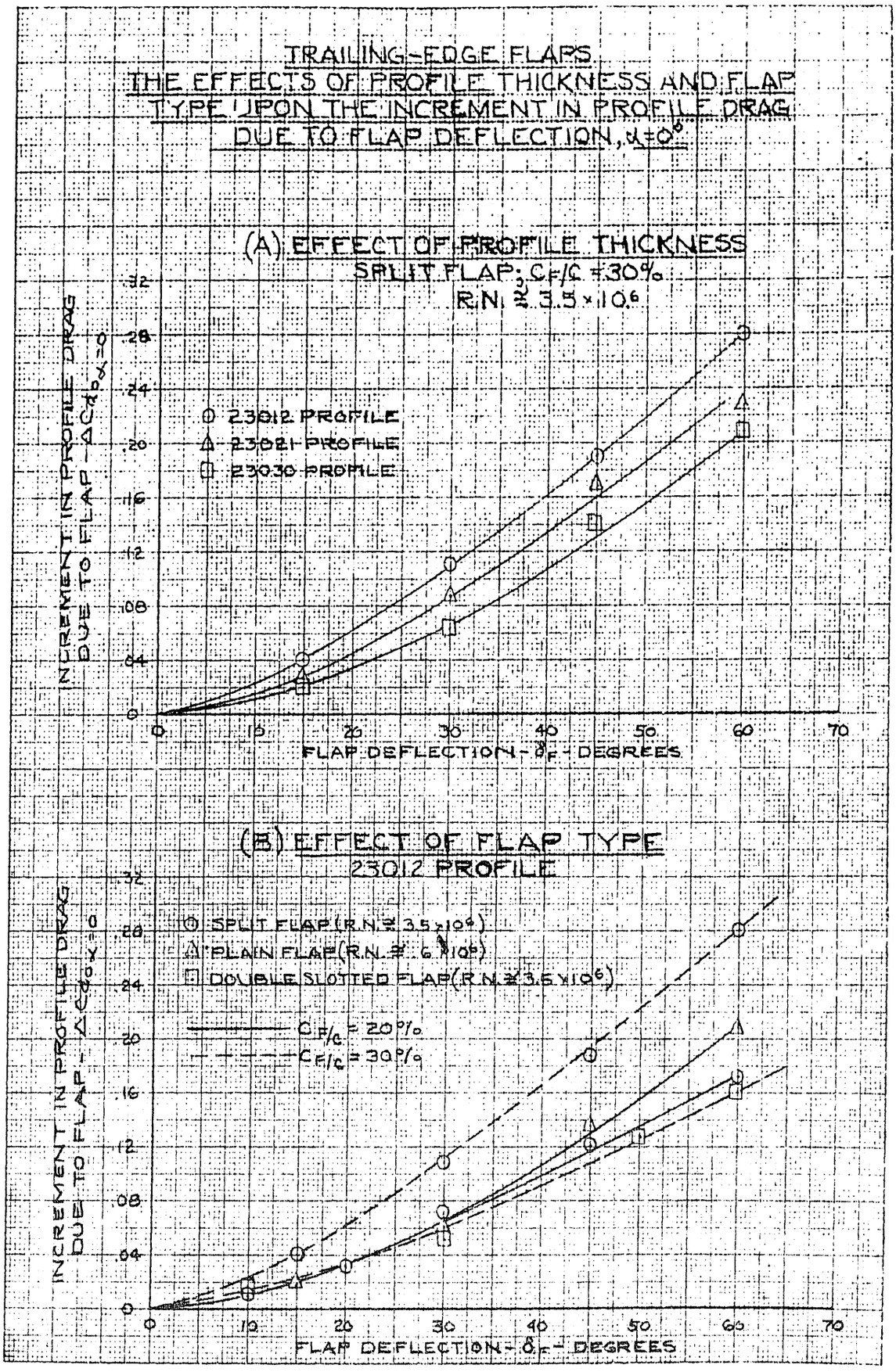

FIG. 89

TRAILING-EDGE FLAPS

THE EFFECTS OF PROFILE THICKNESS AND REYNOLDS NUMBER ON THE MINIMUM-DRAG ENVELOPE POLARS OF PROFILES WITH TRAILING-EDGE FLAPS

(A) EFFECT OF PROFILE THICKNESS

DOUBLE SLOTTED FLAP

$C_{F/c} = .30$, R.N. $= 3.5 \times 10^6$

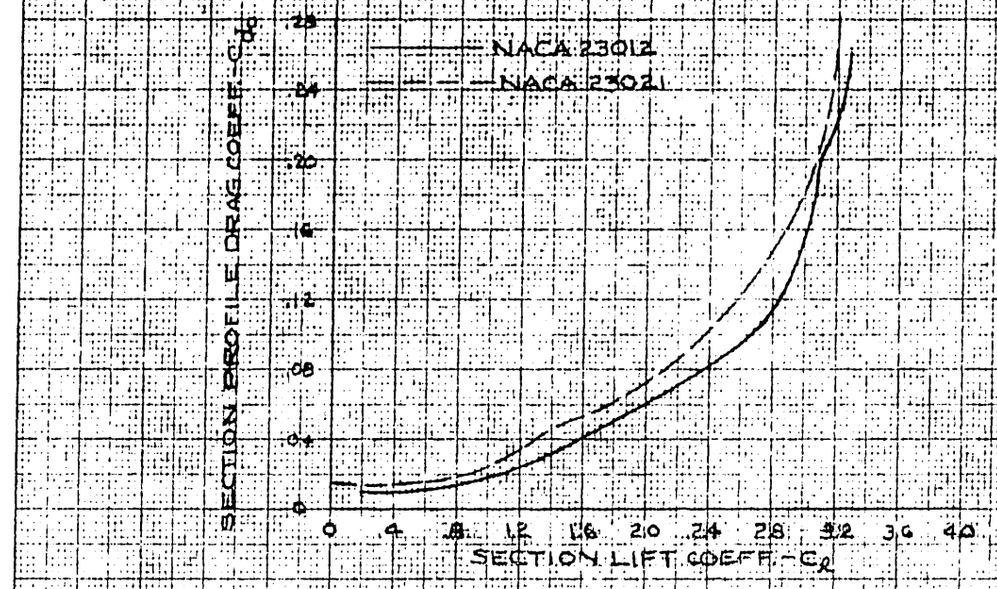

(B) EFFECT OF REYNOLDS NUMBER

PLAIN FLAP

$C_{F/c} = .20$, 23012 PROFILE

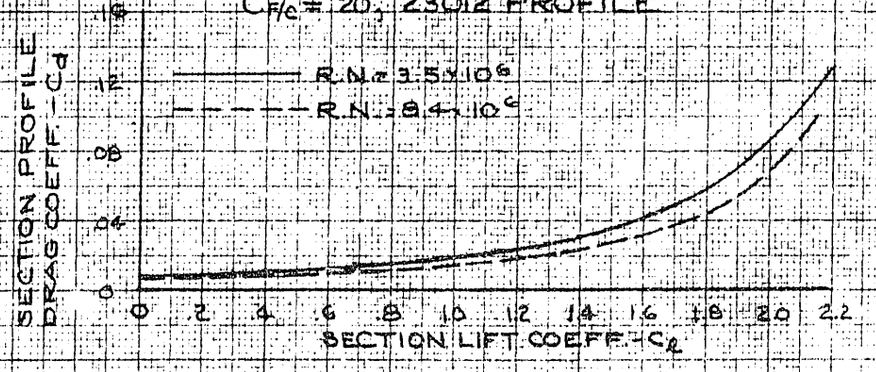

FIG. 80

359-14G
10 X 10 TO THE CM.
KEUFFEL & ESSER CO.

CONFIDENTIAL

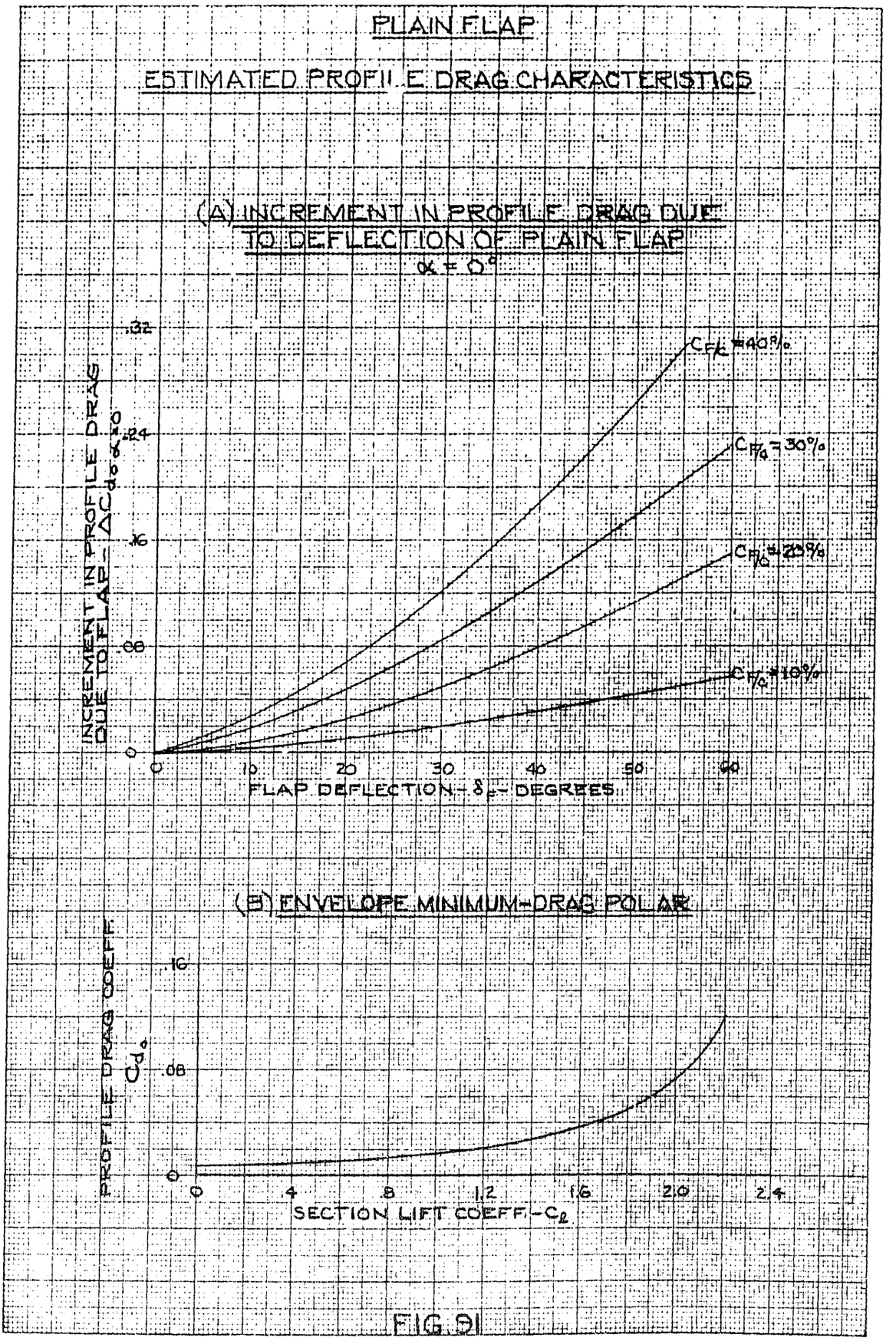

FIG. 91

CONFIDENTIAL

SPLIT FLAP

ESTIMATED PROFILE DRAG CHARACTERISTICS

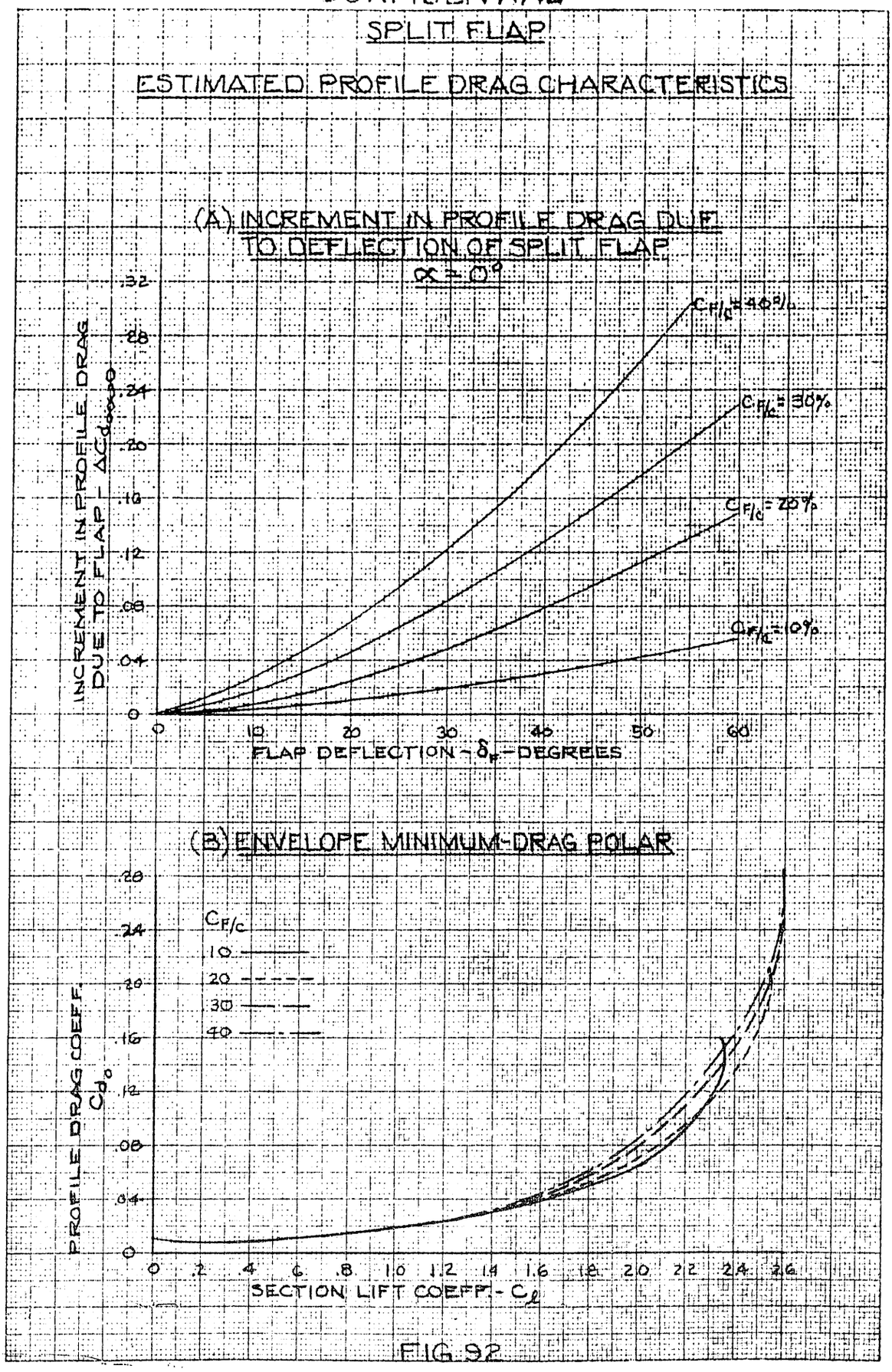

FIG 92

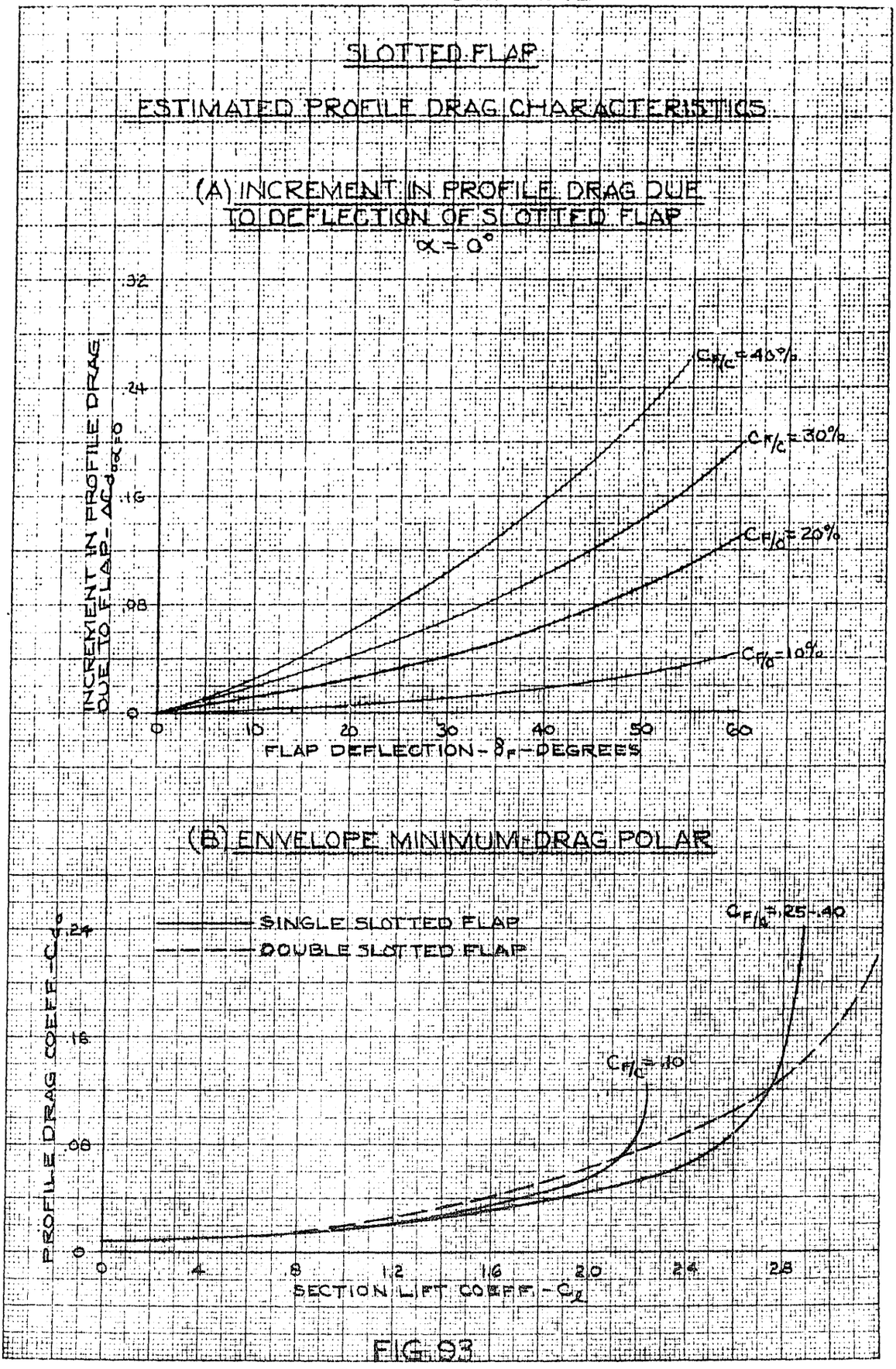
SLOTTED FLAP
ESTIMATED PROFILE DRAG CHARACTERISTICS
(A) INCREMENT IN PROFILE DRAG DUE TO DEFLECTION OF SLOTTED FLAP
α = 0°
INCREMENT IN PROFILE DRAG DUE TO FLAP - ΔC_d0
.32
.24
.16
.08
0
C_F/C = 40%
C_F/C = 30%
C_F/C = 20%
C_F/C = 10%
0
10
20
30
40
50
60
FLAP DEFLECTION - δ_F - DEGREES
(B) ENVELOPE MINIMUM-DRAG POLAR
SINGLE SLOTTED FLAP
DOUBLE SLOTTED FLAP
PROFILE DRAG COEFF. - C_d0
.24
.16
.08
0
C_F/C = .25-.40
C_F/C = .10
0
.4
.8
1.2
1.6
2.0
2.4
2.8
SECTION LIFT COEFF. - C_l

FIG. 93

FIG. 9A

10 X 10 TO THE CM 359-146
KEUFFEL & ESSER CO MADE IN U.S.A.

FIG. 95

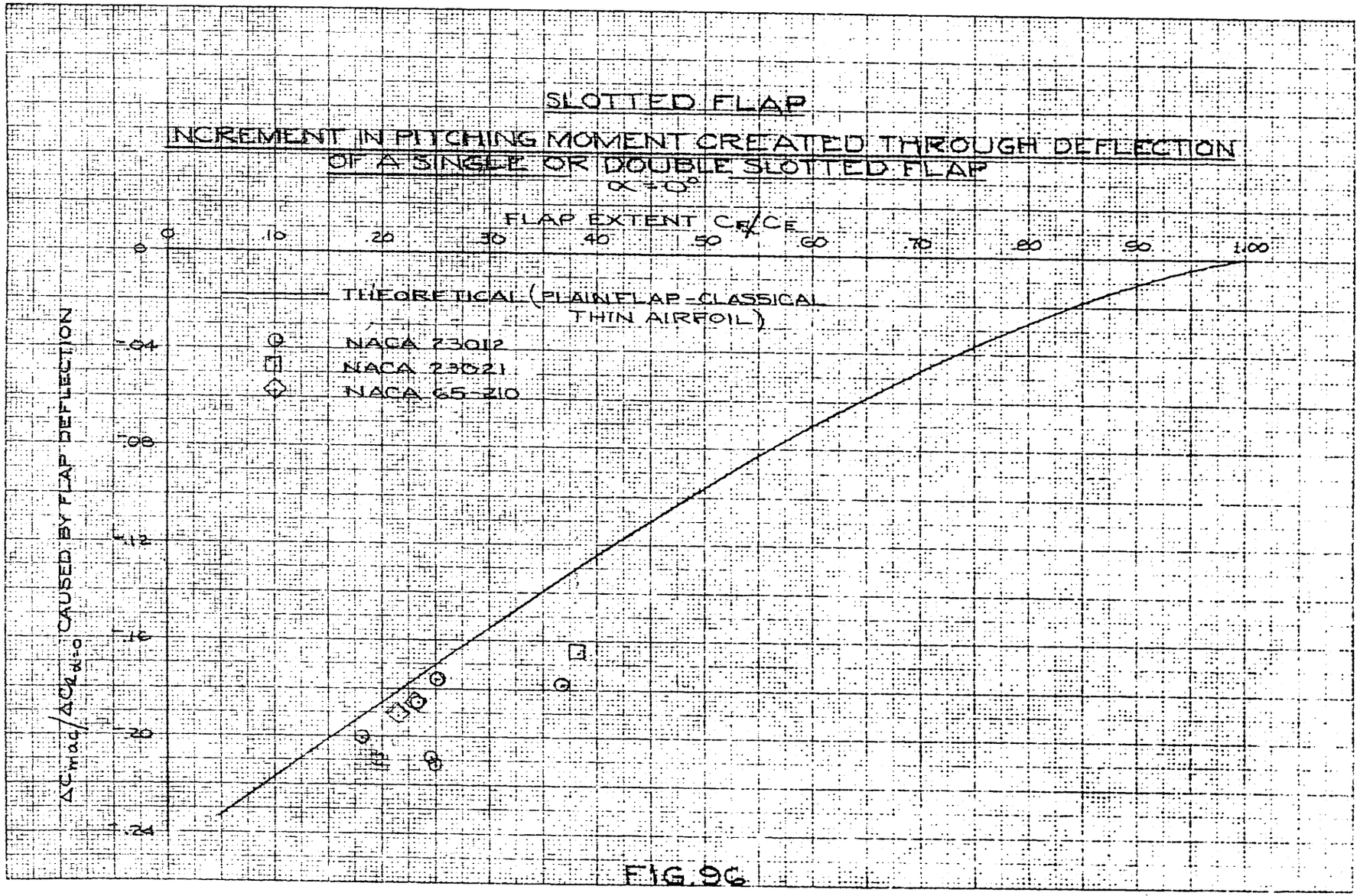

FIG. 96

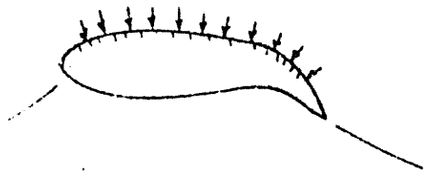

Porous Suction Over Entire Upper Surface

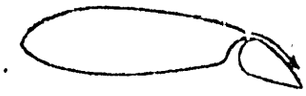

a) Single Slot Blowing

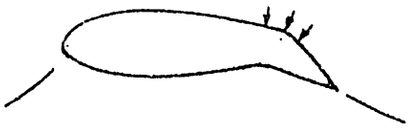

Porous Suction at Flap

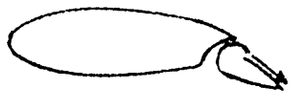

b) Single Slot Blowing

Slot Suction at Flap

a) Multiple Slot Blowing

Cusped Slot Suction

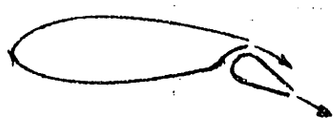

b) Multiple Slot Blowing

Trailing Edge Suction With Split Flap

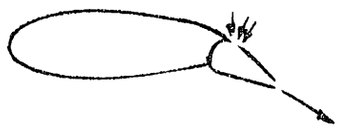

a) Combined Suction & Blowing

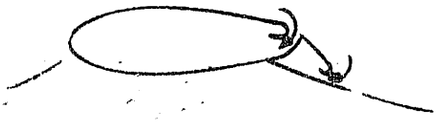

Combined Flap And Trailing Edge Suction

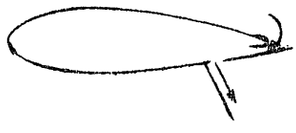

b) Combined Suction & Blowing

TYPICAL POWERED FLAP SYSTEMS

FIG. 97

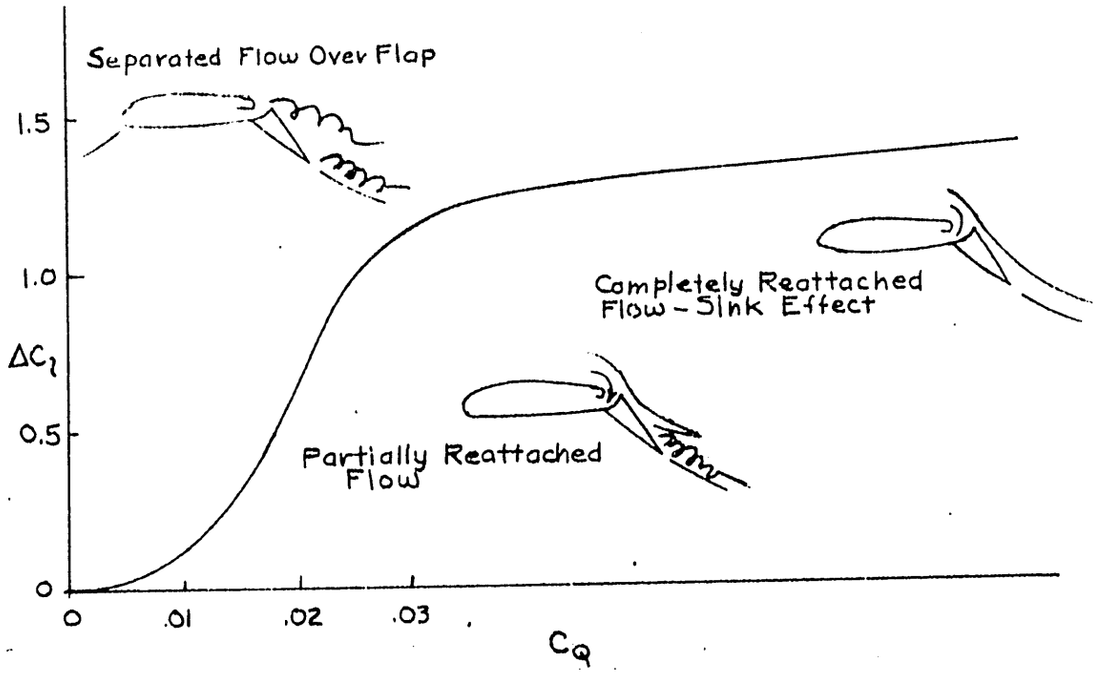

FIG. 98

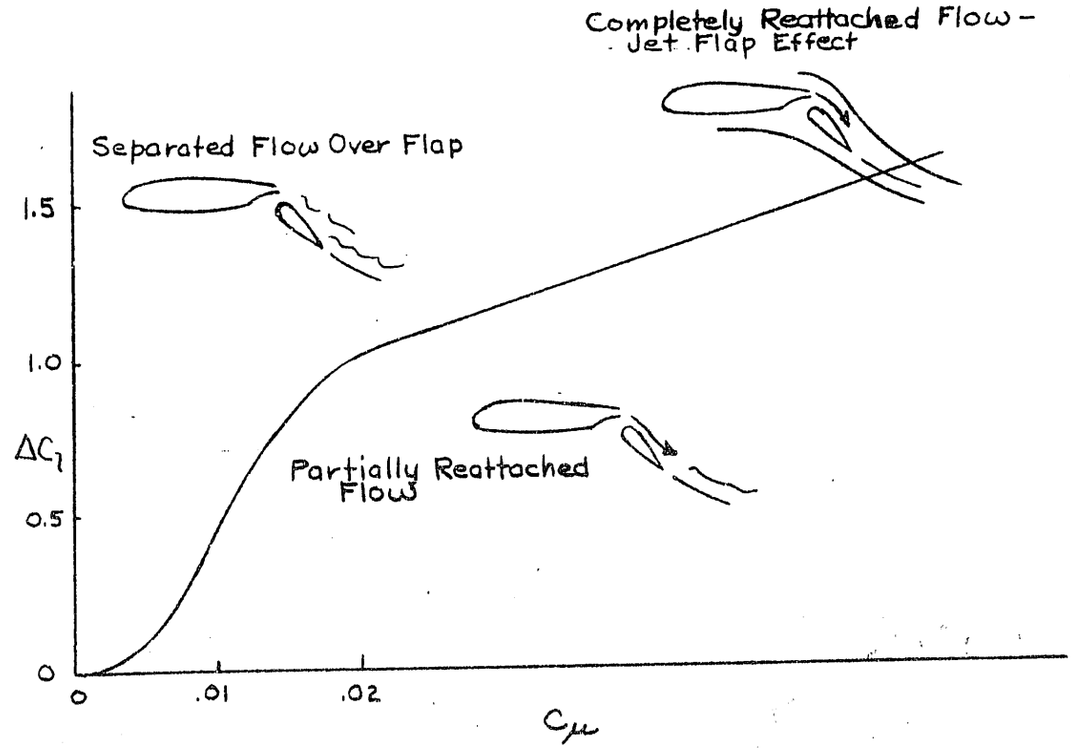

FIG. 99

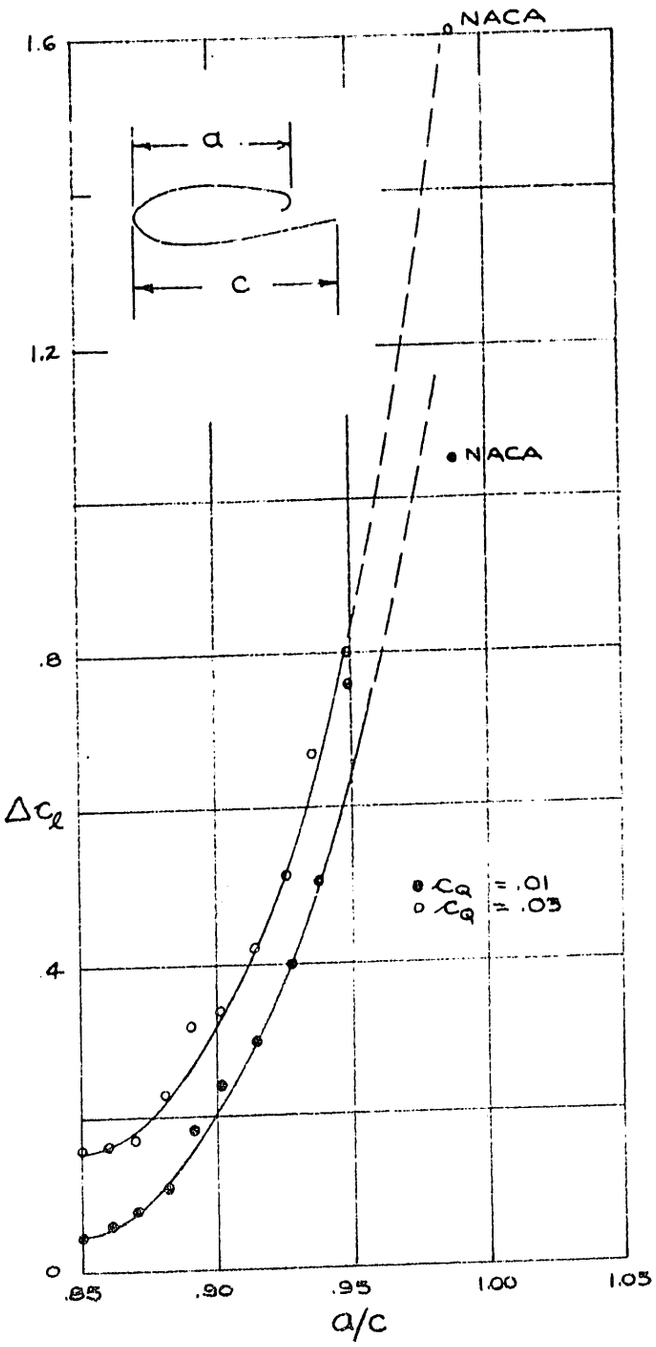

LIFT INCREMENT VS. SLOT LOCATION
SLOT CENTER ON CHORD LINE

FIG. 100

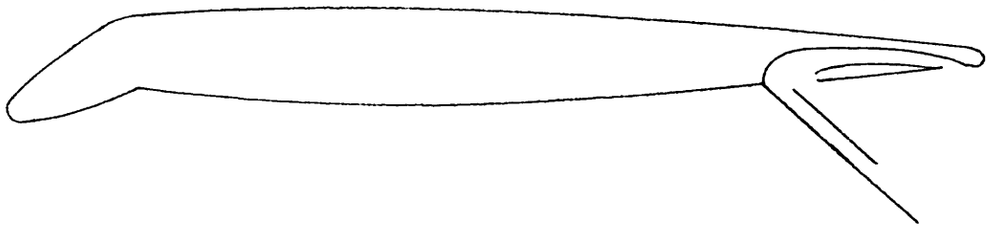

High Pressure Duct

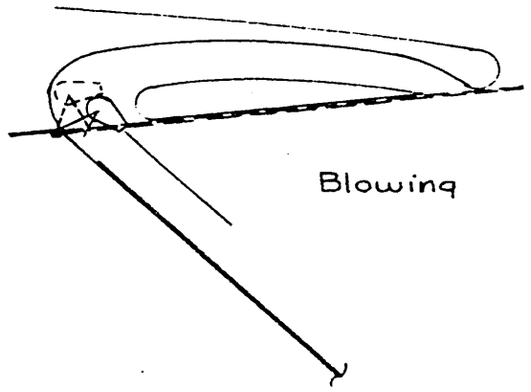

NACA 64A010 EQUIPPED WITH TESABOF

FIG. 101

CUSP SUCTION AIRFOIL

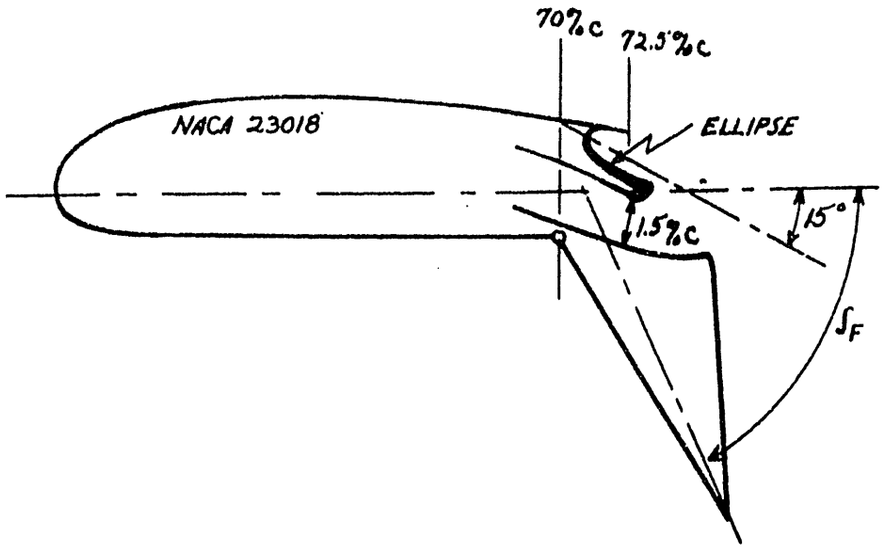

FIG. 102

CUSP SUCTION FLAP WING

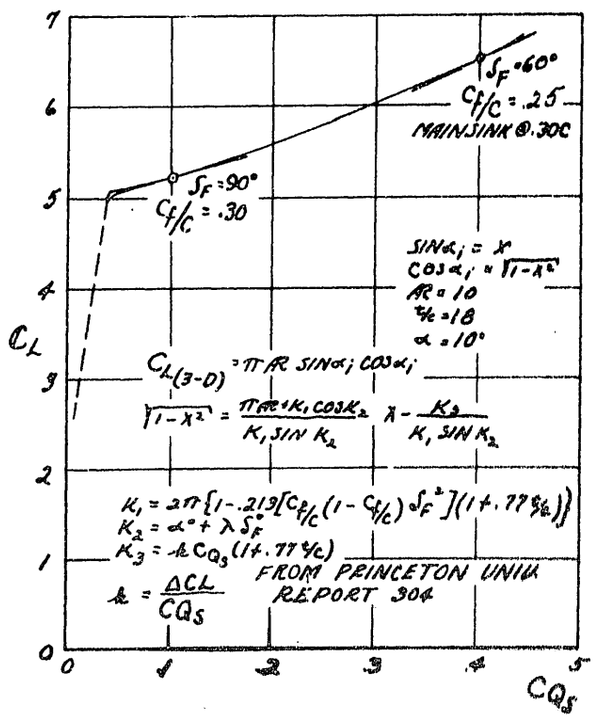

FIG. 103

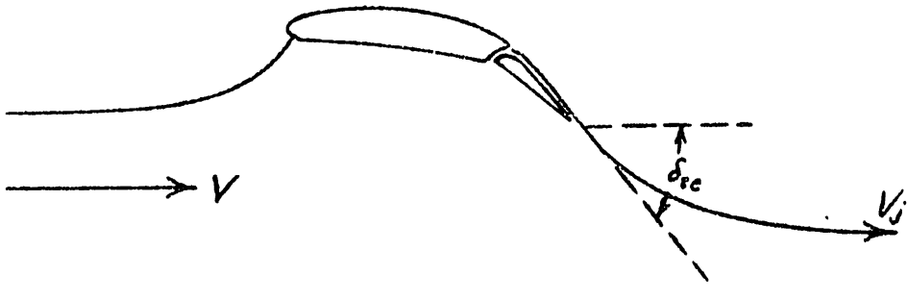

THEORY OF THE FINITE-SPAN BLOWING WING

FIG. 104

JET MOMENTUM LOSS OVER 20% C BLOWING FLAP
(FROM WIND TUNNEL TESTS)

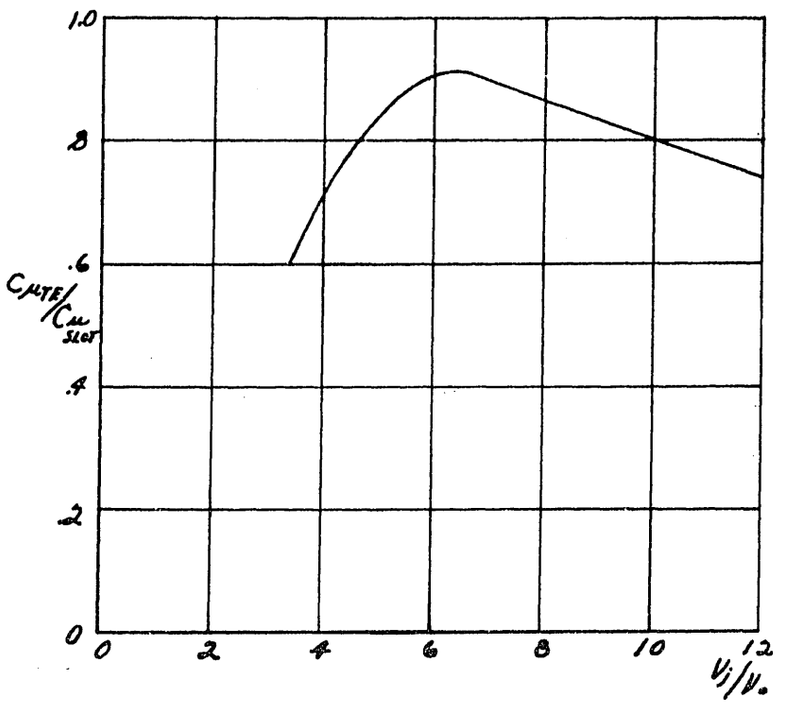

FIG. 105

LEADING-EDGE FLAP TYPES

(a) "DROOP-SNOOT"

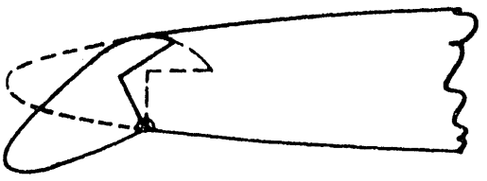

(b) CONTOURED (ARTICULATED) L.E. FLAP

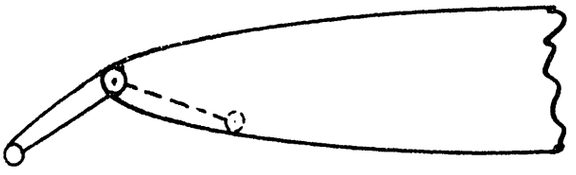

(c) KRÜGER FLAP

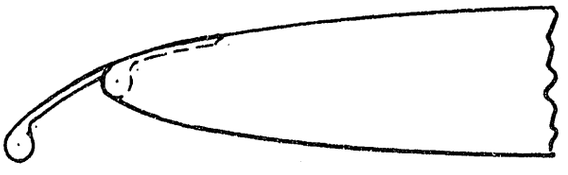

(d) NACA UPPER SURFACE L.E. FLAP

(e) NACA LOWER SURFACE L.E. FLAP

FIG. 106

CONTOURED L.E. FLAP

TYPICAL EFFECT OF LEADING EDGE FLAP DEFLECTION ON L.E. STAGNATION POINT LOCATION AND STALL ANGLE AND TYPE

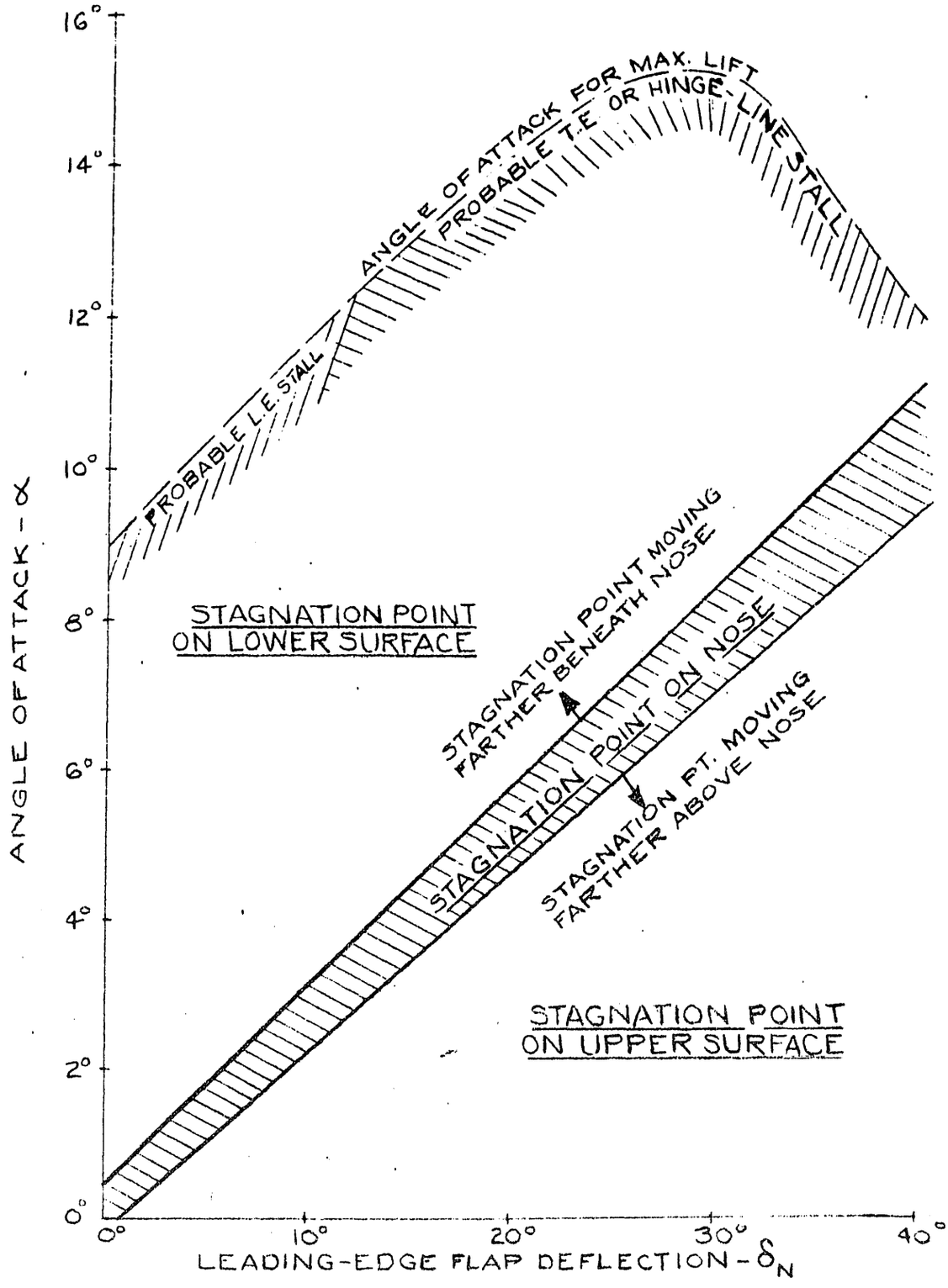

FIG.107 CONFIDENTIAL

CONTOURED L.E. FLAP
TYPICAL VISCID PRESSURE DISTRIBUTIONS

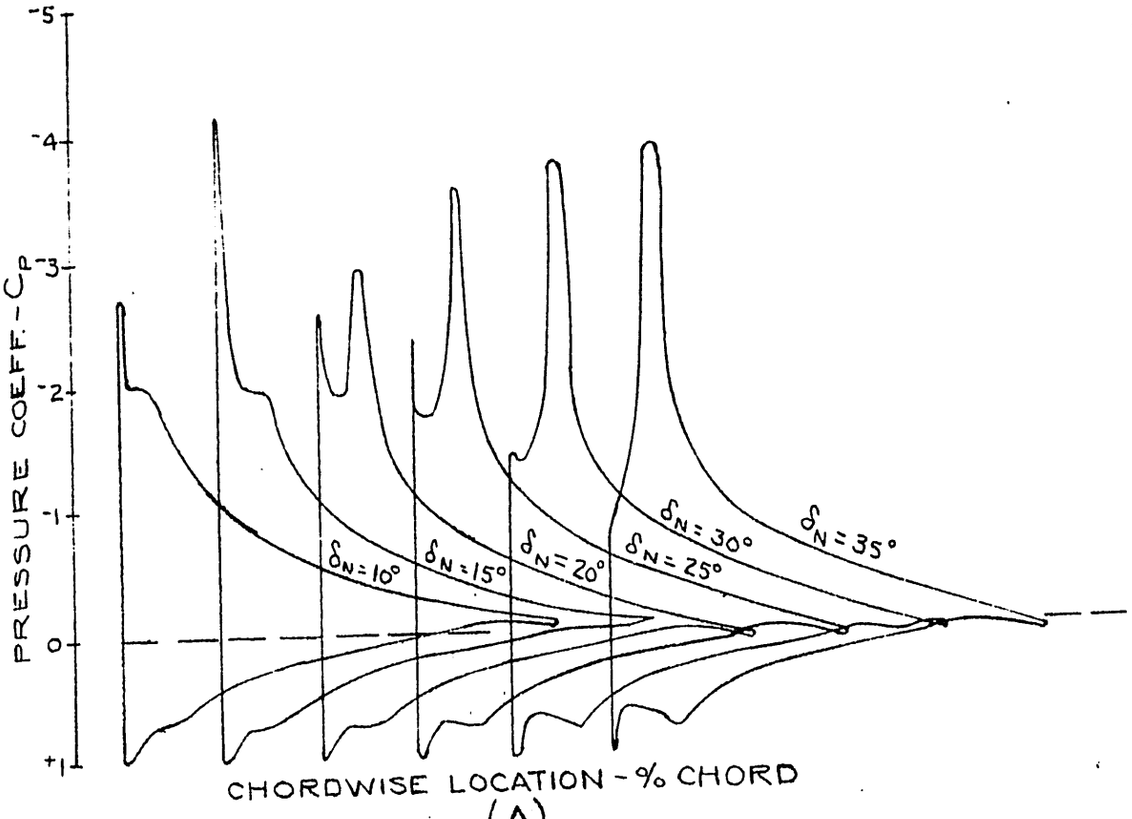

(A)

AS FUNCTION OF L.E FLAP DEFLECTION, ANGLE OF ATTACK BEING CONSTANT (AND GREATER THAN $\alpha_{C_{\ell MAX}}$ FOR BASE PROFILE)

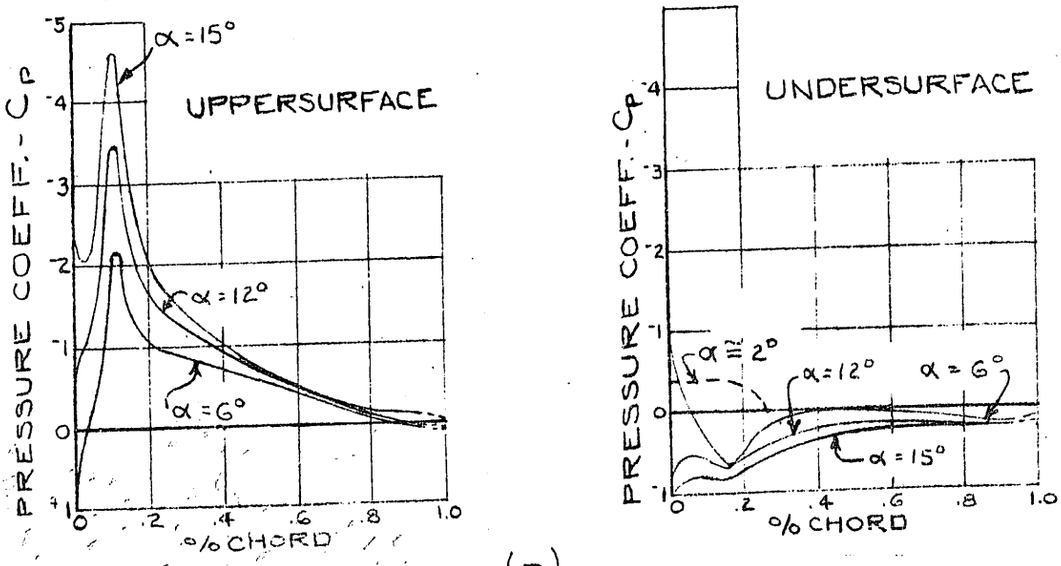

(B)

AS FUNCTION OF ANGLE OF ATTACK, L.E. FLAP DEFLECTION BEING CONSTANT (30°)

FIG. 108

CONTOURED L.E. FLAP
SMOKE PHOTOGRAPHS OF AN NACA 64-010 PROFILE WITH AND WITHOUT LEADING-EDGE FLAP

WITHOUT L.E. FLAP

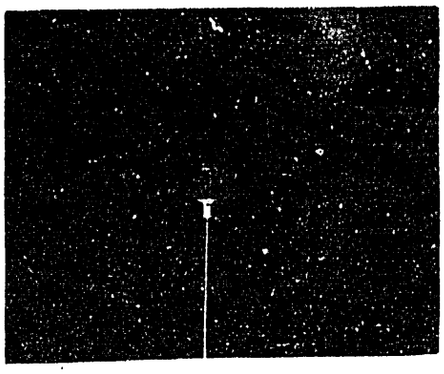

$\alpha = 0°$

WITH L.E. FLAP ($\delta_N = 30°$)

$\alpha = 0°$

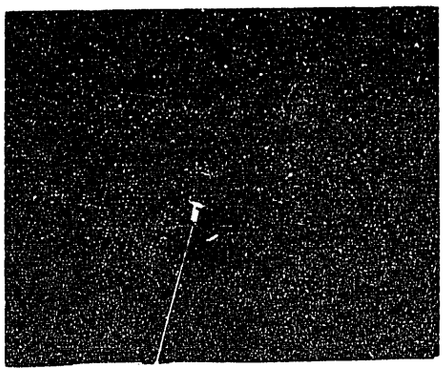

$\alpha = 16°$

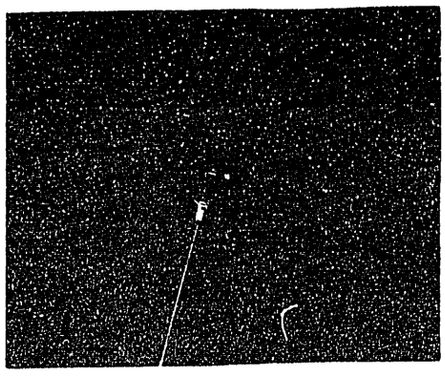

$\alpha = 16°$

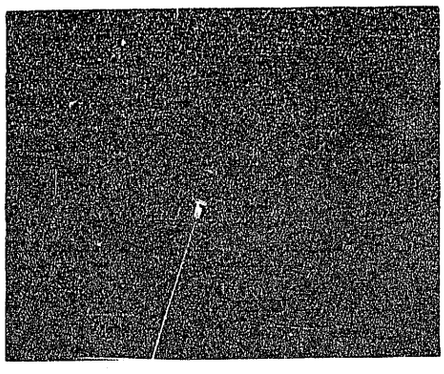

$\alpha = 18°$

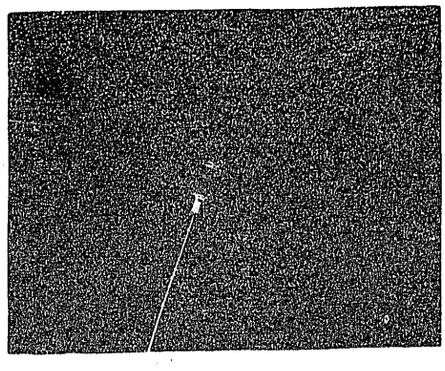

$\alpha = 20°$

FIG. 109

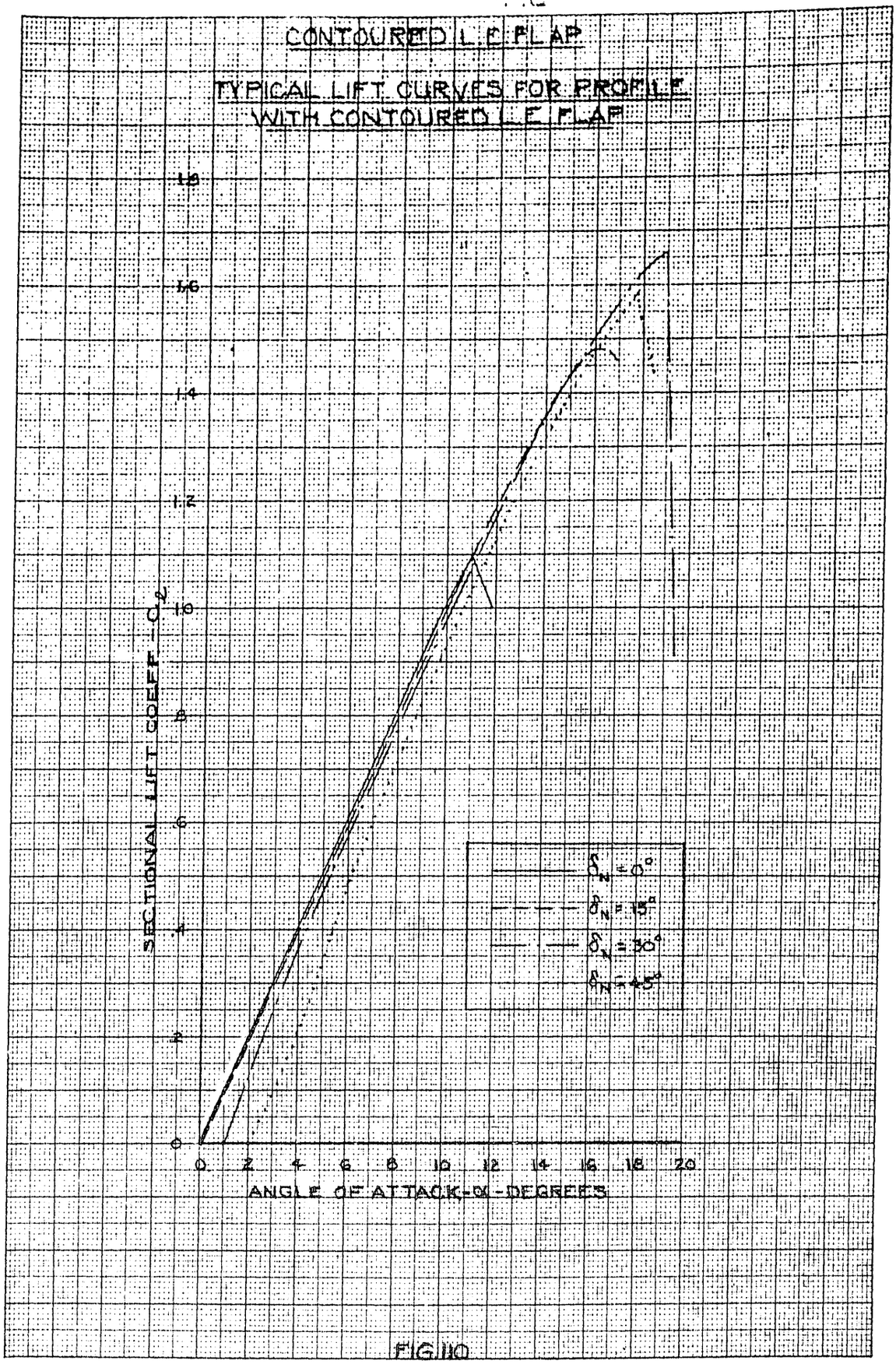

FIG 110

CONTOURED L.E. FLAP
INCREASE IN ANGLE OF ATTACK FOR ZERO LIFT DUE TO INCREASED L.E. FLAP DEFLECTION
(Two-Dimensional)

FIGURE A
Effect of δ_N on $\alpha_{o.L.}$
Flap Chord/Profile Chord ≅ 15%

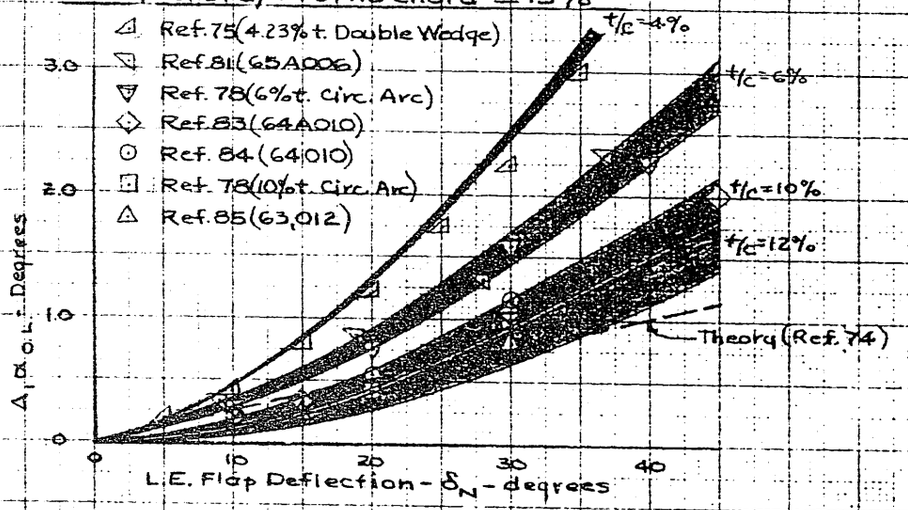

FIGURE B
Effect of C_N/C Ratio on $\alpha_{o.L.}$ — as Incremental Corr. to Fig. A

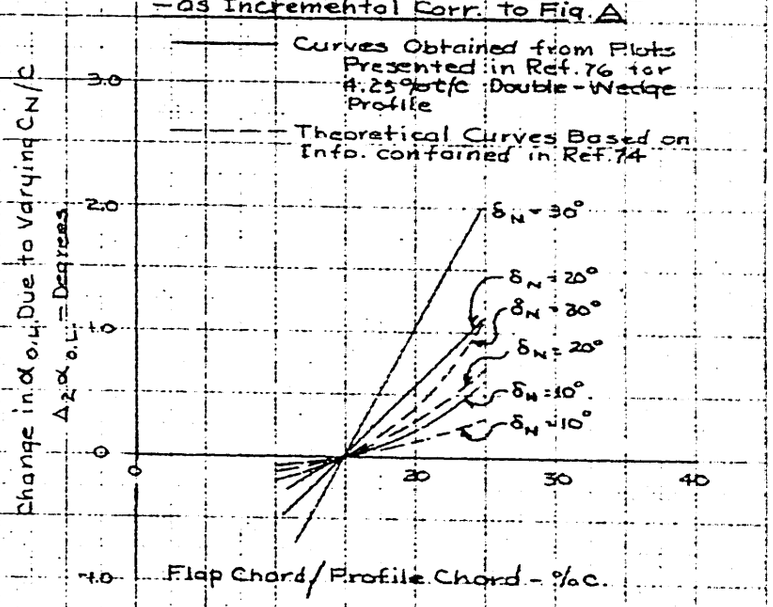

Procedure:

1. Apply only if no radical base profile camber.
2. Assume no R.N. effect.
3. Assume in Fig. B that theoretical curves hold for t/c ≅ 12% and empirical for t/c ≅ 4%.
4. Use following formula:

$$\underbrace{\alpha_{o.L.}}_{\alpha_{o.L.}\,@\,\delta_N} = \underbrace{\alpha_{o.L.}}_{\text{Base Profile}} + \underbrace{\Delta_1\alpha_{o.L.}}_{\text{Fig. A}} + \underbrace{\Delta_2\alpha_{o.L.}}_{\text{Fig. B}}$$

FIG. 111

INCREASE IN LIFT CURVE SLOPE DUE TO INCREASED L.E. FLAP DEFLECTION

(TWO-DIMENSIONAL)

FIGURE A

EFFECT OF δ_N ON LIFT CURVE SLOPE

FLAP CHORD/PROFILE CHORD = 15%

FIGURE B

EFFECT OF C_N/C RATIO ON LIFT CURVE SLOPE INCREMENTAL CORR TO FIG. A

C_l CURVE OBTAINED FROM PLOTS PRESENTED IN REF. 76 FOR 4.23 t/c DOUBLE WEDGE PROFILE

FIGURE C

METHOD OF OBTAINING AND APPLYING SLOPE

PROCEDURE

1. APPLY ONLY IF NO RADICAL BASIC PROFILE CAMBER
2. ASSUME NO R.N. EFFECT
3. ASSUME NO THICKNESS EFFECT
4. USE FOLLOWING FORMULA:

$$C_l = C_{l_0} + \Delta a_0 (\alpha - \Delta\alpha_0)$$

WHERE SLOPE @ δ_N = BASE PROFILE FIG. A FIG. B

5. APPLY DETERMINED SLOPE AS IN FIG. C

FIG 13

FIG. 14

CONTOURED L.E. FLAP

INCREASE IN MAXIMUM SECTIONAL LIFT COEFFICIENT AS A FUNCTION OF L.E. FLAP DEFLECTION-VARIOUS PROFILES

$R.N. = 6 \times 10^6$ $C_N/C = 15\%$

ROUNDED LEADING-EDGE PROFILES — SHARP LEADING-EDGE PROFILES

INCREASE IN MAX SECTION LIFT COEFF $\Delta C_{l_{max}}$

L.E. FLAP DEFLECTION - δ_N - DEGREES

○ 4.23% DOUBLE-WEDGE
□ 8% CIRCULAR-ARC
▽ 10% CIRCULAR-ARC

NOTE: R.N. = 4.9×10^6

FIG. 116

CONTOURED L.E. FLAP
ANGLE OF ATTACK FOR MAXIMUM LIFT AS FUNCTION OF FLAP DEFLECTION FOR CONFIGURATIONS STALLING IN A PURE MANNER

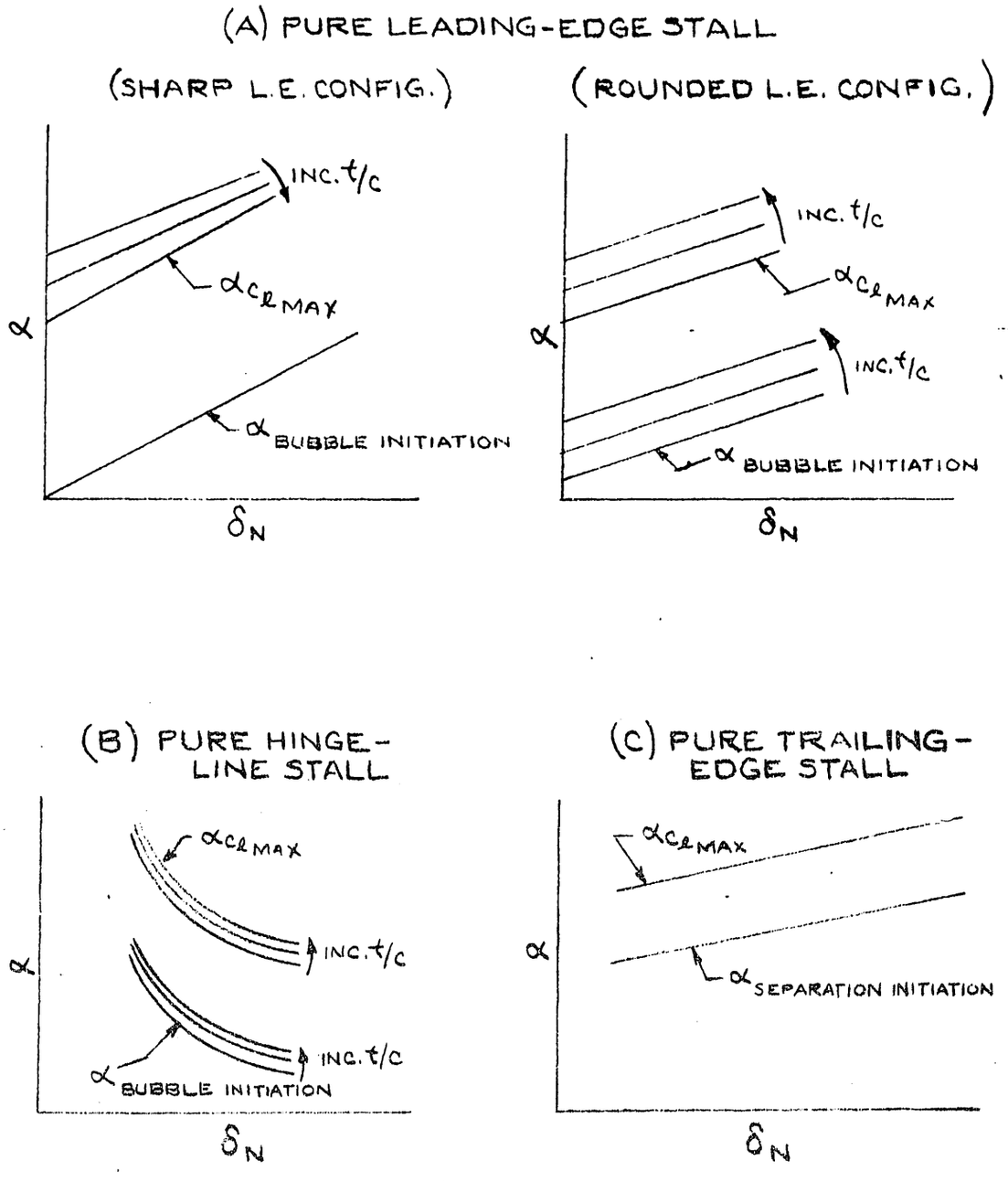

FIG. 117

CONTOURED L.E. FLAP
ANGLE OF ATTACK FOR MAXIMUM LIFT AS FUNCTION OF FLAP DEFLECTION FOR CONFIGURATIONS STALLING IN A COMBINED MANNER

(A) COMBINED LEADING-EDGE AND HINGE-LINE STALL PATTERN

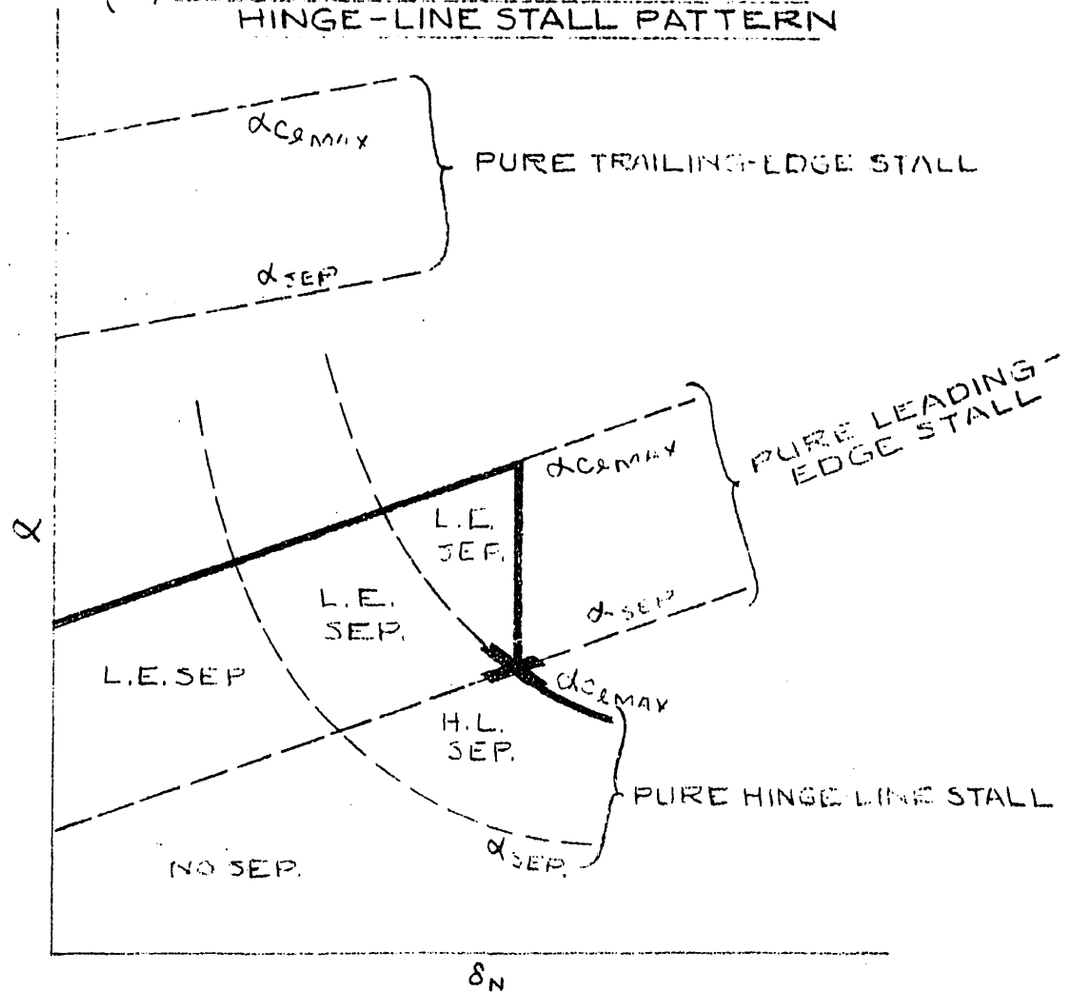

(B) COMBINED LEADING-EDGE AND TRAILING-EDGE STALL

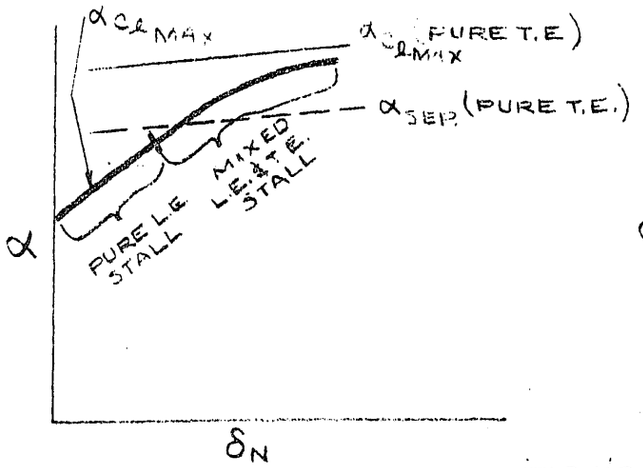

(C) COMBINED TRAILING-EDGE AND HINGE-LINE STALL

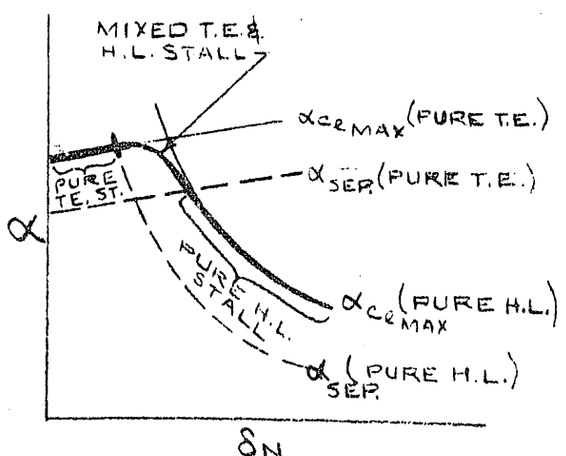

FIG 118

CONFIDENTIAL

CONTOURED L.E. FLAP

ANGLE OF ATTACK FOR MAXIMUM LIFT AS FUNCTION OF FLAP DEFLECTION FOR CONFIGURATIONS OF VARIOUS PROFILE THICKNESSES, STALLING IN A COMBINED MANNER

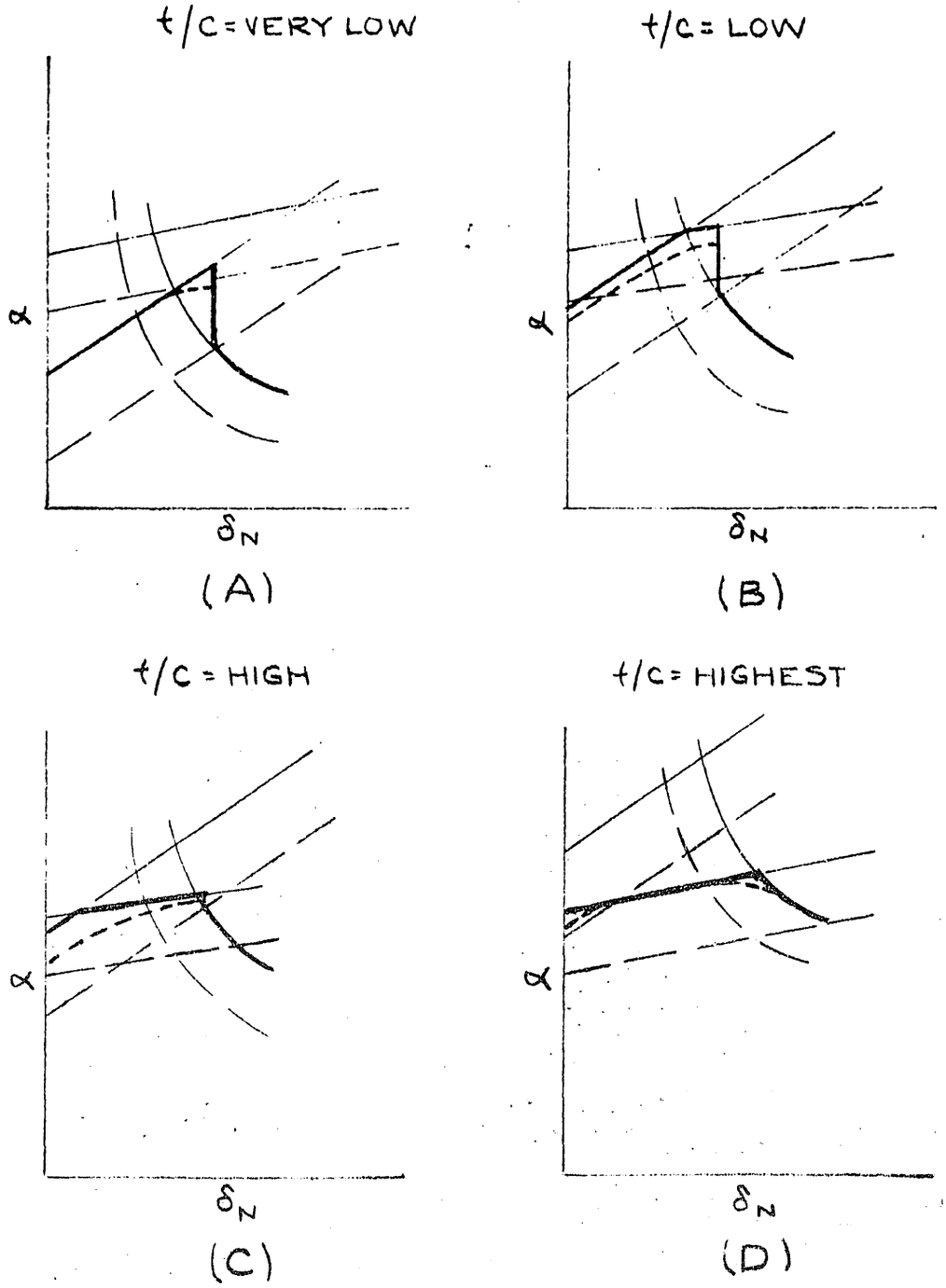

FIG. 119

FIG. 120

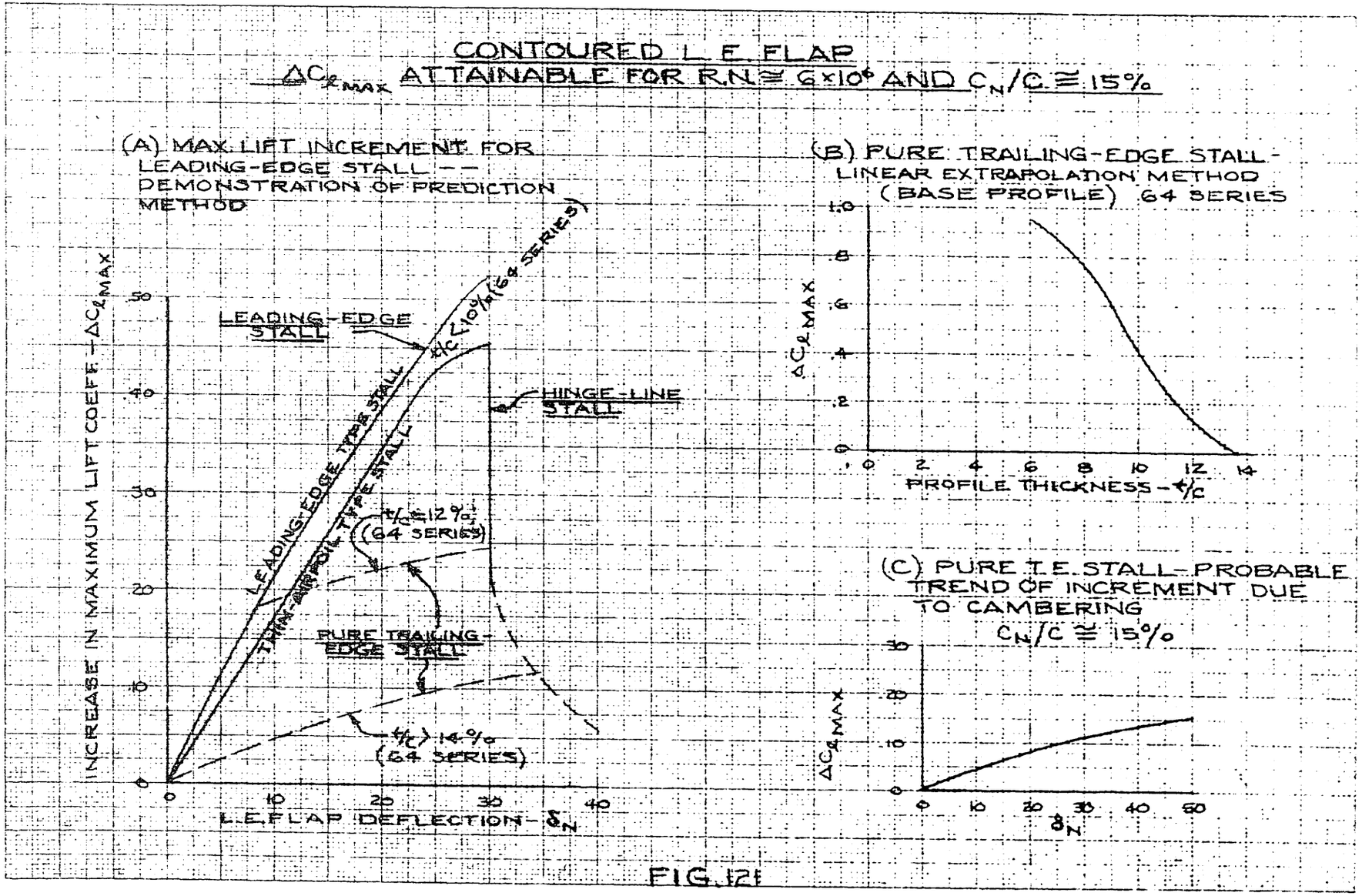

FIG. 12

CONTOURED L.E. FLAP

MAXIMUM SECTION LIFT COEFFICIENT AS A FUNCTION OF REYNOLDS NUMBER

$C_N/C \cong 15\%$

65A006 PROFILE

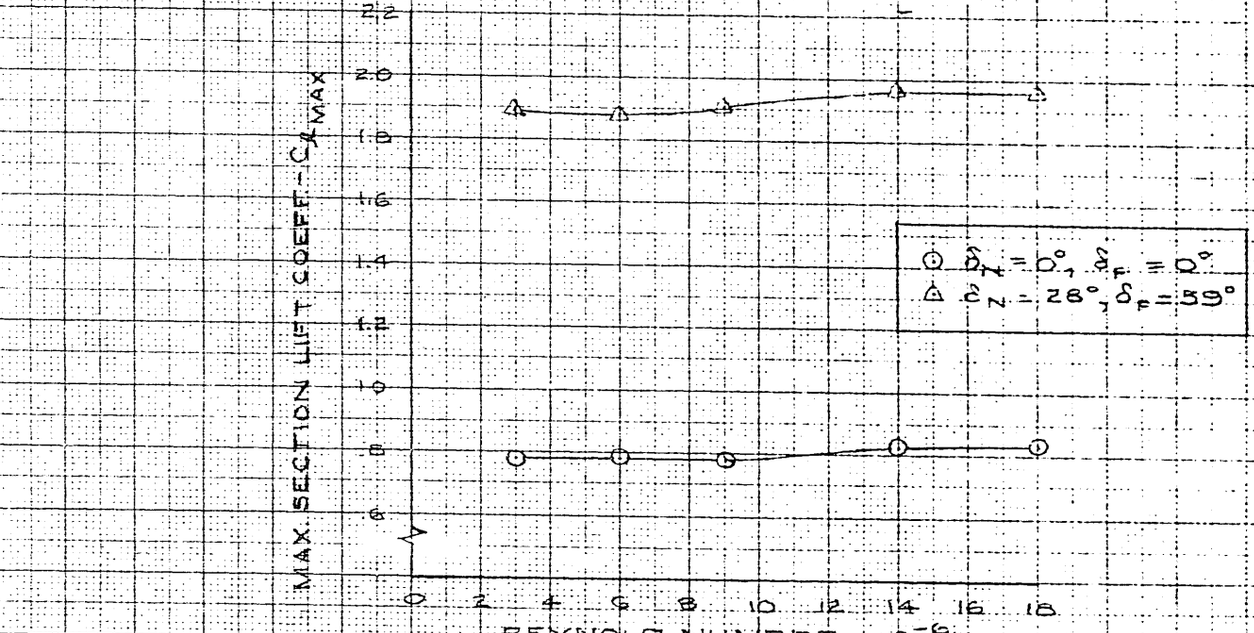

FIG 123

CONTOURED L.E. FLAP

COMPARISON OF 64A010 MAXIMUM LIFT CHARACTERISTICS (@ NEAR OPTIMUM δ_N) WITH CHARACTERISTICS PREDICTED FOR A PURE L.E.-B.L.C. SYSTEM BY THE LINEAR EXTRAPOLATION METHOD

$C_{\ell_{MAX}}$ VS. REYNOLDS NUMBER

$C_N/C \cong 15\%$

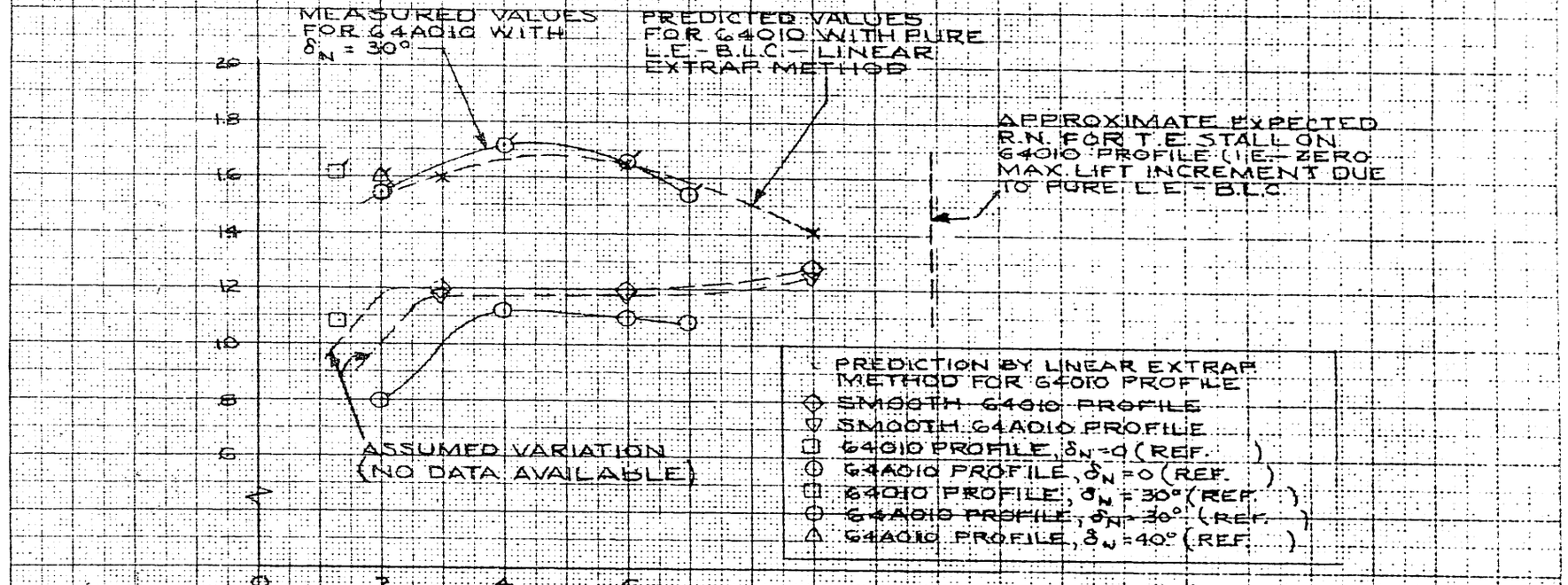

FIG 124

CONFIDENTIAL

CONFIDENTIAL

CONTOURED L.E. FLAP

COMPARISON OF THE MAX. LIFT CHARACTERISTICS OF TWO PROFILES (@ NEAR-OPTIMUM δ_N) WITH CHARACTERISTICS PREDICTED FOR A PURE L.E. B.L.C. SYSTEM BY THE LINEAR EXTRAP METHOD

$C_{\ell_{MAX}}$ VS REYNOLDS NUMBER

$C_N/C \cong 15\%$

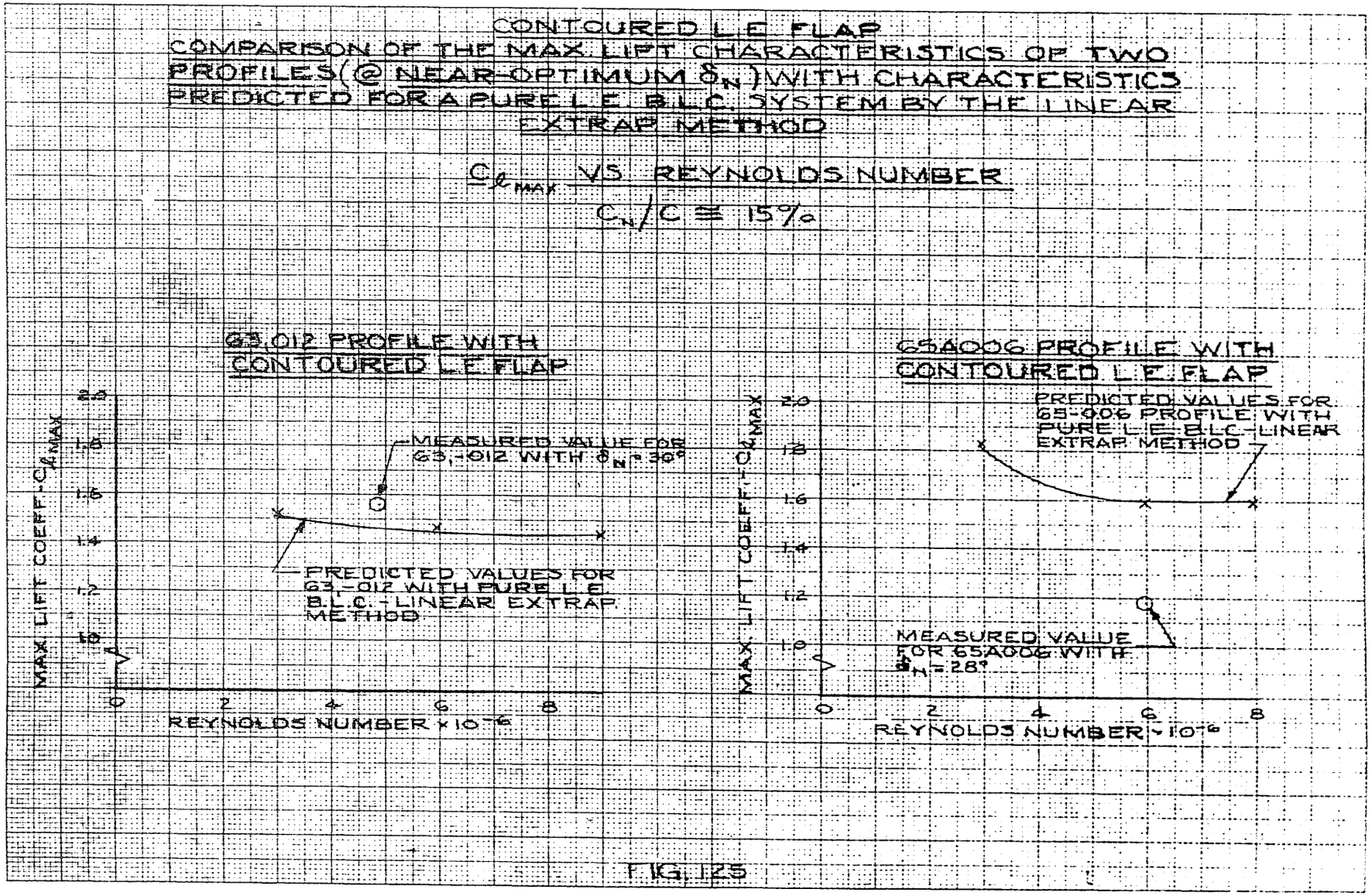

FIG. 125

CONFIDENTIAL

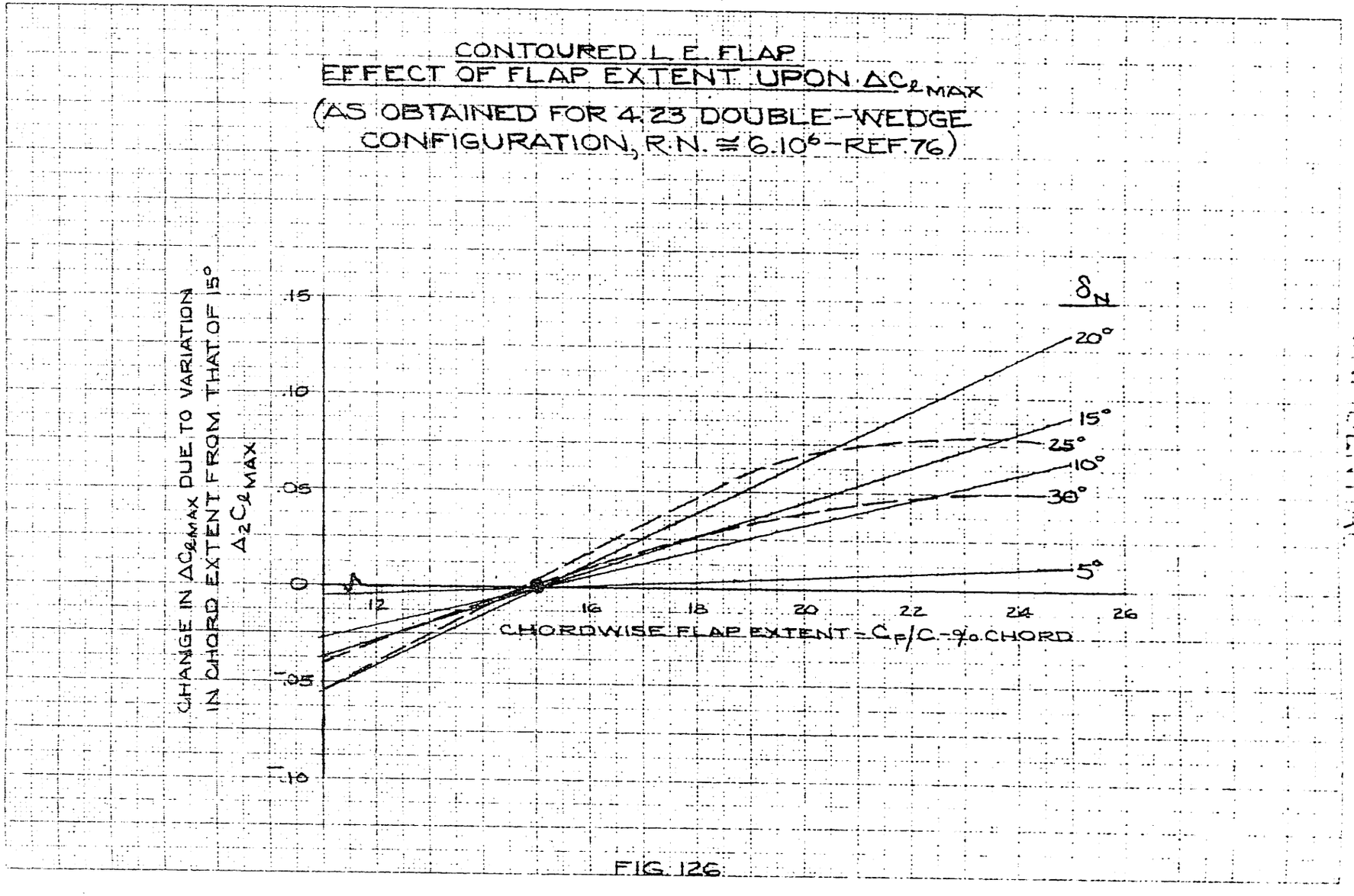

FIG. 126

CONTOURED L.E. FLAP
ESTIMATED $\Delta C_{\ell_{MAX}}$ ATTAINABLE AS FUNCTION OF δ_N, t/c, R.N. AND PROFILE SERIES

PROCEDURE

① USE NO-FLAP DATA FOR BASE PROFILE CHARACTERISTICS
② DETERMINE BASE PROFILE STALL TYPE FROM FIG. 18
③ DETERMINE $\delta_N = 0°$ PURE L.E. STALL $\Delta C_{\ell MAX}$ (FIGS. 24 OR 25).
④ ADD VALUE FROM (B) BELOW TO ③ AND PLOT ON (A).
⑤ IF T.E. STALL LINE, ④, IS, @ $\delta_N = 30°$, AT A $\Delta C_{\ell MAX} > .40$, SUBTRACT .10 ALONG ENTIRE STALL LINE.
⑥ ESTIMATE L.E. STALL LINE, KNOWING C_N/C AND BASE PROFILE STALL TYPE.
⑦ IF T.E. STALL LINE CROSSES L.E. STALL LINE, IT WILL ESTABLISH $\Delta C_{\ell MAX}$ FOR GREATER δ_N'S.
⑧ OCCURENCE OF HINGE-LINE STALL FINALLY LIMITS LIFT INCREASE.

(A) PREDICTION CURVE

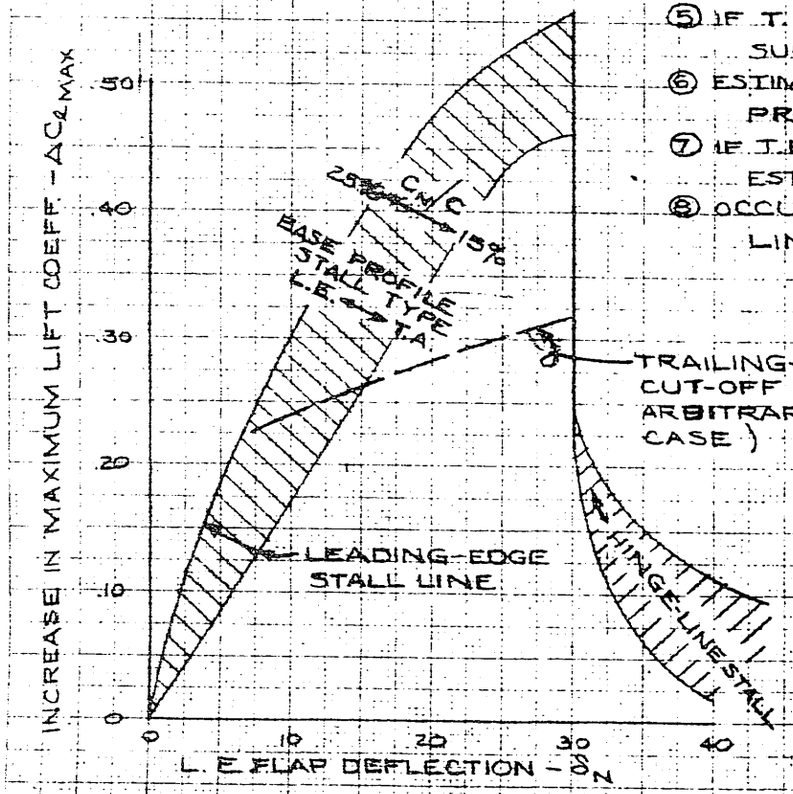

(B) ESTIMATED "CAMBER EFFECT"

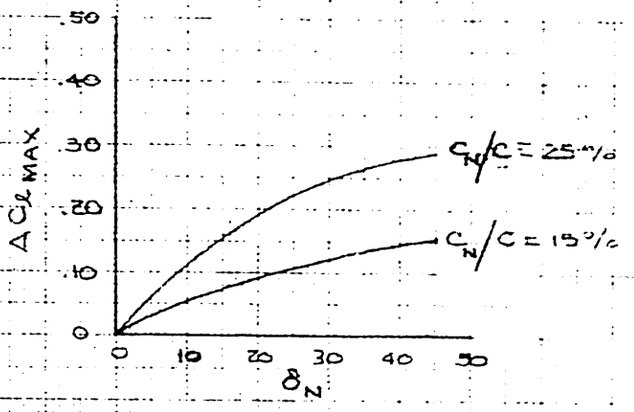

FIG. 127

CONFIDENTIAL

EXTENSIBLE L.E. FLAPS

NOTATION

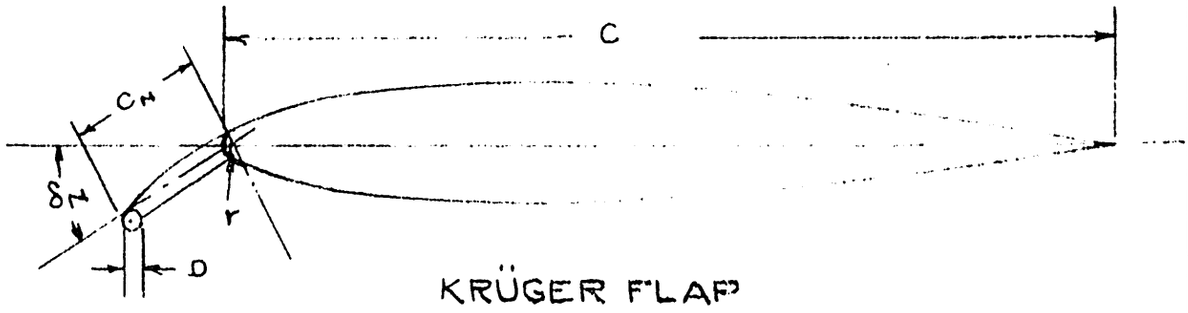

KRÜGER FLAP

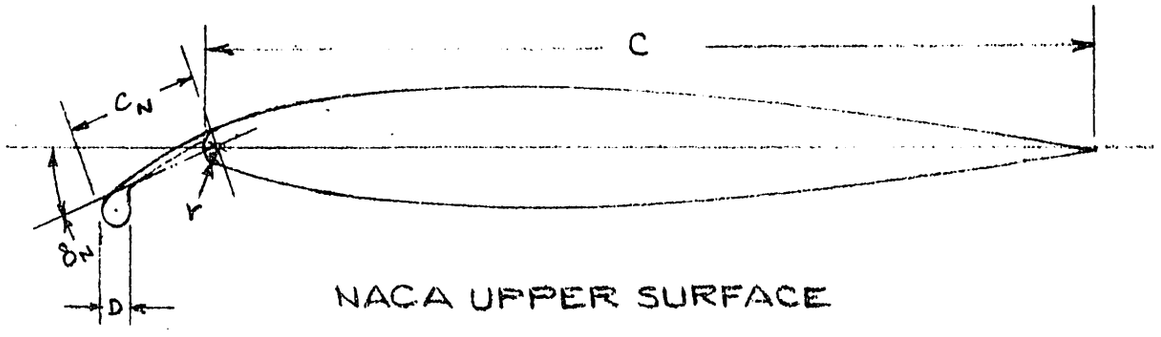

NACA UPPER SURFACE

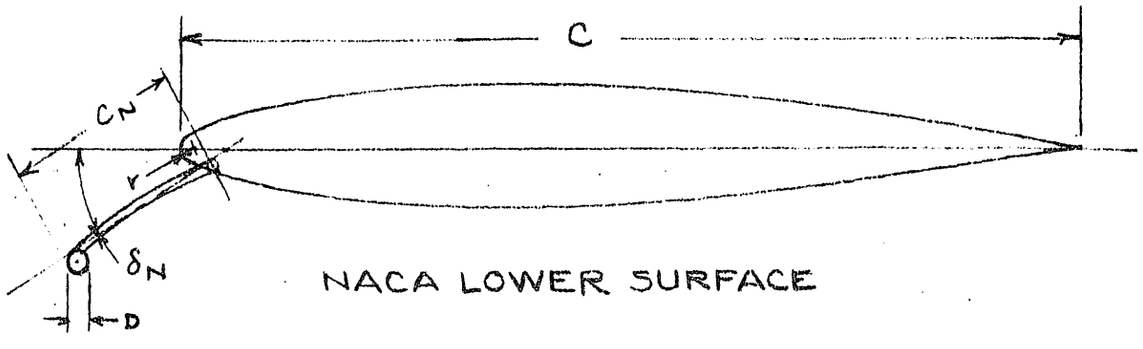

NACA LOWER SURFACE

FIG. 128

EXTENSIBLE L.E. FLAPS
CHANGE IN $C_{L_{MAX}}$ AS FUNCTION OF FLAP DEFLECTION FOR THREE PROFILES OF DIFFERENT SECTION AND REYNOLDS NUMBER

D/C VARIABLE

$C_N/C = .10$

- ○ 64,-012 - NACA LOWER SURFACE FLAP - R.N. ≅ 6×10⁶ - D/C ≅ .016 - REF. 88
- × 64,-012 - NACA UPPER SURFACE FLAP - R.N. ≅ 6×10⁶ - D/C ≅ .020 - REF. 88
- △ 2315 BIS. - KRÜGER FLAP - R.N. ≅ .82×10⁶ - D/C = .008 - REF. 92
- —— 2315 BIS. - KRÜGER FLAP - R.N. ≅ .82×10⁶ - D/C = .024 - REF. 92
- ◇ CHANGED MUSTANG PROFILE (13.5% t/c) - KRÜGER FLAP - R.N. ≅ 2.1×10⁶ - D/C = .017 - REF. 91

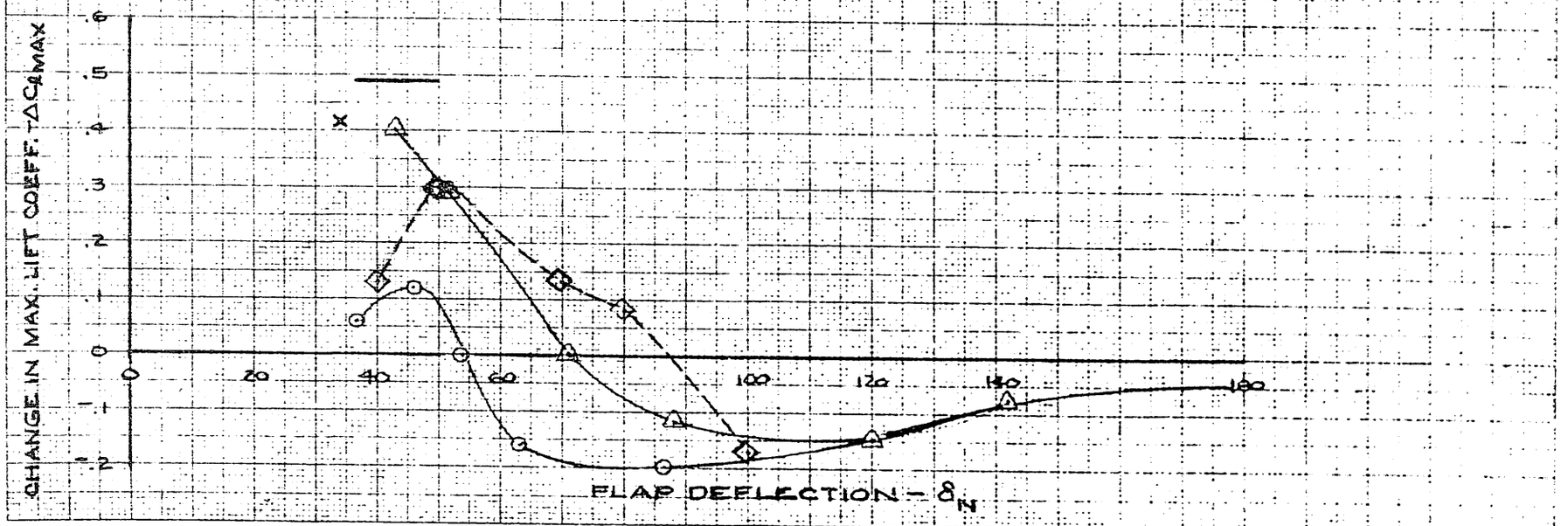

FIG. 129

CONFIDENTIAL

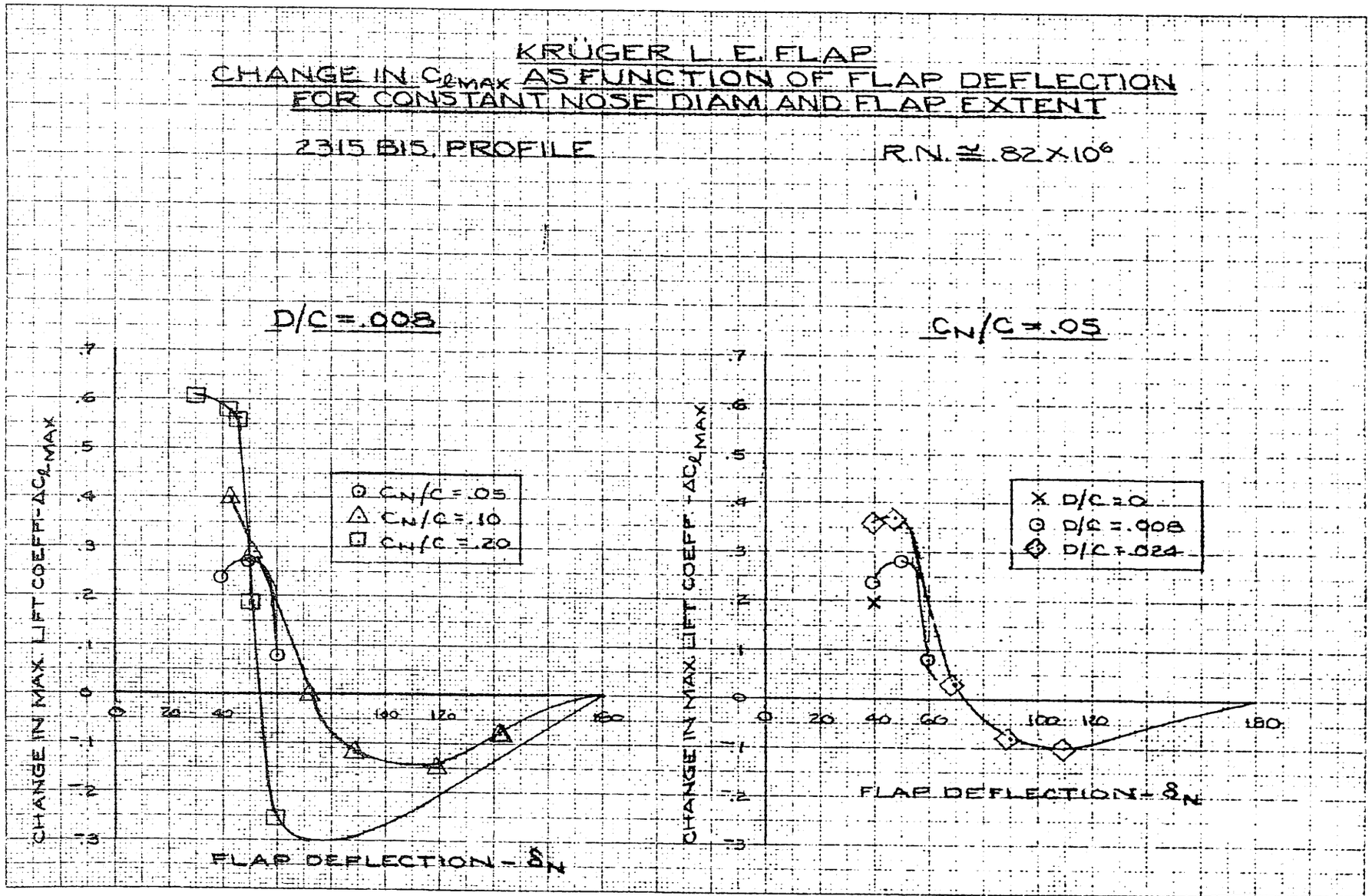

FIG. 130

KRÜGER L.E. FLAP

INCREASE IN $C_{\ell_{MAX}}$ AS FUNCTION OF FLAP EXTENT AND NOSE DIAM.

2315 B15. PROFILE R.N ≅ 8.2×10^6
APPARENT OPTIMUM δ_N

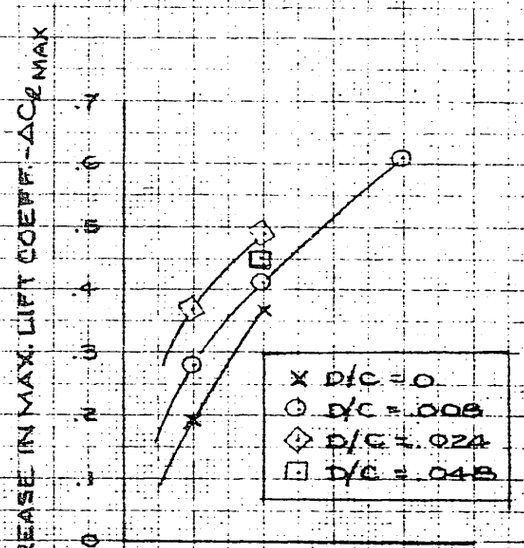

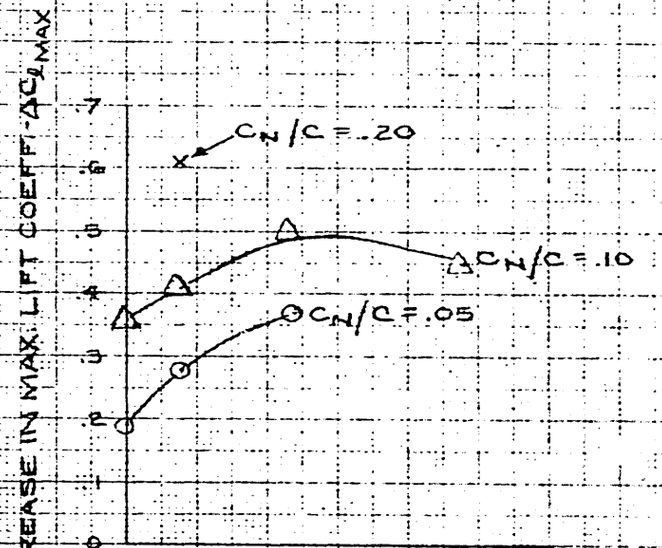

FIG. 131

LEADING-EDGE FLAPS
INCREASE IN MAX. LIFT COEFF. VS. NOSE RADIUS COEFF*

KRÜGER'S DATA (REF 92)
- ⊙ MESSERSCHMITT PROFILE, $t/c = .12$, $c_N/c = .10$, $D/c = .005$, R.N. = ?
- □ MUSTANG-WALZ 2-PROFILE, $t/c = .14$, $c_N/c = .10$, $D/c = .017$, R.N. $= 2.1 \times 10^6$
- △ MUSTANG-WALZ 4-PROFILE, $t/c = .15$, $c_N/c = .10$, $D/c = .030$, R.N. $= .57 \times 10^6$
- ◇ 2315 BIS. PROFILE, $t/c = .12$, $c_N/c = .10$, $D/c = .024$, R.N. $= .82 \times 10^6$

OTHER EXTENSIBLE FLAP DATA (REF. 88)
- × 64, 012 (UPPER-SURFACE), $c_N/c = .10$, $D/c = .020$, R.N. $= 6 \times 10^6$

CONTOURED FLAP DATA
- ○ SHARP-NOSE PROFILES, $c_N/c = .15$, R.N. $= 6 \times 10^6$
- ▽ 63, -012, $c_N/c = .15$, R.N. $= 4.9 \times 10^6$
- △ 65A006, $c_N/c = .15$, R.N. $= 6 \times 10^6$
- ◇ 64A010, $c_N/c = .15$, R.N. $= 6 \times 10^6$

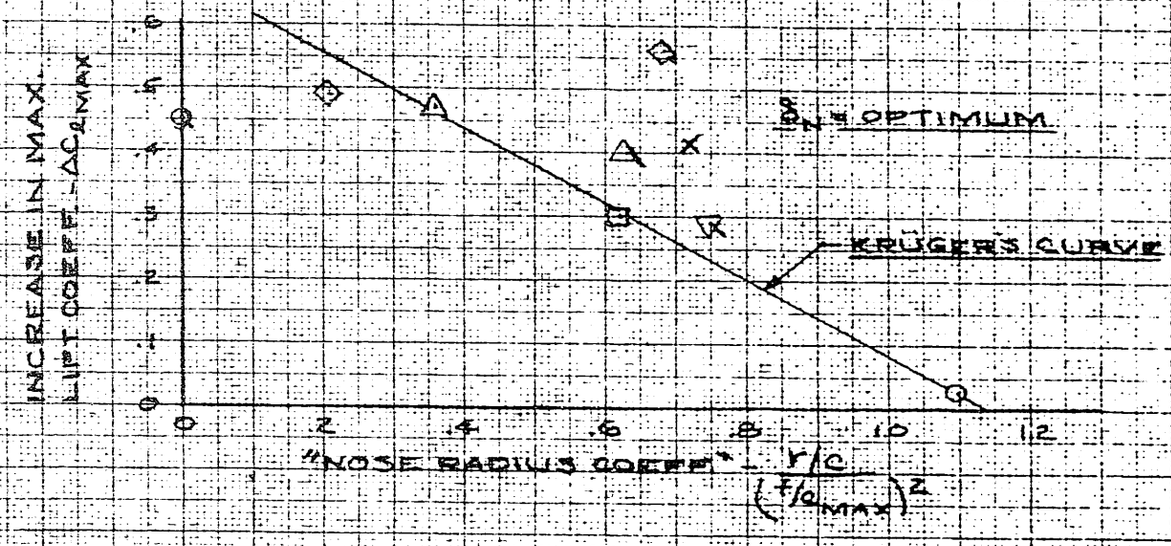

FIG. 132

EXTENSIBLE LEADING-EDGE FLAP
PROBABLE EFFECT OF C_N/C AND D/C UPON THE CHANGE IN MAX. LIFT COEFF. DUE TO FLAP DEFLECTION
(LEADING-EDGE SEPAPATION ONLY)

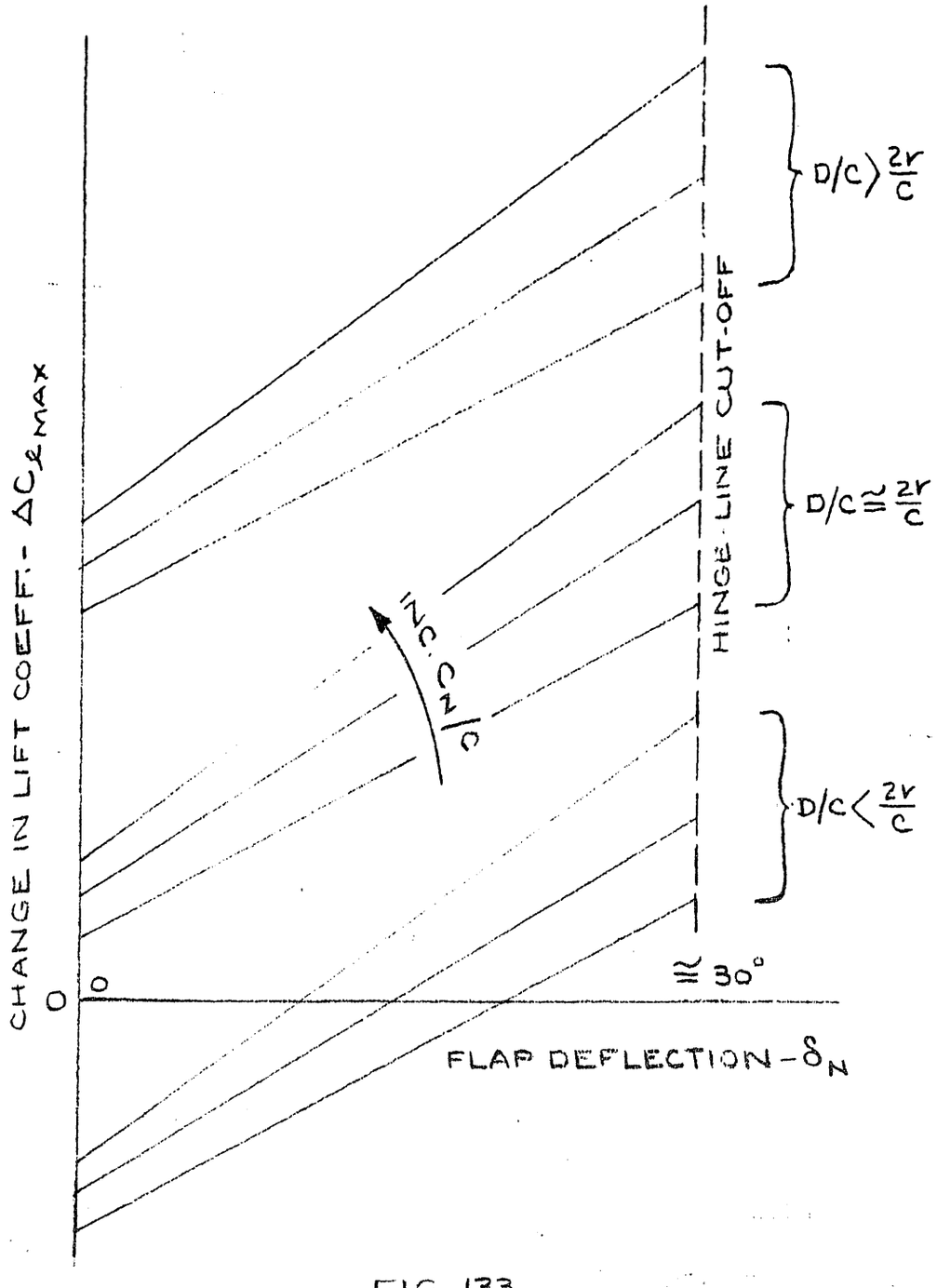

FIG. 133

ARRANGEMENT OF WING AND SLATS

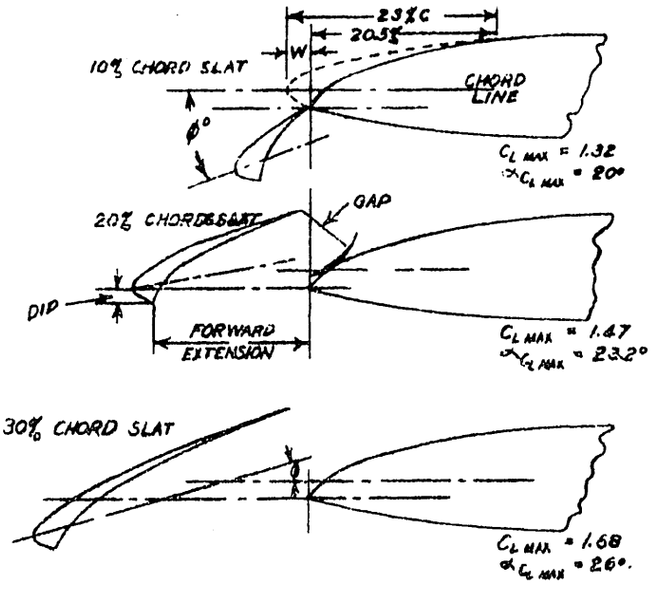

SLOT POSITIONS SHOWN ARE THOSE GIVING HIGHEST $C_{L\,max}$ FOR $\Delta C_L = -0.02$ ON OPENING AT $\alpha = 12°$
10% THICK SYMMETRICAL WING SECTION

FIG. 134

HIGH-LIFT SUCTION SYSTEMS

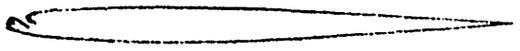

(A) LEADING-EDGE SLOT SUCTION

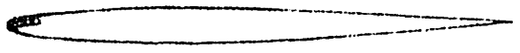

(B) LEADING-EDGE AREA SUCTION

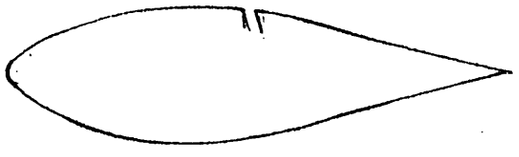

(C) MIDCHORD TYPE SUCTION

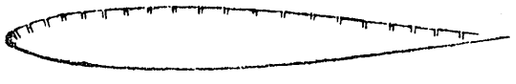

(D) UPPER-SURFACE DISTRIBUTED SUCTION

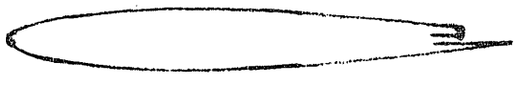

(E) TRAILING-EDGE SUCTION

FIG. 135

LEADING-EDGE SUCTION
TYPICAL APPEARANCE OF $\Delta C_{l\,MAX}$ VS. C_Q CURVE FOR A PROFILE UTILIZING LEADING-EDGE SUCTION

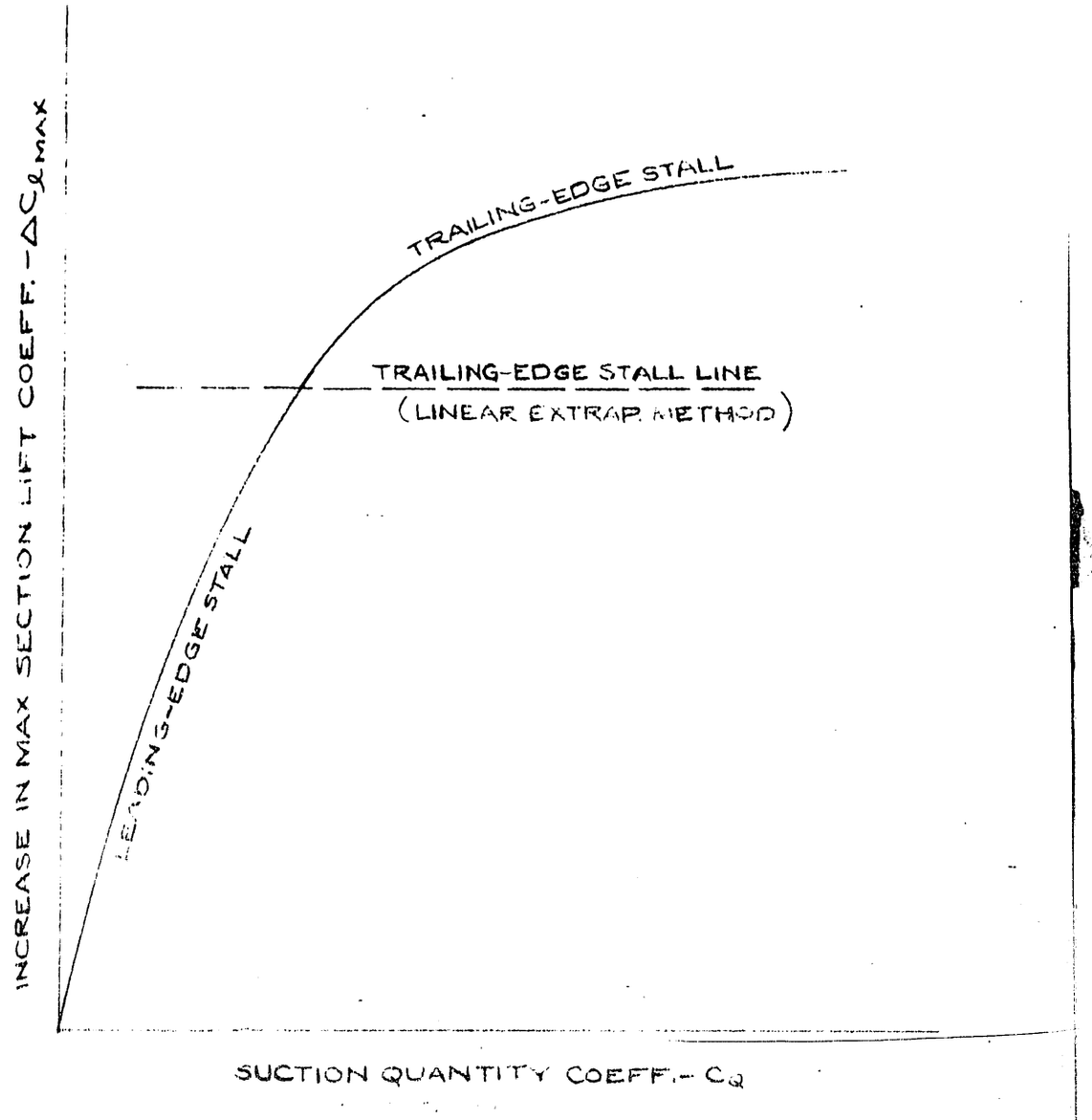

FIG. 136

LEADING-EDGE SUCTION

PARTIAL-CONTROL CONCEPTS OF THE LINEAR METHOD AS APPLIED TO THE TYPICAL CASE OF LEADING-EDGE SUCTION

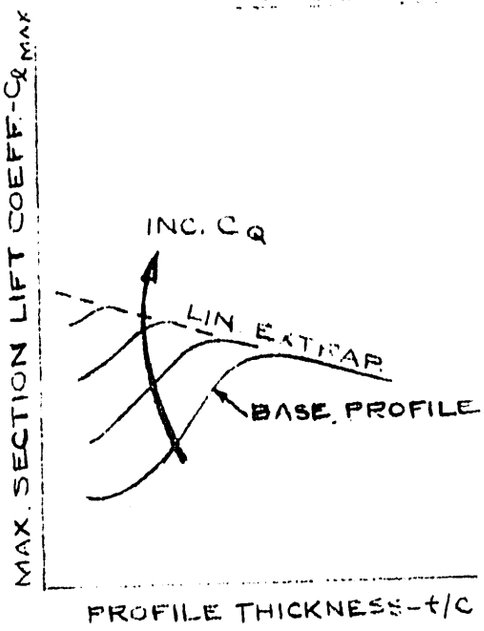

(A) SUCTION OPERATING ON LEADING-EDGE SEPARATION ONLY

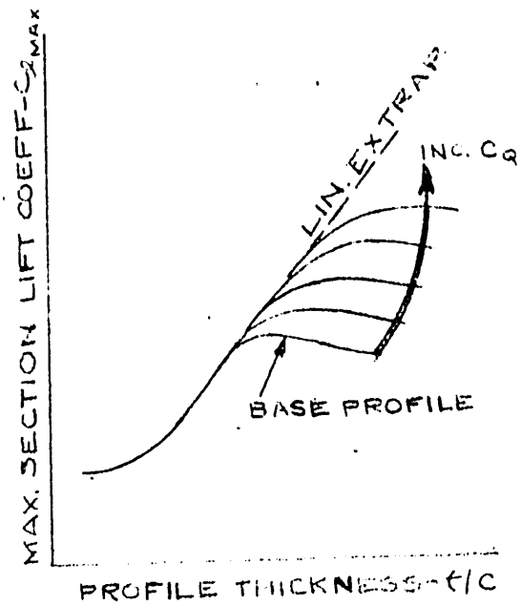

(B) SUCTION OPERATING ON TRAILING-EDGE SEPARATION ONLY

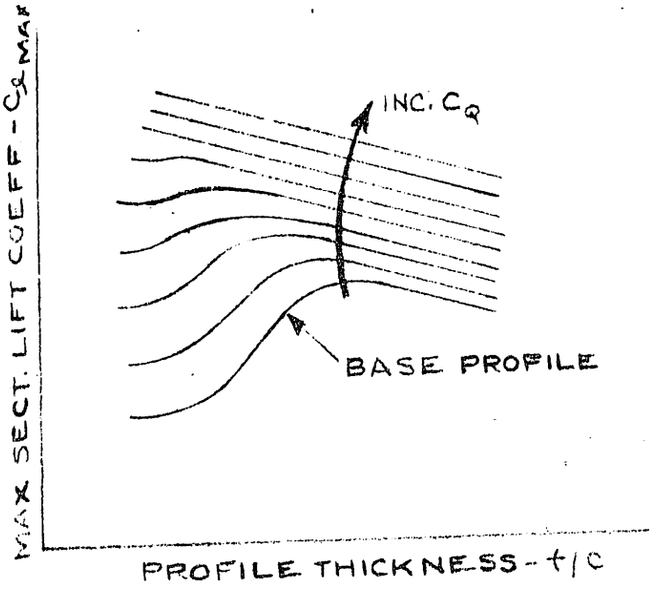

(C) SUCTION OPERATING ON BOTH LEADING-EDGE AND TRAILING-EDGE SEPARATION, BUT MORE EFFECTIVELY ON THE LEADING-EDGE SEP.

FIG. 137

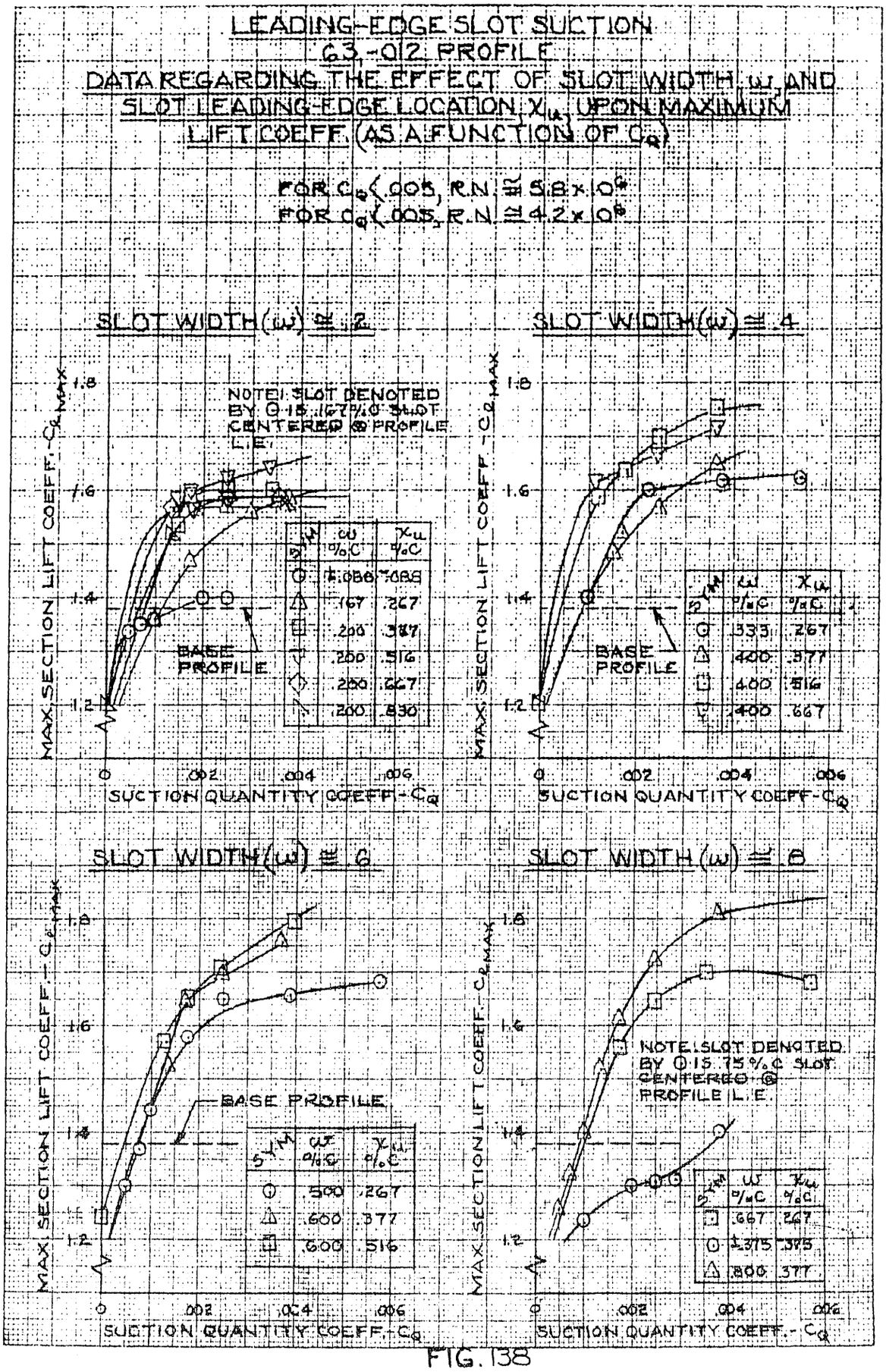

FIG. 138

LEADING-EDGE SLOT SUCTION
63,-012 PROFILE
DATA REGARDING THE EFFECT OF SLOT WIDTH AND SLOT LOCATION UPON MAXIMUM LIFT COEFF. FOR VARIOUS VALUES OF C_Q
R.N. ≅ 5.8×10^6

LINE	C_Q
———	.0015
— — —	.0025
- - - -	.0040

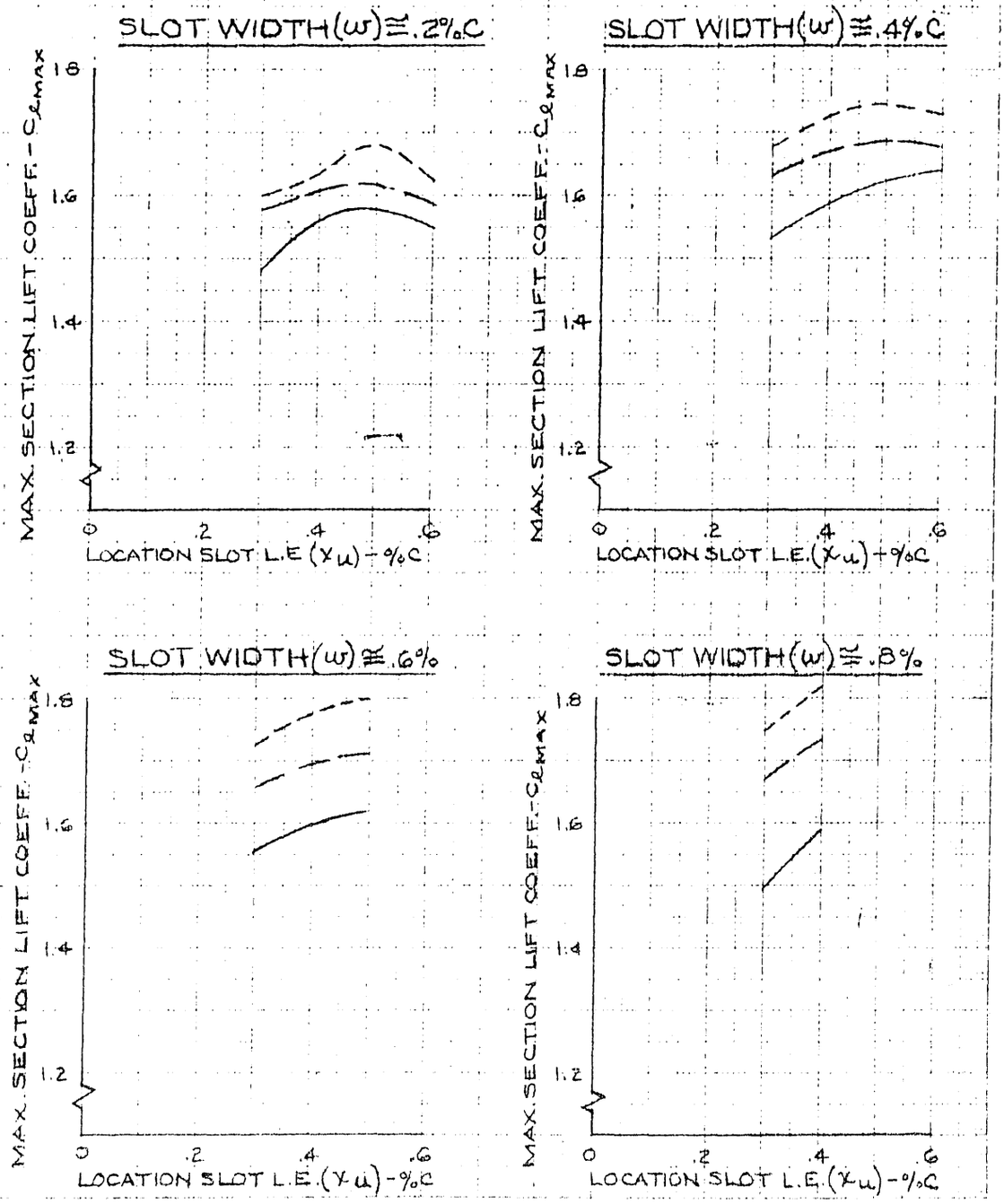

FIG. 139

LEADING-EDGE SLOT SUCTION
63,-012 PROFILE
CROSS-PLOT INDICATING THE EFFECT OF SLOT WIDTH AND SLOT LOCATION UPON MAX. LIFT COEFF. FOR VARIOUS VALUES OF C_Q

R.N. ≅ 5.8×10^6

LINE	LOCATION SLOT L.E. (Y_u)
———	.38 %C
- - - - -	.50 %C

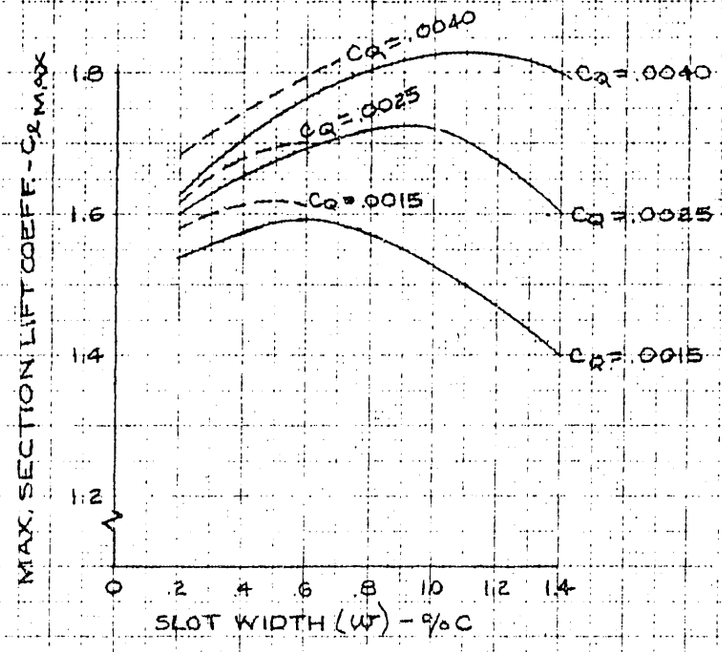

FIG. 140

LEADING-EDGE SLOT SUCTION ADDITIONAL DATA - EARLY EXPERIMENTAL RESULTS (1945-1947)

(A) EARLY BRITISH EXPERIMENTAL INVESTIGATIONS

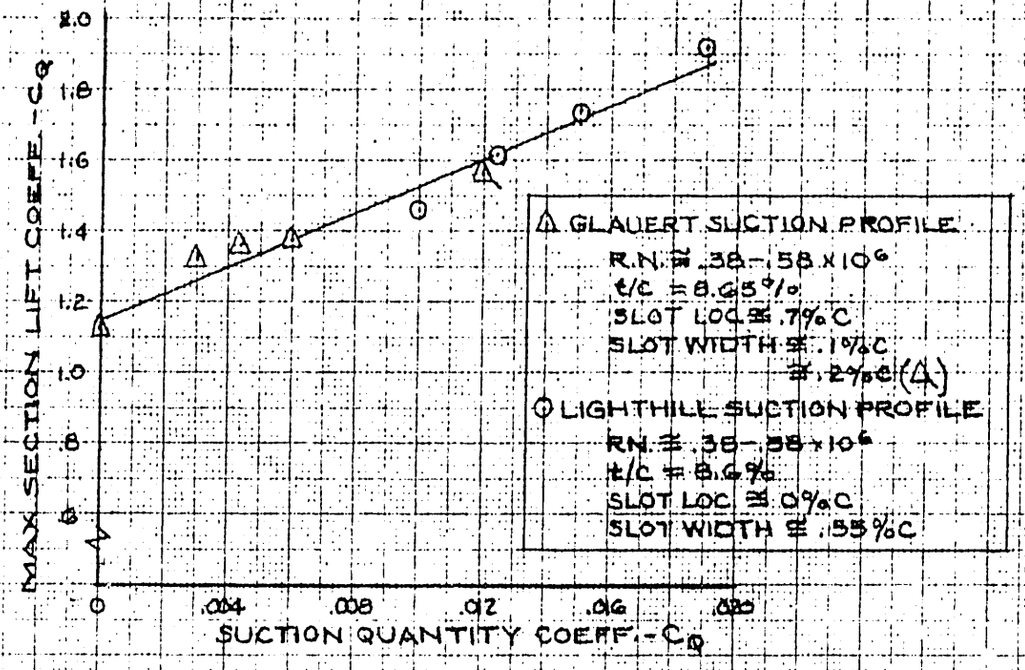

(B) RESULTS OF EARLY GERMAN EXPERIMENTAL INVESTIGATIONS REGARDING OPTIMUM SLOT LOCATION

R.N. ≅ .33 x 10⁶ SLOT WIDTH = ?

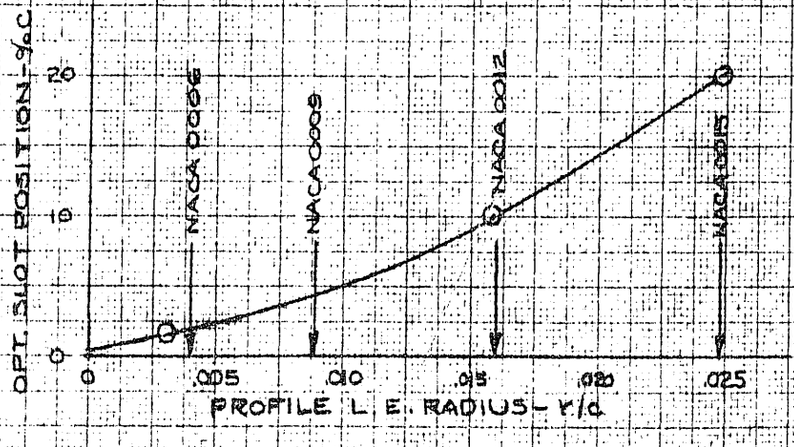

FIG. 14-1

CONFIDENTIAL

LEADING-EDGE AREA SUCTION
VARIOUS TYPES OF PERMEABILITY ARRANGEMENT
AND THEIR TYPICAL EFFECTS UPON THE SHAPE
OF THE CHORDWISE SUCTION VELOCITY DISTRIBUTION

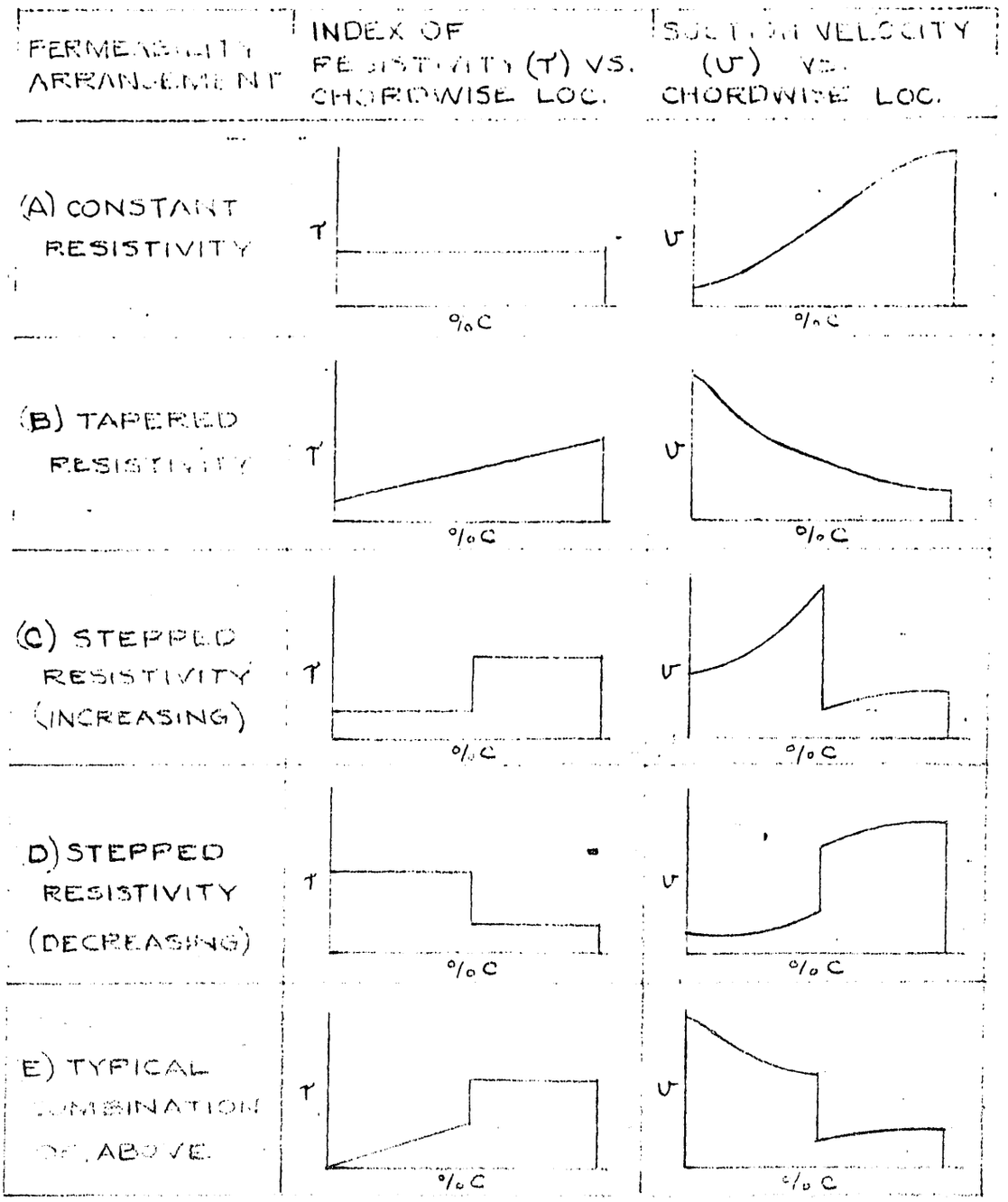

FIG. 142

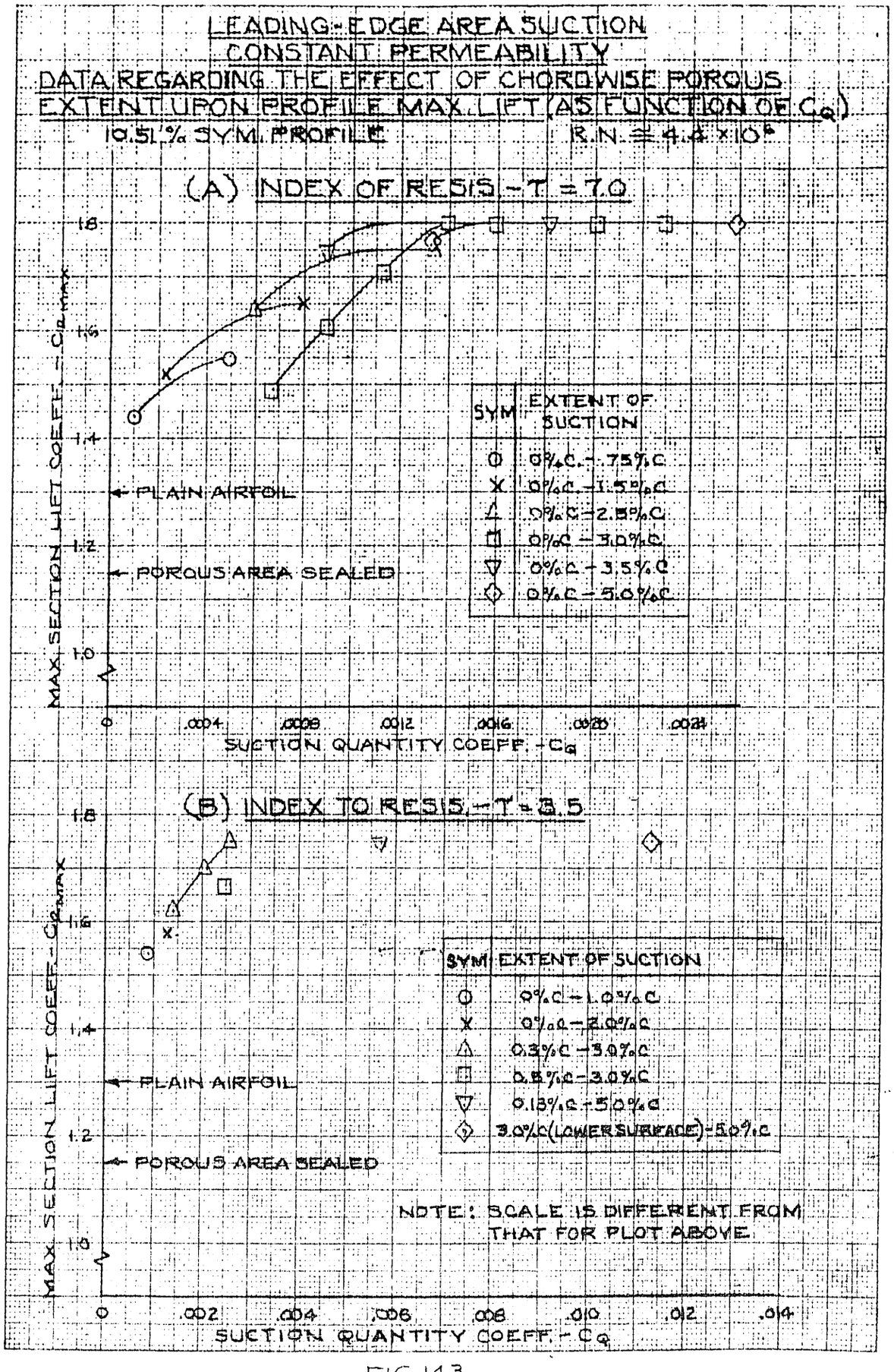

FIG. 143

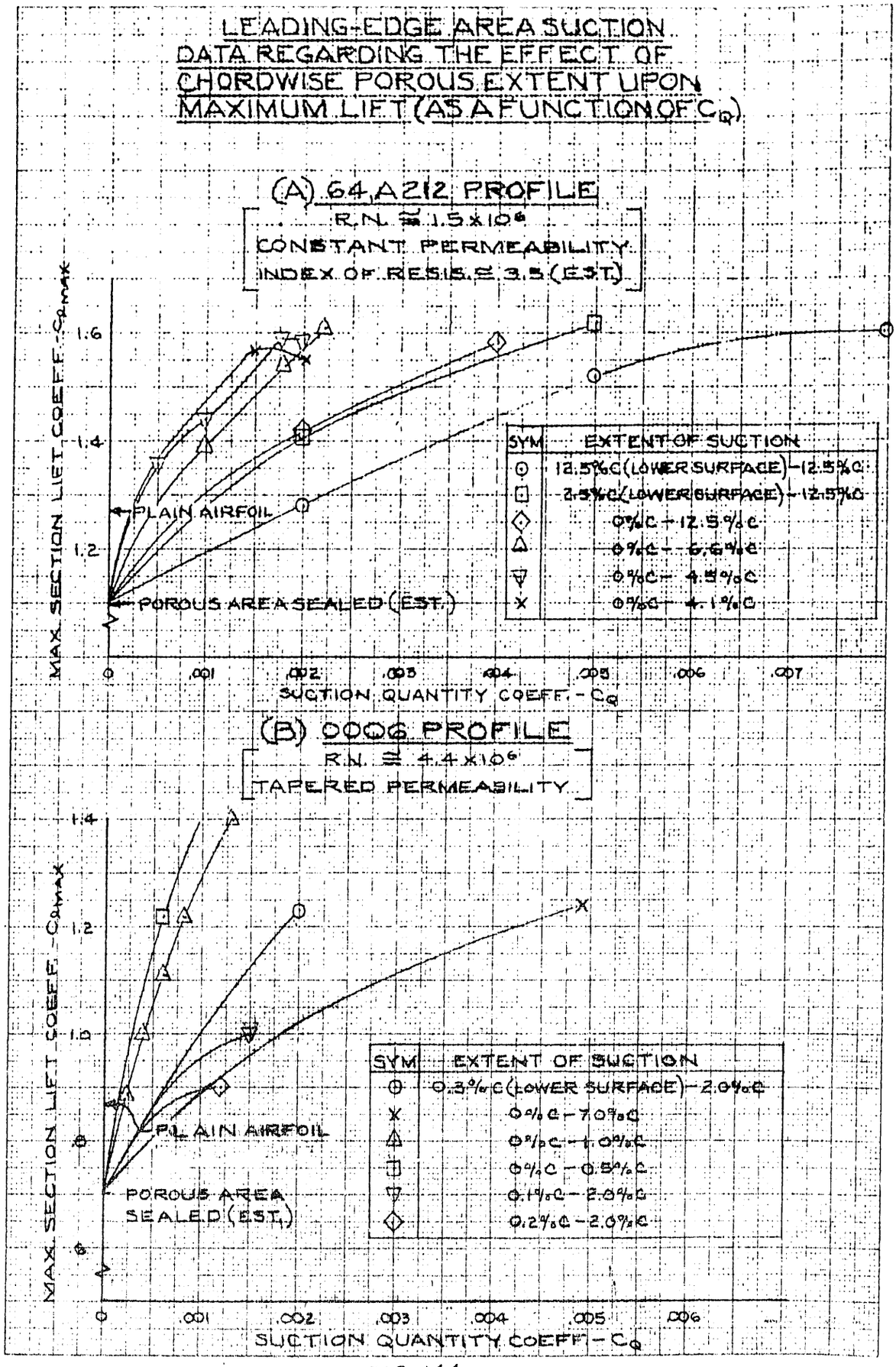

FIG. 144

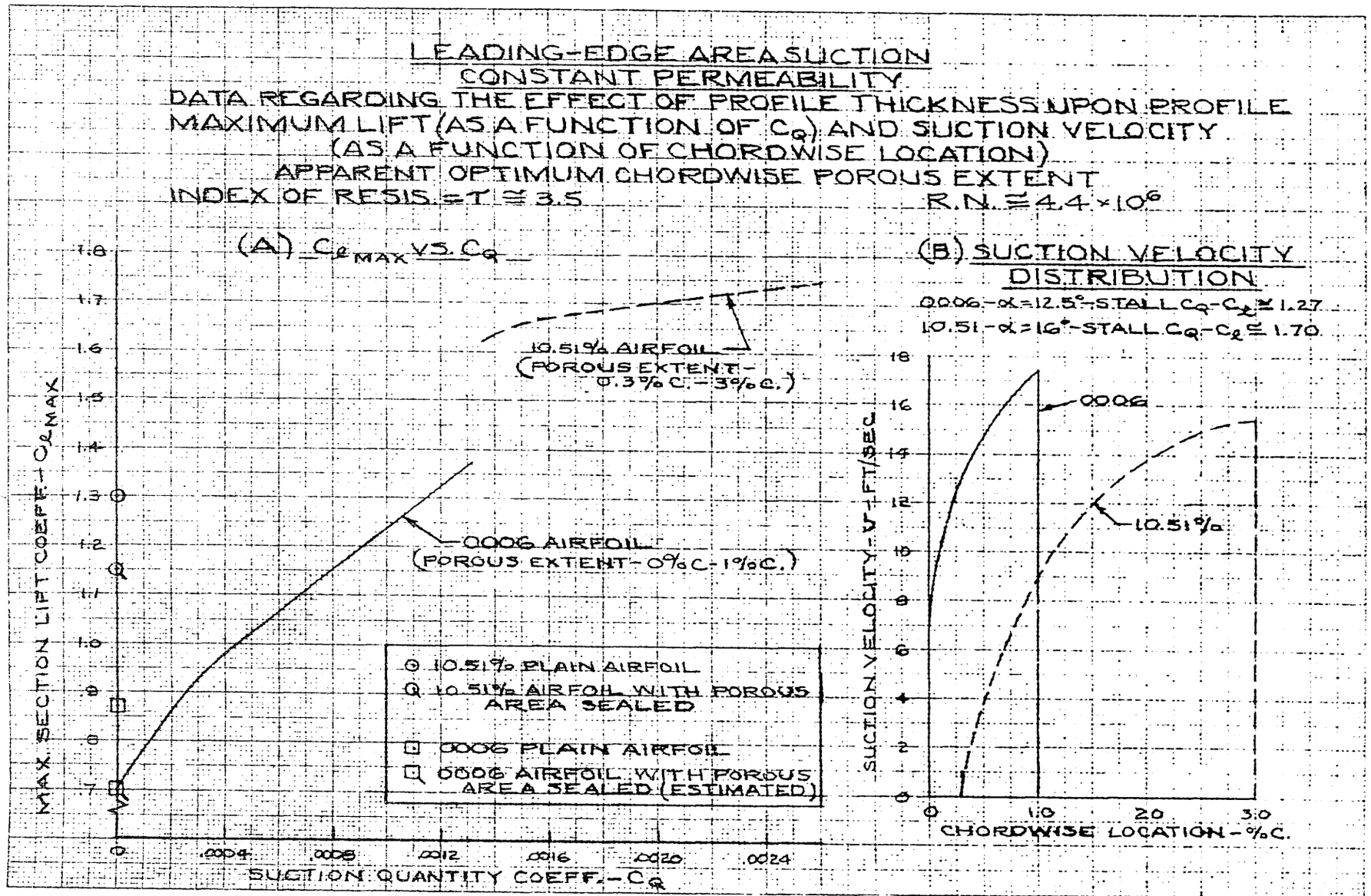

FIG 145

CONFIDENTIAL

LEADING-EDGE AREA SUCTION
CONSTANT PERMEABILITY
DATA REGARDING THE EFFECT OF THE RESISTIVITY OF THE POROUS MATERIAL UPON PROFILE MAXIMUM LIFT (AS A FUNCTION OF C_Q) AND SUCTION VELOCITY (AS FUNCTION OF CHORDWISE LOCATION)

10.51% SYM. PROFILE R.N. ≅ 4.4×10^6

(A) $C_{\ell MAX}$ VS. C_Q

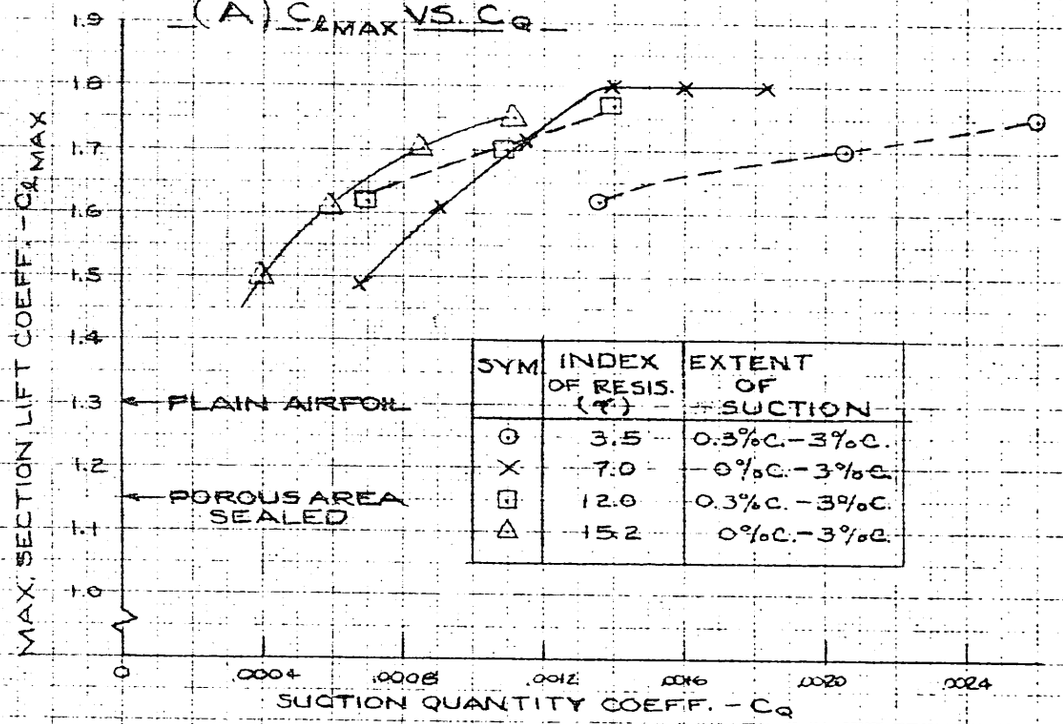

SYM	INDEX OF RESIS. (τ)	EXTENT OF SUCTION
⊙	3.5	0.3%c.-3%c.
×	7.0	0%c.-3%c.
⊡	12.0	0.3%c.-3%c.
△	15.2	0%c.-3%c.

(B) SUCTION VELOCITY DISTRIBUTION

(α = 16°; C_Q = THAT FOR STALL @ 16°; $C_\ell \cong 1.7$)

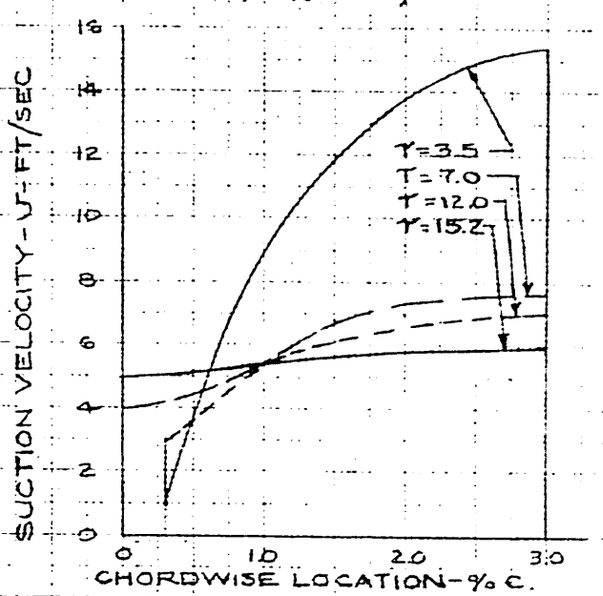

FIG. 146

LEADING-EDGE AREA SUCTION TESTED PERMEABILITY ARRANGEMENTS

REFERENCE	CONFIGURATION	RESIS. DISTRIBUTION
118	C	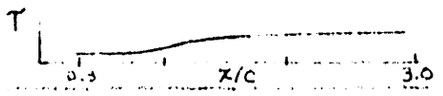
	D	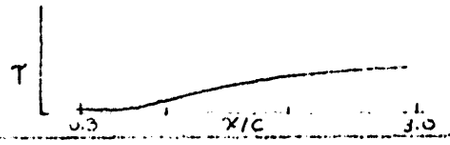
	E	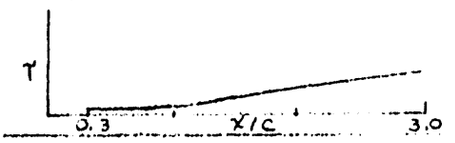
	K	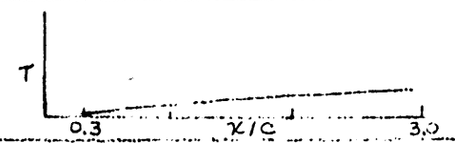
	L	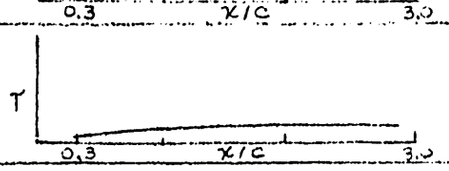
	F	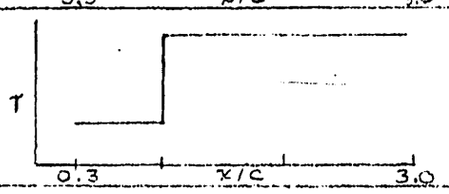
	G	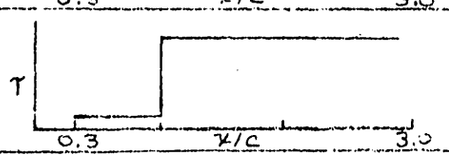
	H	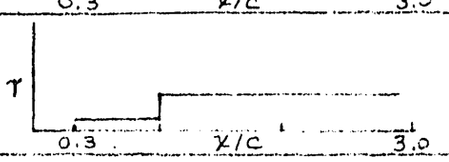
	I	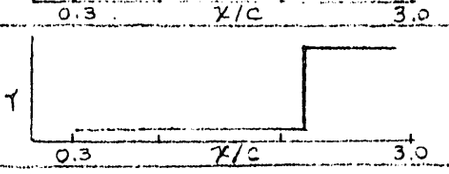
	J	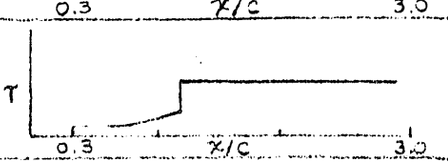
119	TAPERED	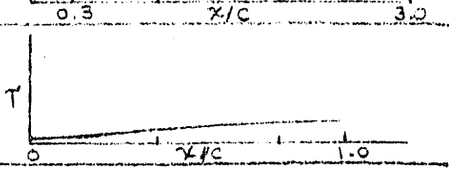

FIG. 147

LEADING-EDGE AREA SUCTION
0006 AIRFOIL
THE EFFECT OF TAPERED PERMEABILITY UPON MAX. LIFT COEFF.
POROUS EXTENT = 0%C-1%C R.N. ≅ 4.4 X 10⁶

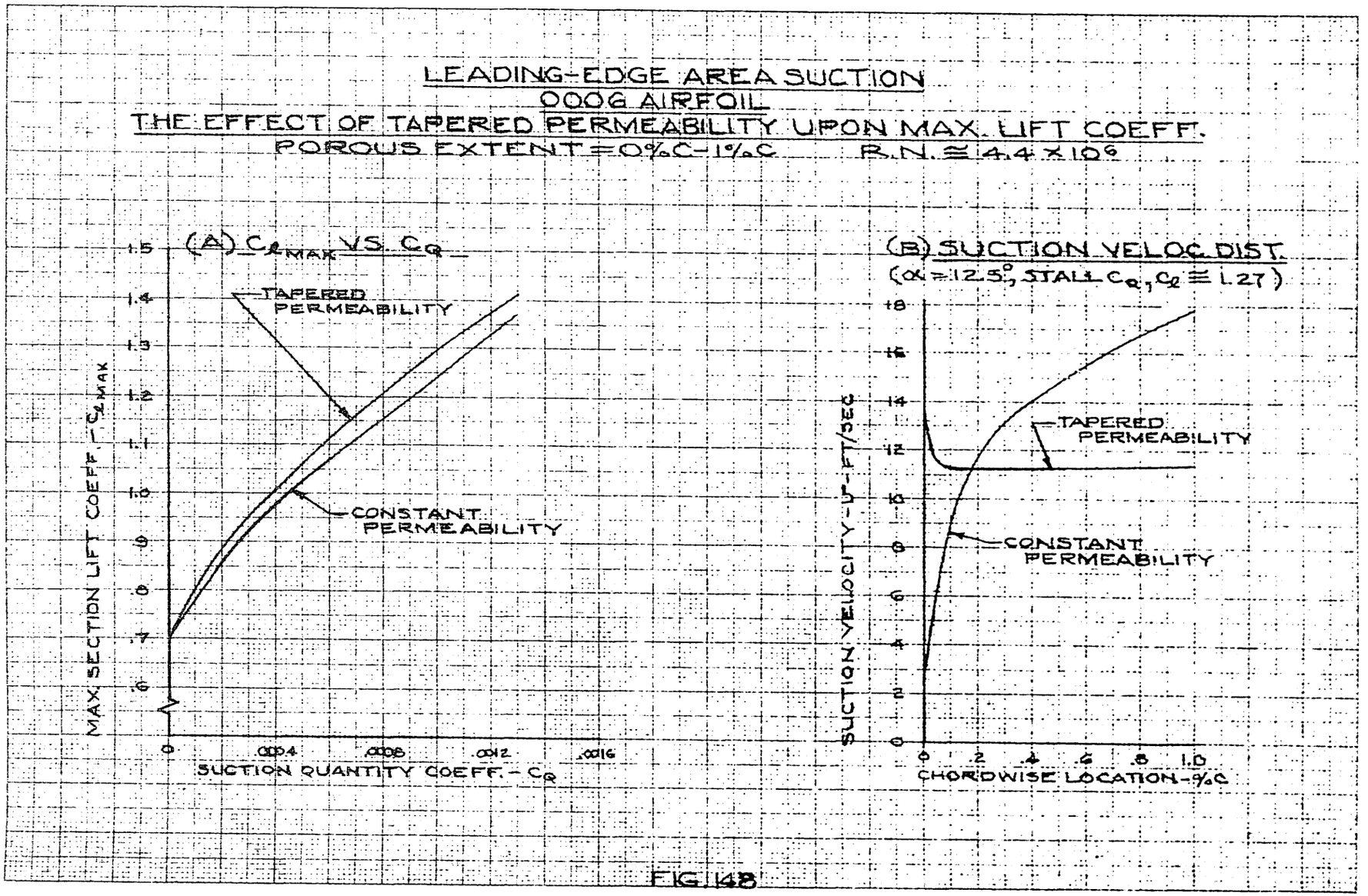

FIG. 148

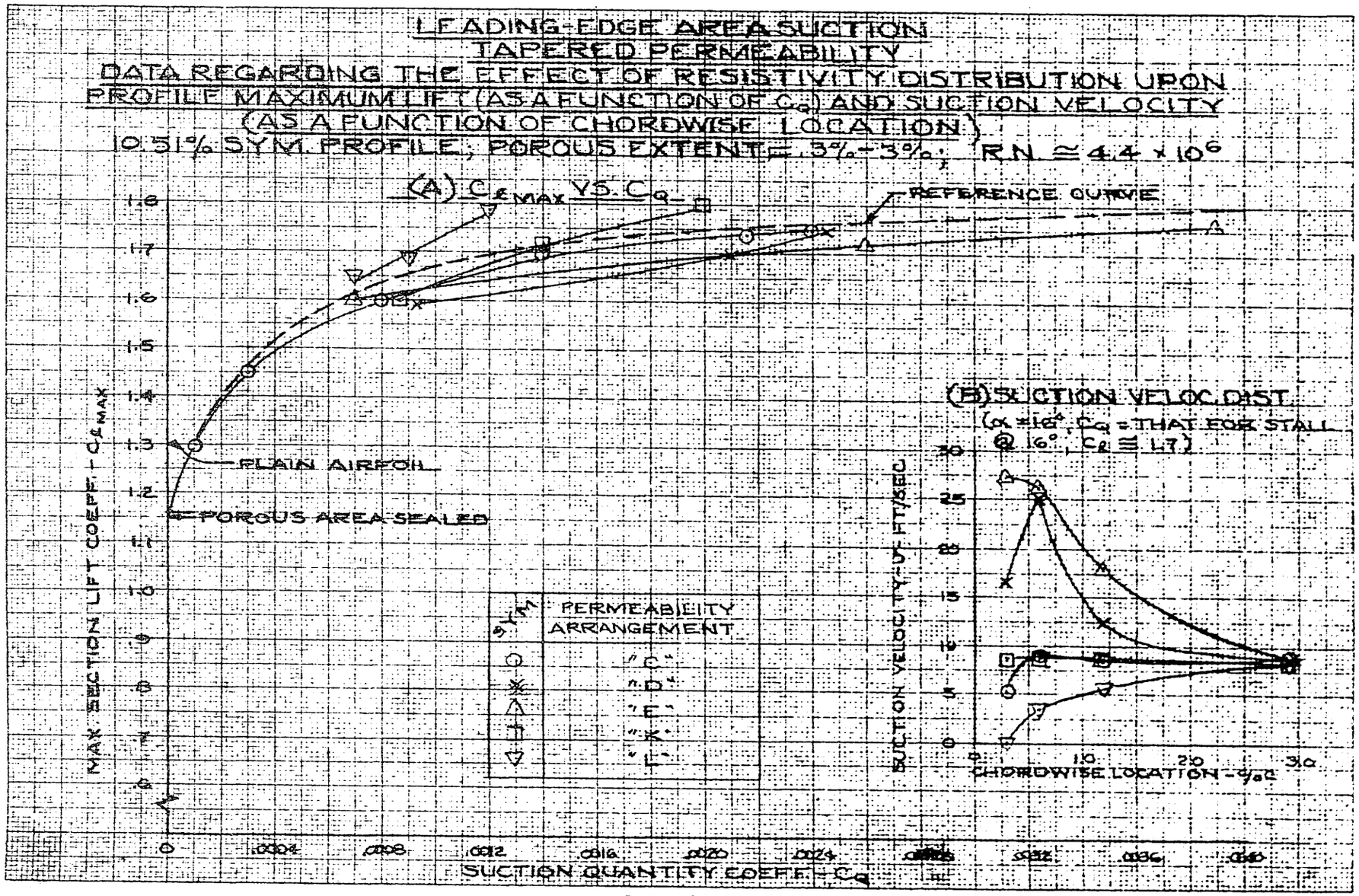

FIG. 149

LEADING-EDGE AREA SUCTION
STEPPED PERMEABILITY

DATA REGARDING THE EFFECT OF RESISTIVITY DISTRIBUTION UPON PROFILE MAXIMUM LIFT (AS A FUNCTION OF C_Q) AND SUCTION VELOCITY (AS A FUNCTION OF CHORDWISE LOCATION)

10.51% SYM. PROFILE; POROUS EXTENT = 3% c - 3% c; R.N. $\cong 4.4 \times 10^6$

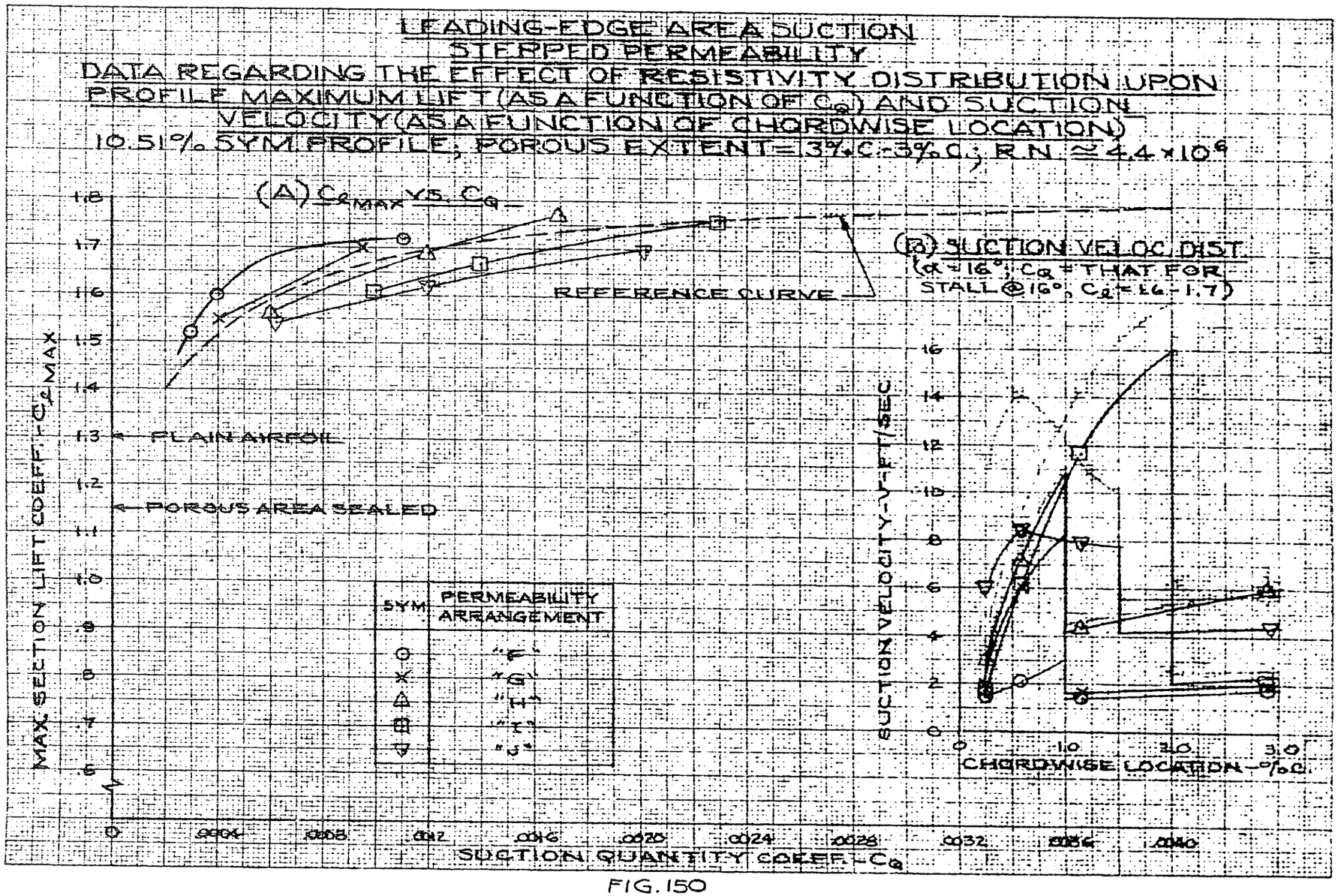

FIG. 150

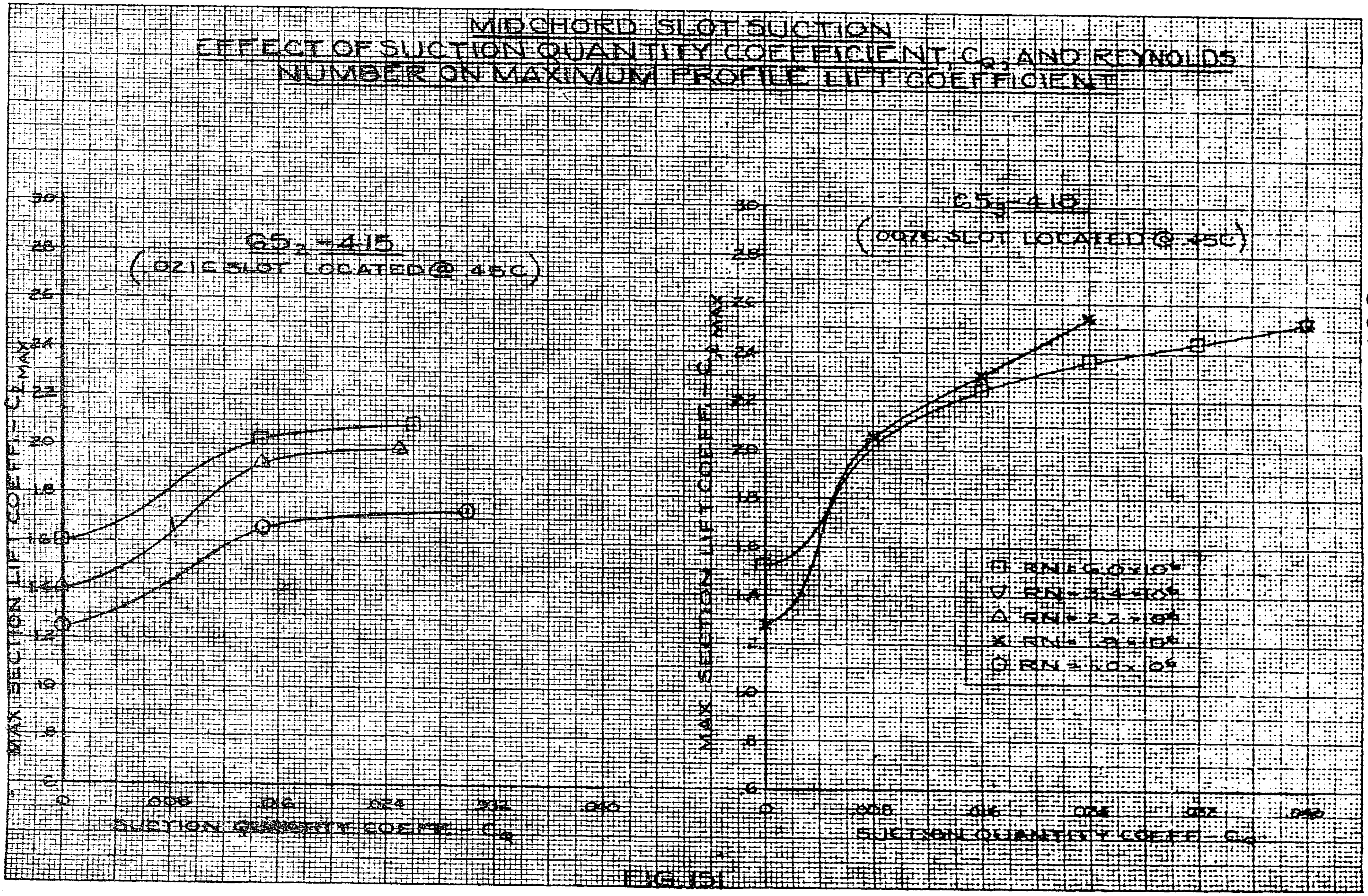

FIG. 151

CONFIDENTIAL

FIG 6b2

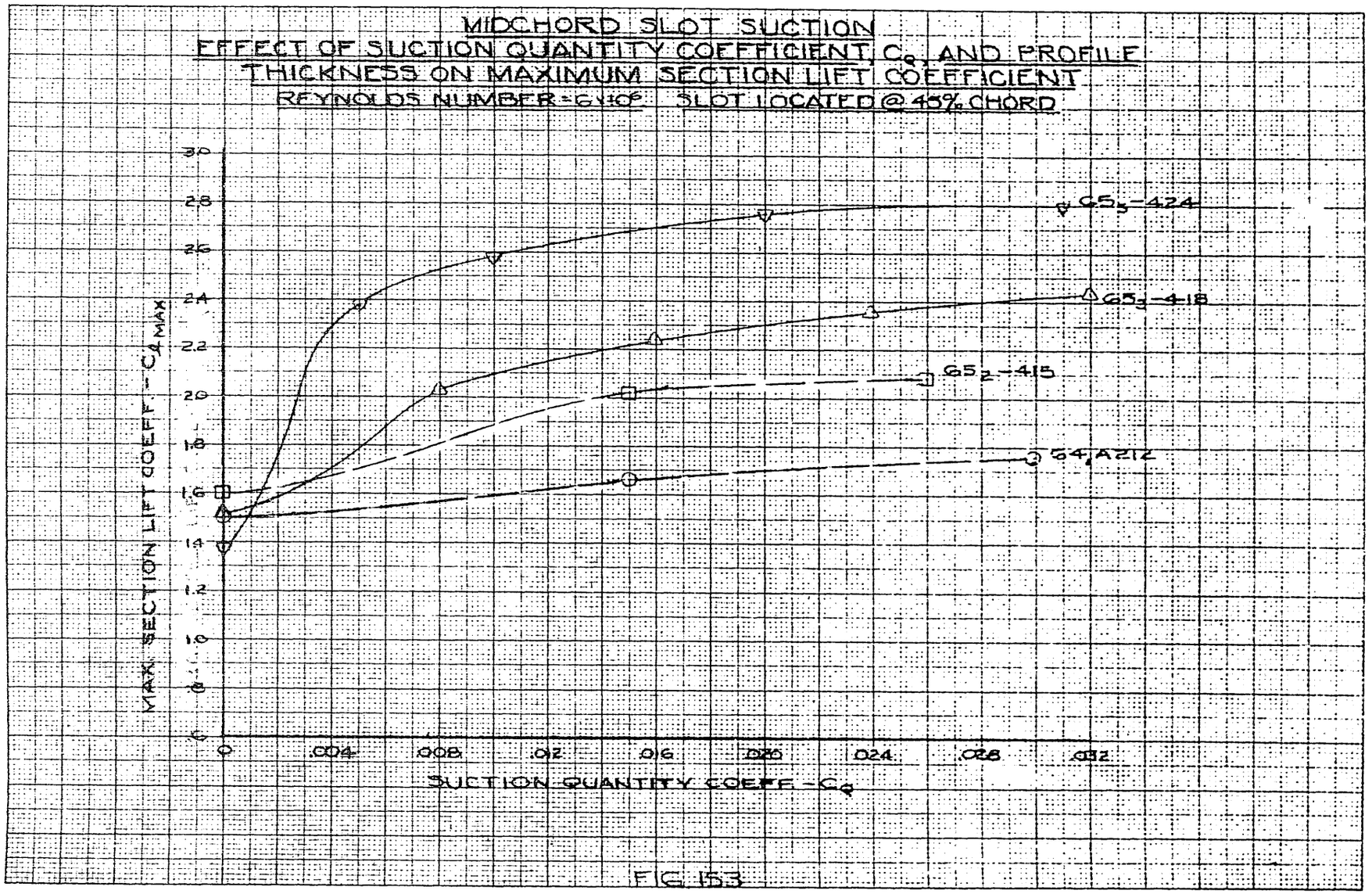

FIG 153

CONFIDENTIAL

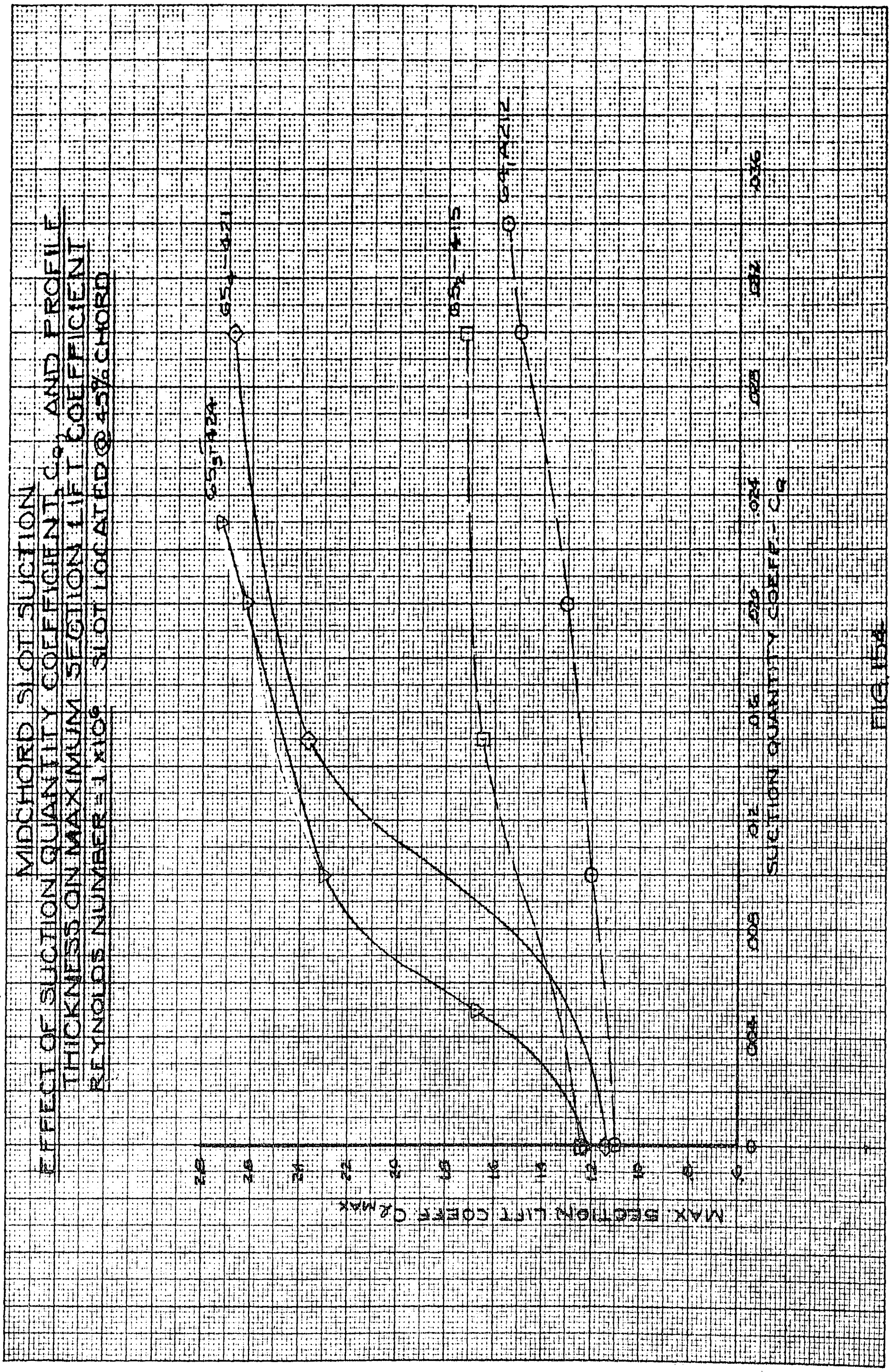

CONFIDENTIAL

MIDCHORD SLOT SUCTION

EFFECT OF SUCTION QUANTITY COEFFICIENT, C_Q, AND PROFILE THICKNESS ON MAXIMUM SECTION LIFT COEFFICIENT - CAMBERED PROFILES

REYNOLDS NUMBER = 6×10^6

SLOT LOCATED @ 45% CHORD

NOTE: DATA POINTS @ 12% t/c ARE FROM TESTS OF 64, A212. ALL OTHER POINTS FROM TESTS OF 65-4 SERIES PROFILES

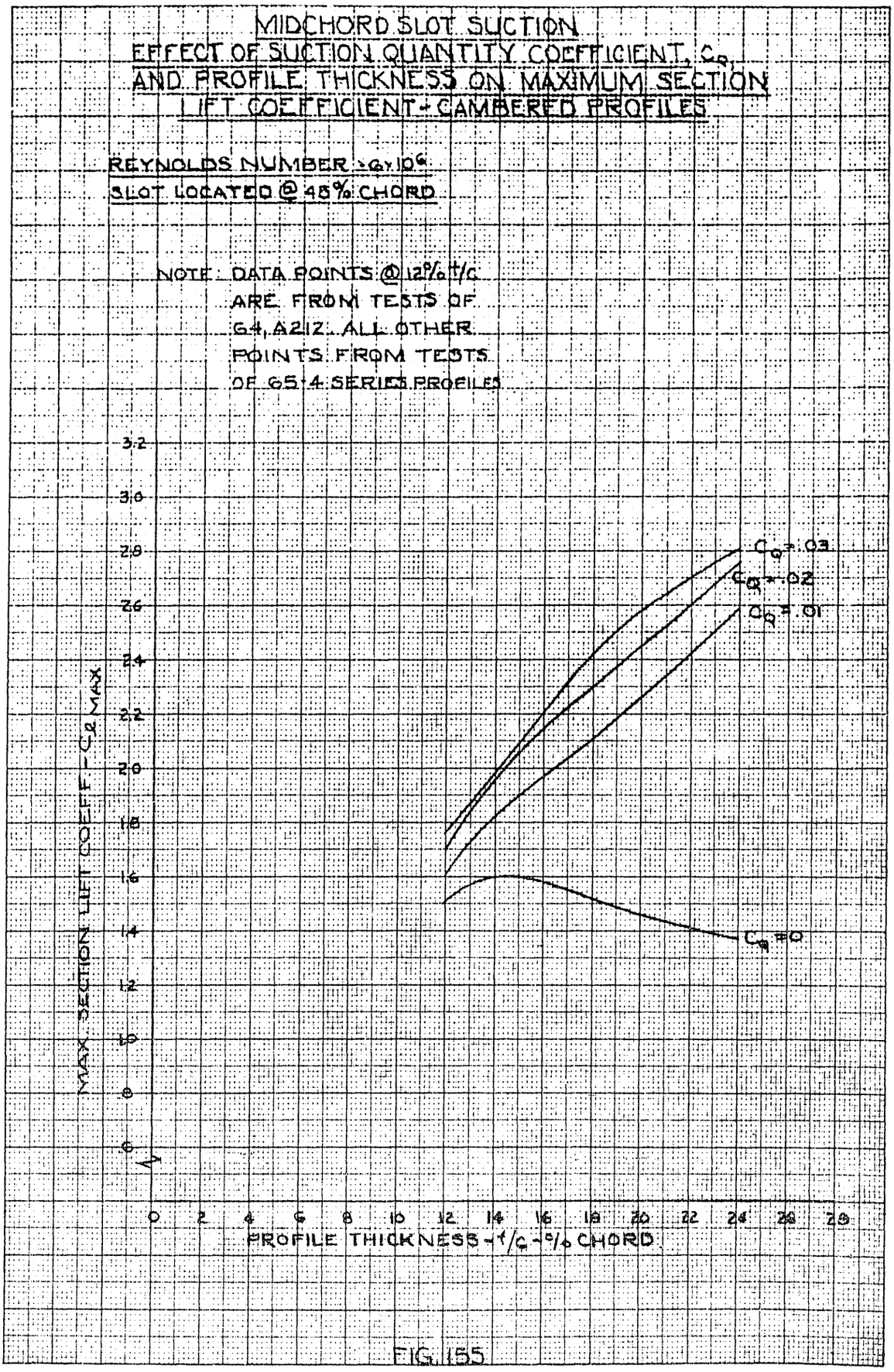

FIG. 155

FIG. 157

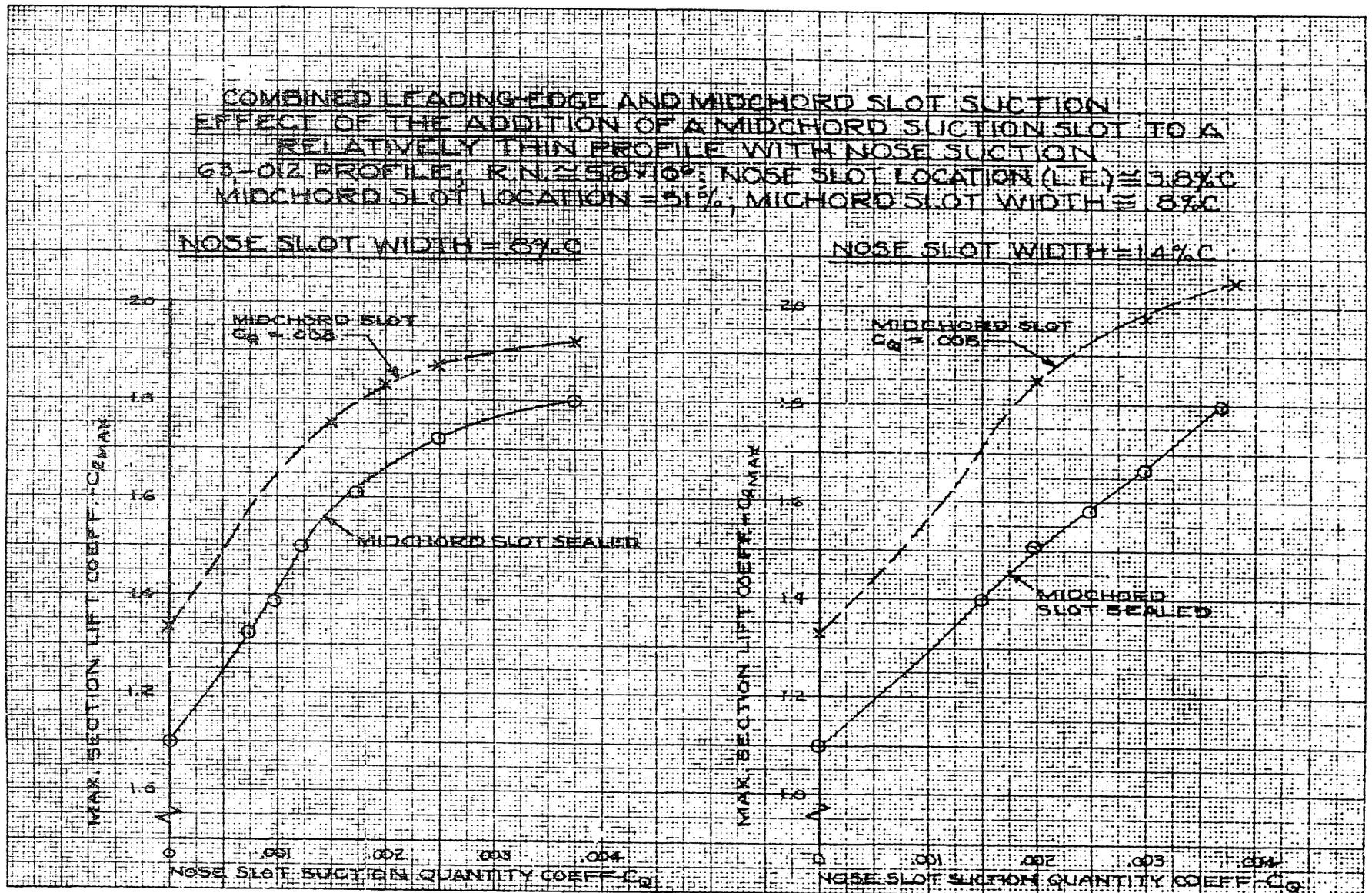

FIG. 158

CONFIDENTIAL

COMBINED LEADING-EDGE AND MIDCHORD SLOT SUCTION
THE EFFECT OF SUCTION FROM VARIOUS
COMBINATIONS OF SLOT LOCATIONS

65_3-018 PROFILE R.N. $\neq 1.0 \times 10^6$

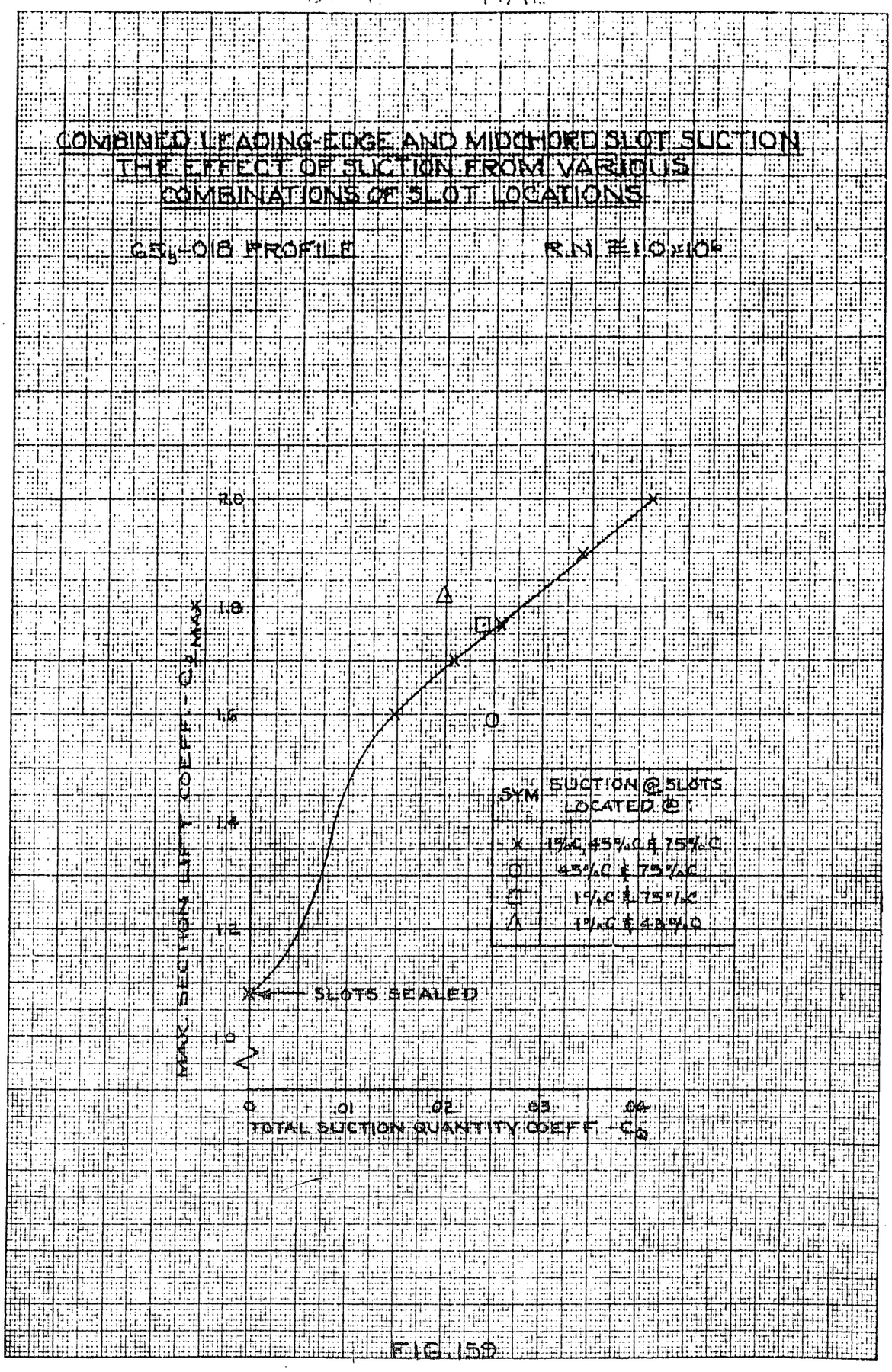

FIG. 159

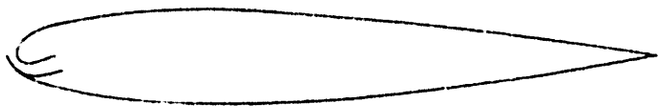

(a) Blowing Slot Under Leading Edge

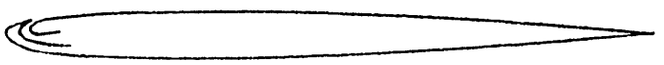

(b) Blowing Slot at Leading Edge

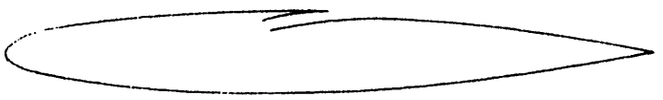

(c) Mid-chord Blowing Slot

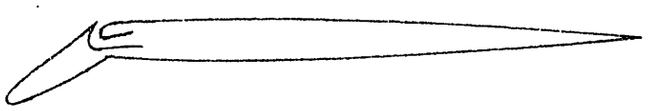

(d) Blowing at Nose Flap Break

FIG. 160

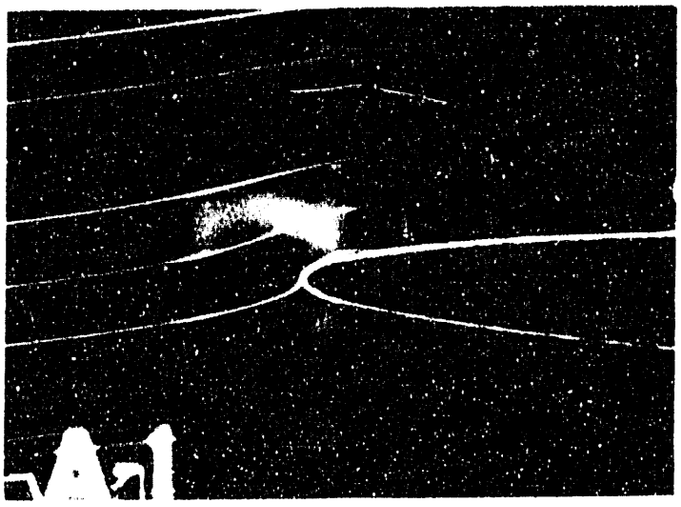

SOLID AIRFOIL AT $\alpha_c = 4°$

(A)

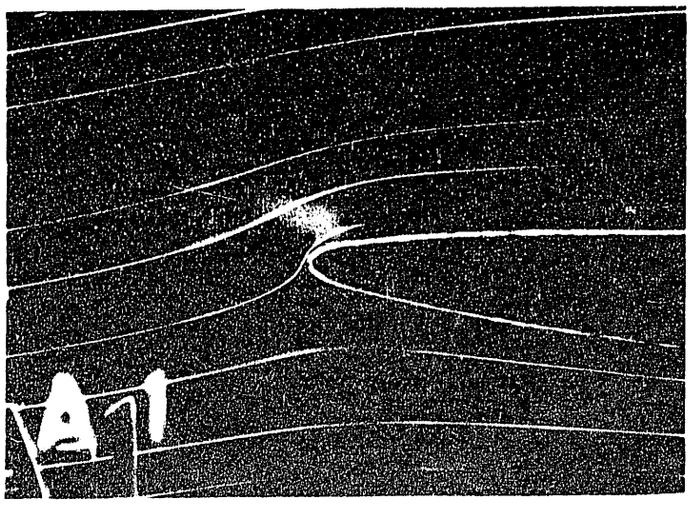

SOLID AIRFOIL AT $\alpha_c = 6°$

(B)

FIG. 161

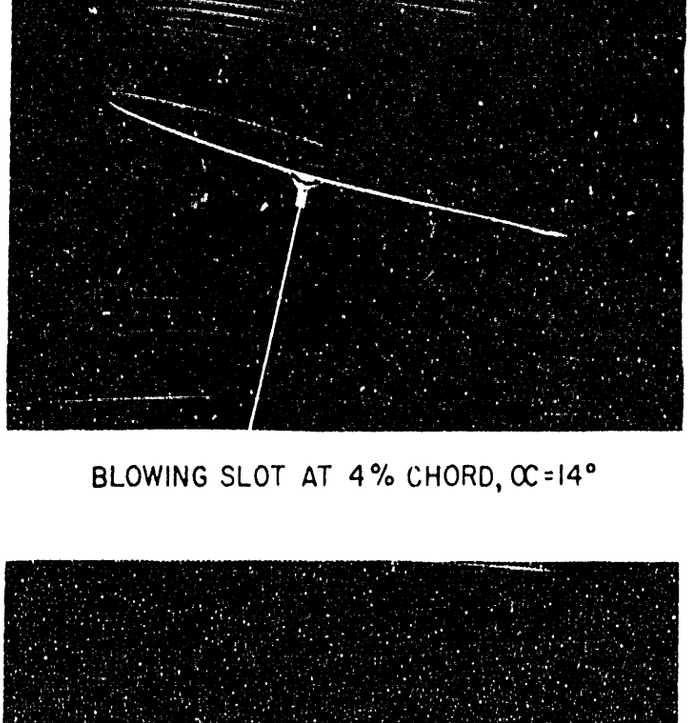

FIG. 162

BLOWING SLOT AT 4% CHORD, $\alpha_c = 14°$

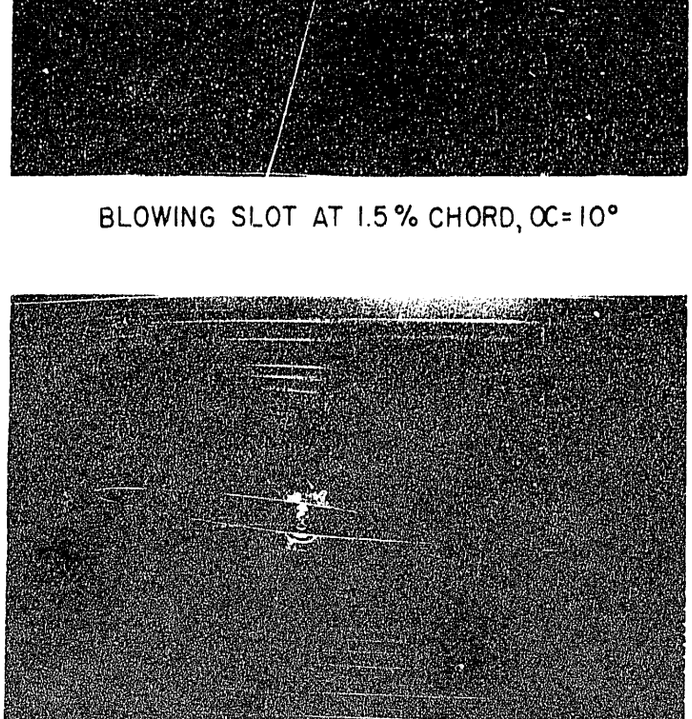

FIG. 163

BLOWING SLOT AT 1.5% CHORD, $\alpha_c = 10°$

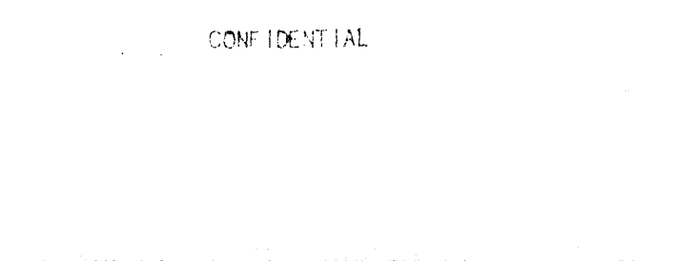

FIG. 164

BLOWING SLOT AT 0% CHORD

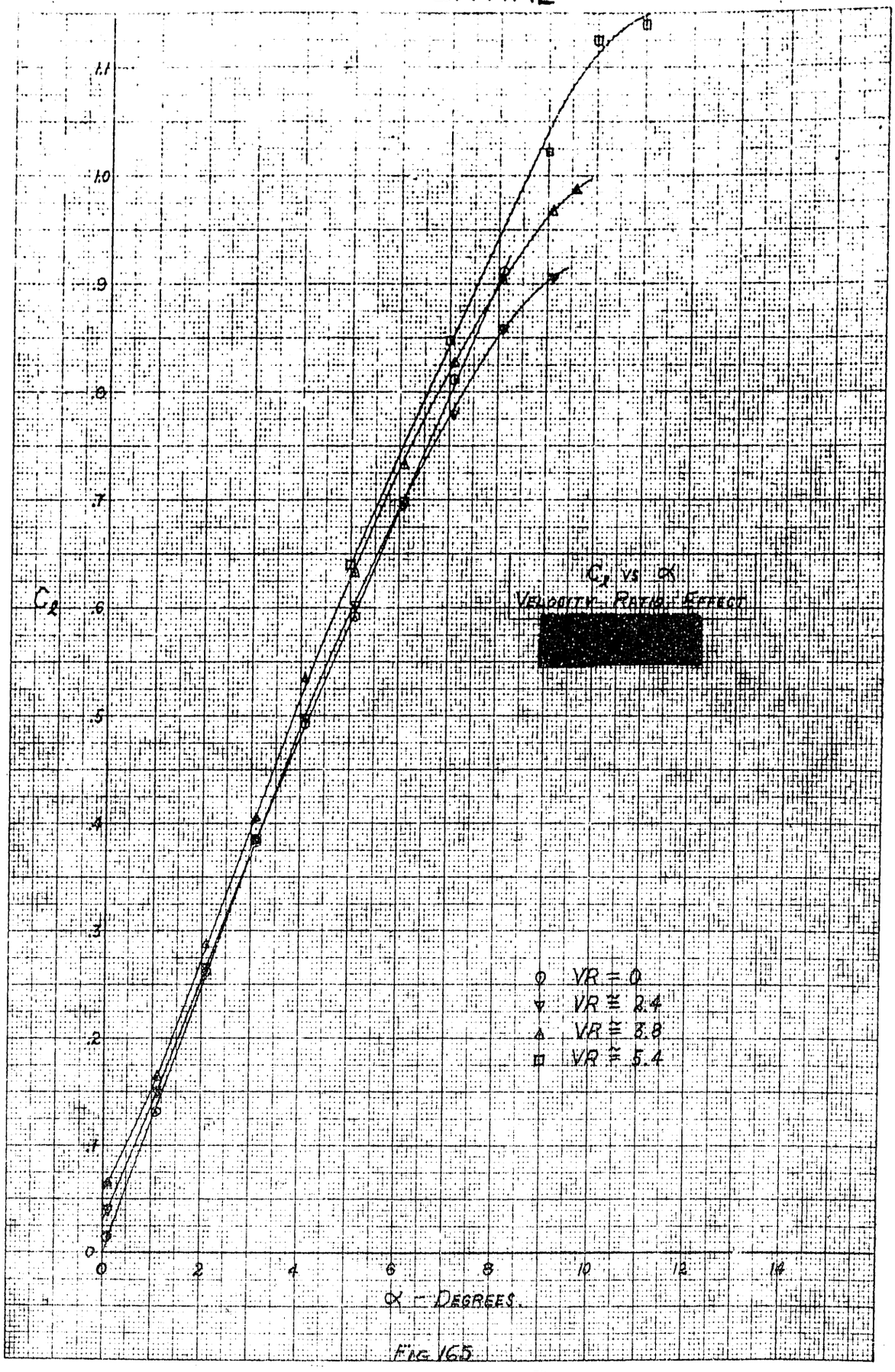
C_L vs α
Velocity Ratio Effect
C_L
α - Degrees
VR = 0
VR ≅ 2.4
VR ≅ 3.8
VR ≅ 5.4
1.1
1.0
.9
.8
.7
.6
.5
.4
.3
.2
.1
0
0
2
4
6
8
10
12
14

Fig. 165

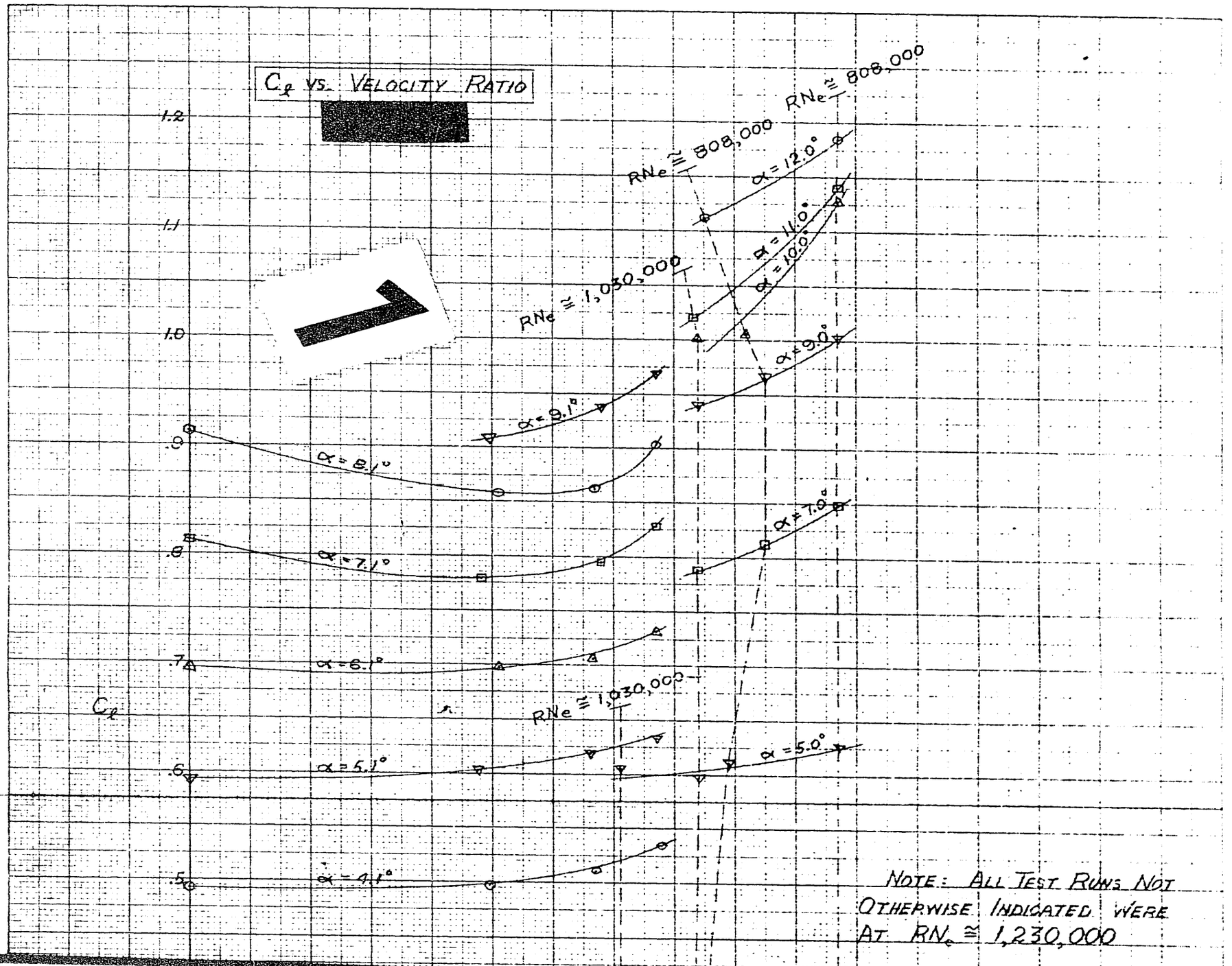

NOTE: ALL TEST RUNS NOT
OTHERWISE INDICATED WERE
AT $RN_c \cong 1,230,000$
$\alpha = 5.0°$
$\alpha = 4.1°$
$\alpha = 3.1°$
$\alpha = 2.1°$
$\alpha = 1.1°$
$\alpha = 1.0°$
$\alpha = 0.1°$
C_N
R_{Nc}
VELOCITY RATIO
FLOW QUANTITY COEFFICIENT = C_Q
.0025
.0050
.0075
.0100
.0125
1
2
3
4
5
6
7
.1
.2
.3
.4
.5
.6

FIG. 166

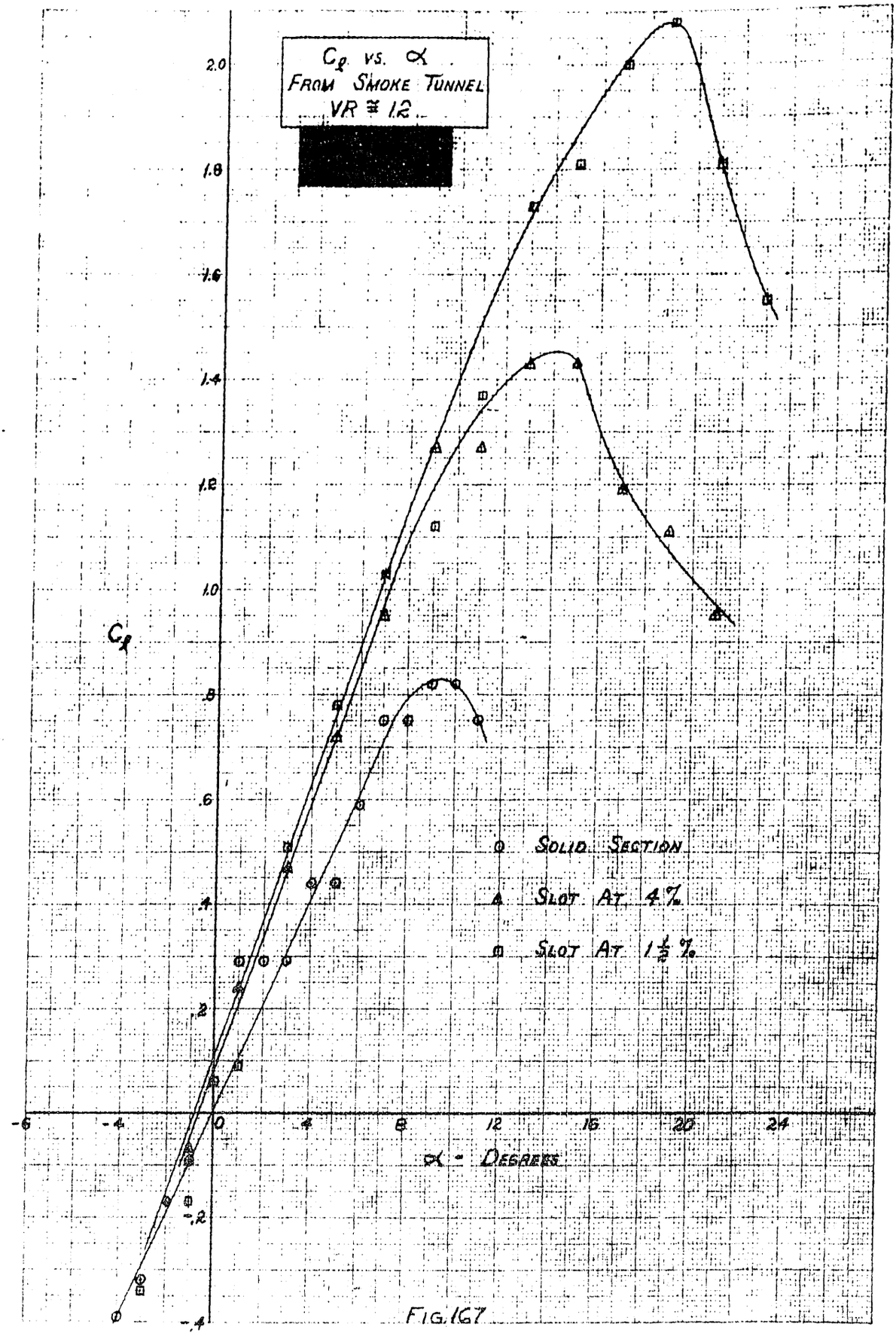

FIG. 167

PRESSURE DISTRIBUTION
$RN_e \cong 1{,}230{,}000$
$VR = 0$

[redacted]

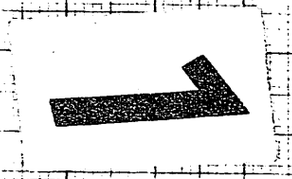

6
5
4
3
C_p

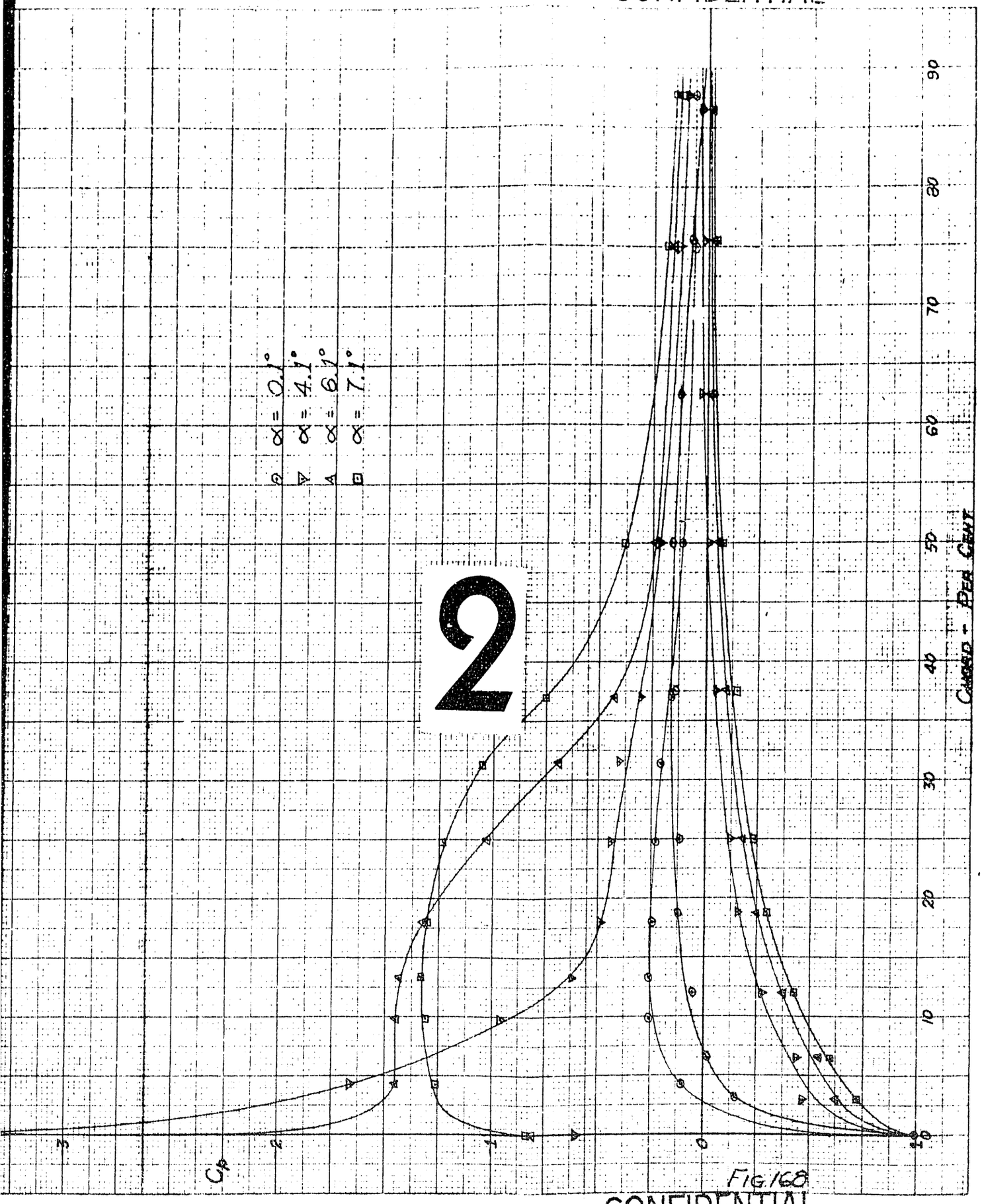

FIG. 168

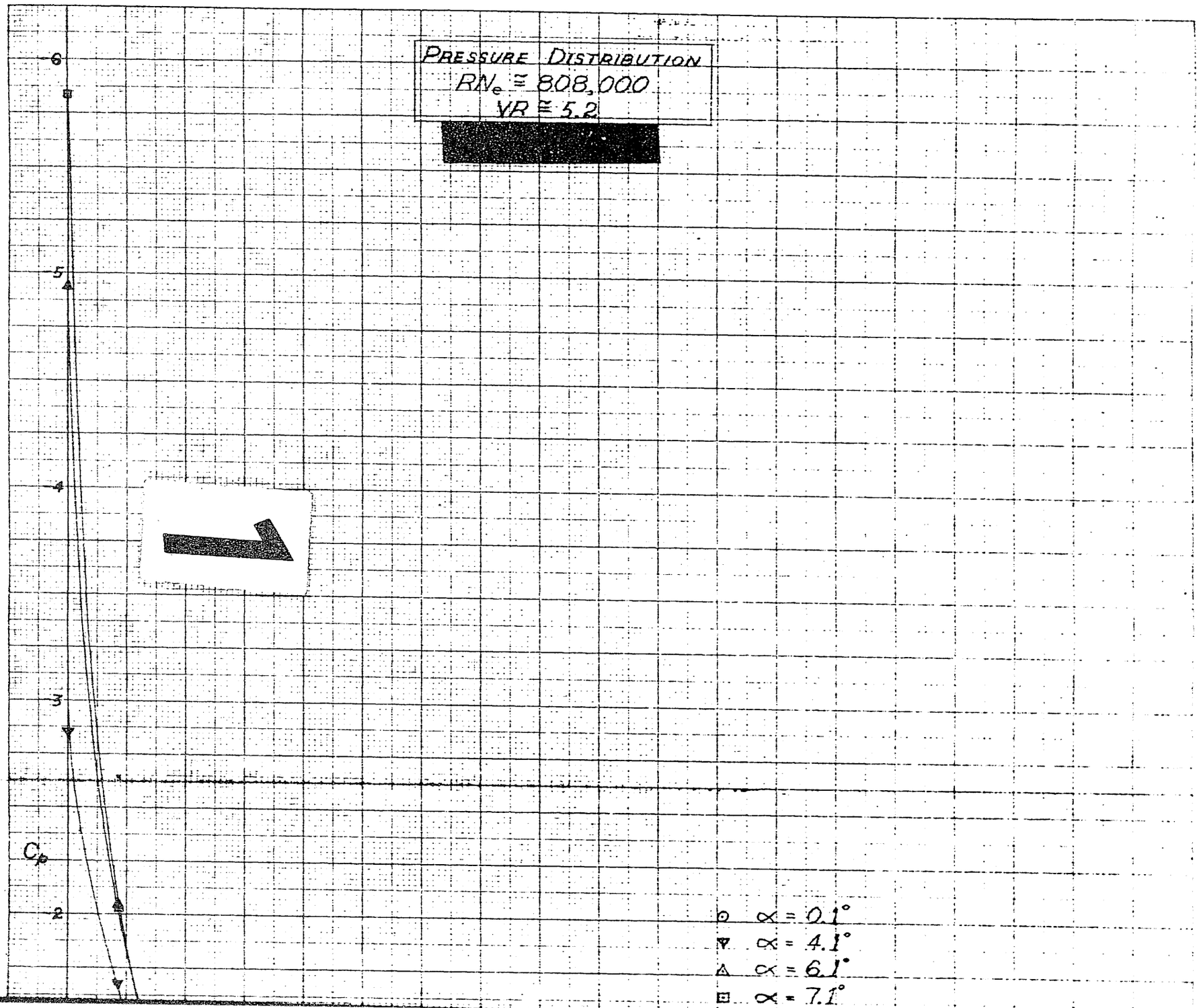

CONFIDENTIAL

FIG. 169

CONFIDENTIAL

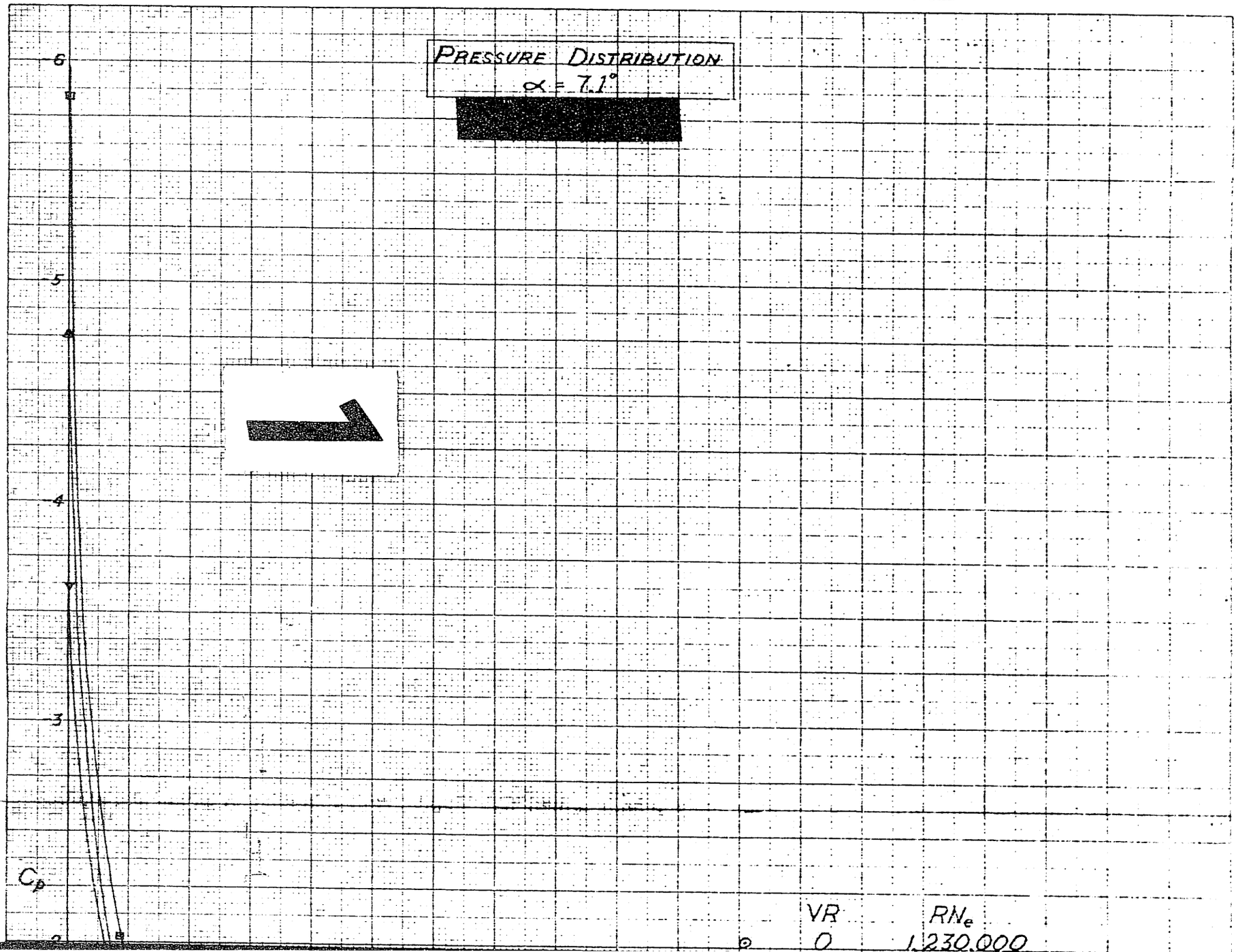

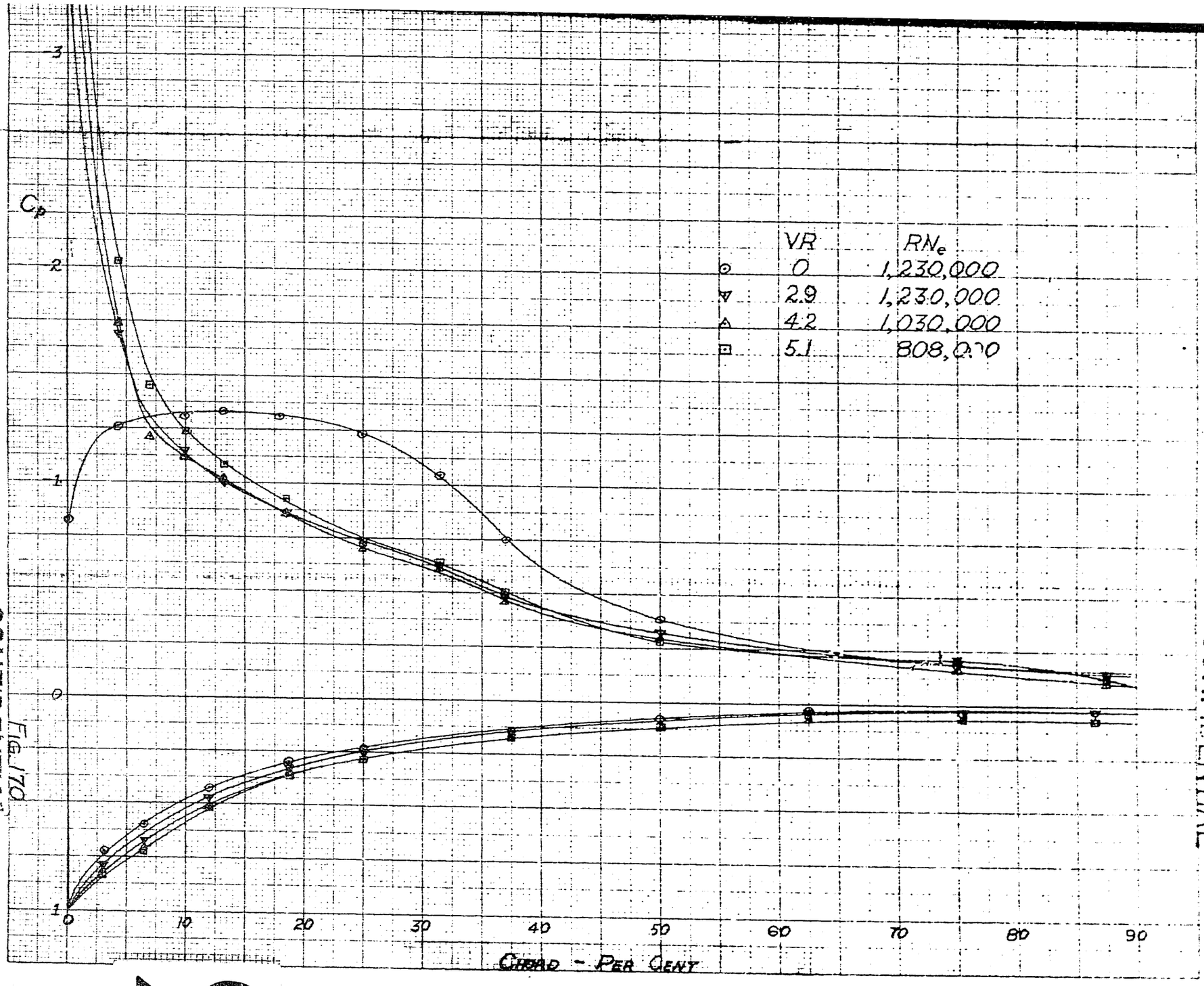

FIG. 170

SLOT CONFIGURATIONS
SIKORSKY BLOWING TESTS

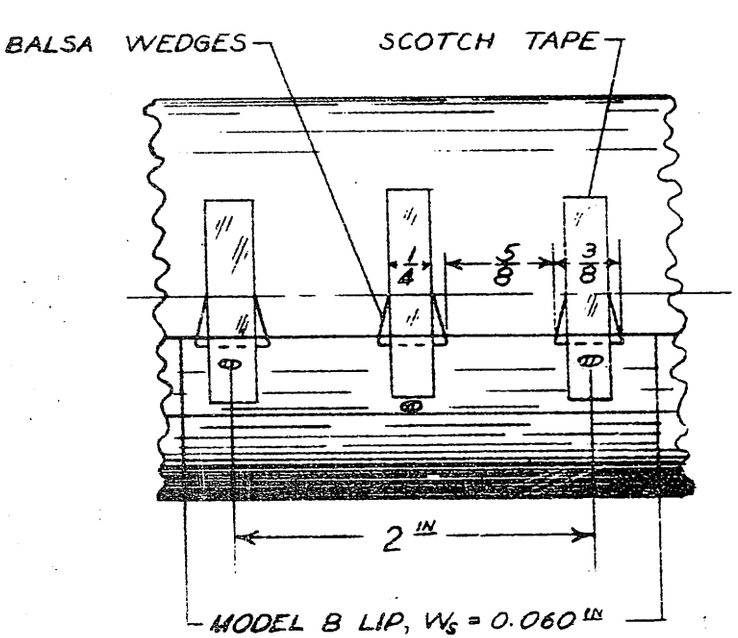

TEST MODEL CONFIGURATION
OF PROTRUDING-LIP SPACED SLOTS

(b)

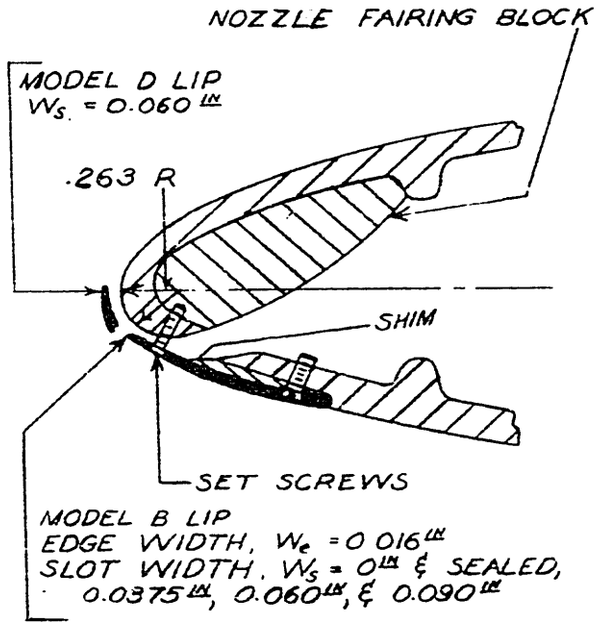

TEST MODEL CONFIGURATIONS
OF PROTRUDING-LIP CONTINUOUS SLOT

(a)

Fig. 171

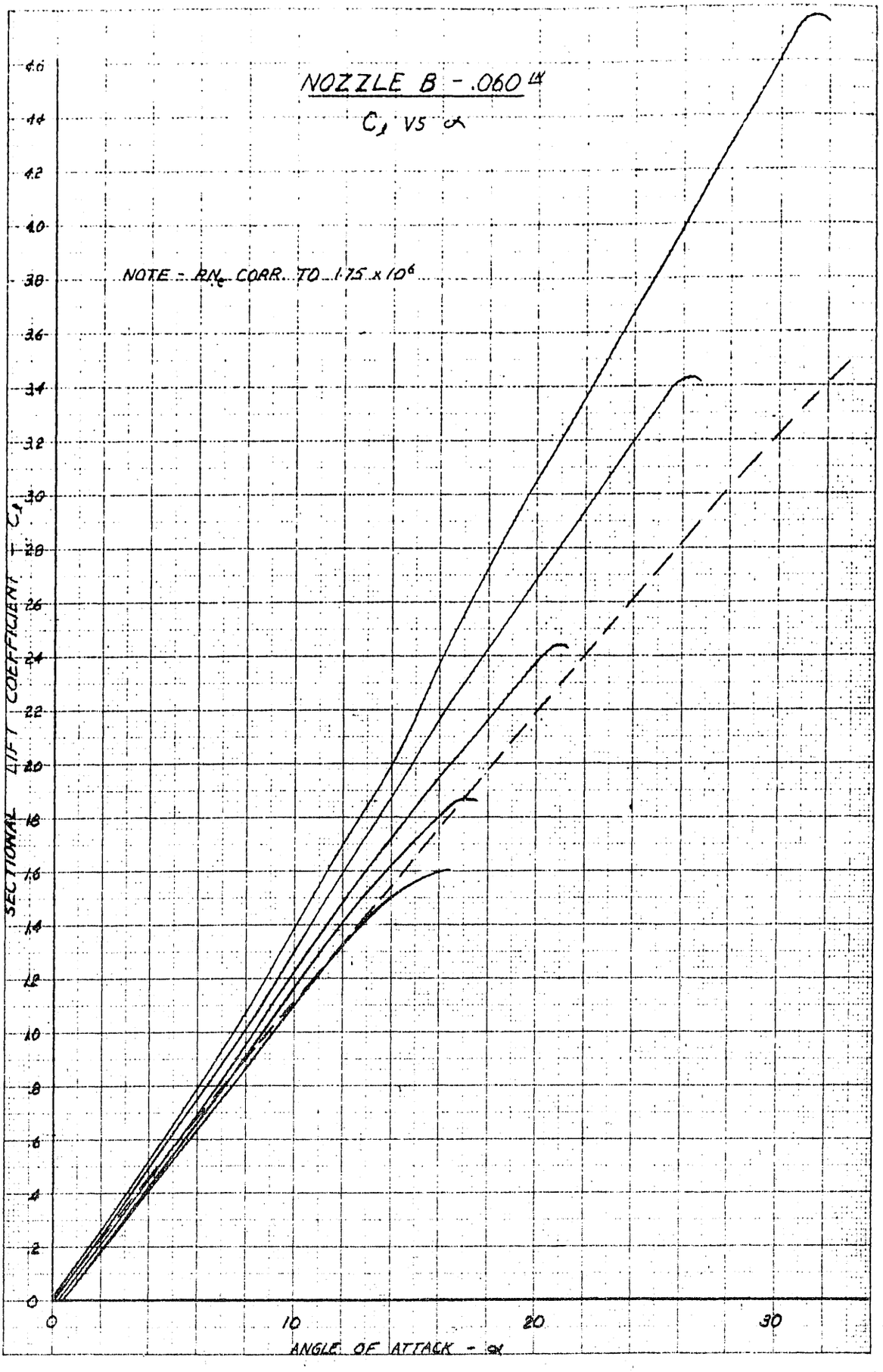

FIG. 172

NOZZLE "B" - .060"

C_l vs. V_j / V_o

NOTE - ALL TEST RUNS NOT OTHERWISE INDICATED WERE @ $RN_c \cong 1{,}250{,}000$

α	SYMBOL
0.6	○
4.6	△
8.6	□
10.6	◇
12.6	▽
14.6	○
15.6	△
16.6	□
17.6	◇
18.6	▽
19.6	○
20.6	△
21.6	□
22.6	◇
23.6	▽
24.6	○
25.6	△
26.6	□
27.6	◇
28.6	▽
29.6	○
30.6	△
31.1	□

TIONAL LIFT COEFFICIENT - C_l

5.0
4.8
4.6
4.4
4.2
4.0
3.8
3.6
3.4
3.2
3.0
2.8
2.6
2.4
2.2
2.0
1.8

$RN_c \cong 600{,}000$: $\alpha = 31.1°$, $30.6°$, $29.6°$, $28.6°$, $27.6°$, $26.6°$

$RN_c \cong 880{,}000$: $\alpha = 25.6°$, $24.6°$, $23.6°$, $22.6°$, $21.6°$, $20.6°$, $19.6°$, $18.6°$, $17.6°$, $16.6°$, $15.6°$, $14.6°$

$RN_c \cong 1{,}100{,}000$

$RN_c \cong 1{,}450{,}000$

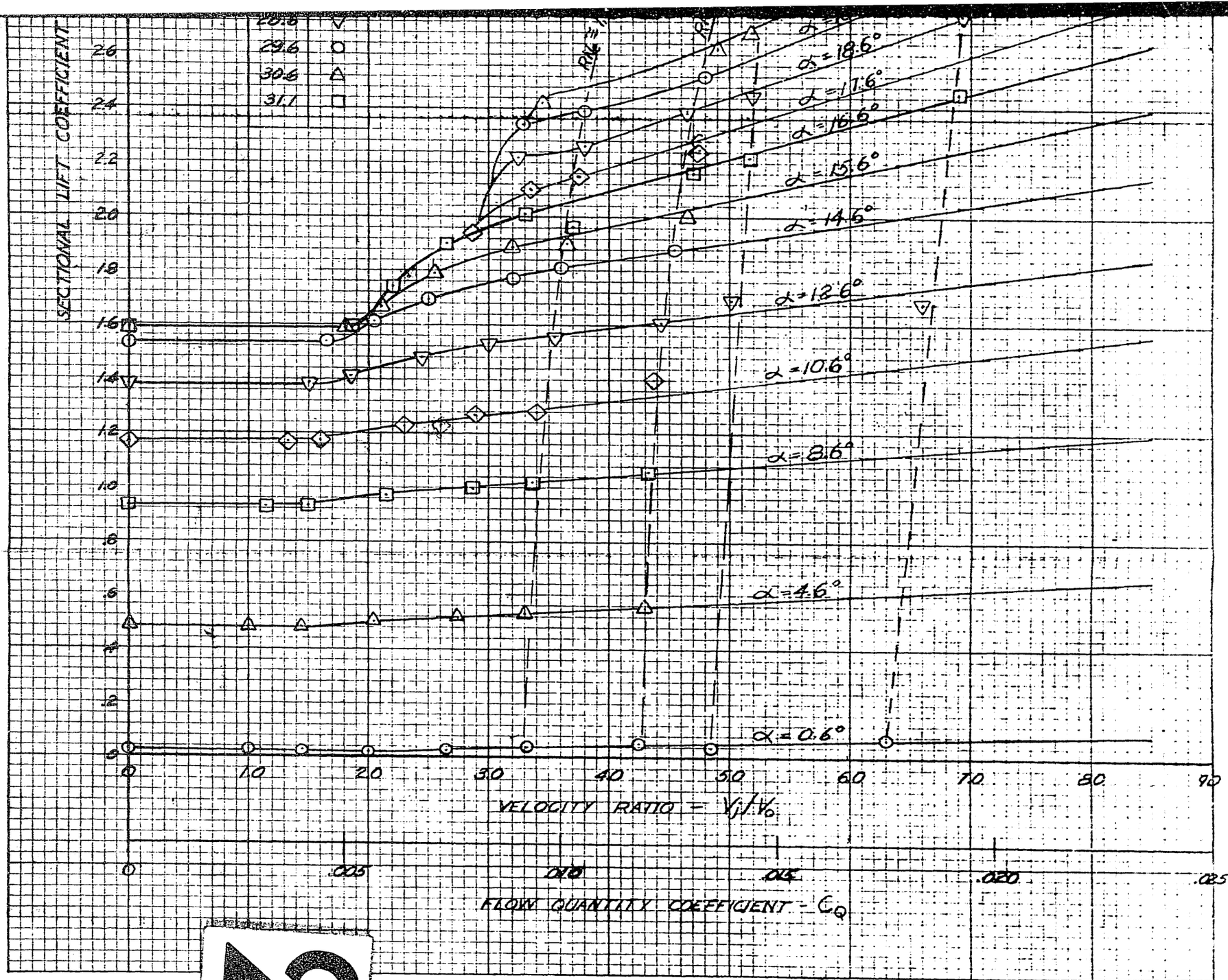
SECTIONAL LIFT COEFFICIENT
RN
29.6
30.6
31.1
α = 18.6°
α = 17.6°
α = 16.6°
α = 15.6°
α = 14.6°
α = 12.6°
α = 10.6°
α = 8.6°
α = 4.6°
α = 0.6°
2.6
2.4
2.2
2.0
1.8
1.6
1.4
1.2
1.0
.8
.6
.4
.2
0
10
20
30
40
50
60
70
80
90
VELOCITY RATIO = Vj/V0
.005
.010
.015
.020
.025
FLOW QUANTITY COEFFICIENT = CQ

FIG. 173

LIFT COEFFICIENT vs. FLOW COEFFICIENT

NACA 0012 R.N. = 1.0 x 10^6
SLOT WIDTH .006 at .45c.

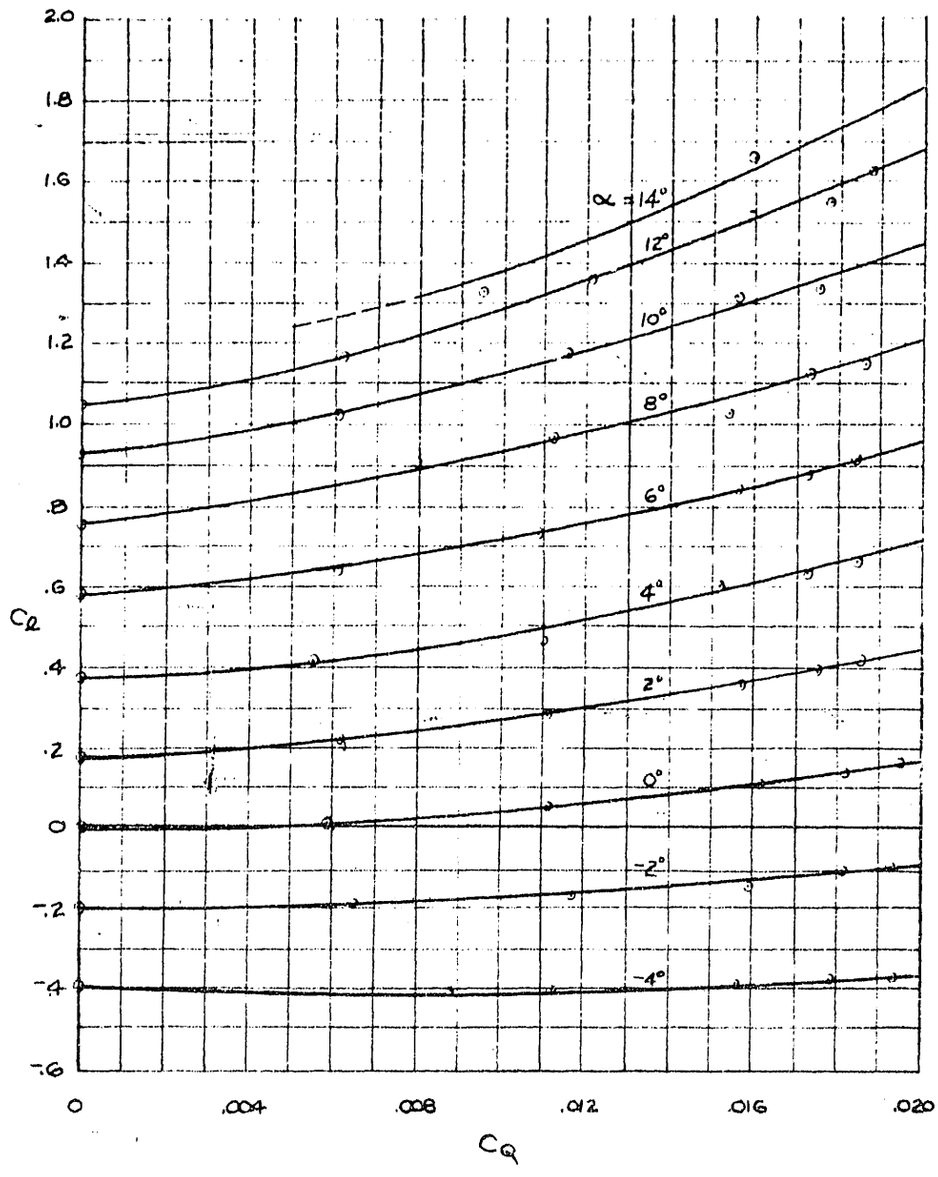

FIG. 174 CONFIDENTIAL

LIFT COEFFICIENT vs. ANGLE OF ATTACK

NACA 0012 R.N. = 1.0×10^6
SLOT WIDTH .006 at .45C

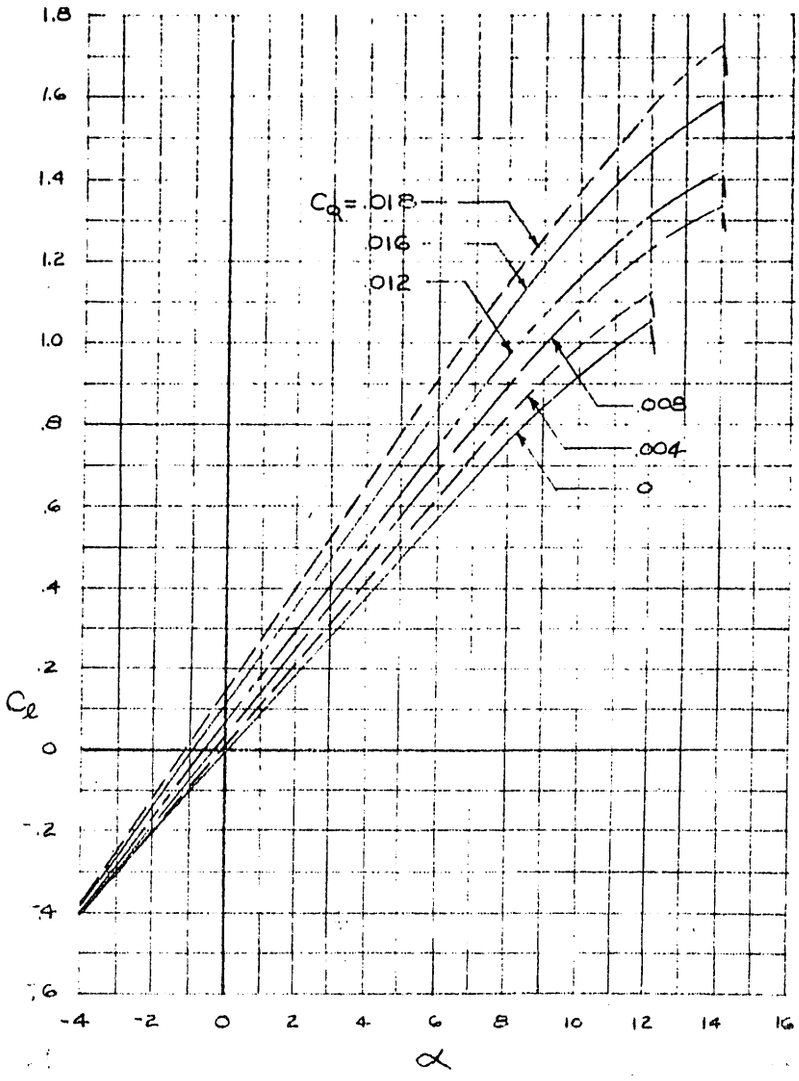

FIG. 175

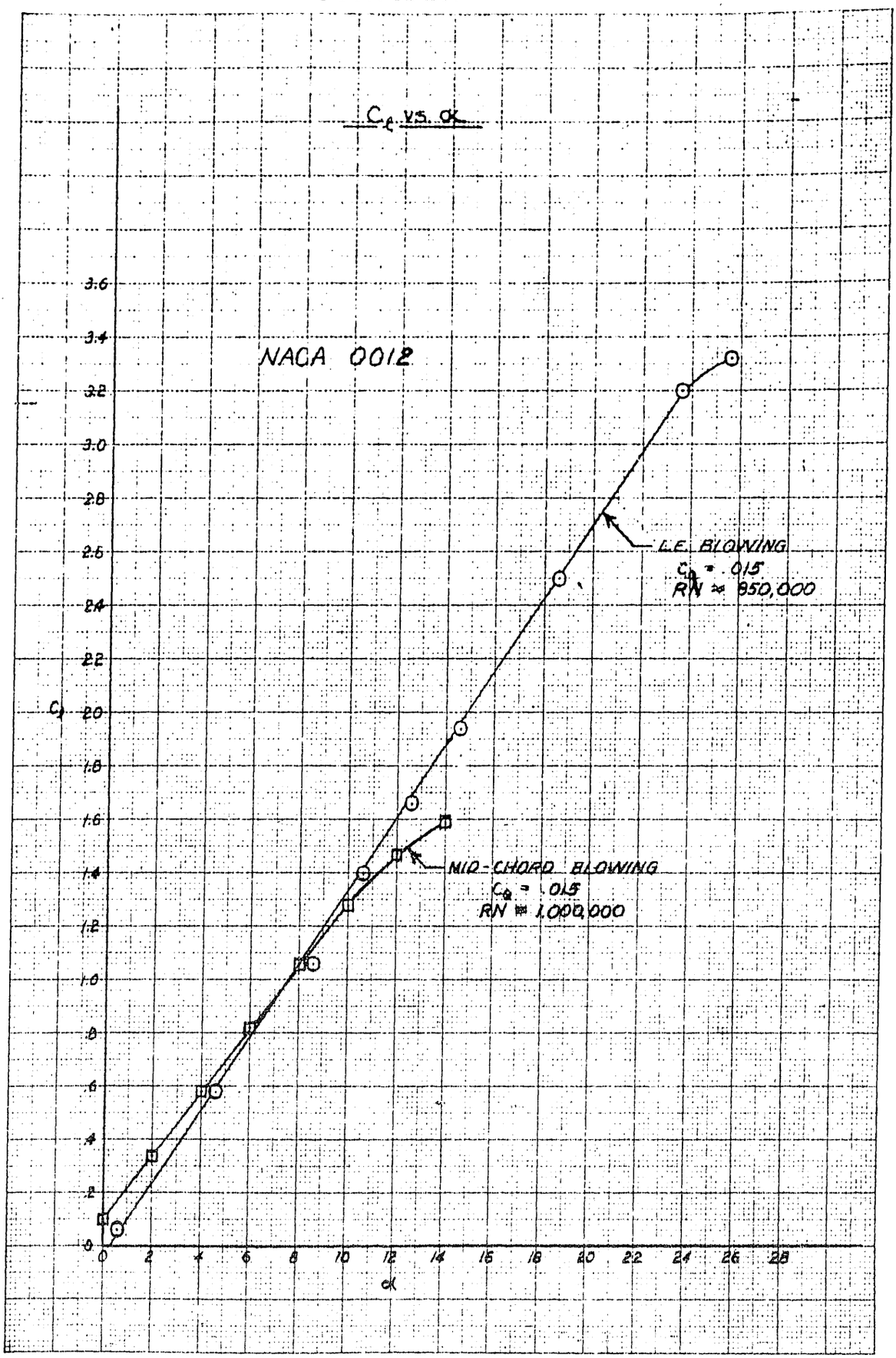

FIG. 176

MODEL GEOMETRY

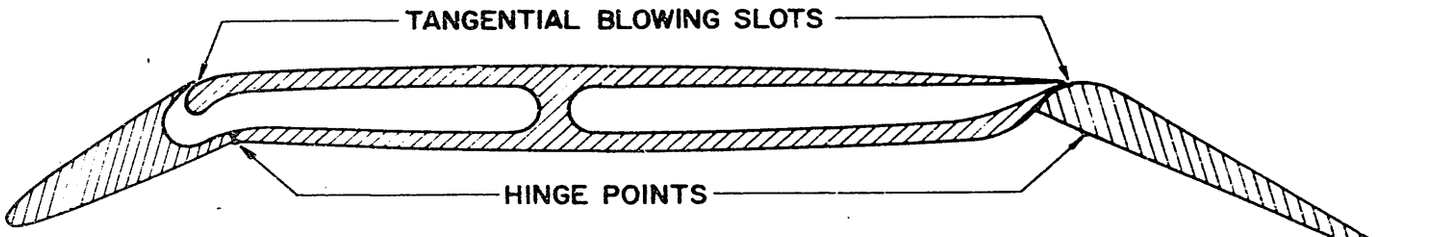

AIRFOIL SECTION-NACA 64-006
CHORD = 16 IN SPAN = 2 IN

δ_N = VARIABLE
δ_F = VARIABLE
$C_N/C = .175$ $C_F/C = .30$

GEOMETRY OF MODEL USED IN SMOKE TUNNEL INVESTIGATION

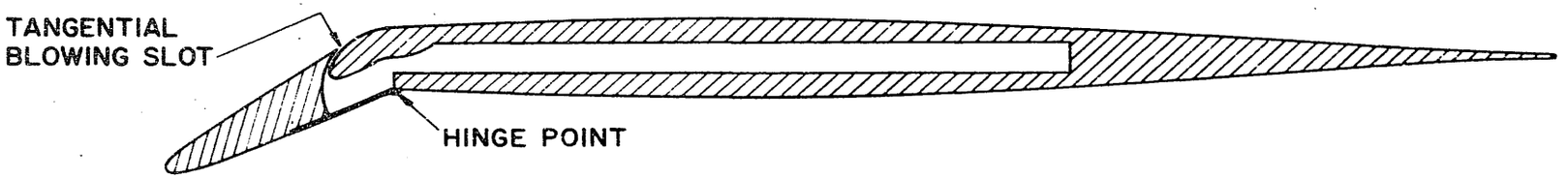

AIRFOIL SECTION-NACA 65-006
CHORD = 16 IN SPAN = 12 3/16 IN

δ_N = VARIABLE
$C_N/C = .175$

GEOMETRY OF 65-006 PROFILE USED IN PRESSURE DISTRIBUTION STUDIES

FIGURE 17

CONFIDENTIAL

CONFIDENTIAL

SMOKE PHOTOS OF A 64-006 PROFILE WITH AND WITHOUT TANGENTIAL BLOWING AT THE 17.5% LOCATION $C_\mu \cong .07$

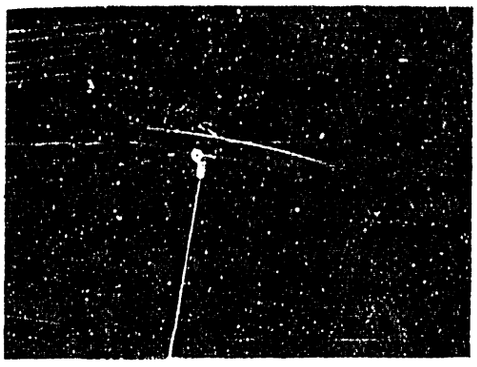

(a) NO BLOWING, $\alpha = 10°$

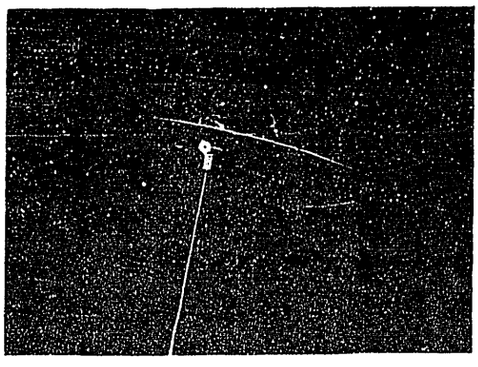

(b) NO BLOWING, $\alpha = 12°$

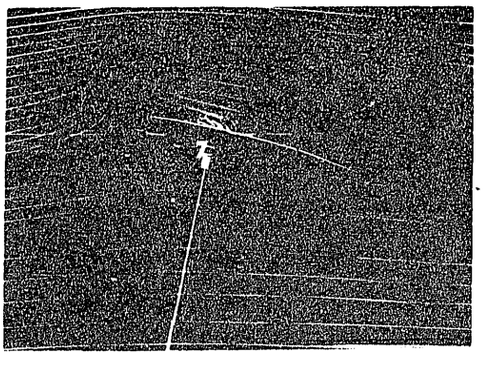

(c) BLOWING, $\alpha = 12°$

FIGURE 178

SMOKE PHOTOS OF A 64-006 PROFILE WITH A 17.5% C. LEADING-EDGE FLAP DEFLECTED 30° WITH AND WITHOUT BLOWING AT THE BREAK OF THE LEADING-EDGE FLAP

$C_\mu \cong .33$

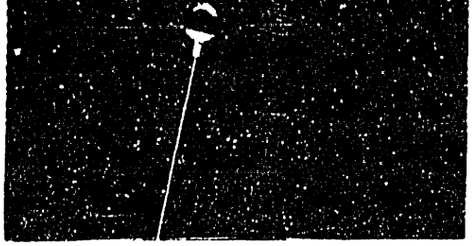

(a) α = 12°

(d) α = 18°

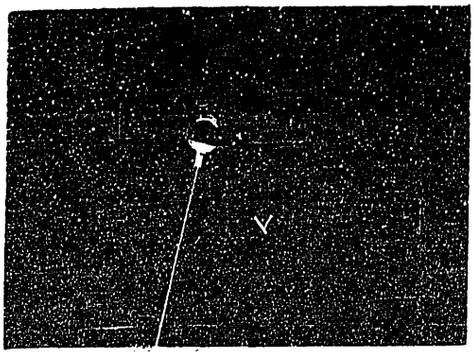

(b) α = 14°

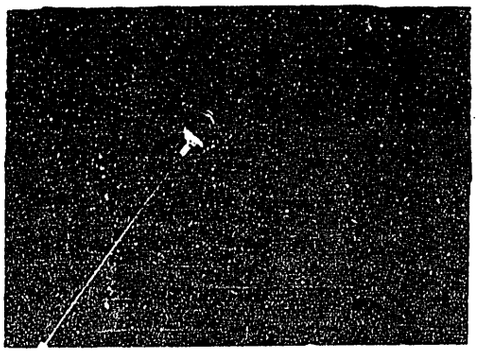

(e) α = 37°

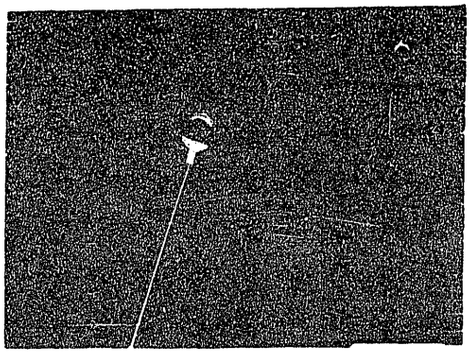

(c) α = 18°

NO BLOWING

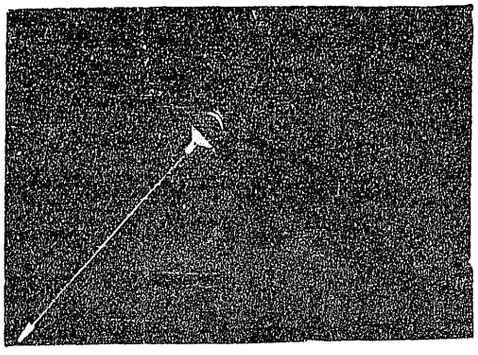

(f) α = 45°

BLOWING AT THE FLAP BREAK

FIGURE 179

SMOKE PHOTOS OF A 64-006 PROFILE WITH
A 17.5%C. LEADING-EDGE FLAP DEFLECTED 30°
AND A 30% PLAIN TRAILING-EDGE FLAP DEFLECTED 30°

TANGENTIAL BLOWING SLOTS ARE
PROVIDED AT THE BREAKS OF BOTH FLAPS

ANGLE OF ATTACK = 20°

C_μ (EACH SLOT) ≅ .07

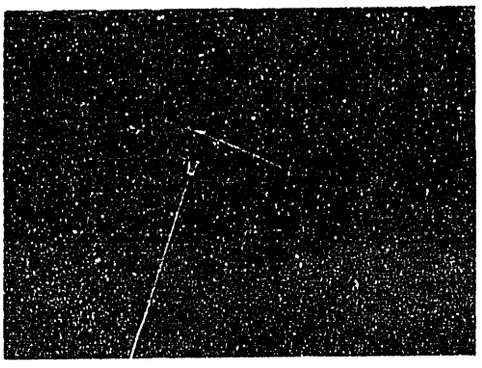

(a) NO BLOWING

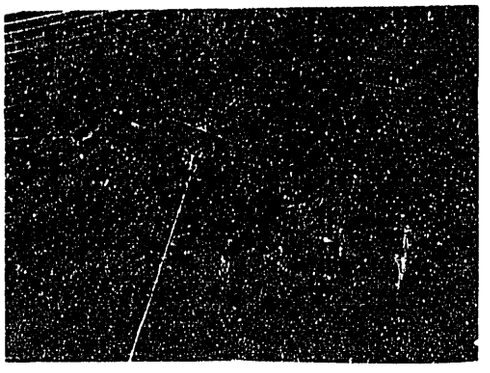

(b) BLOWING AT THE BREAK OF THE TRAILING-EDGE FLAP

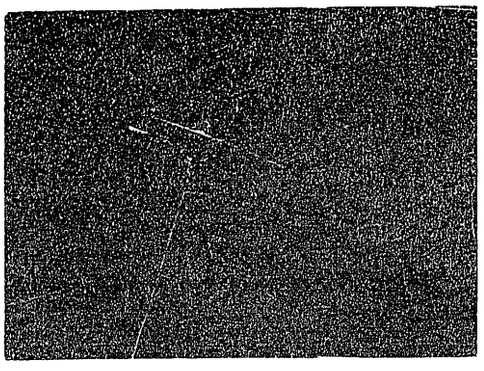

(c) BLOWING AT THE BREAK OF THE LEADING-EDGE FLAP

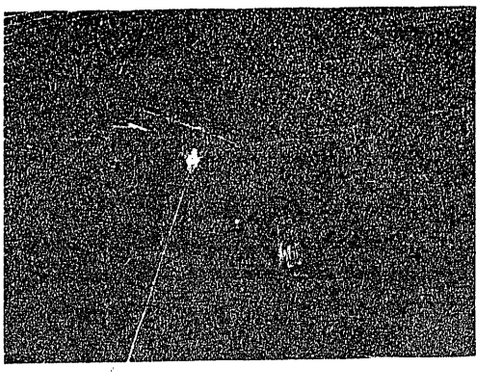

(d) BLOWING AT THE BREAKS OF BOTH FLAPS

FIGURE 180

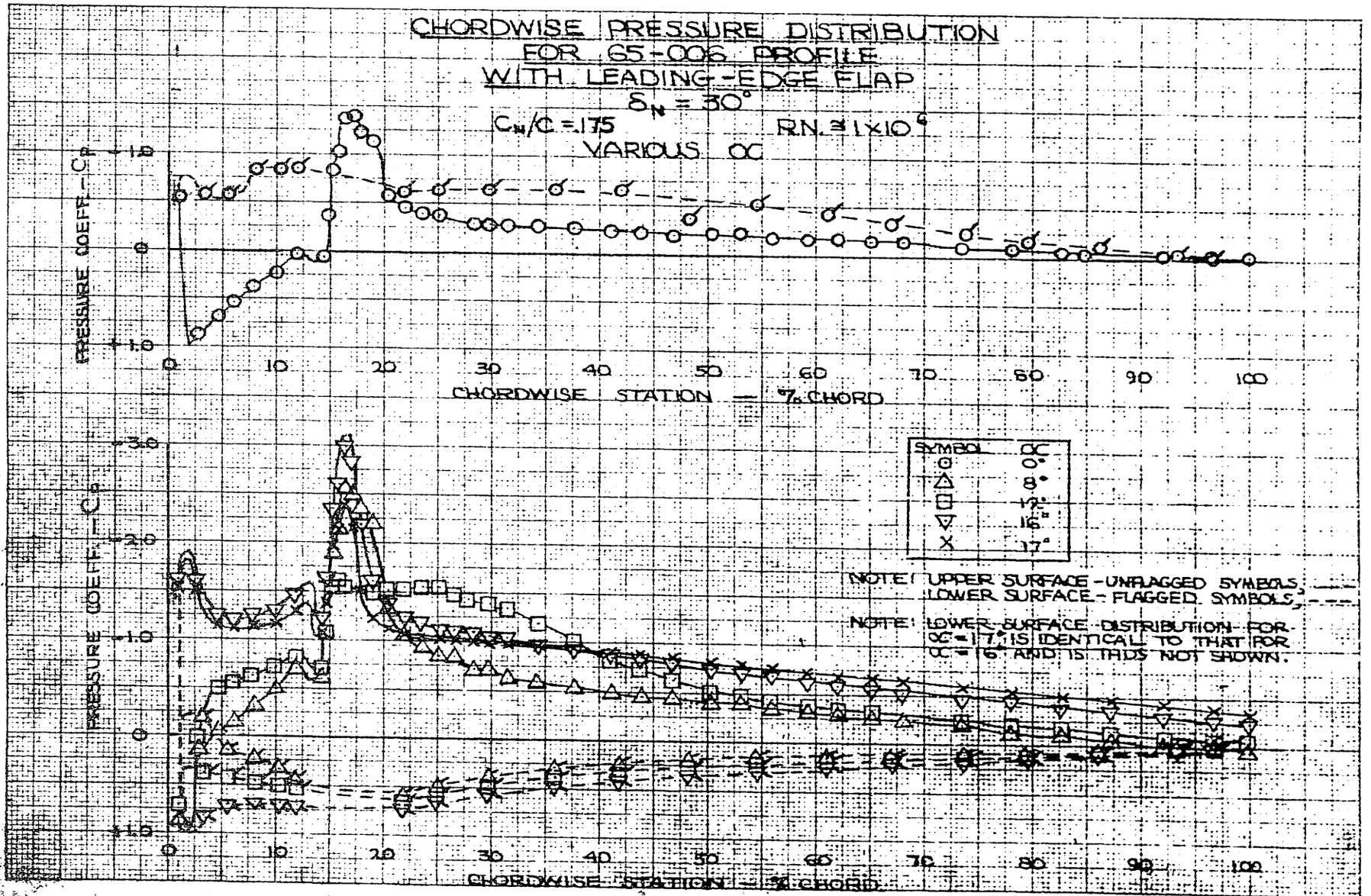

FIG. 181

CONFIDENTIAL

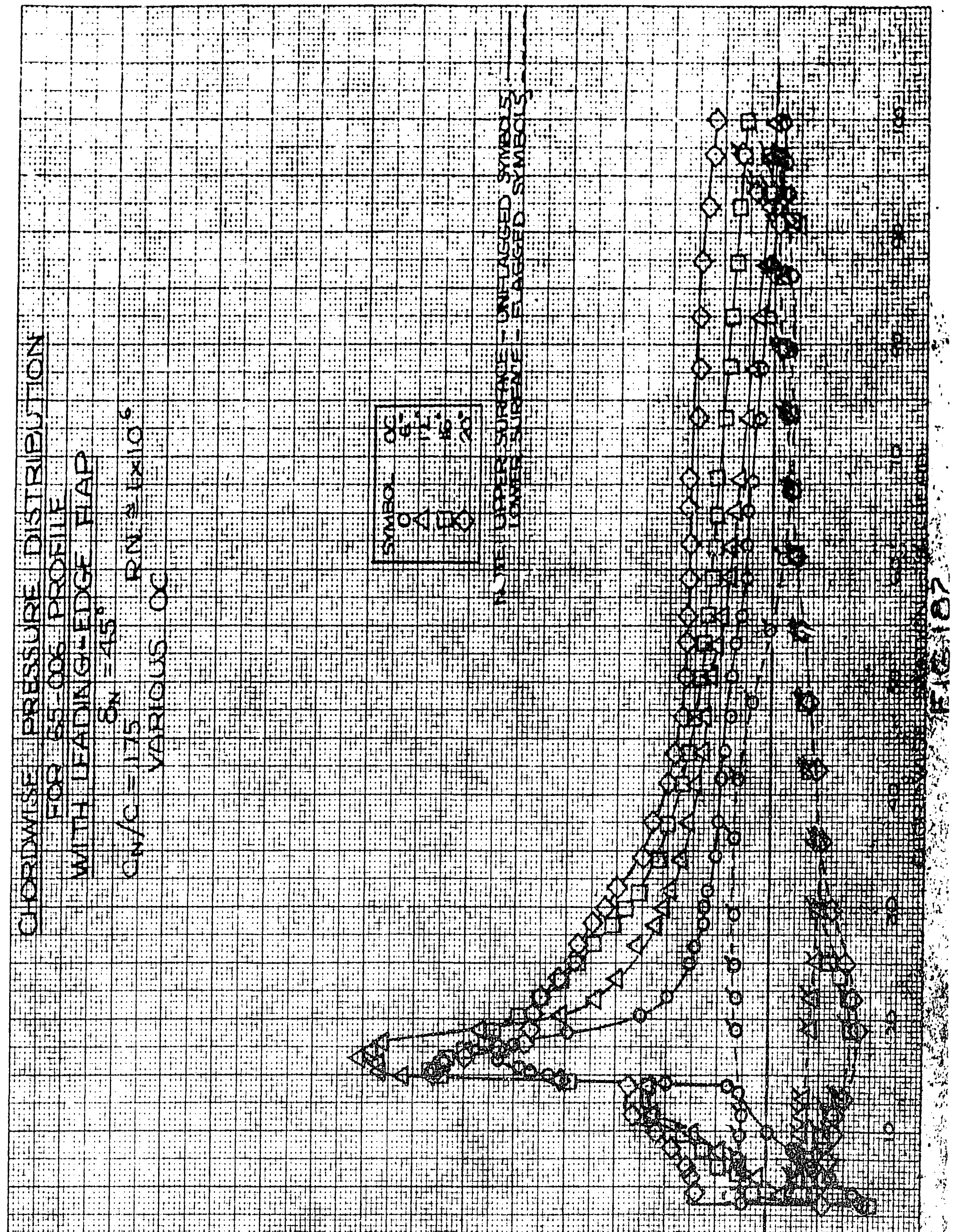

CONFIDENTIAL

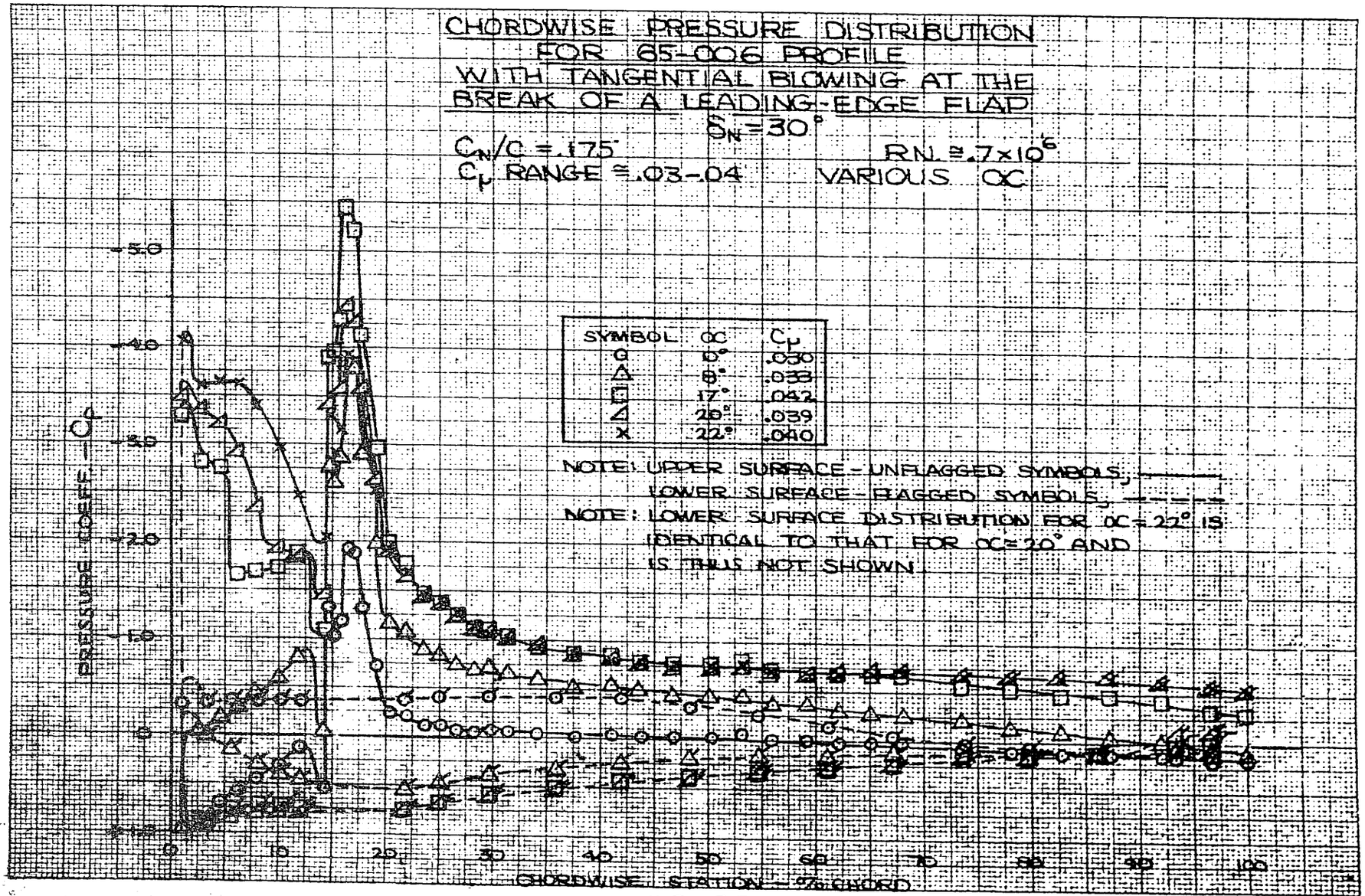

FIG.183

CONFIDENTIAL

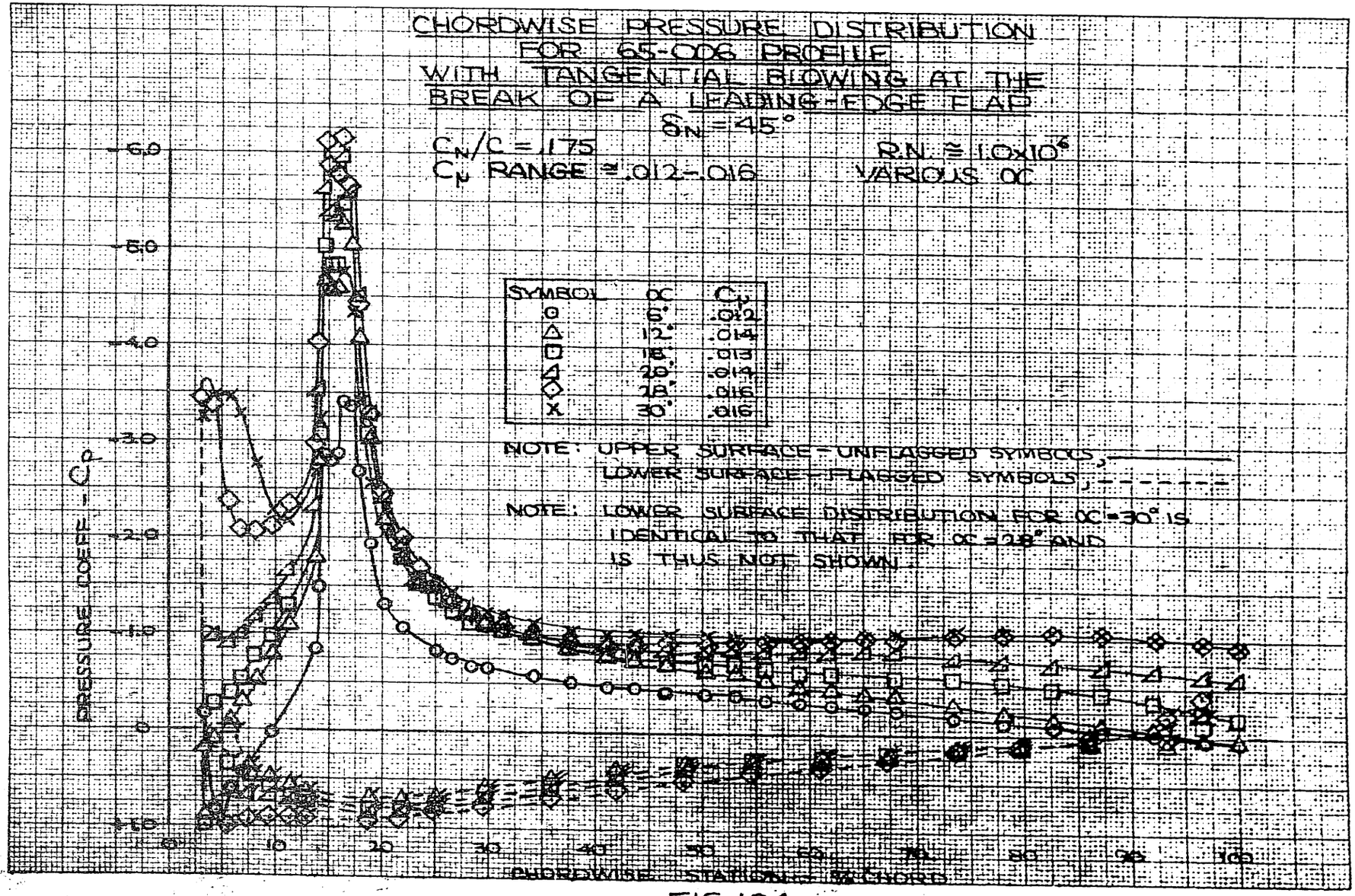

FIG. 184

CONFIDENTIAL

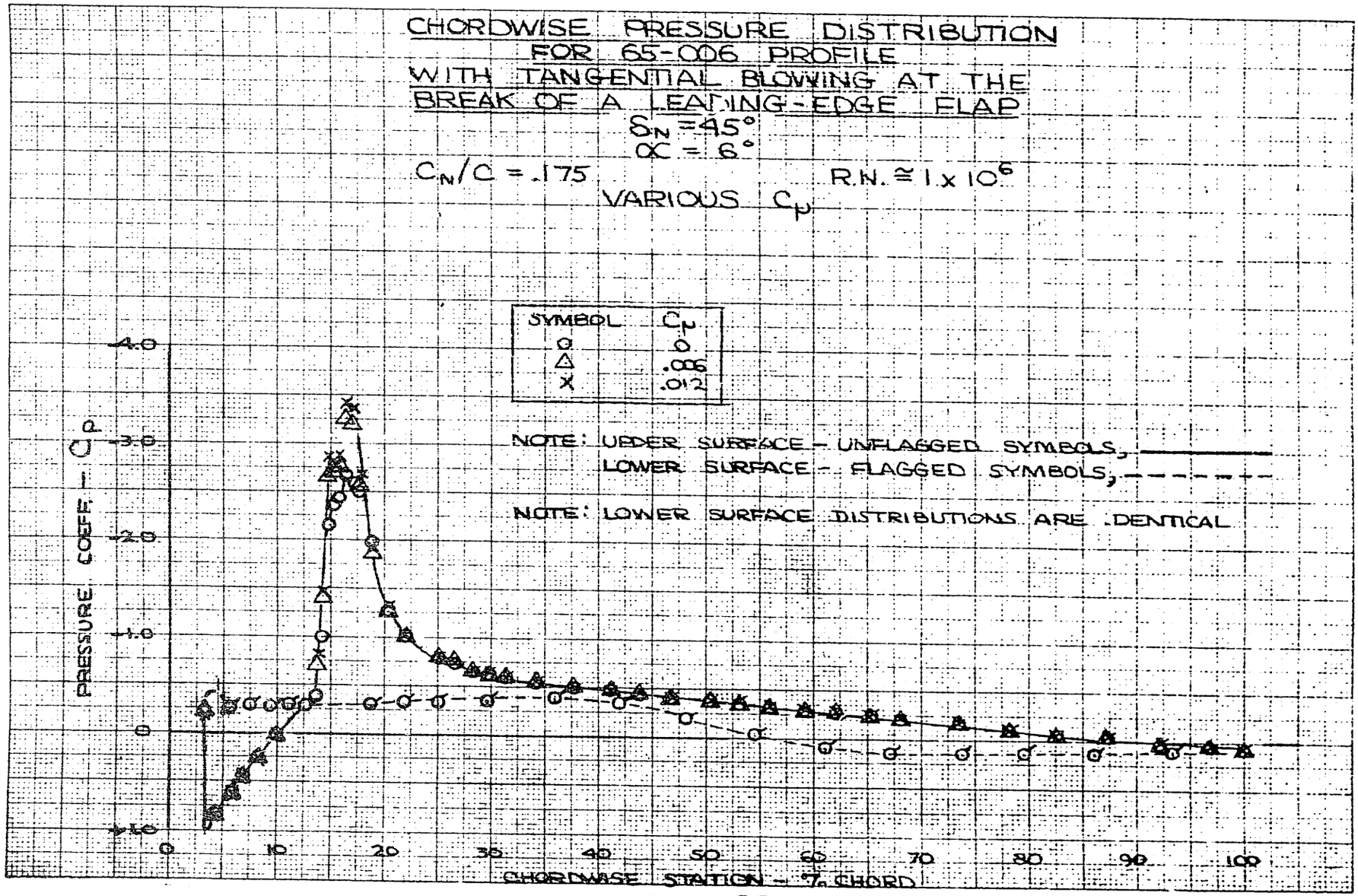

FIG. 185

CONFIDENTIAL

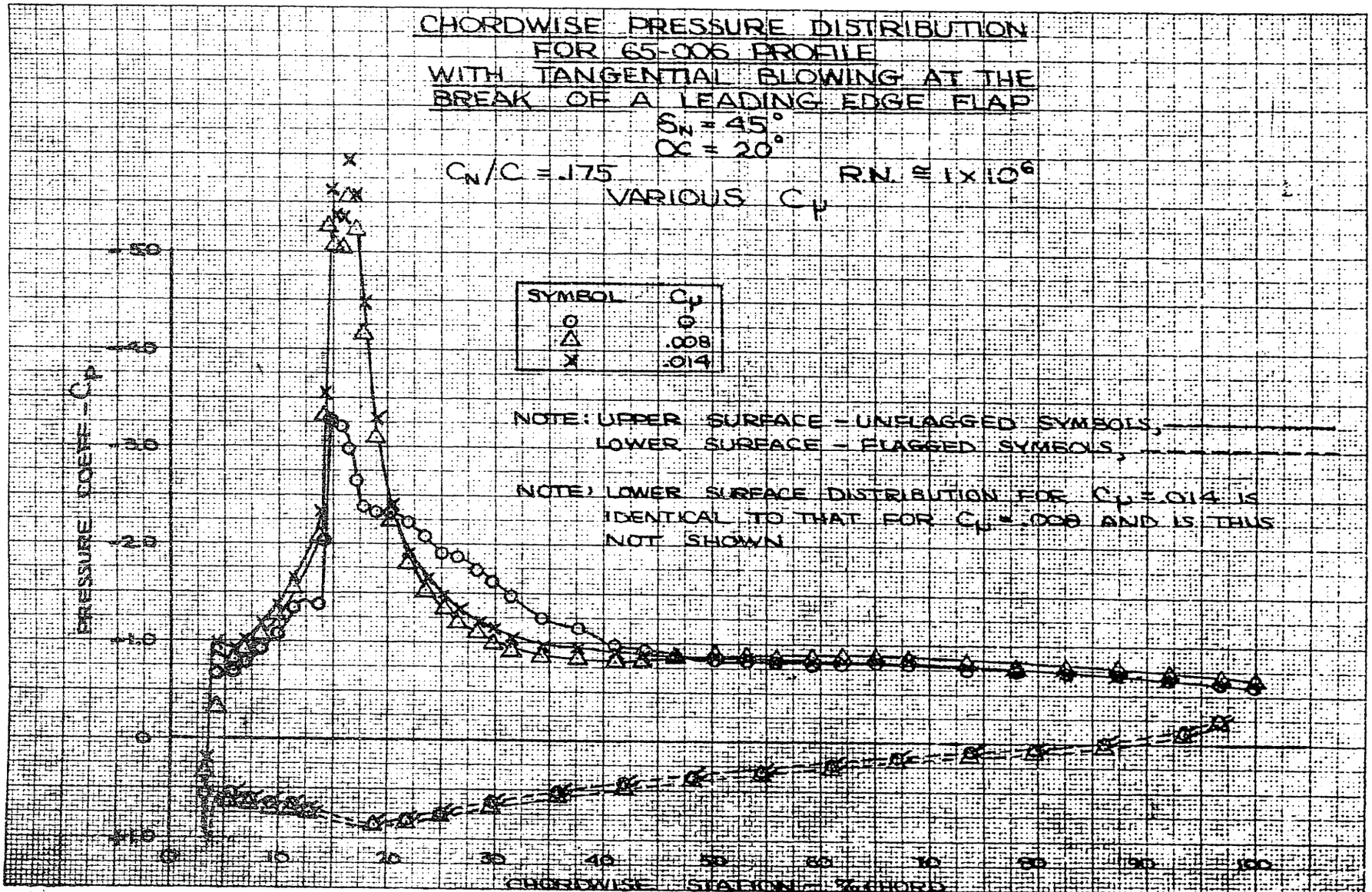

FIG. 186

CONFIDENTIAL

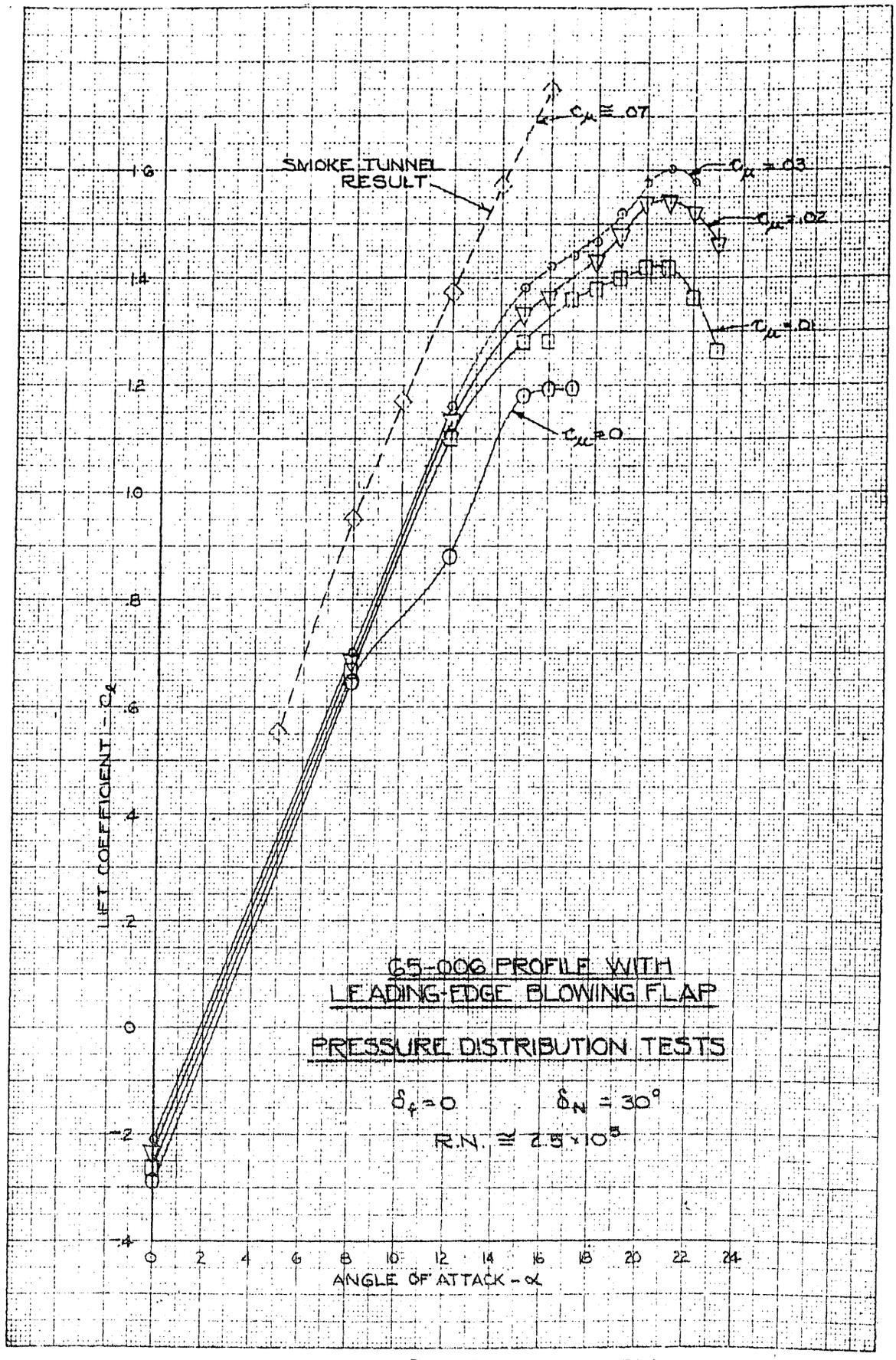

FIG. 187A CONFIDENTIAL

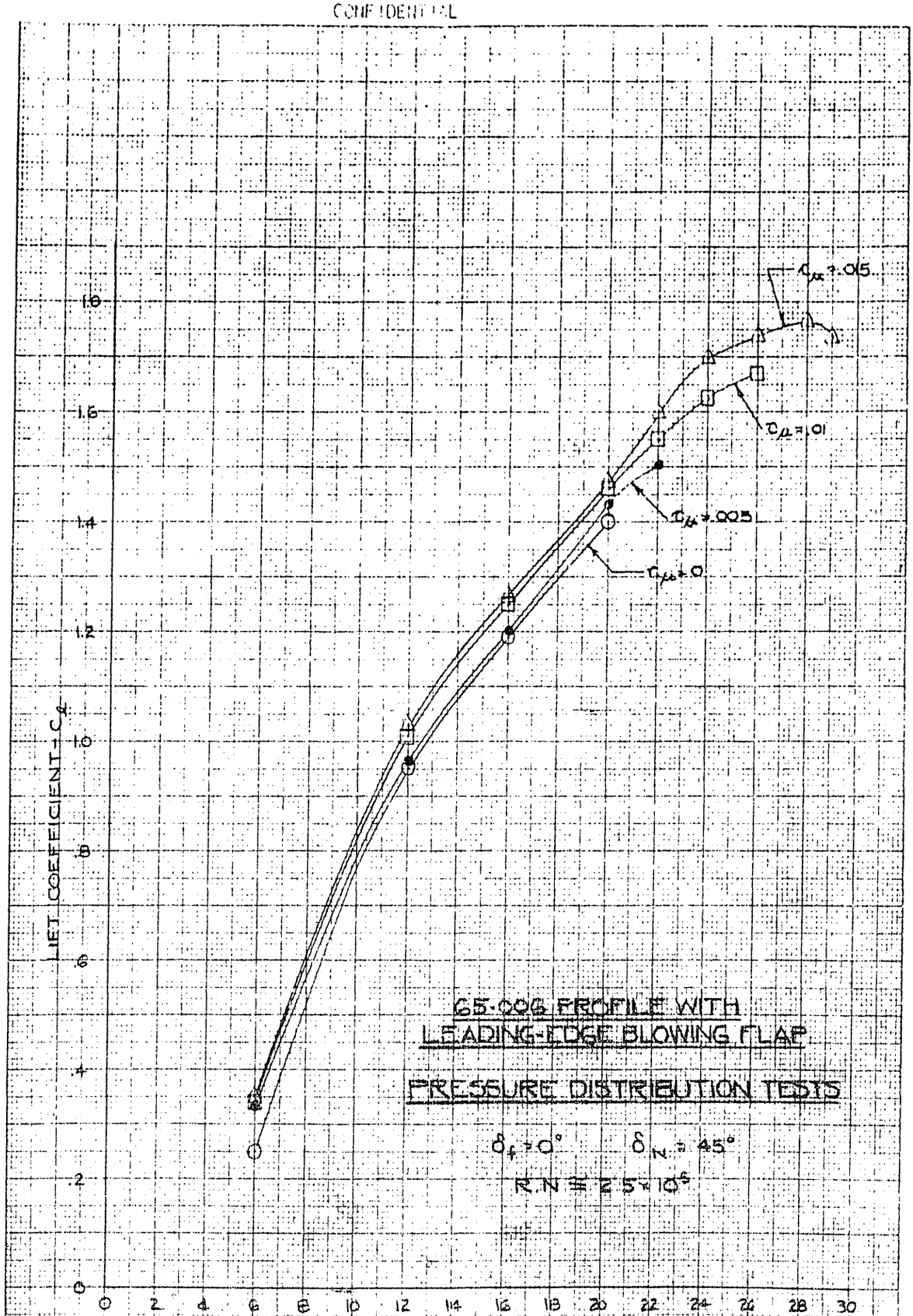
LIFT COEFFICIENT - C_L
ANGLE OF ATTACK - α
$C_\mu = .015$
$C_\mu = .01$
$C_\mu = .005$
$C_\mu = 0$
65-006 PROFILE WITH
LEADING-EDGE BLOWING FLAP
PRESSURE DISTRIBUTION TESTS
$\delta_f = 0°$ $\delta_N = 45°$
$R.N = 2.5 \times 10^6$

FIG. 187B

EMPIRICAL STABILITY BOUNDARY FOR SWEPT BACK, UNCAMBERED, UNTWISTED WINGS (REF 309)

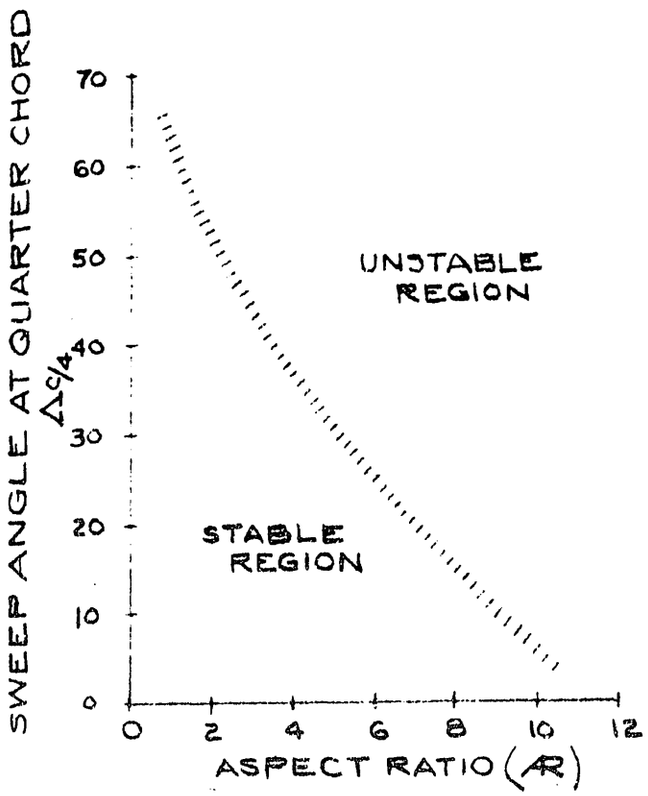

FIG. 188

REVISED STABILITY BOUNDARY BASED ON MOMENT AREAS (REF. 309)

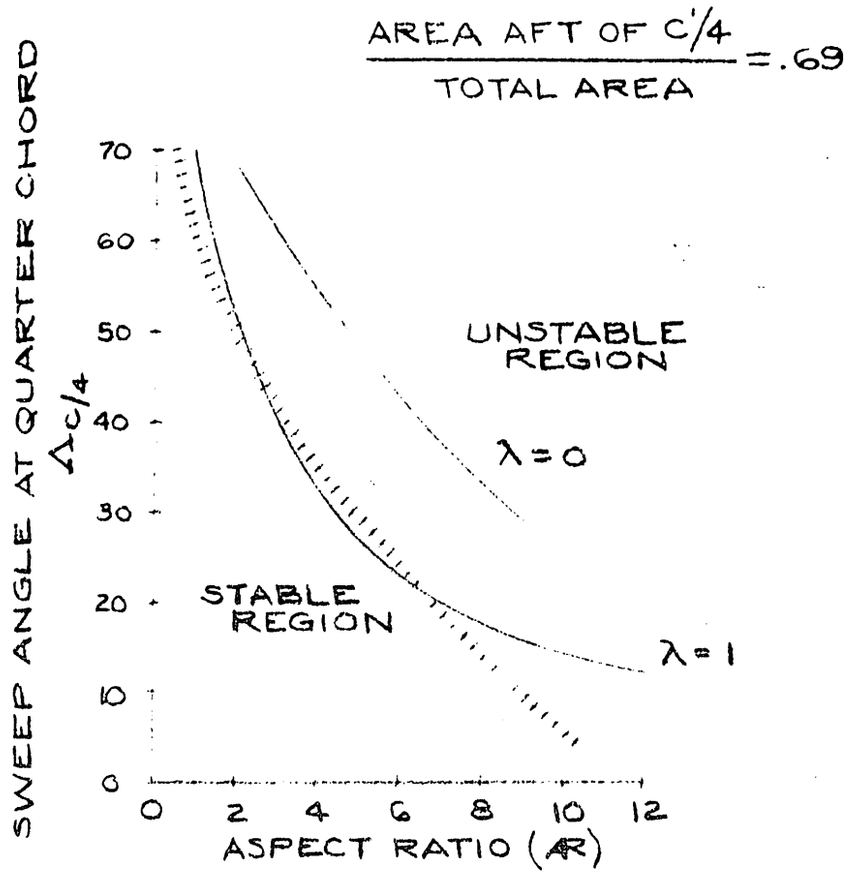

FIG. 189

EMPIRICAL BOUNDARY FOR PREDOMINANT SEPARATION TENDENCIES OF UNCAMBERED, UNTWISTED SWEPT WINGS (REF. 309)

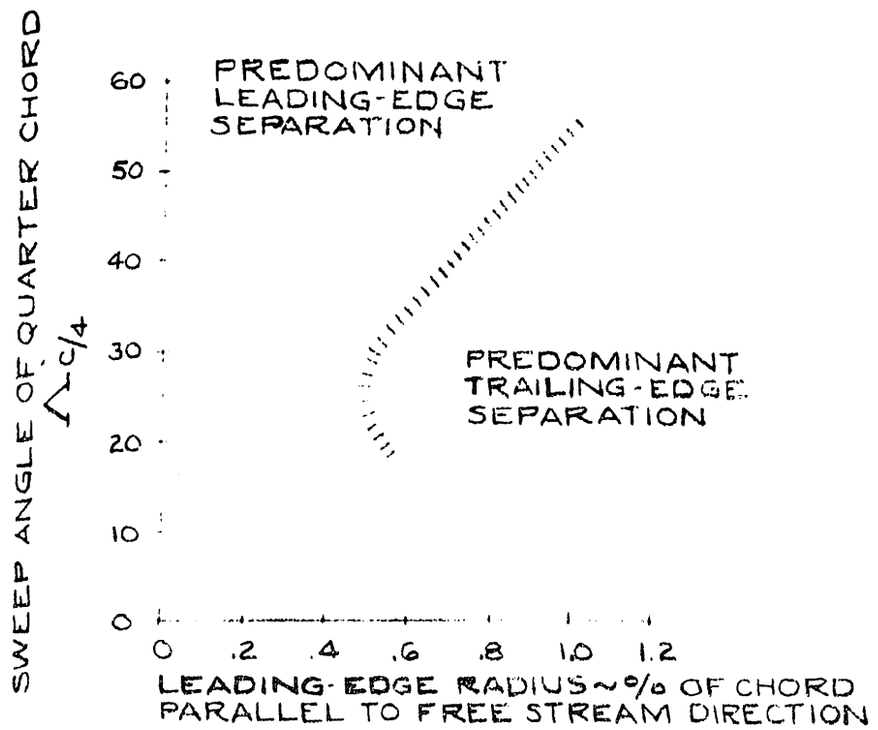

FIG 190

INFLUENCE OF ASPECT RATIO ON $C_{L_{MAX}}$ AND α_{MAX} OF VARIOUS WING PLAN FORMS (REF. 285)

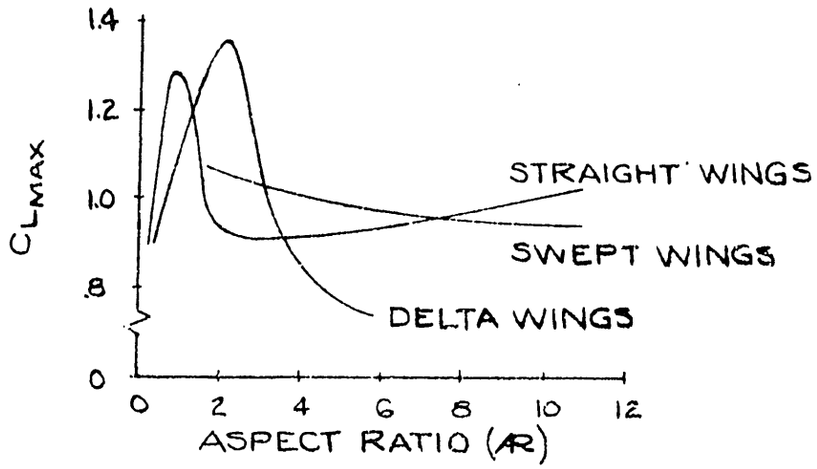

(a)

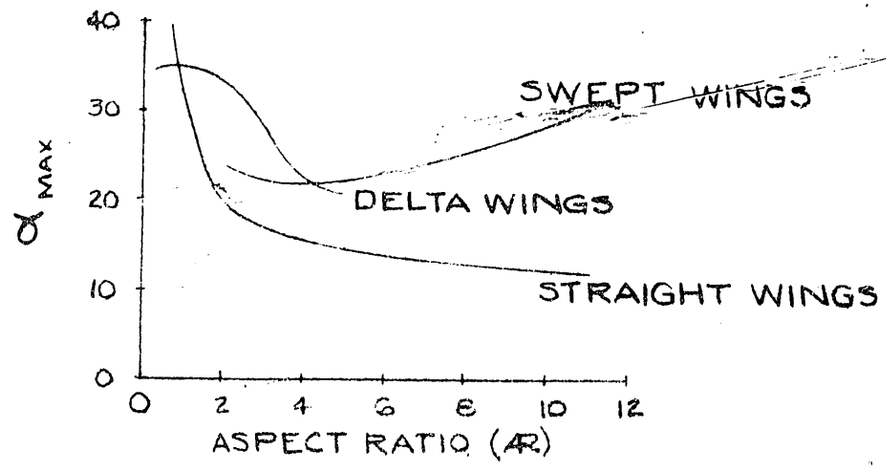

(b)

FIG. 191

VARIATIONS WITH SWEEPBACK ANGLE OF THE RATIO OF MAXIMUM LIFT COEFFICIENT OF THE SWEPT WING TO THE MAXIMUM LIFT COEFFICIENT OF THE EQUIVALENT UNSWEPT WING AS DEFINED BY THEIR LEADING-EDGE RADII. (REF. 309)

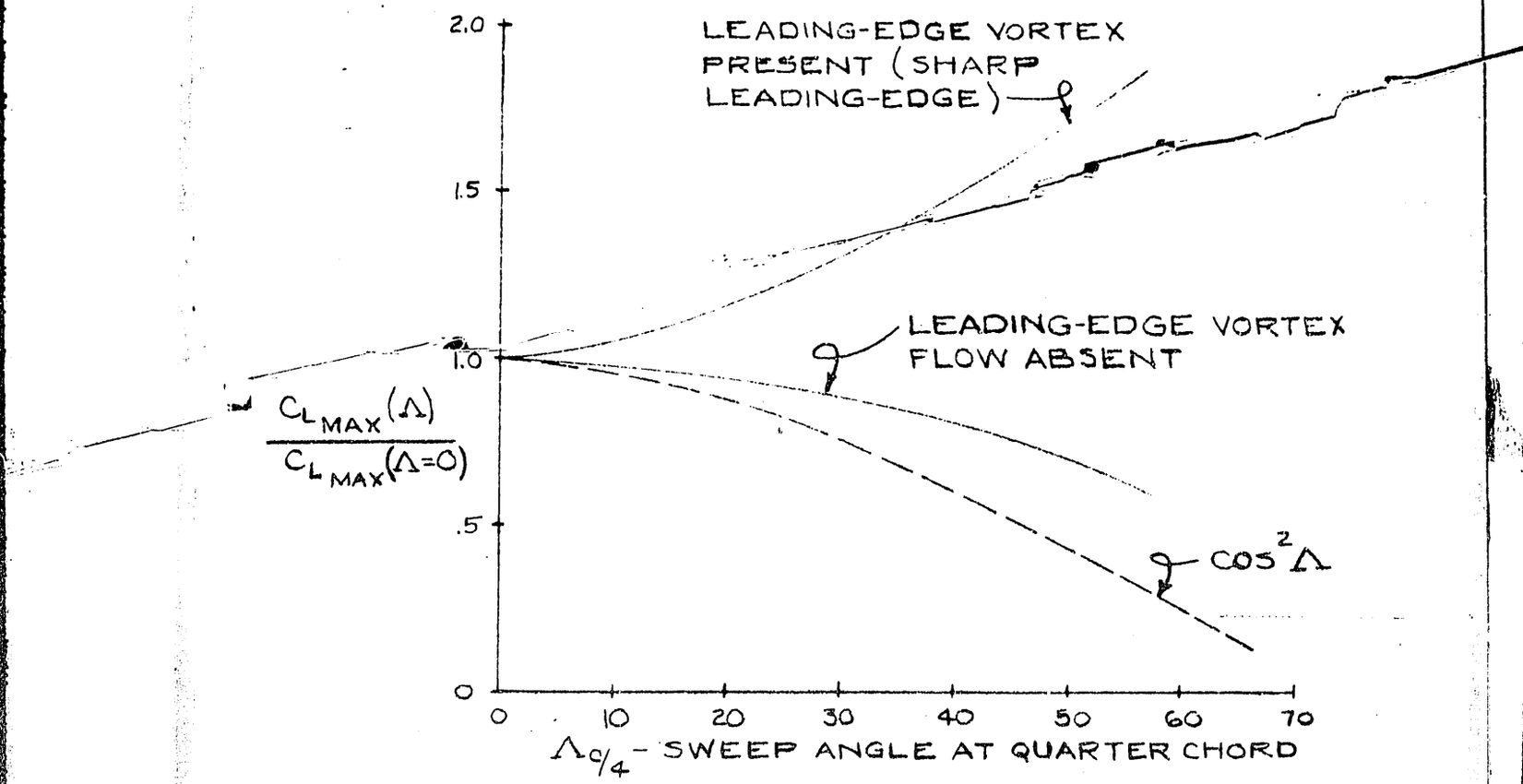

FIG. 192

VARIATION OF THE RATIO OF INFLECTION-LIFT COEFFICIENT TO MAXIMUM LIFT COEFFICIENT WITH SWEEPBACK ANGLE FOR WINGS WHICH EXHIBIT EITHER TRAILING-EDGE SEPARATION OR LEADING-EDGE SEPARATION (REF. 309)

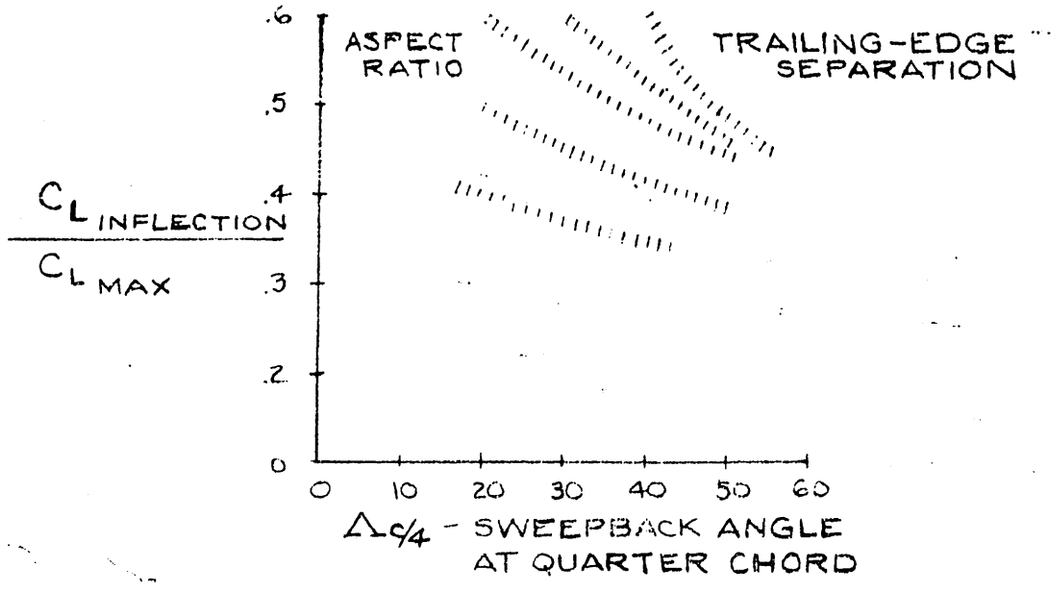

(a)

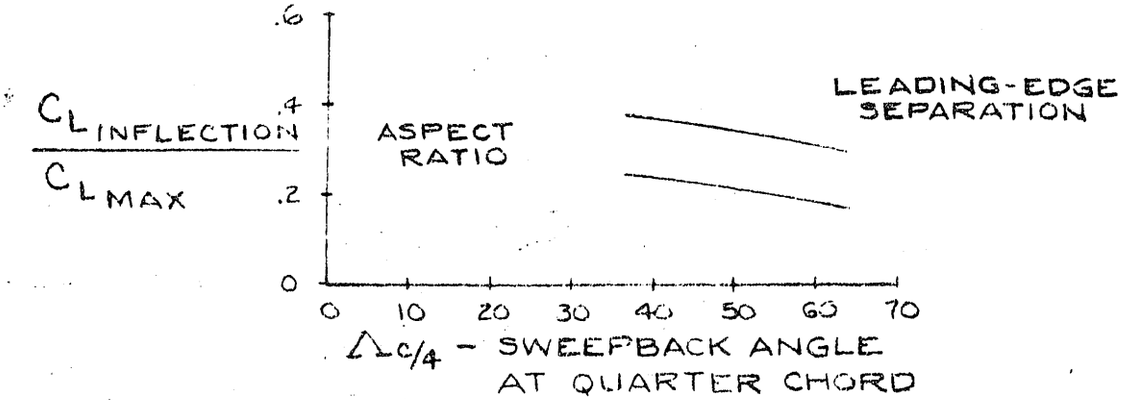

(b)

FIG. 193

INFLUENCE OF THE SWEEPBACK ANGLE ON THE WING MAXIMUM LIFT COEFFICIENT

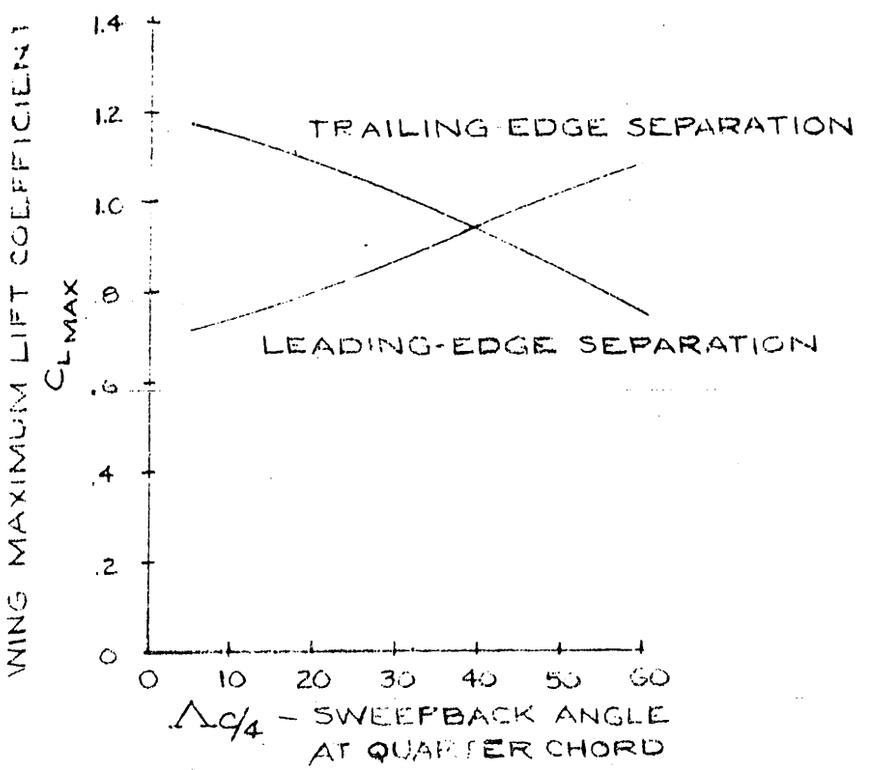

FIG. 194

INFLUENCE OF REYNOLDS NUMBER
ON THE WING MAXIMUM LIFT COEFFICIENT

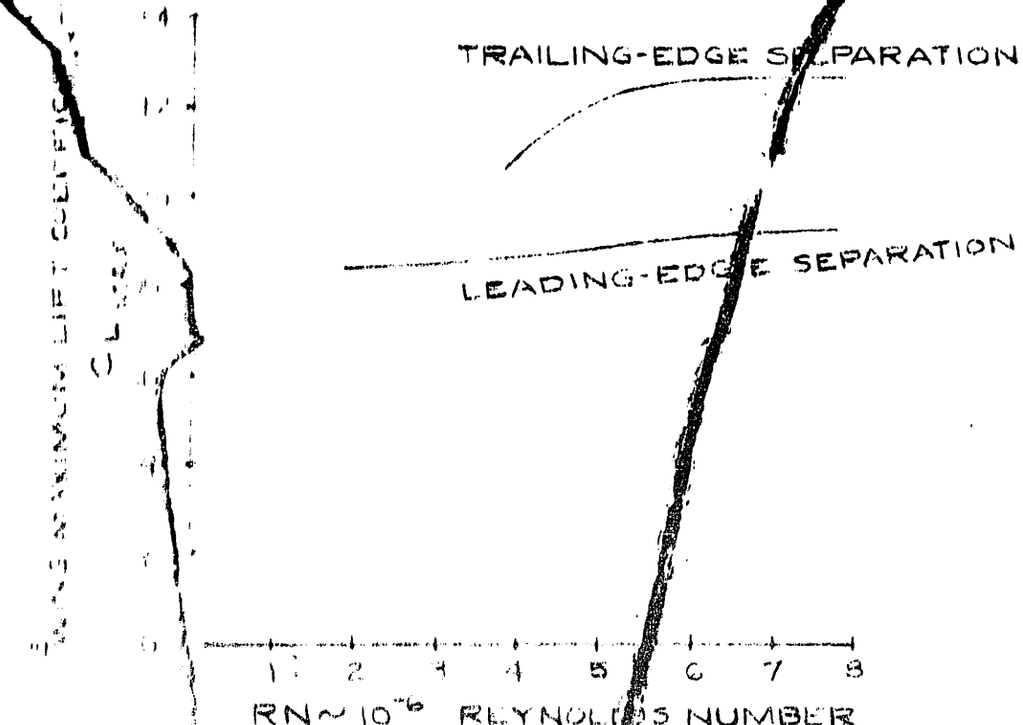

FIG. 19.6

VARIATION WITH SWEEP ANGLE OF MAXIMUM LIFT INCREMENT AND LIFT INCREMENT AT AN ANGLE OF ATTACK OF 0° DUE TO SEMISPAN SPLIT FLAPS FOR TWO FAMILIES OF WINGS. FLAPS DEFLECTED 60°
REF 309.

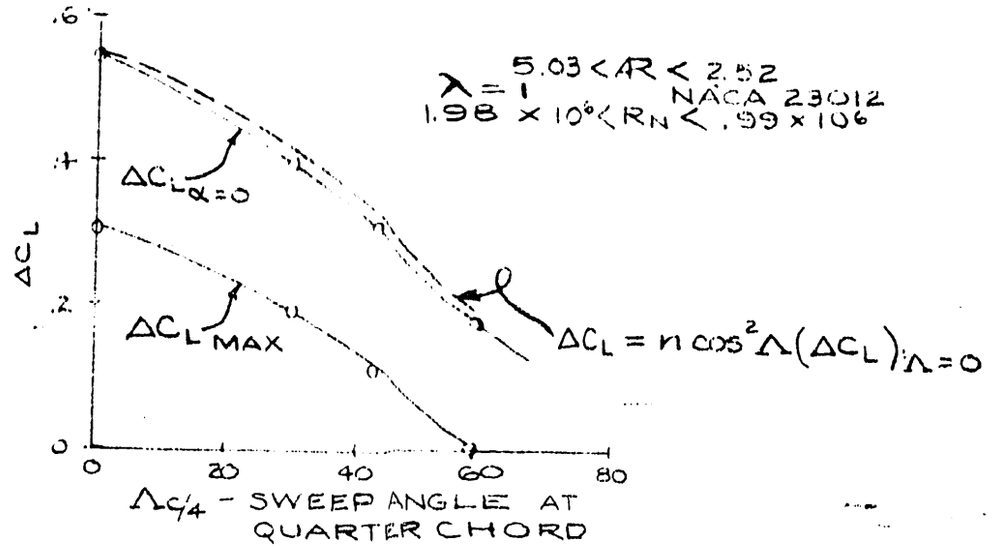

(a)

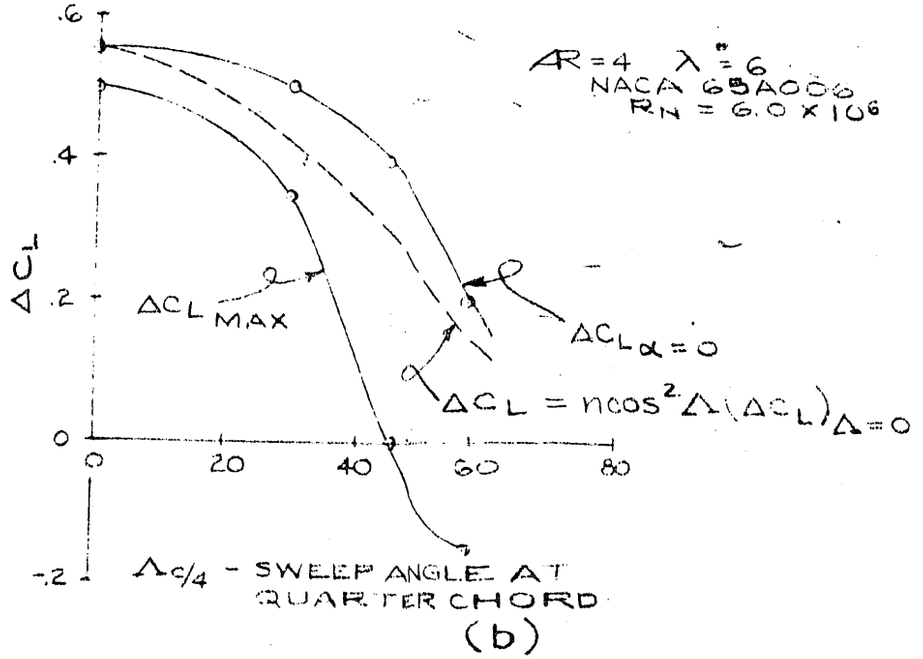

(b)

FIG. 196

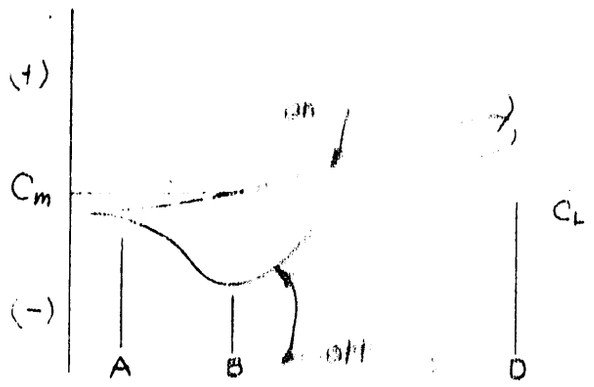

FIG 197